QC
851
.B6
no.1

December 1979
Boulder, Colorado

NOAA/ERL Wave Propagation Laboratory
National Center for Atmospheric Research

PROJECT PHOENIX

The September 1978 Field Operation



QC
851
36
no.1

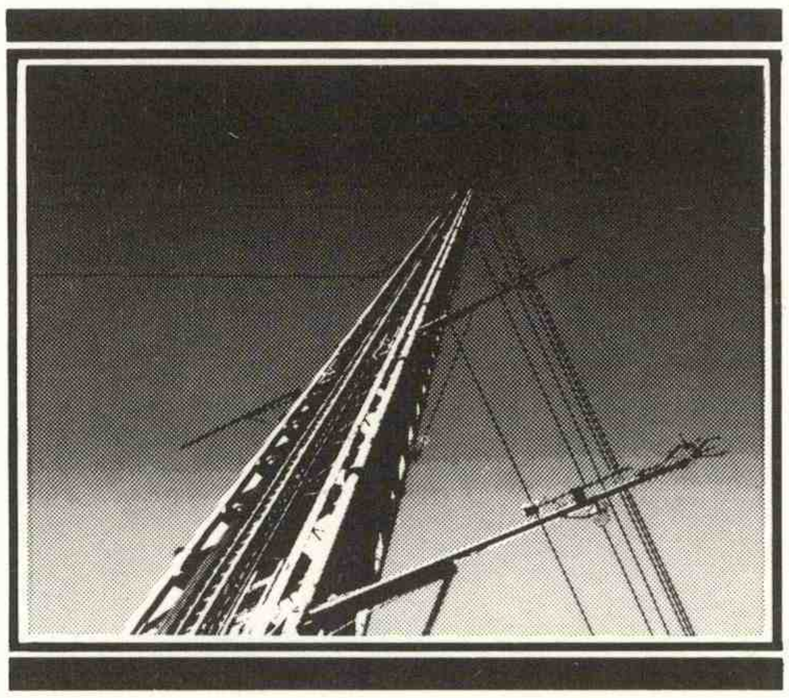
PROJECT PHOENIX

The September 1978 Field Operation

W. H. Hooke, Editor

SILVER SPRING
CENTER
APR 24 1980
N.O.A.A.
U. S. Dept. of Commerce

Report Number One
December 1979



NOAA/NCAR
Boulder Atmospheric Observatory

A joint publication of NCAR and NOAA available from NOAA/ERL, Boulder, CO 80303, and from the NCAR Publications Office, P.O. Box 3000, Boulder, CO 80307.

PO 1226

NOTICE

Mention of a commercial company or product does not constitute an endorsement by NOAA Environmental Research Laboratories or the National Center for Atmospheric Research. Use for publicity or advertising purposes of information from this publication concerning proprietary products or the tests of such products is not authorized.

The National Center for Atmospheric Research is operated by the University Corporation for Atmospheric Research and is sponsored by the National Science Foundation. Any opinions, findings, conclusions, or recommendations expressed in this publication are those of the author(s) and do not necessarily reflect the views of the National Science Foundation.

(Order by SD Stock No. 003-017-00474-1)

For sale by the Superintendent of Documents, U.S. Government Printing Office, Washington, D.C. 20402

PROJECT PHOENIX

The September 1978 Field Operation

Directors:

Peter H. Hildebrand
National Center for Atmospheric Research

William H. Hooke
Robert A. Kropfli
NOAA/ERL Wave Propagation Laboratory

CONTENTS

		Page
Foreword		vii
Preface		ix
Acknowledgments		xiii
Abstract		xiv
1.	Project PHOENIX: Background and Introduction W. H. Hooke, P. H. Hildebrand, and R. A. Kropfli	1
2.	BAO Site, Tower Instrumentation, and PHOENIX Operations J. C. Kaimal and D. E. Wolfe	16
3.	PHOENIX Multiple-Doppler Radar Operations R. A. Kropfli	33
4.	PHOENIX Operations of the NCAR Queen Air Research Aircraft P. H. Hildebrand	57
5.	Microwave Radiometer Studies in PHOENIX M. T. Decker	69
6.	FM-CW Radar Operations During PHOENIX R. B. Chadwick and K. P. Moran	80
7.	TPQ-11 (8mm) Radar Operations During PHOENIX F. Pasqualucci	88
8.	Lidar and Knollenberg Probe Operations During PHOENIX N. L. Abshire and G. M. Lerfald	93
9.	Optical Systems Measuring Surface-Level Convergence During PHOENIX R. B. Fritz and T.-I. Wang	104
10.	Portable Automated Mesonet (PAM) Observations During PHOENIX P. H. Hildebrand	112
11.	The PHOENIX Rawinsonde Data P. H. Hildebrand and R. B. McBeth	117
12.	PHOENIX Lagrangian Turbulence Observations Using Pibals and Tetroons S. R. Hanna	138
13.	Microbarograph Observations During PHOENIX A. J. Bedard, Jr., and C. Ramzy	150
14.	Acoustic Echo Sounder Operations During PHOENIX W. D. Neff and E. H. Brown	157
15.	A Brief Summary of Weather Conditions During PHOENIX D. E. Wolfe	176
16.	PHOENIX Summary Logs W. H. Hooke, P. H. Hildebrand, and R. A. Kropfli	239
17.	Interactive Access to the BAO Data R. S. Lawrence and M. H. Ackley	267

FOREWORD

The Boulder Atmospheric Observatory (BAO) is a unique national facility operated jointly by the National Oceanic and Atmospheric Administration (NOAA) and the National Center for Atmospheric Research (NCAR). The BAO, located 25 km east of the Rocky Mountains near Boulder, Colorado, consists of a 300-m instrumented meteorological tower, an array of ground-based remote and immersion sensing instruments, and a system for acquiring and archiving data. The facility is used for evaluating and testing meteorological instruments including remote sensors and for the study of boundary-layer dynamics, air pollution chemistry, and relationships between these areas of science and larger-scale meteorology.

BAO Reports are intended to document research activity at the observatory in a timely, useful fashion. Subject matter varies, and may include, but need not be limited to, descriptions of instrumentation, summaries of special research projects, manuals of procedures for using BAO facilities, and scientific reports. Their joint publication by NCAR and NOAA reflects the cooperative sponsorship of the BAO by both parent institutions, and a mutual interest in the dissemination of research results from this important national venture. On behalf of both organizations and the BAO staff, we are happy to present this report series.



William H. Hooke (NOAA/WPL)



Robert J. Serafin (NCAR/FOF)

PREFACE

Following more than a year of planning, the Wave Propagation Laboratory of NOAA and the Atmospheric Technology Division of NCAR, together with other agencies and institutions, carried out a major field study at the Boulder Atmospheric Observatory (BAO) during September 1978. Named PHOENIX*, the project used research-instrumented aircraft, a surface meteorological network, radars, lidar, acoustic sounders, microwave radiometers, optical wind sensors, rawinsondes and fixed-level balloons, and the BAO tower itself in amassing the basic data set. PHOENIX comprised numerous experiments, including (i) tests, evaluations, and comparisons of a number of the remote-sensing systems deployed and (ii) efforts to develop a relatively complete data set on the convectively active planetary boundary layer (PBL) and a wide variety of atmospheric processes at work within it. As opportunity permitted, PHOENIX teams also gathered data on cloud formation, development, and structure immediately above the PBL. Ultimate objectives of the work are improved understanding of the boundary layer and the methodology for its study.

At this writing, the data are still being analyzed. Already we can clearly anticipate a number of theoretical and experimental advances that should in time find their way into the open literature. Despite this prospect, however, we believe that the rich PHOENIX data set itself offers further opportunities for independent research, in directions that may have been unforeseen in our original planning or might perhaps lie outside the scope of our own in-house programs and objectives. In a similar way, previous experiments such as the O'Neill, Kansas, Wangara, and Minnesota expeditions have had a lasting impact on the progress of micrometeorology. Long after the corresponding in-house analyses have been completed, theorists have continued to turn to these landmark data

---

* The name PHOENIX has been chosen because the convective planetary boundary layer, like the bird of mythology, rises anew each day out of the "ashes" of the PBL from the previous day.

sets for their model evaluation and testing. In the case of the classic O'Neill experiment, for example, the summary volumes by Lettau and Davidson (1957) made using the data both attractive and convenient.

In order to help make the PHOENIX data similarly available and useful for this purpose to the meteorological community at large, we have prepared this summary document describing the PHOENIX field study. The document is organized as follows: Chapter 1 outlines the historical background and planning preceding the PHOENIX study, and provides a capsule summary of the experimental goals and objectives. The next thirteen chapters describe the specific instruments used in the PHOENIX studies and their mode of operation, and provide sample data outputs. Chapter 15 describes the synoptic weather situation during September. Chapter 16 provides a daily summary log of PHOENIX operations. BAO tower data can be made available through direct computer terminal access; procedures and available graphics are described in detail in Chapter 17. Our hope is that this volume will be followed by another that will summarize in-house scientific findings resulting from the project.

This report differs in one important respect from the O'Neill summaries. There, the full body of the data, formidable though it was, could be tabulated and presented essentially in toto. In PHOENIX, the remote-sensing systems and other instrumentation generated orders-of-magnitude more data, precluding their full presentation here. Instead our goal and hope is to publish what amounts to a catalog or digest of the data that will both accurately convey what is available and give instructions for obtaining it.

A high degree of teamwork and professionalism was displayed by every member of the PHOENIX effort. At no time has any PHOENIX participant given less than the fullest measure of selflessness and cooperation so necessary a part of any successful field program. From the outset we have known that the following PHOENIX data analysis would take place on a shoestring budget in the face of strongly competing demands on the time of every staff member. Through many planning meetings prior to the

experiment and data analysis meetings subject to PHOENIX implementation we have discussed this issue openly and faced it squarely. With management encouragement, the result to date has been a uniformly high degree of dedication to the studies and their ultimate goals and objectives. In this regard a special thanks is due to Robert A. Kropfli of WPL and Peter H. Hildebrand, formerly of the Illinois State Water Survey and now at NCAR, who served with me as directors of the PHOENIX project, in both its planning and operations, and who are now providing much of the commitment and impetus required to keep the data analysis moving forward.

William H. Hooke, Editor
Wave Propagation Laboratory
September 30, 1979

Reference

Lettau, H. H., and B. Davidson, Eds., Exploring the Atmosphere's First Mile, Pergamon, New York (1957).

ACKNOWLEDGMENTS

On behalf of all the PHOENIX participants, we are happy to acknowledge both the financial and moral support provided by NOAA management: Dr. Wilmot N. Hess, Director, ERL; Mr. Joseph O. Fletcher, Deputy Director, ERL; Dr. Alan R. Thomas, Director, Office of Programs; Dr. C. Gordon Little, Director, WPL; and their counterparts in NCAR management: Dr. Francis P. Bretherton, President, UCAR; Dr. John W. Firor, Executive Director, NCAR; Dr. Clifford Murino, Director, ATD; and Dr. Robert J. Serafin, Manager, FOF. Science advances to the extent that such men match a discerning vision with a corresponding commitment of resources, and these men have done so amply, both in fostering the BAO concept and nurturing the resultant facility, and in implementing the PHOENIX project in particular.

On behalf of all the PHOENIX staff (and the WPL Meteorological Radar Program Area especially) we would like to thank the National Science Foundation for its support of radar operations and analysis during this experiment, through Agreement # ATM-7722135 A01. We are grateful for the support received from the staffs of NOAA's Wave Propagation Laboratory, NCAR's Field Observing Facility, and NCAR's Research Aviation Facility, who operated the radars, flew the aircraft, and were responsible for collection of the data sets reported herein. We also gratefully acknowledge the help we received from Steven R. Hanna and his staff at NOAA's Atmospheric Turbulence and Diffusion Laboratory, and from Bruce L. Gary and his staff at NASA's Jet Propulsion Laboratory. We believe that this report and the other scientific publications and papers to follow will repay the faith and support supplied by all these sponsors.

One of us (PHH) would like to acknowledge the vision, encouragement, and support of Dr. Robert J. Serafin and Mr. Richard E. Carbone of NCAR/FOF, and to acknowledge support under NSF grant # ATM-76-24236.

Finally, we also gratefully acknowledge the help of Ms. Jeannette Garing, who performed in an outstanding way, far exceeding the normal requirements of her position, in relieving one of us (WHH) of much of the administrative burden associated with BAO operations and the PHOENIX experiment, and Ms. Mildred Birchfield, for her extraordinary patience and helpfulness in expertly typing and retyping the many versions of this document.

Peter H. Hildebrand
William H. Hooke
Robert A. Kropfli
PHOENIX Directors

ABSTRACT

This report describes the instruments tested and compared and equipment used during Project PHOENIX, a major field study of the planetary boundary layer. The data-gathering systems evaluated include multiple-Doppler radar, microwave radiometer, FM-CW radar, TPQ-11 radar, lidar, optical wind sensors, the Portable Automated Mesonet (PAM), rawinsonde, microbarograph, acoustic sounders, balloons, aircraft, and the 300-m BAO tower. Also provided are a discussion of the project's background and planning, a description of the synoptic weather situation during the experiment, instructions for access to the data, and a daily summary log of PHOENIX operations.

CHAPTER 1

PROJECT PHOENIX: BACKGROUND AND INTRODUCTION

W. H. Hooke[1], P. H. Hildebrand[2], and R. A. Kropfli[1]

1.1 History

The PHOENIX experiment — its organization and goals — is best understood when it is viewed as one step in a progressive sequence of boundary-layer experiments extending nearly thirty years in the past and likely to continue for three decades more. In America, these experiments are rooted in the classic O'Neill and Great Plains programs of the 1950's, and include the 1968 Kansas and 1973 Minnesota studies. They have their counterparts in the research activities of other countries, including, for example, the Kerang, Hay, and Wangara field exercises in Australia. To a considerable extent they have molded the boundary-layer studies carried out as part of major national and international field programs such as BOMEX, IFYGL, AMTEX, METROMEX, and GATE, to name just a few.

Each of these experiments has been motivated primarily by the urgent need to learn more about both physical and chemical boundary-layer phenomena. Without exception, however, these investigations have been severely constrained by the lack of resources and technological capabilities necessary for obtaining an adequate data set. Historically, therefore, boundary-layer studies have been preoccupied with the testing and evaluation of new observing technologies. The early boundary-layer experiments demonstrated the potential of sonic anemometry for highly diagnostic turbulence measurement, while later experiments brought such techniques to their present maturity. The major atmospheric field programs have added a new dimension to planetary boundary-layer (PBL) research through the effective use of instrumented aircraft to provide spatially-averaged data sets representative of conditions over wide areas. The very latest and most sophisticated of these studies have typically featured one or more ground-based remote-sensing systems — such as radars, lidar, or acoustic sounders — which could provide area and volume spatial coverage in some respects surpassing that of the aircraft.

---

[1] Wave Propagation Laboratory, National Oceanic and Atmospheric Administration, Boulder, Colorado 80303.

[2] National Center for Atmospheric Research, Boulder, Colorado 80307.

Difficult as it may have been to introduce new measurement technology in the 1950's, the successful melding of these remote-sensing systems of the 1970's into observing programs poses far greater problems in logistics, operation, and subsequent data processing and interpretation. As a result, the rate at which these new techniques have been integrated into PBL experiments has seemingly been slower. Results to date have been intriguing in some cases, downright exciting in others, but the effective incorporation of these devices into field experiments has proved a relatively stubborn and unyielding problem, requiring considerable planning and experience and a good deal of simple trial-and-error.

By the early 1970's, it had become apparent from such field trials that the pressure-cooker environment of major international experiments, posing inflexible deadlines and requiring tight coordination, was not the ideal arena for mastering the new tools. What was needed was a field site where such tests could be conducted on a more continuous, ongoing basis, allowing greater freedom and flexibility, and fostering a more relaxed atmosphere. It was with this goal and objective in mind that NOAA's Wave Propagation Laboratory (WPL) and NCAR's Field Observing Facility (FOF) began planning for the Boulder Atmospheric Observatory (BAO). Now a reality, the BAO provides just such a free environment for conducting boundary-layer studies while simultaneously evaluating and testing meteorological instrumentation (Hall, 1977; Hooke, 1978; Kaimal, 1978). It provides capabilities both for ongoing, routine experiments and tests as well as special, more concentrated and intense field studies.

The PHOENIX experiment is a good prototype of the latter. In the context of the overall BAO program, the concept of carrying out a major study of the convectively active PBL is natural indeed. Even the very earliest planning documents for the facility and its scientific program spoke of such an experiment. However, amidst budgetary concerns and preoccupation with the very practical matters associated with erecting and instrumenting the BAO tower and developing the automatic data processing (ADP) software, WPL and FOF staff saw little hope of conducting such a convective PBL study at any time prior to 1979.

Nevertheless, in 1977 it became apparent that a prototype experiment could be implemented as soon as the late summer or early fall of 1978. Moreover, at that point we could see that this experiment constituted a useful complement to and extension of a similar study carried out by Hildebrand in May of 1977 in

Oklahoma, where NCAR aircraft, radar equipment, and KTVY-tower instrumentation operated by NOAA's National Severe Storms Laboratory (NSSL) were combined to study the convectively-active PBL. It proved possible to schedule a number of NCAR facilities, including the portable automated mesonet (PAM) network, two Queen Air instrumented aircraft, a rawinsonde, and a C-band radar, for the month of September 1978. The WPL X-band dual Doppler radars and other remote-sensing systems were similarly available. Simultaneously, the Environmental Radiometry Program Area of WPL was able to arrange for the use of microwave radiometers during the same month to carry out radiometric measurements of atmospheric temperature and humidity profiles. Thus, despite relatively short notice, we found it possible to accelerate the scheduling of studies at the BAO by what amounted to a full year.

1.2 Experimental Goals

Prior to the PHOENIX experiment, a number of planning meetings served to identify and highlight a number of major goals. These objectives were quite numerous, but most could be categorized comfortably under three main headings. The first major group of objectives focused on obtaining a definitive, essentially complete, and (where possible) redundant data set on dry PBL dynamics over the BAO terrain. While the experiment concentrated on the convectively active PBL, both for purely historical reasons having to do with the origin of the experiment and because neither WPL nor NCAR could field the crews required for 24-hour-a-day operation, there were a few nighttime observations. The second major group of objectives focused on moist processes — developing a data set on clouds, cloud processes, and cloud environments in the layer directly above the PBL. As it happened, this particular September proved rather dry; however, we were able to carry out cloud studies on several days. Third, and finally, the participating laboratories evaluated, tested, and compared the performance of a wide variety of atmospheric remote sensors.

Before addressing each of these goals in the succeeding sections, we should like to reemphasize that we felt that a primary need in our pursuit of all three objectives was to obtain as much redundancy in the measurement of the relevant atmospheric parameters as possible. Thus, many of the atmospheric variables were measured by two or more methods independently. Each time such redundant information has been available, we have begun our analysis by comparing the various measurements before leaping ahead to atmospheric studies. We anticipated — and

our experience in the data-analysis phase of PHOENIX to date has borne this out — that such comparisons are salutary for several reasons. Initial comparisons almost invariably reveal numerous unacceptable discrepancies, which bring to light errors in the data-processing routines, calibration problems, etc. (Lacking such redundancy, we would have been reduced to spotting such errors solely through checks for internal consistency of the individual data sets, a comparatively weak diagnostic tool.) After all such errors have been tracked down and eliminated, those discrepancies that still remain give a good idea of the uncertainties inherent in each of the several measurement techniques compared. Theorists are then free to focus their time and energy on those actual atmospheric phenomena revealed by all the sensors rather than waste effort in fruitless speculation on those that may be nothing more than artifacts of a particular data set.

1.3 Studies of the Dry Planetary Boundary Layer

1.3.1 Studies of the convective PBL

A major goal — not only the original goal in the very earliest planning of the PHOENIX experiments, but also the goal we felt had to be achieved before we could consider PHOENIX a success — was to study in some detail those physical processes associated with dry convective PBL development. These processes include atmospheric heating adjacent to the earth's surface, the development of turbulence through convective instability, the entrainment of air from the overlying inversion into the resulting mixed layer, the concomitant increase in mixed-layer depth, the triggering of secondary circulations, and the interactions of these with synoptic meteorological settings on the one hand and local terrain influence on the other. Our hope was that the data analysis would provide new physical understanding of these processes and interactions leading to improved parameterizations for use in numerical models. Specific subgoals and objectives for the experiment and data analysis included the following six studies:

i) A study of gross features of the PBL and its temporal development each day at the BAO. The data for this study were to consist of height profiles of mean wind and temperature as functions of time, and estimates of mixed-layer depth, made using records from the tower or X-band and C-band Doppler radars, FM-CW and TPQ-11 radars, aircraft, rawin-

sondes, and acoustic sounders, and following PBL changes throughout the daylight hours.

ii) A study of meso-γ scale (0.1-10 km) PBL features such as roll vortices and gravity waves. Here acoustic-sounder, lidar, FM-CW, TPQ-11, and multiple-Doppler radar data were to be juxtaposed with tower measurements in order to provide time histories as these features developed and passed over fixed points. To supplement this picture, visualizations of the corresponding spatial structure were provided by the multiple pulsed-Doppler radars and instrumented aircraft. The plan called for comparing theoretical and observed spatial and temporal scales, velocity amplitudes, and fluxes associated with the circulations and their internal structure.

iii) A study of PBL entrainment. This is a poorly understood but important process accompanying PBL growth during the morning hours. PHOENIX plans called for NCAR Queen Air flights to probe the entrainment layer intensively, measuring fluxes of heat and momentum, both for comparison with the incomplete theory currently available and for the development of new concepts.

iv) A study of the effects of terrain on convective PBL development. Plans called for careful analysis of aircraft, PAM, and multiple-Doppler radar data, looking first for evidence of terrain effects. This would be followed by efforts to establish precise relationships between PBL depth and the spatial structure and amplitude of geographically stationary secondary circulation patterns on the one hand, and the corresponding features of the underlying topography on the other.

v) A comparison of the Colorado high plains PBL with that over Oklahoma. The Colorado PBL is typically drier, deeper, and subject to lower wind speeds than its Oklahoma counterpart. Juxtaposing the PHOENIX data set with a similar data set obtained one year earlier by Hildebrand in Oklahoma should permit a uniquely detailed comparison of the two regimes.

vi) A study of turbulence velocity and temperature spectra and statistics. We have a good idea of what turbulence velocity and temperature spectra

should look like over smooth terrain (from, e.g., the AFCRL Minnesota experiment). Thus, plans called for using PHOENIX data to assess terrain effects on turbulence spectra, measured by aircraft, radars, and the tower. Study of turbulence variances, covariances, and perhaps higher-order moments should permit us to investigate the applicability of Monin-Obukhov similarity and other scaling over the BAO terrain. In like manner we plan to examine the effect, if any, of the BAO terrain on turbulence energy budgets. Differences between these and their counterparts over idealized terrain could be due to advection effects or to large-eddy production in the surface layer.

1.3.2 Comparison of Eulerian and Lagrangian turbulence statistics

As another goal, we set the development of simultaneous data sets on turbulence statistics in both Eulerian (fixed) and Lagrangian (flow-following) coordinate systems. This particular experiment was led by Dr. Steven R. Hanna, Research Meteorologist at NOAA's Atmospheric Turbulence and Diffusion Laboratory in Oak Ridge, Tennessee, who worked cooperatively with staff from WPL's Meteorological Radar group to obtain Lagrangian statistics on turbulent velocity fluctuations in the PBL by measuring Doppler shifts in X-band radar echoes from constant-level balloons. By using this technique, Hanna and the WPL crew were able to achieve sampling rates one or two orders of magnitude higher than those previously available, which relied upon successive-range-difference data from non-Dopplerized radars. As the data analysis proceeds, the results will be compared with corresponding Eulerian statistics determined by using data collected at fixed levels of the BAO tower. Ultimately it will be desirable to make such comparisons under a wide variety of meteorological conditions, including different times of day and seasons of the year. However, in this experiment the focus was on the convectively active PBL, since during such periods there was much more information on the background meteorological conditions.

1.3.3 Study of the nocturnal PBL

The nocturnal PBL not only poses many challenges to the theorist, defying our complete understanding despite the repeated and concerted efforts of the last several decades, but it also presents many obstacles to those who would observe

it. For example, the strong turbulent mixing characterizing the convectively active PBL is absent at night; what weak mixing still occurs is insufficient either to disperse or maintain aloft the chaff required for X-band pulsed Doppler radar observations. Nevertheless, because of its implications for air-quality meteorology, the need to improve our understanding of the nocturnal PBL is so great that we must begin planning now for a major nocturnal PBL experiment in one or two years' time from this writing. Moreover, while any forthcoming full-scale nocturnal PBL study promises to be rather expensive, we felt that the incremental costs associated with occasionally gathering nocturnal data during the PHOENIX program should be relatively small, given that the requisite physical resources had already been assembled for other purposes. For this reason, even though we did not field the crews necessary to provide for 24-hour-a-day operation throughout September, we did operate during nighttime hours on two evenings. Goals for the nighttime experiments and data analysis included the following:

i) An evaluation of the utility of the WPL multiple X-band Doppler radars (which require chaff for clear-air work) under nocturnal conditions. Unfortunately, this goal could not be achieved. In order to ensure achievement of the goals for the daytime work, we postponed nighttime work until the end of September. By that time all radar crews were experiencing considerable fatigue, and an attempt at 24-hour operation was deemed unwise.

ii) Development of as complete a picture as possible of the nocturnal PBL flow over the BAO terrain, including any circulation that might be associated with the topography and the vertical structure of mean winds and temperature, as well as turbulent properties, including spectra, and energy and momentum budgets. To the extent that the radar data were essential to this picture, this goal was not achieved either; however, some information on surface flows will be provided by analysis of data from NCAR's portable automated mesonet (PAM) network, from the BAO tower, and from the acoustic sounder and FM-CW radar.

iii) Acquisition of a data set tracing the complete diurnal cycle of the PBL, including not only the daytime development of the convectively active PBL, but also the collapse of the convective PBL at dusk, the development of the nocturnal inversion during the hours immediately following,

achievement of steady-state and its episodic interruption as the night progresses, and the breakup of the inversion at dawn. Tower, aircraft, and acoustic-sounder data are being used to investigate these processes.

1.3.4 Study of low-level terrain effects

In April of 1978, a site evaluation experiment was conducted at the BAO in order to gain some preliminary information on the effect of the local terrain on the turbulence characteristics of the area. As one element of this study, P. Kahn and J. A. Businger of the University of Washington observed surface airflow over the BAO terrain, using NCAR's PAM network, deployed on a small grid of very high resolution (element spacing in some cases considerably less than 1 km). During PHOENIX, the PAM system was again deployed around the BAO, this time over a coarser, larger-scale grid. The combined April and September data sets should permit a detailed look at the surface airflow over a 100 km^2 area centered on the BAO, and its relation to the prevailing wind and stability conditions as indicated by aircraft, tower, and X-band dual-Doppler radar data. Such information will be extremely useful in planning for future BAO experiments.

1.3.5 Studies of long-path, near-ground statistics of aerosol distribution

There is considerable interest in, and currently very little data available on, long-path, near-ground statistics of aerosol distribution. To meet this need, the Atmospheric Spectroscopy Program Area of WPL has attempted to record such data by using its pulsed lidar system as targets of opportunity arise, taking such measurements during a number of field experiments whenever the lidar was not required for other purposes. Data on aerosol distribution from Fairplay, Colstrip, NHRE, and the Boulder area have been obtained in this way. While the data obtained during PHOENIX were relatively few in number, they are unique in that they were recorded in conjunction with in-situ data from a Knollenberg probe flown along the lidar beam.

1.3.6 Data sets for the wind-energy community

The wind-energy community has considerable interest in obtaining statistical and climatological data on PBL winds, particularly in the lowest several hundred

meters, for use in the design of wind-powered electrical generators. For this application, the data must include information not only on the mean wind profiles, but also on properties of the turbulent gusts, since the latter can be dominant contributors to airfoil loading and vibrational stresses. Of particular importance in wind-powered generator design are data for extreme wind conditions. On Monday, September 11, 1978, winds picked up considerably at the BAO site following the passage of a small frontal system, and the tower was operated accordingly in its maximum-data-rate mode, in order to collect the desired statistics. In the data-analysis effort WPL is working under the sponsorship of the Battelle Pacific Northwest Laboratories.

1.4 Studies of Clouds and Cloud Environments

A second major goal — and one that rapidly assumed greater importance during the final weeks of the PHOENIX planning, as it became apparent that new remote-sensing systems such as WPL's TPQ-11 eight-millimeter radar could be readied for operation in time for the experiment — was to study in some detail the dynamical and microphysical processes associated with low-level clouds. Clouds play a fundamental role in atmospheric physics, figuring prominently in the atmosphere's radiative budget, and the hydrologic cycle, and affecting weather on all spatial and temporal scales ranging from local short-term events to global climate. However, despite their importance, and the level of effort expended in their study, they remain an area of some ignorance, largely because of the observational challenge they pose. As a result of the remote-sensor development of the last several years, we stand on the threshold of greatly expanded, highly diagnostic capability in our observations of clouds and cloud processes. However, before we can exploit this capability in future cloud-research programs, we must perform a number of calibrations, intercomparisons, and tests.

While Septembers are not ideally suited for cloud studies in Colorado, we did recognize that some cloudy, rainy days might be expected, that such weather would preclude study of the convectively active planetary boundary layer, and that in order to make fullest use of the rather extensive observational capability at the BAO, we had to prepare a cloud observation plan for use should the opportunity arise. Toward this end we developed several specific goals. The first of these called for observations of cumulus clouds in their nascent, growing phase.

In particular, we had hoped to examine regions of horizontal convergence (as indicated by the triangles of optical sensors deployed for measuring horizontal convergence at the earth's surface, the PAM system, and radar data) believed to engender clouds in high humidity. However, apart from one or two days in which cloud cover was essentially total, the humidity remained sufficiently low and synoptic-scale subsidence sufficiently great that skies over the PHOENIX test area remained clear; thus, we never did seriously attempt to observe the development of convective clouds during PHOENIX. We also hoped to examine glaciation in young, growing clouds. It is now believed that glaciation may occur at an earlier stage in cloud development and at warmer temperatures than formerly supposed, possibly because of aerosols of biological origin that might serve as ice nuclei. We had hoped to study such glaciation in young, growing cumuli using lidar, radar, and in-situ data. However, no suitable events occurred during September 1978. A similar plan, calling for study of PBL structure in thunderstorm cold-air outflows, was also abandoned because of the lack of opportunity.

What did occur during this particular September was the development of a stratus deck over the site on a few occasions. WPL took advantage of this opportunity to develop lidar, TPQ-11 radar, multiple Doppler X-band radar, and FM-CW radar data sets on echo returns from the cloud, for comparison with data from a Knollenberg probe flown aboard a light aircraft. From these data sets it is proving possible to compare observed echo strengths with those predicted theoretically from knowledge of the cloud-droplet number densities and size spectra.

1.5 Evaluation and Testing of Remote Sensors and other Meteorological Instrumentation

A third major goal, and perhaps the most important from the point of view of the Wave Propagation Laboratory, was to use PHOENIX to evaluate, test, and compare a wide variety of remote-sensing systems and meteorological instruments. The specific subgoals were numerous, but could be categorized fairly neatly into a series of experiments involving primarily (i) the multiple-Doppler X- and C-band radars, (ii) tests of several microwave radiometers, (iii) checkout of the TPQ-11 radar and comparison of the TPQ-11 radar, lidar, and FM-CW radar with one another, (iv) operation of the FM-CW radar in a VAD mode, (v) comparison of various estimates of horizontal convergence, and (vi) calibration of the BAO acoustic Doppler sounding system. Here we enumerate and expand upon these goals in turn.

1.5.1 Evaluation of multiple-Doppler radar measurement techniques

The original PHOENIX remote-sensing goals called for evaluation of the multiple X- and C-band pulse-Doppler radars with regard to a number of particular aspects of their overall performance. Generally speaking, the evaluations involved comparing radar observations of the convective-PBL motion field on all measurable spatial and temporal scales with other data describing that same motion field, obtained variously by aircraft, FM-CW radar, acoustic echo sounder, and tower instrumentation. For the most part, the radars determined PBL winds by measuring the Doppler shifts detected in the motion of reflective chaff distributed by light aircraft flying within the PBL. However, on many days the radars were able to detect apparent clear-air returns, possibly from insects. Specific goals for the radar work included the following:

i) Comparing radar-derived three-dimensional wind fields with those derived from tower, aircraft, FM-CW, PAM, and acoustic-sounder data.

ii) Testing the effect of different lower-boundary conditions on the velocity-field recovery. In effect, each incorporated BAO topography, PAM data, and other inputs in a different way.

iii) Evaluating a variety of radar time-space sampling modes.

iv) Comparing radar, tower, and aircraft estimates of turbulence quantities such as the eddy dissipation rate ε and Reynolds stresses $\langle u'w' \rangle$, $\langle v'w' \rangle$.

v) Obtaining a data set with which to compare theory (Gal-Chen, 1978a,b; Hane and Scott, 1978; Leise, 1978) for the recovery of mesoscale temperature fields from Doppler-radar winds.

vi) Testing turbulence-parameter extraction from VAD measurements at a single radar site, using a method developed by Srivastava.

vii) Comparing the X-band radar echo strengths with those measured by other radars operating at different frequencies.

1.5.2 Evaluation of radiometric profiling techniques

With its wide variety of atmospheric observations, the PHOENIX experiment provided a good opportunity for a joint study of radiometric techniques for atmospheric profiling planned by WPL and NASA's Jet Propulsion Laboratory. These techniques measure microwave thermal radiation from the atmosphere and infer atmospheric temperature and water vapor profiles as well as line integrals of water vapor and cloud liquid. Five-channel radiometric systems with frequencies in the oxygen-absorption complex near 60 GHz, the water-vapor absorption band near 22 GHz, and the window between these, have demonstrated their usefulness in this application under both clear and cloudy environments. Even with this progress, however, further potential improvement should be attainable. Realizing some of this potential was an important goal of the PHOENIX experiment. Specific subgoals included the following:

i) Improved height resolution of atmospheric temperature and water vapor profiles. Theoretical studies have shown that this is achievable if data from microwave radiometers can be combined with knowledge of inversion or boundary-layer height. These heights can be derived from radar, lidar, and acoustic-echo-sounder data, as well as from in-situ instruments mounted on towers or airborne platforms. Many of these ancillary instruments were operated for this purpose during the PHOENIX experiment.

ii) Intercomparison of several radiometers. In the past, measurements of atmospheric radiation have usually been compared with values computed from rawinsonde data. An examination of radiation measurements from collocated radiometers should give some information on whether the biases derived from radiometer-radiosonde comparisons are due to the radiometric instruments or arise from other sources.

iii) Observation of horizontal atmospheric structure. We planned to test radiometric ability to observe horizontal structure by any of several methods, including elevation scan, time-series analysis, or time-delayed correlation of geometrically-spaced observations. These structures included clumpiness, horizontal gradients, wave motions, and thermal plumes among others. Ultimately, the radiometric data should

be compared with other data on the same structures available from radars, acoustic sounders, and other sources.

iv) Sensing of stratospheric temperatures. Some of the channels of the WPL radiometer were specifically designed to observe radiation from altitudes above the tropopause.

1.5.3 Calibration and comparison of the TPQ-11 radar with other instruments

Just prior to the PHOENIX experiment, WPL completed first-phase development of a new 8.6-mm radar capability suitable for use in cloud studies. As a first step, a conventional TPQ-11 radar was modified in order to achieve a 10-dB gain in sensitivity. The PHOENIX experiment provided an excellent opportunity to compare TPQ-11 data with data from other radars and lidar, as well as with in-situ measurements, in order to verify the nature of the atmospheric processes responsible for the echoes (particle scatter versus refractive-index fluctuations). Specific goals included the following:

i) Comparing TPQ-11 clear-air and cloud echo-returns with FM-CW and lidar data.

ii) Comparing TPQ-11 and lidar data with in-situ (Knollenberg probe) data on cloud-particle number density and size distribution.

1.5.4 Evaluation of FM-CW radar performance

The FM-CW radar team had several main objectives, including the following:

i) Continuing evaluation of the FM-CW radar as a device for detecting low-level wind shear at airports. To do this requires an ability to sense PBL winds at low elevation angles. During the PHOENIX experiment the FM-CW radar measured minimum elevation angles and received power for different azimuths.

ii) Comparing FM-CW wind measurements with wind data from the tower, acoustic Doppler, rawinsonde, aircraft, and dual-Doppler radars.

iii) Determining the angular dependence of FM-CW radar echo returns from stable layers.

iv) Comparing FM-CW estimates of the structure function C_n^2 of the turbulent echo returns and the eddy dissipation rate ε with tower data.

1.5.5 Comparison of various estimates of horizontal convergence

Horizontal convergence of atmospheric surface flows is of considerable interest because of its apparent association with cumulus development. A number of techniques were available during the PHOENIX experiment for measurement of horizontal convergence. These included the multiple Doppler radars, triangles of optical paths for measuring line-integrated surface winds, and the PAM network. Data from all these sensors will be compared as part of the PHOENIX analysis.

1.5.6 Calibration of the BAO acoustic Doppler wind profiling system

One of the remote-sensing systems that is to be a permanent part of the operational BAO is an acoustic-Doppler wind-sensing system. During the month of September one prototype version of this system was operated essentially continuously to permit calibrating it against data from the radars, and the tower.

1.5.7 Calibration of the Sunset VHF radar

The PHOENIX experiment had at its disposal a considerable amount of flight time for NCAR instrumented aircraft. As a result, these could be flown over the Rocky Mountains west of the BAO to obtain wind profiles directly above the Sunset VHF radar system operated there by ERL's Aeronomy Laboratory. The objective of this work was to provide uniquely definitive wind profiles for comparison; previously the group had to rely solely on Denver-area rawinsondes.

1.6 A Final Note of Caution

We regret that we must close this introduction with a caveat. However, despite our best efforts to achieve a consensus prior to the experiment on the

use of Mountain Standard Time (MST) versus Mountain Daylight Time (MDT), we found after the fact that most (but not all) remote-sensor groups used MDT, while the tower data were recorded on MST. Rather than attempt the formidable and unrewarding task of making the two data sets perfectly compatible, we have chosen to simply alert readers and potential users to the problem, suggesting appropriate care in acquiring and using the data.

References

Gal-Chen, T., A method for the investigation of the anelastic equations: implications for matching models with observations, Mon. Weather Rev. 106, 587-606 (1978a).

Gal-Chen, T., Deduction of pressure and density fluctuations using Doppler radars observations: a feasibility study, Preprints 18th Conf. Radar Meteorology, March 28-31, 1978, Atlanta, Georgia, pp. 104-111, American Meteorological Society, Boston, Mass. (1978b).

Hall, F. F., Jr., The Boulder Atmospheric Observatory and its meteorological research tower, Optics News 3, No. 2, 14-18 (1977).

Hane, C. E., and B. C. Scott, Temperature and pressure perturbations within convective clouds derived from detailed air motion information: preliminary testing, Mon. Weather Rev. 106, 654-661 (1978).

Hooke, W. H., The Boulder Atmospheric Observatory, Proc. 3rd U.S. National Conf. on Wind Engineering Research, February 26-March 1, 1978, Gainesville, Florida, pp. 81-88, National Science Foundation, Washington, D.C. (1978).

Kaimal, J. C., NOAA Instrumentation at the Boulder Atmospheric Observatory, Preprints 4th Symposium on Meteorological Observations and Instrumentation, April 10-14, 1978, Denver, Colorado, pp. 35-40, American Meteorological Society, Boston, Mass. (1978).

Leise, J. A., Temperature retrieval from dual-Doppler radar wind field data, Preprints 18th Conf. Radar Meteorology, March 28-31, 1978, Atlanta, Georgia, pp. 94-99, American Meteorological Society, Boston, Mass. (1978).

CHAPTER 2

BAO SITE, TOWER INSTRUMENTATION, AND PHOENIX OPERATIONS

J. C. Kaimal and D. E. Wolfe
Wave Propagation Laboratory
National Oceanic and Atmospheric Administration
Boulder, Colorado 80303

2.1 The BAO Site

The PHOENIX experiment focused on the convective planetary boundary layer above roughly 100 km^2 of the Colorado high plains centered on the Boulder Atmospheric Observatory (BAO). The observatory proper is situated on a section of land (a square 1.0 mi, or 1.6 km, on a side) in gently rolling terrain some 25 km east of the foothills of the Rocky Mountains and some 30 km north of Denver. Figure 2.1 provides a schematic map of the Denver-Boulder area, indicating the BAO location. The town closest to the BAO is Erie, Colorado, some 5 km to the west and some 30 m lower in elevation. Figures 2.2a,b are contour maps of the immediate BAO terrain. From these maps we see that the terrain in the general vicinity of the BAO exhibits a 1%-2% north-south grade, while sloping downward from the tower both to the east and west. Superimposed on this larger-scale topography are a number of smaller-scale features, some of considerable amplitude. Figure 2.3 provides a map of intermediate scale and resolution, which displays the PHOENIX experimental area itself. It also shows the deployment of the three X-band Doppler radars, the PAM network surface stations, and the large optical triangle used in the experiment. Figure 2.4 depicts the BAO-PHOENIX terrain as viewed from the 50-m and 10-m levels of the tower. The 50-m level horizon corresponds more closely to the PHOENIX test area; the 10-m level photographs show more clearly the terrain topography and surface characteristics. Figures 2.5a,b depict aerial and ground views of the BAO tower. Together these photographs should give the reader a general impression of the site and terrain. The ground cover consists primarily of grasses — both wild grasses and crops — broken by small clusters of buildings and trees. The area overlies a coal seam, and here and there one finds evidence of coal-mining activity, such as crushing mills, slag piles, or subsidence.

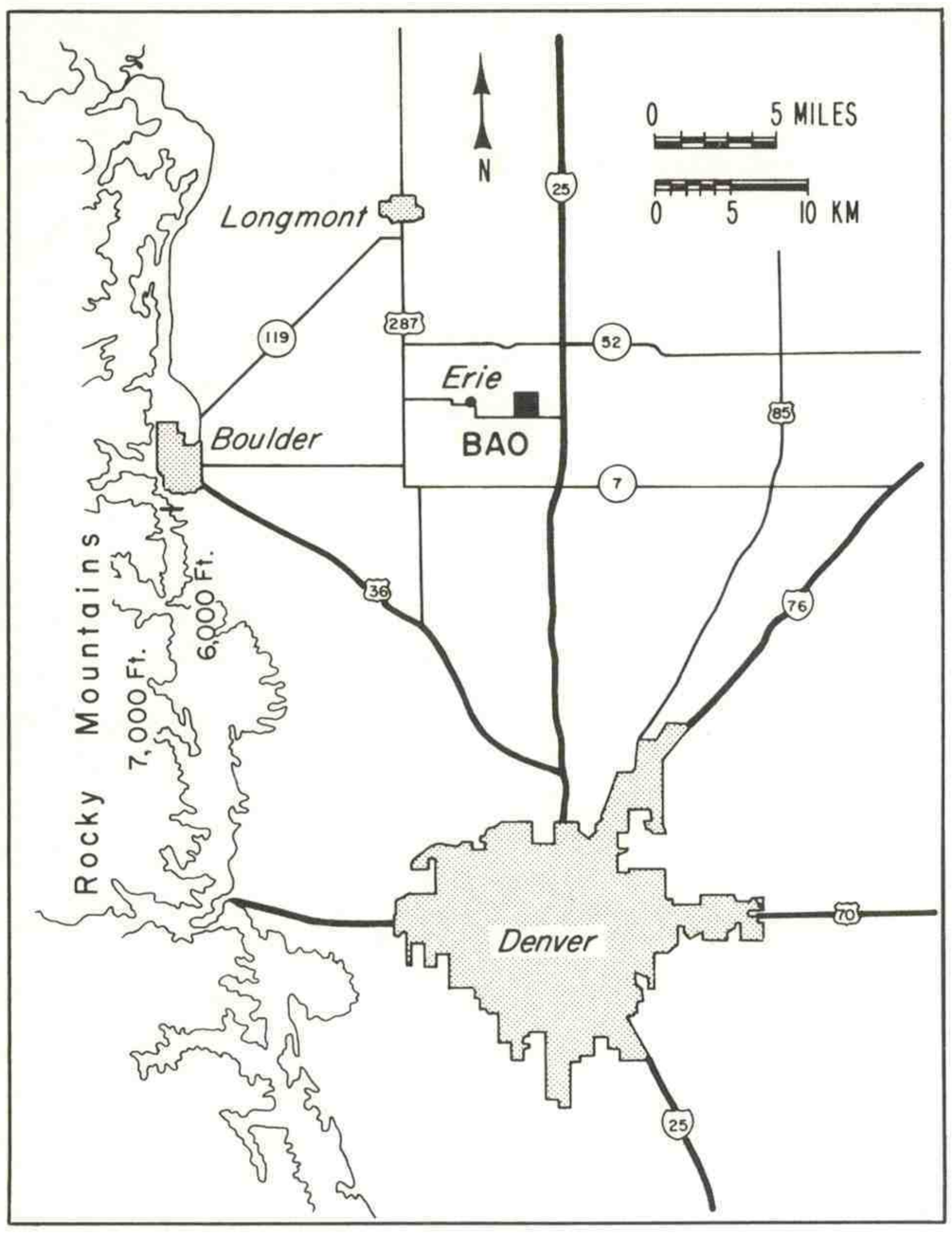


Figure 2.1.--Map showing the geographical relationship of the BAO to Denver and Boulder.

A quantity parameterizing the frictional drag induced by this ground cover in response to atmospheric flows is the so-called "roughness length" z_o. This length scale appears in the formula for the logarithmic wind profile,

$$u = \frac{u_*}{k} \ell n \frac{z}{z_o} \quad ,$$

where u is the mean wind speed at height z, k is von Karman's constant, and u_* is the friction velocity, itself defined by

$$u_* = \sqrt{\tau/\rho} \quad ,$$

where τ is the surface stress and ρ is the atmospheric density. Preliminary results from analysis of site evaluation data collected both during April 1978 and the PHOENIX experiment suggest that at the BAO z_o is somewhat azimuth-dependent, varying from some 2 to 6 cm for west winds to some 30 cm for winds from the south or southeast (S. Schotz and H. A. Panofsky, private communication). At present the possible origin of this anisotropy (e.g., particular terrain features, or perhaps simply the mean terrain slope itself) remains uncertain.

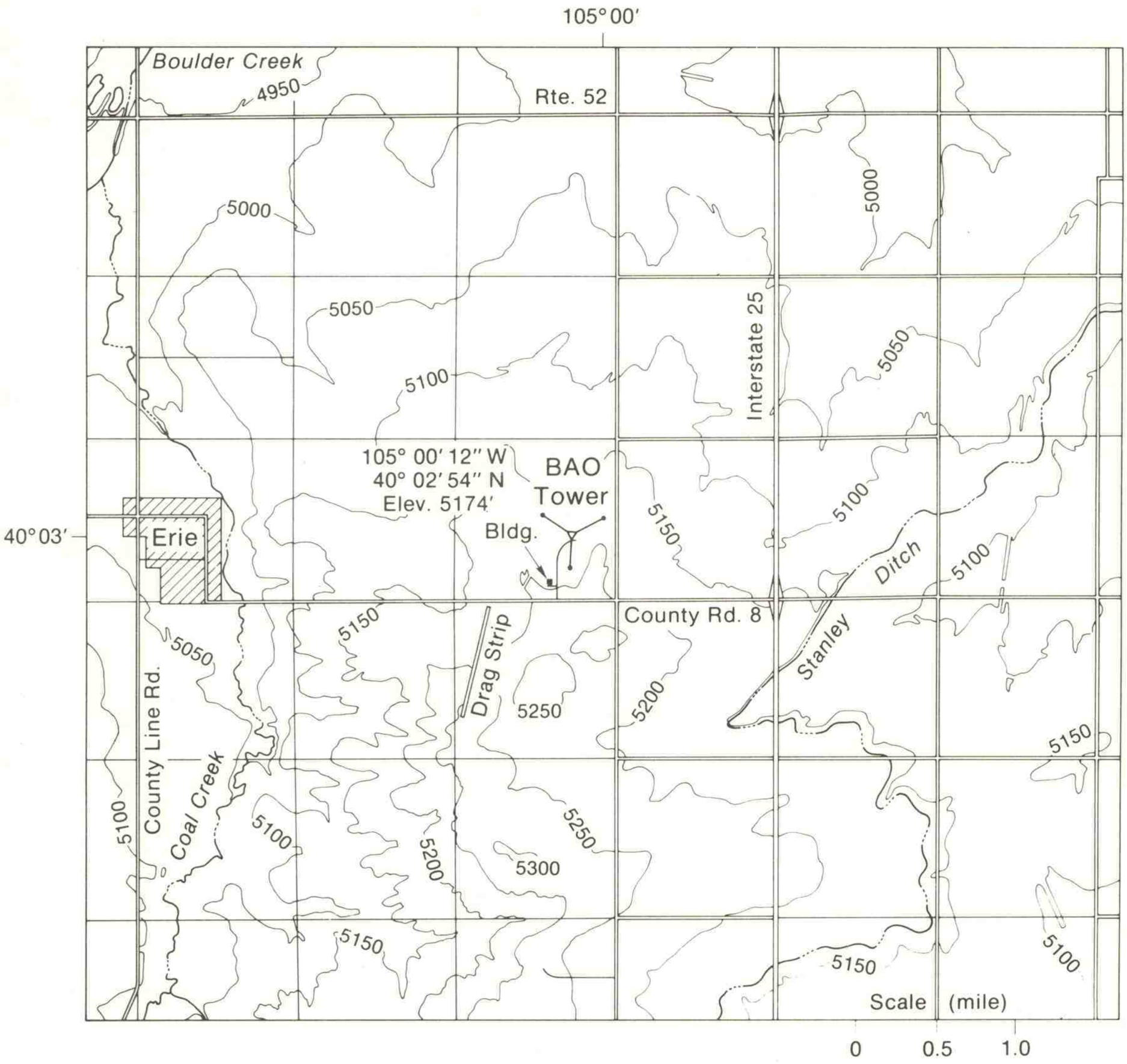


Figure 2.2a.--A conventional contour map of the immediate BAO terrain.

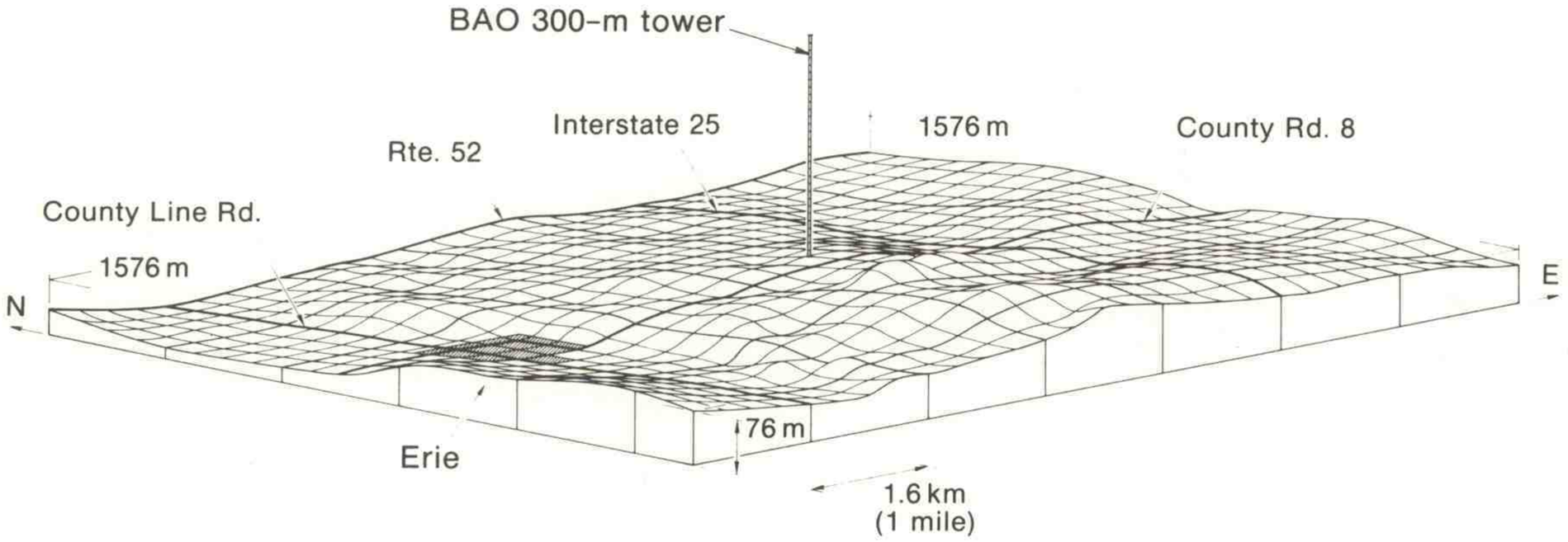


Figure 2.2b.--A 3-D view (exaggerated vertical scale) of the same topography.

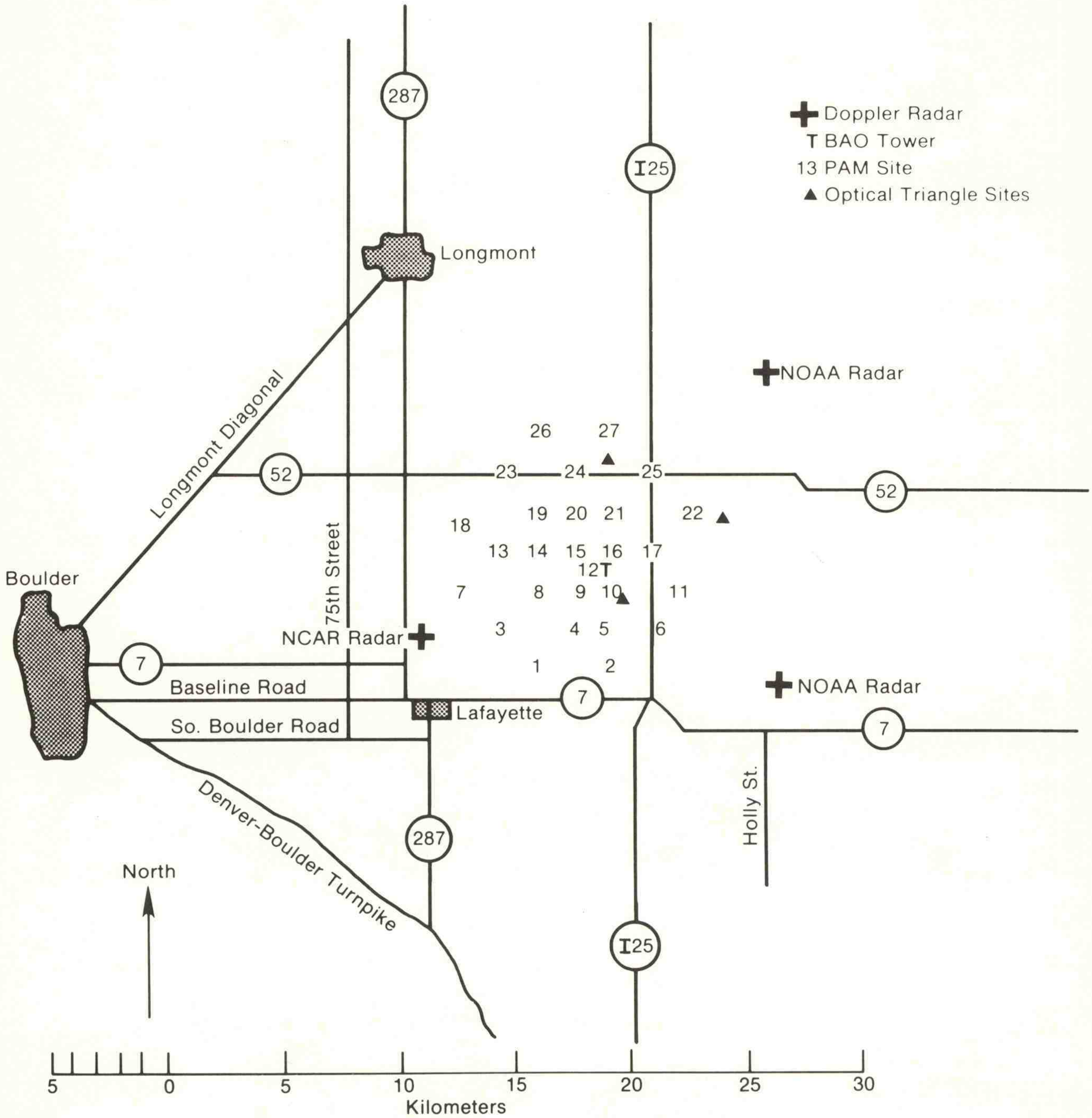


Figure 2.3.--A map of the PHOENIX experimental area, indicating positions of the Doppler radars, the BAO tower, the optical triangle sites, and the PAM network sites (indicated by number).

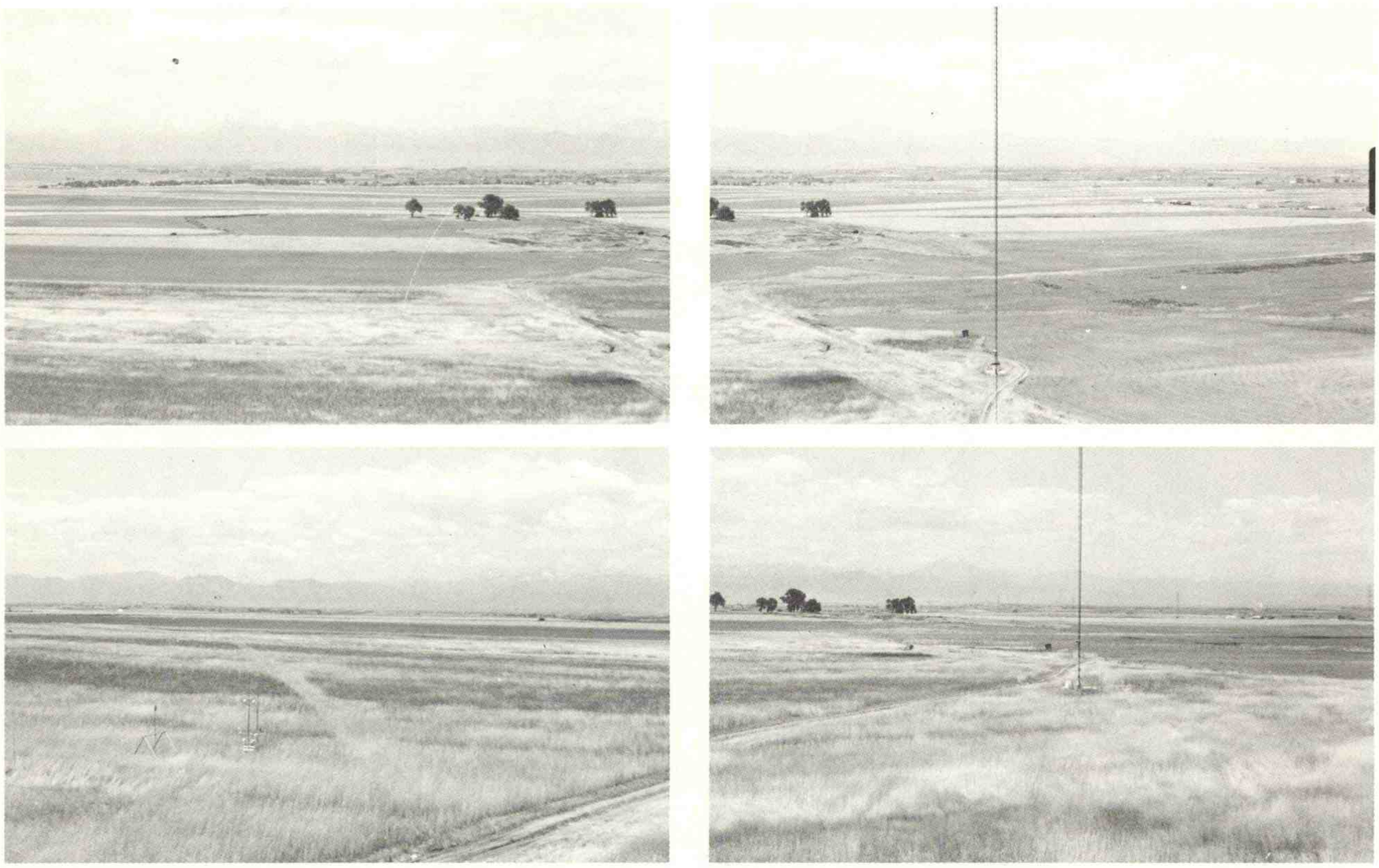
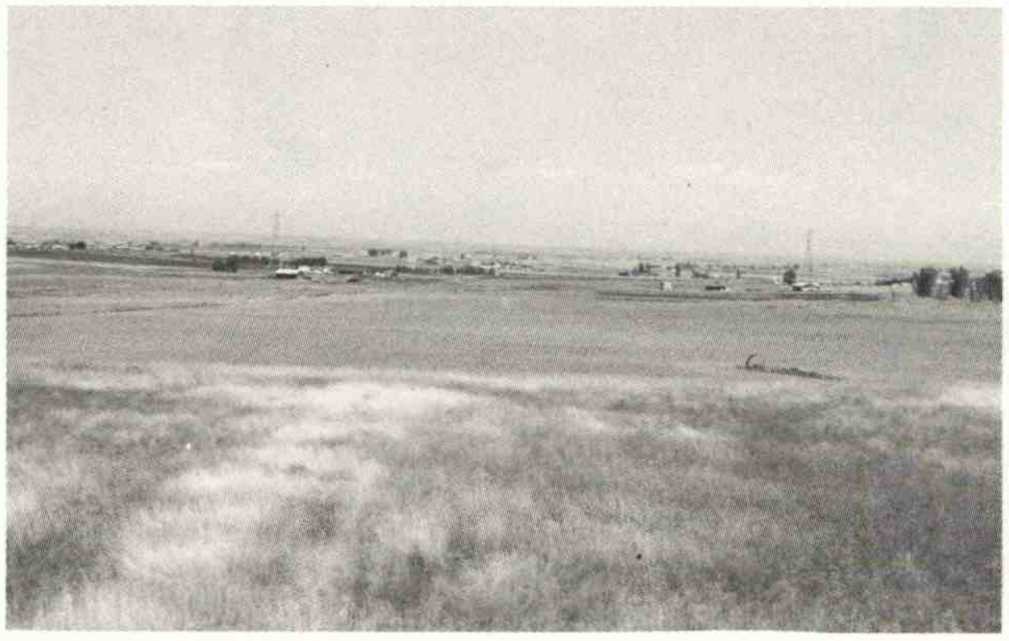
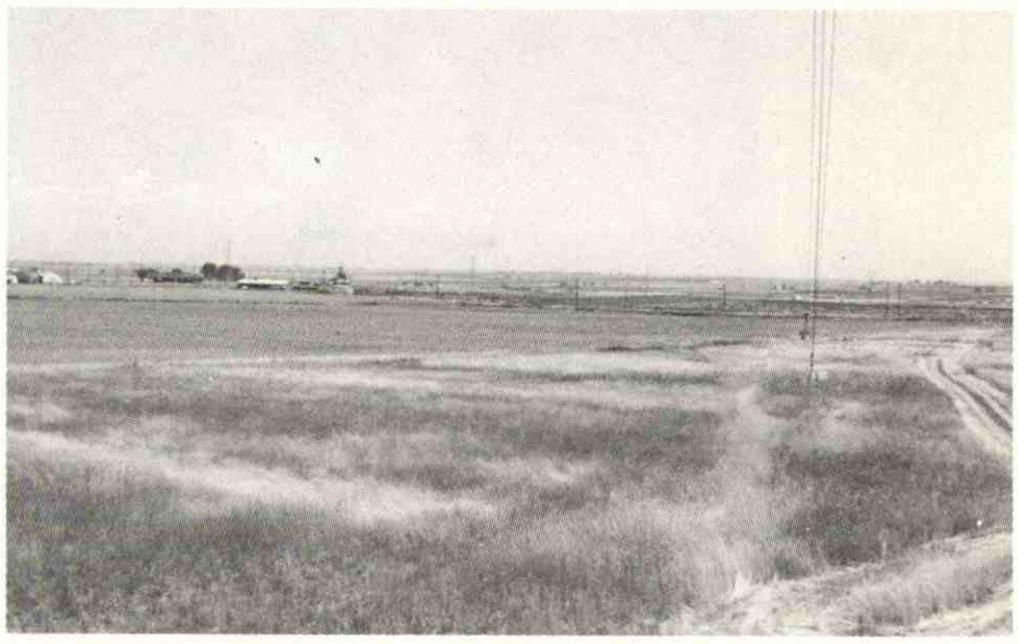


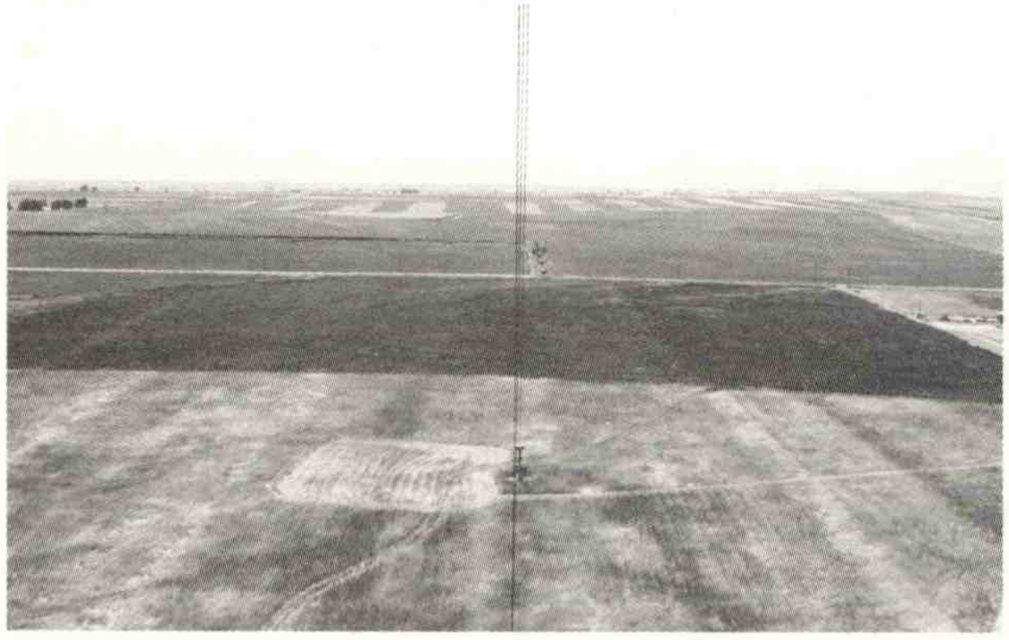
Figure 2.4.--The terrain to the east, southeast, south, and southwest of the BAO tower, as viewed from the 50-m level (row 1) and 10-m level (row 2), and to the west, northwest, north, and northeast, as viewed from the 50-m level (row 3) and 10-m level (row 4).

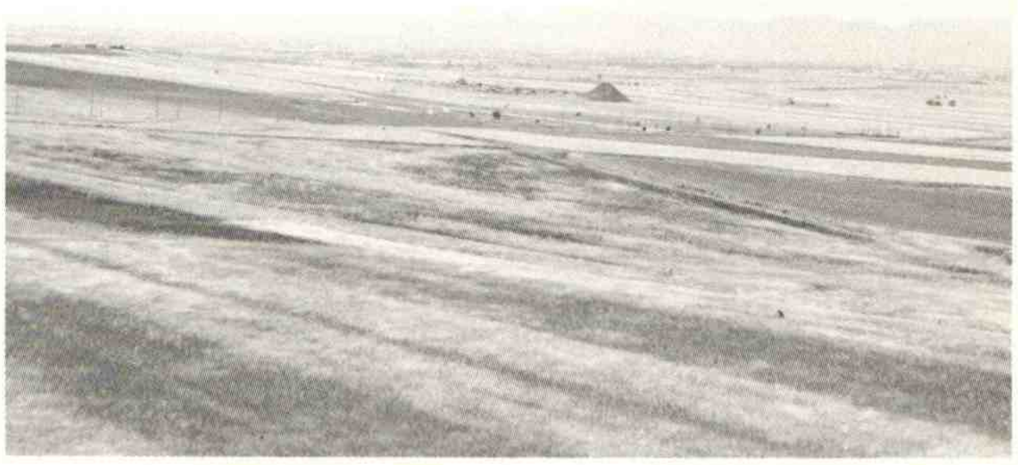


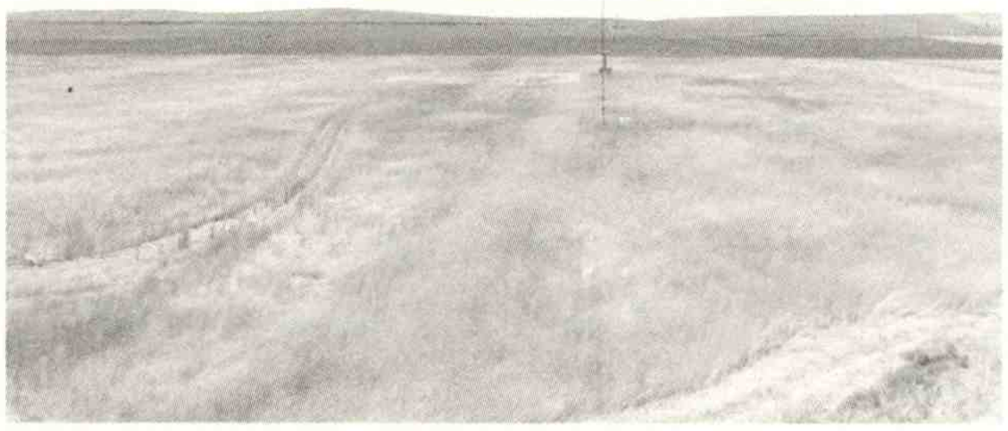














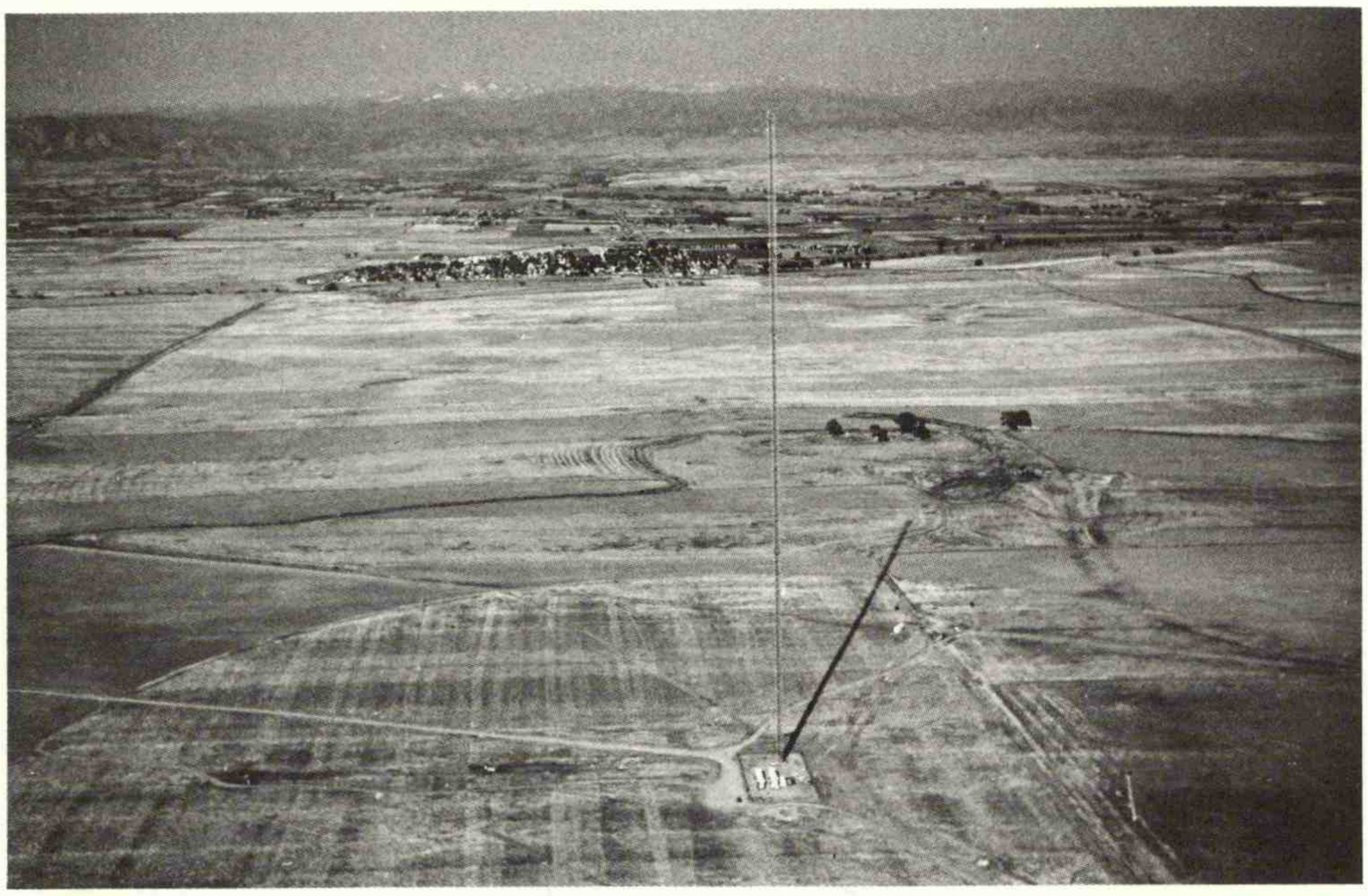


Figure 2.5a.--An aerial view of the BAO tower, taken in the summer of 1978 from an altitude of approximately 300 m, looking toward the west (photograph by Jon Wieringa).

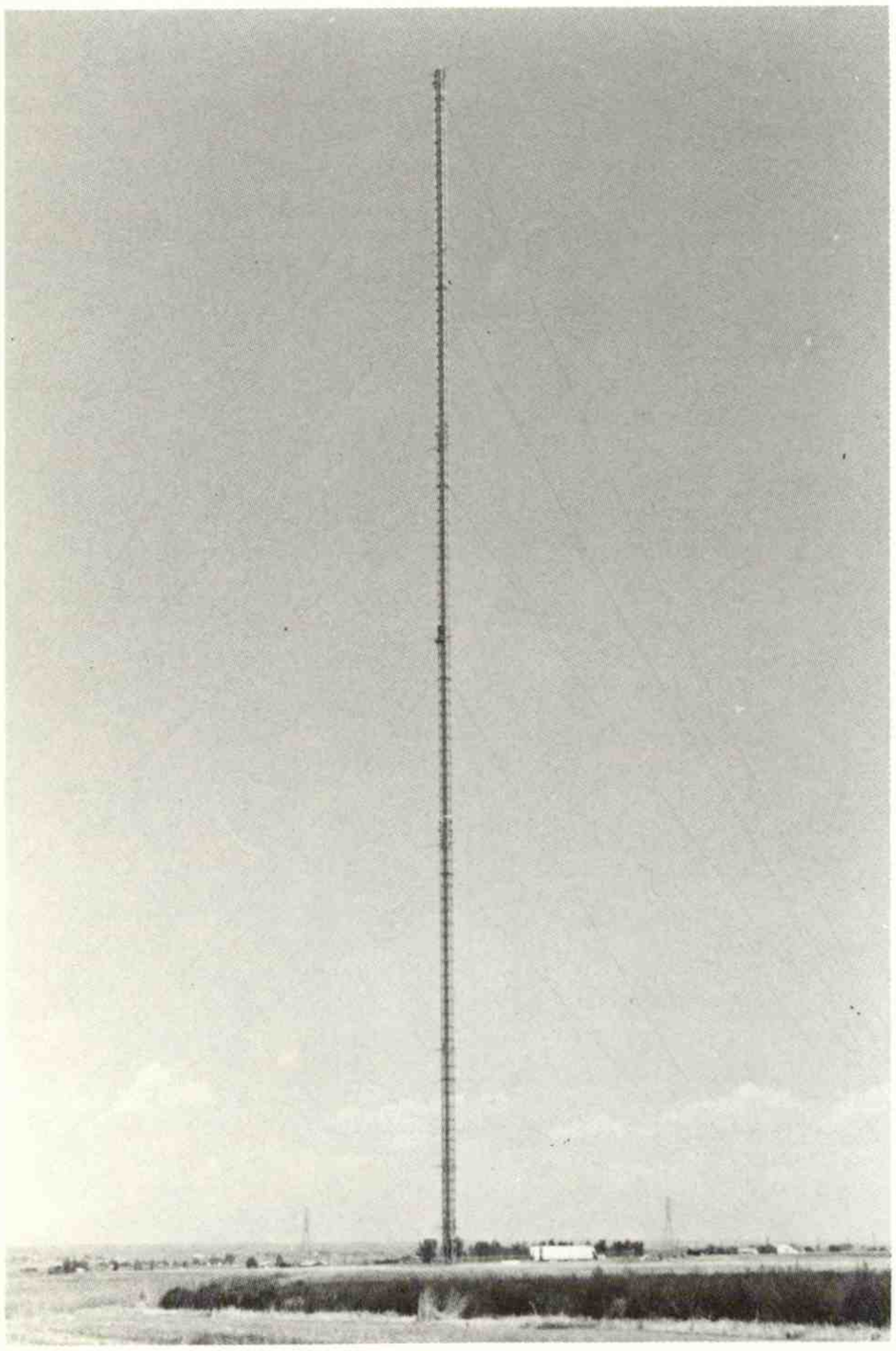


Figure 2.5b.--View of the BAO 300-m tower from ground level.

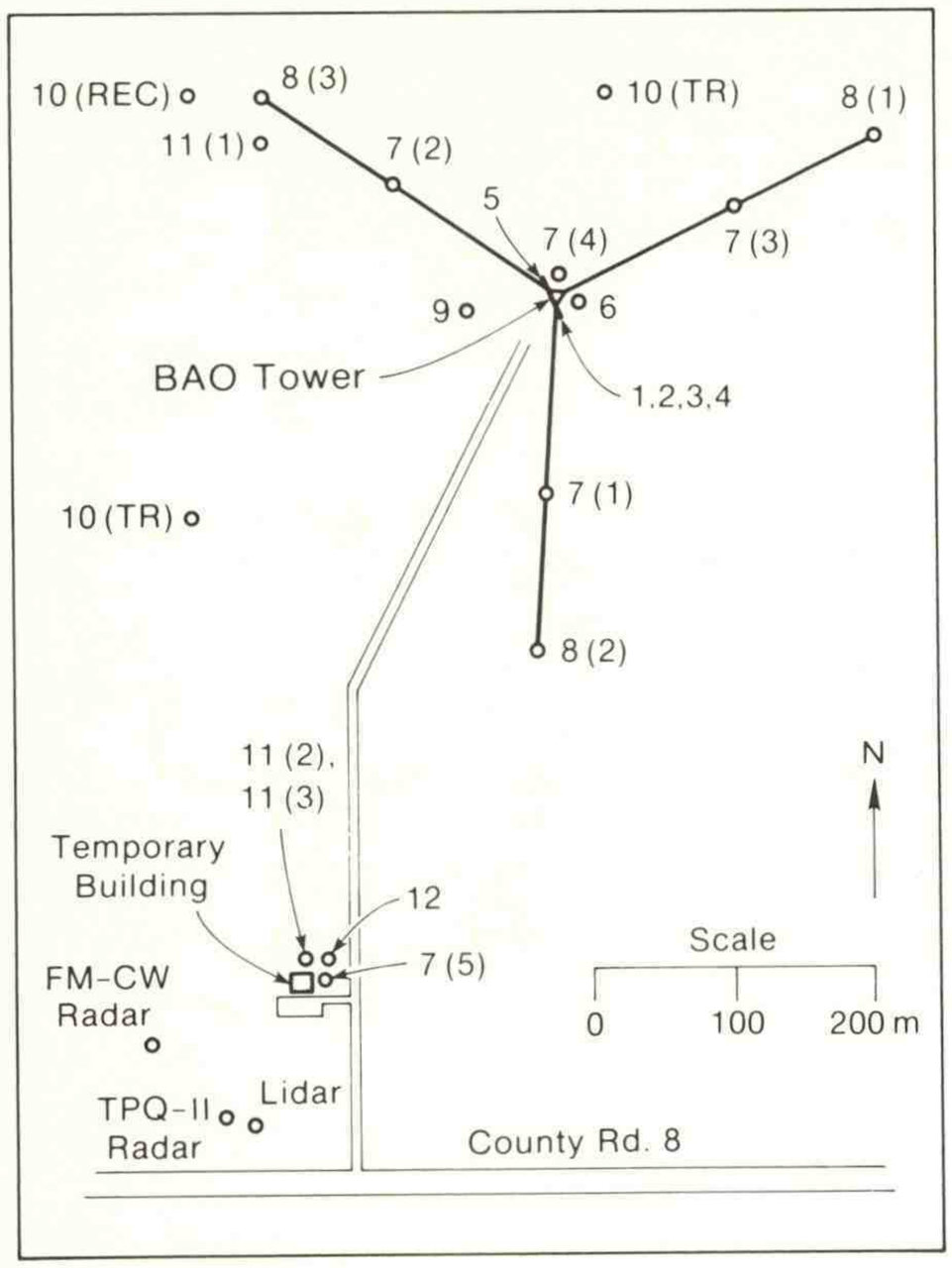


Figure 2.6.--The locations of the tower and major pieces of equipment on the BAO section during PHOENIX. The instruments are keyed to Table 2.1. Survey by W. D. Neff.

Figure 2.6 shows approximate location of the major pieces of equipment on the BAO section during PHOENIX. Central feature of the BAO is of course its instrumented 300-m tower, located and guyed as shown. In addition to the instruments deployed at the eight fixed levels themselves (described in Section 2.2), the tower also offers instruments at the anchors for each of the inner and outer guy wires. At each of the inner-guy anchor points, there is a sensitive microbarograph, described in Chapter 13 of this volume (Bedard, 1979), for the detection of pressure fluctuations associated with small-scale gravity waves propagating over the site. The array of three such instruments provides information on wave amplitude, phase speed, wavelength, period, and direction of propagation. An acoustic echo sounding system was located at each of the outer guy anchors, providing a look at spatial variability and small-scale structures such as gravity waves and thermal plumes over the site. Chapter 14 (Neff and Brown, 1979) summarizes acoustic-sounder studies during PHOENIX. In addition, optical sensors at each of the three outer guy wires formed a triangle for monitoring mean surface winds and small-scale convergence as described in Chapter 9 (Fritz and Wang, 1979).

South by southwest of the tower, near the temporary building providing lab facilities for the BAO, were located the NCAR rawinsonde system and WPL's FM-CW

radar, TPQ-11 radar, and pulsed lidar system. Two of the microwave radiometers used in the experiment were deployed just outside (to the north) of the temporary building. The third system and the van housing its electronics were deployed a few yards southeast of the northwest guy anchor of the tower. The locations of all the instruments are indicated on the map (which is keyed to Table 2.1).

2.2 Tower Instrumentation

Use of instrumented meteorological towers has been pivotal to the success of many of the early boundary-layer experiments mentioned in Chapter 1 (Hooke et al., 1979). In some respects, the 300-m BAO tower may be thought of as the culmination of such tower experiments. Worldwide, only a few instrumented towers can claim to be taller, while none supports anything like the sophisticated complement of instruments available at the BAO. Thus, the BAO tower and its instrumentation are without peer.

For the PHOENIX experiment, the tower was instrumented at eight fixed levels, at heights of 10, 22, 50, 100, 150, 200, 250, and 300 m. The instrumentation at each of the eight levels is essentially identical. It consists of sonic anemometry for measuring the mean and fluctuating components of the wind along three orthogonal axes, a quartz thermometer for accurately measuring mean temperature, platinum-wire thermometry for measuring temperature fluctuations, and a dew-point hygrometer for measuring mean relative humidity. Kaimal (1978) has provided further details concerning the tower instrumentation. In addition, for this experiment, propeller-vane anemometers provided redundant wind-speed and direction measurements at all levels with the exception of 150 m and 250 m. These yielded mean wind profiles used to test the procedures for correcting sonic anemometer data (vulnerable to a slight velocity defect when the wind direction is along one of the anemometer axes) and to test wind profiles obtained from an acoustic Doppler-sounding system. With the exception of the dewpoint hygrometer, which was mounted on the northwest boom, all tower sensors were mounted on the southeast boom. Figure 2.7 depicts the instrument configuration typical of each level. Surface measurements supporting those taken on the tower included mean atmospheric pressure and incoming solar radiation.

Table 2.1 provides a complete list of BAO sensors operated during the PHOENIX experiment together with information on their response characteristics, sampling rate, and location. Figures 2.6 and 2.7 are keyed to this table.

Table 2.1.--BAO sensors operated during the PHOENIX experiment

Sensor	Parameter(s) measured	Response characteristic	Rate at which sampled	Location
Sonic anemometer	u,v,w	0.05 Hz block-average	10 Hz	SE boom (all levels)
Propeller-vane anemometer	S,D	2.4 m distance constant	1 Hz	SE boom (all except 150 and 250 m levels)
Platinum wire thermometer	0	5-10 Hz cut-off	10 Hz	SE boom (all levels)
Quartz thermometer	T	1 min time constant	1 Hz	SE boom (all levels)
Cooled-mirror hygrometer	T_d	1 s cycle time	1 Hz	NW boom (all levels)
Absolute pressure	P		1 Hz	Surface (below van)
Fluctuating pressure	P		1 Hz	Surface (5 locations)
Optical triangle	S,D, Conv, C_N^2	Spatial average over 450 m equilateral triangle	1 Hz	Surface (outer anchor points)
Solar	R	about 5 min	1 Hz	Surface
Acoustic Doppler	u,v			(REC)=receiver (TR)=transmitter
Microwave radiometer	T,q			(1) NEMS (2) SCAMS (3) MTS

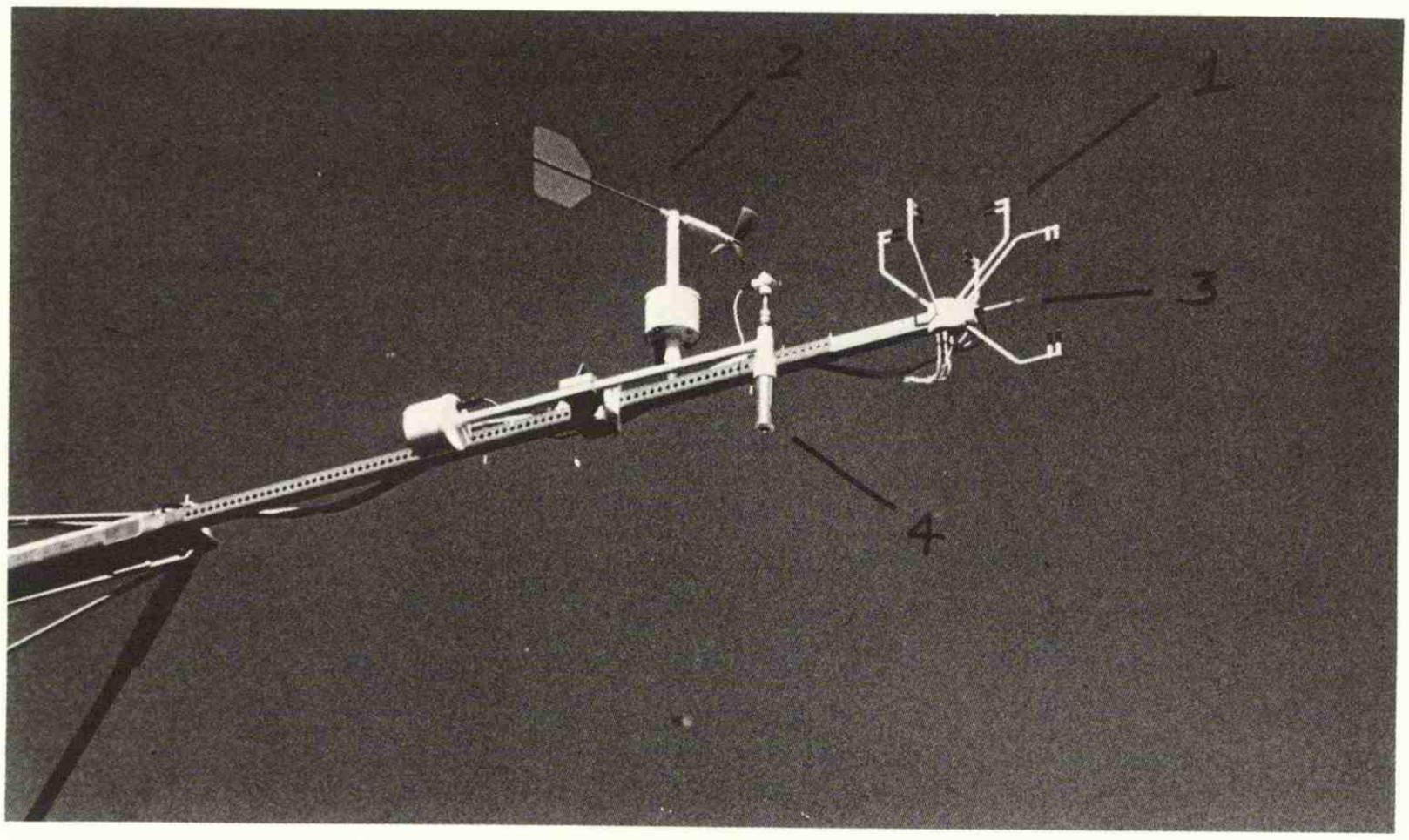


Figure 2.7.--Tower southeast boom configuration for the PHOENIX experiment. Sonic anemometry, propeller vane anemometer, and quartz and fast-response temperature sensors are shown; the dewpoint hygrometer was mounted on the northwest boom (not shown). Instrumentation of other levels was essentially identical. Sensor numbers are keyed to Table 2.1.

Although BAO data-acquisition chores are now handled by a PDP 11/34 minicomputer housed in the temporary building shown in Figure 2.6, at the time of the PHOENIX experiment data acquisition was controlled by an XDS-920 computer housed in a trailer at the base of the tower. In addition to recording the raw data on digital magnetic tape for later processing and analysis, the computer printed out data summaries every 20 min, listing means, variances, fluxes, and Obukhov length. A sample listing for one such period is shown in Figure 2.8; Table 2.2 explains the symbols used.

2.3 BAO Tower-PHOENIX Operations

In the course of the PHOENIX experiment, tower measurements were recorded in either one of two modes. During those times when the multiple Doppler X-band radars and the NCAR aircraft were recording, all raw BAO tower data, whether recorded at a 1 Hz or 10 Hz rate, were stored digitally on magnetic tape, with 20-min summaries displayed in real time on the line printer. These periods or runs were marked by a prefix "R" (e.g., Run R1, R2, etc.), denoting recording of "raw" data; typically they were confined to daylight hours between 0800 and 1600 MDT.

Table 2.2.--Summary sheet explanation

1. AVERAGED PARAMETERS

VWES	Horizontal wind component from west (sonic).
VSOU	Horizontal wind component from south (sonic).
W	Vertical wind component (sonic).
VH	Horizontal wind speed (sonic).
AZ	Horizontal wind direction (sonic).
PVS	Horizontal wind speed (prop-vane).
PVD	Horizontal true wind direction (prop-vane).
T	Temperature (quartz thermometer).
TD	Dew point (dew point hygrometer).
L	Obukhov length.

2. 2nd AND 3rd MOMENTS

UU, VV, WW, TT, UV, UW, UT, VT, UW, WT
UVW, UWW, VWW, UUW, VVW, WWW, UWT, VWT, WWT, WTT

WHERE:

U	(=u) Longitudinal wind component (sonic)	referenced to 10 m
V	(=v) Lateral wind component (sonic)	mean wind direction
W	(=w) Vertical wind component (sonic)	
T	(=θ) Temperature (platinum wire)	

3. OPTICAL TRIANGLE

V	wind speed	(from measurements
AZ	wind direction (CW)	along legs of an
CONV	convergence	equilateral triangle,
CN-SQR	structure parameter for refractive index x 10^{12}	450 m on each side, centered on tower.)

4. RMS PRESSURE VALUES

STN 1, STN 2, STN 3, STN 4, STN 5.	(from microbarograph stations around the tower.)

5. PRESSURE

mean surface pressure

6. SOLAR RAD

mean solar radiation (direct and diffuse)

BOULDER ATMOSPHERIC OBSERVATORY DATA SUMMARY

AVERAGING PERIOD= 20.00 MIN 26 SEP 78 640 MST

Z[M]	VWES	VSOU	W	VH	AZ	PVS	PVD	T	TD	L
10	-0.26	2.34	-0.07	2.35	174.	2.24	172.	11.89	7.62	15.98
22	-0.42	3.87	-0.12	3.89	174.	3.77	173.	13.46	7.96	-2.47
50	0.68	2.82	-0.13	2.90	193.	2.83	194.	14.50	4.48	*******
100	1.61	1.36	-0.12	2.11	230.	2.11	230.	15.22	1.34	*******
150	2.13	-0.60	-0.06	2.22	286.	******	****	16.69	-1.73	*******
200	2.60	-2.85	-0.22	3.86	318.	4.26	307.	17.17	-1.65	*******
250	2.89	-3.51	-0.27	4.55	321.	******	****	18.50	-3.85	*******
300	2.15	-2.66	-0.12	3.42	321.	4.07	331.	18.55	-3.92	*******

Z[M]	UU	VV	WW	TT	UV	VW	UT	VT	UW	WT
10	0.1112	0.0740	0.0267	0.1034	-0.0121	-0.0002	0.0050	-0.0339	-0.0110	-0.0060
22	0.0228	0.0144	0.0053	0.0500	0.0022	0.0013	0.0161	-0.0007	-0.0016	0.0022
50	0.0919	0.0598	0.0116	0.0988	0.0023	-0.0013	-0.0688	0.0146	0.0072	-0.0015
100	0.1767	0.0313	0.0054	0.1163	0.0176	-0.0005	-0.1266	-0.0022	0.0010	-0.0005
150	0.1061	0.1430	0.0170	0.0437	0.0892	0.0133	-0.0585	-0.0575	0.0112	-0.0048
200	0.5532	0.3183	0.0355	0.2985	-0.3418	-0.0214	-0.3641	0.2115	0.0403	-0.0293
250	0.1468	0.0421	0.0204	0.0123	-0.0306	0.0014	0.0234	-0.0118	0.0139	0.0018
300	0.2766	0.3177	0.0435	0.0438	-0.2578	-0.0083	0.0693	-0.0842	0.0171	0.0022

Z[M]	UVW	UWW	VWW	UUW	VVW	WWW	UWT	VWT	WWT	WTT
10	0.00072	-0.00360	-0.00075	0.00262	-0.00023	0.00058	-0.00279	0.00098	0.00459	-0.00152
22	-0.00022	0.00040	0.00013	0.00001	-0.00011	0.00009	0.00053	-0.00004	-0.00012	0.00044
50	-0.00111	-0.00197	-0.00025	-0.00158	0.00123	0.00052	0.00109	0.00152	0.00284	0.00025
100	0.00013	-0.00028	0.00043	0.00160	0.00017	-0.00011	-0.00058	-0.00013	0.00051	0.00012
150	-0.00011	-0.00053	0.00006	-0.00279	0.00004	-0.00003	0.00134	-0.00013	0.00080	-0.00054
200	0.00508	-0.00487	0.00281	-0.00439	-0.00386	0.00102	0.00753	-0.00794	0.00399	-0.00948
250	0.00094	-0.00247	0.00012	-0.00365	-0.00005	-0.00015	-0.00051	-0.00002	-0.00025	0.00008
300	-0.00140	0.00663	-0.00804	0.00397	-0.00284	0.00286	-0.00086	0.00227	0.00254	-0.00071

OPTICAL TRIANGLE

V [M/SEC]	AZ[DEG]	CONV[1/SEC]	CN-SQR*10**12
1.09	195.	-0.00059	0.00673

RMS PRESSURE VALUES [MICROBARS]

STN 1	STN 2	STN 3	STN 4	STN 5
2.167	1.905	1.379	2.220	1.543

PRESSURE[MB]
844.14

SOLAR RAD[LY/MIN]
0.18

Figure 2.8.--A sample data summary for a 20-min tower run during PHOENIX. Table 2.2 explains the symbols used.

In the alternate mode, which encompassed much of the remaining time, only the 20-min summary data listed on the line printer were stored on magnetic tape. Run numbers for these periods were marked by the prefix "A" (e.g., Run A1, A2, etc.) denoting "average" data storage only. Lists of prefix "R" and "A" runs, giving the run durations as well as the ranges of wind speed and direction (taken from the 20-min summaries) for each, are given in Tables 2.3 and 2.4. Data were also recorded on paper strip charts, facilitating equipment checkouts and permitting rapid verification of shifts in wind speed and direction, PBL depth, and other parameters.

It should be noted that although data were recorded on a nearly continuous basis, there were numerous time intervals, primarily during the nighttime hours, when wind azimuths were such that winds blew through the tower toward the

Table 2.3.--PHOENIX raw data runs

Run no.	Start Time* (Date)	End Time* (Date)	Wind speed Range (m s^{-1})	Wind direction Range (°)	Direction shift
R1	0900 (9/1)	1140 (9/1)	2-6.0	160-200	CW
R2	0720 (9/5)	1440 (9/5)	0-6.0	340-120	CW
R3	0700 (9/6)	0740 (9/6)	1-5.0	320	
R4	0800 (9/6)	1400 (9/6)	0-4.5	350-110	CW
R5	0740 (9/11)	1500 (9/9)	2-5.0	350-120	CW
R6	0500 (9/11)	0740 (9/11)	0-7.0	270-165	CCW
R7	0800 (9/11)	1300 (9/11)	0-26.0	216-280	CW
R8	1300 (9/11)	1540 (9/11)	15-22.5	280-270	CCW
R9	1600 (9/11)	2120 (9/11)	7.5-25.0	270-260	CCW
R10	2140 (9/11)	0820 (9/12)	0-18.0	260-150	CCW
R11	0620 (9/18)	1600 (9/18)	0-12.0	240-350	CCW
R12	0840 (9/19)	1540 (9/19)	2-8.0	140-060	CCW
R13	0800 (9/20)	1320 (9/20)	0-3.5	140-180	CW
R14	1320 (9/20)	1600 (9/20)	0-3.0	190-230	CW
R15	0740 (9/21)	1540 (9/21)	0-2.5	350-110	CW
R16	1540 (9/21)	1820 (9/21)	0-3.0	110-340	CCW
R17	0740 (9/22)	1820 (9/22)	0-3.5	190-090	CCW
R18	0700 (9/25)	0940 (9/25)	1-6.5	190-160	CCW
R19	0500 (9/26)	0920 (9/26)	0-5.0	280-010	CW
R20	0940 (9/26)	1640 (9/26)	0-6.5	070-020	CCW
R21	1720 (9/26)	2240 (9/26)	0-9.0	070-360	CW
R22	2300 (9/26)	1220 (9/27)	0-10.0	010-100	CCW
R23	1300 (9/27)	1720 (9/27)	2-12.0	100-180	CW
R24	1740 (9/27)	1900 (9/27)	5-12.5	170	

*All times MST.

Table 2.4.--PHOENIX average data runs

Run no.	Start Time* (Date)	End Time* (Date)	Wind speed Range (m s^{-1})	Wind direction Range (°)	Direction Shift
A1	1600 (9/6)	0900 (9/7)	0.-16.	80-20	CW
A2	2200 (9/7)	0900 (9/8)	0.-4.5	200-40	CW
A3	1400 (9/8)	0700 (9/9)	4.-15.5	90-350	CCW
A4	1520 (9/9)	1840 (9/9)	2.5-8.	90-180	CW
A5	2120 (9/9)	0440 (9/11)	.5-13.	**	--
A6	0840 (9/12)	1200 (9/12)	2.-6.	100-20	CCW
A7	1620 (9/12)	1300 (9/13)	.5-8.	330-120	CW
A8	1800 (9/13)	1120 (9/14)	1.-7.	30-140	CW
A9	1640 (9/14)	0920 (9/15)	0.-5.5	340-260	CCW
A10	0940 (9/15)	1300 (9/15)	2.5-4.	140-100	CCW
A11	1520 (9/15)	1700 (9/17)	2.-14.5	**	--
A12	1620 (9/18)	0820 (9/19)	4.-12.5	60-160	CW
A13	1600 (9/19)	0740 (9/20)	1.-4.	290-30	CW
A14	0040 (9/21)	0720 (9/21)	1.5-4.5	180-350	CW
A15	1920 (9/21)	0720 (9/22)	1.5-4.5	350-190	CCW
A16	1840 (9/22)	1400 (9/24)	1.5-10.5	**	--
A17	2220 (9/24)	0640 (9/25)	1.5-7.5	200-180	CCW
A18	1940 (9/25)	0440 (9/26)	0.-4.5	200-340	CW
A19	1920 (9/27)	1000 (9/28)	3.0-11.5	200-300	CW

*(MST)

**Weekend run

instruments, seriously contaminating the measurements. Thus, for wind directions from the north, specifically from the 100° sector between 320° and 60° east of north, the fast-response sensors exhibit spurious high-frequency fluctuations, characteristic of tower interference. Such conditions usually began to occur at twilight, persisting during the nighttime hours until sometime after sunrise. However, as the convective planetary boundary layer would become established, the winds invariably returned to favorable directions. During the daytime hours under near-calm conditions, the winds would occasionally make brief excursions into the unwanted sector, but these occurrences were relatively rare and easy to identify on the strip-chart records.

2.4 Data Availability

At this writing, PHOENIX BAO tower data are available on disk storage of the BAO ADP system at the Wave Propagation Laboratory. The system, which consists of a PDP 11/70 and extensive peripherals, permits extremely rapid and convenient processing of these data, offering a number of convenient analysis routines, including spectral, statistical, and graphics packages. In fact, the data offer a unique opportunity for direct access by remote computer terminal. Features of the PDP 11/70 and instructions for access may be found in Chapter 17 (Lawrence and Ackley, 1979) of this volume. For further information, the interested reader is referred to the senior author (commercial phone (303) 499-1000 ext. 6263, FTS 323-6263).

Acknowledgments

In any operation as complex as the BAO, the system is no better than its operating staff. For this reason we were particularly fortunate to have the aid of the BAO staff — Bob Krinks, Jim Newman, and Norbert Szczepczynski. Without their help, consultation, and dedication throughout the many long hours involved, this experiment could not have been a success.

References

Bedard, A. J., Jr., Microbarograph observations during PHOENIX, Chapter 13, in Project PHOENIX: The September 1978 Field Operation, W. H. Hooke, Ed., NOAA/NCAR Boulder Atmospheric Observatory Rept. No. 1, available from NOAA/ERL, Boulder, Colo., and from NCAR Publications Office, Boulder, Colo. (1979).

Fritz, R. B., and T.-I. Wang, Optical systems measuring surface-level convergence during PHOENIX, Chapter 9, in Project PHOENIX: The September 1978 Field Operation, W. H. Hooke, Ed., NOAA/NCAR Boulder Atmospheric Observatory Rept. No. 1, available from NOAA/ERL, Boulder, Colo., and from NCAR Publications Office, Boulder, Colo. (1979).

Hooke, W. H., P. H. Hildebrand, and R. A. Kropfli, Project PHOENIX: background and introduction, Chapter 1, in Project PHOENIX: The September 1978 Field Operation, W. H. Hooke, Ed., NOAA/NCAR Boulder Atmospheric Observatory Rept. No. 1, Available from NOAA/ERL, Boulder, Colo., and from NCAR Publications Office, Boulder, Colo. (1979).

Kaimal, J. C., NOAA instrumentation at the Boulder Atmospheric Observatory, Preprints Fourth Symposium on Meteorological Observations and Instrumentation, April 10-14, 1978, Denver, Colorado, pp. 35-40, American Meteorological Society, Boston, Mass. (1978).

Lawrence, R. S., and M. H. Ackley, Interactive computer access to BAO data, Chapter 17, in Project PHOENIX: The September 1978 Field Operation, W. H. Hooke, Ed., NOAA/NCAR Boulder Atmospheric Observatory Rept. No. 1, available from NOAA/ERL, Boulder, Colo., and from NCAR Publications Office, Boulder, Colo. (1979).

Neff, W. D., amd E. H. Brown, Acoustic-echo sounder operations during PHOENIX, Chapter 14, in Project PHOENIX: The September 1978 Field Operation, W. H. Hooke, Ed., NOAA/NCAR Boulder Atmospheric Observatory Rept. No. 1, available from NOAA/ERL, Boulder, Colo., and from NCAR Publications Office, Boulder, Colo. (1979).

CHAPTER 3

PHOENIX MULTIPLE-DOPPLER RADAR OPERATIONS

Robert A. Kropfli
Wave Propagation Laboratory
National Oceanic and Atmospheric Administration
Boulder, Colorado 80303

3.1 Introduction

Although dual-Doppler radars have been developed primarily to study motion fields within precipitating clouds (e.g., Miller and Strauch, 1974; Miller et al., 1975; Kropfli and Miller, 1976; Dye et al., 1978), the same radars have also been applied in PBL studies, both in small experiments (e.g., Wilson, 1970; Frisch and Clifford, 1974; Gossard and Frisch, 1976) and as part of large field programs (e.g., Kropfli and Kohn, 1978). In such studies the radars use either natural aerosols, such as snowflakes (Wilson, 1970), or artificial chaff (e.g., Gossard and Frisch, 1976; Kropfli and Kohn, 1978) as tracers, deducing wind velocities from the Doppler shifts measured in the echoes from these targets. Scanning the radars through large volumes has provided a tremendous step forward in our visualization of boundary-layer flow fields.

To appreciate more concretely the advantages and shortcomings that multiple-Doppler radars portend for PBL studies, it may be illuminating to consider the following illustration, drawn from PHOENIX data. We may begin by noting that the BAO tower represents in some sense a culmination of in-situ micrometeorology. Sonic anemometry and fast-response temperature sensors at eight fixed levels provide information about the turbulent airflow past the tower with unprecedented accuracy and detail. Now picture what two or three Doppler radars, operated in concert, achieved during the PHOENIX experiment. Together they provided information on the three components of the wind flow throughout a volume some 7 to 14 km on a side (depending upon the scan mode) and extending throughout the entire PBL depth, typically 1 to 2 km. Within this volume, the radars provided velocity estimates on a 200-m grid, resolving wavelengths as small as 600 m. Thus, the data set they provided may be thought of as equivalent to that from roughly 1000 towers, each some 1000 to 2000 m high and each instrumented at from five to ten

levels! Figures 3.1a-e show sample wind fields prevailing over the PHOENIX experimental area during just one 2-min interval, as derived by the Doppler-radar technique. They reveal considerable small-scale structure in the flow field — a richness and texture that we know must be present in any high-Reynolds-number flow, but that is impossible to visualize in detail without the aid of the radars or their equivalent. By contrast, the BAO tower could provide only a single wind vector on each of these plots, and hence no insights into the spatial variability of the flow (except most indirectly and uncertainly, through the application of Taylor's hypothesis to time series of the tower data). The usefulness of data from a single tower, such as the BAO, or its shorter predecessors in Kansas and Minnesota, lies in the fact that they may be taken to be representative of conditions over wide areas. This will be true to the degree that the terrain is essentially homogeneous and that the prevailing meteorological conditions are nearly stationary. Unfortunately, both of these are rather specialized conditions, achieved only rarely in practice, and impose corresponding limitations on the scope of PBL issues that tower research can address. However, with radar capability for developing detailed spatial pictures well in hand, it becomes practicable for the first time for the meteorological research community to address itself to the study of the PBL over inhomogeneous terrain and to examination of the effects of nonstationary flows on the PBL. The former problem has immense practical importance; for example, it bears on the study of urban circulations and on the environmental quality impacts of ore and energy extraction in mountainous terrain. Similarly, the latter problems are of interest in studies of such phenomena as frontal development and motions and severe-storm dynamics.

Regrettably, the situation is neither so simple, nor so unmitigatedly bright, as it might appear from the above discussion. For example, the radars provide no direct information on either mean or fluctuating temperature and humidity, parameters readily measured by in- situ instrumentation. Moreover, radar wind estimates represent volume averages over cubes typically 200 m on a side, the order of the outer scale of the PBL turbulence. By contrast, sonic anemometry and fast-response temperature systems on the tower measure fluctuations on scales as small as 1 m. While it is true that some information on these smaller scales is implicit in each radar echo return, this link is only indirect. Furthermore, at low elevation angles, radar estimates of wind speed are vulnerable to contamination by ground clutter, leading to underestimates in the wind speeds. Thus, despite the wealth of data provided by the radars in comparison with those available from

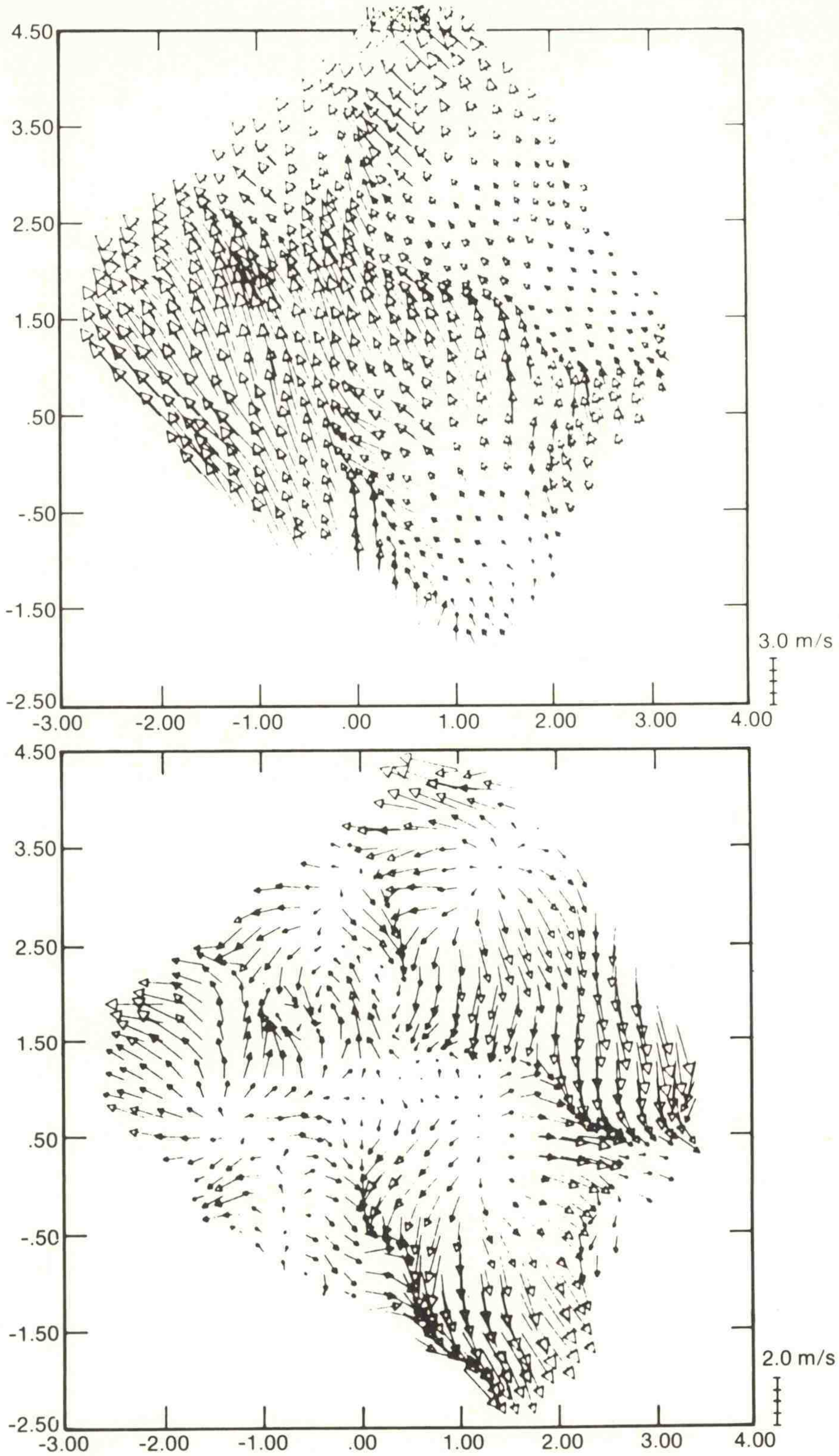


Figure 3.1a.--Total and eddy (volume mean removed) wind fields at 1516 MDT on September 21, 1978, at z = 0.1 km. Arrow lengths are proportional to wind speed. The area covered by the plot amounts to some 50 km^2. Geographic north is toward the top of the figure; the BAO tower is at the origin.

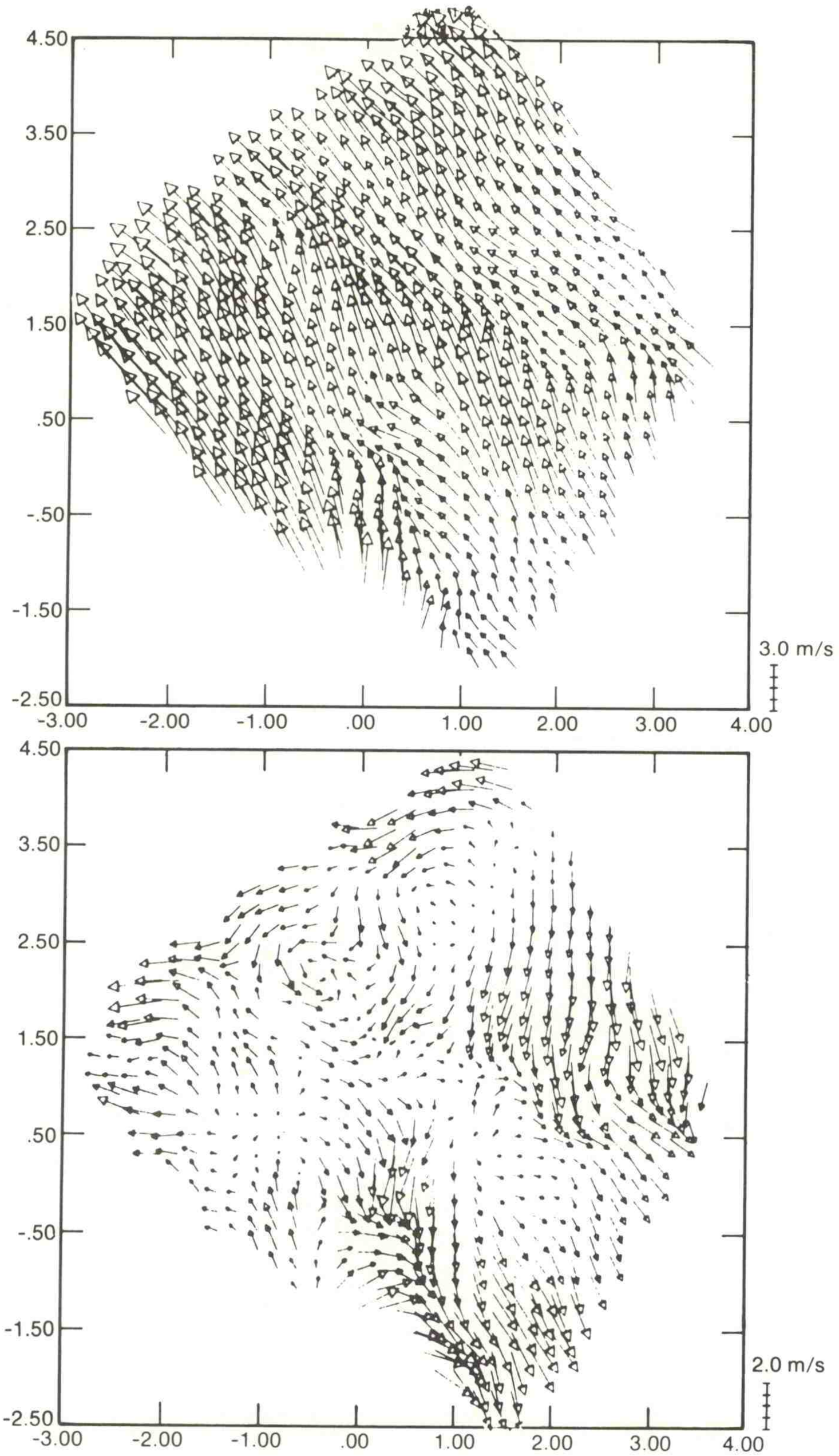


Figure 3.1b.--Same as Figure 3.1a but at z = 0.3 km.

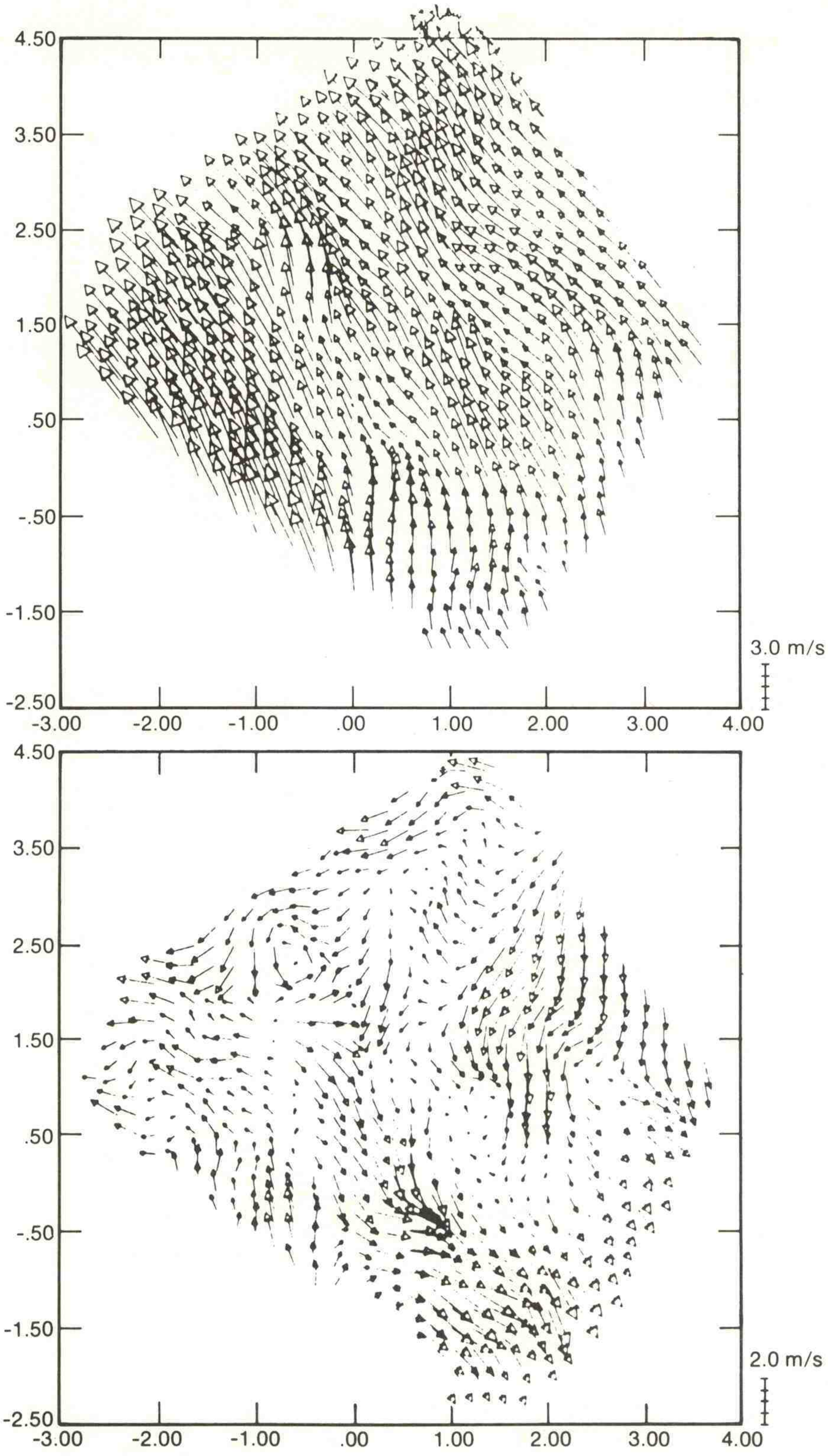


Figure 3.1c.--Same as Figure 3.1a but at z = 0.5 km.

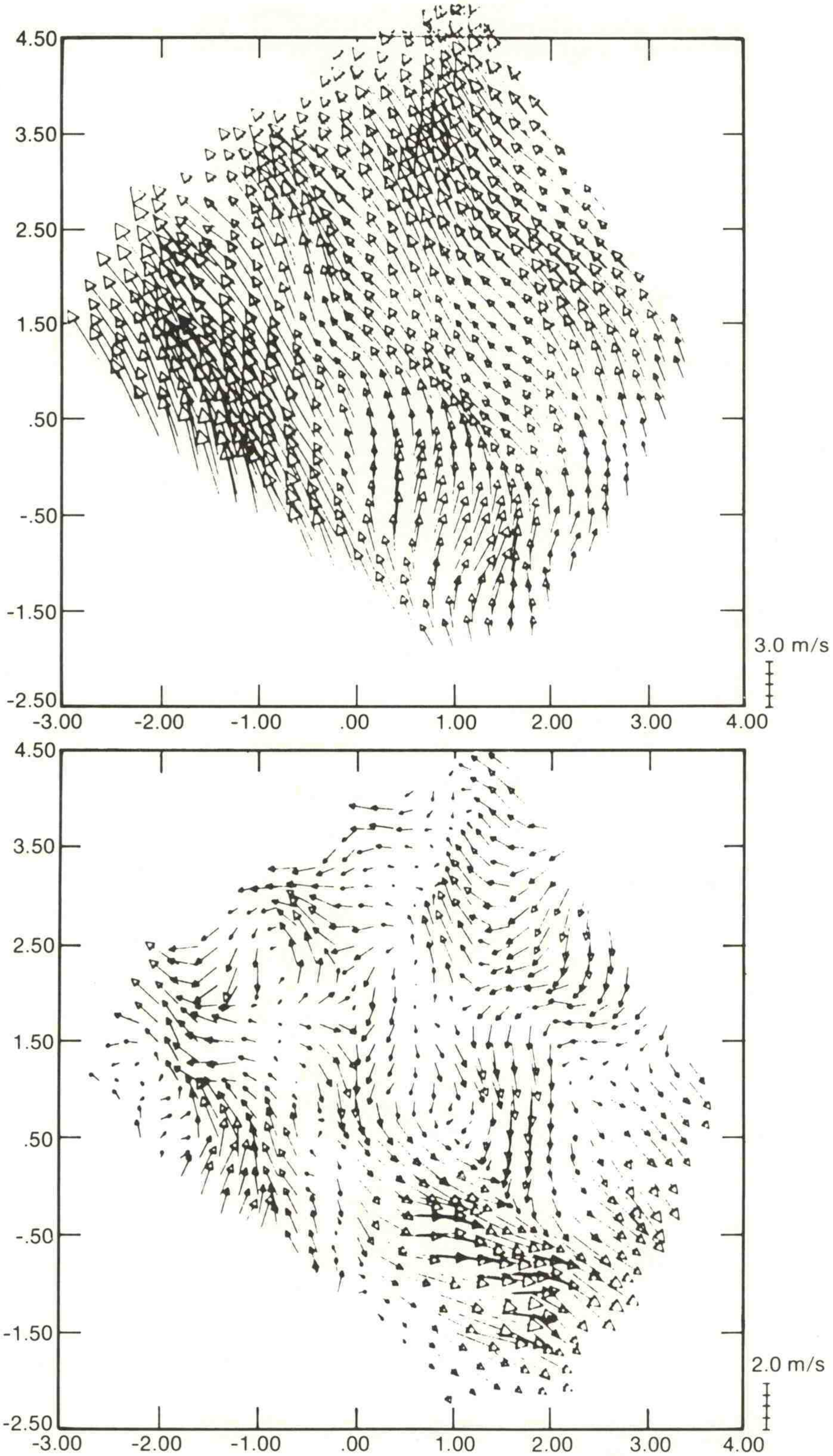


Figure 3.1d.--Same as Figure 3.1a but at z = 0.7 km.

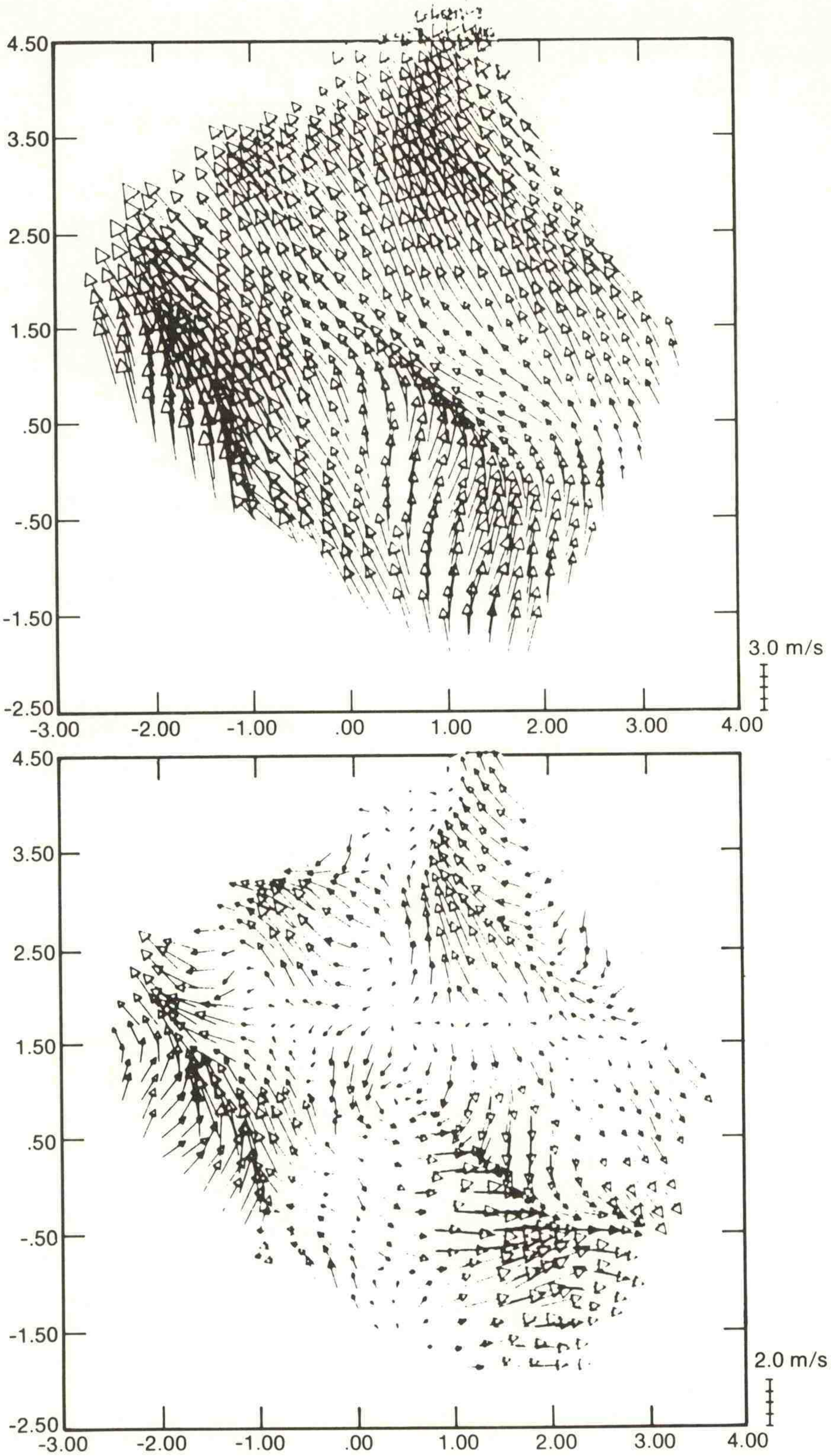


Figure 3.1e.--Same as Figure 3.1a but at z = 0.9 km.

the in-situ instrumentation, to dispense with the BAO tower and others like it would be premature. Rather the accuracy of the radar measurements should be carefully assessed by comparison with both tower and aircraft data.

Accordingly, the goals for the PHOENIX multiple-Doppler radar systems were many and varied. On the one hand, the radars were used in the relatively glamorous work of exposing and monitoring spatial and temporal variability in PBL airflow around the BAO. Should the radar data prove of sufficiently high quality, they will even be used to test novel concepts for retrieving PBL temperature fields suggested by Gal-Chen (1978a,b) and Leise (1978). On the other hand, they were used for more routine but nonetheless important matters such as examining the effects of ground clutter and the assumed lower boundary conditions on radar wind retrievals and the effect of using selected pairs of radars rather than the full triad. In addition, radar velocity data are being compared with aircraft and tower data recorded simultaneously, in order to calibrate radar wind retrievals and to evaluate the radar's ability to estimate Reynolds stresses, eddy dissipation rates, and other turbulence quantities. It should be emphasized that the success of these more ordinary activities is absolutely critical in establishing sound theoretical and experimental footing for quantitative application of radar data in future PBL studies.

3.2 The Doppler Radar Systems

One C-band and two X-band Doppler radars were operated in concert for this experiment. Two were identical NOAA systems operating at a wavelength λ of 3.22 cm, peak transmitted power of 20 kW, pulse width of 1.0 μs, and beamwidth of 0.8°. By contrast, the NCAR CP-4 C-band radar unit provided a wavelength of 5.49 cm, peak transmitted power of 316 kW, pulse duration of 1.0 μs, and beamwidth of 1.0°. Despite the fact that the chaff cutter used to disperse the chaff providing the targets for all radars was optimized for the WPL radars of shorter wavelength, chaff echo strength proved entirely adequate for the NCAR unit. A number of other radar and scanning parameters are computer-controllable over a wide range, providing considerable versatility. Table 3.1 lists some of the NOAA and NCAR radar parameters selected for the PHOENIX experiment. One of the two NOAA units is shown in Figure 3.2; the appearance of the NCAR unit is essentially similar.

Table 3.1.--NOAA and NCAR radar parameters

Parameter	NOAA	NCAR
Pulse repetition period	900 μs	1000 μs
Number of samples per estimate	64,128	64,128
Number of range gates	32-96	1024
Range gate separation	1 μs	1 μs
Antenna scan rate	4°-8°/s	4°-12°/s

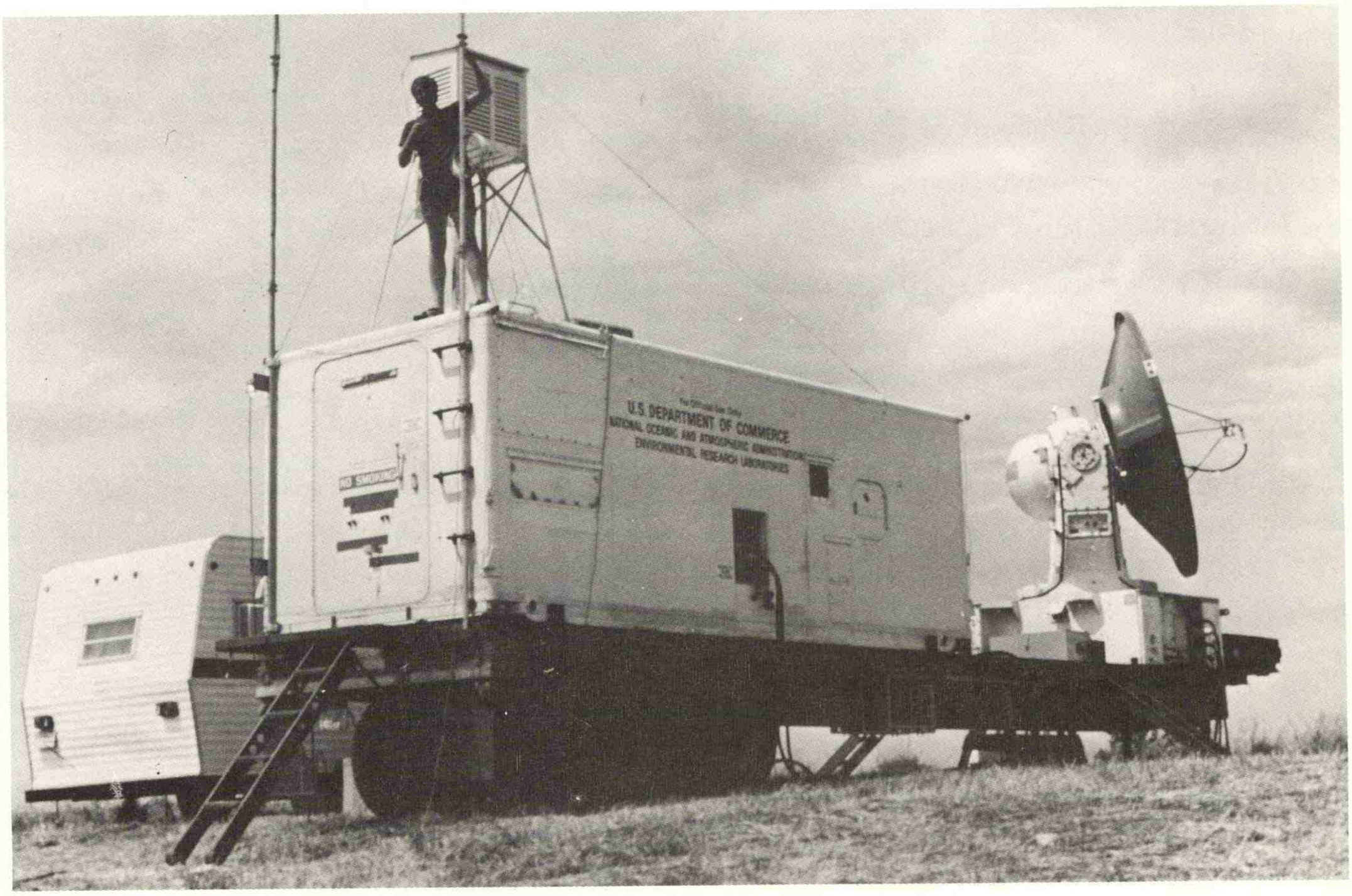


Figure 3.2.--One of a matched pair of NOAA X-band Doppler radars used during PHOENIX.

3.3 Radar Site Selection

To meet all the PHOENIX experimental objectives required measurements of air motions from 1 to 250 min in period and 0.2 to 10 km in spatial dimension. In order to cover this wide range, we found it optimal to locate each of the three radars about 10 km from the BAO tower. This configuration permitted various combinations of the three radars to scan an area of several hundred square kilometers while allowing observations of air motions at scales as small as a few hundred meters. Siting the radars equidistant from the tower also had the important advantage of equalizing the radial and tangential dimensions of the radar pulse volumes at the BAO. Thus, radar sample volumes associated with each radar were about 150 m in all dimensions at the tower. Consequently, the pulse volume filtering near the tower was similar for all radars.

Following the initial planning, we considered it very important for the radars to be able to measure wind fields along the entire height of the BAO tower, in order to make definitive comparisons. For this reason we initially chose radar sites offering an unobstructed view of the tower. However, during the first week of PHOENIX operations it became apparent that the velocity measurements from these sites were being biased excessively by ground clutter. We therefore identified new sites promising less clutter, redeployed the radars, and operated during the last two weeks of the experiment from these new locations. The new sites are indicated on the map in Figure 2.3 of Chapter 2 (Kaimal and Wolfe, 1979). While not offering a clear view of the tower base, these new sites had a close-in horizon that successfully suppressed most of the clutter except for the tower itself. These sites were much improved and the radar analysis effort currently emphasizes data taken during the last two weeks of the experiment.

Data were restricted to areas for which the normalized variance of the horizontal components $[\sigma^2(u) + \sigma^2(v)]/\sigma^2(v_R)$ was less than unity, so that an accurate horizontal velocity field could be used to compute the vertical component from an integration of the continuity equation. In determining these areas, we have assumed that the interpolation scheme used to transform data to a rectangular grid would average over at least four radar estimates of the radial velocity, v_R. Thus, the statistical error is reduced by a factor of two from curves given by Bohne and Srivastava (1975).

Although three radars were usually in operation during PHOENIX, many analyses will involve only two radars since the third adds little accuracy to vertical velocity estimates for the low elevation angles typically used in the PBL work. A direct measurement of w is not possible in this situation. However, the presence of the third radar extended the viable dual-Doppler analysis areas greatly and will provide velocity measurements in areas that might have been blocked by hills had only two radars been used.

3.4 Radar Scan Modes

The two NOAA radars operated during the entire PHOENIX experiment in the Coplan scanning mode. Specifically, they scanned in tilted planes passing through the baseline between them. NCAR's CP-4 radar operated most of the time in the constant elevation mode and on a few occasions in the Coplan mode with a baseline parallel to the baseline of the other two radars.

The radar objectives outlined in Chapter 1 (Hooke et al., 1979) could not have been achieved with a single scan mode because of the limited rate at which the radars acquire velocity samples. As a result, constraints were placed on scanning by the required accuracy (determined by the dwell time), the temporal and spatial resolution, and the largest scales desired. Five different scan modes were devised to satisfy all the objectives and, in addition, allow us to evaluate the relative merits of different radar sampling schemes for future experiments.

The routine that was followed throughout the experiment was to go through two cycles of sometimes four and sometimes five scan modes as rapidly as possible. Taking two identical volume scans in rapid succession has, in effect, given us the redundant data set that will be helpful in distinguishing mere peculiarities in the data from unusual features in the flow field. Each pair of scans was completed in about 3 min and the entire sequence was completed in 15 to 20 min. All scans were predetermined to reduce operator errors. Decisions on exactly which of these predetermined scans were to be used were based on the previous scans and on reports of PBL depth from the aircraft and other remote sensors at the tower. Samples of the five scan types are shown in Figures 3.3-3.6. (The scan volumes sampled by the 100- and 200-series scans are essentially identical, although the cell sizes within each volume are different.) Table 3.2 summarizes the five different scan types.

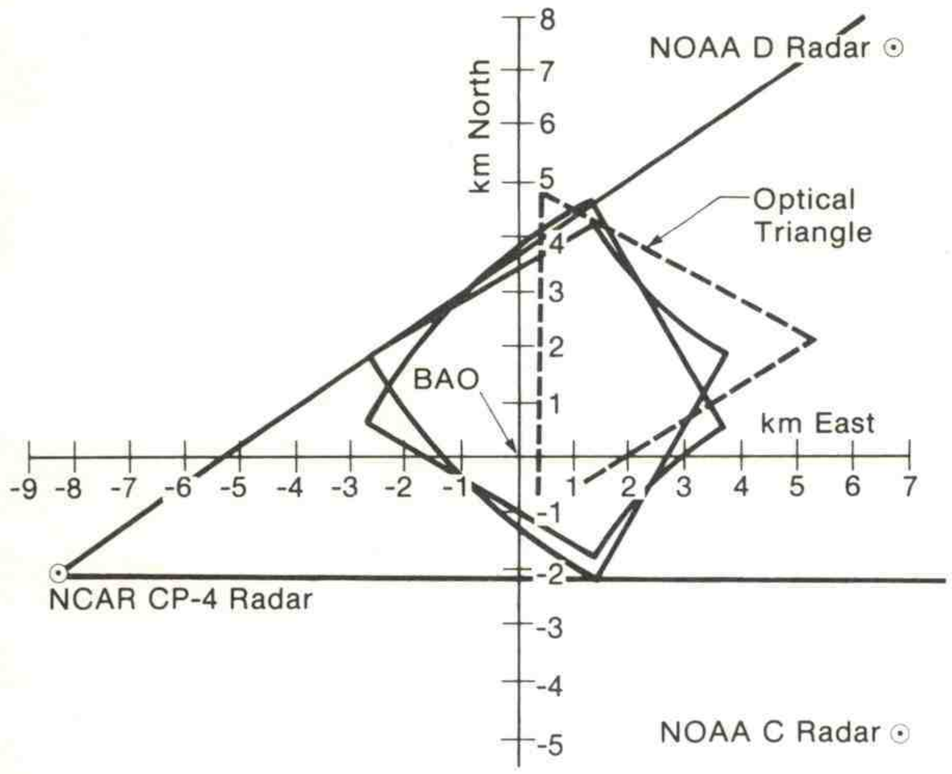


Figure 3.3.--Area covered by the 100- and 200-series radar scans.

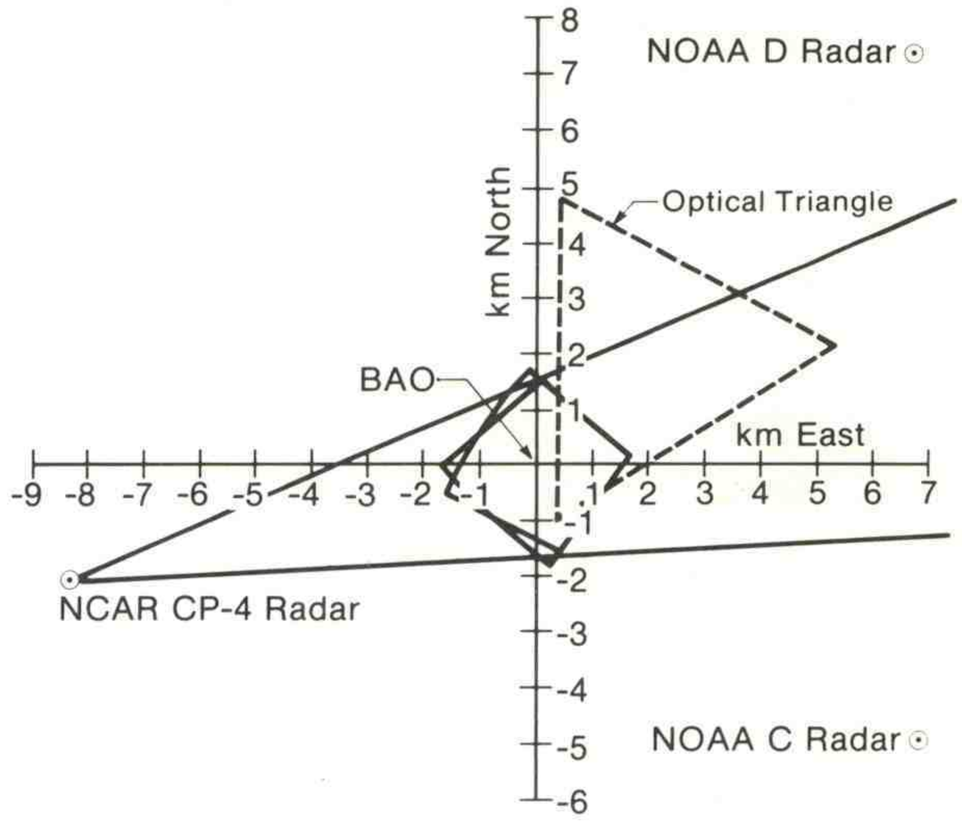


Figure 3.4.--Area covered by the 300-series radar scan.

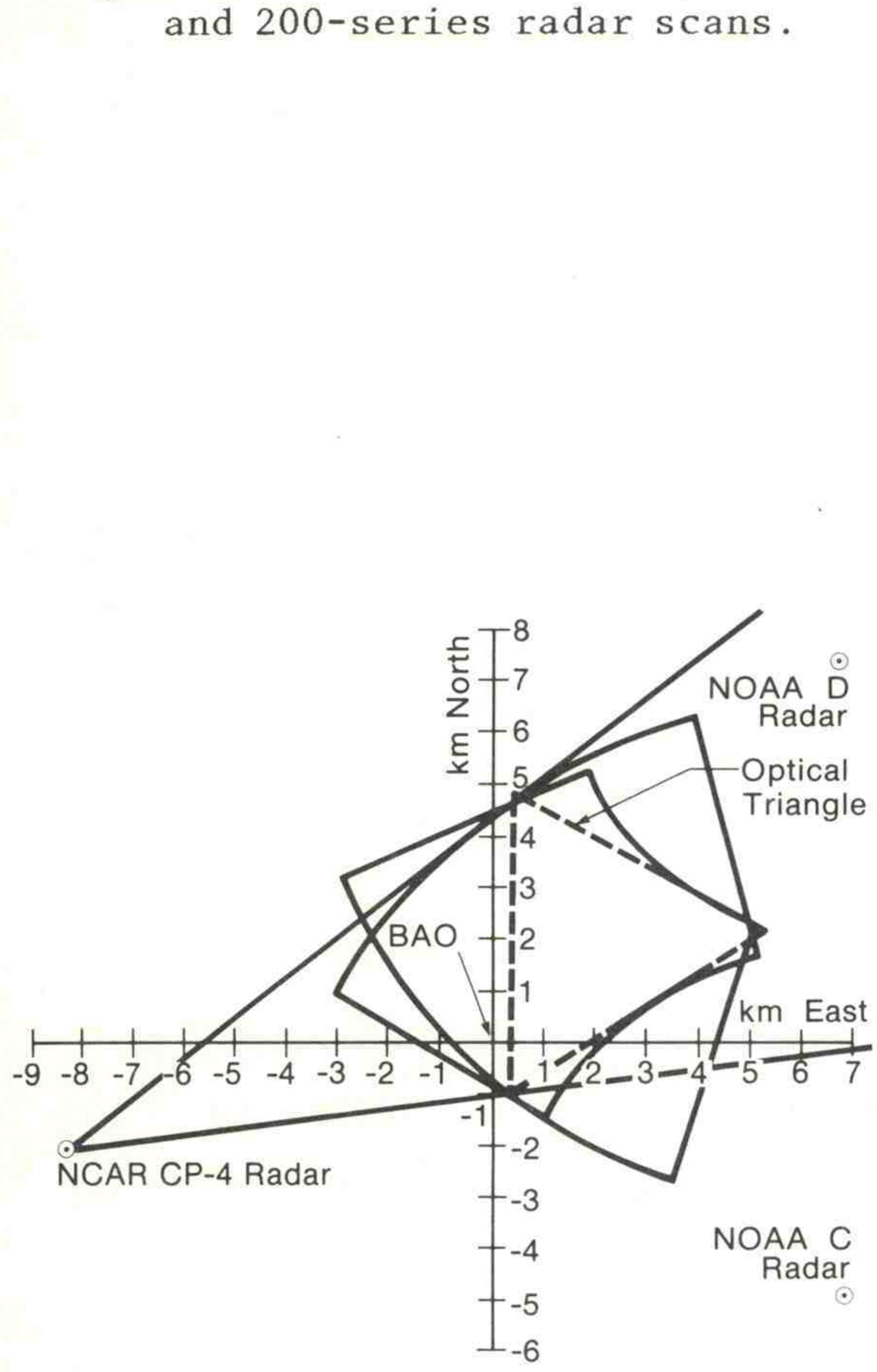


Figure 3.5.--Area covered by the 400-series radar scan.

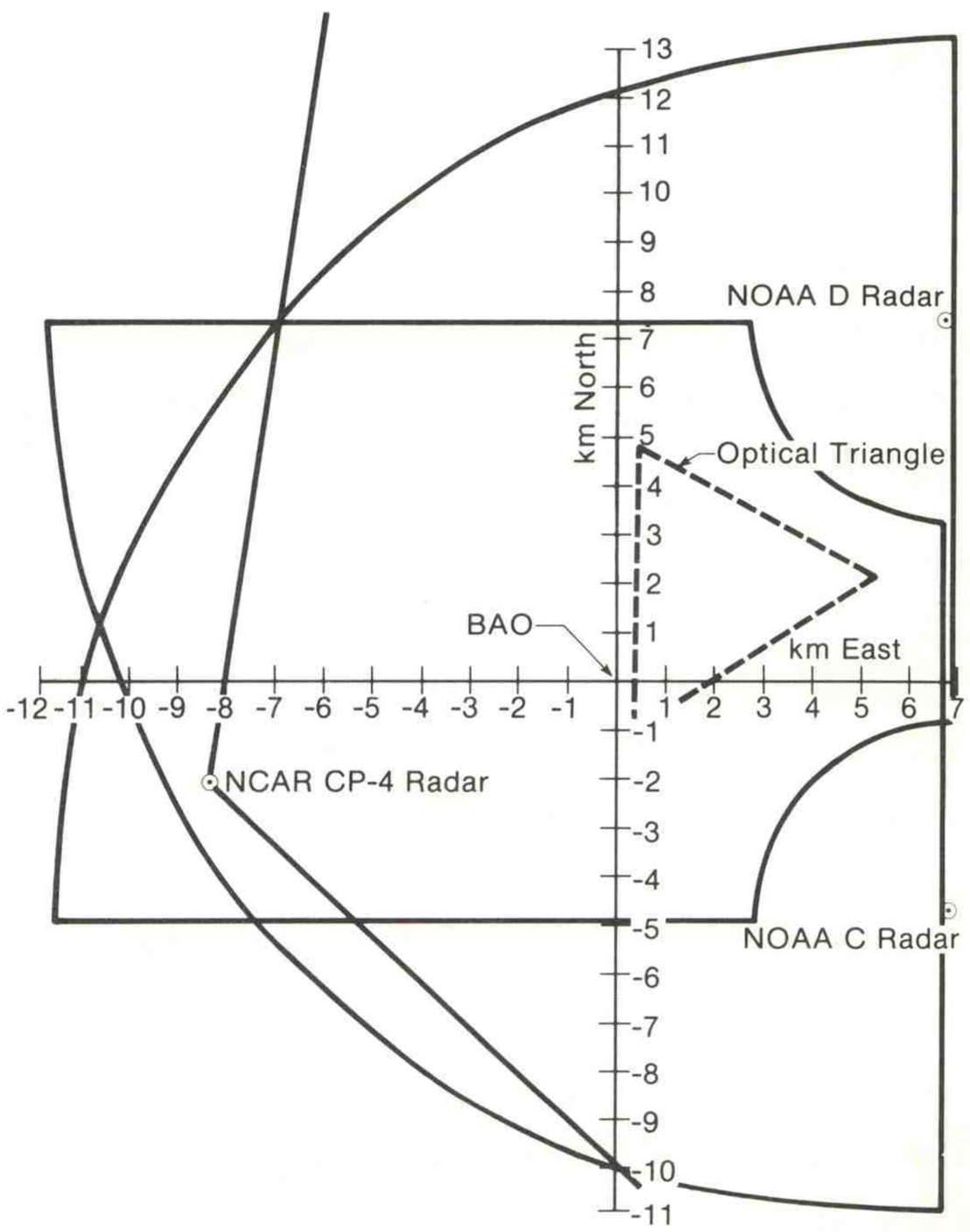


Figure 3.6--Area covered by the 600-series radar scan.

Table 3.2--Radar scan modes

Scan number/Name	Volume time (s)	Sample density (Number/km^3)	Area covered (km^2)
100/Standard	72<T<96	170<N<270	20<A<110
200/Fast-Standard	40<T<80	300<N<400	20<A<110
300/Over-Sampled	40<T<90	600<N<1300	A ≅ 4
400/Optical triangle	50<T<180	160<N<300	A ≅ 25
600/Large Scale	140<T<180	80<N<160	A = 270

3.5 Error Analysis

While areas for acceptable scanning have been computed for errors normalized to the variance of the spectral mean, one can use the standard relationship (appropriate for high signal-to-noise ratio)

$$\sigma^2(v) = \frac{\sigma_v \lambda}{8\sqrt{\pi}\ T_D}$$

to compute the absolute variance or expected error in the radial velocity. Here σ_v is the Doppler width, λ is the radar wavelength, and T_D is the dwell time. Figure 3.7 shows how $\sigma(v)$ varies with pulse period for 64 and 128 samples/estimate, assuming a wavelength of 3 cm and spectral width of 1 m s^{-1}.

Data-recording considerations at the NOAA radars indicated that a pulse period of 900 μs gave the largest dwell and hence the smallest error, and yet maximized the data rate. This point is indicated by an X on the curves in Figure 3.7. Thus, we can see the expected error for high signal-to-noise ratios was 0.13 m s^{-1} for 128 samples and 0.19 m s^{-1} for 64 samples. The signals from chaff were usually very strong (>10 dB), justifying the use of this approximation.

Applying the results of Figure 4 of Bohne and Srivastava (1975) to the PHOENIX experiment, we find that for the three-radar case, the minimum value of the sum of the normalized variances of the two velocity components,

$$\frac{\sigma^2(u) + \sigma^2(v)}{\sigma^2(v_R)},$$

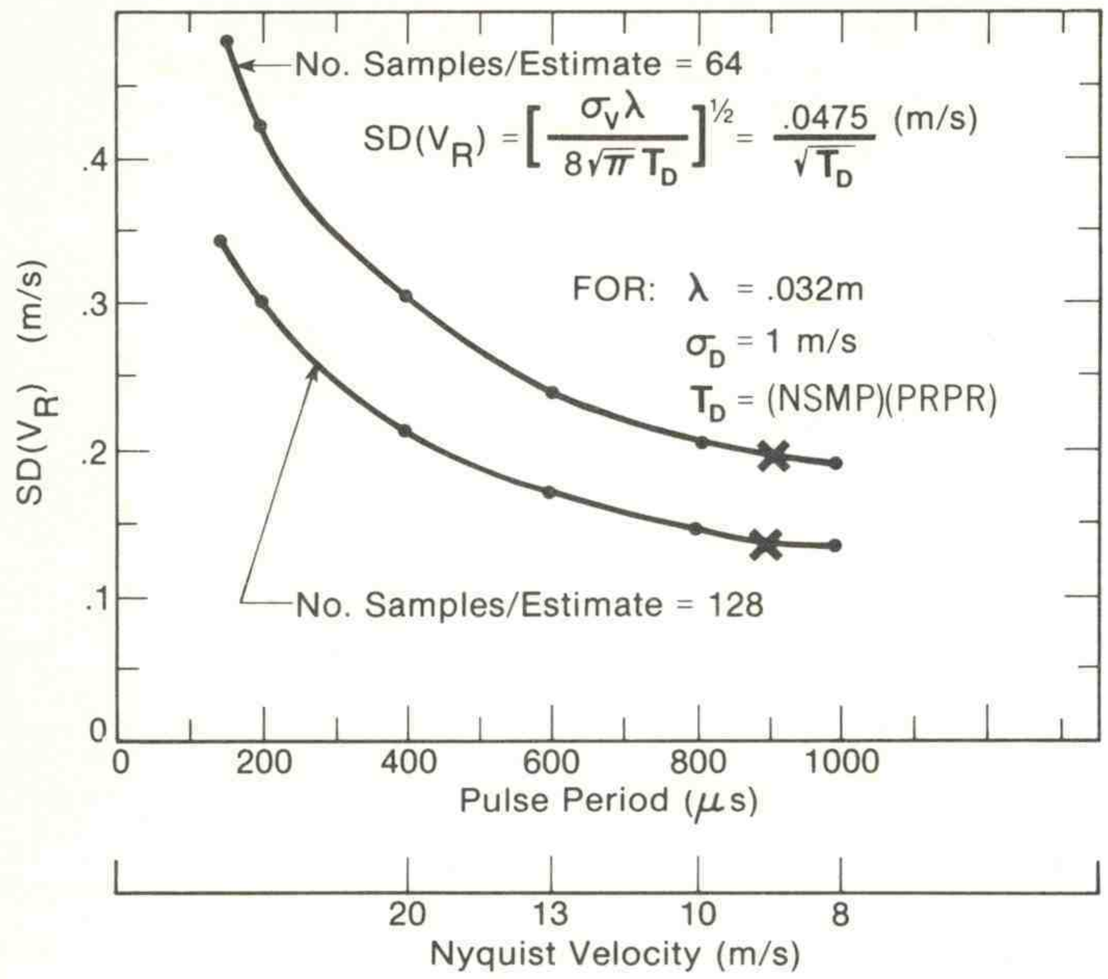


Figure 3.7.--Expected standard deviation of radial velocity estimate as a function of radar pulse period for 128 and 64 samples per estimate and large signal-to-noise ratio.

is about 1.4 in the vicinity of the BAO tower before any variance reduction is achieved in the interpolation process. The weighting done in the interpolation to a common grid will reduce this normalized variance still further. Specifically, the grids chosen for the various scan types would reduce these variances by a factor of at least 4 in the vicinity of the tower. Thus, for the two cases indicated in Figure 3.7 the expected errors in the horizontal wind would be on the order of 0.1 m s^{-1} for large signal-to-noise ratio. A corresponding analysis for the two-radar solution yields a similar result in the vicinity of the tower. An analysis of the random errors in estimates of w leads to an expected error of 0.2 m s^{-1} near the 1-km level.

3.6 Chaff Dispersal

Chaff was dispersed over an area several hundred square kilometers in extent by means of a chaff cutter flown aboard a small single-engine aircraft. A continuous line of 1.5-cm chaff was distributed for several hours at a time along cross-wind flight legs. Usually the flight patterns were adjusted to dispense chaff about 30 to 45 min upwind of the target area. When the winds were weak and variable in direction, a zig-zag pattern covering an appropriate box was chosen. Convective activity was usually sufficiently strong between 1100 and 1730 each day to distribute the chaff uniformly throughout the PBL in the test area. Radar echoes from the resulting chaff cloud were usually at least 10 dB above the noise over most of the region of interest.

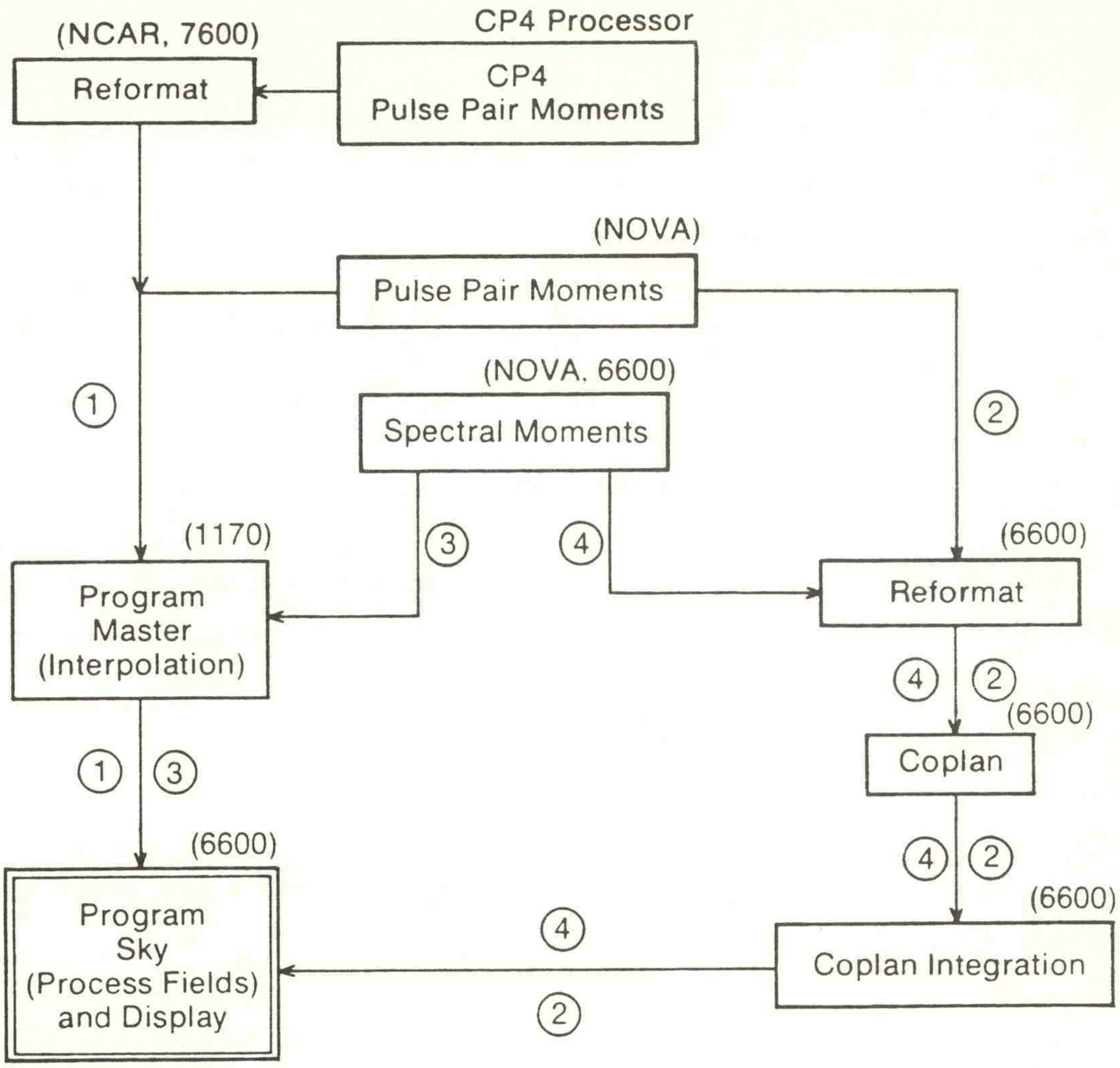


Figure 3.8.--Alternative software "paths" leading to the display program Sky.

3.7 Radar Data Processing and Analysis

The block diagram in Figure 3.8 indicates a number of the possible processing schemes that might be used to produce the desired velocity fields. Nominally, they all lead to the same result; however, each involves differing amounts of complexity and computer effort. The software for all of these schemes is nearly complete; tests are being run to establish which procedure will be used routinely on the bulk of the PHOENIX data. The circled numbers indicate the possible paths in the order of increasing complexity and required computer resources.

Path 1 is the simplest and most straightforward and involves only three steps. First, pulse-pair estimates of radial velocity are generated by using

NOVA software currently available in the radar. The pulse-pair tapes are then interpolated to a Cartesian grid with program Master on the BAO PDP 11/70 computer, and a CDC 6600-compatible tape is also generated on the 11/70. Finally, this tape is read by program Sky, which carries a wide variety of operations and develops displays for the Cartesian fields.

If our ongoing quality checks indicate that unacceptable errors arise from the two-radar approximations inherent in path 1, we plan to fall back on path 2. Here a reformat stage precedes the conventional Coplan and Coplan Integration programs. As in path 1 the fields are subsequently manipulated and displayed in Sky on the 6600.

Should it happen that the biasing effects of ground clutter cannot be properly removed in paths 1 and 2 by discriminating on the basis of the signal-to-clutter ratio in Sky, spectral lines in the vicinity of the DC component will have to be removed and moments then computed from the corrected spectra. This will be costly and time-consuming; we will avoid it if we can. If the simple two-radar approximation to the horizontal wind fields proves sufficiently accurate, Master will be used as in path 1. This path is shown as path 3.

Finally, should the ground clutter problem prove solvable only by spectral analysis and should we simultaneously find that the two-radar approximation is inadequate, we will use path 4. This is the least economical path, of course, as it is the most complex and time-consuming.

At the time of this writing, the software necessary for all the above processing schemes is complete, with the exception of the algorithms responsible for removing ground clutter from the spectral-moment estimates. We are currently evaluating the feasibility of operationally running such algorithms.

3.8 Radar Data Samples

Radar data may of course be displayed in a wide variety of formats. Although the material below is by no means exhaustive, it is at least indicative of the displays that are available. The basic displays are similar to those shown in Figures 3.1a-e. However, different resolutions are also available, as indicated

in Figures 3.9a-c. The high-resolution display resulted from a 300-series scan of the type shown in Figure 3.4, while the medium-resolution display was derived from a 200-series scan, indicated in Figure 3.3. The low-resolution, high-area coverage display utilized data from the 600-series scan shown schematically in Figure 3.6. This last display also indicates those areas covered by the higher-resolution scans above. All scans were made within an 8-min time frame, and hence reveal certain similar features shown in different amounts of detail. However, nonstationarity of the flow field has also resulted in certain differences.

Other data displays are also available. Figure 3.10 shows the velocity field in vertical planes cutting through the PHOENIX experimental volume, revealing closed circulation patterns of updrafts and downdrafts characteristic of the thermal convection regime. Figure 3.11 shows plots of flow-field horizontal divergence revealed at two different heights. Such plots typically reveal that in the convectively-active PBL, regions of surface convergence are associated with regions of upper-level divergence and vice versa, as one expects from typical convective flow patterns associated with thermal plumes and roll vortices.

Figure 3.12 demonstrates that there are considerable scan-to-scan consistency and correlation between the PBL airflows. By contrast, Figure 3.13 shows that after tens of minutes, the flow pattern has experienced considerable changes. The careful analysis of both the stationary (and hence presumably terrain-linked) and evolving aspects of PBL flows will be the focus of much of the PHOENIX analysis.

3.9 Radar Operations

Table 3.3 lists the approximate radar operating times for the PHOENIX experiment. For the most part, all three radars were operating during these periods. The data gap from September 15 to 18 corresponds to the period during which the radar positions were changed in order to improve ground-clutter characteristics. As a rule, radar operations coincided with other PHOENIX operations, primarily flights of the NCAR research aircraft. As a result, most of the time intervals shown contain gaps of 1 or 2 h duration, corresponding to aircraft refueling.

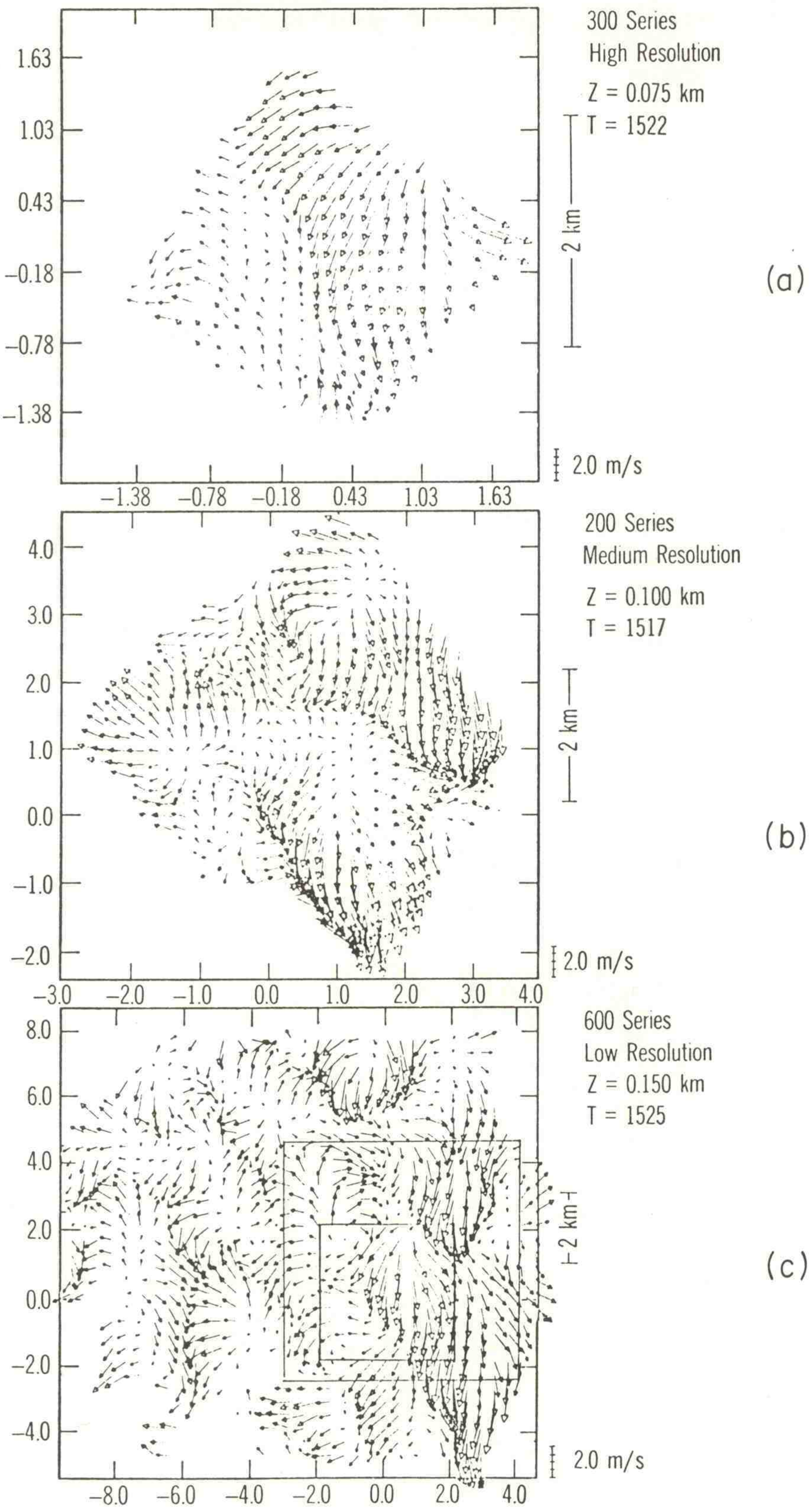


Figure 3.9.--Examples of (a) high-resolution (300-series), (b) medium-resolution (200-series), and (c) low-resolution (600-series) wind fields at the lowest levels (and nearly the same time).

Table 3.3.--PHOENIX multiple-Doppler radar operating times

Date (September 1978)	(MDT)
1	1053-1621
5	1120-1618
6	0956-1539
8	1109-1503
9	0958-1410
15	1429-1614
18	1352-1655
19	1058-1539
20	1027-1240
21*	1117-1729
22*	1144-1838
25*	1315-1737
26*	1045-1842
27*	1101-1704

* Data that have been reduced to first and second moments and have been interpolated to the standard series grids, so that they are relatively convenient for use. All other data are still in raw form.

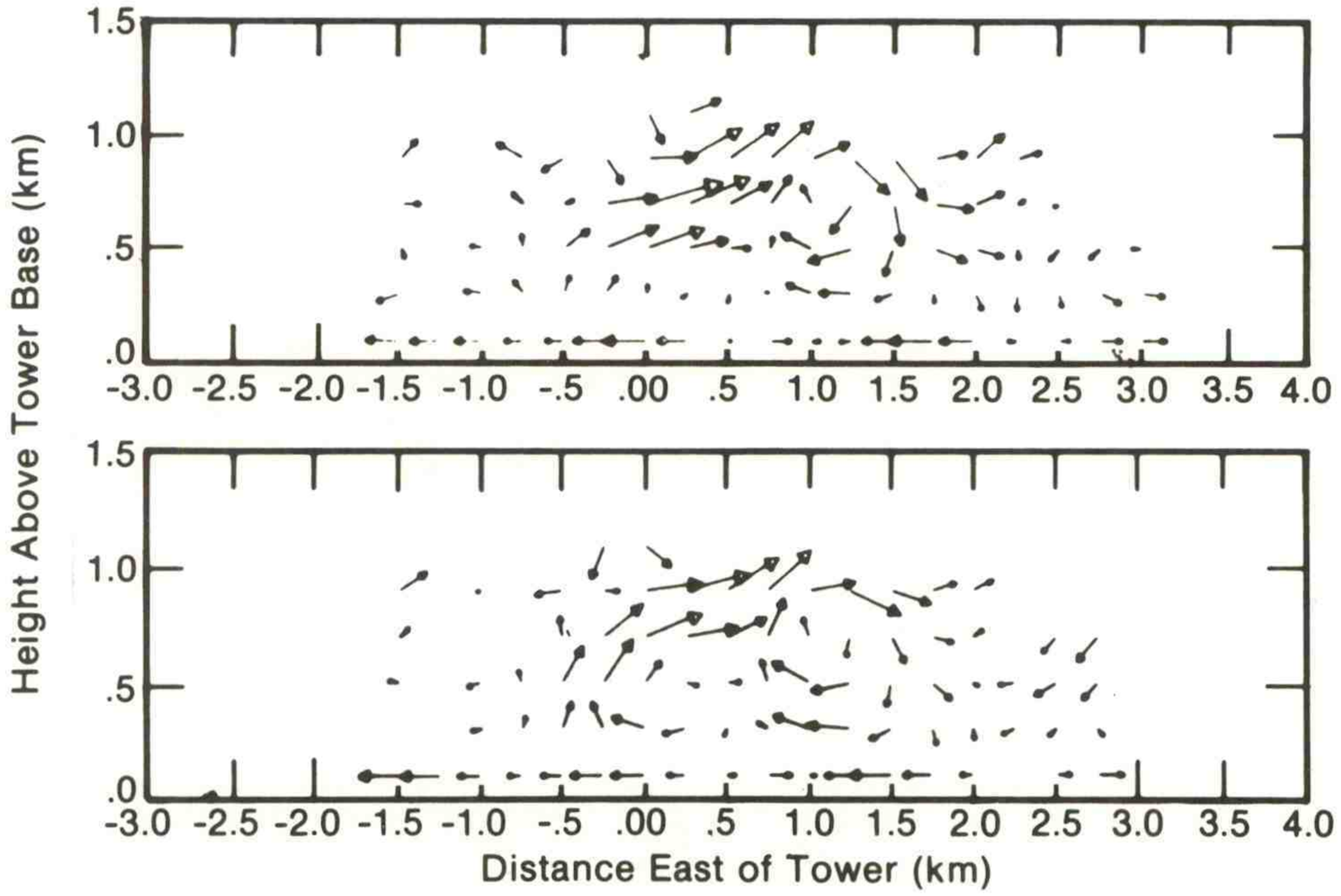


Figure 3.10.--Vertical (XZ) sections through the wind field at 1531 and 1533 MDT on September 21, 1978, for Y = 0.5 km.

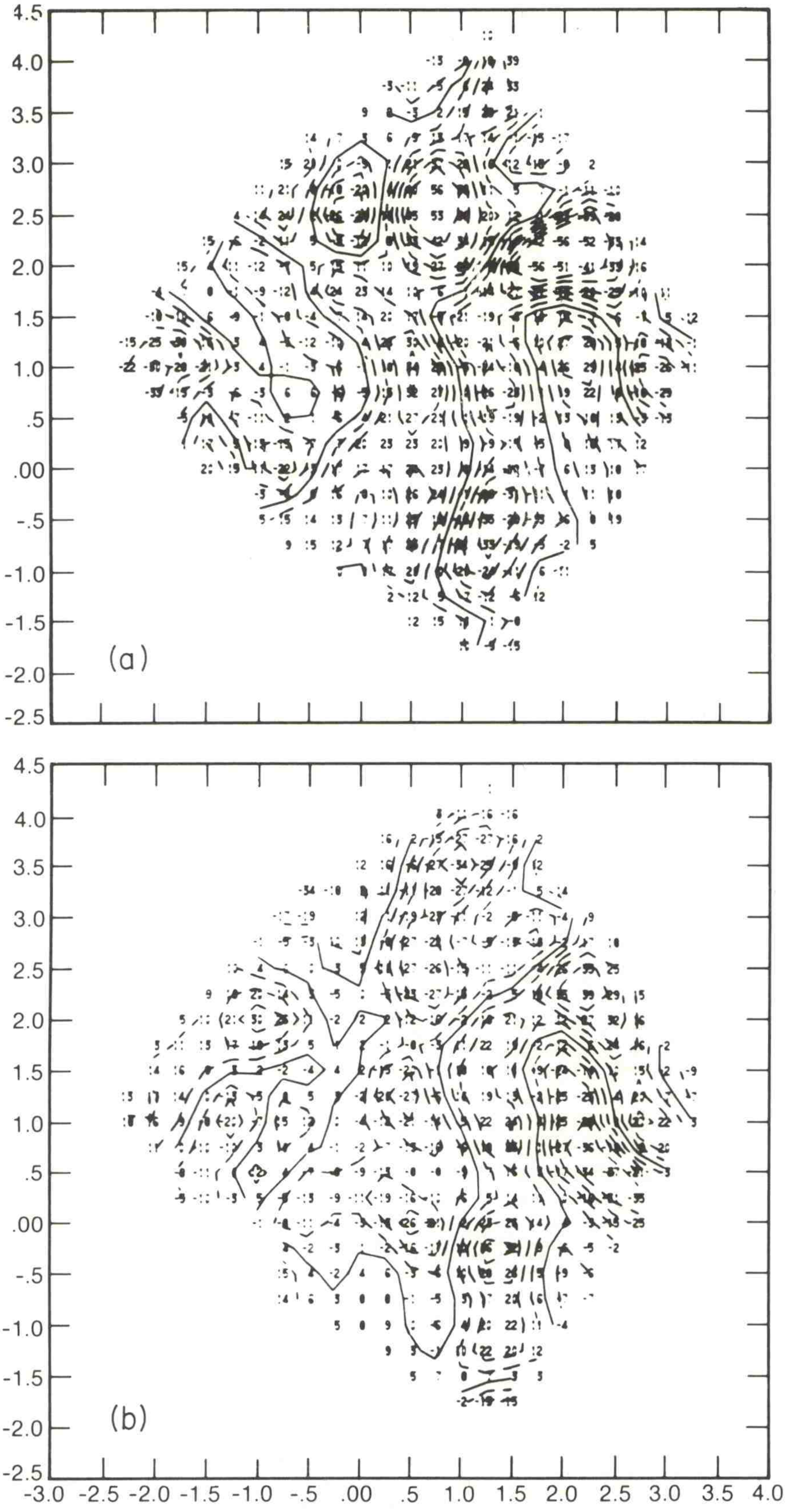


Figure 3.11.--Computed divergence fields at (a) Z = 0.1 km and (b) Z = 0.7 km for 1556 MDT, September 21, 1978. Contours denote each 10^{-4} s^{-1}.

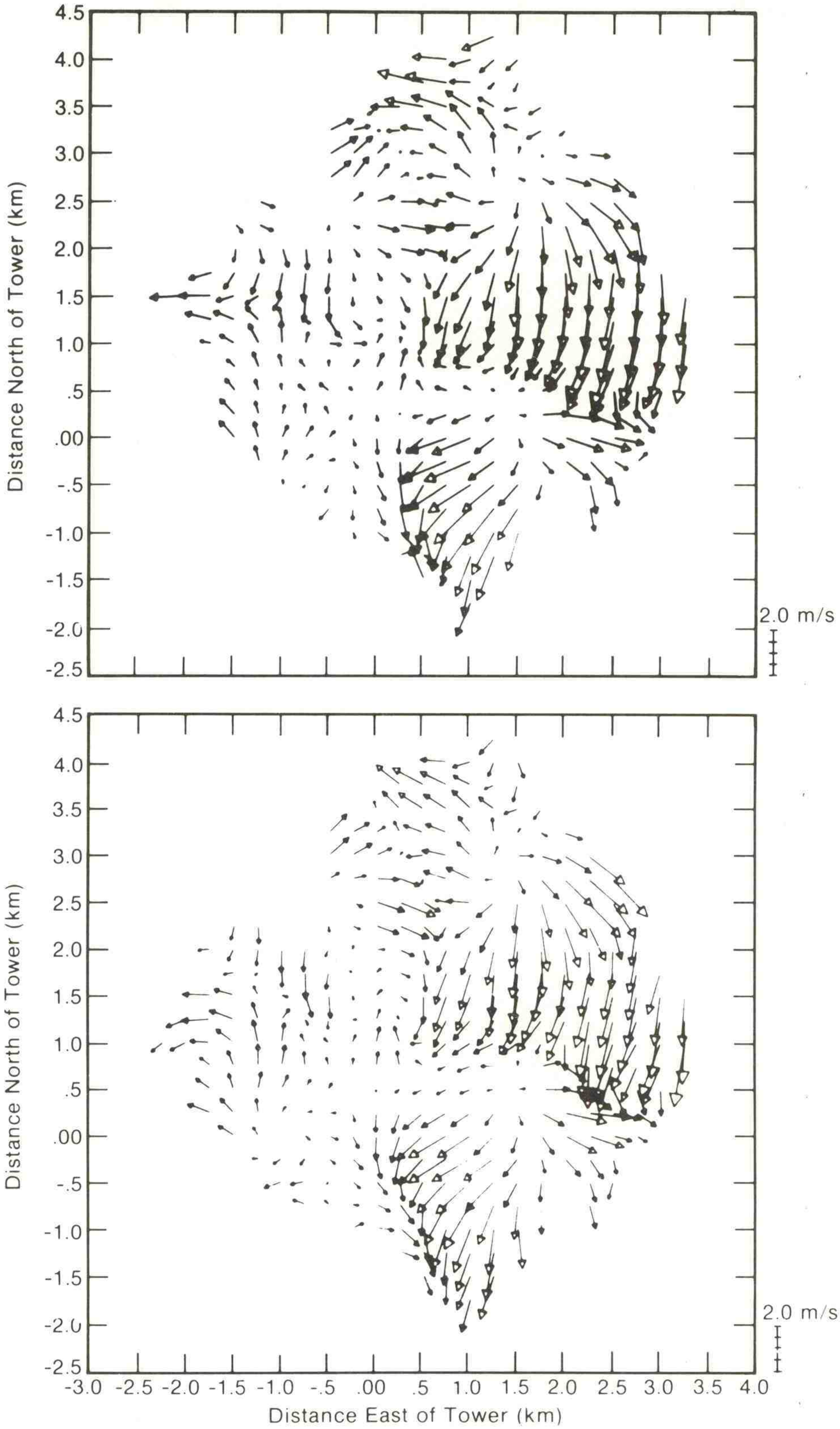


Figure 3.12.--Horizontal eddy wind fields (volume mean removed) for Z = 0.1 km at 1512 MDT and 1513 MDT on September 21, 1978. Note the good scan-to-scan correlation.

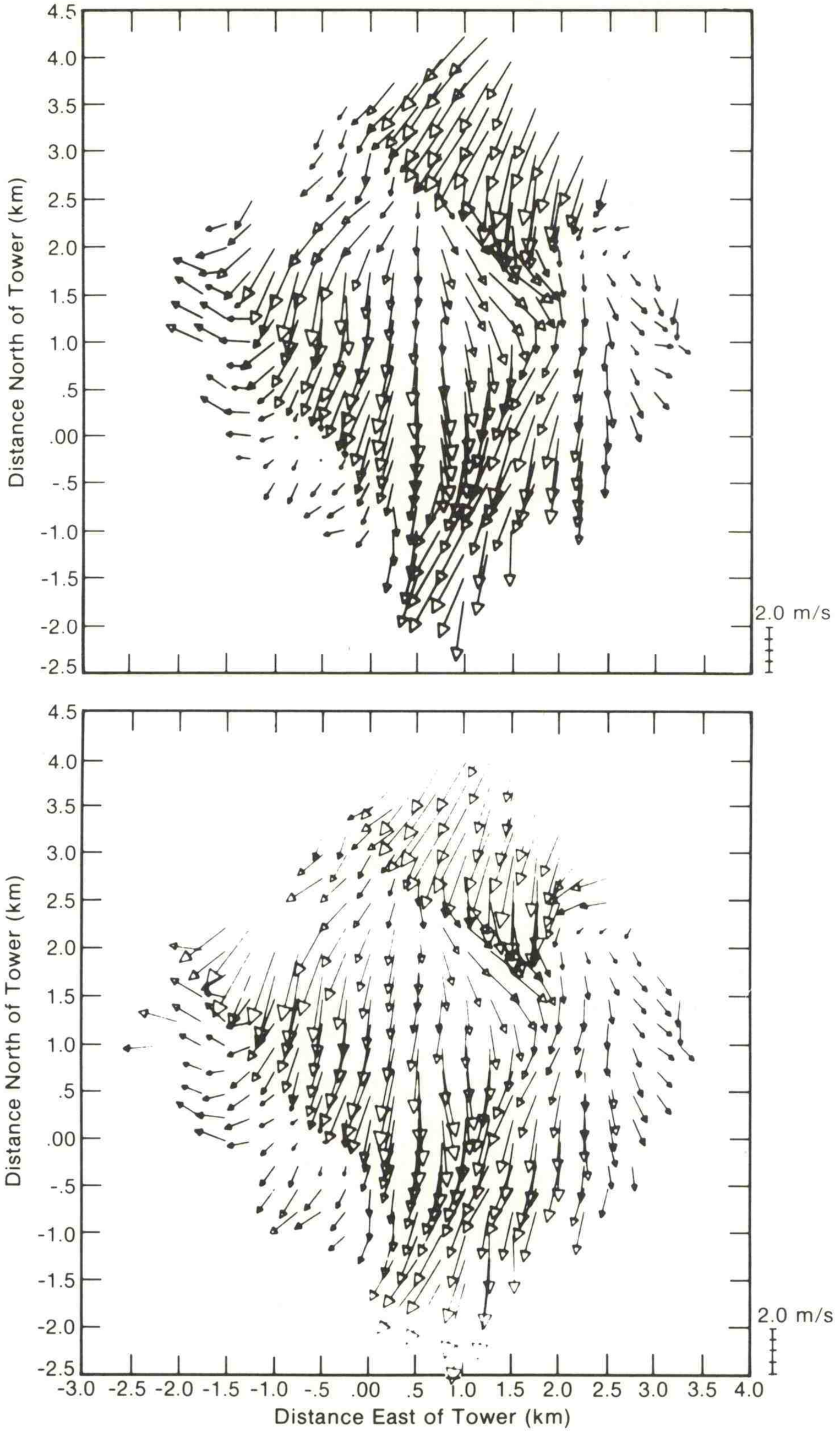


Figure 3.13.--Same as Figure 3.12 but for 1531 MDT and 1533 MDT. Again there is good scan-to-scan correlation, but the circulation has evolved significantly from that 20 min earlier.

At this writing, not all of the data are in a form equally convenient for outside use. Those time intervals marked by an asterisk refer to data reduced to first and second moments, and interpolated to the standard series grids. These data are in a form relatively convenient for analysis. To bring the other data into this form would require considerable computer processing. For further information, the interested reader is referred to the author (commercial phone (303) 499-1000 ext. 6235, FTS 323-6235).

Acknowledgments

The assistance and support of the NOAA/WPL and NCAR/FOF radar staffs are gratefully acknowledged. In particular, Bruce Bartram, Nancy Bowden, Carroll Campbell, Jack Hanchett, Jay Miller, Bill Moninger, Sue Stippich, Dick Strauch, and Bruce Sweezy from NOAA/WPL and Brian Lewis and Dale Zalewski from NCAR/FOF put in many long hours while operating radars throughout the experiment. Without their excellent support, the multiple-Doppler radar portions of the experiment would not have been so successful.

Robert S. Lawrence piloted the great majority of the chaff dispersal flights; Garner T. McNice and Stephen M. Wandzura substituted on occasion. We would like to take this opportunity to extend our thanks to these men for their help with this tedious and unrewarding task.

References

Bohne, A. R., and R. C. Srivastava, Random errors on wind and precipitation fall speed measurement by a triple Doppler radar system, The University of Chicago Laboratory for Atmospheric Probing, Technical Report No. 37, 44 pp. (1975).

Dye, J. E., L. J. Miller, B. E. Martner, and Z. Levin, Growth and recirculation of precipitation in an evolving convective storm, Preprints Conf. on Cloud Physics and Atmospheric Electricity, July 31-August 4, 1978, Issaquah, Wash., pp. 528-533, American Meteorological Society, Boston, Mass. (1978).

Frisch, A. S., and S. F. Clifford, A study of convection capped by a stable layer using Doppler radar and acoustic echo sounders, J. Atmos. Sci. 31, 1622-1628 (1974).

Gal-Chen, T., A method for the investigation of the anelastic equations: implications for matching models with observations, Mon. Weather Rev. 106, 587-606 (1978a).

Gal-Chen, T., Deduction of pressure and density fluctuations using Doppler radar observations: a feasibility study, Preprints 18th Conf. Radar Meteorology, March 28-31, 1978, Atlanta, Georgia, pp. 104-111, American Meteorological Society, Boston, Mass. (1978b).

Gossard, E. E., and A. S. Frisch, Kinematic models of a dry convective boundary layer compared with dual-Doppler radar observations of wind fields, Boundary-Layer Meteorol. 10, 311-330 (1976).

Hooke, W. H., P. H. Hildebrand, and R. A. Kropfli, Project PHOENIX: background and introduction, in Project PHOENIX: The September 1978 Field Operation, W. H. Hooke, Ed., NOAA/NCAR Boulder Atmospheric Observatory Rept. No. 1, available from NOAA/ERL, Boulder, Colo., and from NCAR Publications Office, Boulder, Colo. (1979).

Kaimal, J. C., and D. E. Wolfe, BAO site, tower instrumentation, and PHOENIX operations, Chapter 2, in Project PHOENIX: The September 1978 Field Operation, W. H. Hooke, ed., NOAA/NCAR Boulder Atmospheric Observatory Rept. No. 1, available from NOAA/ERL, Boulder, Colo., and from NCAR Publications Office, Boulder, Colo. (1979).

Kropfli, R. A., and N. M. Kohn, Persistent horizontal rolls in the urban mixed layer as revealed by dual-Doppler radar, J. Appl. Meteorol. 17, 669-676 (1978).

Kropfli, R. A., and L. J. Miller, Kinematic structure and flux quantities in a convective storm from dual-Doppler radar observations, J. Atmos. Sci. 33, 520-529 (1976).

Leise, J. A., Temperature retrieval from dual-Doppler radar wind field data, Preprints 18th Conf. Radar Meteorol., March 28-31, 1978, Atlanta, Georgia, pp. 94-99, American Meteorological Society, Boston, Mass. (1978).

Miller, L. J., and R. G. Strauch, A dual Doppler radar method for the determination of wind velocities within precipitating weather systems, Remote Sensing Environ. 3, 219-235 (1974).

Miller, L. J., J. D. Marwitz, and J. C. Fankhauser, Kinematic structure of a Colorado thunderstorm, Preprints 16th Conf. Radar Meteorol., April 22-24, 1975, Houston, Texas, pp. 128-133, American Meteorological Society, Boston, Mass. (1975).

Wilson, D. A., Doppler radar studies of boundary layer word profile and turbulence in snow conditions, Preprints 14th Conf. Radar Meteorol., November 17-20, 1970, Tucson, Arizona, pp. 191-196, American Meteorological Society, Boston, Mass. (1970).

CHAPTER 4

PHOENIX OPERATIONS OF THE NCAR QUEEN AIR RESEARCH AIRCRAFT

Peter H. Hildebrand
National Center for Atmospheric Research
Boulder, Colorado 80307

Aircraft use in boundary-layer experiments has a long history, dating back to the classic O'Neill experiment itself, when nervy pilots flew a PBY-6A as low as 15 m above the deck to compare aircraft data with those from sonic anemometry and surface instrumentation (Bunker, 1957). The same experiment featured an L-20 liaison-type plane flying at levels from 15 to 150 m above the surface in order to monitor PBL temperature and humidity structure (Harney and Rounds, 1957). During the ensuing decades, as micrometeorological emphasis has shifted from the surface boundary layer to the planetary boundary layer surmounting it, from surface fluxes of momentum and energy to the interaction of the PBL with the entire free atmosphere above, and as airborne meteorological instrumentation has become increasingly sophisticated and reliable, research aircraft have come to play an ever more important role in PBL studies. Such aircraft offer numerous advantages for PBL investigations. First, and perhaps most fundamentally, they offer the research meteorologist access to the great heights of interest in PBL work, not only probing through the entire depth of the mixed layer, which may extend as high as several kilometers in extreme cases, but also penetrating into the overlying free atmosphere. Second, they offer the advantages of wide areal coverage, providing line averages of meteorologically significant quantities such as fluxes of momentum and heat, and offering diagnostic capabilities for the study of spatial inhomogeneity in these parameters. And finally, they provide approximately instantaneous spatial scans (deriving from aircraft airspeeds an order of magnitude larger than wind velocities typically encountered), obviating the need for indirect inferences from single-tower data relying on a relatively shaky application of Taylor's hypothesis. As a result, use of such research aircraft has proved increasingly popular despite their high operational costs. Relatively modern studies such as those by Lenschow (1970, 1972, 1973), Bean et al. (1972, 1975), and Pennell and LeMone (1974) serve to illustrate the power of this approach.

Unique though their intrinsic capabilities may be, research aircraft offer still more when coordinated in their use with operations of ground-based remote sensors, such as Doppler radars. Although currently able to measure a wider variety of turbulence and mean-flow parameters than these remote sensors, they are unable to provide the complete volume coverage the radars obtain with ease. It was the goal of the PHOENIX experiment to exploit this synergism in the study of the PBL and its circulation systems.

To measure PBL structure in PHOENIX, we used two Queen Air research aircraft, furnished by the Research Aviation Facility of NCAR and denoted as N304D and N306D. Basic aircraft capabilities and instrumentation have been summarized by Burris et al. (1973). Lenschow et al. (1978) provide an updated report on the velocity-sensing systems on board, while Duncan and Brown (1978) describe the currently-used data acquisition system. For PHOENIX, the planes were instrumented nearly identically. Both measured temperature, humidity, winds (both mean and fluctuating parts of the three wind components u, v, and w), pressure, refractive index, and aircraft position (latitude, longitude, and altitude). Both operated forward-pointing time-lapse cameras. In addition, N306D carried a downward-pointing infrared surface temperature sensor. All data were sampled at 20 Hz; at the aircraft cruising speed of some 75 m s^{-1}, this would correspond to a spatial resolution of 4 m along the flight path. Most measurements were made redundantly with several types of sensors. All instruments were calibrated both before and after the experiment, and every day of flight included aircraft intercomparisons and a tower flyby, as well as other calibration procedures. Figure 4.1 shows the two aircraft flying past the BAO at 300-m altitude in the course of one of the calibration runs.

The daily flight plans involved four basic types of flight patterns. The vertical cross sections of these flights are illustrated in Figure 4.2. A plan view of the flight is shown in Figure 4.3. The bulk of the data were collected by alternating the flux flight pattern (Figure 4.2a), with the sounding pattern (Figure 4.2b). In the flux pattern the aircraft flew constant-altitude flight levels of about 30-km length. The flight altitudes ranged from somewhat above the PBL-capping inversion to just 150 m above the ground, with two or three flight altitudes concentrated at the inversion itself. The idea was to use data from the mid-PBL altitude, together with current theoretical understanding of the mixed

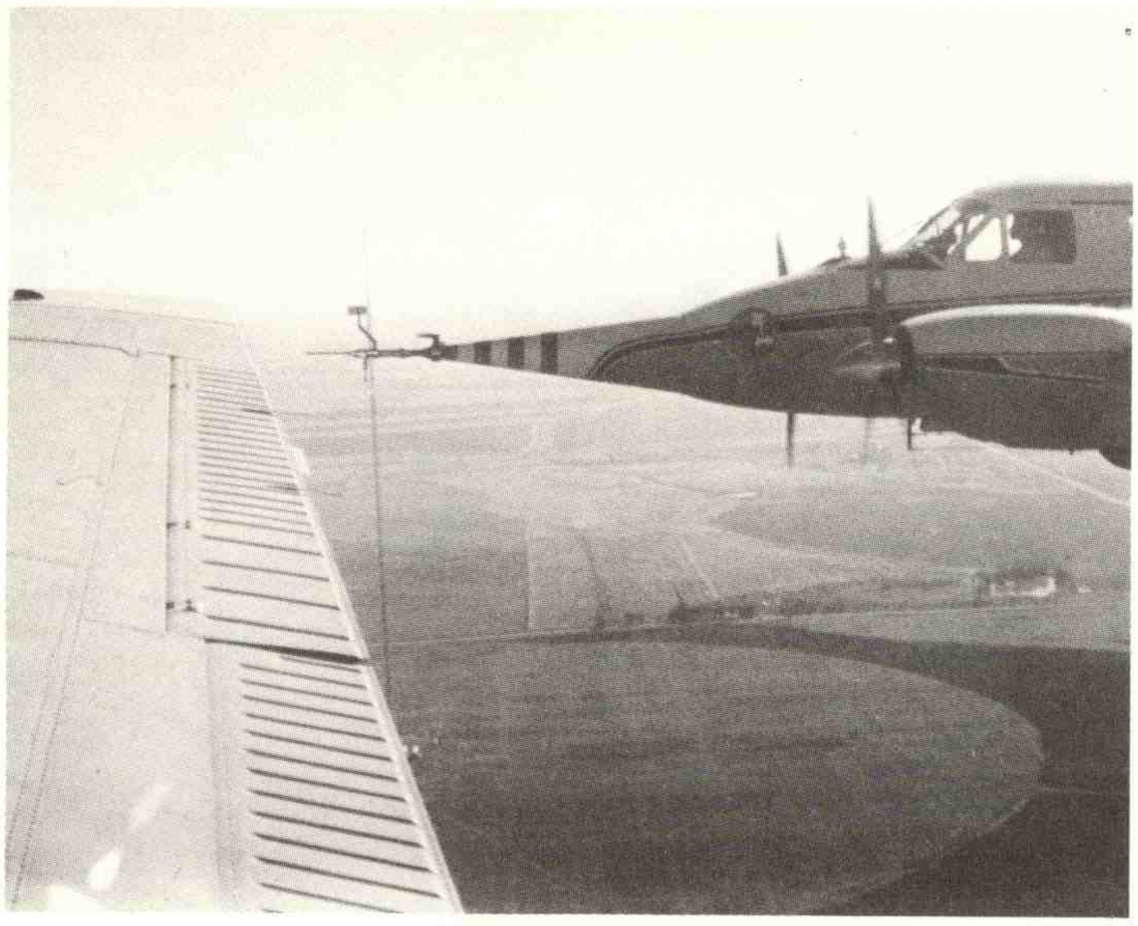


Figure 4.1.--NCAR aircraft N304D and N306D making a 300-m altitude calibration run past the BAO tower (background) prior to one of the PHOENIX operations.

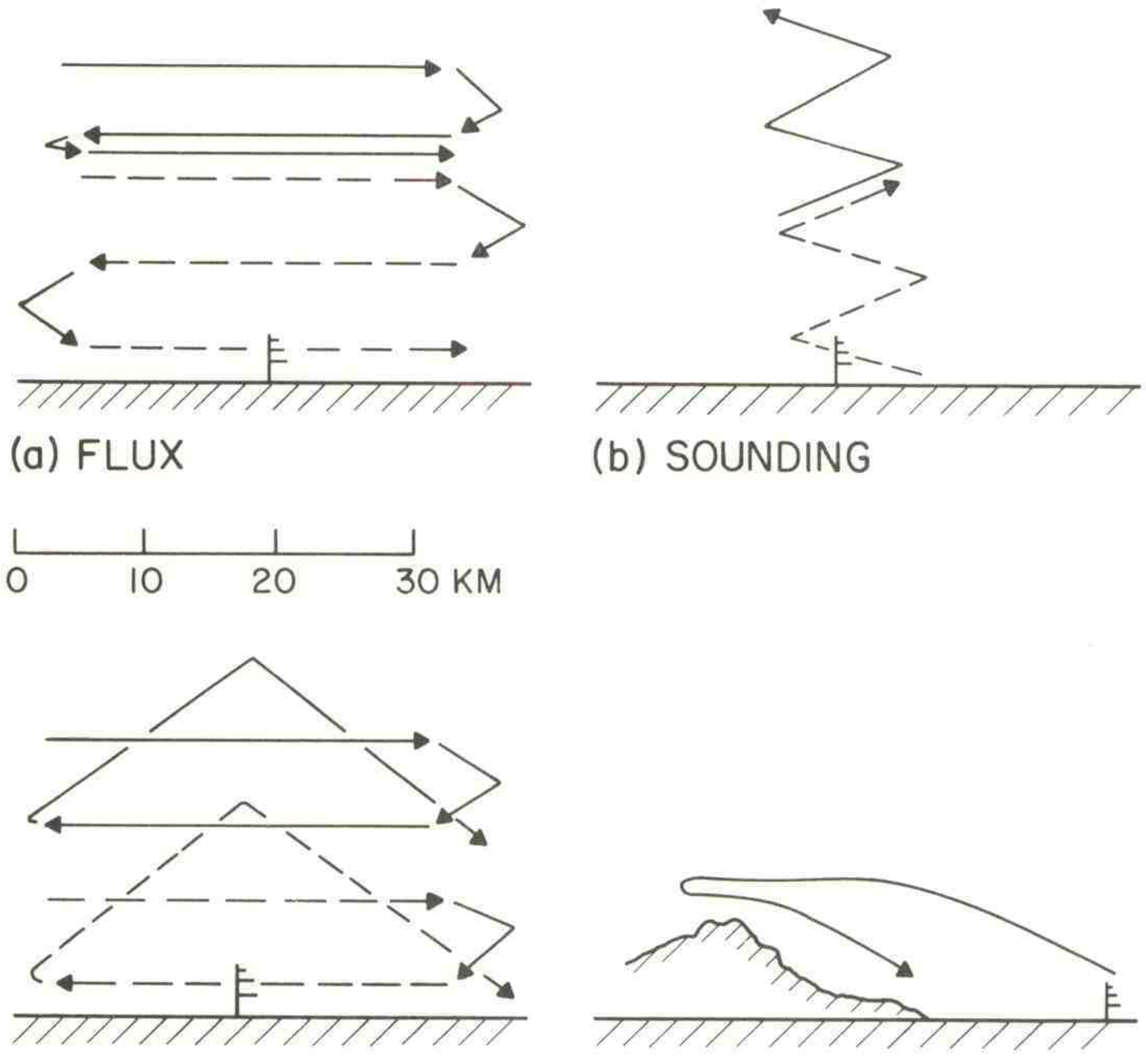


Figure 4.2.--The aircraft flight patterns as viewed in the vertical plane. BAO tower location is indicated schematically by the short vertical line at the surface. Flight paths for the two aircraft are indicated by solid and dashed lines respectively. A plan view of the flight paths showing their horizontal extent is given in Figure 4.3.

layer, to define conditions through the convectively active PBL as a whole, while using the data gathered at higher levels to resolve fine detail within the so-called entrainment layer that caps the PBL, in order to glean a better understanding of its workings and the processes active within it. In most cases, the two aircraft operated together, one flying nearly directly above the other, executing north-south and east-west flight legs at each level before changing altitudes.

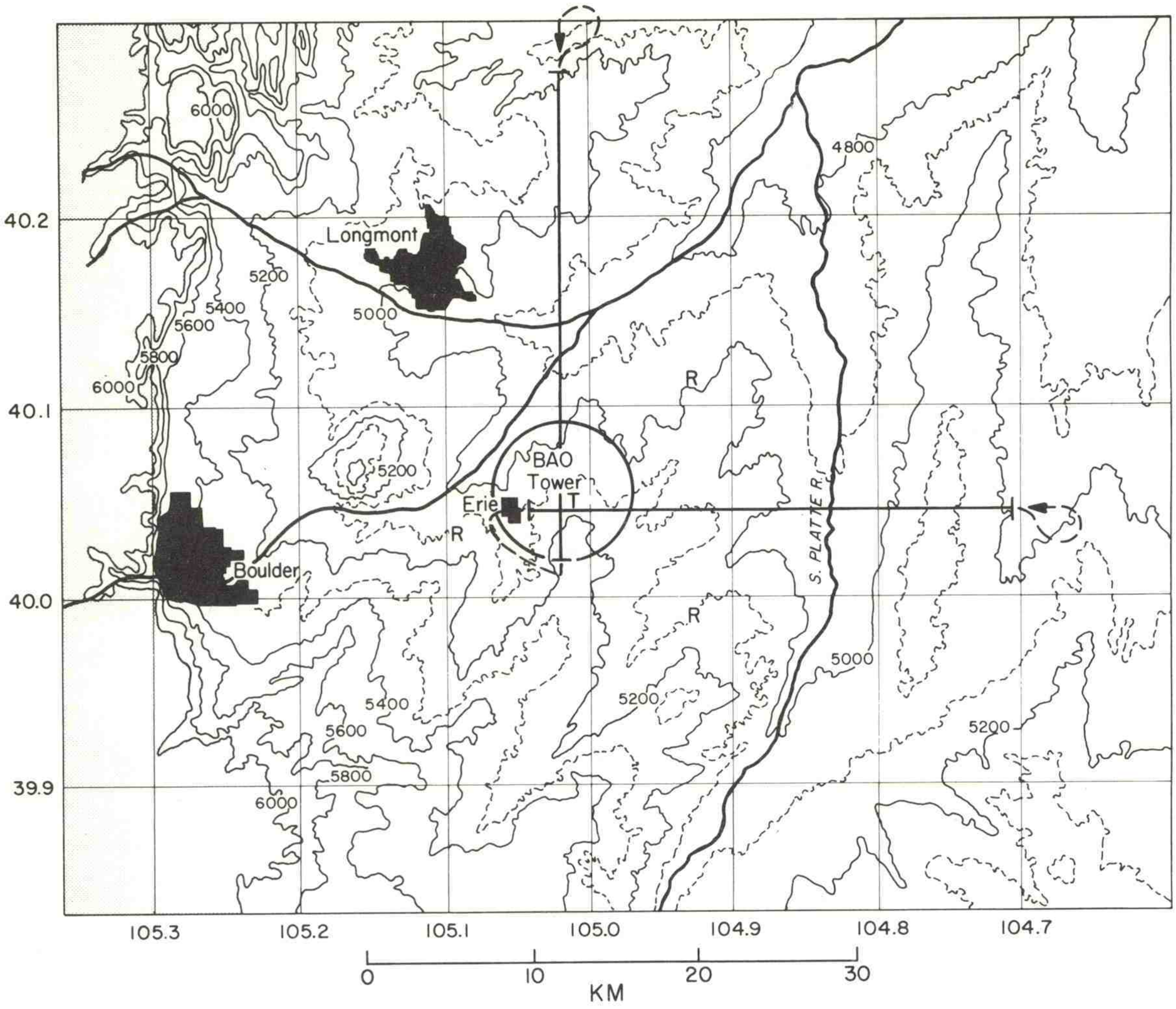


Figure 4.3.--A plan view of the radar flight paths, indicating their position and orientation relative to the BAO and the multiple-Doppler radars (R's).

However, in some cases, particularly on flights during September 21, 22, 26, and 27, only one aircraft was airborne at a given moment. In those cases, flight legs were flown in only one direction, that is, either E-W or N-S; the choice in these cases was based upon radar-observed structure in the air motion.

In flying the sounding pattern, the aircraft flew an ascent at 150 m/min in a box pattern from ground level to a maximum altitude which was above the highest flux pattern level. Following the box ascent, a quick spiral descent was frequently made in the same area, although in some cases the spiral descent was omitted to save time. Again in order to save time, in all cases for which both aircraft were available, the sounding was broken into two altitude ranges. In such cases one aircraft would fly immediately above the other.

The third type of flight pattern was the cross-section pattern illustrated in Figure 4.2c. This pattern, used only on September 22, 26, and 27, was designed to provide measurements of PBL structure late in the afternoon, after the ground had begun cooling and PBL growth had halted. Very little is known about mixed-layer breakdown in the afternoon; this pattern was considered to provide our best chance of observing the salient features of PBL evolution during such periods. While executing this pattern, both aircraft flew horizontal flight legs in two directions (N-S and E-W) and at two levels, the four total levels being spread throughout the PBL. Following the horizontal legs, both aircraft would fly a sawtooth pattern, as illustrated, in both the N-S and E-W directions.

The final data collection flight pattern (Figure 4.2d) extended over the Rocky Mountains; it was designed to measure characteristics of the airflow over the mountains as part of ongoing efforts to assess the impact of the Rockies on BAO micrometeorology. This pattern was flown at about noon on occasions when both aircraft were operating. In this case, one aircraft would fly the mountain pattern while the other flew a sounding alone.

The flights for the entire experiment are summarized in Table 4.1. In general, the flights prior to September 21 began at about 0900 MDT and lasted until about 1600 MDT in the afternoon. These flights consisted of flux and sounding flight patterns, with two of each pattern made in alternation on both morning and afternoon flights. On many days, a mountain flight was made by one aircraft at the end of the morning flight.

The flights made on September 21, 22, 26, and 27 lasted longer, extending from about 0900 through about 1900 MDT. On these days, single aircraft frequently flew morning and early-afternoon flights in which flux and sounding flight patterns were alternated twice. For the third flight of each day, both aircraft flew flux, cross-section, and sounding patterns, switching from flux to cross-section patterns when it appeared PBL growth had terminated with the onset of surface cooling.

On September 28, a series of horizontal E-W flight legs of approximately 15-km length, and at altitudes ranging from 3 to 6 km MSL, were flown over the NOAA Sunset radar located 20 km west of Boulder, in order to provide calibration data for the radar.

Table 4.1--Summary of PHOENIX flights

Date Sept. '78	Horizontal legs Time (MDT)	Flight levels (K ft MSL)	Soundings Time (MDT)	Max. Alt. (K ft)	Over mountains Time (MDT)
1	0918-1010	8.7, 8.5, 8.3, 7.5, 6.5, 6.0	0839-0855	10.5	
			1016-1035	14	
	1042-1133	12.5, 11.5, 10.0, 9.0, 7.0, 5.7	1138-1204	14	
5	0923-1023	7.5, 7.0, 7.0, 6.5, 0.5, 6.5	0851-0904	10.5	
			1026-1045	12	
	1045-1136	7.5, 7.0, 7.0, 6.5, 0.5, 5.7	1143-1205	12	Aborted
			1431-1450	14	
	1452-1540	14, 12.5, 10.5, 9, 7.5, 5.7	1544-1615	14	
6			0850-0901	10	
	0921-1014	9, 8, 7, 6.1, 0.5, 0.65	1019-1037	12	
	1044-1135	9, 8, 7, 6.5, 6.0, 5.7	1138-1156	12	1138-1207
			1319-1331	14	
	1331-1404	9, 7.8, 7, 5.7	1411-1422	14	
	1433-1524	14, 12, 10.5, 9, 7.5, 5.7	1527-1541	14	
8			1146-1216	20	
9	0913-1006	9, 8.5, 8, 7.5, 6.5, 5.7	0838-0855	10.5	
	1040-1130	9, 8, 7, 6.5, 6, 5.7	1013-1033	12	1133-1203
			1136-1157	12	
	1349-1404	7.5, 6.5, 5.7	1333-1348	9	
	1452-1543	10, 11.5, 8.5, 7, 6.5, 5.7	1430-1444	14	
			1547-1554	14	
21	1000-1040	9, 8, 7, 6-6.5, 5.7	0905-0921	10.5	
	1110-1200	10.5, 9, 8, 7.2, 6.5, 5.7	1050-1102	12	
			1204-1232	14	
	1504-1543	9, 8, 7, 5.7	1446-1455	12	
	1559-1701	9, 8.5, 8, 7, 6, 5.7	1544-1558	14	
			1701-1726	14	
22			0926-0950	10.5	
	0958-1041	6.5, 6.3, 0.5	1044-1104	12	
	1109-1146	6.5, 6.2-6.0, 5.7	1147-1159	12	
			1332-1345	12	

Table 4.1--Summary of PHOENIX flights--Continued

Date Sept. '78	Horizontal legs Time (MDT)	Flight levels (K ft MSL)	Soundings Time (MDT)	Max. Alt. (K ft)	Over mountains Time (MDT)
22 (cont.)					
	1406-1440	8.8, 8, 7, 6, 5.7,	1442-1507	14	
	1507-	10.5, 9, 7.5, 5.7	1536-1546	12	
			1642-1701	10	
	1702-1747	10, 8.5, 7, 5.7, 5.7-11	1702-1747	11	
			1748-1754	12	
	1756-1840	10, 8.5, 7, 5.7, 5.7-11	1756-1840	11	
26			0903-0919	12	
	0924-1005	7, 6.5, 6, 5.8, 5.7	1006-1021	10	
	1042-1112	7, 6.5, 6, 5.8, 5.7, 6.0	1112-1128	14	1128-1148
	1301	10.5, 9, 7.5, 6.5, 5.7	1241-1300	12	
	1301-1348	10.5, 9, 7.5, 6.5, 5.7	1351-1412	12	
	1413-1456	10.7, 10.5, 9, 7.7, 6.5, 5.	1457-1521		
			1610-1629	12	
	1647-1738	10.5, 9, 7.5, 5.7, 5.7-12	1647-1738	12	
			1746-1804	12	
	1811-1846	9, 0.5, 0.5-12	1811-1846	12	
27			0921-0937	12	
	0944-1024	7, 6.3, 6, 5.8, 5.7	1024-1033	10	
	1037-1116	7.5, 7, 6.8, 6.3, 6.0, 5.7	1121-1140	12	1140-1210
	1314-1354	8.3, 7.8, 7.0, 6.3, 5.7	1257-1312	12	
	1412-1444	9.0, 8.5, 8.0, 6.0	1356-1409	12	
	1508-1522	12, 11	1445-1508	14	
	1646-1719	13.5, 12	1625-1646	14	
	1740-1820	12, 10, 8, 6, 5.7 5.7-12	1740-1820	12	
	1821-1831	6.5, 6.5			

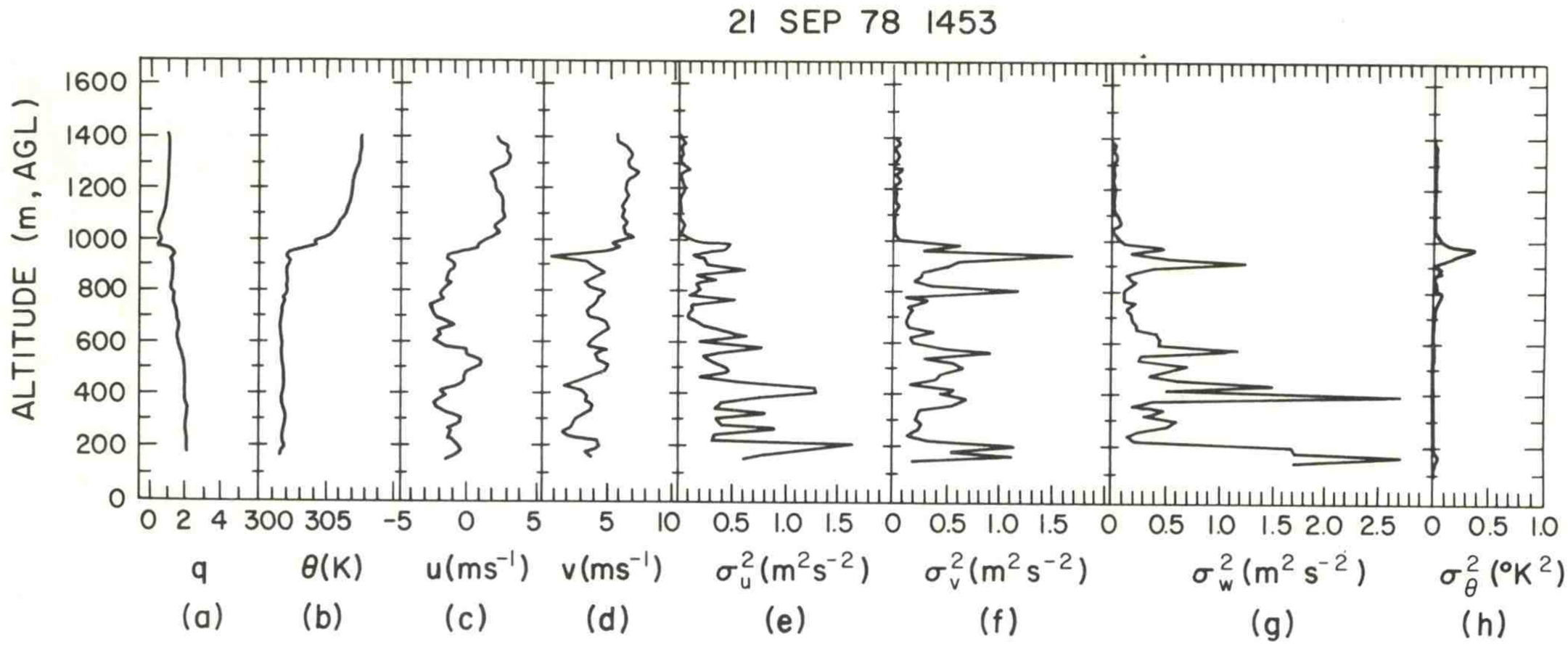


Figure 4.4.--A vertical sounding taken by NCAR Queen Air N306D on September 21, 1978, from 1453-1500 MDT: (a) relative humidity, (b) equivalent potential temperature, (c) east-west wind component, (d) north-south wind component, (e) east-west velocity variance over successive 20-m height intervals, (f) north-south velocity variance over successive 20-m height intervals, (g) vertical velocity over successive 20-m height intervals, (h) equivalent potential temperature variance over successive 20-m height intervals.

Data from all flights were recorded digitally, using the data acquisition system described by Duncan and Brown (1978). Some examples of the data displays currently available are shown here. Figures 4.4a-h show height profiles obtained during a vertical sounding, taken by N306D on September 21, 1978, from 1453 to 1500 MDT. Figures 4.4a-d show height profiles of equivalent potential temperature, relative humidity, and mean u and v components of wind, respectively. Figures 4.4e-h show variances calculated from the same sounding taken from data in successive 20-m height intervals for all three velocity components as well as equivalent potential temperature. The presence of steep gradients in the four mean quantities and the sudden diminution of all variances point unambiguously to the 1300-m level as the vertical limit of the mixed layer.

Figures 4.5a,b show time series in vertical velocity and equivalent potential temperature taken from a horizontal flight leg on September 21, 1978, between 1009 and 1013 MDT. Figures 4.6a,b show vertical-velocity and equivalent-potential temperature spectra deduced from these time series; Figure 4.6c shows the velocity-temperature cospectrum. Data similar to these should be available from all aircraft runs; for further information the interested reader is referred to the author (commercial telephone (303) 494-5151 ext. 78-31).

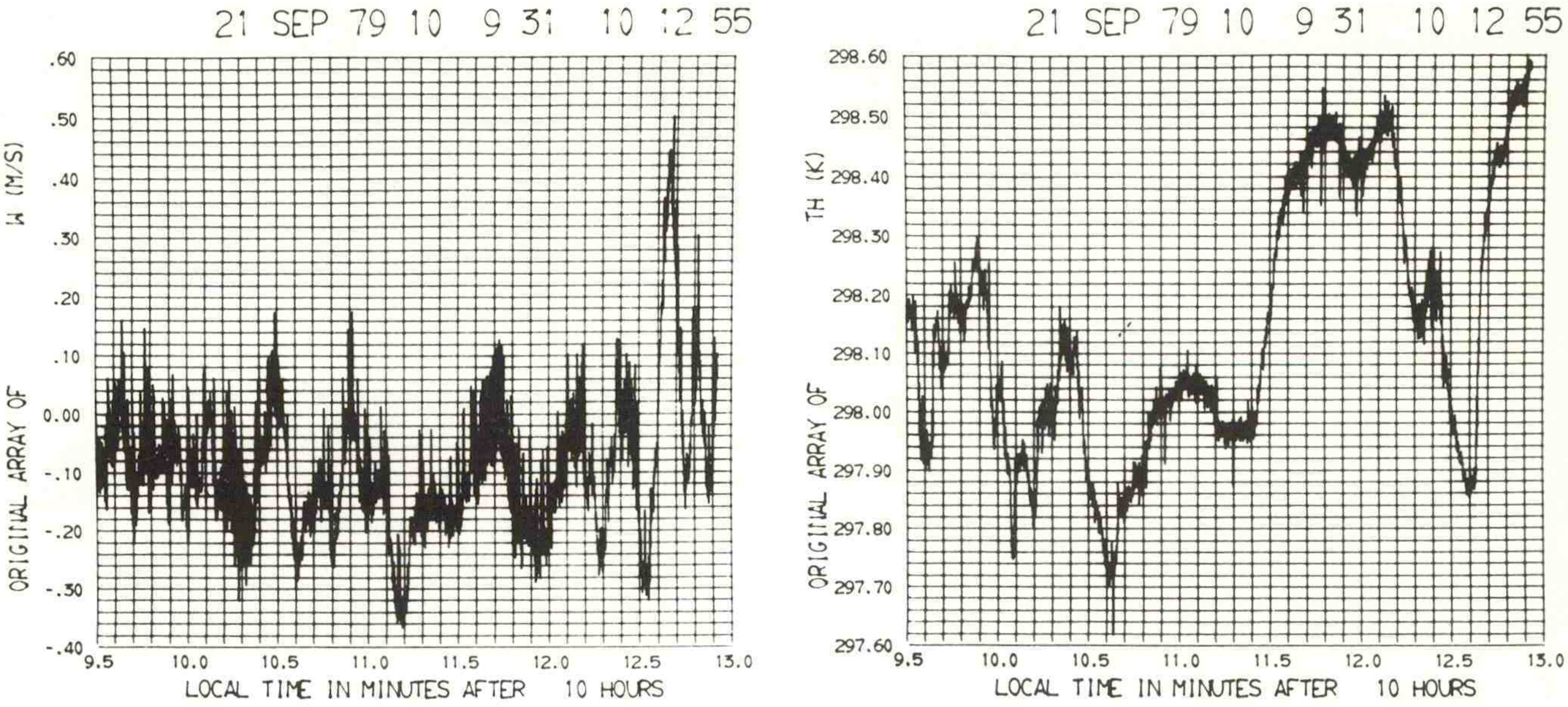


Figure 4.5.--Time series in (a) vertical velocity and (b) equivalent potential temperature taken during a horizontal flight leg on September 21, 1978, from 1009 to 1013 MDT.

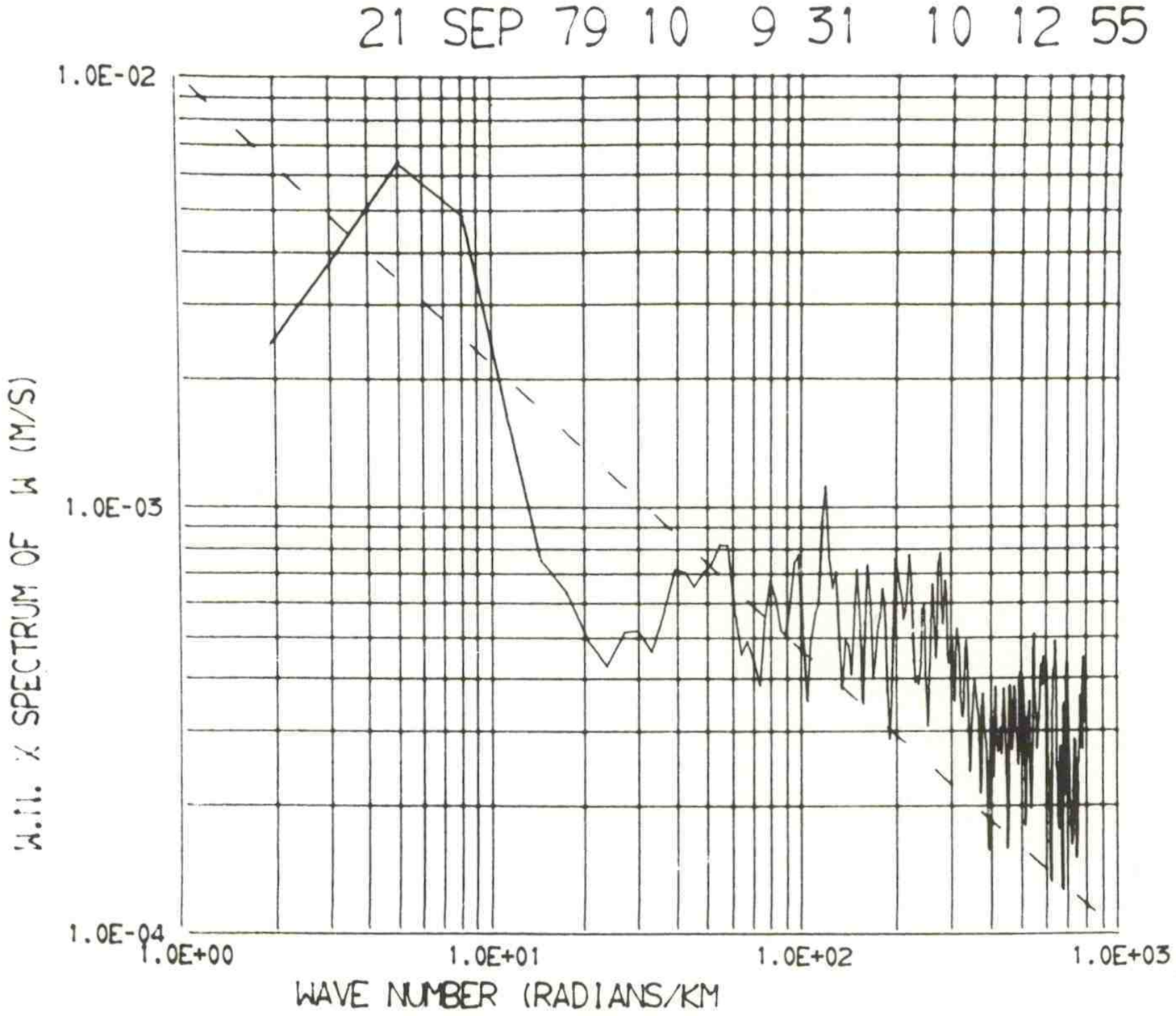


Figure 4.6a.--Vertical-velocity spectrum deduced from the time series of Figure 4.5a.

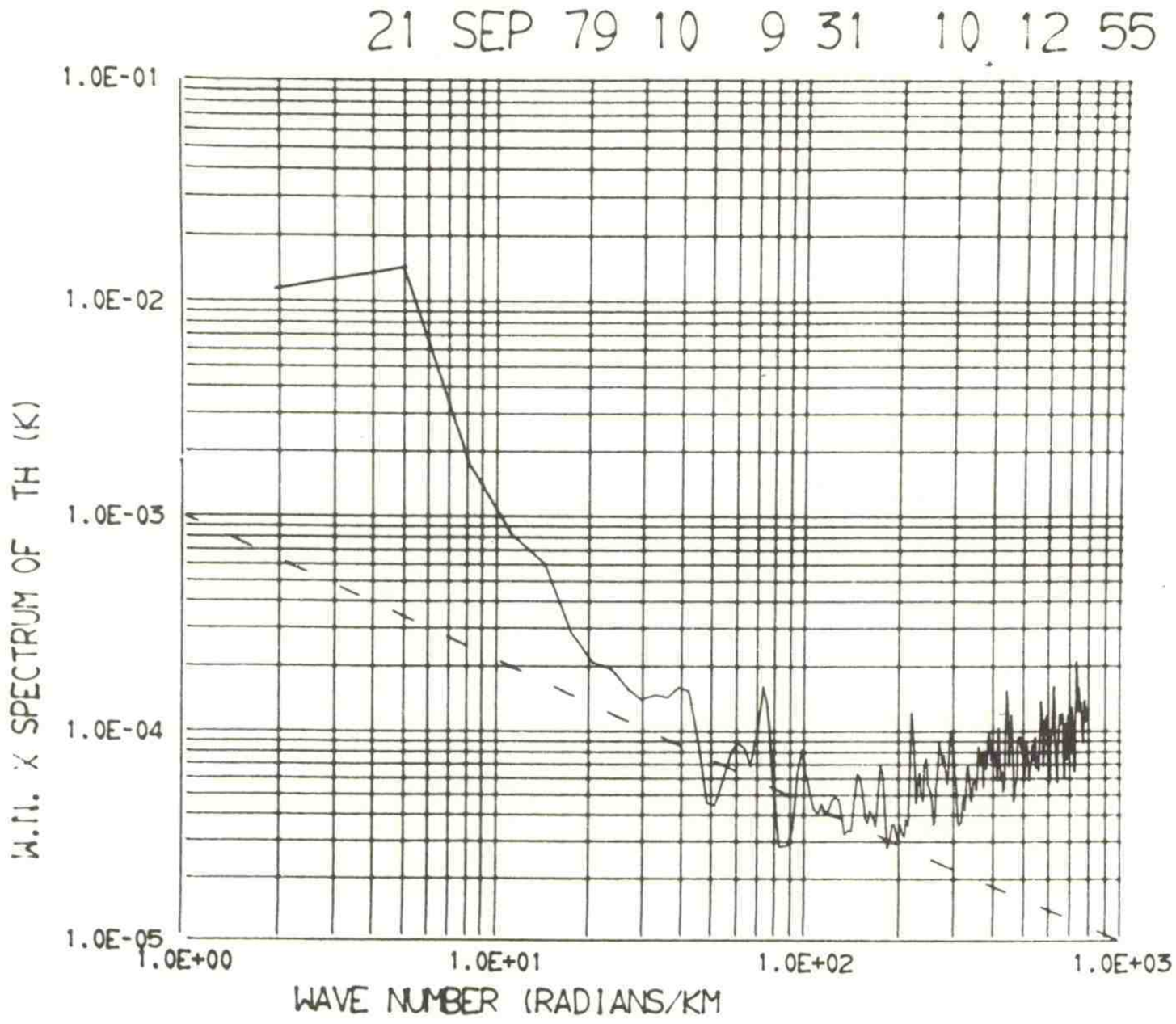


Figure 4.6b.--Equivalent potential temperature spectrum deduced from the time series of Figure 4.5b.

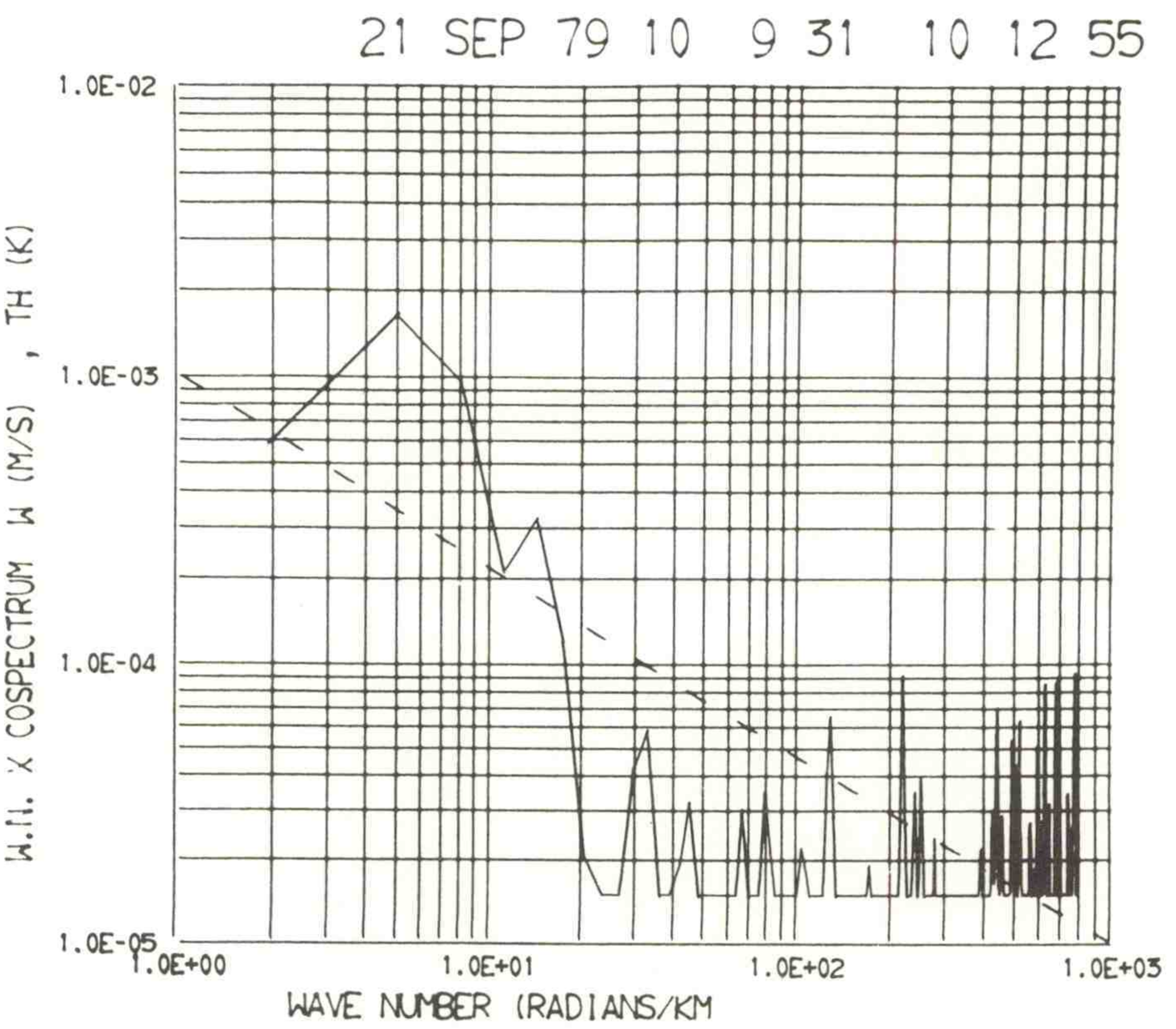


Figure 4.6c.--The velocity-temperature cospectrum for the two time series.

Acknowledgments

The assistance and support of the NCAR Research Aviation Facility staff is gratefully acknowledged. In particular, Pete Orum and Bill Zinser repeatedly flew the required flight paths with necessary precision, Carl Mohr and Dan Breed willingly donated their excellent on-board support in operating the in struments, and Paul Spyers-Duran and other RAF engineering and support staff worked the long hours necessary to provide the quick-look data and calibrated instruments on board the aircraft.

References

Bean, B. R., R. Gilmer, R. L. Grossman, R. McGavin, and C. Travis, An analysis of airborne measurements of vertical water vapor flux during BOMEX, J. Atmos. Sci. 29, 860-869 (1972).

Bean, B. R., C. B. Emmanuel, R. Gilmer, and R. E. McGavin, Spatial and temporal variations of the turbulent fluxes of heat, momentum, and water vapor over Lake Ontario during IFYGL, NOAA Tech. Rept. ERL 313-WMPO 5, 57 pp. (1975).

Bunker, A. F., Aircraft (PBY-GA) fluctuation and flux data — Woods Hole Oceanographic Institution, Chapter 5.3, Exploring the Atmosphere's First Mile, Vol. I., Lettau and Davidson, Eds., Pergamon, New York (1957).

Burris, R. H., J. C. Covington, and M. N. Zrubek, Beechcraft Queen Air aircraft, Atmos. Technol. 1, 25-30, National Center for Atmospheric Research, Boulder, Colorado (1973).

Duncan, T. M., and R. C. Brown, A data acquisition system for airborne meteorological research, Bull. Am. Meteorol. Soc. 59, 1128-1134 (1978).

Harney, P., and W. Rounds, Jr., Aerograph (L-20) temperature and humidity data, Chapter 6.5, Exploring the Atmosphere's First Mile, Vol. I, Lettau and Davidson, Eds., Pergamon, New York (1957).

Lenschow, D. H., Airplane measurements of planetary boundary layer structure, J. Appl. Meteorol. 9, 874-884 (1970).

Lenschow, D. H., The measurement of air velocity and temperature using the NCAR Buffalo aircraft measuring system, NCAR Tech. Note EDD-74, 39 pp. (1972).

Lenschow, D. H., Two examples of planetary boundary layer modification over the Great Lakes, J. Atmos. Sci. 30, 569-581 (1973).

Lenschow, D. H., C. A. Cullian, R. B. Friesen, and E. N. Brown, The status of air motion measurements on NCAR aircraft, Preprints 4th Symp.on Meteorological Observations and Instrumentation, April 10-14, 1978, Denver, Colorado, pp. 433-438, American Meteorological Society, Boston, Mass. (1978).

Pennell, W. T., and M. A. LeMone, An experimental study of turbulence structure on the fair weather trade wind boundary layer, J. Atmos. Sci. 31, 1308-1323 (1974).

CHAPTER 5

MICROWAVE RADIOMETER STUDIES IN PHOENIX

M. T. Decker
Wave Propagation Laboratory
National Oceanic and Atmospheric Administration
Boulder, Colorado 80303

5.1 Introduction and Background

Microwave radiometers infer atmospheric properties such as temperature structure, water-vapor distribution, and liquid water content through measurement of apparent sky brightness at different radio frequencies and zenithal look angles. The last several decades have seen such techniques metamorphose from mere concepts offering intriguing potential to tools of practical operational value. They have found their most glamorous application on satellites, but ground-based systems have also received considerable attention and demonstrated significant promise (e.g., Westwater et al., 1975; Decker et al., 1978a,b; Westwater and Guiraud, 1978). Despite this interest and progress, microwave radiometry is not customarily thought of as a tool for boundary-layer research. Indeed, it has thus far proved only marginally useful in that role.

The fact is, however, that radiometric retrievals of atmospheric temperature profiles are rather sensitive to the thermal structure of the planetary boundary layer. Moreover, even the most rudimentary information about the PBL, for example, its height, can provide significant improvement in the accuracy of the radiometric temperature retrievals (Westwater, 1978). From our parochial point of view, then, the question has been not so much what radiometry could do for PHOENIX, but rather what PHOENIX could do for radiometry. PHOENIX operations, in their normal course, provided a number of independent estimates of PBL height, including measurements from the BAO tower, the aircraft, the multiple-Doppler X-band radars, the TPQ-11 radar, the FM-CW radar, acoustic sounders, and lidar. The simultaneous use of all these systems provided an opportunity to determine which might be optimal for hybrid use with radiometry in temperature profiling. Factors investigated included all-weather capability, unambiguity in PBL-height determination, and overall accuracy. Moreover, PHOENIX operations customarily provided two

rawinsonde flights each day, yielding another estimate of PBL thickness, and permitting a check on radiometrically retrieved profiles to tropopause heights.

In effect, then, the PHOENIX experiment provided an excellent opportunity for carrying out a study previously planned by WPL in cooperation with the Jet Propulsion Laboratory (JPL). JPL personnel brought and operated two instruments for PHOENIX use (the so-called SCAMS and NEMS radiometers); WPL operated a third (the MTS system). The systems provided operating frequencies at the water-vapor absorption line near 22 GHz, in the oxygen absorption complex between 50 and 60 GHz, and in the window-region between these absorption bands. In addition, WPL operated a two-channel (20.6 and 31.65 GHz) radiometer, which continually monitored the zenith atmosphere at the Denver Weather Service Field Office at Stapleton Airport, some 30 km south of the BAO. (The radiometer had been installed there previously to provide estimates of total atmospheric water vapor content and liquid water content for comparison with operational estimates of these quantities.) While it happened that this system was intermittently down for about a week during the PHOENIX experiment, there is still some overlap of data.

5.2 The SCAMS Radiometer

The scanning microwave spectrometer (SCAMS) system is a ground-based version of the radiometer flown aboard Nimbus 6. Staelin et al. (1975b) describe the instrument in some detail. This five-channel system makes simultaneous measurements of atmospheric radiation at frequencies of 22.235, 31.65, 52.85, 53.85, and 55.45 GHz. The instrument scans in a vertical plane from a zenith angle of 58.3°, through the zenith, and to 28.1° on the other side of zenith. The scan is stepped in 7.2° increments with a dwell time of about 1 s at each step. Two additional steps are used to point the antennas at calibration targets, and the entire sequence is repeated approximately once each 16 s. During the PHOENIX experiment, the instrument was located on the north side of the temporary building at the BAO (Figure 2.6), with vertical scan plane oriented to contain the line joining the SCAMS system with the NEMS radiometer located near the northwest guy-anchor of the BAO tower. Figure 5.1 shows the SCAMS instrument in place at the BAO.

During BAO operations, the SCAMS system was operated (and calibrated) in two modes. In the first mode, essentially that described above, the instrument was configured as shown in Figure 5.1 and Figure 5.2a. In the second mode, one of the

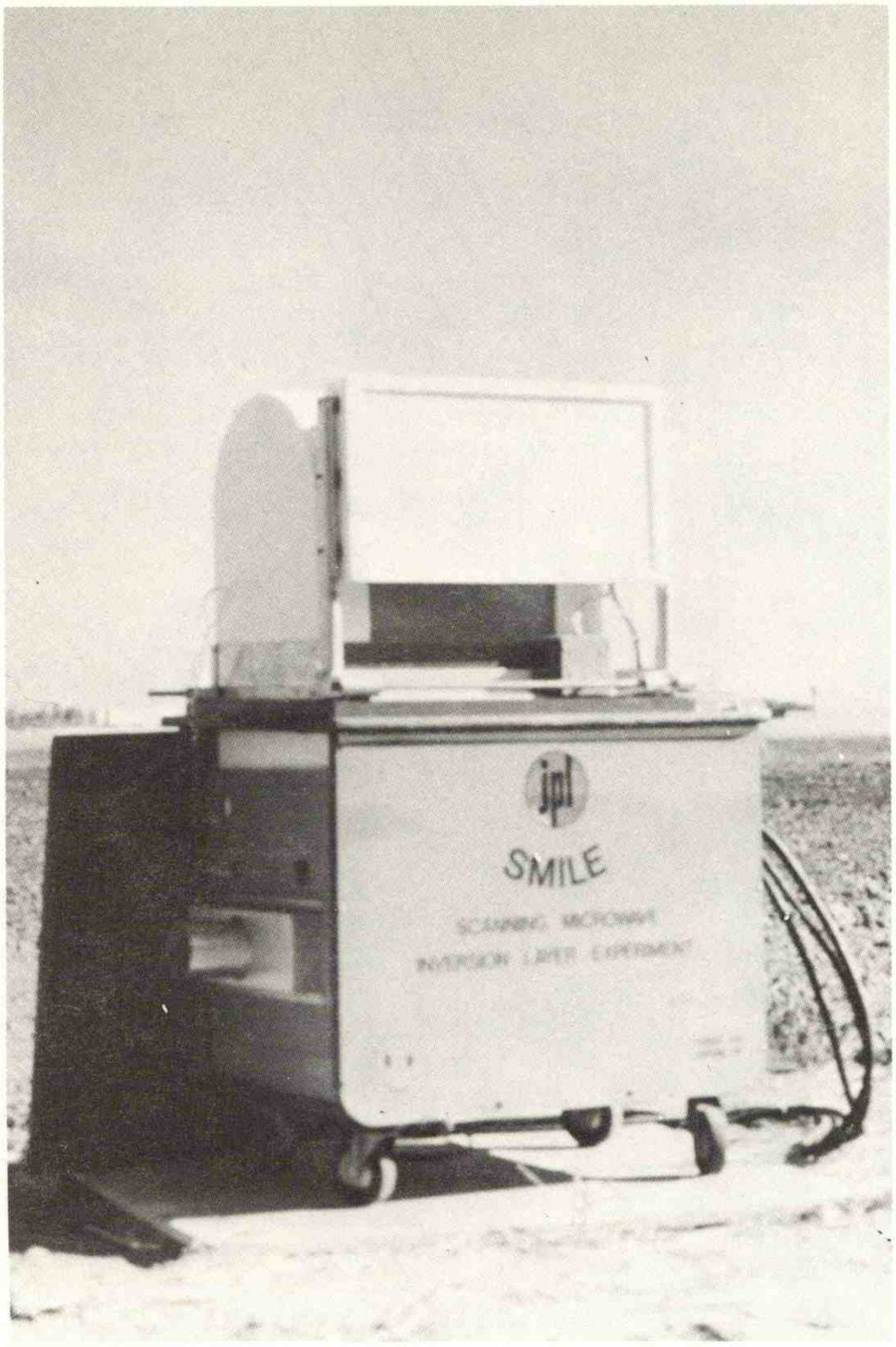
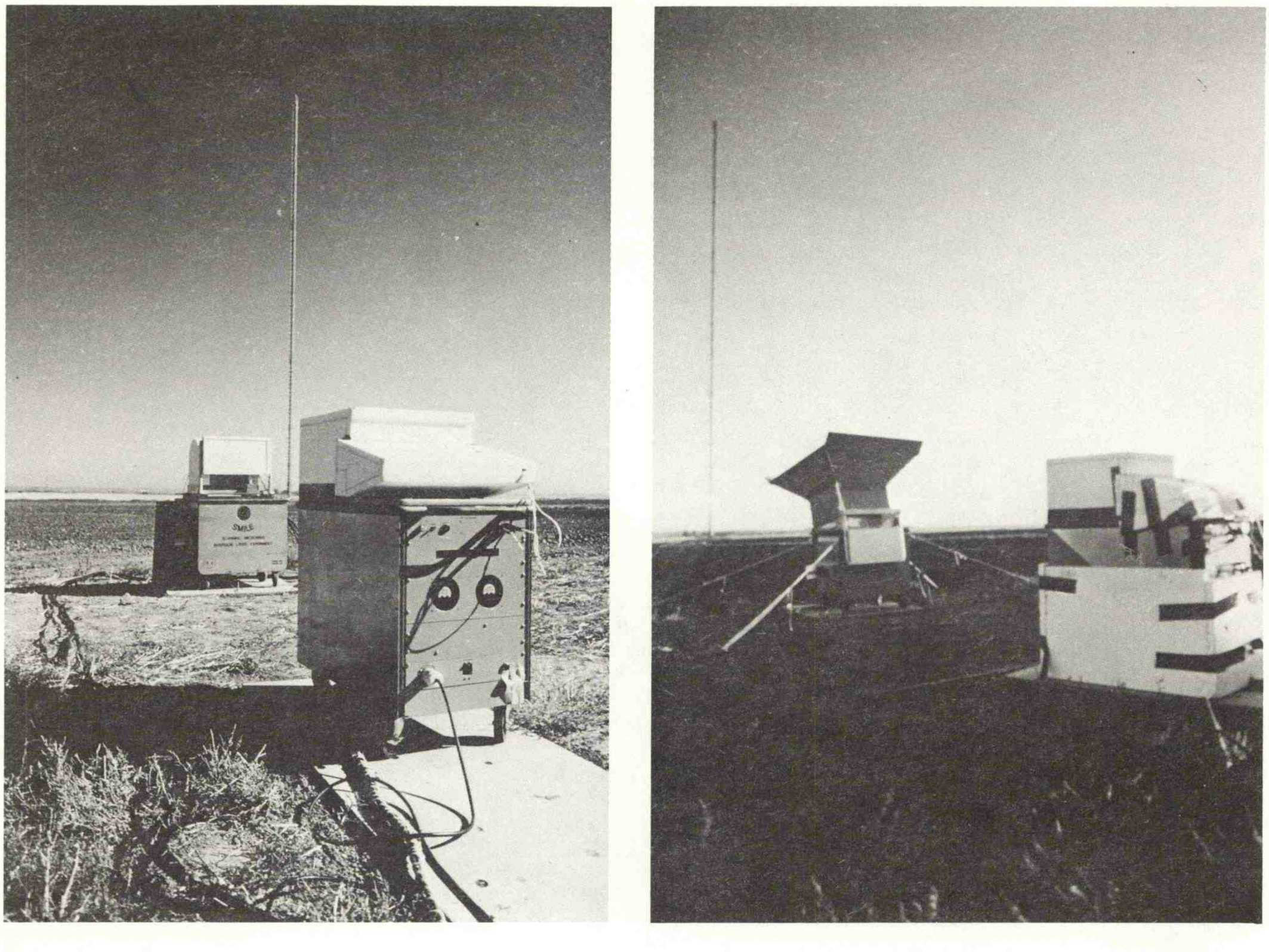


Figure 5.1.--The Jet Propulsion Laboratory SCAMS radiometer at the BAO during PHOENIX.

two calibration targets was removed, and the system fitted with an inverted metal pyramid over the antennas, as shown in Figure 5.2b. This had the effect of reducing radiation into sidelobes from the ground (which has a much higher temperature than the air, at least during the daytime), replacing radiation originating in the atmosphere itself. Calibration of the 22.235 and 31.65 GHz channels was then performed in the "tipping curve" mode in which the curve of sky brightness temperature versus number of air masses is forced through the background cosmic radiation value at zero air mass. This method of calibration, however, was inappropriate for higher frequencies. During PHOENIX, the system would typically be operated in the latter mode for some 4 h at a stretch, punctuated by 20-min runs in the first configuration.



a b

Figure 5.2.--(a) The SCAMS (background) and MTS (foreground) radiometers in place at the BAO. (b) The same two systems — the SCAMS system modified as described in Section 5.2 and the MTS system insulated to minimize thermal problems.

5.3 The NEMS Radiometer

The Nimbus E microwave spectrometer (NEMS) is a ground-based version of the microwave radiometer flown aboard Nimbus 5. For partial descriptions of the instrument the reader is referred to Rosenkranz et al. (1972) and Staelin et al. (1973). Waters et al. (1975) and Staelin et al. (1975a) have published results obtained with the satellite system itself. It is a five-channel system operating at frequencies of 22.235, 31.4, 53.65, 54.9, and 58.8 GHz. During most of the PHOENIX observing periods, observations were made with the instrument pointing at the zenith, with several elevation-angle scans made each day for calibration purposes. Data output occurs every 4 s. During PHOENIX the NEMS system was located

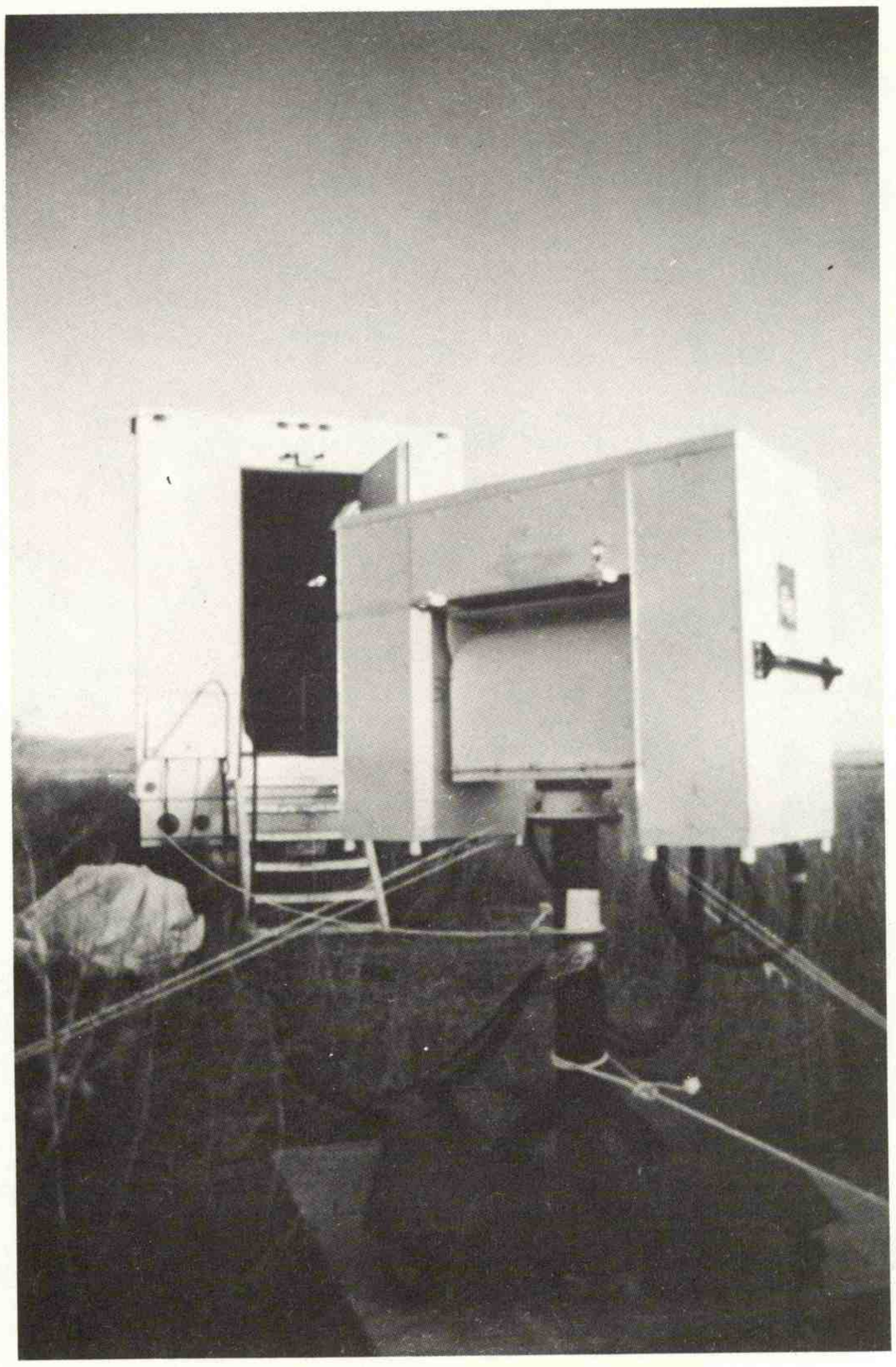


Figure 5.3.--The Jet Propulsion Laboratory NEMS radiometer deployed at the BAO for the PHOENIX experiment.

near the northwest guy anchor of the BAO tower, some 800 m to the north of SCAMS. Figure 5.3 shows the NEMS radiometer deployed for PHOENIX with the van housing its electronics in the background.

5.4 The MTS Radiometer

The microwave temperature sounder (MTS) radiometer is a 12-channel instrument with all channels in the oxygen absorption complex. Figure 5.4 shows the instrument and its associated electronics. Three of the channels (at 52.85, 53.85, and 55.45 GHz) are identical with corresponding channels of the SCAMS instrument. A fourth channel at 53.331 GHz has the same bandwidth characteristics as the preceding three. The frequency locations of the remaining eight channels are determined by the oxygen absorption lines at 53.067 and 53.596 GHz. Channels of narrow

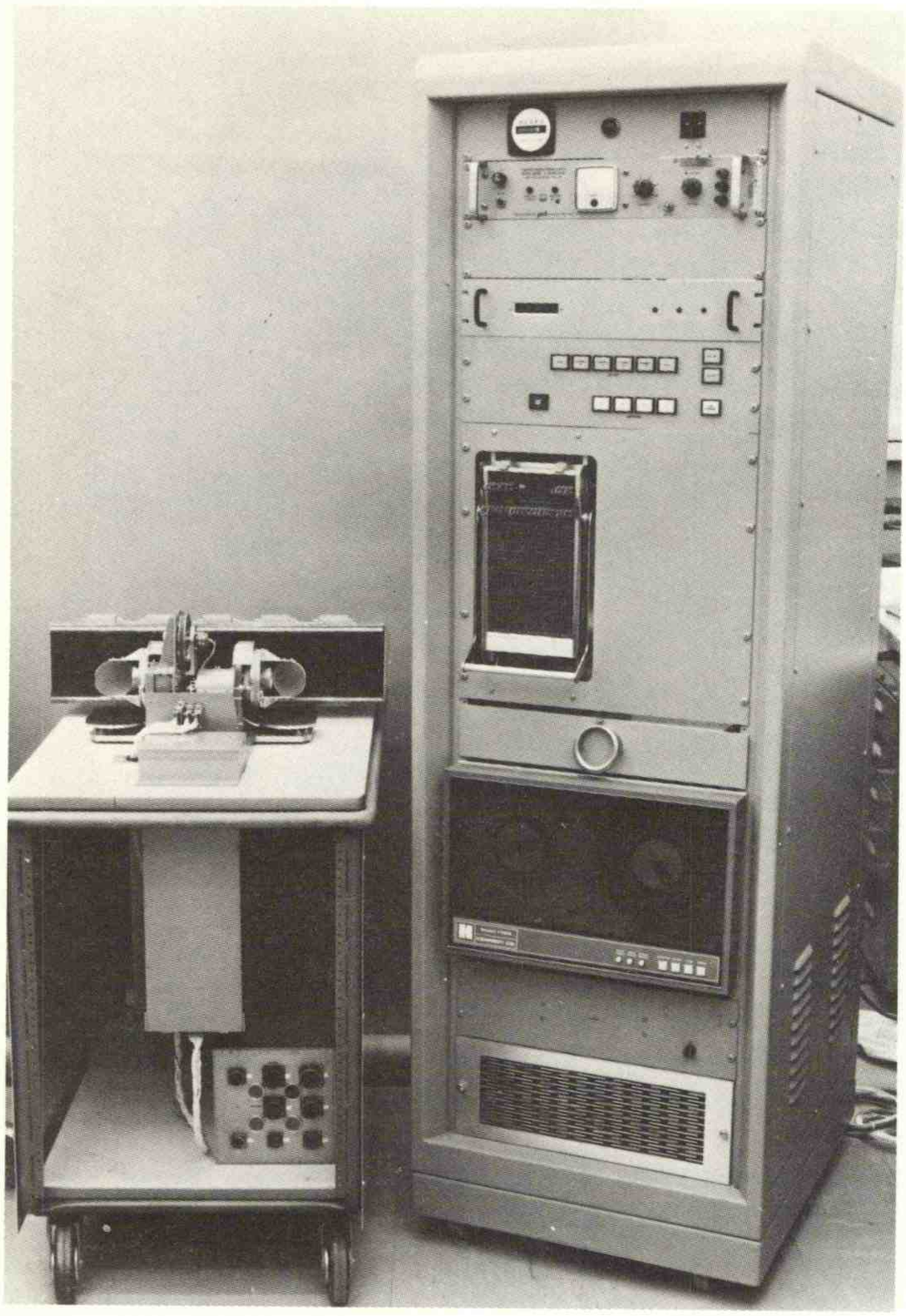


Figure 5.4.--The MTS system — radiometer itself and associated electronics.

bandwidth sensing at frequencies near the peaks of these lines are designed to obtain temperature information from altitudes above the tropopause. Channels centered progressively farther out on the wings of these lines contain information about temperatures at successively lower heights. During PHOENIX, the instrument scanned in the same vertical plane as the SCAMS system, with steps of 9.47° through zenith angles of ±47.4°. Dwell time at each step in the scan was approximately 1 s, with measurements being made simultaneously at all 12 frequencies. The scans were repeated every 15 s. In operation during the PHOENIX experiment, the MTS radiometer was sited near the SCAMS system. Figure 5.2 shows both systems in place. The early MTS configuration was that shown in Figure 5.2a; however, in order to control certain thermal problems, it proved necessary to insulate the system with plastic foam as shown in Figure 5.2b.

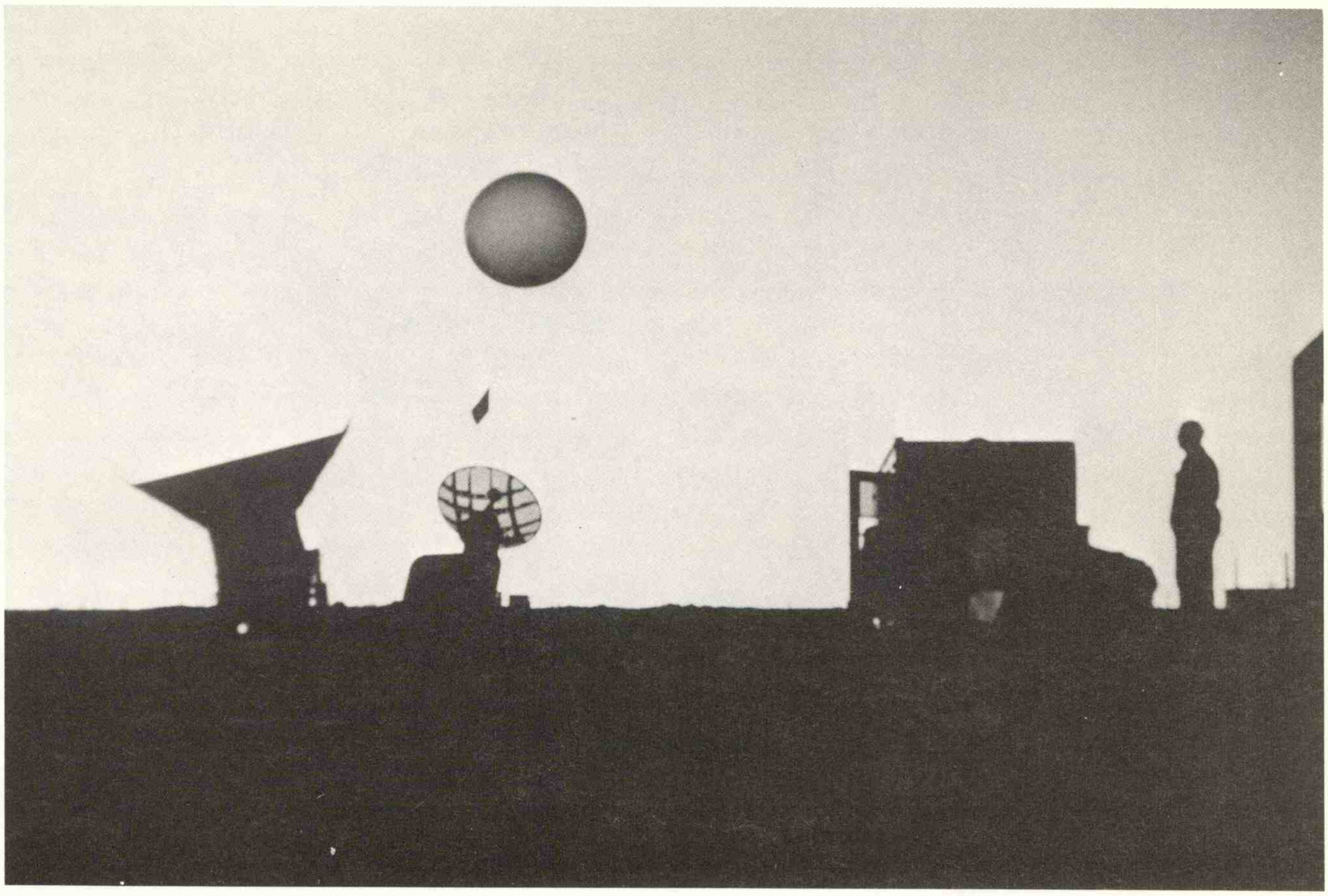


Figure 5.5.--A predawn rawinsonde launch during PHOENIX. SCAMS and MTS radiometers are silhouetted in the foreground.

5.5 PHOENIX Operations

Nominal operating periods for the radiometry during PHOENIX were from 0600 to 1400 MDT during each day from September 5 to September 28, excluding Saturdays and Sundays. Figure 5.5 shows one of the predawn radiosonde launches from the radiometer sites near the temporary building. Tables 5.1-5.4 give operating periods for each of the systems. It should be noted, however, that at this writing not all the data have been checked for quality. It may be that some of the periods included here correspond to bad or unusable data. A continuous data run was made from 0600 MDT on September 26 to 1800 MDT on September 27.

5.6 Data Analysis to Date

Raw data from the three radiometers were recorded on magnetic tape; procedures for reading and converting the data to brightness temperatures are available.

Table 5.1.--Operating times for SCAMS radiometer

Date (September)	Time (MDT)	Date (September)	Time (MDT)
5		17	
6	0608-1804	18	0551-1601
7	0601-1432	19	0531-1647
8	0546-1221	20	0610-1057, 1238-1931
9		21	0755-1932
10		22	0720-1534
11	0534-1320	23	
12	1202-1410	24	
13	0540-1403	25	0616-1439
14	0533-1401	26	0710-2012
15	0536-1409	27	0001-0308, 0519-1852
16		28	

Table 5.2.--Operating times for NEMS radiometer

Date (September)	Time (MDT)	Date (September)	Time (MDT)
5		17	
6	0913-1038, 1554-2400	18	0559-1541
7	0000-0334, 1002-1701	19	0551-1948
8	0547-1358	20	0619-2400
9		21	0000-0458
10		22	0653-1438
11	0552-2400	23	
12	0000-1356	24	
13		25	0646-1410
14	0544-1309	26	0641-2400
15	0559-1336	27	0000-0644
16		28	0613-1250

Table 5.3.--Operating times for MTS radiometer

Date (September)	Time (MDT)	Date (September)	Time (MDT)
5	0610-1436	15	0600-1355
6	1140-1355	16	
7	0748-1112	17	
8	0640-1302	18	0601-1400
9		19	0600-1617
10		20	0605-1555
11	0634-1110	21	0605-1625
12	0732-1400	22	0605-1555
13	0600-1306	23	
14	0615-1355	24	
		25	0606-1400
		26	0606-2400
		27	0000-1900
		28	0600-1158

Table 5.4.--Operating times for Denver 2-channel radiometer

Date (September)	Time (MDT)	Date (September)	Time (MDT)
5	0000-1930	16	
6	0730-2400	17	
7	0000-2400	18	
8	0000-2400	19	2200-2300
9	0000-2400	20	0030-0700
10	0000-24--	21	1900-2400
11	0000-2400	22	0000-0600, 1800-2400
12	0000-2400	23	0000-2400
13	0000-1830 power failure	24	0000-2400
14	1530-2400	25	0000-2400
15	0000-1800 power failure	26	0000-2400
		27	0000-2400
		28	0000-2400

*Down time due to RF interference from fire watch transmitter.

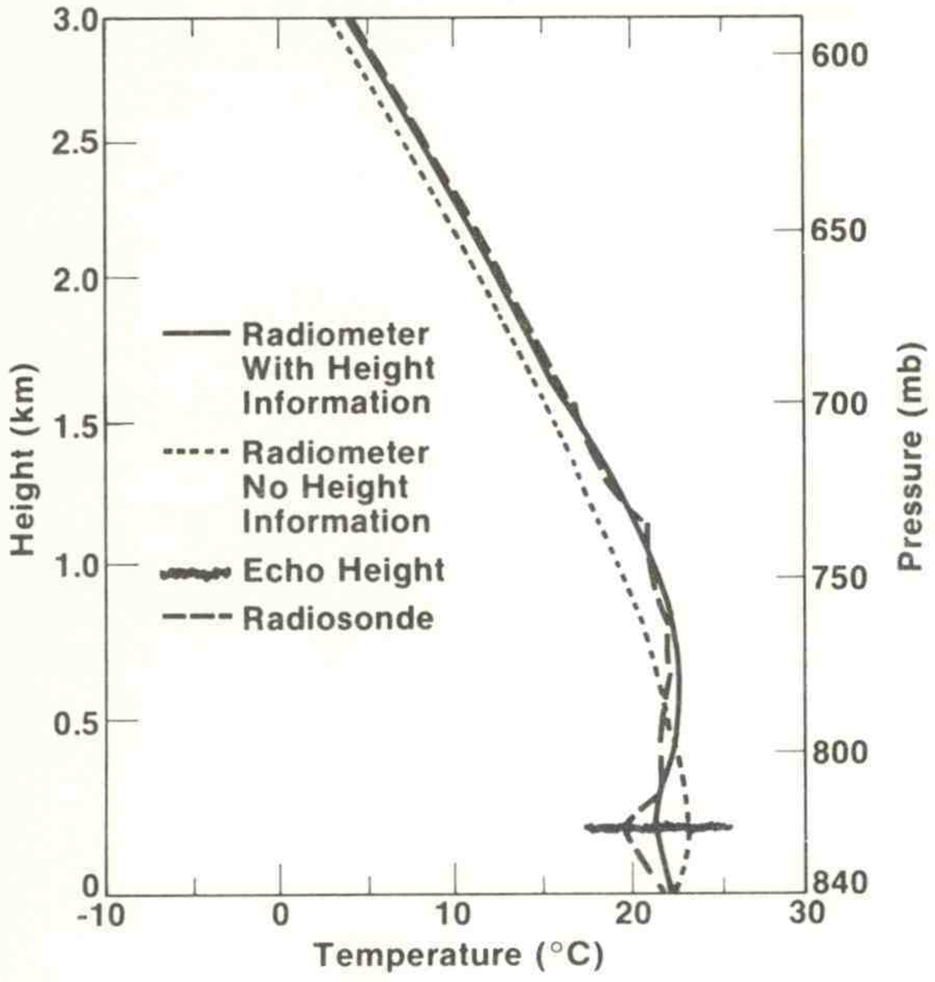


Figure 5.6.--Sample comparison of rawinsonde and radiometer data from the PHOENIX experiment.

Most of the SCAMS data have been processed to yield brightness temperatures for 7-min averaging periods. Preliminary processing of the NEMS data is complete and the data can be obtained in various formats. The MTS data for 1 h following 32 of the 38 rawinsonde launches have been examined in some detail and are available in fairly convenient form. Figure 5.6 compares sample rawinsonde and radiometer (SCAMS) data from PHOENIX, retrieved both with and without the aid of active-sensor supplementary information. For further information, readers may consult the author (commercial phone (303) 499-1000 ext. 6550, FTS 323-6550).

Acknowledgments

We wish to thank C. E. (Bud) Case of our group for checkout and operation of the MTS radiometer, and Bruce Gary of the Jet Propulsion Laboratory and other JPL staff — Noboru Yamane, Steve Bednarczyk, Richard Wetzel, and Dave Pettersen — for their generous aid and participation in preparation, field, and analysis phases of the PHOENIX experiment.

References

Decker, M. T., E. R. Westwater, and F. O. Guiraud, Experimental evaluation of ground-based microwave radiometric sensing of atmospheric temperature and water vapor profiles, J. Appl. Meteorol. 17, 1788-1795 (1978a).

Decker, M. T., E. R. Westwater, and F. O. Guiraud, Tests of microwave radiometric sensing of atmospheric temperature and water in the Gulf of Alaska, Preprints 4th Symp. on Meteorological Observations and Instrumentation, April 10-14, 1978, Denver, Colorado, pp. 148-149, American Meteorological Society, Boston, Mass. (1978b).

Rosenkranz, P. W., F. T. Barath, J. C. Blinn III, E. J. Johnston, W. B. Lenoir, D. H. Staelin, and J. W. Waters, Microwave radiometric measurements of atmospheric temperature and water from an aircraft, J. Geophys. Res. 77, 5833-5844 (1972).

Staelin, D. H., A. H. Barrett, J. W. Waters, F. T. Barath, E. J. Johnston, P. W. Rosenkranz, N. E. Gant, and W. B. Lenoir, Microwave spectrometer on the Nimbus 5 satellite: meteorological and geophysical data, Science 182, 1339-1341 (1973).

Staelin, D. H., A. L. Cassel, K. F. Kunzi, R. L. Pettyjohn, R. K. L. Poon, and P. W. Rosenkranz, Microwave atmospheric temperature sounding: effects of clouds on the Nimbus 5 satellite data, J. Atmos. Sci., 32, 1970-1976 (1975a).

Staelin, D. H., A. H. Barrett, P. W. Rosenkranz, F. T. Barath, E. J. Johnson, J. W. Waters, A. Wouters and W. B. Lenoir, The scanning microwave spectrometer (SCAMS) experiment, Nimbus 6 Users Guide, Goddard Space Flight Center, Greenbelt, Md. (1975b).

Waters, J. W., K. F. Kunzi, R. L. Pettyjohn, R. K. L. Poon, and D. H. Staelin, Remote sensing of atmospheric temperature profiles with the Nimbus 5 microwave spectrometer, J. Atmos. Sci. 32, 1953-1969 (1975).

Westwater, E. R., Improved determination of vertical temperature profiles of the atmosphere by a combination of radiometric and active ground-based remote sensors, Preprints 4th Symp. on Meteorological Observations and Instrumentation, April 10-14, 1978, Denver, Colorado, pp. 153-157, American Meteorological Society, Boston, Mass. (1978).

Westwater, E. R., J. B. Snider, and A. V. Carlson, Experimental determination of temperature profiles by ground-based microwave radiometry, J. Appl. Meteorol. 14, 524-539 (1975).

Westwater, E. R., and F. O. Guiraud, Ground-based passive microwave sensing of water vapor and cloud liquid, Preprints 4th Symp. on Meteorological Observations and Instrumentation, April 10-14, 1978, Denver, Colorado, pp. 150-152, American Meteorological Society, Boston, Mass. (1978).

CHAPTER 6

FM-CW RADAR OPERATIONS DURING PHOENIX

R. B. Chadwick and K. P. Moran
Wave Propagation Laboratory
National Oceanic and Atmospheric Administration
Boulder, Colorado 80303

6.1 FM-CW Radar in Boundary-Layer Studies

From its inception, the frequency-modulated, continuous-wave (FM-CW) radar has had a remarkable impact on boundary-layer studies. Previously, powerful microwave pulsed radars had been used to monitor clear-air atmospheric structures (e.g., Hardy et al., 1966; Hardy and Katz, 1969). However, these were limited in their ability to probe the planetary boundary layer (PBL) for two reasons. First, they could not resolve spatial scales smaller than 100 to 200 m. Second, they could not examine the structure of the lowermost atmosphere because of the masking effects of ground clutter. Thus, when Richter (1969) developed a vertically pointing FM-CW radar system, combining the high sensitivity necessary for detection of clear-air echoes with ultra-high resolution (<1 meter) and essentially no ground clutter, he opened up tremendous new opportunities for PBL research. A spurt of papers quickly followed (e.g., Atlas et al., 1970; Gossard et al., 1970, 1971; Bean et al., 1971) describing the use of the new tool in studying a variety of micrometeorological processes rendered observable for the first time. Recently, however, FM-CW systems have enjoyed an added dimension: Doppler wind-measurement capability (e.g., Chadwick et al., 1976a,b; Chadwick and Strauch, 1979). Thus, in high-resolution studies of atmospheric structure, the radar may be operated in the range-only mode (to measure reflectivity as a function of range); in wind profiling, the radar is operated in the range-Doppler mode (to measure the Doppler velocity spectrum for each range interval). The two modes of operation use the same equipment, differing only in sweep rates and sampling schemes.

In the range-only mode of operation, the antennas are usually pointed vertically, typically providing a maximum range of about 3 km or less in clear air, but much greater in the presence of targets such as hydrometeors, chaff, and insects. The WPL equipment provides 500 range cells within this altitude, yielding cells

and hence resolution about 6 m or less in range. The beamwidth is some 0.05 radians, so that the interrogated cells are generally shaped like thin discs. In the range-only mode of operation, the output displays show regions of enhanced atmospheric refractive-index fluctuations. The time history of these records reveals the advection of structures passing overhead within the PBL during the observation period, as well as non-stationarity in the PBL itself (associated, for example, with the rise of the convectively-mixed layer during the morning hours). From the resulting data set it is very easy to discern layers of high refractive-index variability and the behavior of these layers during the day.

In the range-Doppler mode the antenna can either be aligned in a given fixed direction or scanned in azimuth. As in the range-only mode, the maximum range for clear-air measurements is again 3 km or less. The number of range gates and the number of spectral points are variable, subject to the constraint that the product of range cells and the number of spectral points per range cell must equal 500, which is the number of points available at the output of the signal processor. Normally, ten range cells with 50 spectral points each are used, providing radial wind velocity measurements at equally spaced intervals out to the maximum range. Such a measurement yields only the radial component of the wind, i.e., the wind component parallel to the antenna beam direction. To derive profiles of the total vector wind, the airspeeds are measured with the radar looking in two or more directions. Horizontal homogeneity of the wind field within the scanning volume is assumed. Wind-velocity measurements made while the radar antenna is scanning azimuthally yield a so-called velocity-azimuth display (VAD). Total wind profiles as well as convergence profiles and estimates of shearing and stretching deformation can be obtained from a VAD scan.

As indicated above in passing, the optically clear air targets for the FM-CW radar are half-radar-wavelength Fourier components of fluctuations in refractive index associated with atmospheric turbulence. Of course the radar detects other targets, including hydrometeors, insects, clouds, aircraft, and balloons. As a rule these other targets produce radar echoes of sufficiently distinctive character that they are readily distinguishable from clear-air returns, so that no misinterpretations arise. Indeed, to the extent that insects and chaff follow the mean flow, they simply increase the signal-to-noise ratio and actually aid the wind measurement process. However, when the backscattered power exceeds a certain level, the signal processor saturates and quantitative wind and backscatter

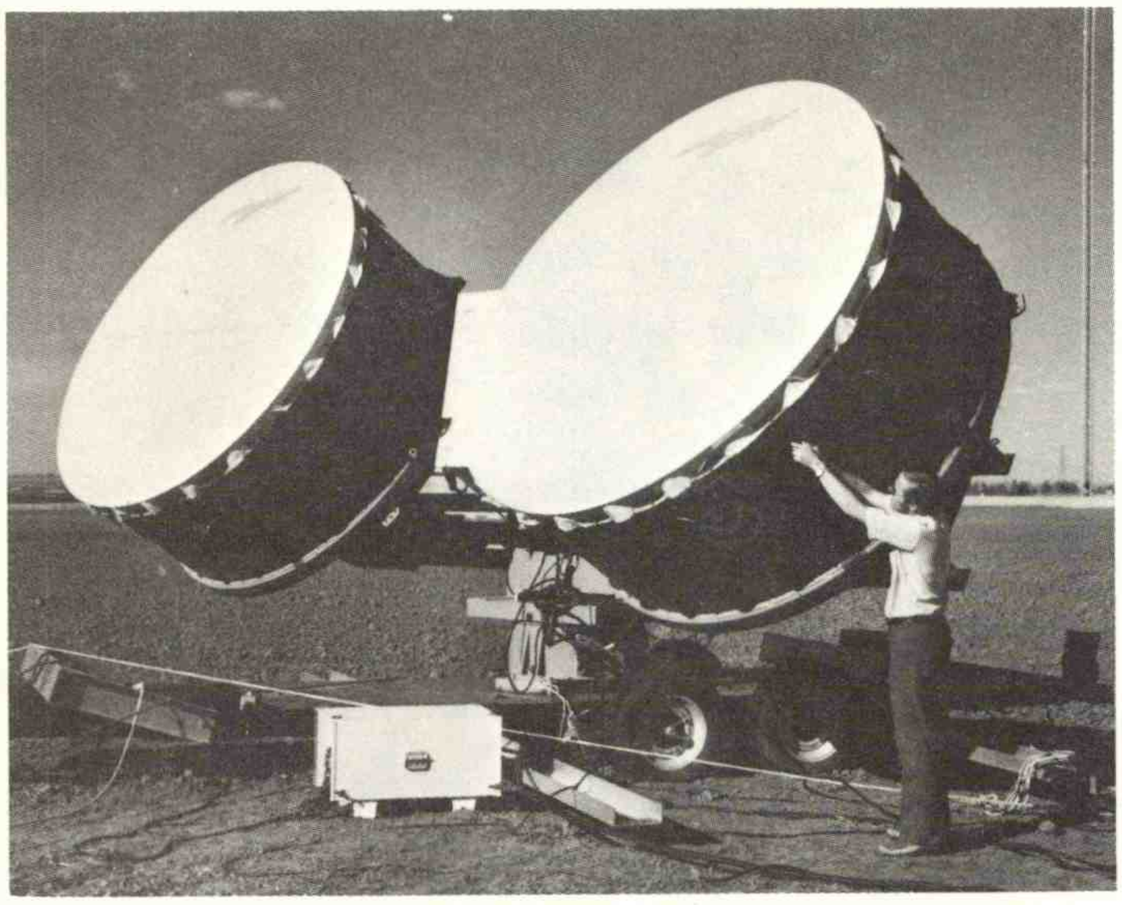


Figure 6.1.--The transmitting and receiving antennas for the WPL FM-CW radar. The BAO 300-m tower is in the background. Another trailer, not shown, houses the radar transmitter and receiver electronics as well as a digital data acquisition system.

intensity measurements deteriorate in quality and reliability. This was often the case during PHOENIX operations when heavy concentrations of chaff were dispersed by aircraft over the BAO site in support of the dual-Doppler radar studies.

6.2 Details of the WPL FM-CW Radar

The Wave Propagation Laboratory FM-CW radar is mobile and transported on two trailers. Figure 6.1 shows the radar receiving and transmitting antennas and their mount, with the BAO tower in the background. The radar transmitter, receiver, and data processing electronics are housed in a trailer that is not shown. The major parameters describing system performance are listed in Table 6.1. Table 6.1 gives no maximum range for the system, since this depends upon atmospheric conditions and/or the availability of suitable targets, factors that vary diurnally and seasonally. However, as mentioned above, the WPL FM-CW radar capabilities permit measurements to heights typically 2 to 3 km during the month of September. Chadwick et al. (1978) have recently compiled a climatology and statistics for clear-air radar returns in the Colorado boundary layer.

Table 6.2 is a log of FM-CW radar operations during the PHOENIX study, indicating the time intervals during which the equipment was running, the mode of operation, and auxiliary comments on such matters as atmospheric conditions and outages resulting from excessive chaff densities. Figure 6.2 illustrates the photographic output typical of range-only operation. Figure 6.3 shows a sample of

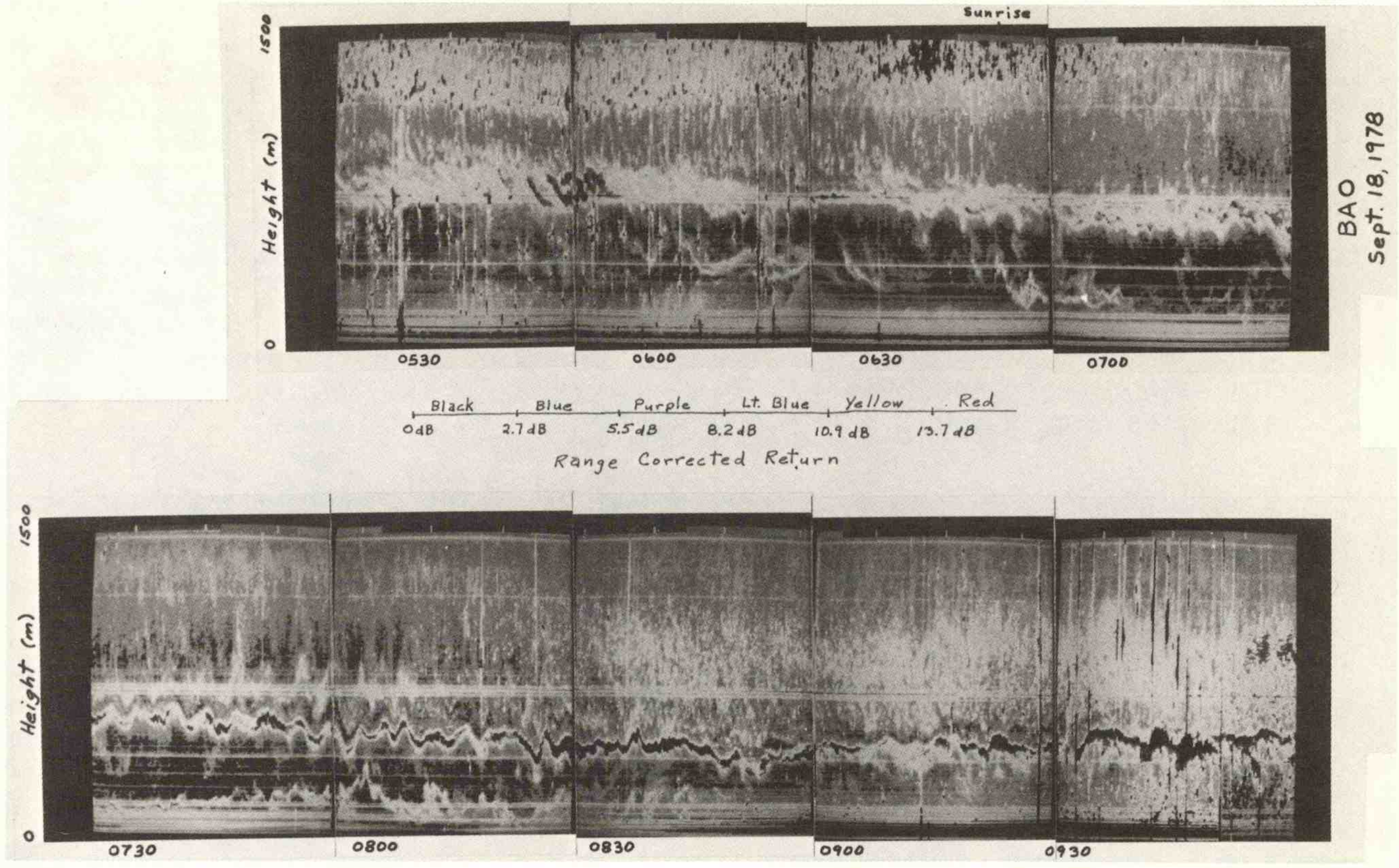


Figure 6.2.--A sample of range-reflectivity data from the FM-CW radar. The large-amplitude gravity-wave event revealed by the data (especially prominent between 0700 and 0900 MDT) is currently under intensive investigation.

Table 6.1.--FM-CW radar performance parameters

Average transmitted power	200 W
Antenna diameter	2.44 m
Wavelength	10 cm
Receiver noise figure	2.2 dB
Minimum range	15 m
Minimum detectable signal	-155 dBm
Range resolution (adjustable)	$\geq$ 1.65 m
Velocity resolution (adjustable)	$\geq$ 3 cm s^{-1}

Table 6.2.--FM-CW radar operations during PHOENIX

Date (Sept. '78)	Time (MDT)	Mode[1,2,3]	Comments
4	1808-2400	R, 0-500 m	Good layer starts at 0800
5	0000-1059	R, 0-500 m	Stopped by chaff drifting overhead
	1059-1140	R, 0-1000 m	Strong, active return at 500 m
	1316-1400	R, 0-1000 m	
6	0853-1040	R, 0-500 m	Same chaff return
	1040-1049	R, 0-1000 m	
	1050-1142	R, 0-1500 m	Same chaff return
	1156-1321	R, 0-1500 m	
	1321-1431	R, 0-2500 m	Stopped by chaff
	1708-2400	R, 0-5000 m	
7	0000-1003	R, 0-500 m	Good layer starts at 0700
	1536-1710	R, 0-3000 m	Very strong layer at 2000 m
	1710-1755	R, 0-3000 m (90°, 70°)	Alternated between two elevation angles to determine angular dependence of echo return
	1826-2400	D, 0-4500 m (90°) V_{max}=4.91 m s^{-1}	
8	0000-0810	D, 0-4500 m (90°) V_{max}=4.91 m s^{-1}	
	0822-1257	R, 0-2500 m	Strong return at about 1500 m
10	1822-2400	R, 0-1000 m	
11	0000-1038	R, 0-1000 m	
	1536-1614	VAD, 0-500 m, V_{max}=10.54 m s^{-1}	
	1614-1639	VAD, 0-2500 m, V_{max}=10.54 m s^{-1}	Strong winds and directional shear
12	1038-1114	R, 0-1500 m	
	1150-1327	D, 0-500 m (el 75°, as 270°) V_{max}-10 m s^{-1}	
	1115-2400	R, 0-1500 m	
13	0000-0909	R, 0-1500 m	Layer at 700 m
	0939-2400	R, 0-2500 m	Few insects at start
14	0000-0845	R, 0-2500 m	
	1631-2400	R, 0-2500 m	Strong returns at 2000 m

[1]R = range-only
[2]D = Doppler
[3]VAD = variable-azimuth display

Table 6.2.--FM-CW radar operations during PHOENIX--Continued

Date (Sept. '78)	Time (MDT)	Mode	Comments
15	0000-1007	R, 0-2500 m	Strong returns at night, layer in morning
	1456-2400	R, 0-3000 m	Saturated 2000-2400
16	0000-1207	R, 0-3000 m	
	1224-1242	VAD, 0-1500 m (el 69.3°) V_{max}=10 m s^{-1}	
	1242-2400	D, 0-1500 m (el 110°), az 90°) V_{max}=10 m s^{-1}	
17	0000-1111	D, 0-1500 m (el 110°, az 90°) V_{max}=10 m s^{-1}	
	1123-2400	R, 0-1500 m	One hour of saturation around 1500; several layers from 1600 to 1900
18	0000-1124	R, 0-1500 m	Single, strong layer throughout period gravity waves 0600
	1137-1440	R, 0-2500 m	
	1451-1550	D, 0-4500 m (el 120°, az 90°) V_{max}=10 m s^{-1}	
	1555-1620	VAD, 0-4500 m (el 70°0) V_{max}=10 m s^{-1}	Strong wind shear
	1650-1721	R, 0-3500 m	
	1728-2400	R, 0-2500 m	
19	0000-0344	R, 0-2500 m	
	0344-1005	R, 0-2500 m	Some equipment problems
	1116-1133	R, 1000-4000 m	Stopped because of chaff
	1155-1618	R, 1000-4000 m	Cloud returns
	1635-2400	R, 0-1500 m	Long periods of saturation
20	0000-0850	R, 0-1500 m	Long periods of saturation
	1155-1200	R, 0-4500 m	Clouds and inversion layer
	1207-1354	R, 0-3500 m	Clouds and inversion layer
	1354-1633	R, 0-3500 m	
	1638-1729	R, 0-1500 m	
	1729-2400	R, 0-1500 m	Transmitter off, noise only
21	0000-0938	R, 0-1500 m	Transmitter off, noise only
	0951-1115	R, 0-1500 m	Rising inversion layer
	1115-1124	R, 0-1500 m	Chaff
	1124-1357	R, 0-1500 m	Rising layer with occasional chaff
	1738-2400	R, 0-1500 m	Some strong "blobs"

Table 6.2.--FM-CW radar operations during PHOENIX--Continued

Date (Sept. '78)	Time (MDT)	Mode	Comments
22	0000-0705	R, 0-1500 m	
	0705-0920	R, 0-1500 m	Some equipment problems
	1314-2400	R, 0-2500 m	Strong returns
23	0000-1155	R, 0-2500 m	Strong layers
	1200-1215	R, 0-4500 m	Layer at 2500 m
24	1757-2400	R,0-1500 m	
25	0000-0819	R, 0-1500 m	"Blobs" between 0400 and 0600
	0823-0844	R, 0-500 m	Numerous insects
	0844-0921	R, 0-1000 m	Layer above 700 m
	0926-1111	R, 0-2500 m	Persistent layer
	1111-1217	R, 0-2500 m	Layer at about 1500 m
	1658-2400	R, 0-1500 m	Chaff overhead
26	0000-0942	R, 0-1500 m	Saturated until about 0700 Extremely strong layers between 0700 and 1000
	0949-1108	R, 0-4500 m	Stopped because of chaff
	1708-2350	R, 0-2500 m	Strong returns

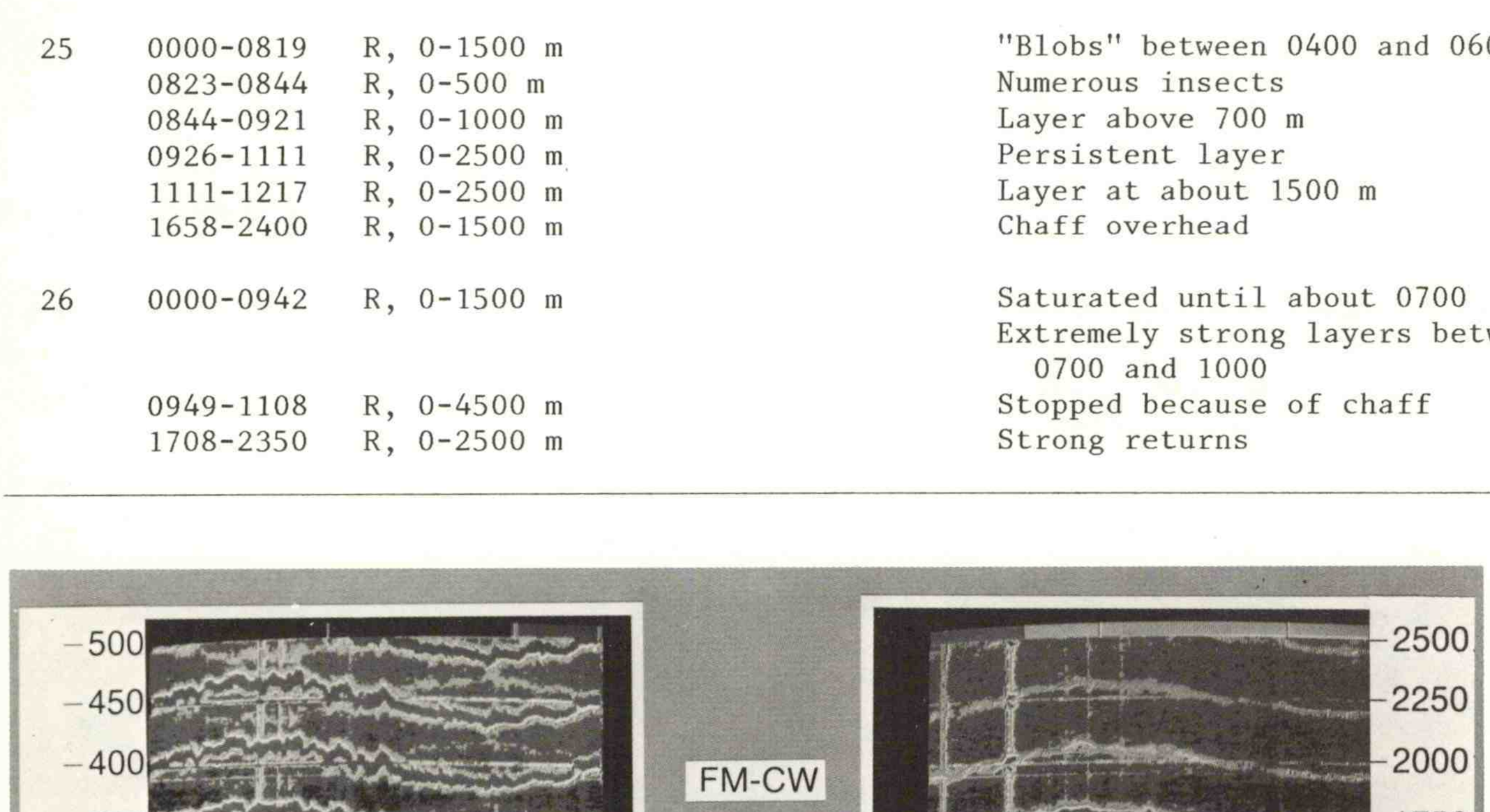


Figure 6.3.--A velocity-azimuth display from the FM-CW radar.

the photographic range-velocity data. For further information the interested reader should consult the author (commercial phone (303) 499-1000 ext. 6318, FTS 323-6318).

References

Atlas, D., J. I. Metcalf, J. H. Richter, and E. E. Gossard, The birth of "CAT" and microscale turbulence, J. Atmos. Sci. 27, 903-913 (1970).

Bean, B. R., R. E. McGavin, R. B. Chadwick, and B. D. Warner, Preliminary results of utilizing the high resolution FM radar as a boundary layer probe, Boundary-Layer Meteorol. 1, 466-473 (1971).

Chadwick, R. B., K. P. Moran, R. G. Strauch, G. E. Morrison, and W. C. Campbell, Microwave radar wind measurements in the clear air, Radio Sci. 11, 795-802 (1976).

Chadwick, R. B., K. P. Moran, R. G. Strauch, G. E. Morrison, and W. C. Campbell, A new radar for measuring winds, Bull. Am. Meteorol. Soc. 57, 1120-1125 (1976b).

Chadwick, R. B., K. P. Moran, G. E. Morrison, and W. C. Campbell, Measurements showing the feasibility for radar detection of hazardous wind shear at airports, Air Force Geophysical Laboratories technical report AFGL-TR-78-0160, Hanscom AFB (1978).

Chadwick, R. B., and R. G. Strauch, Processing of FM-CW Doppler radar signals from distributed targets, IEEE Trans. Aerospace Electronic Systems AES-15, 185-188 (1979).

Gossard, E. E., J. H. Richter, and D. Atlas, Internal waves in the atmosphere from high-resolution radar measurements, J. Geophys. Res. 75, 3523-3536 (1970).

Gossard, E. E., D. R. Jensen, and J. H. Richter, An analytical study of tropospheric structure as seen by high-resolution radar, J. Atmos. Sci. 28, 794-807 (1971).

Hardy, K. R., D. Atlas, and K. M. Glover, Multi-wavelength backscatter from the clear atmosphere, J. Geophys. Res. 71, 1537-1552 (1966).

Hardy, K. R., and I. Katz, Probing the clear atmosphere with high power high resolution radars, Proc. IEEE 57, 468-480 (1969).

Richter, J. H., High resolution tropospheric radar sounder, Radio Sci. 4, 1261-1268 (1969).

CHAPTER 7

TPQ-11 (8 mm) RADAR OPERATIONS DURING PHOENIX

F. Pasqualucci
Cooperative Institute for Research in Environmental Sciences
University of Colorado
Boulder, Colorado 80309

One of the more novel remote-sensing systems operated during PHOENIX was the surplus TPQ-11 (8 mm) radar (Petrocchi and Paulsen, 1966) modified and upgraded by WPL and CIRES for use in cloud studies. The chief advantage of the TPQ-11 for this purpose is its operating frequency of 35 GHz, which permits detection of cloud droplets too small to be sensed by radars operating at lower frequencies. The WPL modifications improve both system reliability and performance, increasing the receiver sensitivity by some 13 dB and reducing the minimum detectable signal to -110 dBm. Table 7.1 gives the parameters of the modified TPQ-11 equipment. The equipment at its PHOENIX site is shown in Figure 7.1.

During the PHOENIX experiment the modified TPQ-11 system proved it was able to detect clear-air returns through the depth of the planetary boundary layer.

Table 7.1.--WPL TPQ-11 radar parameters

Parameter	Value
Peak transmitted power	100 kW
Antenna diameter	2.06 m
Wavelength	8.6 mm
Receiver noise figure	4.5 dB
Minimum detectable signal	-110 dBm
Pulse width	0.5 μs
Pulse repetition period	1 ms

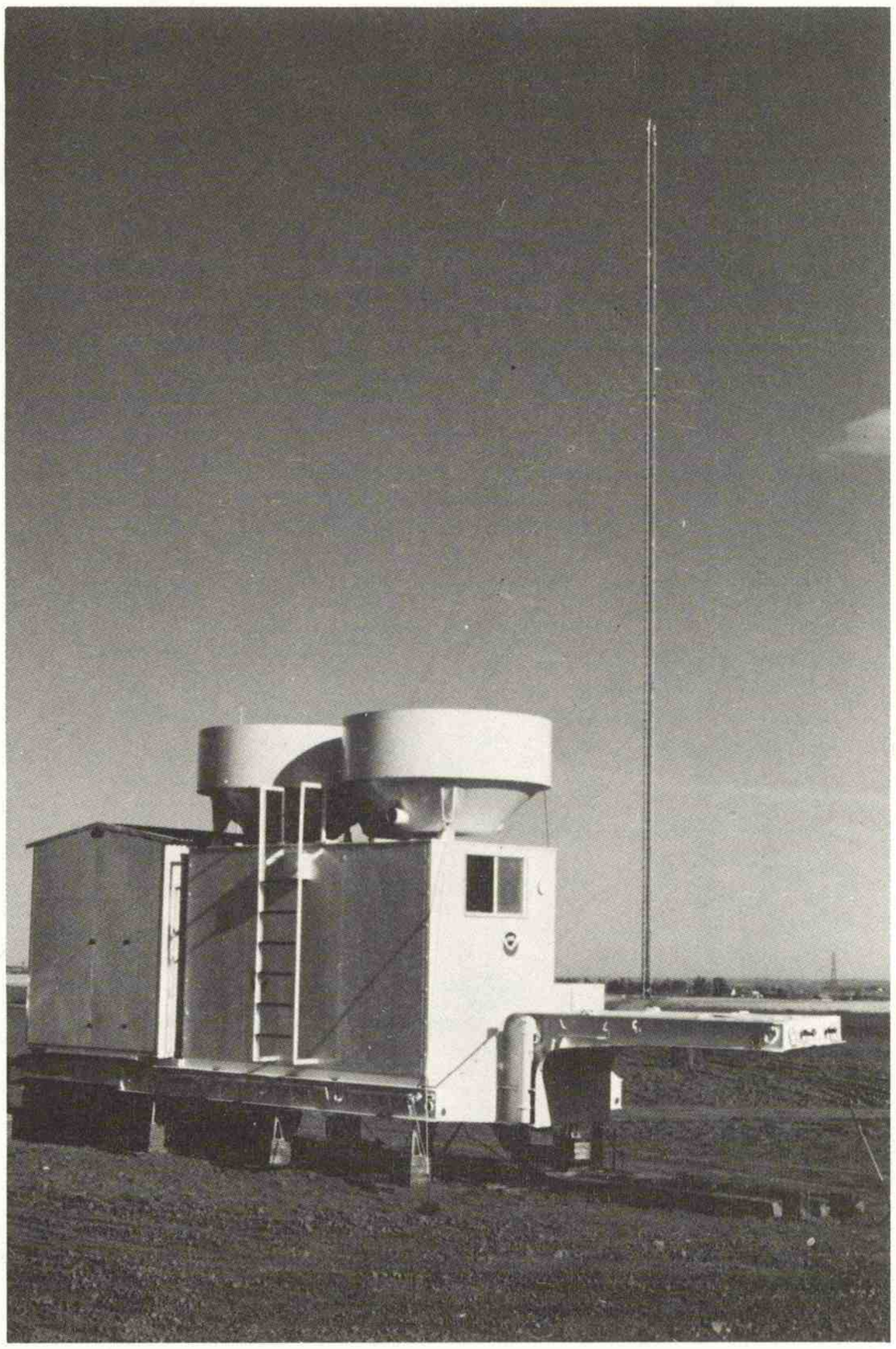


Figure 7.1.--The WPL-modified TPQ-11 radar system on site at the BAO. The 300-m tower is in the background.

Thus, during September the system played a part in both clear-air and cloud studies. The radar was operated in the vertically pointing mode, providing data on echo intensity as a function of height above the radar and of time. Table 7.2 is a log of the radar operations. The PHOENIX experiment took place just as the modified TPQ-11 became operational, and before any digital data acquisition system for the radar had been developed. Thus, all data acquired during PHOENIX were analog. Two facsimile recorders were used to archive the data, so that either one or two records are available for each run, depending upon the type of observation made and on the meteorological situation. The first recorder was used in a "threshold" mode, recording all signal returns stronger than -110 dBm. The second recorder was used in a "quantized" mode, processing and displaying

data from the returned echoes according to four levels of intensity:

-108 dBm > Level 1
- 93 dBm > Level 2 $\geq$ -108 dBm
- 83 dBm > Level 3 $\geq$ - 93 dBm
Level 4 $\geq$ - 83 dBm.

Figure 7.2 shows a sample facsimile record obtained from clear-air returns. As it happens, the record reveals a rather large-amplitude wave event, which is currently under study by other WPL and CIRES researchers. The cloud data have all since been digitized. Figure 7.3 shows a sample of the cloud records obtained

Table 7.2.--Summary of TPQ-11 radar operations

Date	Time (MDT)	Threshold mode record	Quantized mode record	Other observations
9/ 1/78	0815 - 1535	yes	no	
9/ 5/78	0840 - 1700	yes	no	
9/ 6/78	0840 - 1545	yes	no	
9/ 7/78	1200 - 1400	yes	no	
9/ 8/78	0913 - 1540	yes	no	
9/ 9/78	0850 - 1627	yes	no	
9/11/78	0950 - 1715	yes	no	
9/14/78	1115 - 1506	yes	no	
9/15/78	0922 - 1628	yes	no	
9/17/78	1100 - 1300	yes	yes	
9/18/78	0855 - 1725	yes	yes	
9/19/78	1000 - 1645	yes	yes	good clouds (digitized records available)
9/20/78	0956 - 1618	yes	yes	good clouds (digitized records available)
9/21/78	0908 - 1515	yes	no	
9/22/78	0915 - 1815	yes	yes	
9/26/78	0750 - 2133	yes	yes	good cirrus after 6 pm
9.27/78	0900 - 1940	yes	yes	
9/28/78	1011 - 1745	yes	yes	

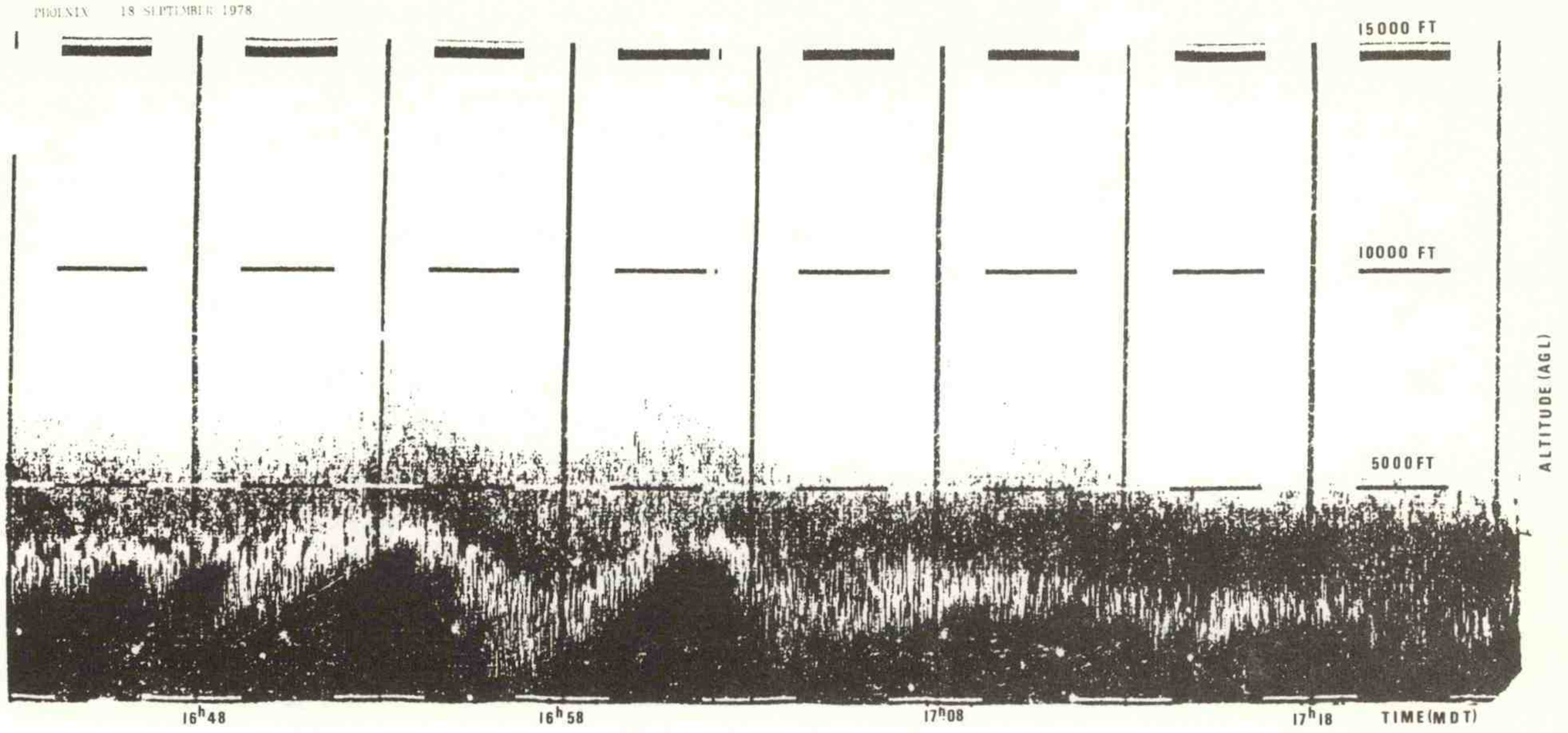


Figure 7.2.--A sample TPQ-11 radar facsimile record with clear-air returns, revealing a range-amplitude gravity-wave event.

during PHOENIX. For further information the interested reader should consult the author (commercial phone (303) 499-1000, ext. 6207, FTS 323-6207).

Reference

Petrocchi, P. J., and W. H. Paulsen, Meteorological significance of vertical density profiles of clouds and precipitation obtained with the AN/TPQ-11 radar, Proc. 12th Radar Meteorology Conf., Norman, Oklahoma, pp. 467-472, American Meteorological Society, Boston, Mass. (1966).

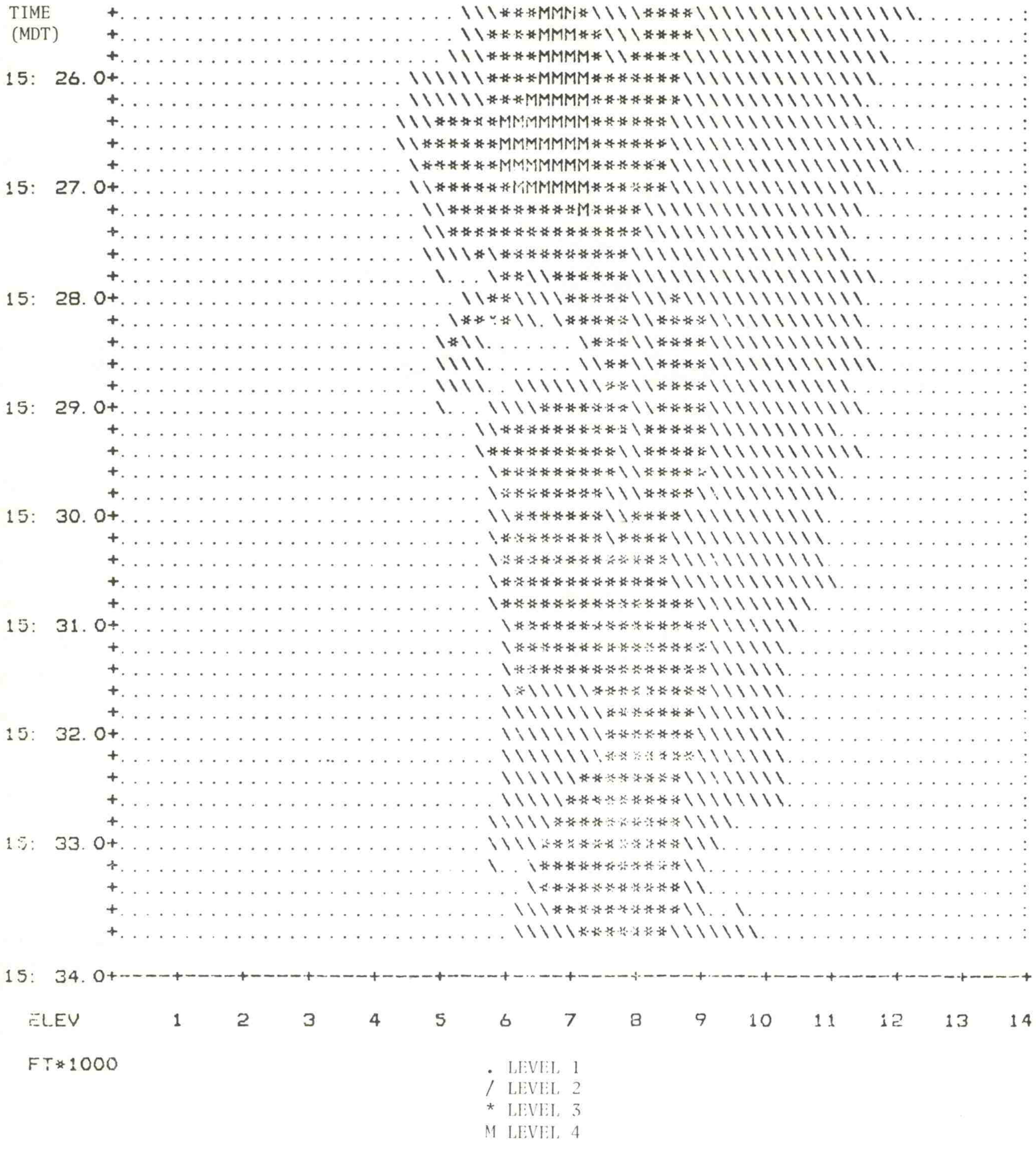


Figure 7.3.--A digital record of TPQ-11 radar echoes from cloud.

CHAPTER 8

LIDAR AND KNOLLENBERG PROBE OPERATIONS DURING PHOENIX

N. L. Abshire and G. M. Lerfald
Wave Propagation Laboratory
National Oceanic and Atmospheric Administration
Boulder, Colorado 80303

8.1 Introduction

Lidar techniques offer a wealth of opportunities for atmospheric study in general and PBL observations in particular, as indicated in reviews over the last decade by Collis (1969), Hall (1974), and Derr et al. (1974). These include quantitative monitoring of structure and circulations within the convective PBL (e.g., Kunkel et al., 1977), aerosol-loading in the polluted urban environment (e.g., Derr et al., 1976), and dispersal of plumes of pollutants from localized sources (e.g., Abshire et al., 1978). Lidar data and radar data are typically complementary rather than merely redundant. Clear-air radar studies of the convective PBL have been most effective in revealing structure near the inversion or entrainment layer above the PBL, where strong ambient humidity gradients produce correspondingly large refractive-index fluctuations (e.g., Konrad, 1970; Hardy, 1972). By contrast, lidar data tend to fill in the mixed-layer structure (e.g., Kunkel et al., 1977), since lidar echo returns result from dust and aerosols lifted from the surface by PBL winds. Thus, in the PHOENIX experiment, with its focus on the comparison of different types of remote-sensing measurements, lidar studies were considered to be a highly desirable part of the operations from the very earliest planning stages. In this chapter we describe the WPL lidar system used in PHOENIX and present a brief log of lidar operations.

8.2 The Lidar System

The particular lidar used during PHOENIX was a two-wavelength pulsed system, which, together with such ancillary equipment as an IR radiometer, several photometers, a microwave radar, and an acoustic echo sounder, constituted a facility developed for use in air-quality studies (e.g., Derr et al., 1976; Lerfald et al., 1977; Abshire et al., 1978). The facility, which for the most part is mounted

Table 8.1.--WPL lidar parameters

	6943 Å Wavelength	3482 Å Wavelength
Peak pulse power	150 MW	15 MW
Range resolution	5 m	5 m
Angular resolution	1 mrad	1 mrad
Pulse repetition frequency	0.1 Hz	0.1 Hz

in a trailer and a van, is transportable from site to site, although unsuited for mobile operation. Figure 8.1 provides a cutaway schematic view of the facility; Figures 8.2a,b show the system as deployed just before and during the PHOENIX experiment, respectively. The heart of the system is a ruby lidar, which can be operated at two frequencies, either simultaneously or individually. Table 8.1 lists the lidar parameters. The receiver system can detect return signals either

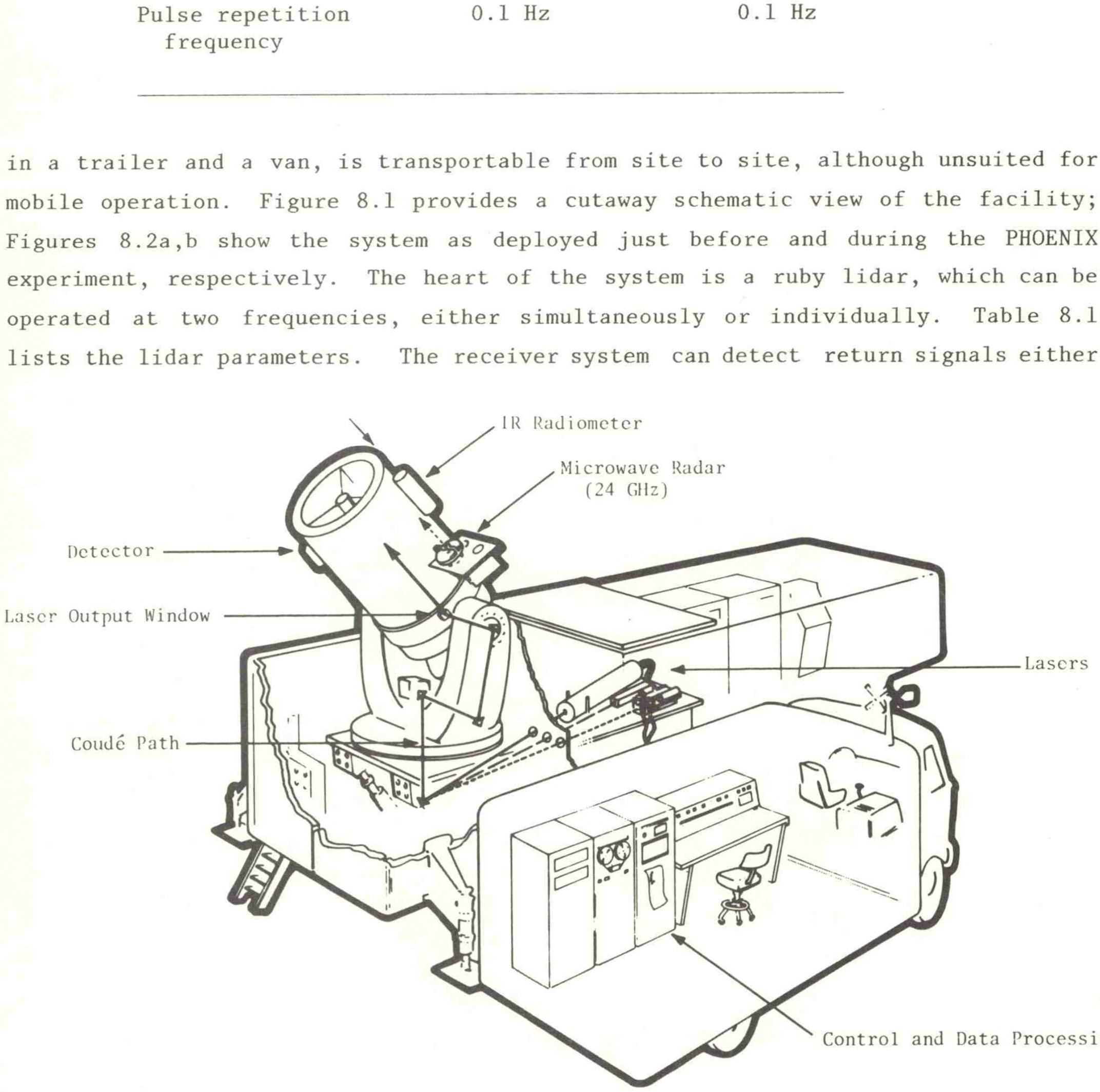


Figure 8.1.--Cutaway view (schematic) of the WPL pulsed-lidar system and its ancillary remote sensors.

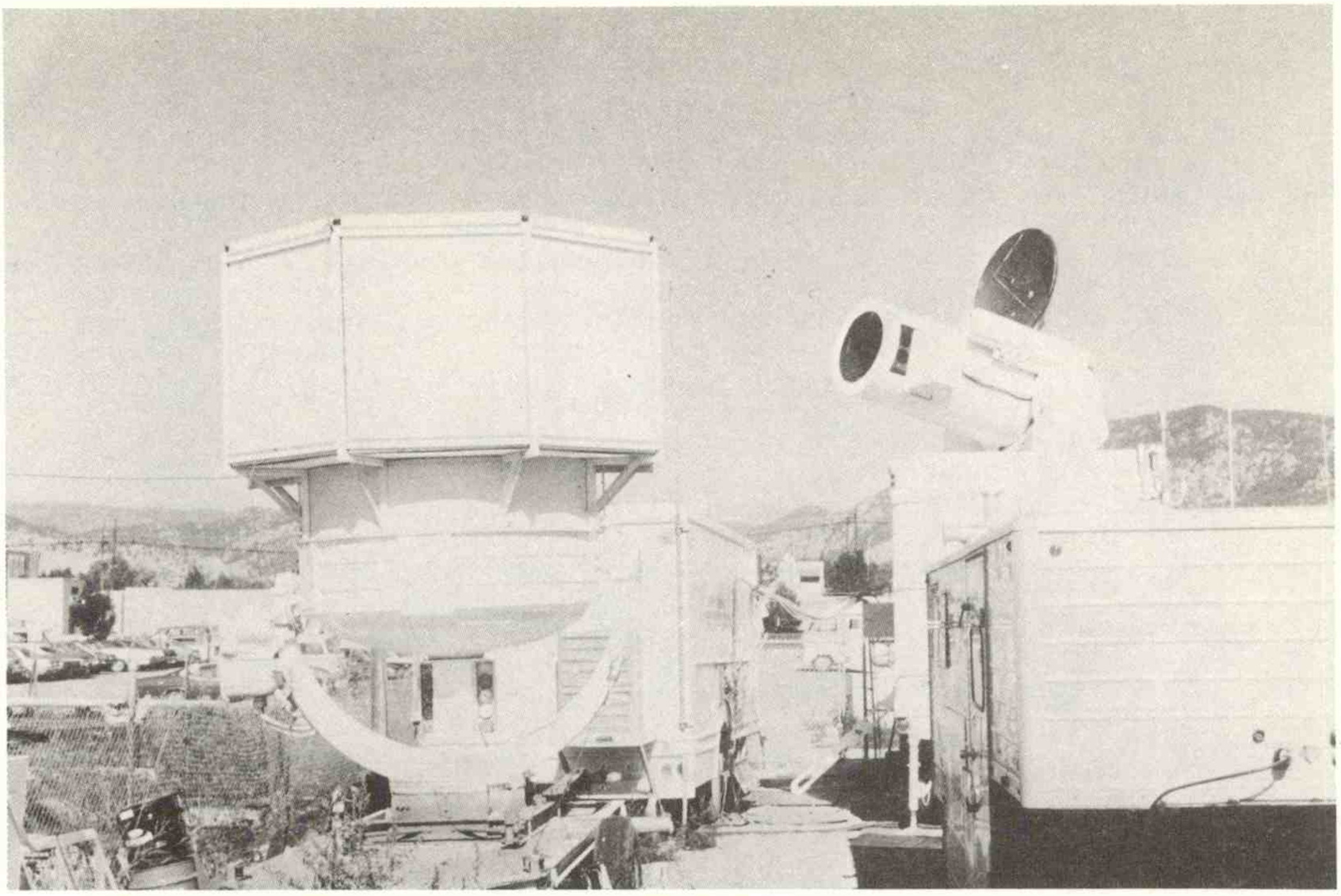


Figure 8.2a.--The WPL pulsed-lidar remote sensing system, with microwave radar antenna mounted above the receiving telescope, and ancillary acoustic echo-sounding antenna in the foreground.



Figure 8.2b.--The WPL pulsed-lidar system deployed at PHOENIX. The all-sky camera is in the foreground. Auxiliary photometers are visible on top of the trailer. The TPQ-11 radar is at the right.

at both wavelengths, or at one wavelength polarized to be both perpendicular and parallel to the polarization of the transmitted beam. At the front end of the receiver system is a Newtonian-mount telescope with a 70-cm mirror diameter and 203-cm focal length; the whole is mounted on a converted Nike-Ajax antenna mount with 1-mil pointing accuracy. The IR radiometer, mounted on the yoke of the lidar system, gives the continuous background temperature of targets scanned by the lidar.

The facility also includes solar irradiance instrumentation: 2π pyranometer, pyrheliometer, IR pyrheliometer, dual-wavelength sun photometer, solar aureole photometer, eight-channel sun photometer (described further below), and two time-lapse cameras. The eight-channel photometer consists of eight optical filters, which are switched automatically in front of a light-sensitive detector. The filters each have a bandpass of about 0.01 μm and are centered at the following wavelengths: 3170 Å, 3329 Å, 3820 Å, 5011 Å, 5960 Å, 8753 Å, 9411 Å, and 10623 Å. The field of view is 1.5°. Dynamic range covers five orders of magnitude (twelve optical thicknesses) with a resolution of about 2%. Lerfald et al. (1977) describe the instruments further, briefly giving performance parameters.

The extinction of solar radiation in nine wavelength bands (the eight listed above plus an IR channel) has been determined from the solar radiometer data. One of these bands (9411 Å) can be used to measure the total atmospheric precipitable water vapor, while the others yield the wavelength dependence of optical extinction caused by aerosol and cloud particles. The aureole photometer measures the angular scattering function from the edge of the sun's disc to 8° above and below sun center. Work is now under way to apply inversion techniques to the extinction and angular scatter data to infer the size distributions of aerosol and cloud particles.

8.3 The Particle-Sampling Probes

To advance beyond the relatively sterile development of remote sensors such as lidar and radar to their fruitful exploitation requires a thorough understanding of the atmospheric scattering mechanisms producing the echo returns. In the case of lidar, particles are known to be the major contributors to scatter. However, the quantitative verification of the theory requires detailed measurements not only of particle number densities but also of particle size distributions



Figure 8.3.--A sample of 2-D particle-sampling probe data obtained during the PHOENIX experiment.

and shapes, and these measurements must be made within the relatively inaccessible lidar sampling volume itself. Such in-situ verification poses a formidable challenge. We were fortunate indeed to have at our disposal three in-situ atmospheric sampling systems designed for this purpose: a two-dimensional (2-D) optical array spectrometer, a forward scattering spectrometer probe (FSSP), and an active scattering aerosol spectrometer (ASAS). Knollenberg (1976) describes the instruments and gives a few additional references. The 2-D probe extends the principle of standard optical array spectrometers, which size in one dimension only. Using a photodiode array and photodetection electronics, together with high-speed front end memory, it records image slices across each particle; these

can be built up into a 2-D picture. Figure 8.3 shows flight data imagery obtained during PHOENIX from this probe. The FSSP sizes particles by measuring the amount of light scattered into its collecting optics during particle interaction through a focused laser beam. The ASAS uses the active open cavity of a gas laser to provide a particle illumination source sufficiently intense for detection of particles in the submicron range. Together, the three instruments measured particles in the size range from 0.8 μm to 6400 μm, providing data useful not only for lidar studies but for radar calibrations and comparisons as well. During PHOENIX, all three instruments were mounted aboard a small, single-engine aircraft and flown in the lidar sampling volume.

8.4 Lidar Goals

As indicated in Chapter 1, lidar goals for the PHOENIX study were rather numerous. They included the following:

i) Observations of the dynamics of the convective PBL — layer rise and evolution, the development of structures within the PBL, etc. — in support of the major PHOENIX objectives.

ii) Simultaneous operation with FM-CW (10-cm), TPQ-11 (8-mm), and 3-cm dual- Doppler radars to measure backscatter cross sections in clouds as a function of wavelength.

iii) Comparison of lidar and radar data with measurements on particle concentrations and size distributions, humidity, and glaciation.

iv) Using data from (ii) and (iii) above to examine the nature of the scatter from clouds (coherent versus incoherent, dependence upon size-spectra of the cloud particles, etc.).

v) Combined solar-radiation and cloud microphysics measurements.

vi) Simultaneous measurements of long-path, near-ground statistics of aerosol distribution using both the lidar and the airborne Knollenberg probe.

8.5 Lidar and Aircraft Operations During PHOENIX

The varied lidar goals described in the previous section resulted in a corresponding variety of operation modes. During the first 25 days of September, the lidar was operated in the dual polarization configuration. Scanning procedures ranged from vertical probes of the same volume illuminated by the TPQ-11 8-mm radar for calibration, to scans of small, building clouds in order to study glaciation, to measurements near the sun to correlate with solar radiation measurements. During the last three days of the experiment, the lidar was used to execute the same studies, this time in the dual-wavelength mode. The photometers, the two pyrheliometers, and one of the time-lapse cameras were all mounted on a solar tracker and operated whenever the lidar itself was in use. The second time-lapse camera was configured to photograph the vertical hemisphere from sunrise to sunset. The acoustic sounding system was deployed to provide vertical profiles, pulsed at a 0.1-Hz rate 24 hours a day.

During PHOENIX, a Cessna 206 turbo-charged aircraft carried the particle-sampling spectrometers. The aircraft worked in four operational modes:

i) Ascending or descending at 1 m s^{-1} in a 1.5-kilometer diameter spiral above the lidar and 8-mm radar, sampling every second.

ii) Ascending or descending in a spiral along the straight line joining the lidar and the sun.

iii) Penetration of cumulus clouds as they were building.

iv) With the lidar pointing just above the horizon, flying at 150 m AGL along the lidar axis.

Data taken by the lidar and solar irradiance instruments were digitized and stored on nine-track digital tape. Along with the data, the data acquisition system also recorded several bookkeeping quantities, such as time of day, laser power, outside temperature, and telescope positions. Table 8.2 summarizes the lidar and aircraft operations, specifying the various operational modes of both the lidar and the airborne instrumentation.

Table 8.2.--PHOENIX lidar log

Date (Sept.)	Time (MDT)	Laser	Solar	Atmospheric Conditions	Aircraft Location Comments	Flight Information
1	0800-1330	V[1]-DP[2]	Yes	Clear	None	
5	0900-1050	V-DP	Yes	Light haze	None	
6	0850-1132	V-DP	Yes	Light haze	None	
	1132-1640	None	Yes	Fog	BP & BAO	
8	0900-1430	V-DP	Yes	Haze	BAO	Data on paper tape only
	1430-1441	Cir-Sun	Yes	Haze w/some Cu.	None	
	1441-1410	V-DP	Yes	Haze w/high Cirrus	None	
	1520-1525	Near sun	Yes	Haze w/Cu.	None	
11	0900-0955	V-DP	Yes	Haze w/Cu. to west	None	
	1007-1048	Near sun	Yes	High winds & dust	None	
	1050-1138	V-DP	Yes	30-40 MPH winds	None	
14	0900-1004	V-DP	Yes	Hazy (heavy)	None	
	1030-1233	Near sun	Yes	Hazy (heavy)	Ft. Lupton, BAO, Denver	
	1537-1710	None	No	Hazy (heavy)	BAO & Arapahoe, Peak	
17	1117-1240	V-DP	Yes	Cloud Cover 1800 M	None	
	1240-1930	None	Yes		None	
18	0845-0938	V-DP	No	Overcast 150 M	BAO	
	0940-0945	Near sun	Yes	Clearing w/haze	BAO	
	0948-1354	V-DP	Yes	Partly cloudy w/haze	BAO	
	1355-1404	Near sun	Yes	Partly cloudy w/haze	None	
	1410-1615	V-DP	Yes	Partly cloudy	BAO	
	1620-1650	Cloud-DP	Yes	Partly cloudy	In cloud	
	1100-1723	V-DP	Yes	Partly cloudy	BAO	
19	1000-1210	V-DP	No	Overcast 2.4 km	BAO	
	1212-1229	Near sun	Yes	Clearing	BAO	
	1230-1607	V-DP	Yes	P. cloudy to overcast	BAO	
20	1000-1440	V-DP	At 1340	Overcast	BAO	
	1402-1507	Near sun	Yes	Clearing	BAO	
	1510-1610	V-DP	Yes	Partly cloudy	BAO	
21	0845-1135	V-DP	Yes	Clear	None	
	1200-1230	None	Yes	Clear	None	
	1230-1437	V-DP	Yes	Clear w/haze	None	
22	1025-1337	V-DP	Yes	Haze (heavy)	At BAO-1318 MDT	
	1340-1453	Near sun	Yes	Partly cloudy w/haze	BAO	
	1500-1515	V-DP	Yes	Hazy	BAO	
	1517-1629	Near sun	Yes	Hazy	BAO	
26	0900-1020	V-DW[3]	Yes	Hazy	BAO	
	1020-1165	Power	Failure			
	1115-1131	V-DW	Yes	Hazy	BAO	
	1137-1321	10°	Yes	Hazy	500 ft off ground	
	1440-1601	D-DW	Yes	Hazy	BAO	
	2020-2218	V-DW	Yes	Thin cloud	None	
27	1400-1645	V-DW	Yes	Thin cirrus	BAO	
	1700-1850	Clouds-DW	Yes	Thin cirrus	In clouds	
28	0400-0700	V-DW	On at 0650	Clear	BAO	
	0700-1129	V-DW	Yes	70% cloud	BAO at 1002 MDT	
	1130-1500	None	Yes	Partly cloudy	None	
	1500-1630	V-DP	Yes	Overcast	BAO	
	1730-1850	Cloud-DP	Yes	Partly cloudy	Chasing clouds	

[1]V = Vertical
[2]DP = Dual Polarization
[3]DW = Dual Wavelength

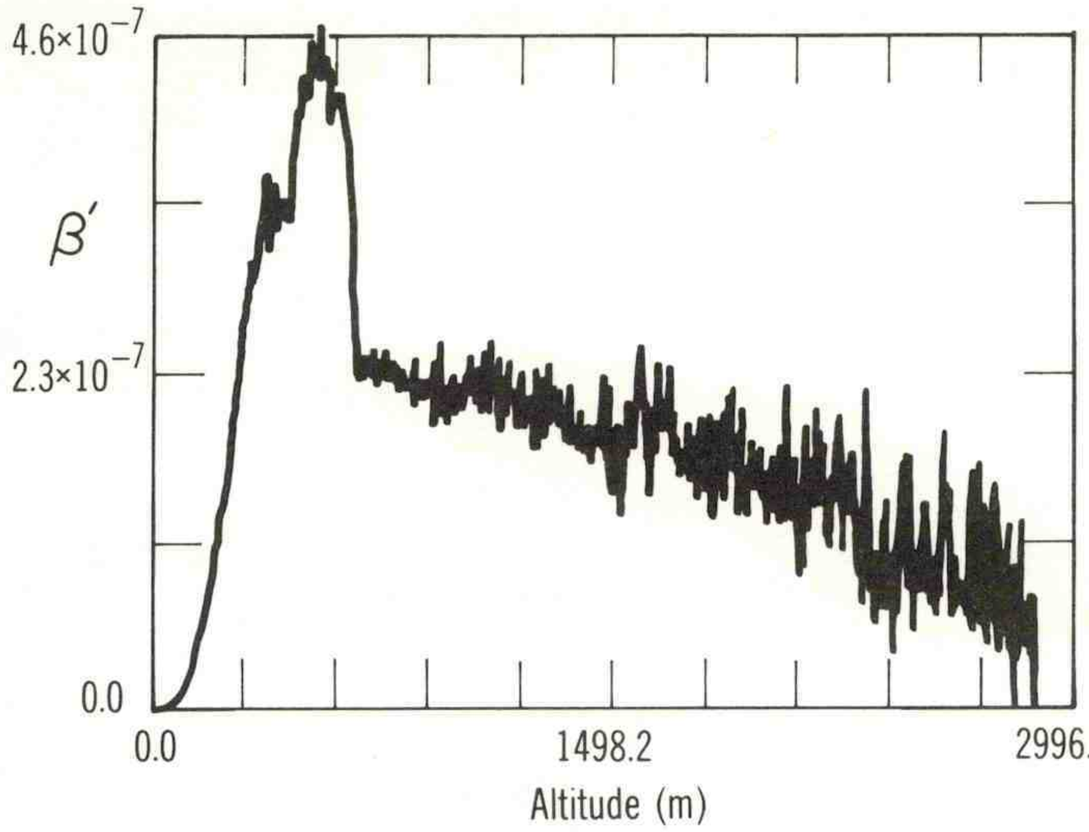


Figure 8.4.--Backscatter lidar echo strength as a function of altitude above the lidar. Echoes reveal the top of the mixed layer to be some 600 m above ground level.

Data analysis is carried out after the fact with the help of a minicomputer. Field data tapes are first copied and the original tapes preserved on archive; bad data are eliminated through checks for quality and faults. Calibration and instrument factors are then applied. For the lidar data, the R^{-2} factor is removed, other calibrations and corrections are applied, and the backscatter coefficients calculated. From this (in the case of dual polarization) the depolarization ratio and other quantities of interest can be calculated, displayed, or stored on disk or tape. Lerfald et al. (1977) cover the complete data analysis procedure. Figure 8.4 gives an example of PHOENIX data, revealing the depth z_i of the inversion layer. Time series of such data are currently being compared with time series from other PHOENIX instrumentation to yield z_i estimates for use in dynamical studies and to help us understand idiosyncracies of the different instruments. For further information the interested reader should consult N. L. Abshire, (commercial phone (303) 499-1000, ext. 6596, FTS 323-6596).

8.6 Preliminary Results

While it is not the purpose of this document to present detailed analysis results, Table 8.3 lists the types of results available to date and the approximate amount of data currently available.

Table 8.3.--Lidar PHOENIX results

Type	No. of days analyzed
Lidar backscatter coefficients	9
In-situ probe particles size distributions and shapes: (0.1-23 μm radii)	11
In-situ probe, particle size distributions and shapes: (13-3200 μm radii)	2
Wavelength dependence of solar extinction	10
Angular scatter from about sun: (aureole radiometer)	7
Precipitable water vapor by optical solar extinction	12

Acknowledgments

We thank Ed Neish, owner and pilot of the Cessna 206 instrumented with the in-situ probe apparatus, for his expert handling of the aircraft in executing the various flight patterns required. We also gratefully acknowledge the help of Viola Hunt, who did much of the Knollenberg data processing. Dick Cupp, Hans Erickson, and Terry McNice put in many long hours operating and maintaining the system.

References

Abshire, N. L., V. E. Derr, G. M. Lerfald, G. T. McNice, R. F. Pueschel, and C. C. Van Valin, Aerosol characterization at Colstrip, Montana, Spring and Fall, 1975, NOAA Tech. Memo. ERL WPL-33 (1978).

Collis, R.T.H., Lidar, Adv. Geophys. 13, 113-139 (1969).

Derr, V. E., M. J. Post, R. L. Schwiesow, R. F. Calfee, and G. T. McNice, A theoretical analysis of the information content of lidar atmospheric returns, NOAA Tech. Rept. ERL 296-WPL 29 (1974).

Derr, V. E., G. T. McNice, N. L. Abshire, R. E. Cupp, R. F. Calfee, and M. J. Ackley, Lidar observations of atmospheric particulates near Denver, Colorado, Symposium Proceedings, Denver Air Pollution Study-1973, EPA-600/9-76-007a, pp 51-86 (1976).

Hall, F. F., Jr., Laser systems for monitoring the environment, Laser Applications 2, 161-225, Academic, New York (1974).

Hardy, K. R., Studies of the clear atmosphere using high power radar, Chapter 14, in Remote Sensing of the Troposphere, V. E. Derr, Ed., Chapter 14, U.S. Govt. Printing Office (1972).

Knollenberg, R. G., Three new instruments for cloud physics measurements: the 2-D spectrometer, the forward scattering spectrometer probe, and the active scattering aerosol spectrometer, Preprints International Conference on Cloud Physics, July 26-30, 1976, Boulder, Colorado, pp. 554-561, American Meteorological Society, Boston, Mass. (1976).

Konrad, T. G., The dynamics of the convective process on clear air as seen by radar, J. Atmos. Sci. 27, 1138-1147 (1970).

Kunkel, K. E., E. W. Eloranta, and S. T. Shipley, Lidar observations of the convective boundary layer, J. Appl. Meteorol. 16, 1306-1311 (1977).

Lerfald, G. M., V. E. Derr, R. F. Pueschel, and R. L. Hulstrom, Final report on Phase I of solar radiation atmospheric transmission research, NOAA Tech. Memo. ERL WPL-18 (1977).

CHAPTER 9

OPTICAL SYSTEMS MEASURING SURFACE-LEVEL CONVERGENCE DURING PHOENIX

R. B. Fritz and T.-I. Wang
Wave Propagation Laboratory
National Oceanic and Atmospheric Administration
Boulder, Colorado 80303

9.1 Introduction and Background

During the past decade, the Optical Propagation Program Area of WPL has developed a line-of-sight optical method for measuring atmospheric winds. Basically, the system observes scintillation patterns induced in an optical beam by atmospheric turbulence and monitors the advection of the patterns across the beam. In this way it provides a line-average estimate of the winds transverse to the beam. Lawrence et al. (1972) describe the basic technique; Ochs et al. (1976) discuss the modifications and extensions required over long paths, where scintillation-saturation effects may enter under strongly turbulent conditions. Although the standard approaches have used light sources such as lasers, incandescent lamps, and even LED's, it is possible to make such measurements by using passive observations of a natural scene (Clifford et al., 1975).

Although wind-sensing systems of this type have found many applications, both civilian and military, the application with perhaps the greatest potential is the measurement of horizontal convergence. Estimating this atmospheric quantity with point sensors is expensive and fraught with uncertainty. At best, such procedures require long averaging times, precluding any hope of studying short-lived fluctuations and small-scale structure in the convergence pattern. By contrast, arrays of optical wind sensors forming cl sed paths measure horizontal surface convergence with a high degree of confidence. The horizontal convergence measured in this way usually correlates very well with independent measurements of vertical velocity fluctuations measured in the same volume. To the extent that atmospheric flows on most scales of geophysical interest are incompressible,

we should find that

$$\nabla_h \cdot \underset{\sim}{u} = - \frac{\partial w}{\partial z} ,$$

where $\underset{\sim}{u}$ is the atmospheric velocity, w is the vertical component of that velocity, and z is the vertical axis. Early tests by Kjelaas and Ochs (1974) proved this to be the case for boundary-layer applications.

9.2 The PHOENIX Systems

In the PHOENIX experiment, WPL used two triangular arrays of optical sensors for measurement of surface-level convergence and divergence. The smaller of the two triangles is the system permanently operated as an integral part of the BAO facility itself. It is equilateral, 450 m on a side, with sensors and light sources housed in metal enclosures atop 4-m pedestals at each of the outer guy anchors of the BAO tower. The locations are as indicated in Figure 2.6 of Chapter 2 (Kaimal and Wolfe, 1979). Data from each receiver are archived by the BAO data processing facility. The size of this array lends itself well to the study of extremely localized patterns of horizontal convergence and divergence such as are associated with the development of thermal plumes. Figure 9.1 shows one of the BAO sensor units.

The larger triangle, consisting of legs approximately 6 km in length, was centered just northeast of the BAO site, as indicated in Figure 2.3 of Chapter 2 (Kaimal and Wolfe, 1979). Site selection was constrained by requirements for unobstructed visibility and power availability. The incandescent light sources and receivers were housed in temporary shelters located on private property rented for the month of September. Figure 9.2 shows one of the sites used as part of the larger triangle. Some of the shelters were less conventional. Figure 9.3 shows an interior view of the optical system in place in an abandoned building constituting the northwest vertex of the triangle. Data from these receivers were recorded on analog strip chart recorders and on digital recorders for after-the-fact, off-line processing in Boulder. Standard procedures for changing the tape cassettes and calibrating the system interrupted data acquisition for approximately one hour at midday on even-numbered September dates. For the most part, the systems operated unattended.

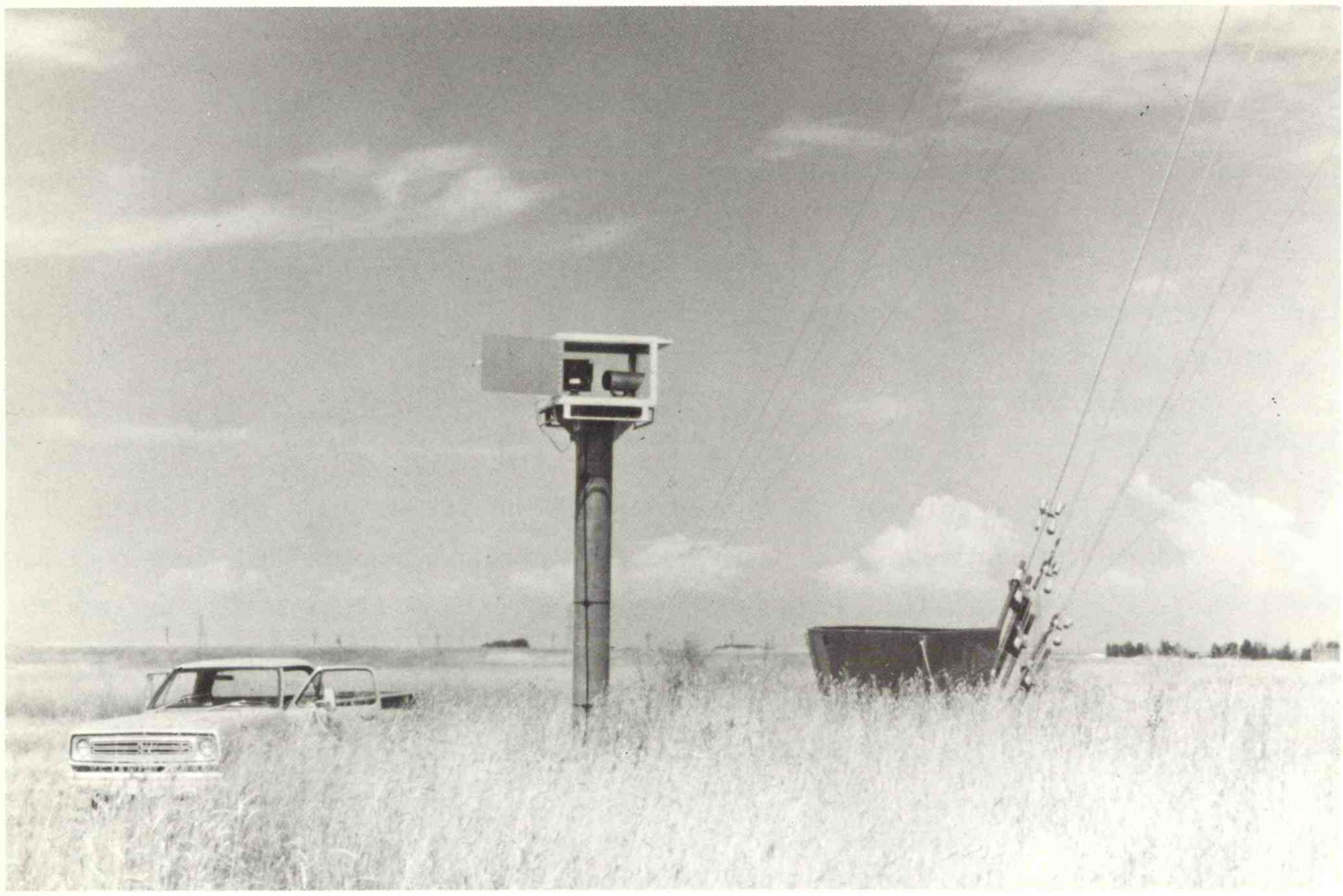


Figure 9.1.--Light source and optical receiver at one of the BAO optical triangle sites. Shelter panels have been pulled back to reveal the instrumentation.

9.3 Wind-Velocity and Convergence Estimates

Since the optical system measures the path-averaged horizontal wind component perpendicular to each side of the triangle, it is possible to determine the two components of the mean horizontal wind velocity, or, equivalently, the horizontal mean wind speed and direction, by combining data from any two sides. For the larger triangle, each combination of two sides was used, yielding three quasi-independent estimates of the mean wind vector for comparison.

Horizontal convergence was calculated by combining data from all three sides of each triangle according to the formula

$$\text{convergence } (s^{-1}) = \frac{\sum_{i=1}^{3} u_i L_i}{A} ,$$

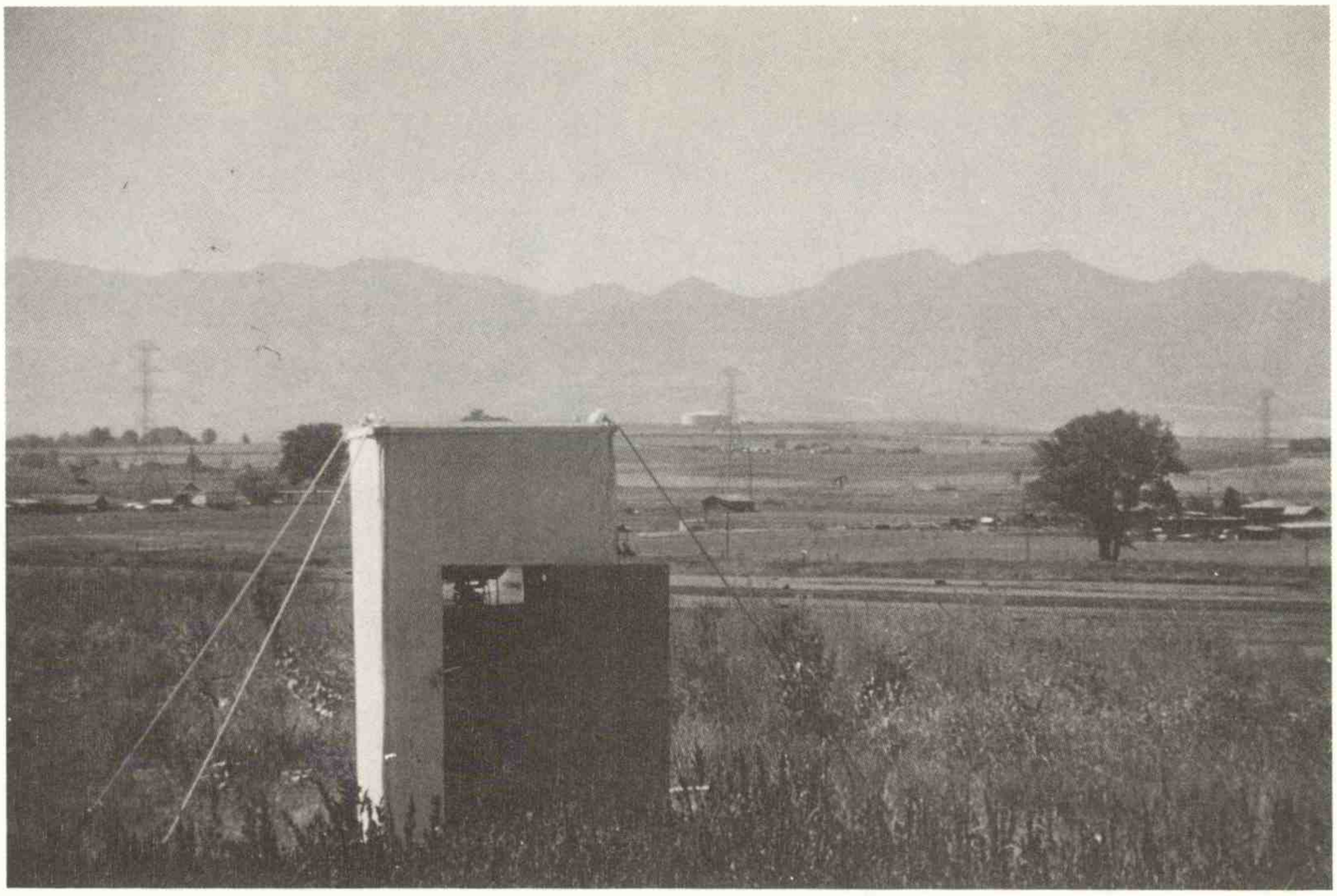


Figure 9.2.--Light source and optical receiver at the east vertex of the large optical triangle. A small shelter protects the system from the elements.



Figure 9.3.--Optical receiver at the northwest vertex of the large optical triangle. Here shelter is provided by an abandoned house.

where $u_i \equiv$ inward wind component across the i^{th} side,
$L_i \equiv$ length of the i^{th} side, and
$A \equiv$ area enclosed by the triangle.

Here A (smaller triangle) = 8.775×10^4 m^2, while A (larger triangle) = 15.42×10^6 m^2. Thus, the area of the larger triangle is some 176 times that of the smaller.

The accuracy of measurements made on the larger triangle was limited by the digital recorders; the accuracy of measurements made on the smaller triangle was limited by receiver sensitivity. Receiver full-scale velocities were set at 10 m s^{-1} on the larger triangle and at 20 m s^{-1} on the smaller triangle. Values higher than the 10 m s^{-1} limit were reached on only two days, one of which was September 11, a day marked by a high wind event at the BAO site. If we assume that the wind components were measured to an accuracy of $\pm$ 0.05 m s^{-1}, then, for the scale of the larger triangle, convergence could be estimated to an accuracy of $\pm 6 \times 10^{-5}$ s^{-1}. Assuming the same crosswind component accuracy for the smaller triangle implies a convergence estimation to within $\pm 8 \times 10^{-4}$ s^{-1}.

9.4 PHOENIX Operations

Data from the larger triangle were recorded on analog charts beginning on September 1 and on the digital system beginning September 4. Apart from shorter interruptions (e.g., the tape changes and calibration mentioned above, or problems occurring near sunset when light scattered through the shelter window would confuse the receiver at the eastern site), the system was operated 24 hours a day until October 2, 1978, with the exceptions listed in Table 9.1.

Table 9.1.--Data outages, 6-km optical triangle

Duration (Times in MST)	Cause
Sept 5 (1800) until Sept 6 (1130)	Cable broken at one site
Sept 11 (1100) until Sept 11 (1830)	High winds, data off scale
Sept 18 (0200) until Sept 18 (0900)	Visibility lost because of fog
Sept 27 (1445) until Sept 28 (1200)	Power failure at one site

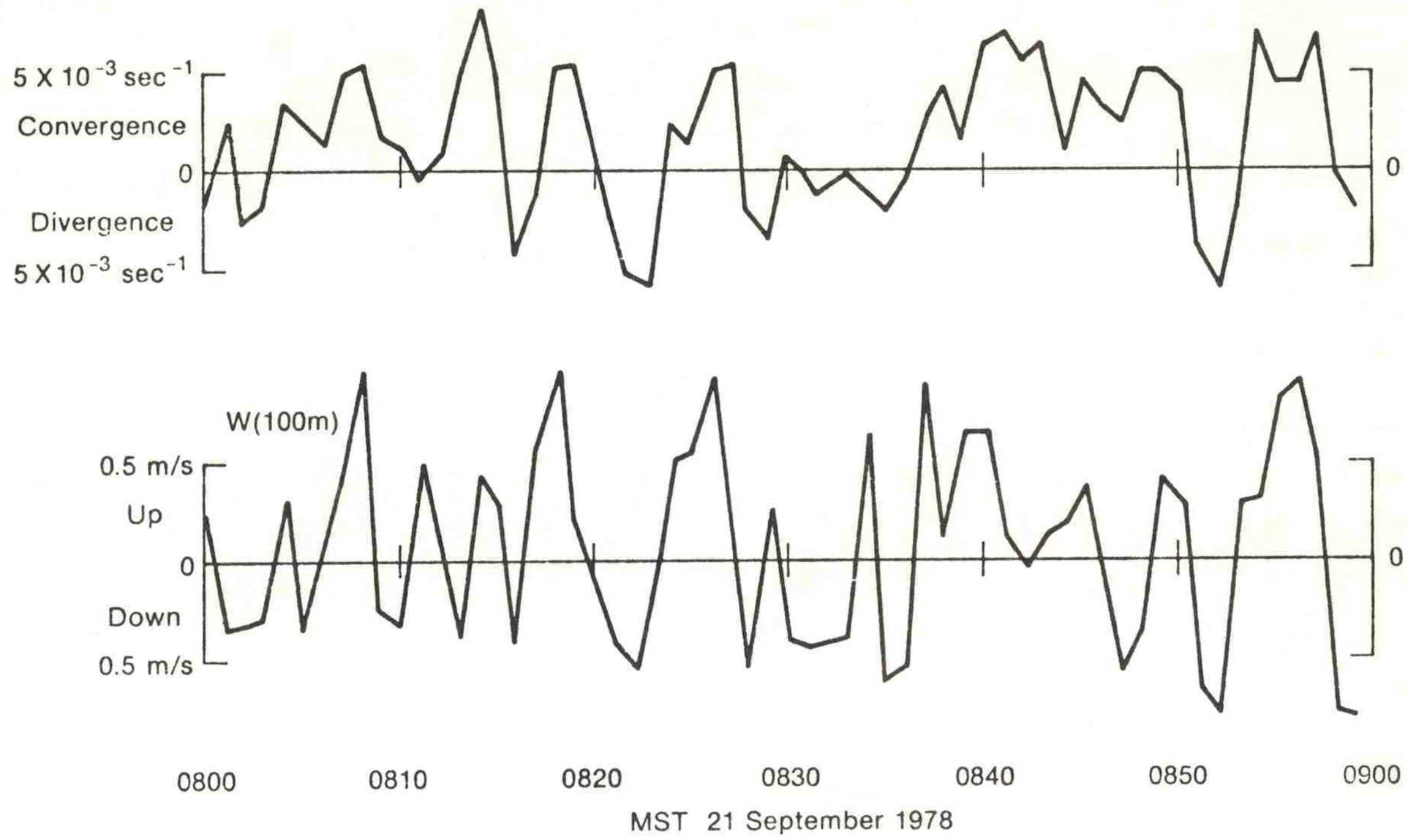


Figure 9.4.--Time series of output from the small optical triangle for a 1-h period, compared with vertical velocity fluctuations recorded at the 100-m level of the BAO tower. Note the good (albeit imperfect) correlation. Tsay et al. (1980) give more comparisons and full discussion.

Data from the smaller triangle were archived together with other data taken at the BAO site whenever the tower instrumentation was up and operating (Tables 2.3 and 2.4 of Chapter 2 [Kaimal and Wolfe, 1979]).

Figure 9.4 shows sample output from the smaller triangle, comparing horizontal convergence with data on vertical velocity fluctuations from the BAO tower. Figure 9.5 shows a data sample from the larger triangle. Figure 9.6 shows a summary of convergence estimates from the larger triangle, plotted as a function of wind azimuth. Although the results display considerable scatter, as one would expect, they also demonstrate a definite influence of wind direction on convergence, possibly terrain-related. The problem is currently under investigation. For further information the interested reader should consult R. B. Fritz (commercial phone (303) 499-1000, ext. 6523, FTS 323-6523).

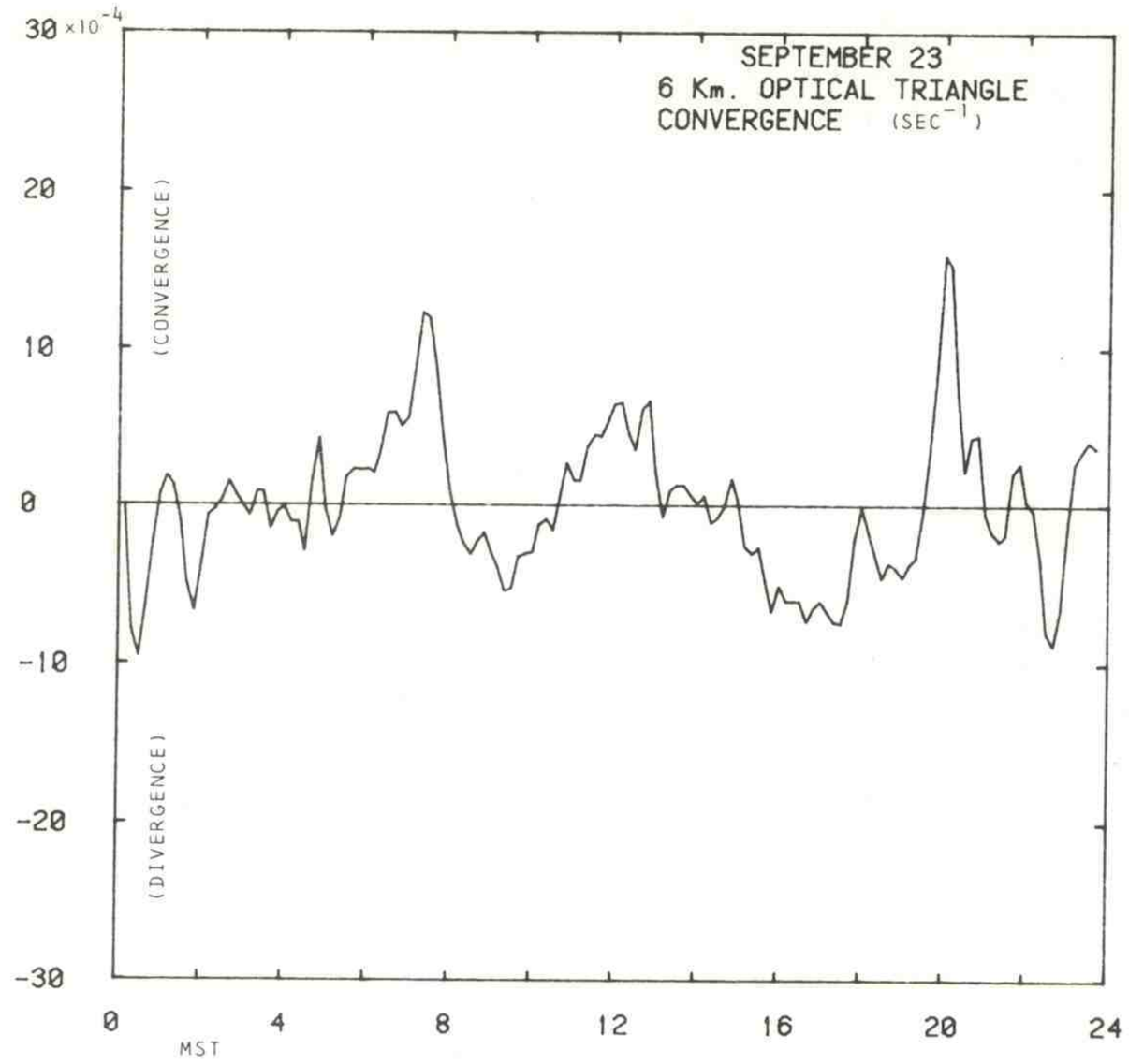


Figure 9.5--One full 24-h period of convergence data from the large optical triangle.

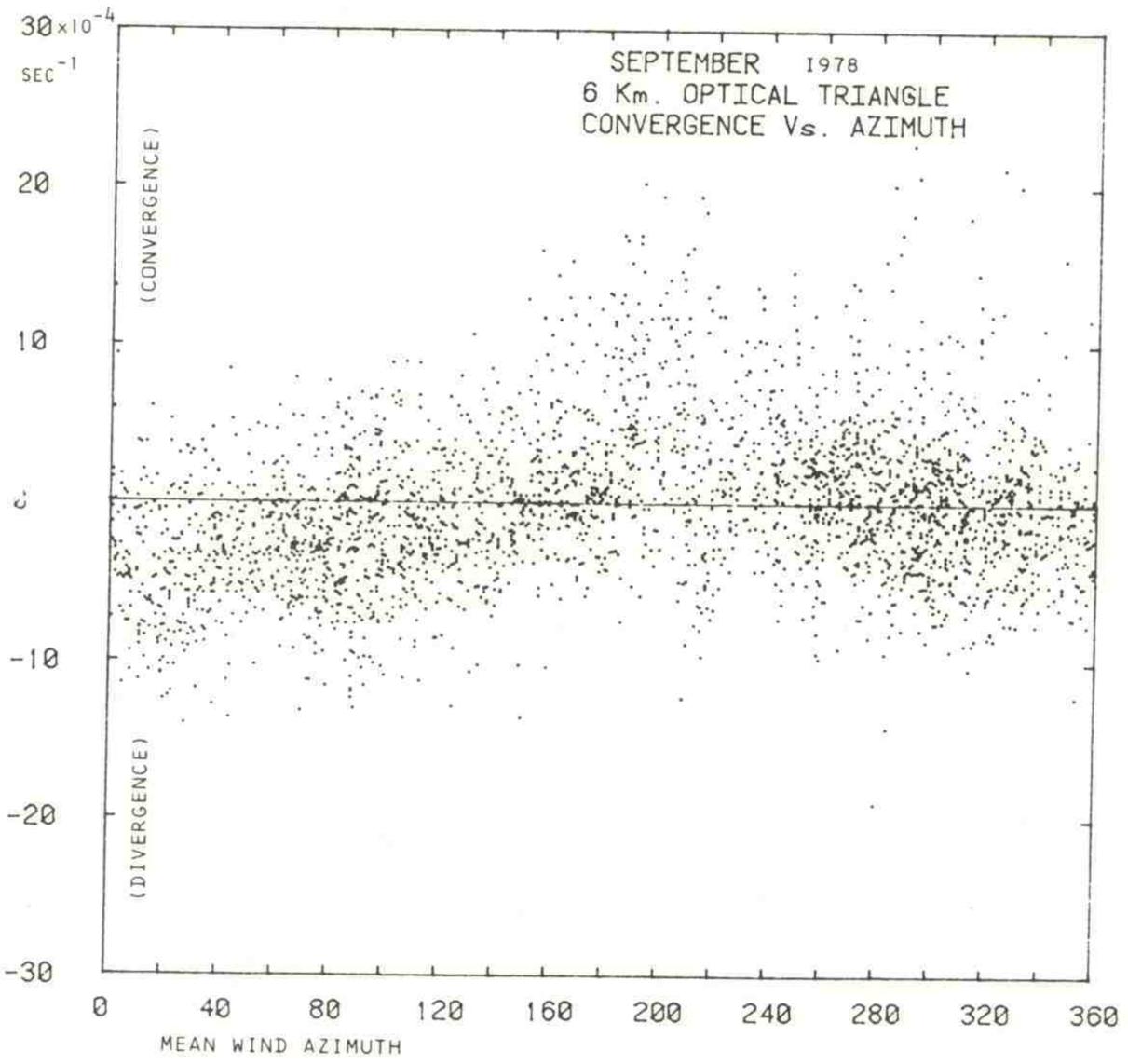


Figure 9.6.--Horizontal convergence as a function of wind direction measured by the 6-km triangle. Points are 10-min averages for the entire month.

Acknowledgments

We wish to acknowledge Gerald R. Ochs and Mu-King Tsay for their help in the system development and data analysis. Ron Quintana did most of the system installation.

References

Clifford, S. F., G. R. Ochs, and T.-I. Wang, Optical wind sensing by observing the scintillations of a random scene, Appl. Optics 14, 2844-2850 (1975).

Kaimal, J. C., and D. E. Wolfe, BAO site, tower instrumentation, and PHOENIX operations, Chapter 2, in Project PHOENIX: The September 1978 Field Operation, W. H. Hooke, Ed., NOAA/NCAR Boulder Atmospheric Observatory Rept. No. 1, available from NOAA/ERL, Boulder, Colo., and from NCAR Publications Office, Boulder, Colo. (1979).

Kjelaas, A. G., and G. R. Ochs, Study of divergence in the boundary layer using optical propagation techniques, J. Appl. Meteorol. 13, 242-248 (1974).

Lawrence, R. S., G. R. Ochs, and S. F. Clifford, Use of scintillations to measure average wind across a light beam, Appl. Optics 11, 239-243 (1972).

Ochs, G. R., S. F. Clifford, and T.-I. Wang, Laser wind sensing: the effects of saturation of scintillation, Appl. Optics 15, 403-408 (1976).

Tsay, M.-U., T.-I. Wang, R. S. Lawrence, G. R. Ochs, and R. B. Fritz, Wind velocity and convergence measurements at the Boulder Atmospheric Observatory using path-averaged optical wind sensors, unpublished manuscript (1980).

CHAPTER 10

PORTABLE AUTOMATED MESONET (PAM) OBSERVATIONS DURING PHOENIX

Peter H. Hildebrand
National Center for Atmospheric Research
Boulder, Colorado 80307

10.1 Introduction and Background

Arrays of surface instrumentation have long played a unique role in atmospheric studies by virtue of the spatial picture they provide. The vast majority of array data has been amassed from operational networks. The data sets have provided many insights and fostered many advances over the past decade, but for some modern purposes they suffer from several deficiencies. Often, the operational networks are not maintained in sufficiently good condition to provide data of research quality. Designed more for ruggedness and durability, they lack the precision, accuracy, and sensitivity required for research work. Moreover, the spacing between the array elements is typically too large to provide the resolution required for micrometeorological or even mesoscale work. Furthermore, data from such arrays are rarely available in forms amenable to quick, facile computer processing. Operational networks also tend to be rooted in place; rarely are they redeployed to meet temporary needs.

NCAR's Portable Automated Mesonet (PAM) system was designed to overcome these deficiencies. The PAM system consists of some 25 to 30 individual stations, each instrumented to provide wind speed and direction, temperature, relative humidity, and rain. The individual stations communicate these data by radio link to a central site or base station, where the data are monitored in real time and recorded digitally for subsequent analysis. The entire system is transportable; installation typically requires only a few days. Brock and Govind (1977) describe the system and its available outputs in some detail, including instrument characteristics — resolution, range, and sampling rates.

The PAM system was of interest to PHOENIX experimenters for a number of reasons. First, the stations provided an excellent look at the effects of topography on surface airflow in the vicinity of the BAO site. As mentioned in

Chapter 1 (Hooke et al., 1979), the effects of terrain on BAO data are of considerable interest. At issue were questions such as these:

To what extent do BAO data provide results of general validity that could be applied to flat terrain?

To what extent do they reflect terrain idiosyncracies

When (what time of day, what season) and under what conditions (prevailing wind, temperature stratification, etc.) are terrain effects most marked? When are they negligible?

What can we learn about terrain forcing from BAO data?

At this writing these questions remain unresolved, but are being actively investigated. The September PAM data should prove extremely useful in answering some of these questions. They complement a data set obtained with PAM at the BAO in April 1978. The April study deployed the PAM stations in a finer grid; the September study extends the area of coverage to about 100 km^2.

In addition to providing data of atmospheric interest per se, the PAM data also provide a means of refining the lower boundary condition used in the analysis of the X-band radar data. Instead of having to settle for an assumption that the underlying surface is horizontal, permitting no vertical velocity, or extrapolating from elevated winds (free from ground clutter) determined by radar in order to estimate surface winds (shielded by ground clutter), we can use the known surface wind field in computations, and check the validity of the alternative procedures.

10.2 PAM Operations During PHOENIX

Figure 2.3 of Chapter 2 (Kaimal and Wolfe, 1979) shows the locations of PAM stations during PHOENIX. For the most part these were deployed at intersections of roads (spaced 1 mi apart); one was situated at the BAO site. Figure 10.1 shows an individual PAM station on-site at PHOENIX. Apart from a few minor outages of individual stations, the PAM system was up and operating through most of September. Table 10.1 is a log of the system operation.

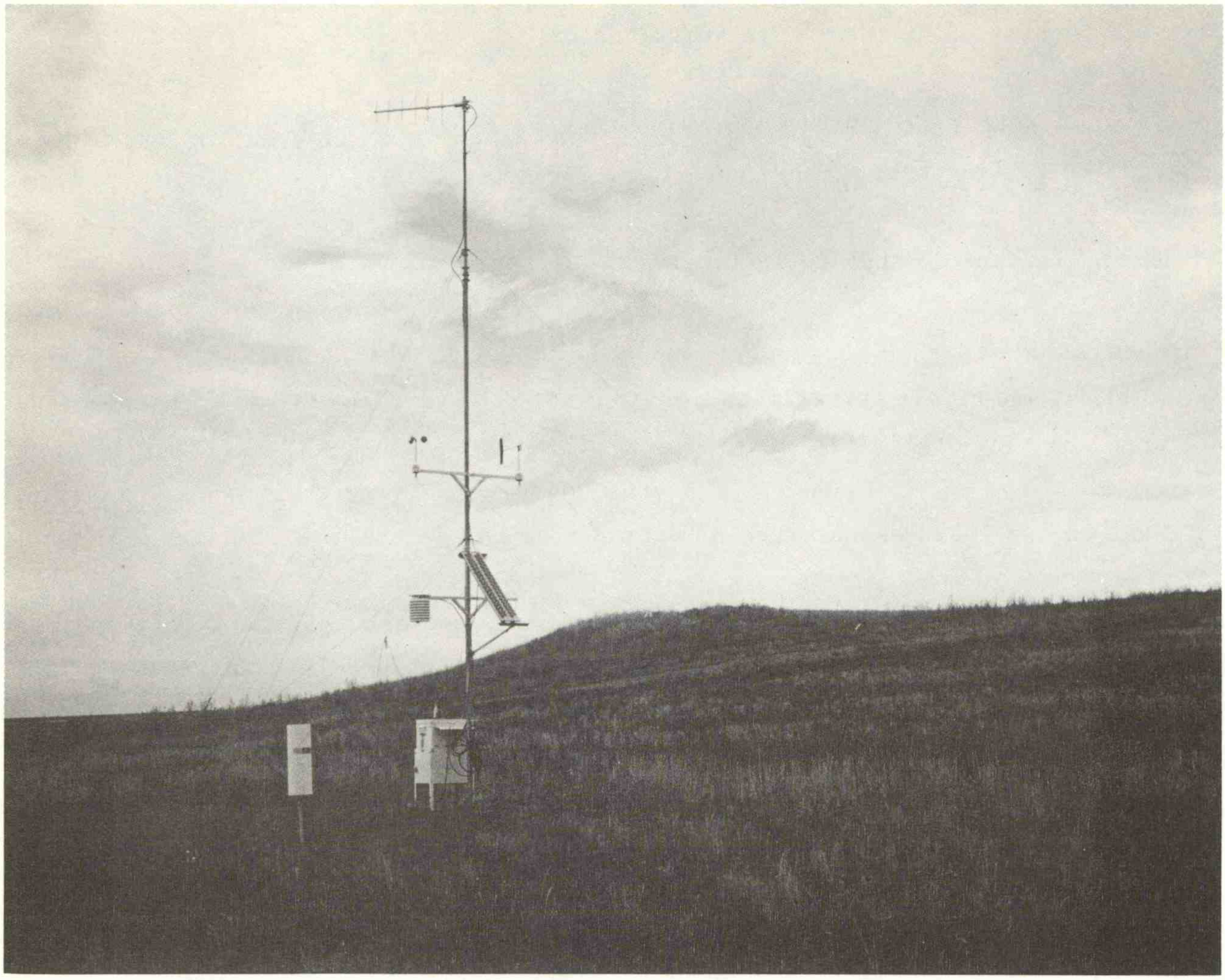


Figure 10.1.--One of the NCAR PAM stations deployed during PHOENIX.

Table 10.1.--PAM operation during the PHOENIX experiment, September 1978

Starting time (MDT)/date	Ending time (MDT)/date
0859/September 1	0842/September 7
0953/September 7	0535/September 11
0801/September 11	0459/September 21
0847/September 21	0912/September 29

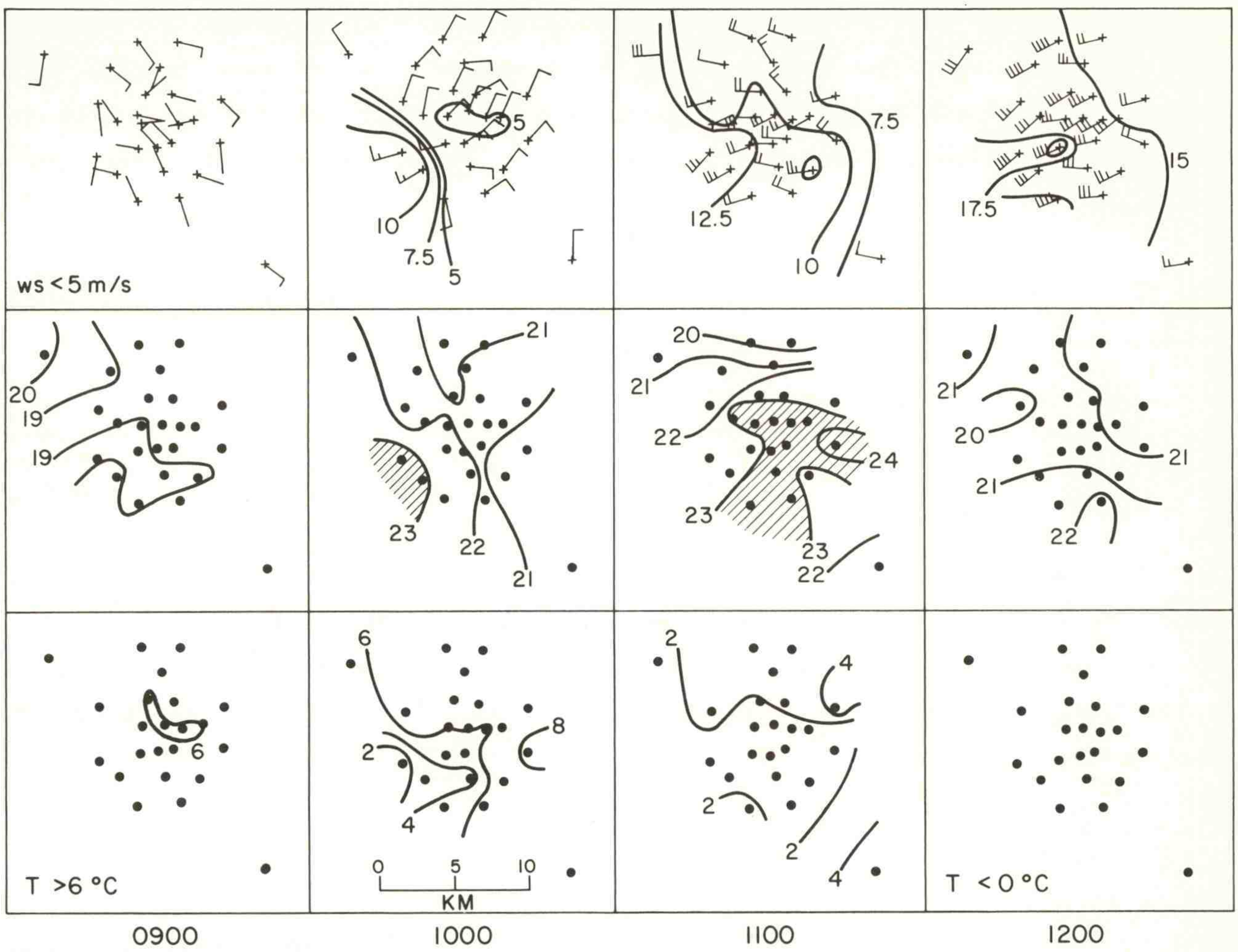


Figure 10.2.--Maps of the surface wind field on the PHOENIX test area on September 11, 1978, showing slow passage of a frontal system. Similar displays can be obtained for any other time interval of interest.

The output displays routinely available for PAM data are many and varied; Brock and Govind (1977) provide examples of most of the important ones. We have reproduced here maps of the surface wind field in the BAO vicinity on September 11, 1978, the high-wind date discussed by Wolfe in Chapter 15. The maps in Figure 10.2 which were produced at hourly intervals show southeasterly winds prevailing over the site in the early morning, shifting to easterly and northeasterly just before the arrival of the front associated with the front-range downslope winds. The front enters the western end of the array shortly before 1000 (MDT) and propagates through the array during the next hour, until at the end of the period the entire array is under the influence of the strong westerly flow. The accompanying temperature and dewpoint maps in the second and third rows of the

figure reveal the temperature perturbation and large drop in dewpoint that accompany the front. The hatched area, in which the temperature exceeds 23°C, moves through the PHOENIX area following the front; this is thought to result from turbulent mixing of potentially warm air initially lying above the PBL-capping inversion.

For further information the interested reader should consult the author (commercial telephone (303) 494-5151, ext. 78-31).

Acknowledgments

The assistance and support of the NCAR/FOF PAM staff are gratefully acknowledged. In particular, Ed Elsberry, Ken St. John, and Mike Williams helped deploy the network, and Gerry English, Steve Semmer, Paul Alhstrom, and Paula Rubin put in the long hours necessary to operate and maintain the PAM system through the experiment.

References

Brock, F. V., and P. K. Govind, Portable automated mesonet in operation, J. Appl. Meteorol. 16, 299-310 (1977).

Hooke, W. H., P. H. Hildebrand, and R. A. Kropfli, Project PHOENIX: background and introduction, Chapter 1, in Project PHOENIX: The September 1978 Field Operation, W. H. Hooke, Ed., NOAA/NCAR Boulder Atmospheric Observatory Rept. No. 1, available from NOAA/ERL, Boulder, Colo., and from NCAR Publications Office, Boulder, Colo. (1979).

Kaimal, J. C., and D. E. Wolfe, BAO site, tower instrumentation, and PHOENIX operations, Chapter 2, in Project PHOENIX: The September 1978 Field Operation, W. H. Hooke, Ed., NOAA/NCAR Boulder Atmospheric Observatory Rept. No. 1, available from NOAA/ERL, Boulder, Colo. and from NCAR Publications Office, Boulder, Colo. (1979).

CHAPTER 11

THE PHOENIX RAWINSONDE DATA

Peter H. Hildebrand and Robert B. McBeth
National Center for Atmospheric Research
Boulder, Colorado 80307

In support of PHOENIX studies in general, but as an integral part of the radiometric studies in particular, rawinsonde observations were taken routinely at the BAO site. The equipment used was a standard GMD rawinsonde system owned and operated by NCAR's Field Observing Facility (FOF). During the month there were some 38 flights; starting times and dates are recorded in Table 11.1. After-the-fact data analysis followed routine procedures. A number of errors crept in to the original data analysis; we now believe that most of the obvious errors in the temperature and humidity data have been rectified, thanks to checking by M. T. Decker in the course of his radiometric data comparisons and by D. E. Wolfe. Figures 11.1-11.38 provide rawinsonde wind, temperature, and humidity profiles for all 38 flights, plotted on skew T/log p diagrams. Wind vectors are plotted as a function of pressure, with arrows indicating directions from which the wind was blowing. North is to the top of each figure.

For further information the interested reader should consult the senior author (commercial telephone (303) 494-5151, ext. 78-31).

Acknowledgments

The assistance and support of NCAR/FOF staff in providing rawinsonde support for PHOENIX are gratefully acknowledged. In particular, Gerry Albright tirelessly and carefully operated the rawinsonde unit for all launches in the experiment.

Table 11.1.--PHOENIX rawinsonde flights

Flight No.	Date (Sept.)	Time (MDT)	Flight No.	Date (Sept.)	Time (MDT)
1	5	0951	20	19	0958
2	5	1344	21	19	1343
3	6	0959	22	20	0956
4	6	1349	23	20	1351
5	7	0642	24	21	1081
6	7	0956	25	21	1350
7	8	0636	26	22	1119
8	8	1059	27	22	1406
9	9	1001	28	25	0651
10	9	1400	29	25	1007
11	11	1002	30	25	1340
12	12	0633	31	26	0642
13	12	0945	32	26	1054
14	13	0633	33	26	1452
15	13	0942	34	27	0705
16	14	0633	35	27	1051
17	14	0943	36	27	1445
18	15	1005	37	28	0651
19	18	0958	38	28	1034

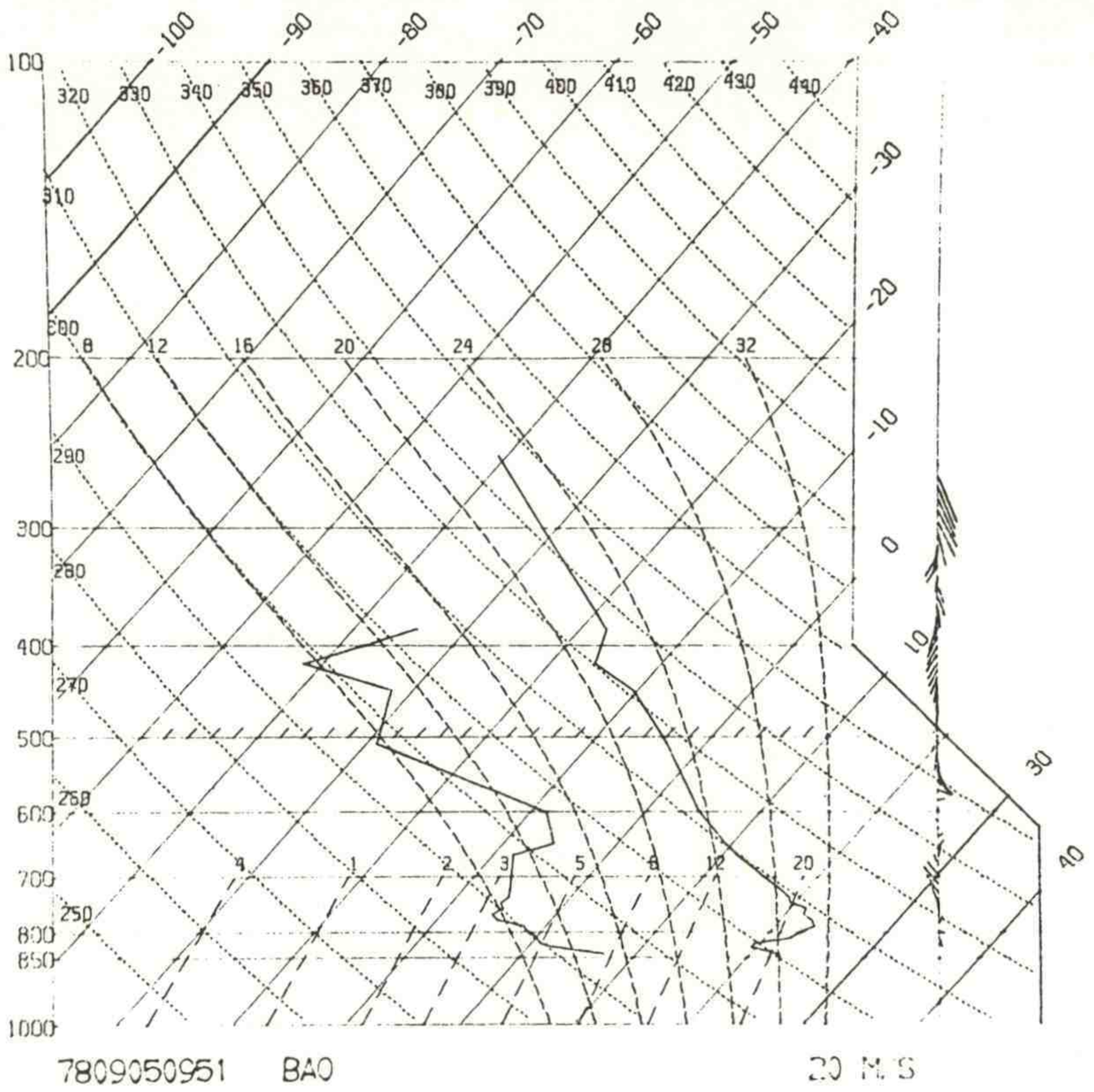


Figure 11.1.--PHOENIX rawinsonde flight number 1.

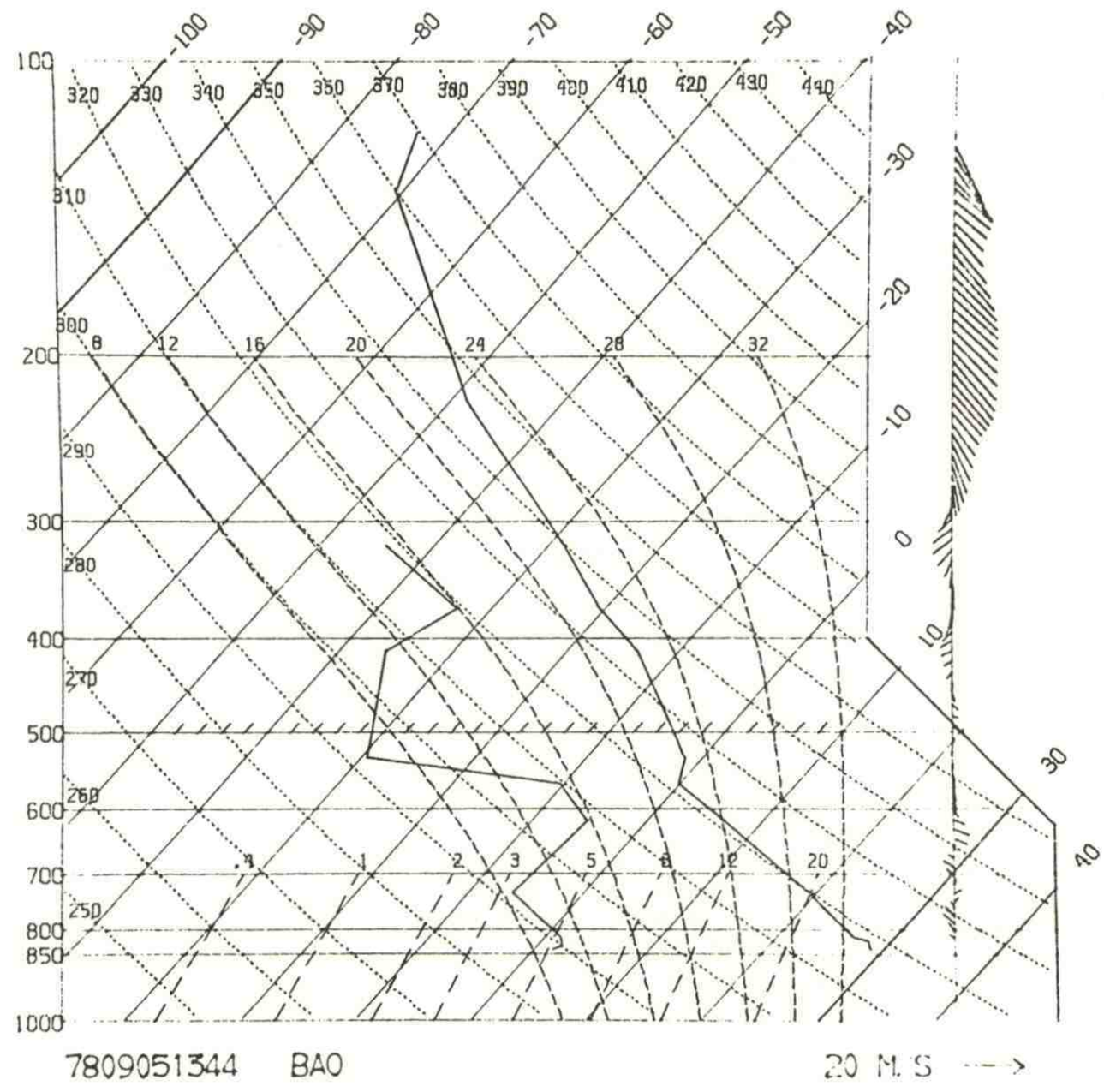


Figure 11.2.--PHOENIX rawinsonde flight number 2.

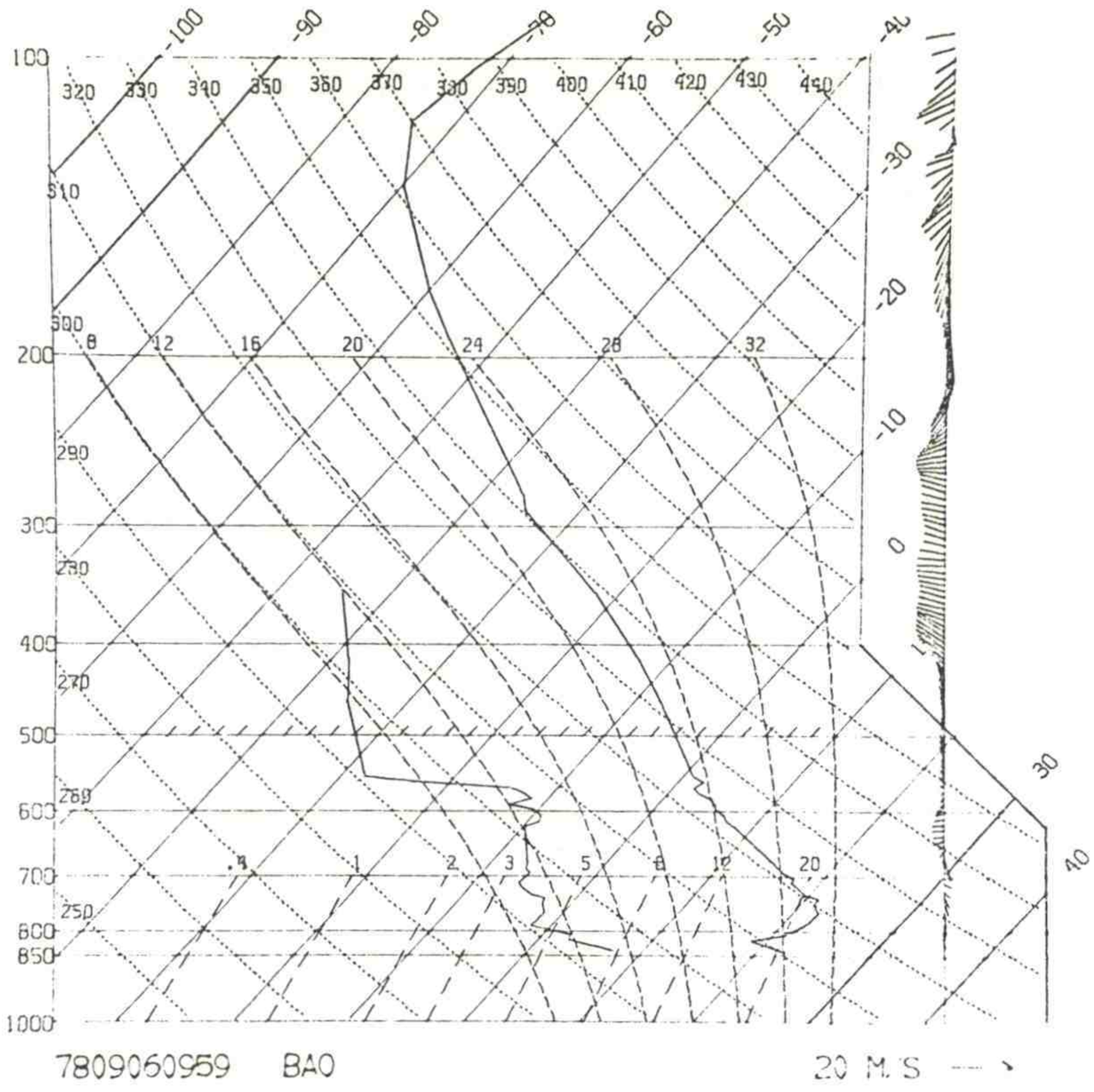


Figure 11.3.--PHOENIX rawinsonde flight number 3.

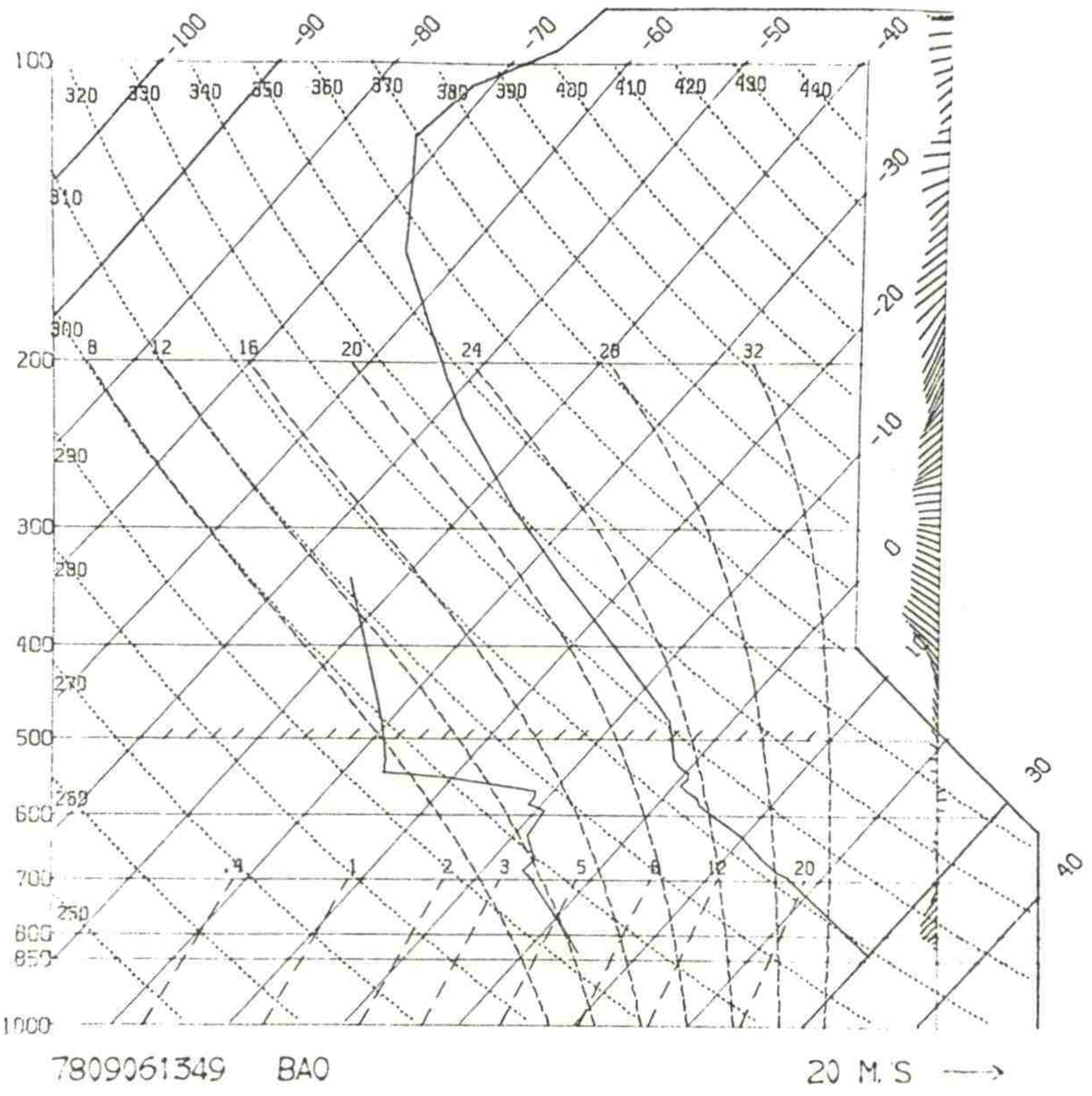


Figure 11.4.--PHOENIX rawinsonde flight number 4.

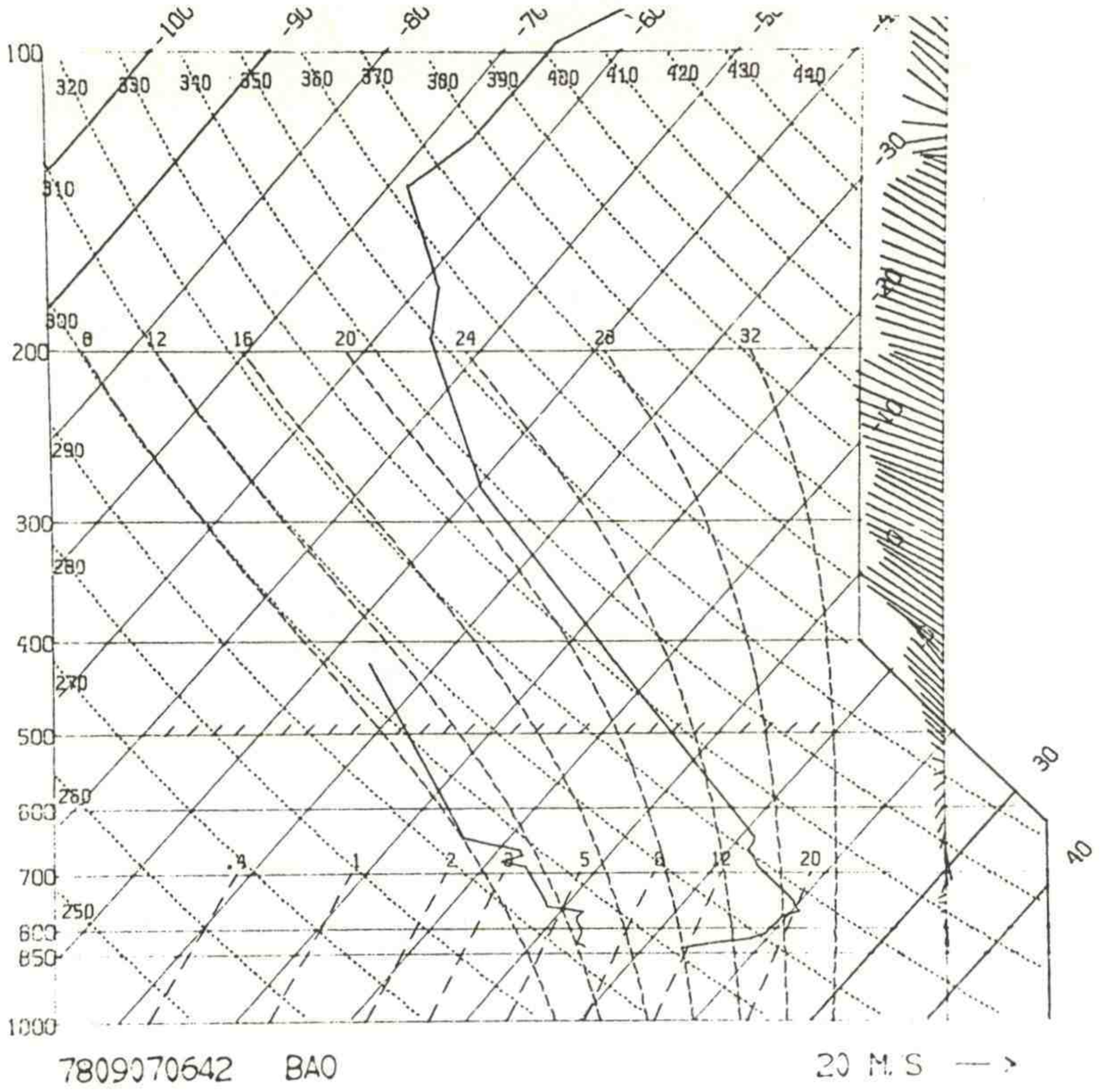


Figure 11.5.--PHOENIX rawinsonde flight number 5.

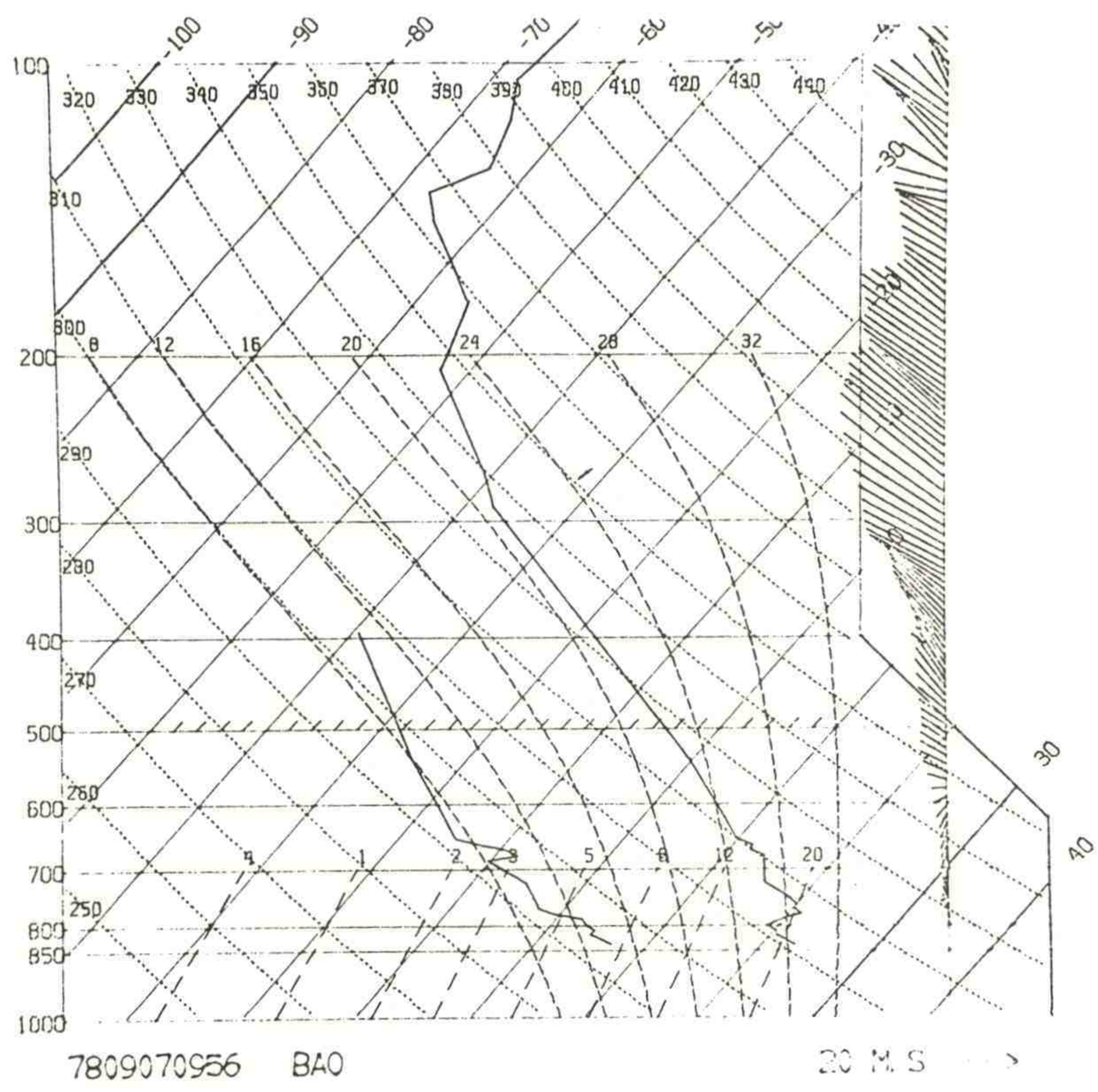


Figure 11.6.--PHOENIX rawinsonde flight number 6.

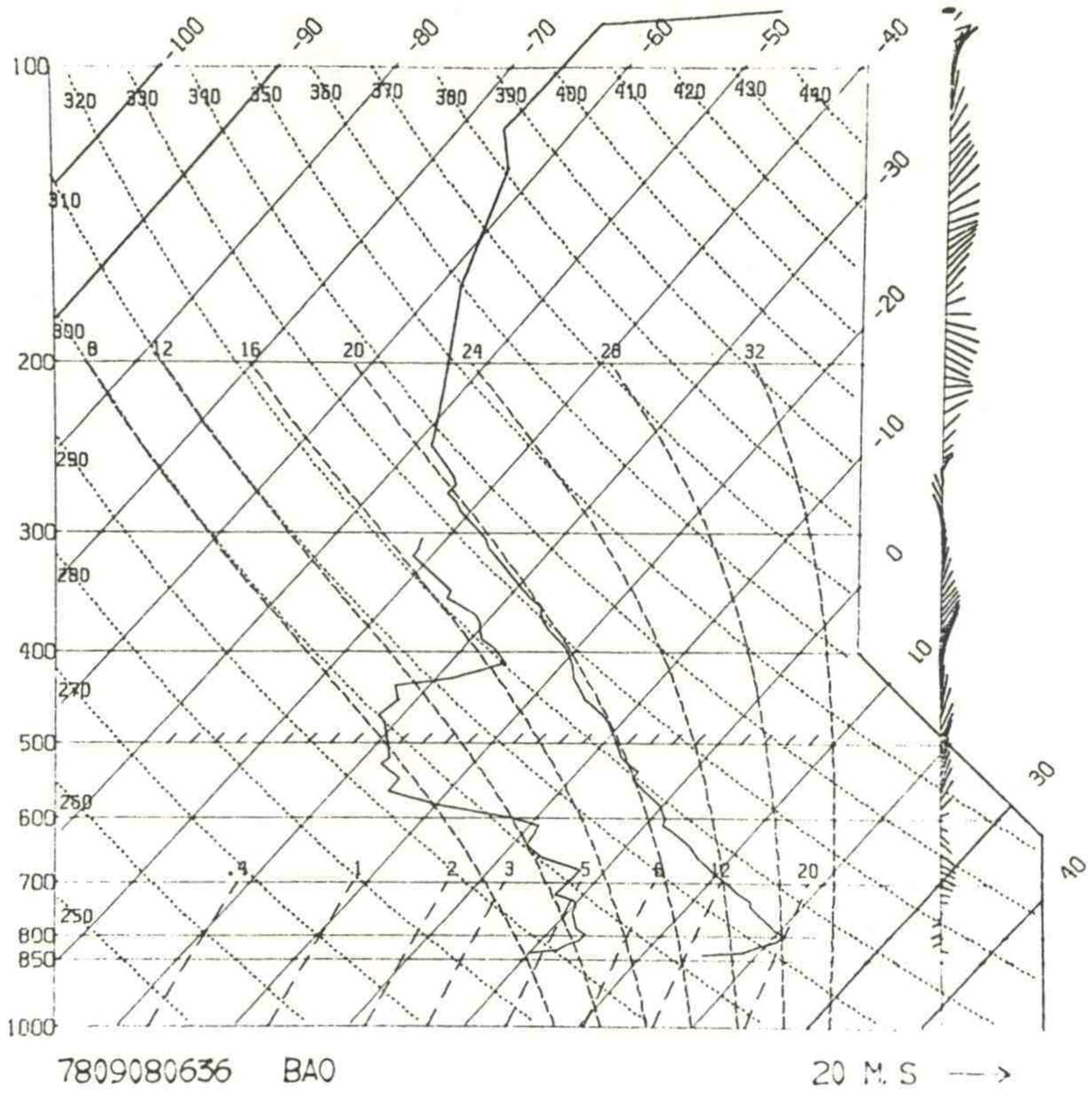


Figure 11.7.--PHOENIX rawinsonde flight number 7.

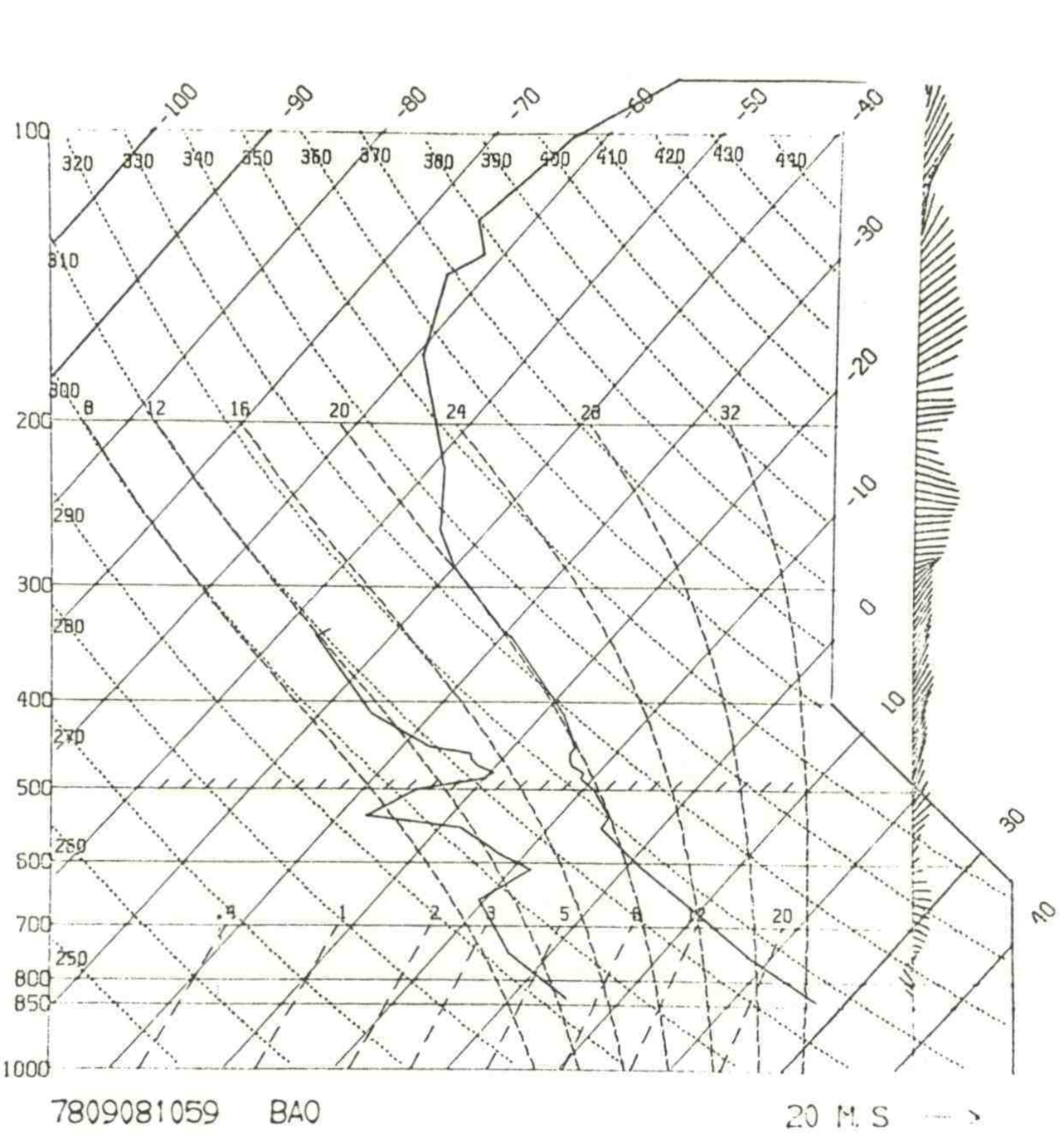


Figure 11.8.--PHOENIX rawinsonde flight number 8.

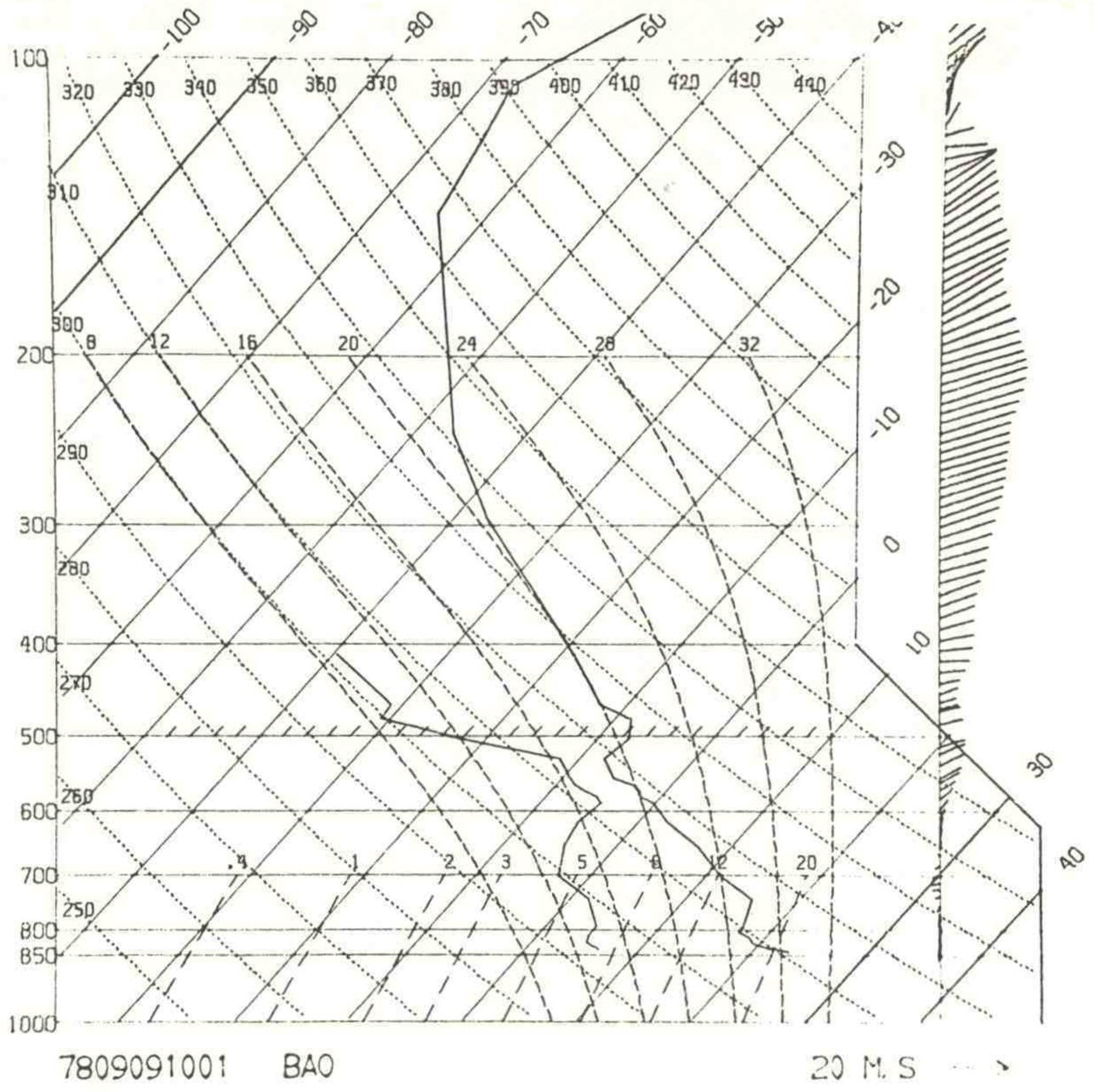


Figure 11.9.--PHOENIX rawinsonde flight number 9.

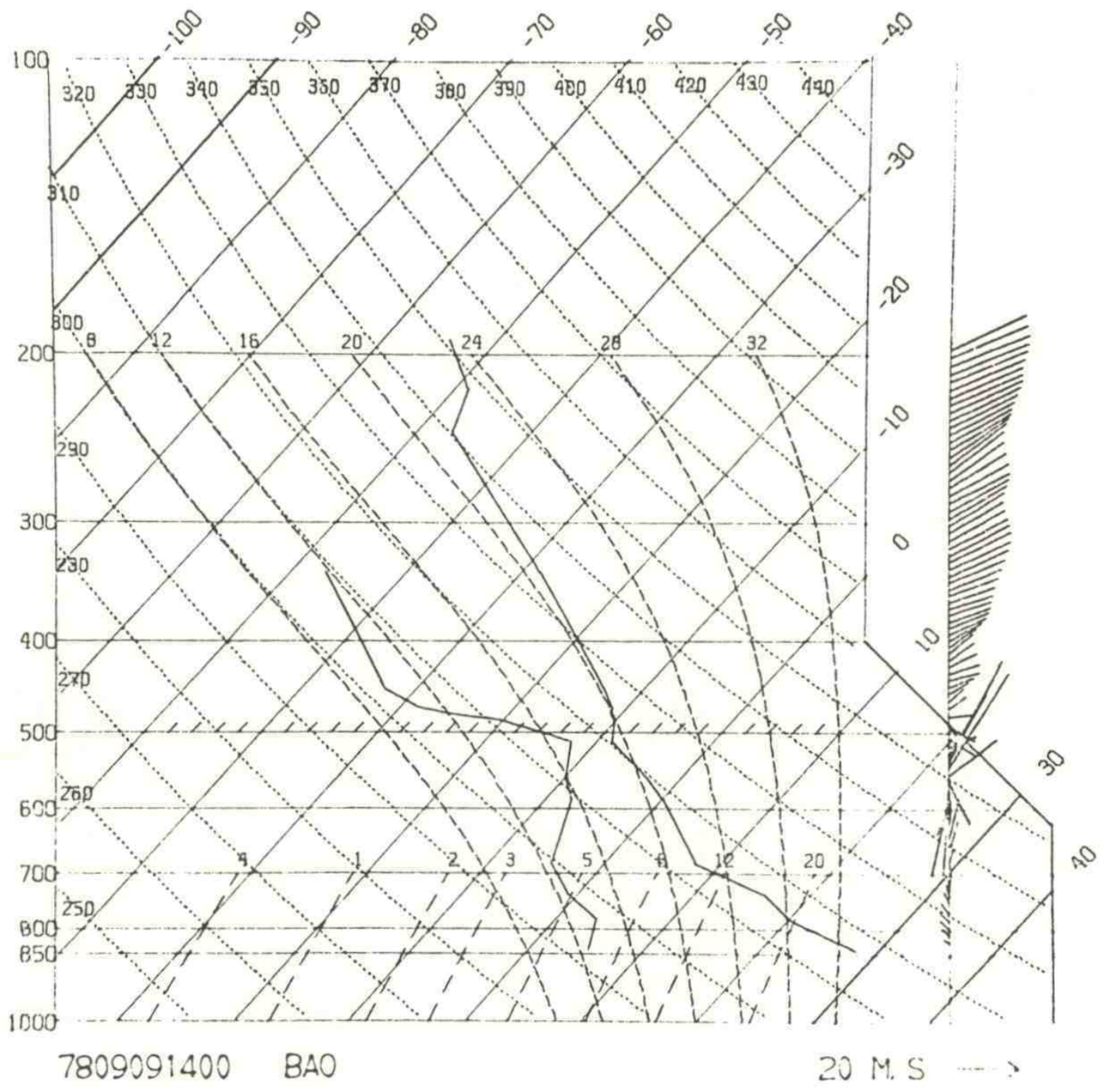


Figure 11.10.--PHOENIX rawinsonde flight number 10.

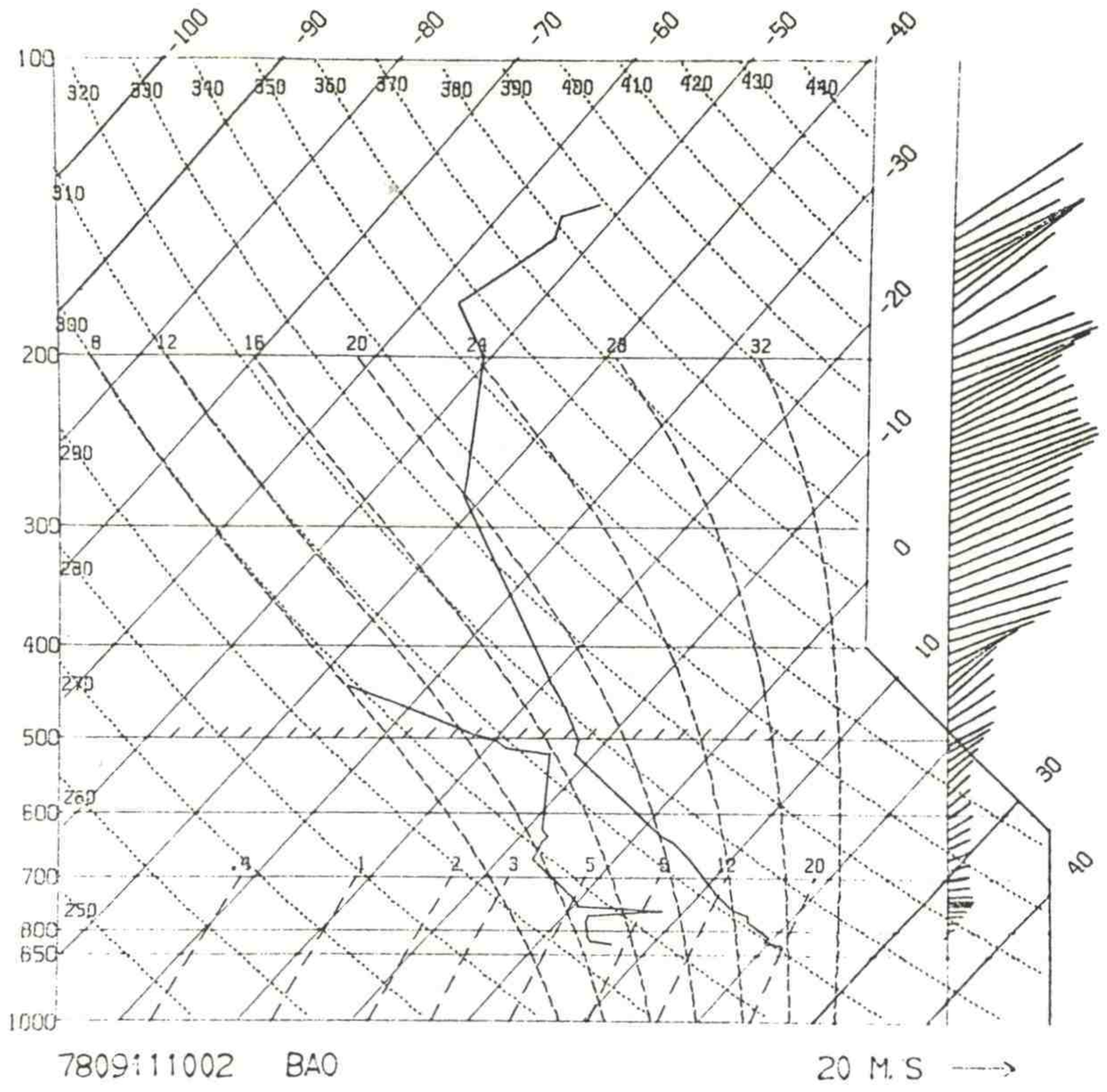


Figure 11.11.--PHOENIX rawinsonde flight number 11.

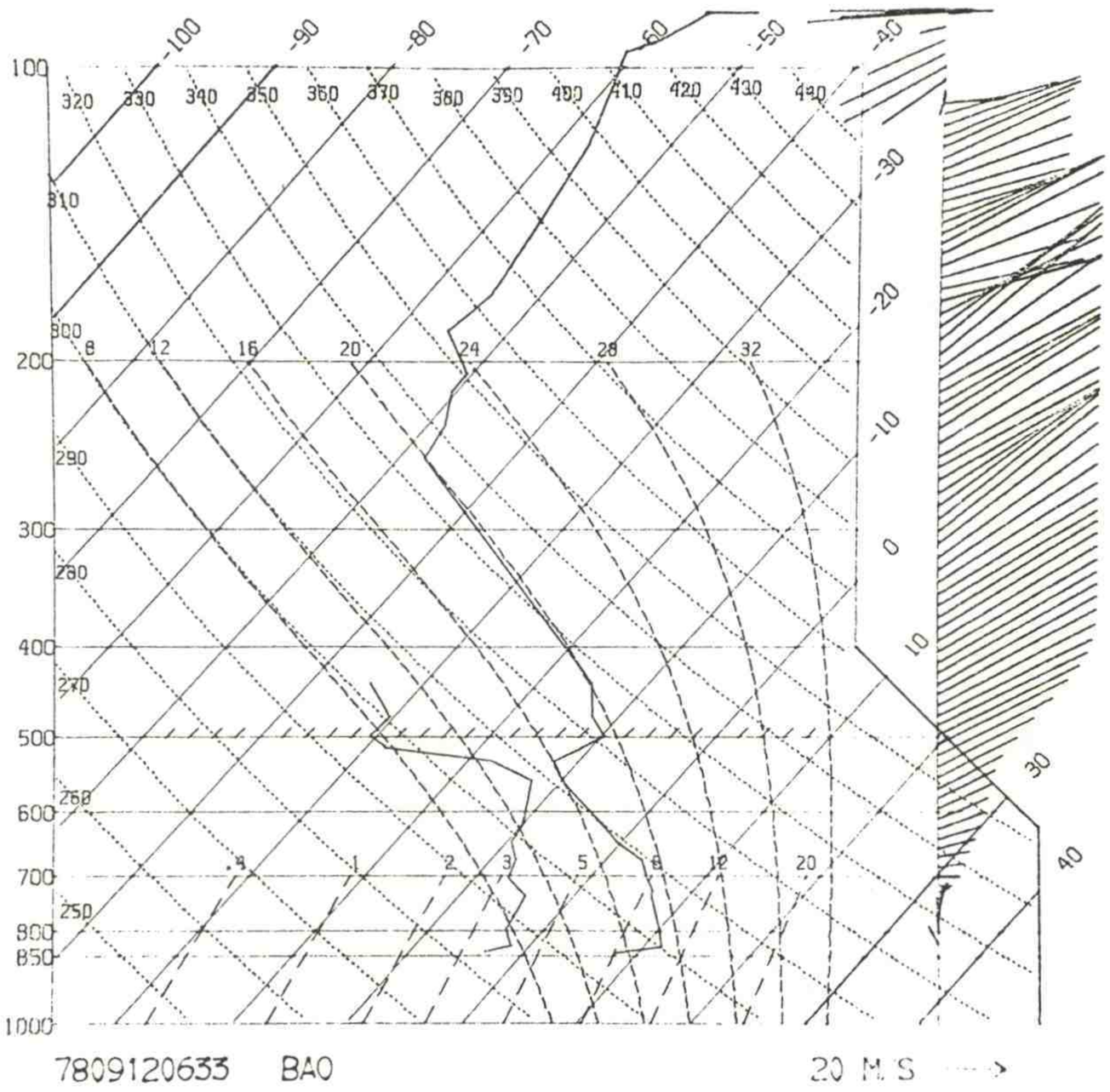


Figure 11.12.--PHOENIX rawinsonde flight number 12.



Figure 11.13.--PHOENIX rawinsonde flight number 13.

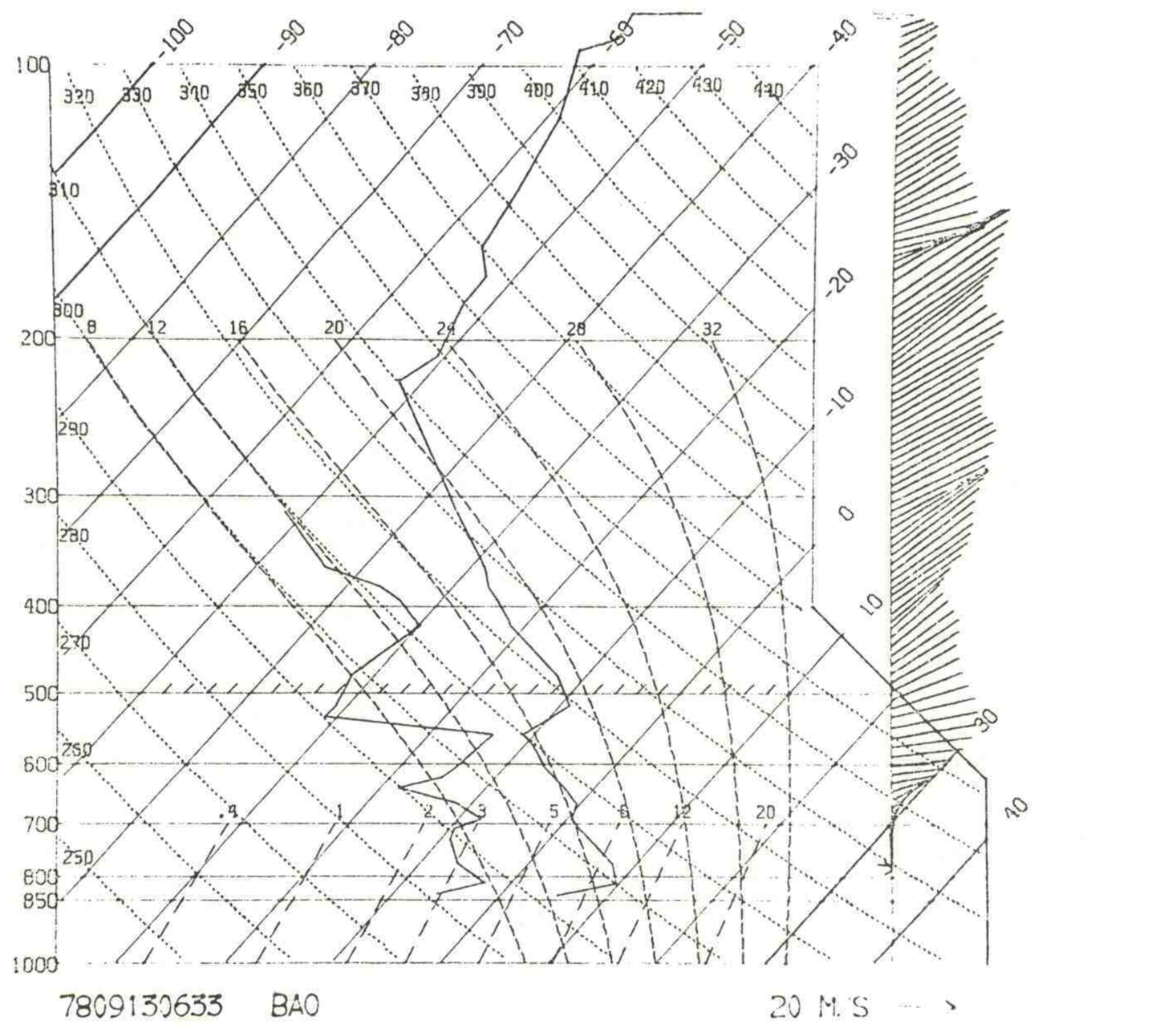


Figure 11.14.--PHOENIX rawinsonde flight number 14.

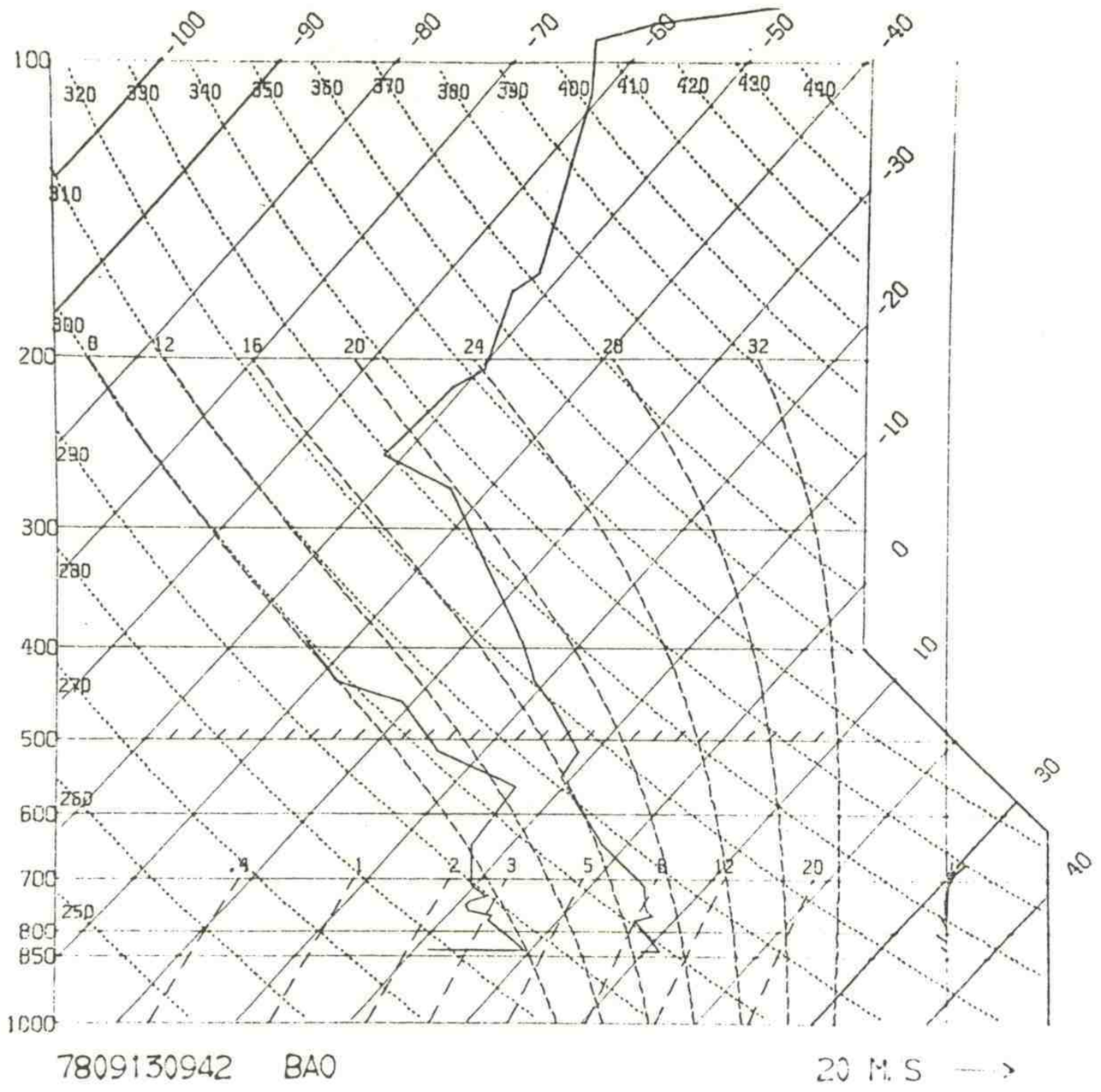


Figure 11.15.--PHOENIX rawinsonde flight number 15.

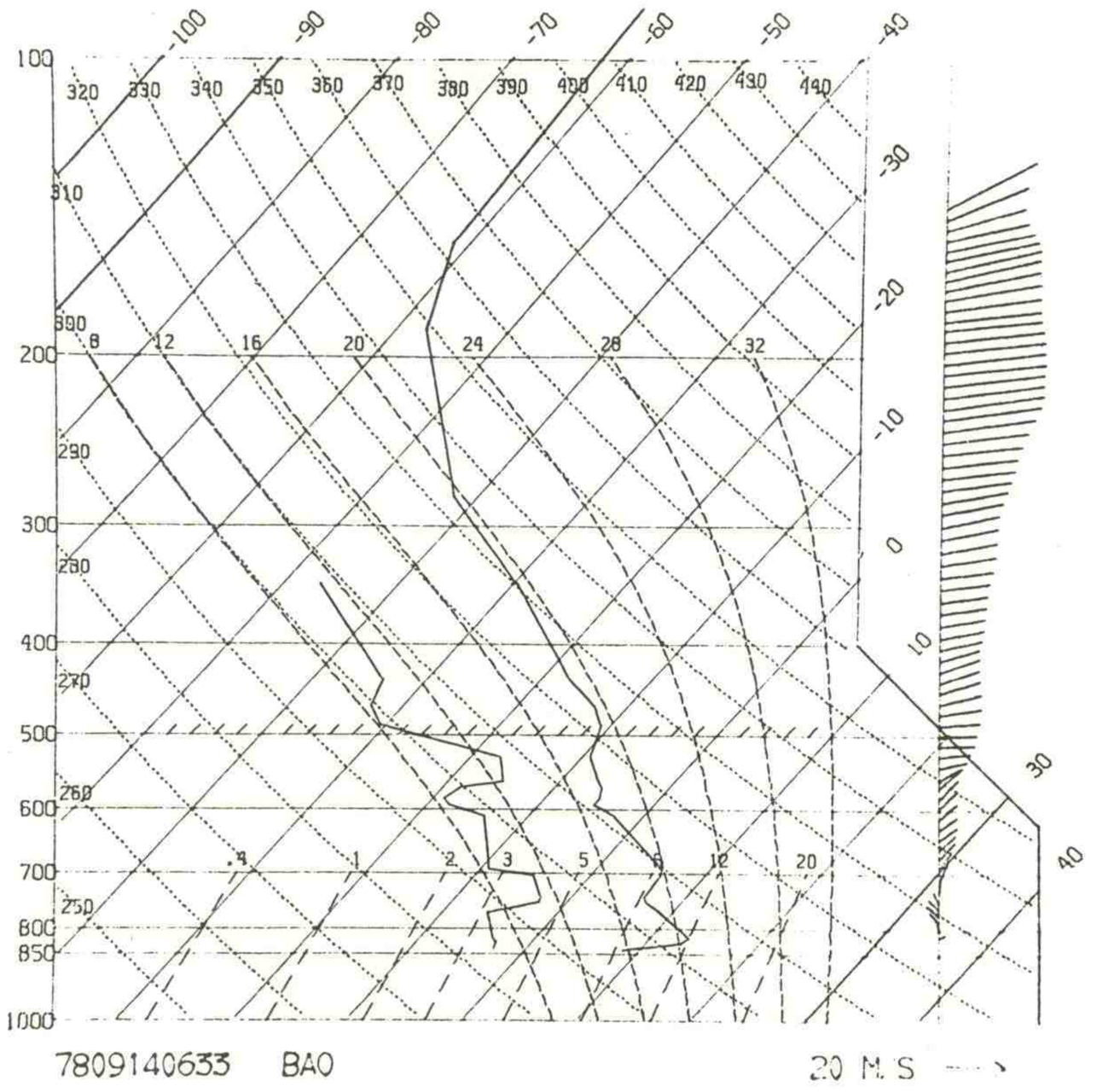


Figure 11.16.--PHOENIX rawinsonde flight number 16.

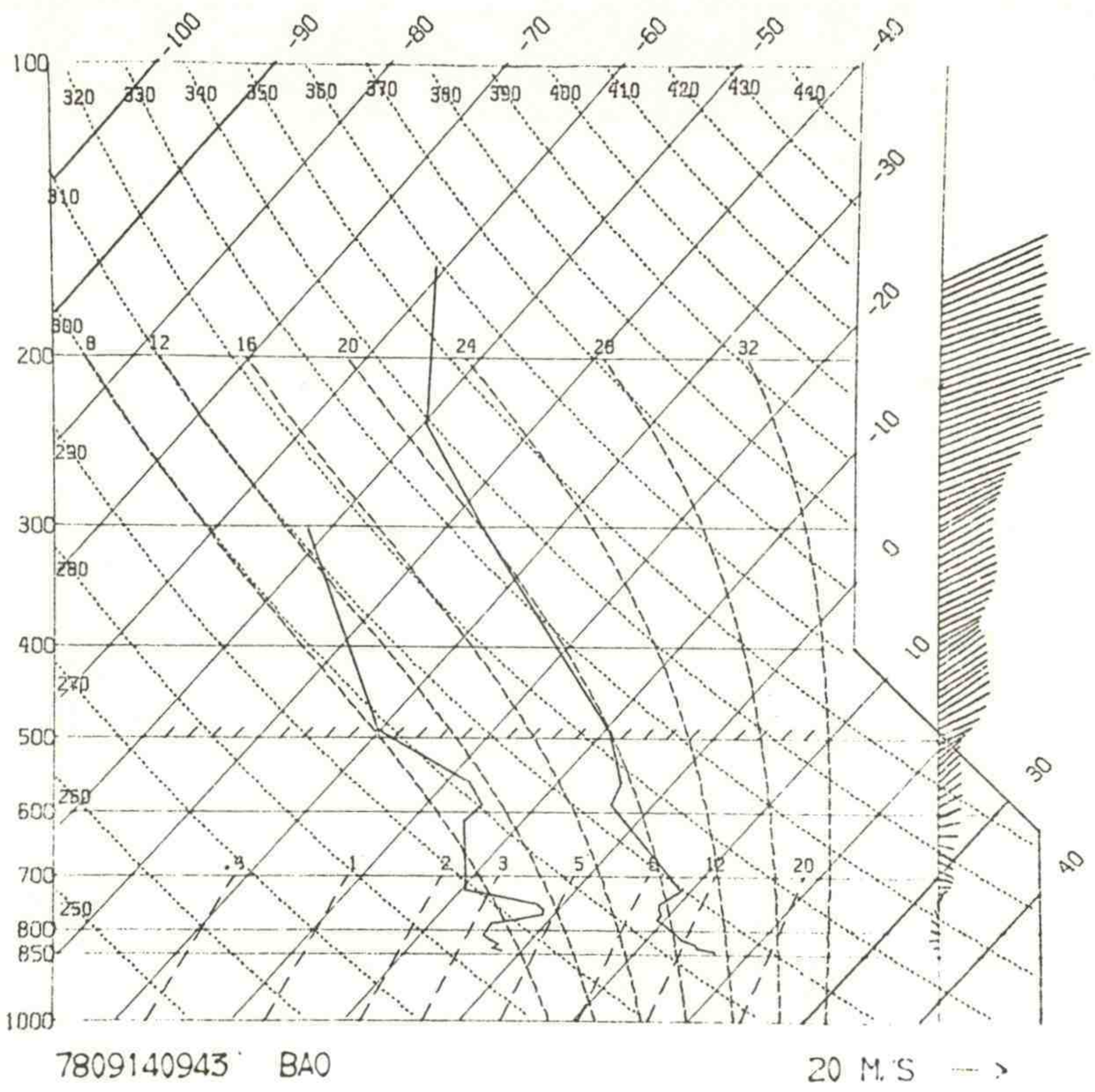


Figure 11.17.--PHOENIX rawinsonde flight number 17.

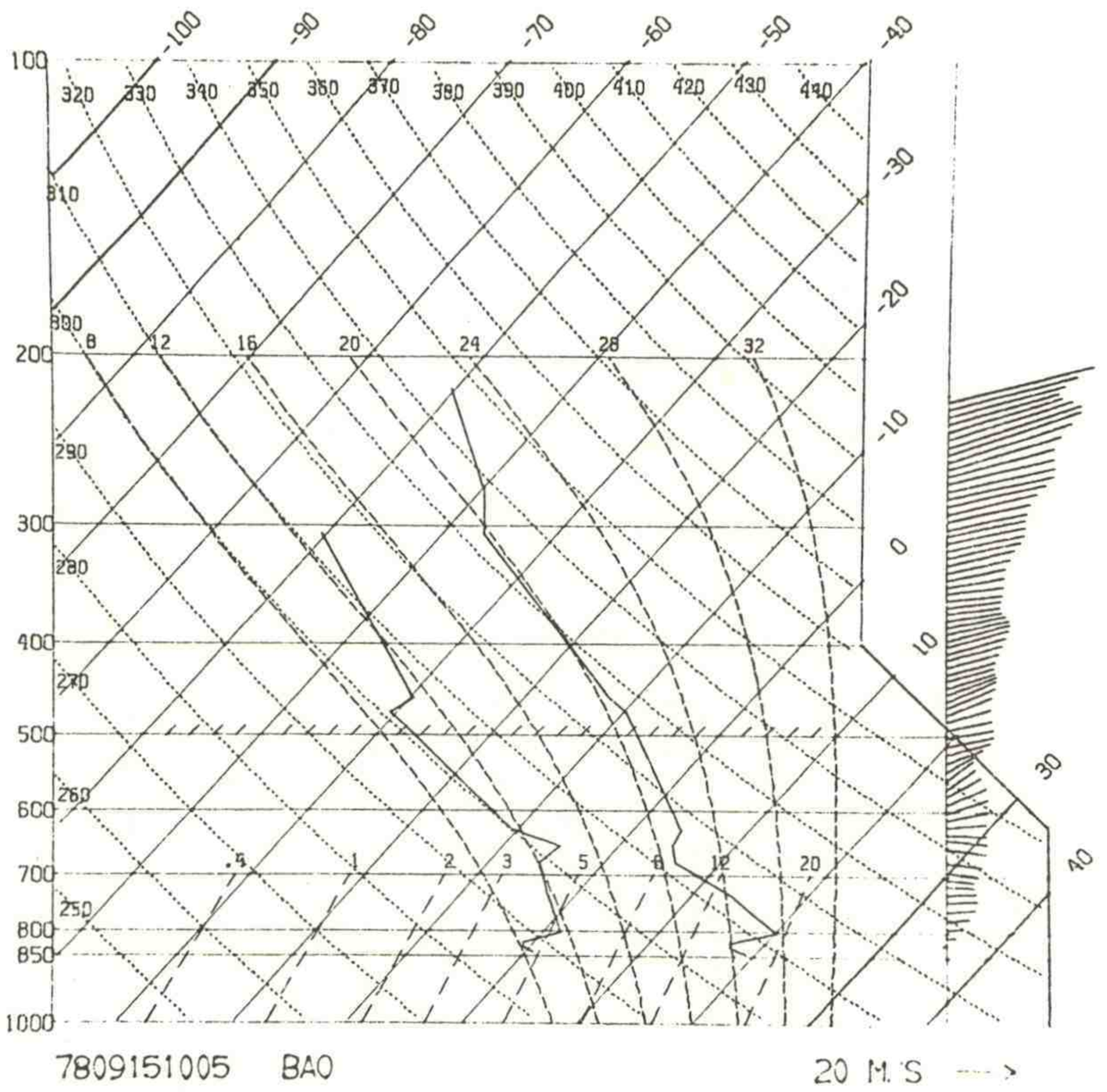


Figure 11.18.--PHOENIX rawinsonde flight number 18.

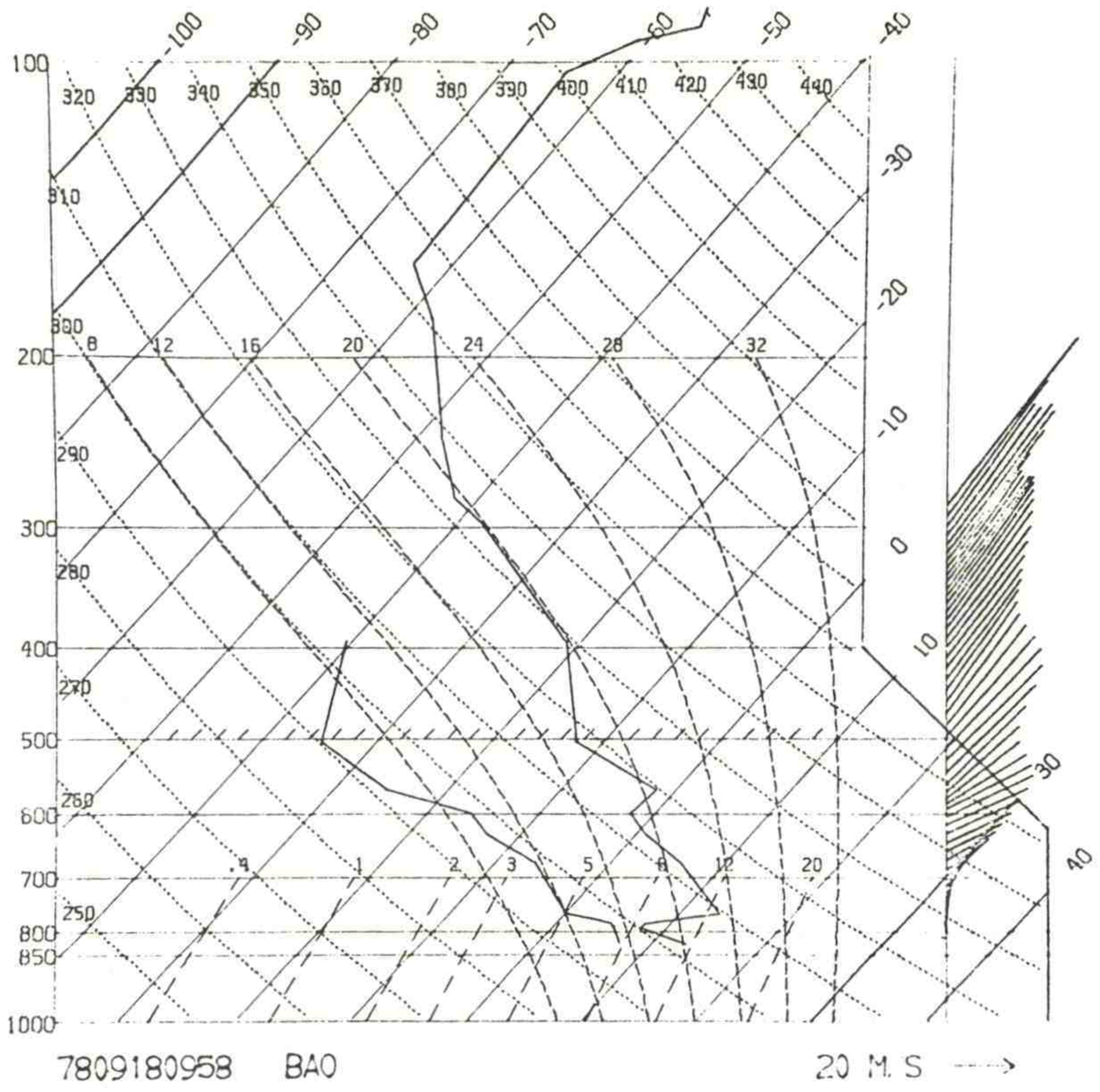


Figure 11.19.--PHOENIX rawinsonde flight number 19.

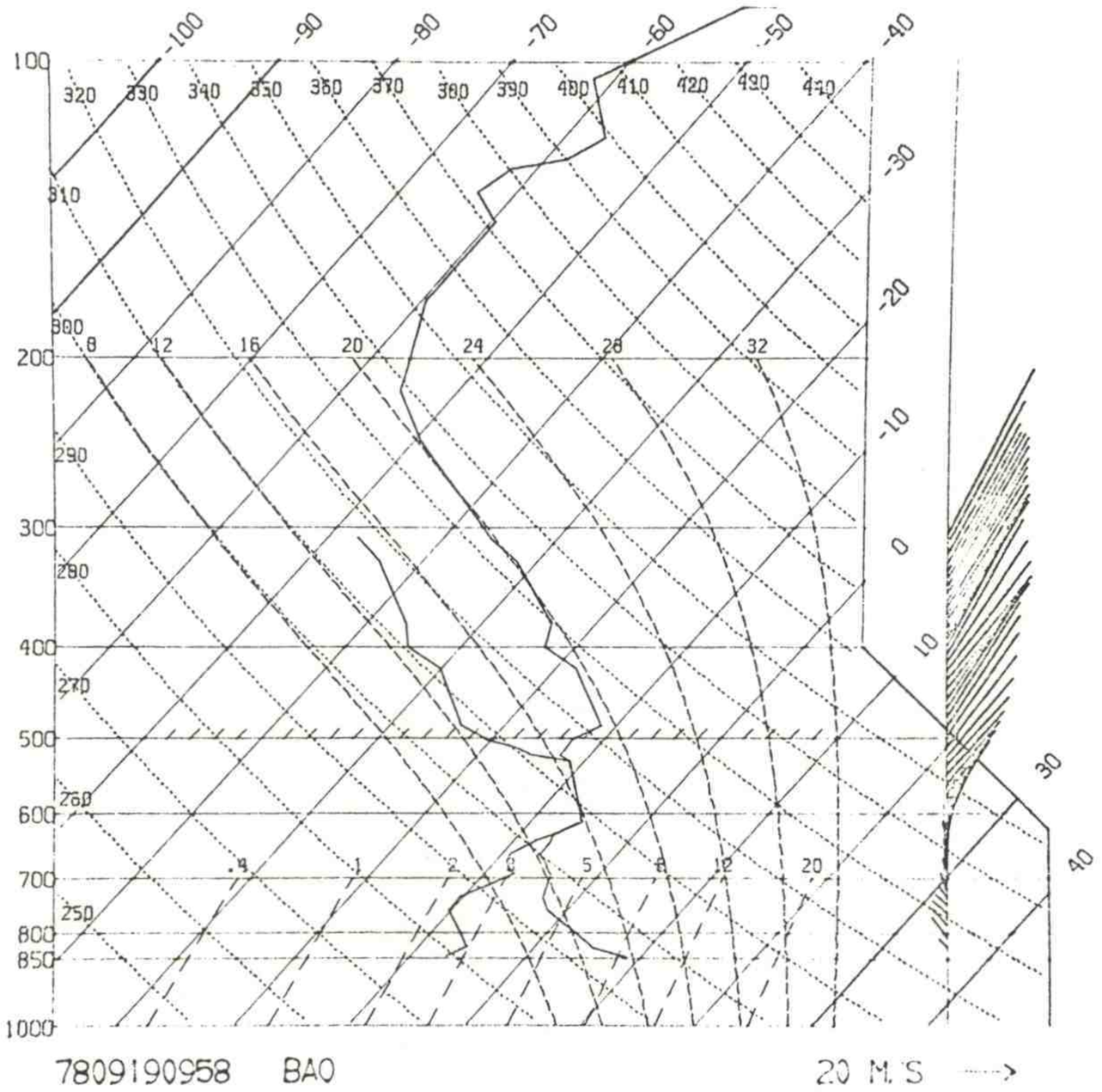


Figure 11.20.--PHOENIX rawinsonde flight number 20.

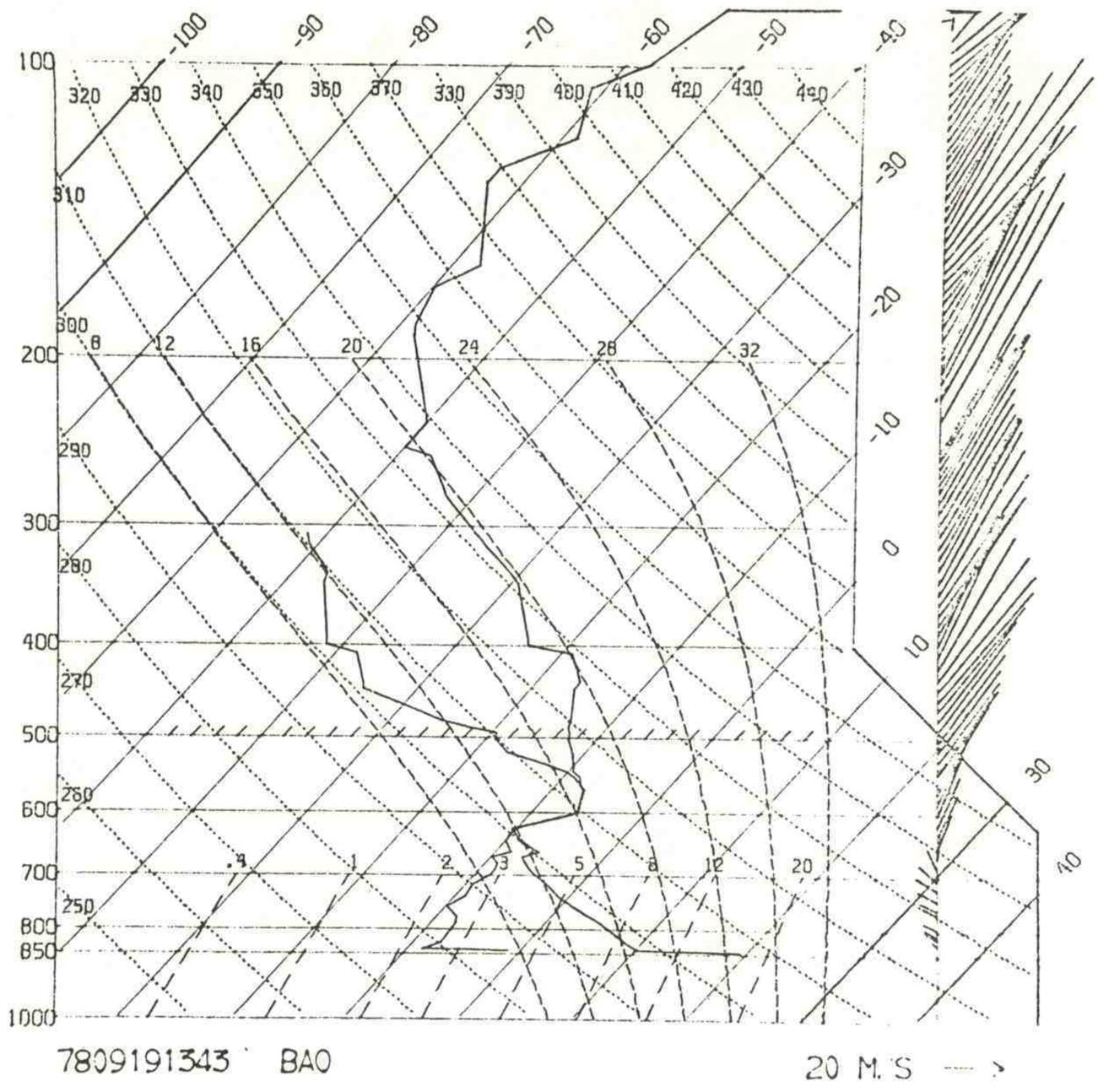


Figure 11.21.--PHOENIX rawinsonde flight number 21.

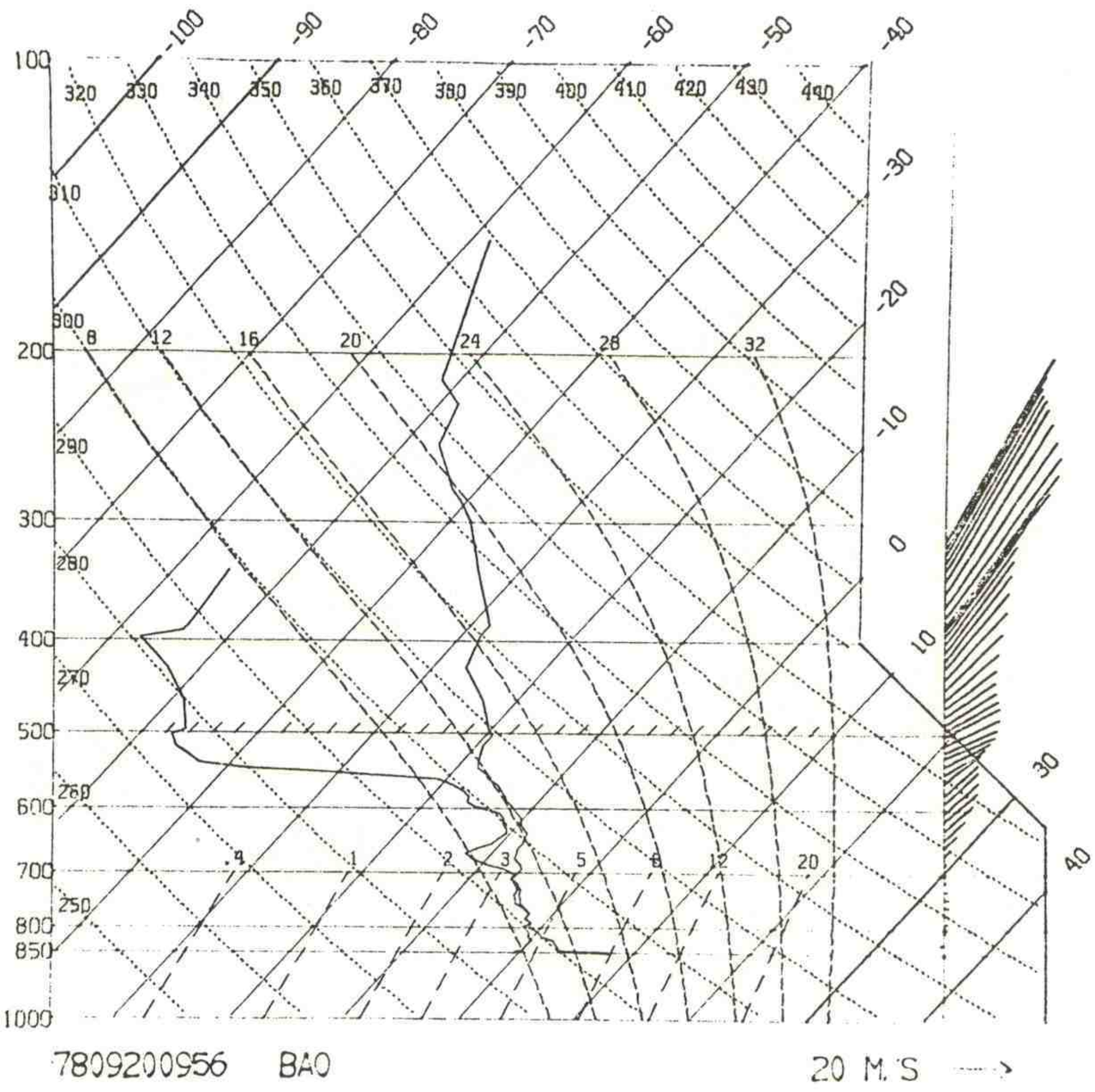


Figure 11.22.--PHOENIX rawinsonde flight number 22.

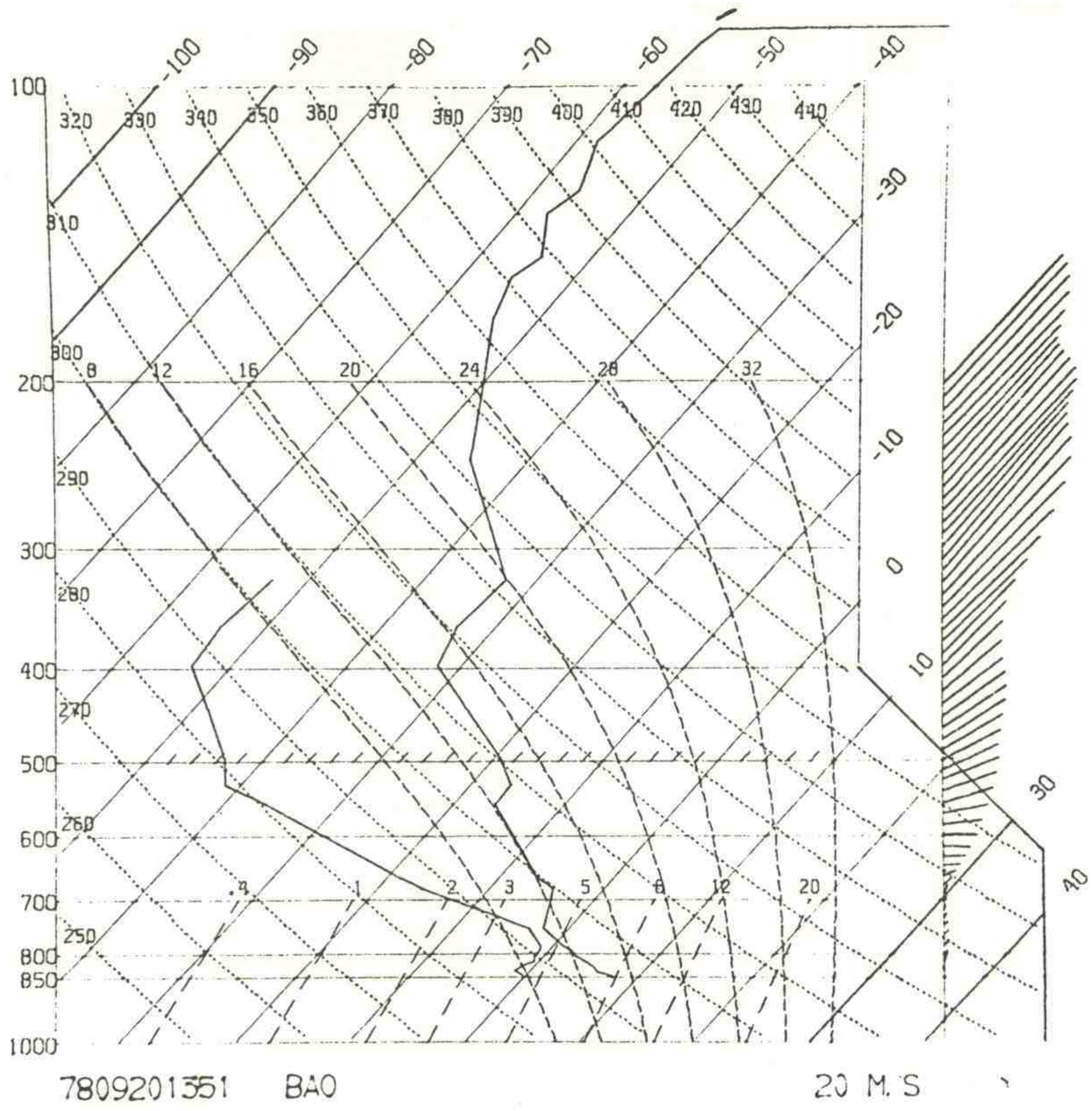


Figure 11.23.--PHOENIX rawinsonde flight number 23.

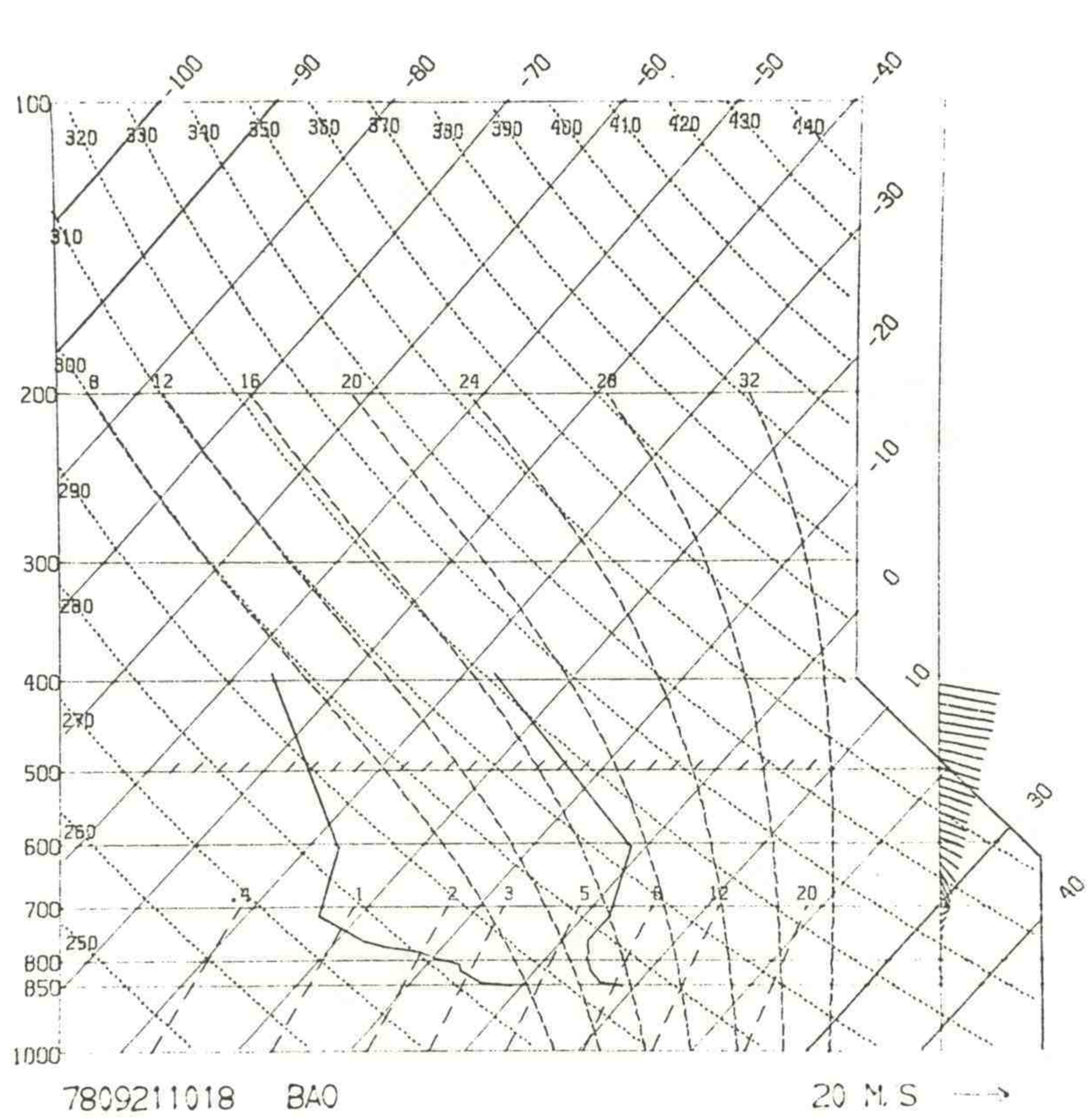


Figure 11.24.--PHOENIX rawinsonde flight number 24.

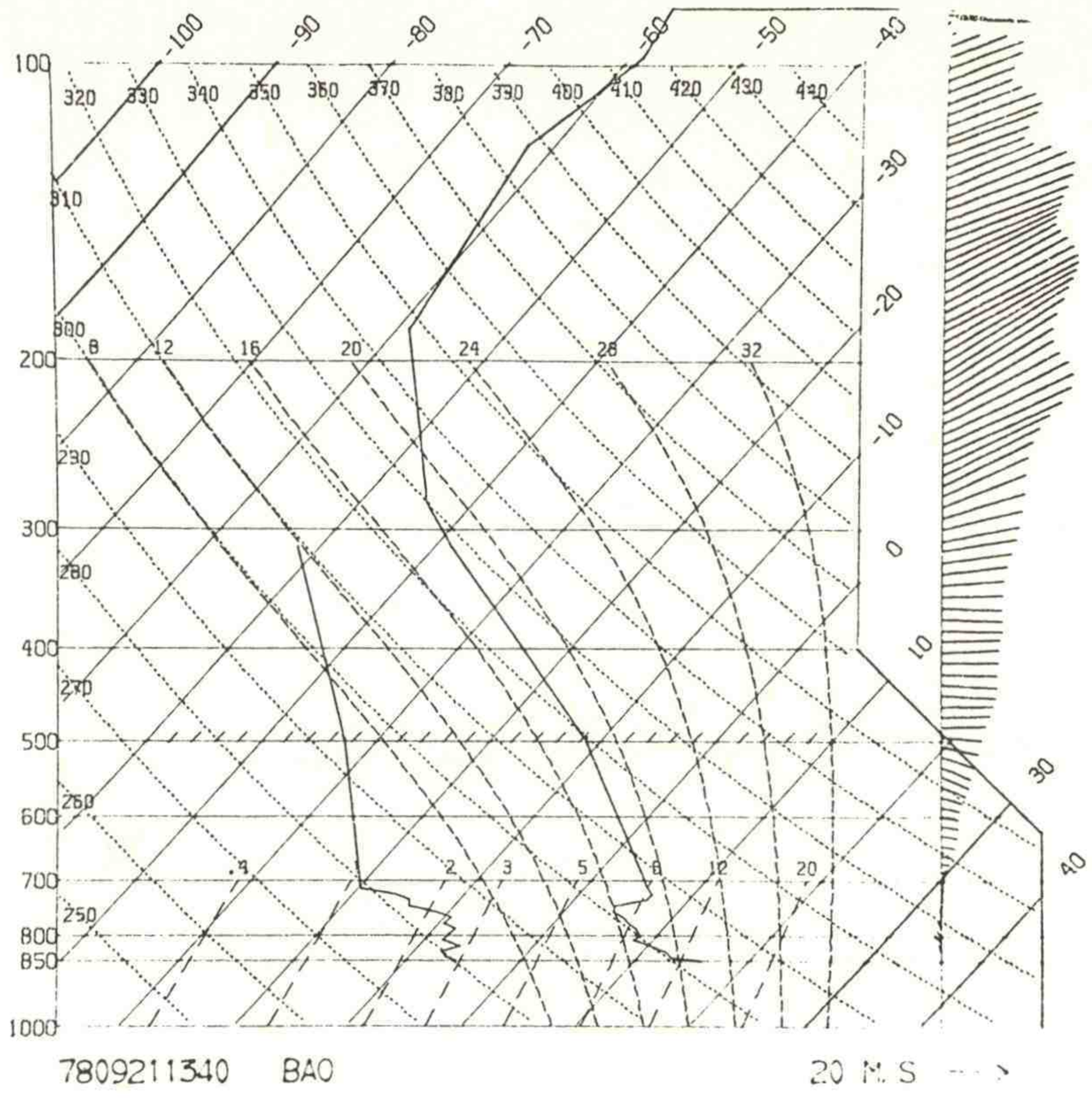


Figure 11.25.--PHOENIX rawinsonde flight number 25.

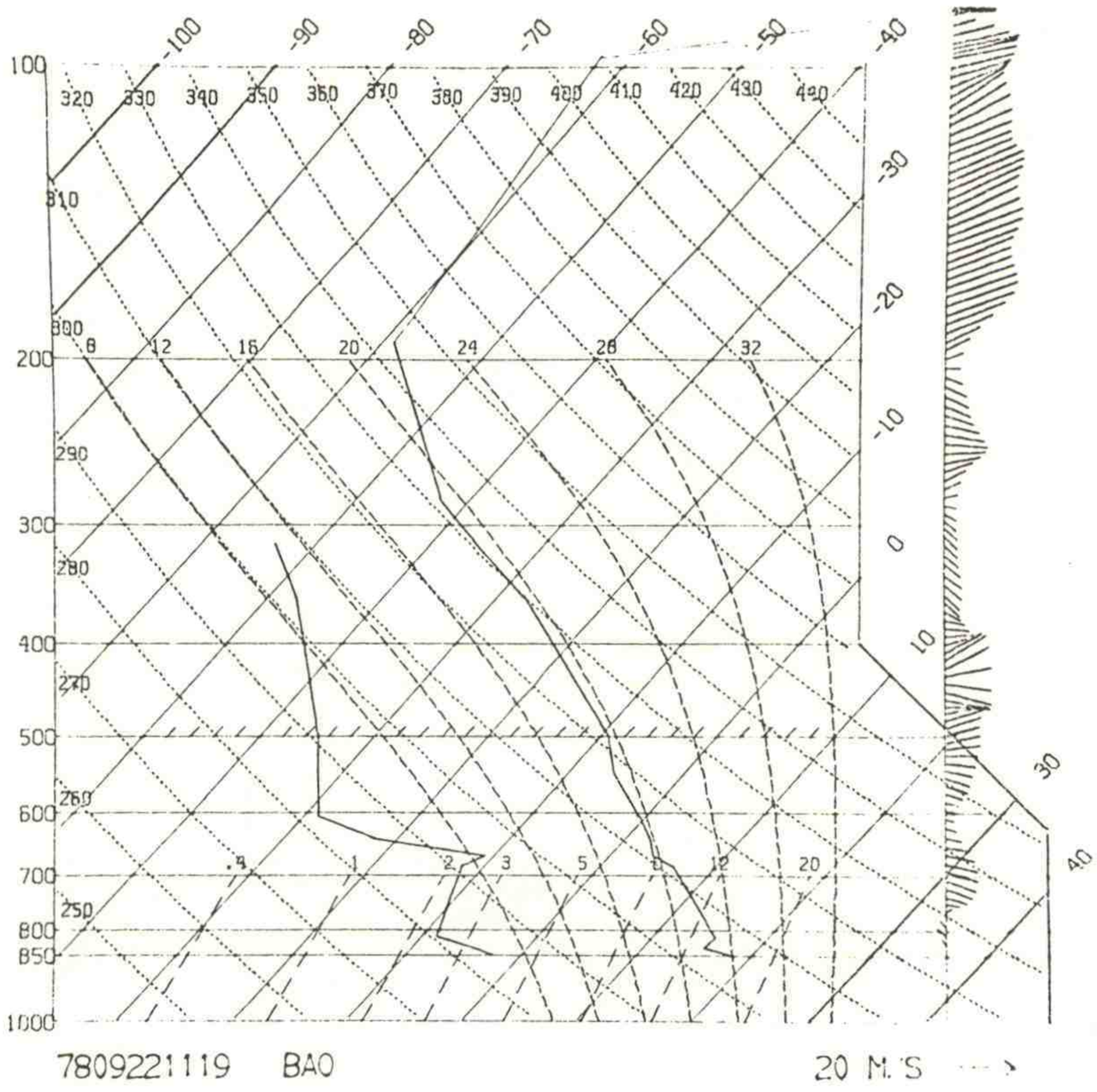


Figure 11.26.--PHOENIX rawinsonde flight number 26.

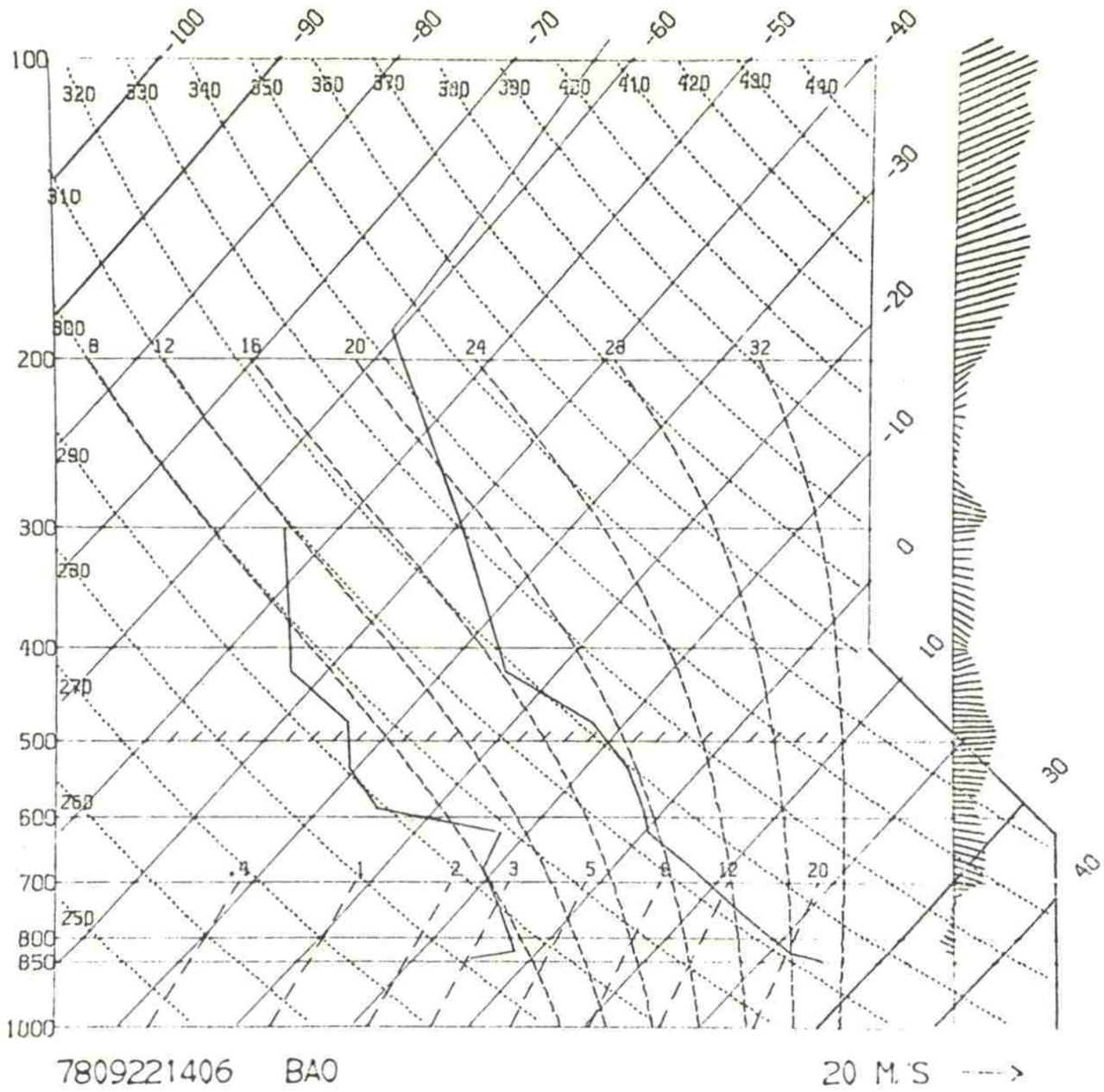


Figure 11.27.--PHOENIX rawinsonde flight number 27.

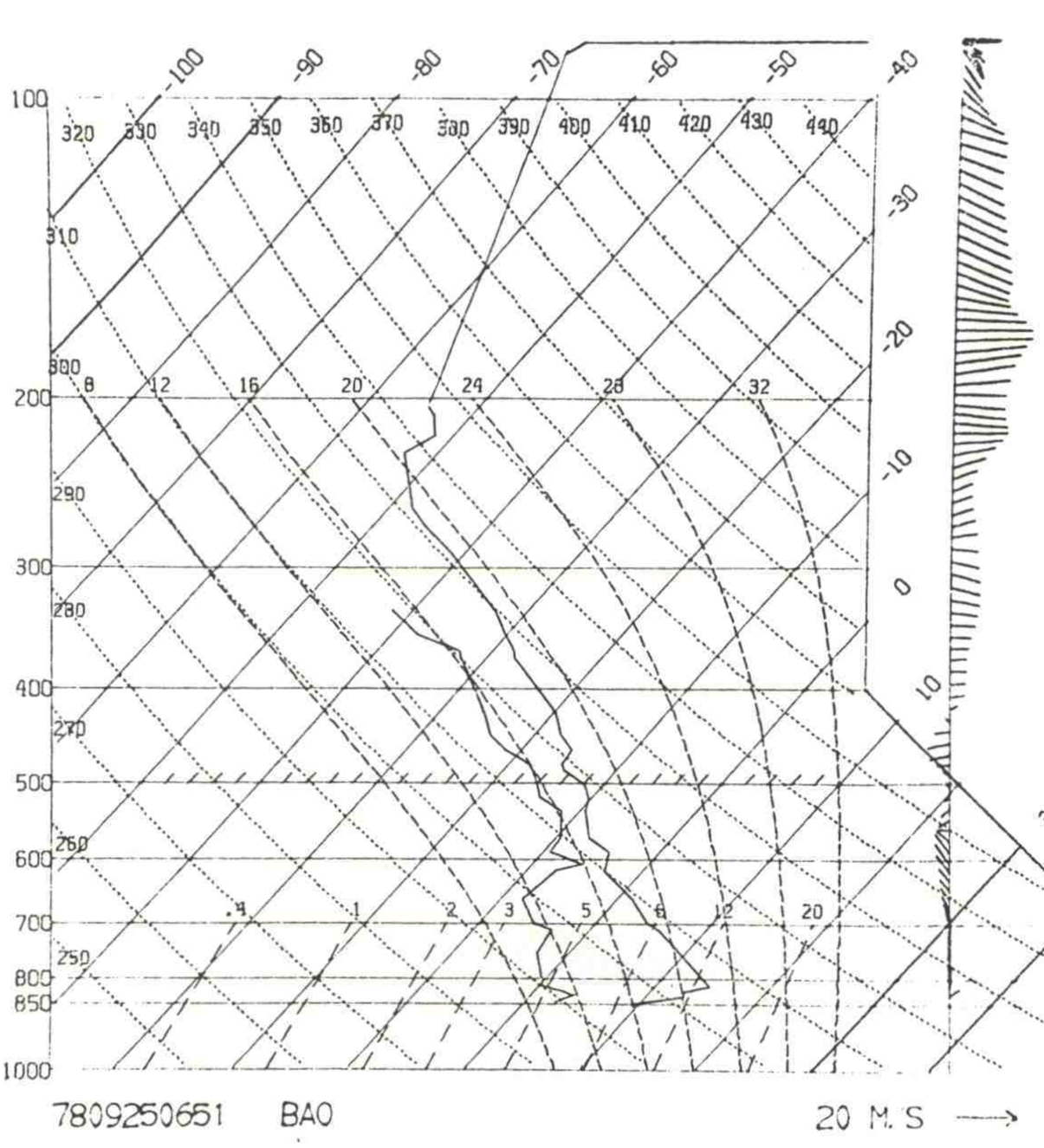


Figure 11.28.--PHOENIX rawinsonde flight number 28.

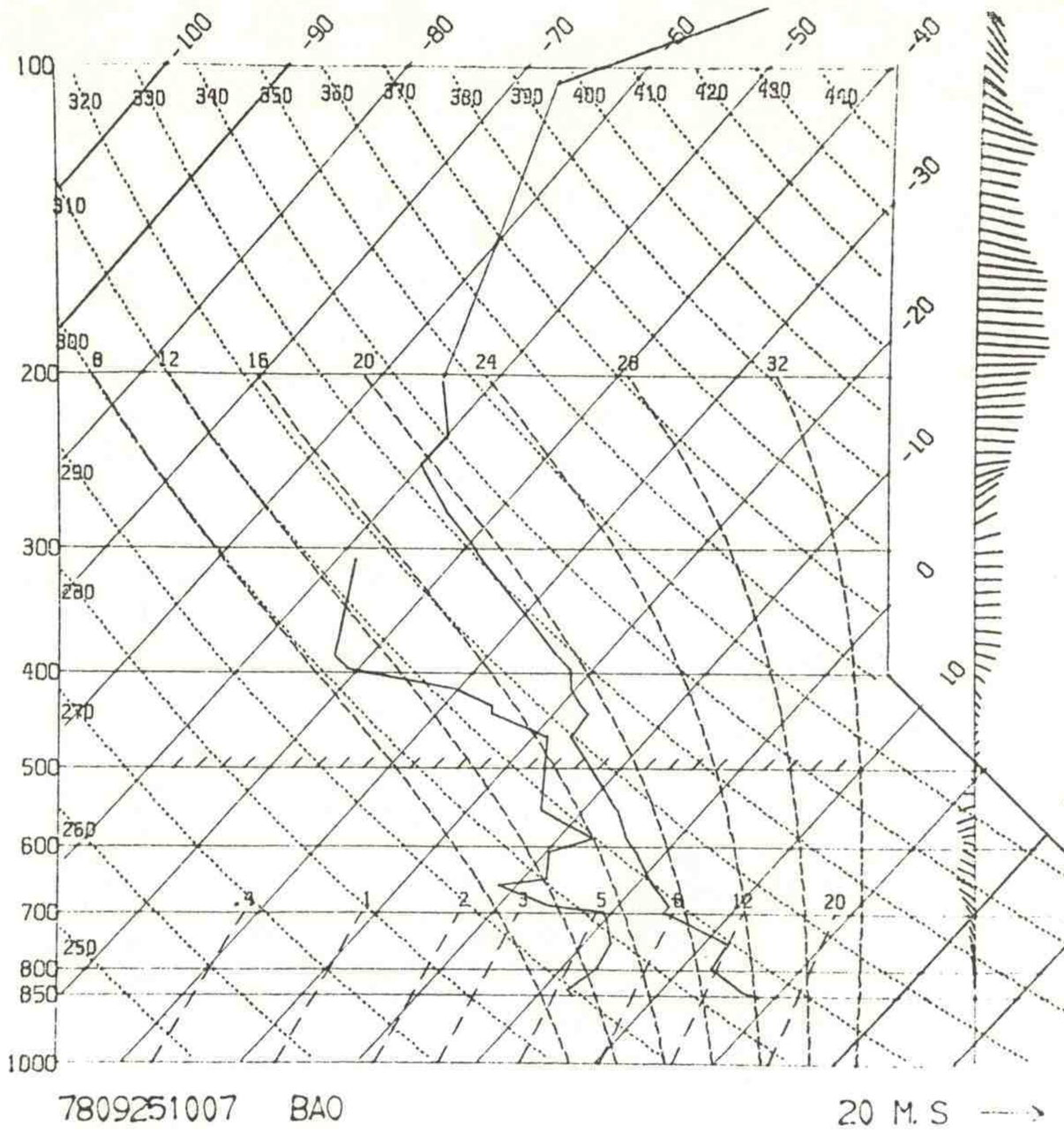


Figure 11.29.--PHOENIX rawinsonde flight number 29.

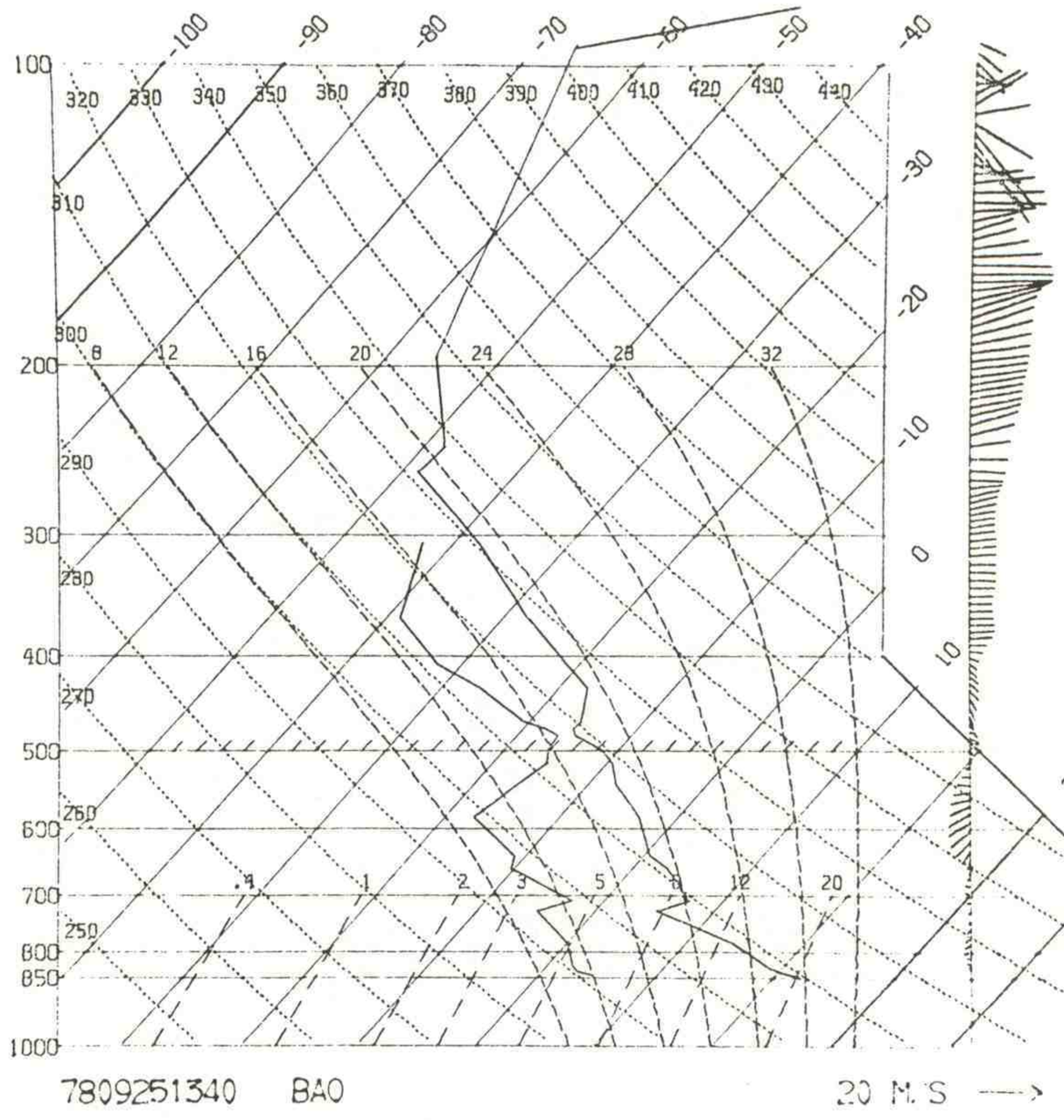


Figure 11.30.--PHOENIX rawinsonde flight number 30.

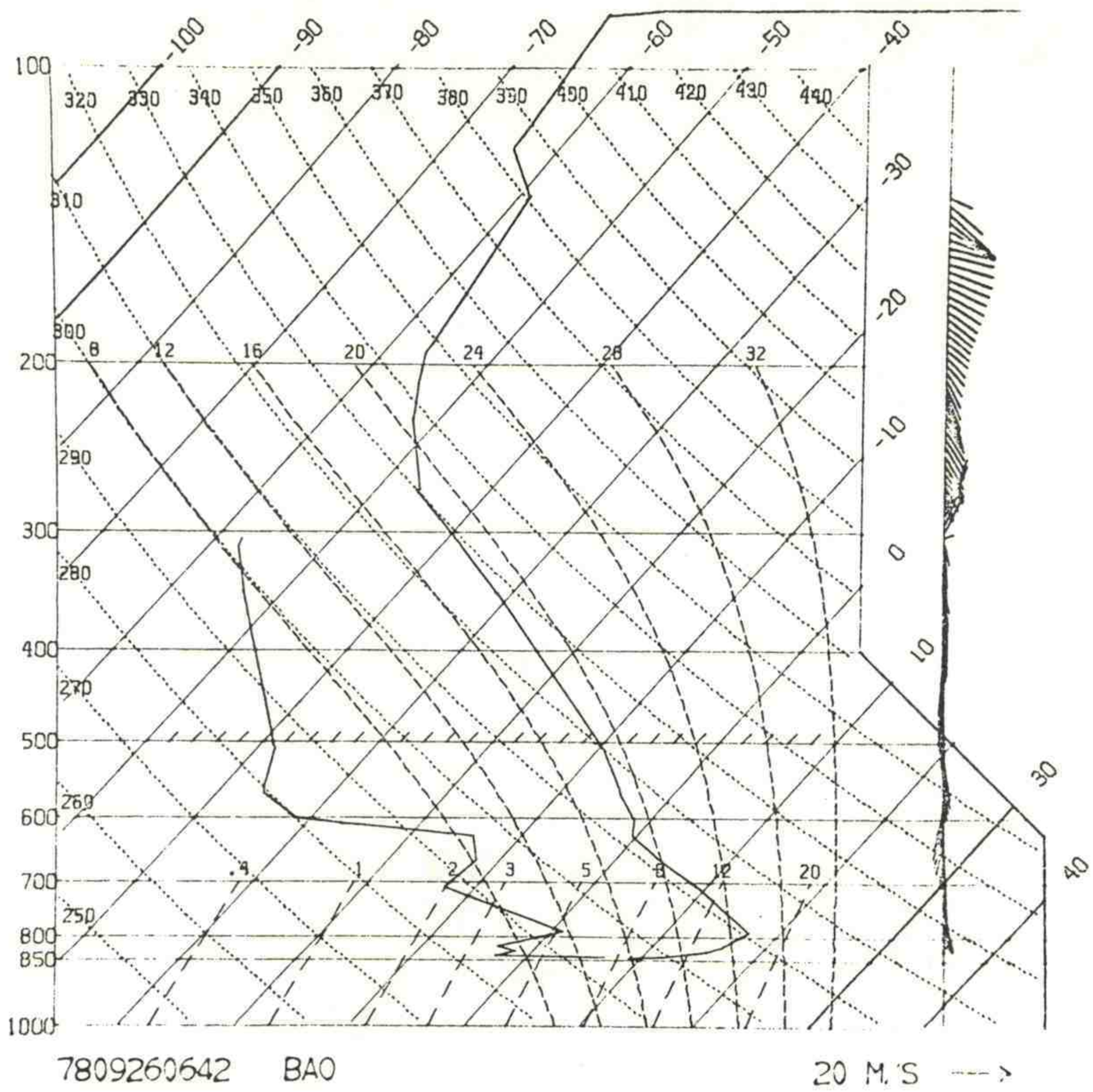


Figure 11.31.--PHOENIX rawinsonde flight number 31.

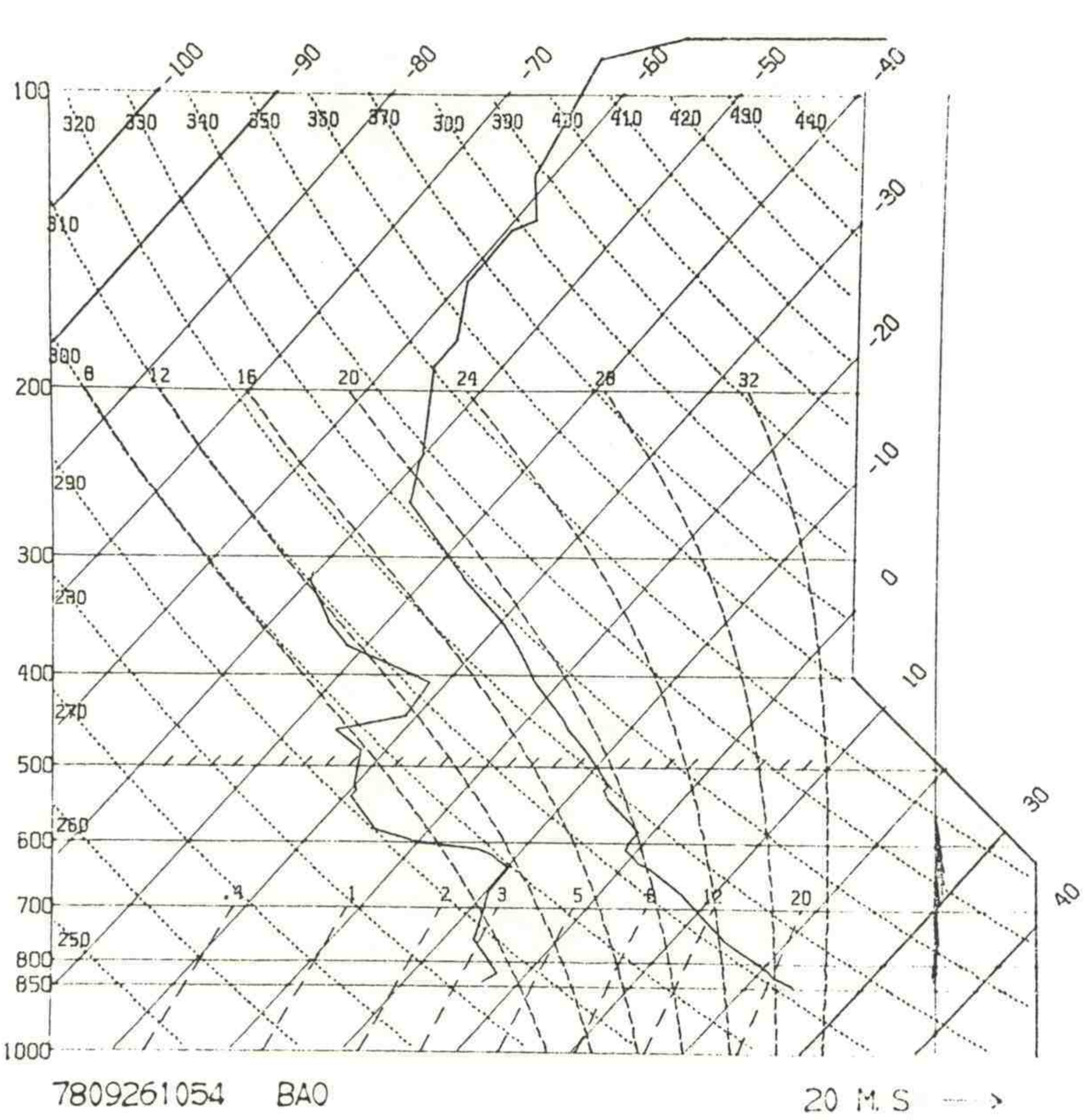


Figure 11.32.--PHOENIX rawinsonde flight number 32.

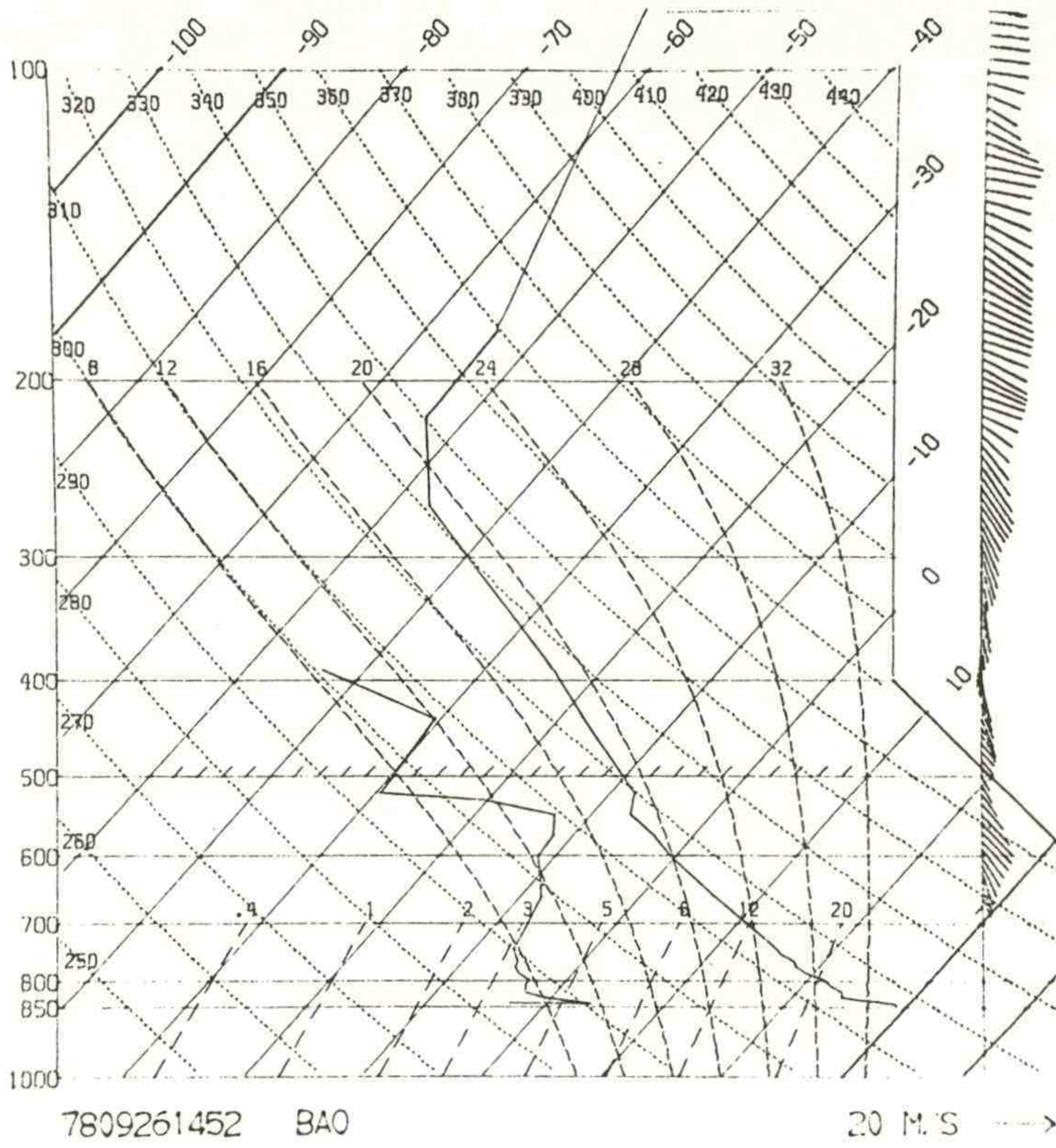


Figure 11.33.--PHOENIX rawinsonde flight number 33.

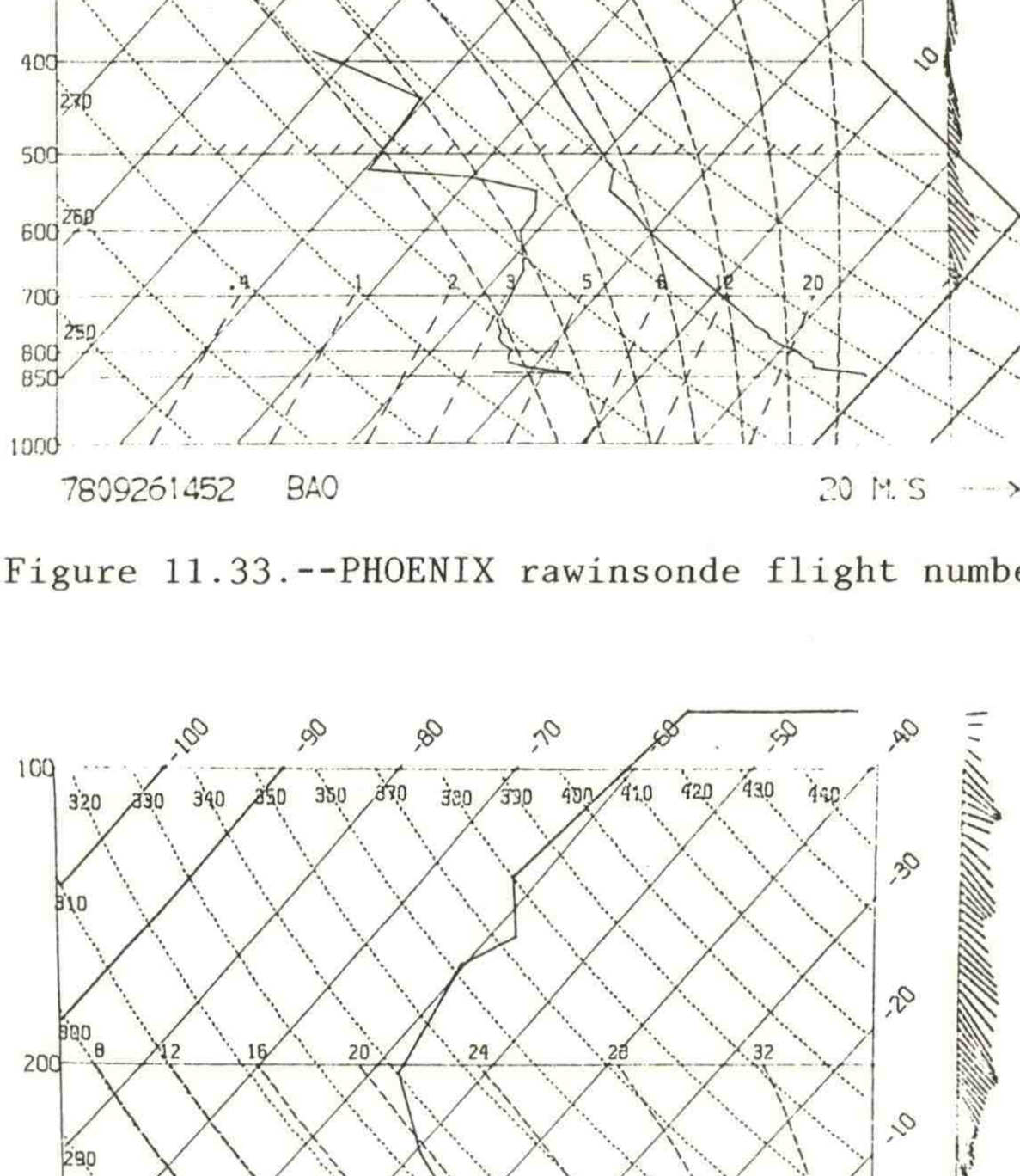


Figure 11.34.--PHOENIX rawinsonde flight number 34.

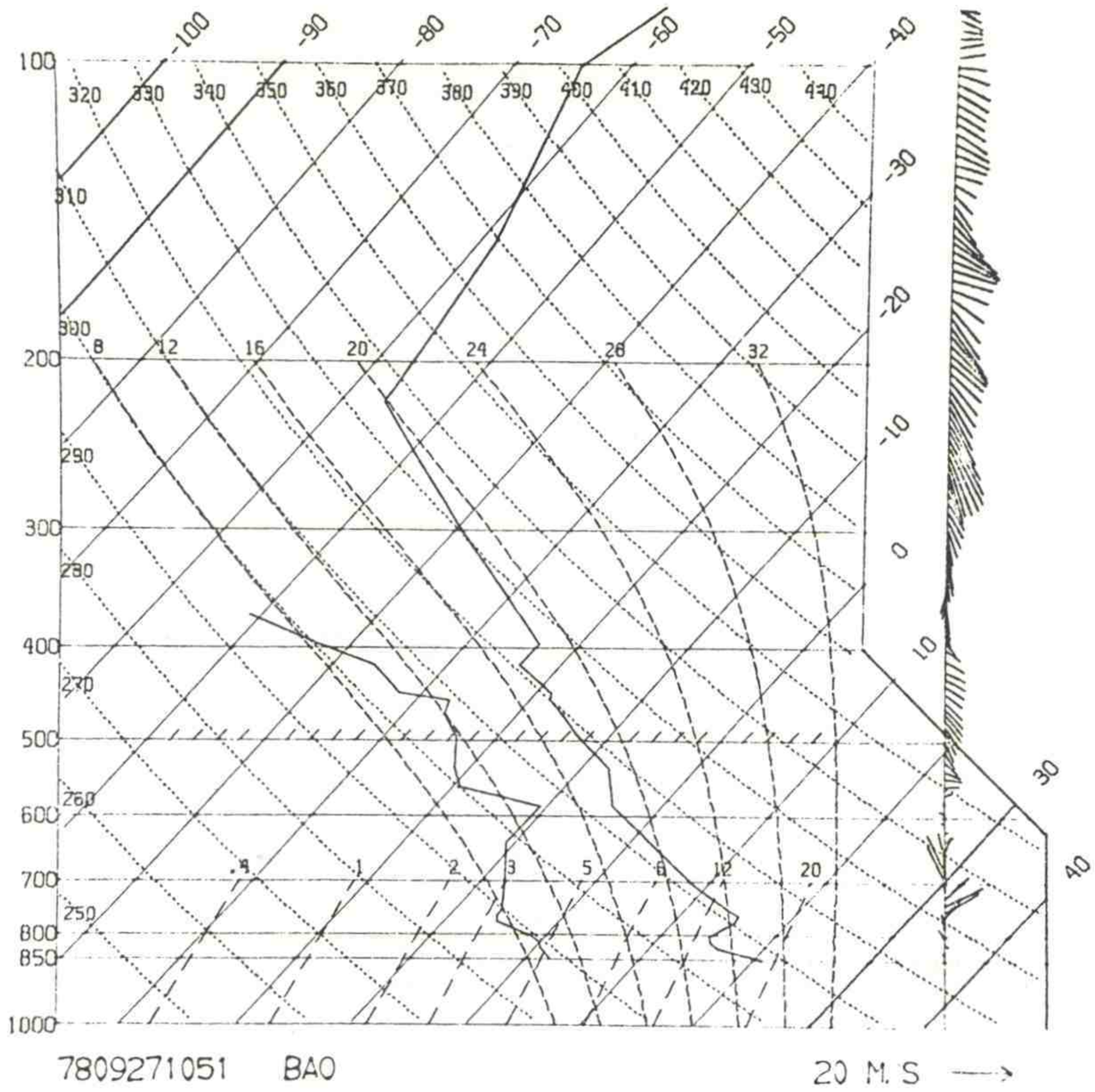


Figure 11.35.--PHOENIX rawinsonde flight number 35.

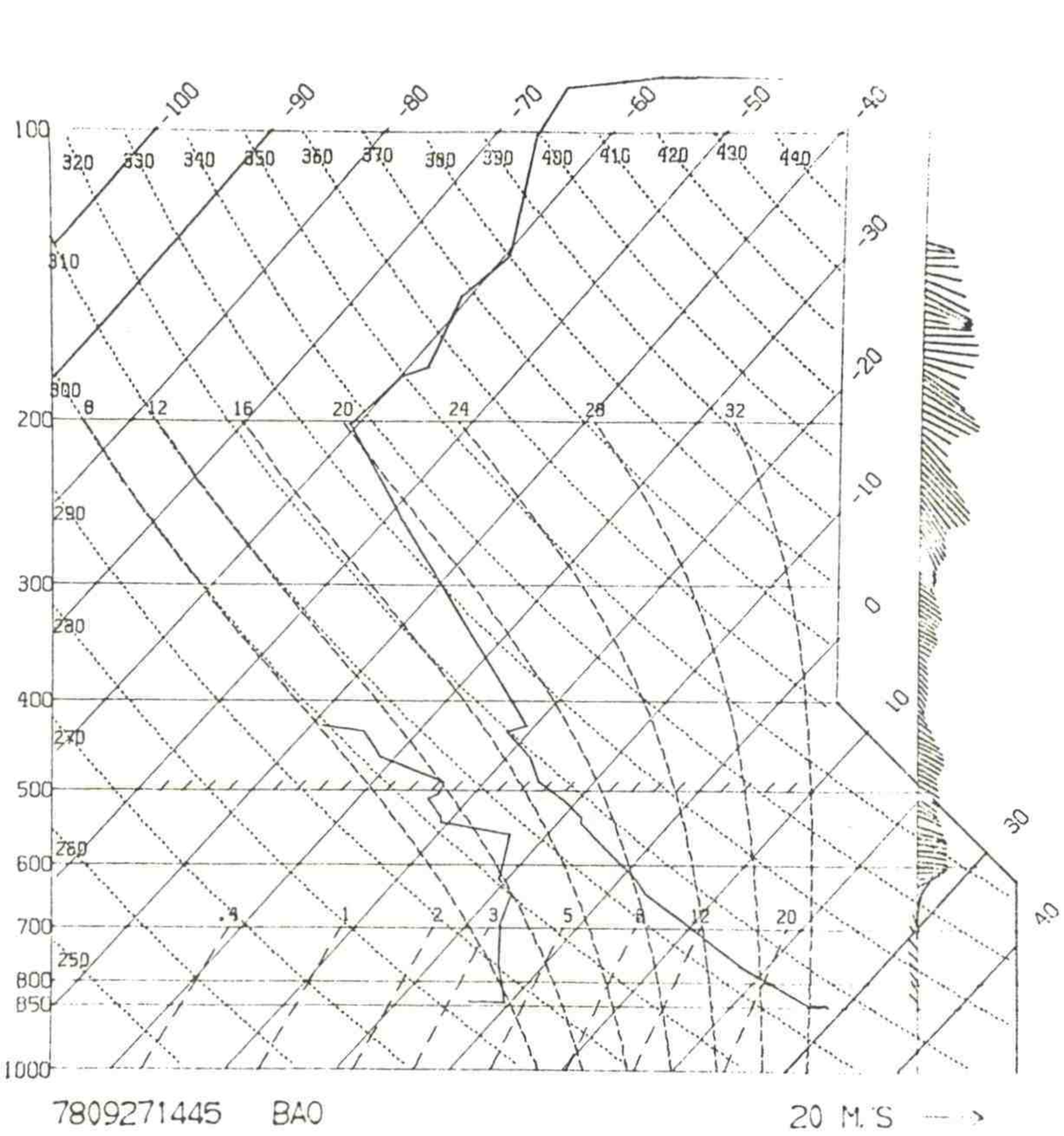


Figure 11.36.--PHOENIX rawinsonde flight number 36.

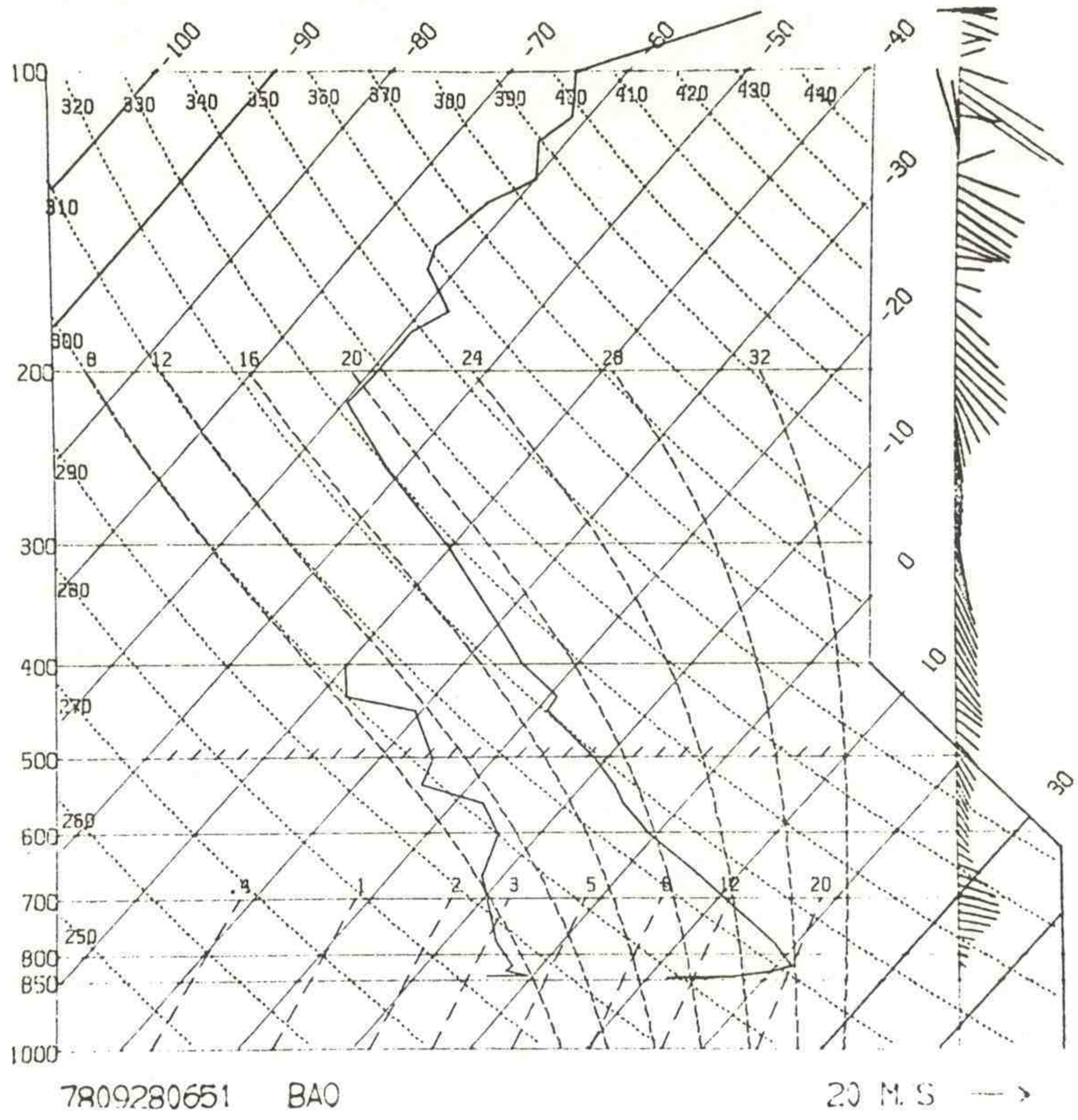


Figure 11.37.--PHOENIX rawinsonde flight number 37.

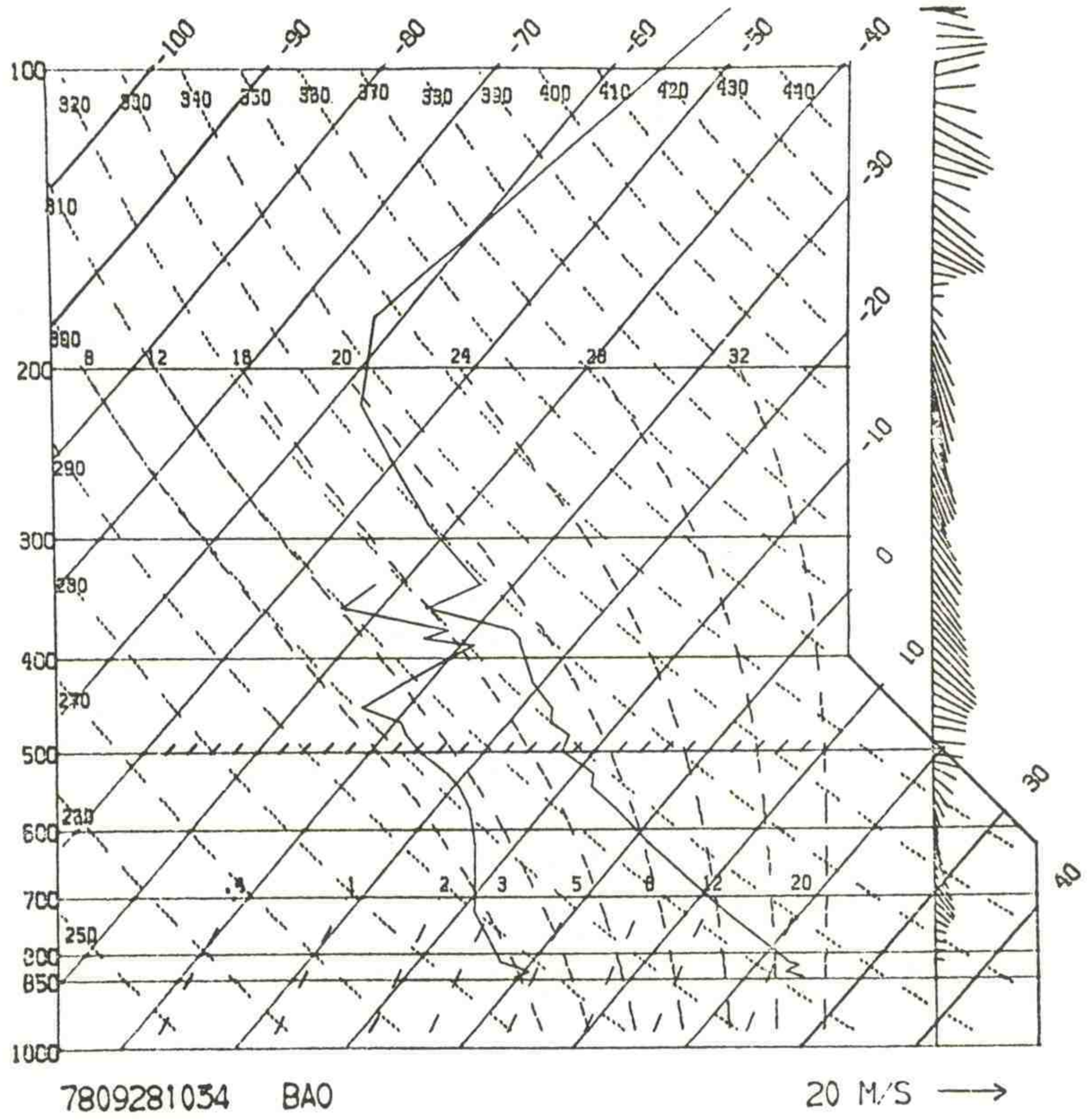


Figure 11.38.--PHOENIX rawinsonde flight number 38.

CHAPTER 12

PHOENIX LAGRANGIAN TURBULENCE OBSERVATIONS USING PIBALS AND TETROONS

Steven R. Hanna
Atmospheric Turbulence and Diffusion Laboratory
National Oceanic and Atmospheric Administration
Oak Ridge, Tennessee 37830

12.1 Introduction

To complement Eulerian turbulence observations made during Project PHOENIX by WPL remote sensors, instruments on the WPL 300-m tower, and the NCAR aircraft, we have developed a method of tracking balloons by radar that permits Lagrangian turbulence observations. The resulting measurements enable us to compare Lagrangian and Eulerian time scales and determine the shape of the Lagrangian energy spectrum. This knowledge should further our understanding of the structure of turbulence and hasten the development of diffusion models (Pasquill, 1974).

Two types of Lagrangian measurements were made during PHOENIX. In the first method, standard 30-g pilot balloons (pibals) were made neutrally buoyant and tracked by double theodolites. In the second method, tetroons were inflated so as to float at tower-top level (300 m) and were tracked by the WPL dual-Doppler radar system. During two 5-day periods, 13 tetroons and 20 pilot balloons were tracked.

Because spectral analysis was a primary tool in data handling, it was important to have complete periods of data records free from gaps or significant errors. Thus, much of the data processing to date has been spent filling the gaps and evaluating the quality of the data. In determining the most useful method of spectral analysis, we evaluated Blackman-Tukey Fourier analysis, two types of Fast Fourier Transforms and the relatively new technique of Maximum Entropy Spectral Analysis. We have completed analysis of the balloon data and are currently comparing them with the tower and aircraft data.

12.2 Experimental Procedure

12.2.1 Neutral pilot balloons

Standard 30-g pilot balloons were made neutrally buoyant in a van parked near one of the theodolites. In order to keep the temperature in the van as close to the outside temperature as possible, the van was either parked in the shade, or the windows and doors were opened. White balloons were used as often as possible because red or black balloons tend to react to solar radiation by heating up and rising during any degree of cloudiness.

Balloons were released at a height of about 100 m through the use of a lift-balloon release system. This system is illustrated in Figures 12.1 and 12.2. The lift balloon was an over-inflated 30-g pilot balloon tied to fishing line wound on a heavy-duty spinning reel. A 6-cm diameter plastic ring was tied to the lift balloon. The neutral balloon system consisted of the 30-g neutral balloon tied to a toy balloon with a glass capillary tube in its neck. The toy balloon was blown up inside the plastic ring so that it was tight against the ring, and the neck of the toy balloon stretched over the end of the glass tube. When the system was sent aloft, the end of the glass tube was freed. About one minute was required for the toy balloon to deflate enough to slip out of the plastic ring, thus releasing the neutral balloon. This technique is adapted from an idea put forth by Longhetto (1971).

Two double theodolite baselines were set up, one 544 m long on the north-south road just west of the 300-m tower and the other 590 m long on the east-west road just north of the tower. There was less than a 1-m difference in elevation between the theodolites on each baseline. The crews at each theodolite consisted of an operator, who also read the elevation angle, and an extra person to read the azimuth angle and operate the radio and tape recorder. Balloons were released near one of the theodolites by a person from the theodolite crew. The timing interval of 15 s was maintained by a stopwatch and radio communications. Data were recorded by voice on cassette recorders.

A summary of the dates and times of the pilot balloon runs, and the measured mean elevation, wind speed, wind direction, and σ_w are given in Table 12.1. The 300-m tower was operating during all the runs, and on September 21 and 22 the

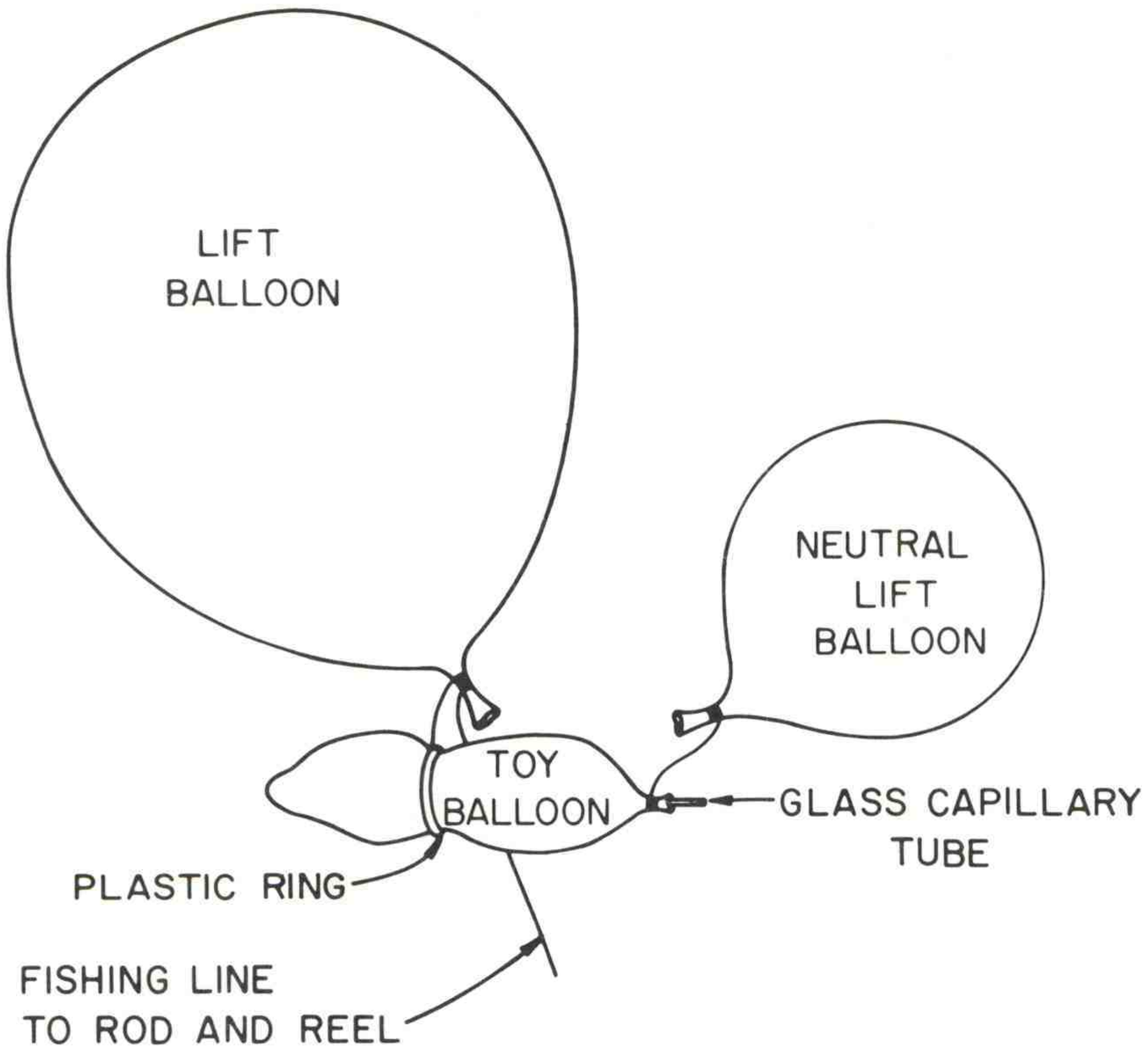


Figure 12.1.--Diagram of lift and release mechanism for neutral pilot balloons.

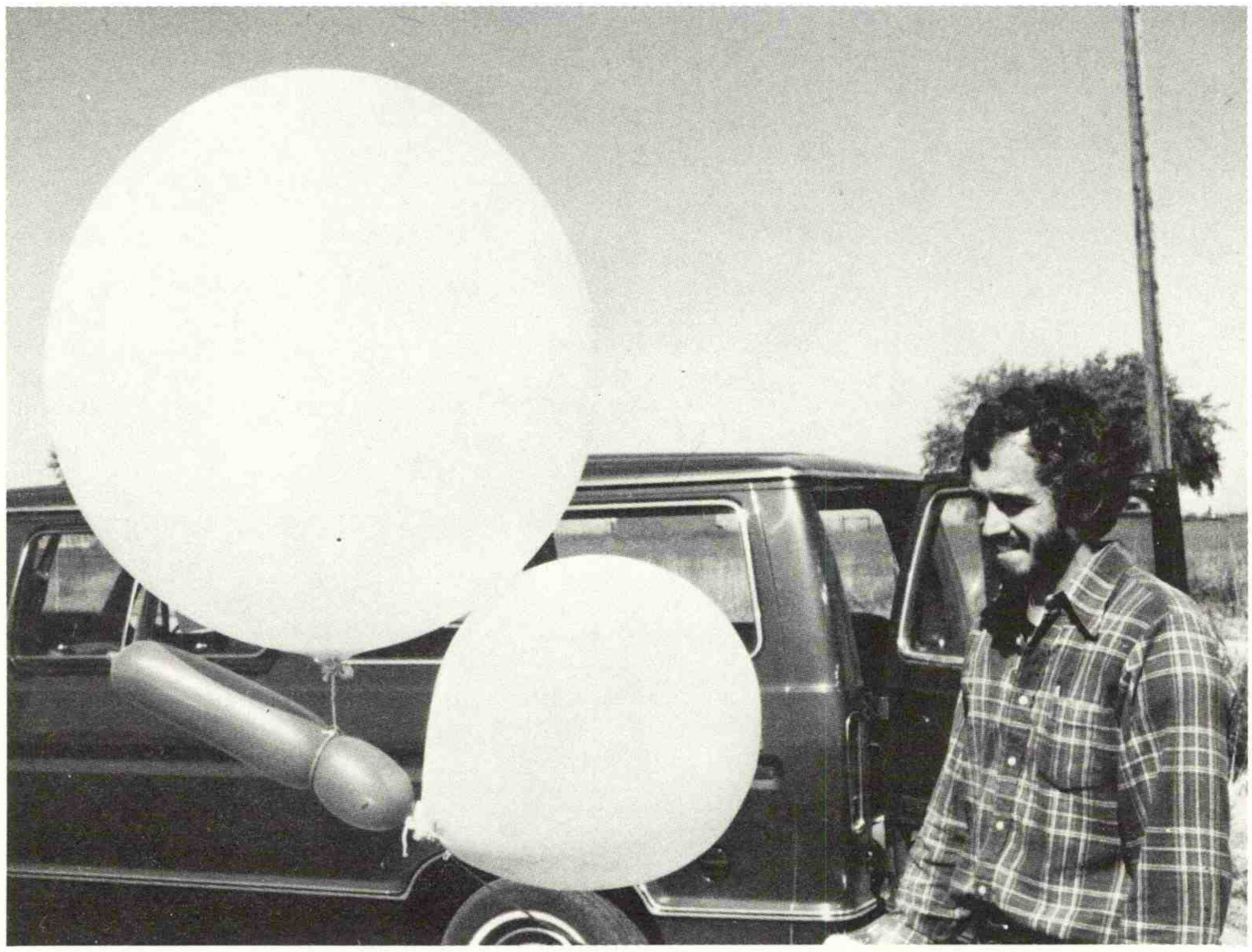


Figure 12.2.--Lift balloon system.

Table 12.1.--Summary of Boulder neutral pilot balloon runs

Run no.	Date (Sept. 1978)	Time MDT	Mean elevation (m)	Mean wind speed and direction	σ_w (m/s)
181	18	1645-1710	600	6.0 NNE	.94
191	19	0950-0956	200	Record too short for analysis	
192	19	1030-1054	600	6.9 SE	.59
193	19	1125-1154	300	6.7 ESE	1.13
194	19	1340-1359	800	6.6 SE	1.35
195	19	1425-1454	800	3.4 ESE	.84
196	19	1520-1550	900	4.9 E	1.17
197	19	1606-1636	800	4.0 E	.92
201	20	1515-1543	800	2.6 SSW	.72
202	20	1613-1631	600	2.3 WSW	.84
211	21	1030-1059	200	1.7 NNW	.85
212	21	1130-1157	300	1.4 SW	.97
213	21	1300-1321	500	1.8 SSE	1.66
214	21	1400-1425	600	2.9 SSE	1.69
215	21	1445-1455	600	Record too short for analysis	
216	21	1530-1554	600	3.8 S	1.43
217	21	1620-1634	120	2.1 NE	.58
221	22	0930-1013	100	1.3 SSE	.69
222	22	1100-1153	120	1.5 ESE	.89
223	22	1212-1242	300	2.8 SE	1.12

NCAR aircraft were flying patterns overhead. Thirty-minute runs were the goal, although the balloon was lost sooner in many cases; and on September 22 we obtained two runs of 50-min duration. Because of the good visibility and absence of obstructions on the horizon, we could easily follow the balloons to quite low elevations.

12.2.2 Tetroons

Tetroons (i.e., super-pressurized polyester film bags) with 1-m^3 displacement (pictured in Figure 12.3) were tracked during two periods: August 29 to September

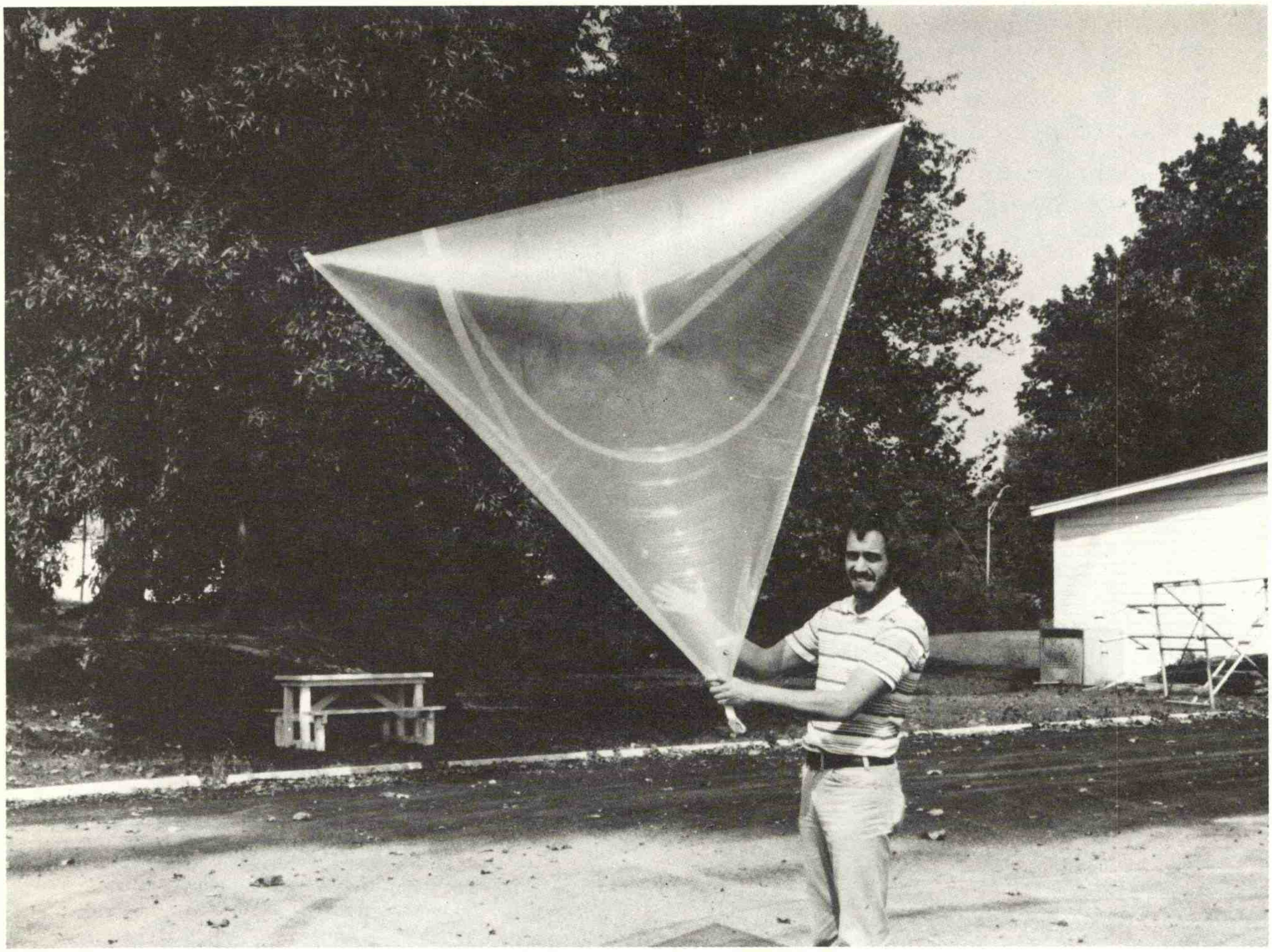


Figure 12.3--Tetroon.

1 and September 18 to September 20. (Because the dual-Doppler radars had as their first priority studies of the convective PBL in support of aircraft operations, the tetroon tracking had to fit into periods of low activity during PHOENIX. Dr. R. A. Kropfli was very helpful in designing the tracking technique and coordinating the experiments.)

The Doppler radar gives accurate velocities of the tetroon in the radial direction from the radar at sampling rates up to 10 Hertz. Components of the wind velocity (u and v) can be calculated if radars at two positions are operating. At low tetroon elevations (300 m) and distances from the radar of 10 km, we feared that ground clutter might be a problem. Thus, one purpose of this experiment was to determine whether this procedure was useful at all.

Tetroons were inflated following procedures recommended by Hoecker (1975). To aid in radar tracking, a pinch of 1.5-cm metallic chaff was blown into the tetroon and another pinch was glued to each of the four sides with rubber cement. The first tetroon was released near Radar 3 to test the radar's ability to detect it. All subsequent tetroons were released from the operations building near the 300-m tower, about 10 km NW of Radar 3 and 10 km SW of Radar 4. A mean flight elevation of 300 m was intended, but convective conditions and inflation problems resulted in a wider range of heights than desired. Three tetroons flew at heights of about 100 to 200 m and were never satisfactorily located by the radars.

The dates and times of the tetroon runs, the number of radars operating, and measurements of mean elevation, wind speed, wind direction, and σ_w are given in Table 12.2. During the August runs the tower was not operating, but during the September runs it provided continuous data. No NCAR aircraft runs coincided with these periods. Run durations ranged from about 10 min to about 50 min, and all data were recorded on magnetic tape. The major data of interest were 0.5-s averages of radial velocity and corresponding signal intensities. The data could have been recorded at a rate of 10 Hz but we expected that the inertia of the tetroon would smooth out such rapid fluctuations in speed.

12.3 Data Analysis

12.3.1 Neutral pilot balloons

The tape-recorded voice records of angles were transcribed onto data sheets. Simple transpositions were corrected and the data keypunched onto computer cards. A standard double theodolite program was used to calculate balloon position (x, y, z) and speed components (u, v, w). We found that if the difference between the azimuth angles of the two theodolites was less than about 3°, as usually occurs at the end of a 30-min run with strong winds, significant errors were introduced into the data. For runs where winds were light, the velocity records should be quite accurate. Total number of data records per run ranged from 80 to 200.

Plots of balloon positions were drawn for all runs; an example is shown in Figure 12.4. The theodolite crews were amazed by the bouncy behavior of the

Table 12.2.--Summary of Boulder tetroon runs

Tetroon no.	Date (1978)	Times of good data (MDT)	Radars operating	Mean elevation (m)	Mean wind speed and direction (m/s)	σ_v (m/s)
1	8/29	1207-1232	3	300	0.4 NE	1.81
2	8/29	1548;	Fair to poor data quality			
3	8/30	1439-1522	3,4	350	3.6 N	1.50
4	8/30	1535;	Fair to poor data quality			
5	8/31	1228;	Fair data quality; tetroon sucked into cloud			
6	8/31	1335-1405	3	400	5.0 SE	1.34
7	8/31	1435				
8	8/31	1515				
9	8/31	1605-1659	3	800	7.7 WSW	
10	9/1	1301-1324	3,4	2000	4.3 NW	1.55
11	9/18	1358-1420	3,4	300	10 N	0.66
12	9/18	1551-1610	3,4	220	11 NNE	1.45
13	9/20	1334-1423	3,4	300	1.3 SSW	.77

balloon on convective days, when it would rise and fall between the ground and an elevation of several hundred meters with a period of 5 to 10 min. In some cases, the balloon would sit on the ground for several seconds, then suddenly get caught by a thermal and rise at a rate of up to 5 m/s.

Wind speed data were analyzed with a straightforward, Blackman-Tukey type of Fourier transform (Jenkins and Watts, 1968), a Fast Fourier Transform (FFT), and a Maximum Entropy Spectral Analysis (MESA) computer program. The particular version of the FFT algorithm used (Singleton, 1969) requires data record lengths with a maximum prime factor of 7. The advantage of the MESA technique (Ables, 1974) is that it has more resolution at low frequencies, for periods near the data record length. For comparison purposes, run 222 was also analyzed by using

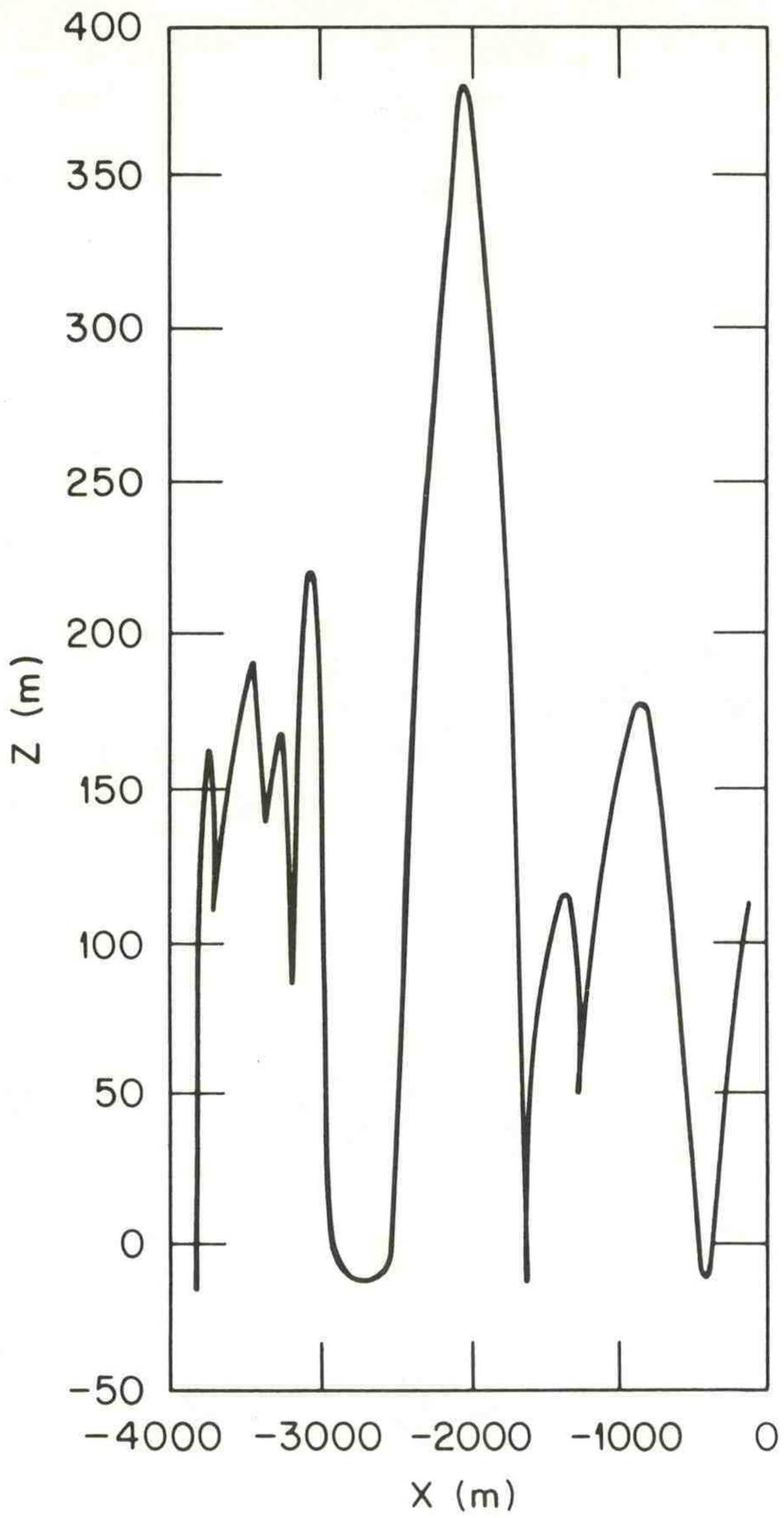


Figure 12.4--Height of neutral balloon 222 as a function of distance east of release point. The terrain slopes downwind in this direction, resulting in readings less than zero on the four occasions that the balloon came to the ground.

an FFT routine requiring a data record length of 2^n. Five different spectra calculated from the vertical speed data in run 222 are plotted for intercomparison in Figure 12.5. The Blackman-Tukey method clearly involves more spectral smoothing than the other four programs, which more or less agree with each other on the locations and magnitudes of the bumps and dips in the spectrum. The FFT (2^n) program has a region of disagreement with the others at frequencies of about .004 to .006 Hz. The frequency carrying peak energy in this example is about .0025 Hz, corresponding to a period of 400 s. The Lagrangian time scale is equal to about 1/5 or 1/6 of the period with peak energy, or about 80 s. The spectral slope in the inertial subrange at high frequencies is close to the theoretical prediction of -1 (Corssin, 1963).

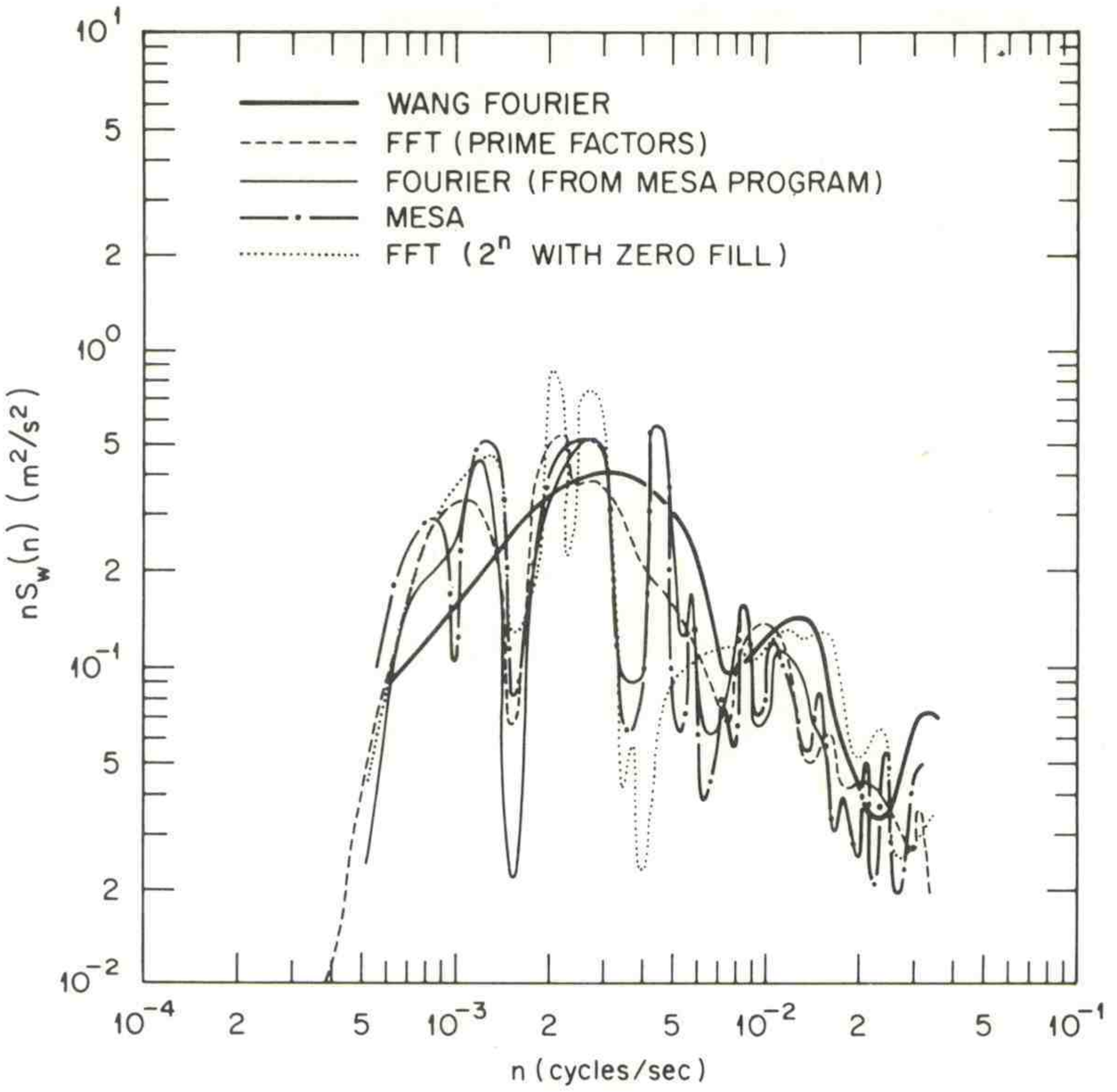


Figure 12.5.--Vertical velocity energy spectra for neutral balloon 222, calculated by five different computer programs. The Fourier (from MESA program) curve agrees with the MESA curve in regions where it is not marked.

12.3.2 Tetroons

Magnetic tapes with radial velocity, signal intensity, and radar angle and range information were received from R. A. Kropfli of WPL about one month after the completion of the experiment. Velocity and intensity printouts were first visually searched for bad or suspect data. A set of criteria was developed for each run such that if the intensity were below some critical value or if the velocity differed from the previous velocity by some critical value, then that velocity was blanked out and replaced by a new velocity linearly interpolated between the previous velocity and the next "good" one. We found that the lower the signal intensity, the greater the random error component in the velocity; this appears in the analyzed spectrum as high frequency energy.

Radar-angle data were used to plot balloon positions, as shown in Figure 12.6. Because the radar was scanning, these traces are sometimes irregular. We

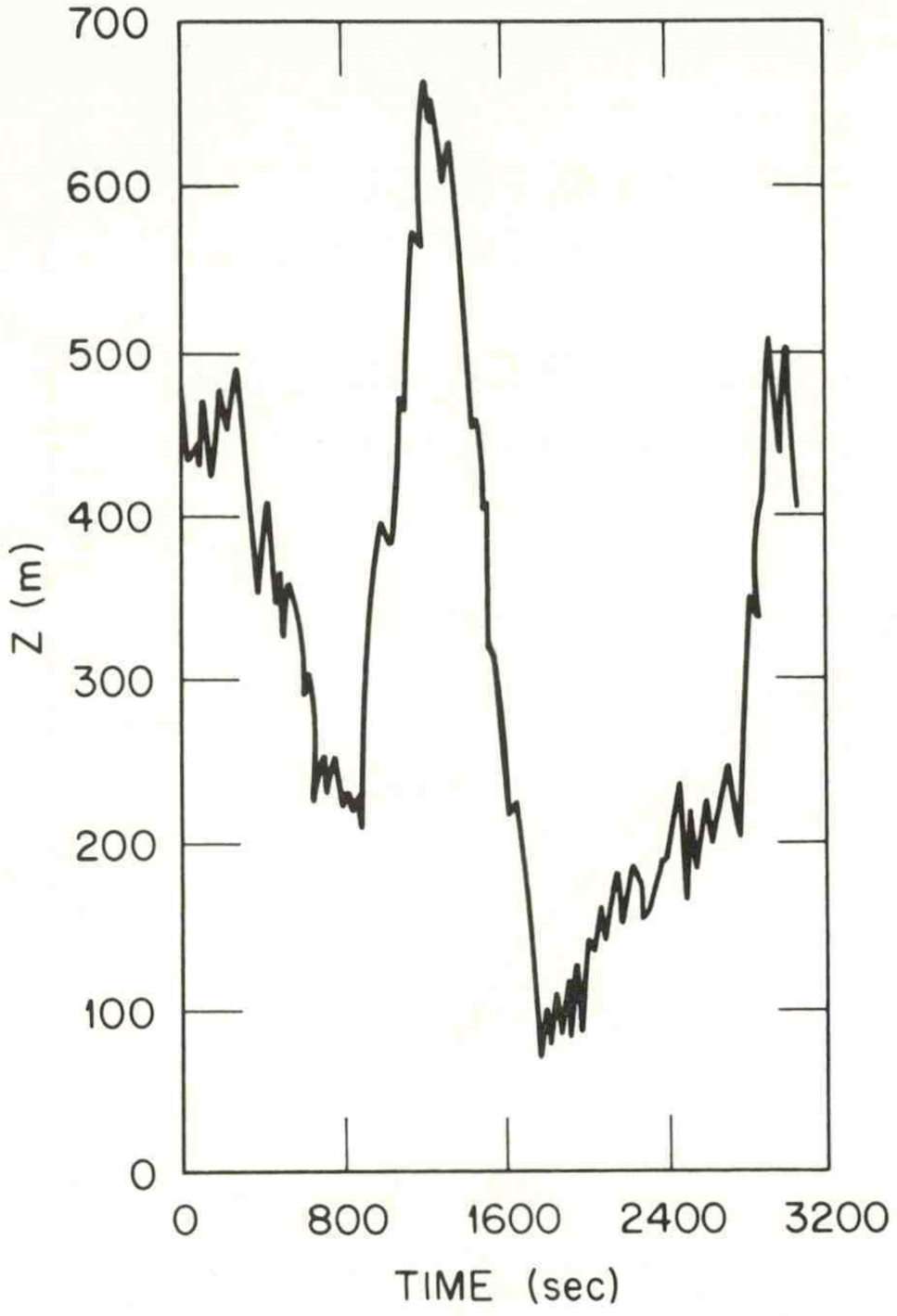


Figure 12.6.--Height of tetroon 13 as a function of time, as observed by radar 4.

found that most of the balloons reached an equilibrium level within the mixed layer.

Sample spectra from tetroon 13 are plotted in Figure 12.7. The MESA program was not applied to these data, since time limitations hold it to records shorter than about 500 points. An average curve for radars 3 and 4 is drawn, as well as a curve obtained from the Blackman-Tukey Fourier Transform program applied to 60-s averages. The FFT spectrum places two peaks at .0007 and .0025 Hz, and the Blackman-Tukey spectrum places a peak at .0025 Hz, the same as the example in Figure 12.5. The spectra follow a -1 slope in the frequency range between .01 and .1 Hz. We attribute the increase in slope at higher frequencies to poor response of the bulky tetroon to eddies of the same size as or smaller than the tetroon.

12.4 Further Analysis

Nearly all of the pilot balloon and tetroon data have been analyzed. Tower velocity spectra were received in May 1979 on magnetic tapes from J. C. Kaimal,

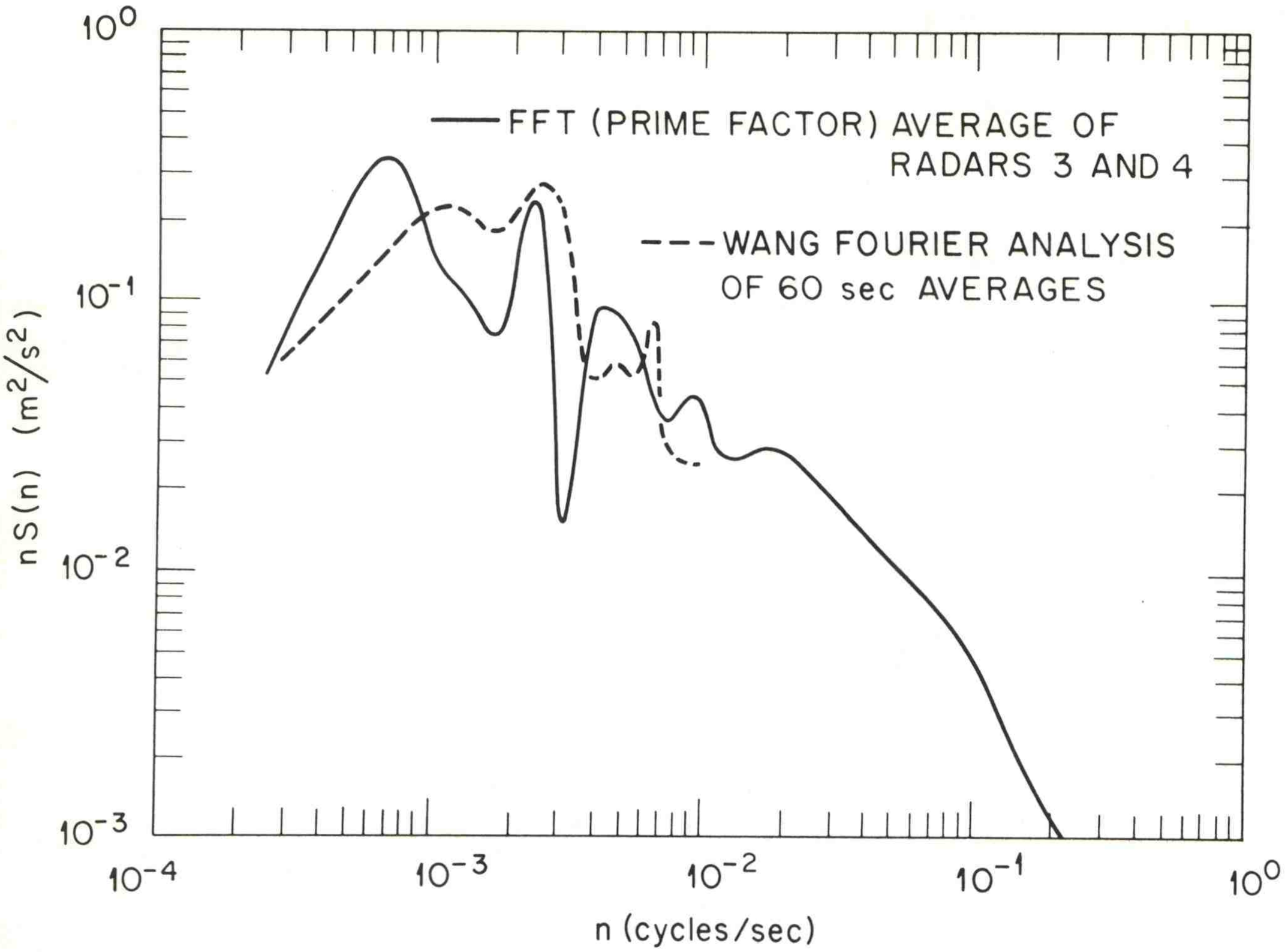


Figure 12.7.--Energy spectra for radial speed component of tetroon 13.

D. E. Wolfe, and J. M. Young of WPL. However, the low-frequency ends of the spectra must still be estimated by using 10-s average velocity data on another tape. P. H. Hildebrand has sent the NCAR-aircraft velocity spectra and they are being analyzed. Time or length scales and spectral shapes of the balloon, tower, and aircraft spectra will be compared. Methods of estimating these scales based on mixing depth and surface layer measurements will be tested.

Acknowledgments

The double theodolite crews included H. Snodgrass, L. Nipper, M. Hall, and J. Waite of ATDL. H. Snodgrass and D. Elliott of ATDL performed most of the computer operations. B. Rust of ORNL guided us in the application of the MESA program.

Many persons at WPL and NCAR contributed to this study. I especially express my appreciation to W. H. Hooke of WPL for administrative arrangements, to R. A. Kropfli of WPL for arranging and coordinating the radar experiment, to D. A. Haugen and J. C. Kaimal of WPL for providing the tower data, and to P. H. Hildebrand of NCAR for providing the aircraft data.

This research was performed under an agreement between the National Oceanic and Atmospheric Administration and the Department of Energy.

References

Ables, J. G., Maximum entropy spectral analysis, Astron. Astrophys. Suppl. 15, 383-393 (1974).

Corssin, S., Estimates of the relation between Eulerian and Lagrangian scales in large Reynolds number turbulence, J. Atmos. Sci. 20, 115-119 (1963).

Hoecker, W. H., A universal procedure for deploying constant volume balloons and for deriving vertical air speeds from them, J. Appl. Meteorol. 14, 1118-1124 (1975).

Jenkins, G. M., and D. G. Watts, Spectral Analysis and Its Applications, Holden-Day, San Francisco, 525 pp. (1968).

Longhetto, A., Some improvements in the balanced pilot balloons technique, Atmos. Environ. 5, 327-331 (1971).

Pasquill, F., Atmospheric Diffusion, second edition, John Wiley and Sons, New York, 429 pp. (1974).

Singleton, R. C., An algorithm for computing the mixed radix Fast Fourier Transform, IEEE Trans. on Audio and Electroacoustics AU-17, 93-102 (1969).

CHAPTER 13

MICROBAROGRAPH OBSERVATIONS DURING PHOENIX

Alfred J. Bedard, Jr., and Carl Ramzy
Wave Propagation Laboratory
National Oceanic and Atmospheric Administration
Boulder, Colorado 80303

A number of studies (e.g., Hooke et al., 1972; Beran et al., 1973; Hooke et al., 1973; Merrill, 1977; Bedard and Sanders, 1978) have demonstrated the utility of arrays of sensitive microbarographs used in conjunction with surface-based remote sensors to study boundary-layer phenomena in general and wave motions in particular. Accordingly, the very earliest BAO planning called for such instrumentation there as part of the permanent operation. An array some 200 m on a side was deployed at the site in time for the PHOENIX experiment (arrays smaller than 1 km are useful for the study of small-scale gravity waves generated by instability of the PBL itself).

Figure 2.6 of Chapter 2 of this volume (Kaimal and Wolfe, 1979) shows the microbarographs to be located near the inner guy anchors of the tower itself, at the base of the tower, and near the temporary building at the entrance to the site. Figure 13.1 shows a shelter housing one of the instruments. The basic instrument measures the pressure difference between two sides of a diaphragm. One side is exposed to the outside air and the other is exposed to a backing volume connected to the outside air by a slow leak. Thus, at low frequencies, it functions as a barovariograph, measuring not pressure itself but the time rate of variation of pressure. The cross-over frequency separating pressure from time-rate-of-change of pressure measurement is 0.02 Hz. For frequencies of interest the instrument can respond to pressure changes as small as 0.1 μb or less. The specific instrument itself has been described by Cordero et al. (1957), Cook and Bedard (1971), Georges and Young (1972), and Bedard (1973, 1975); these and the paper by Hooke (1975) give further references. Figure 13.2 shows this instrument inside a shield designed to minimize thermal effects.

Table 13.1 is a log of microbarograph-array operations during September 1978. Apart from minor outages, operation was continuous after 1500 MDT on

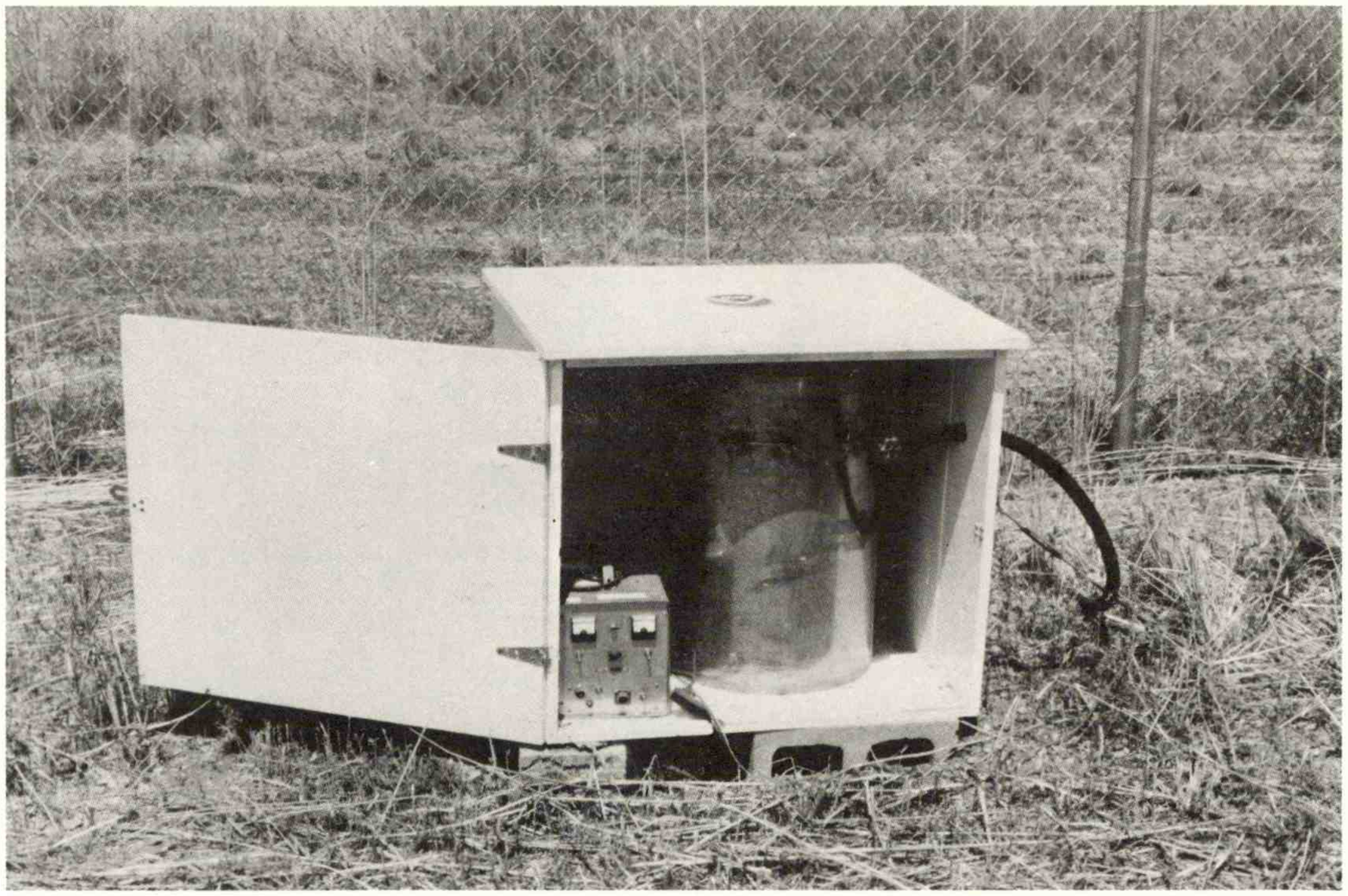


Figure 13.1.--A shelter housing one of the sensitive microbarographs at the BAO. The door has been opened to reveal the microbarograph itself, housed in a large, stainless steel drum, and some of the associated electronics.

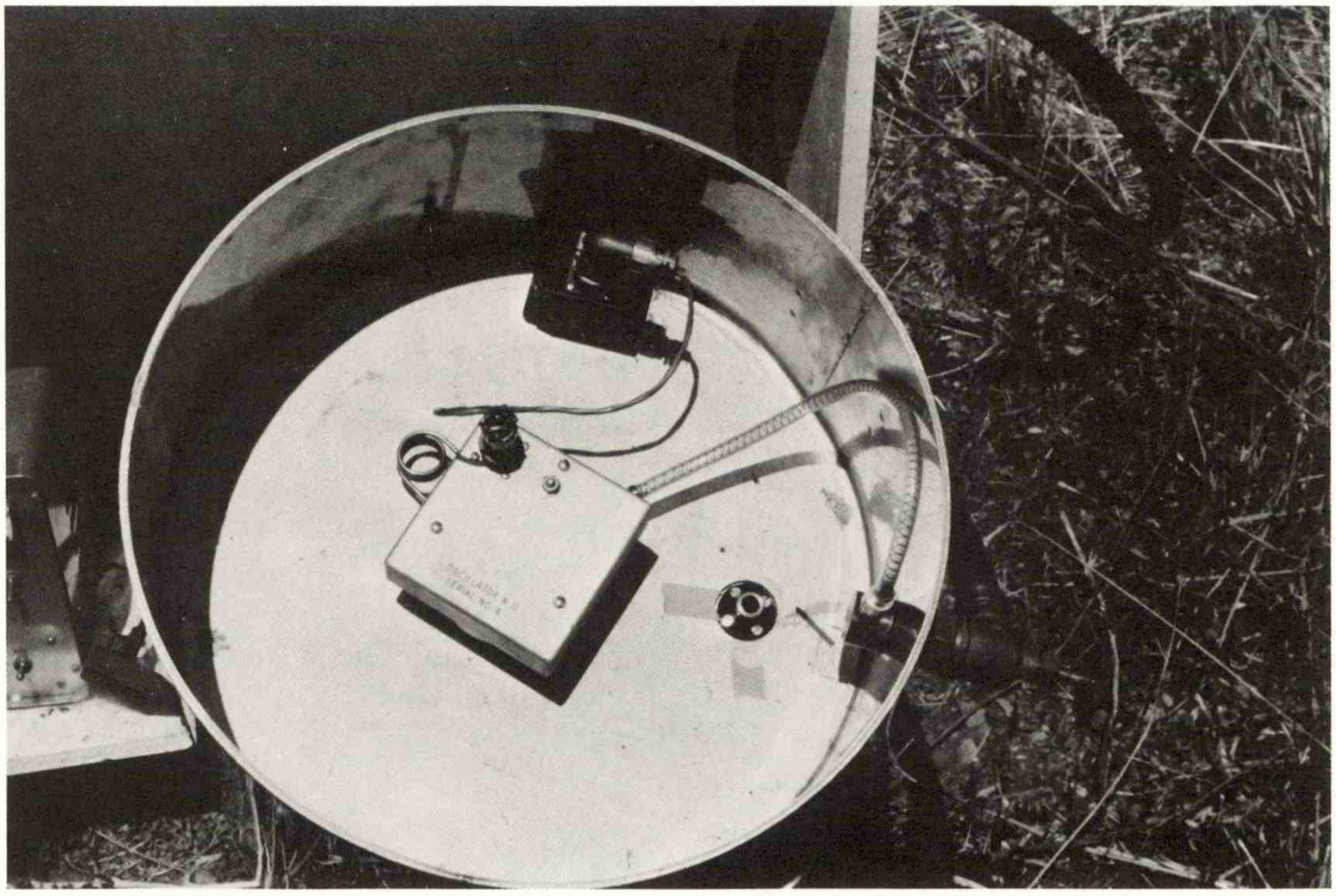


Figure 13.2.--Steel drum with top removed to reveal the microbarograph diaphragm housing, mounted atop the backing volume.

Table 13.1.--WPL microbarograph operations during PHOENIX

Date (1978)	Time (MDT)	Comments[1, 2, 3]
Sept. 1	1925-2100	Wave activity (5-15 min periods)
	2145-2240	Start of large amplitude waves with HF
Sept. 2	0040-0115	Start of large amplitude waves (5-10 min)
	0540-0700	Wave activity (5-10 min)
	1620	Start of HF noise
	1900-2000	Waves (10-15 min) with HF
	2030-2040	Wave train
	2053	Large pulse followed by Hf lasting until 2200
	2230	Pulse, HF noise to 0140 Sept. 3
Sept. 3	0140-0400	Waves showing poor correlation
	0645-0820	Waves (15 min)
	1240-2000	HF large amplitude noise
	2100-2215	HF Correlation (1 min)
	2215-0000	LP Correlation (10-15 min)
Sept. 4	0000-0200	Correlation, short period (~2 min)
	0800	Start of low-level, HF noise
	2000	Sudden start of HF energy, duration - 20 min
	2100-2300	Waves with HF noise
	2310	Pulse-10 min long
	2330-0300	Waves
Sept. 5	1615-1630	LP with HF noise
	1840	End of HF
	2000	Start of HF
	2240-2315	Infrasound riding on waves
Sept 6.	0000-0035	HF riding on LF
	0000-0300	LP waves
	0650-0800	LP waves
	1900	Sudden start of large amplitude HF energy
	2100-2110	LP waves with HF noise
	2250-2330	LP waves with HF noise
Sept. 7	0100-0320	LP waves
	0600-0800	Good waves
	0800	Start HF noise
	1800	Start large amplitude HF fluctuations
	2100-2300	LP waves with HF noise

[1]Times indicated in parentheses are the periods predominant in the recordings.
[2]HF = high frequency
[3]LP = long period

Table 13.1.--WPL microbarograph operations during PHOENIX--Continued

Date (1978)	Time (MDT)	Comments
Sept. 8	0300	Pulse
	0200-0900	Excellent waves
	2210	Sudden start of HF fluctuations
Sept. 9	0030-0200	Good gravity waves with some HF
	1700-2000	Very good waves
	2000-2140	Outage
	2300-2359	Small, short period waves
Sept. 10	0000-0030	Waves with HF
	0300-1000	Good waves
	0900	Start of HF
	1250	Large pressure change
	1440-1700	Large waves
	1840-2359	Huge waves
Sept. 11	0000-0130	Huge waves continued
	0200-0400	Waves (not large) no HF
	0400-0430	Large wave with HF
	0700-1000	Excellent waves
	1000-	HF noise most of the rest of day
Sept. 12	0100-0800	Waves
	0800-0845	Large amplitude waves
	0900-1800	Noise
	1800-2359	Waves
Sept. 13	0345-0700	Waves
	0700-0830	Good waves
	1800-2359	Waves (impulse 2300)
Sept. 14	0000-1000	Waves
	1000-1400	Increased noise
	1800-2000	LP waves (good)
Sept. 15	0100-0900	Waves
	0748	Impulse
	2005	Pressure jump followed by HF
	2135	Impulse
	2220	Impulse
	2255	Single wave
	2320	Start HF (large amplitude)
Sept. 16	0100-0300	Waves
	0600-0900	Waves (especially 0805-0820)
	1850-2200	Waves with HF
	2230-2355	Waves (excellent)

Table 13.1.--WPL microbarograph operations during PHOENIX--Continued

Date (1978)	Time (MDT)	Comments
Sept. 17	0000-0100	Waves
	0100-1200	Waves (good with HF)
	1900	Impulse (start of HF)
	2000-2355	Good waves
Sept. 18	0000-0700	Waves with HF - good
	0700-0900	Waves, excellent
	1130	Wave with HF
	1700-1830	Waves, excellent
	2000-2355	Waves with HF
Sept. 19	1440-1700	Some waves
	1700-2355	Sporadic, excellent waves
Sept. 20	0000-0700	Low level waves
	0930	Spike
	1830-2355	Low level waves
Sept. 21	0000-0900	Sporadic waves
Sept. 22	0800-0900	Good wave activity
Sept. 23	0000-0900	Good waves
	0715	Start HF
	2115	Incoherent wave train
	2200	Pressure pulse
Sept. 24	0100-0900	LP waves
	0830	Start HF
	2020	Start HF
Sept. 25	0000-0100	Wave activity
	0350	Impulse
	0650	Slow moving impulse
	2115	Large impulse
Sept. 26	0200	Short period, small waves (infrasound?)
	0420-0800	0540-excellent
	2020	Start LP waves
	2300-2355	Waves
Sept. 27	0030-1000	Waves
	1800	Start HF noise

Table 13.1.--WPL microbarograph operations during PHOENIX--Continued

Date (1978)	Time (MDT)	Comments
Sept. 28	0100-1100	Excellent waves
	1840	Impulse
	2000	"
	2045	"
	2100	"
	2200	Impulse followed by HF waves
	2300	Impulse
Sept. 29	0200-0330	Waves
	0330	Impulse (with start of HF noise)
	0330-0900	Very good waves
	1925	Impulse
Sept. 30	0000-0600	Low level waves
	2225-2355	Very good waves
Oct. 1	0000-0600	Very good waves

September 1. The comments on the wave activity take into account both amplitude and the degree of correlation between the sites.

References

Bedard, A. J., Jr., The DC pressure summator; theoretical operation, experimental tests and possible practical uses, Fluid. Q. 9, 26-51 (1977).

Bedard, A. J., Jr., The design of a temperature-independent DC flow resistor, Fluid. Q. 5, 31-50 (1973).

Bedard, A. J., Jr., and M. J. Sanders, Jr., Thunderstorm-related wind shear detected at Dulles International Airport using a Doppler acoustic/microwave radar, a monostatic sounder and arrays of surface sensors, Preprints Conference on Weather Forecasting and Analysis and Aviation Meteorology, October 16-19, 1978, Silver Spring, Maryland, pp. 347-352, American Meteorological Society, Boston, Mass. (1978).

Beran, D. W., W. H. Hooke, and S. F. Clifford, Acoustic echo-sounding techniques and their application to gravity-wave, turbulence, and stability studies, Boundary-Layer Meteorol. 4, 133-153 (1973).

Cook, R. K., and A. J. Bedard, On the measurement of infrasound, Geophys. J. R. Astron. Soc. 26, 5-11 (1971).

Cordero, F., H. Matheson, and D. P. Johnson, A nonlinear instrument diaphragm, J. Res. Natl. Bur. Stand. 58, 333-337 (1957).

Georges, T. M., and J. M. Young, Passive sensing of natural acoustic-gravity waves at the earth's surface, Chapter 21, in Remote Sensing of the Troposphere, V. E. Derr, Ed., U. S. Govt. Printing Office (1972).

Hooke, W. H., Sensitive microbarographs used to study atmospheric gravity waves, Preprints 3rd Symp. on Meteorol. Observations and Instrumentation, February 10-13, 1975, Washington, D. C., pp. 175-178, American Meteorological Society, Boston, Mass. (1975).

Hooke, W. H., J. M. Young, and D. W. Beran, Atmospheric waves observed in the planetary boundary layer using an acoustic sounder and a microbarograph array, Boundary-Layer Meteorol. 2, 371-380 (1972).

Hooke, W. H., F. F. Hall, Jr., and E. E. Gossard, Observed generation of an atmospheric gravity wave by shear instability in the mean flow of the planetary boundary layer, Boundary-Layer Meteorol. 5, 29-42 (1973).

Kaimal, J. C., and D. E. Wolfe, BAO site, tower instrumentation, and PHOENIX operations, Chap. 2, in Project PHOENIX: The September 1978 Field Operation, W. H. Hooke, Ed., NOAA/NCAR Boulder Atmospheric Observatory Rept. No. 1, available from NOAA/ERL, Boulder, Colo., and from NCAR Publications Office, Boulder, Colo. (1979).

Merrill, J. T., Observational and theoretical study of shear instability in the air flow near the ground, J. Atmos. Sci. 34, 911-921 (1977).

CHAPTER 14

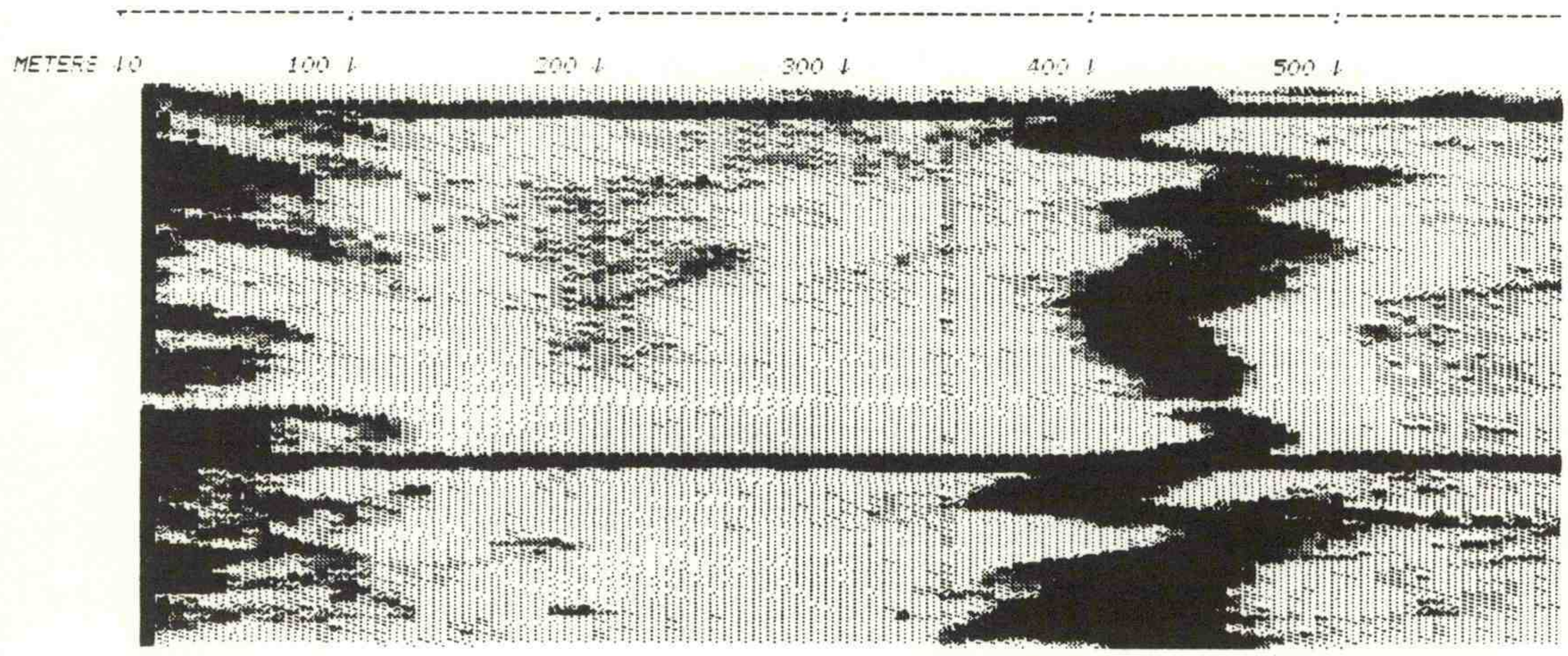
ACOUSTIC ECHO SOUNDER OPERATIONS DURING PHOENIX

W. D. Neff and E. H. Brown
Wave Propagation Laboratory
National Oceanic and Atmospheric Administration
Boulder, Colorado 80303

From the time of their introduction in the late 1960's (McAllister, 1968; McAllister et al., 1969), acoustic echo sounders have offered tremendous potential for boundary-layer flow visualization and for quantitative studies (Little, 1969). During the 1970's, some of that potential has been realized (e.g., Beran et al., 1971; Hooke et al., 1972; Beran et al., 1973; Hooke et al., 1973; Hall et al., 1975, 1976; Gaynor, 1977; Neff, 1978; Neff and Hall, 1978; Gaynor and Mandics, 1978), although much remains to be done. Brown and Hall (1978) provide an up-to-date review. Accordingly, a major activity at the Boulder Atmospheric Observatory (BAO) is the operation and testing of acoustic echo sounders in conjunction with the in-situ sensors on the BAO tower. The acoustic sounders serve three purposes. First, they provide a ready visualization of micrometeorological conditions prevailing over the site, revealing convection, stable layers, gravity-wave activity, and frontal passages, among others. Second, they provide three-component wind speeds to altitudes of about 500 m, thus effectively extending the height of the volume monitored by BAO instruments. And third, they provide research data in their own right: acoustic-sounding records for comparison with tower in-situ data and interpretation.

The Wave Propagation Laboratory took the PHOENIX experiment as an opportunity to test a preliminary version of an evolving microcomputer method for Doppler wind-velocity profiling. The method turned out to be subject to a bias under low signal-to-noise levels that rendered it somewhat unreliable for standard BAO operations (and it produced Doppler data unsuitable for detailed presentation here); the processing algorithms have since been modified to remove this bias. For a more detailed comparison of acoustic-sounder and tower velocity measurements, the interested reader is referred to a forthcoming report on the recent WMO/CIMO comparison of low-level sounding systems, held at the BAO during August-September 1979.

Despite the unreliability of the Doppler data, the acoustic sounding systems did provide a rough indication of wind speeds above tower height as well as useful digital data on C_T^2 profiles throughout the experiment. Figures 14.1a,b show samples of the digital output. Both analog and digital facsimile data are also available for the period. Figure 14.2 provides analog facsimile records for the experiment period, included here to aid the interested reader in selecting time intervals for study. In addition to the data reproduced here, data are available from a mobile acoustic echo sounder, located at Gunbarrel, some 10 km from the BAO. The WPL lidar group also operated its acoustic sounder from a site adjacent to the lidar, just south of the temporary building. Figure 14.3 shows brief logs of the operations of various acoustic systems.



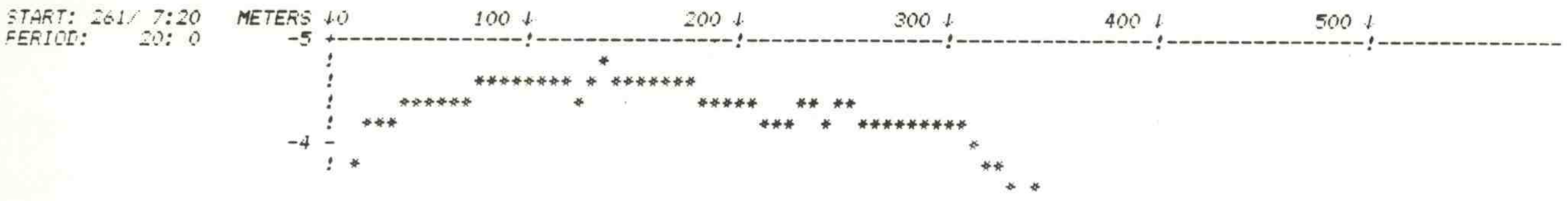


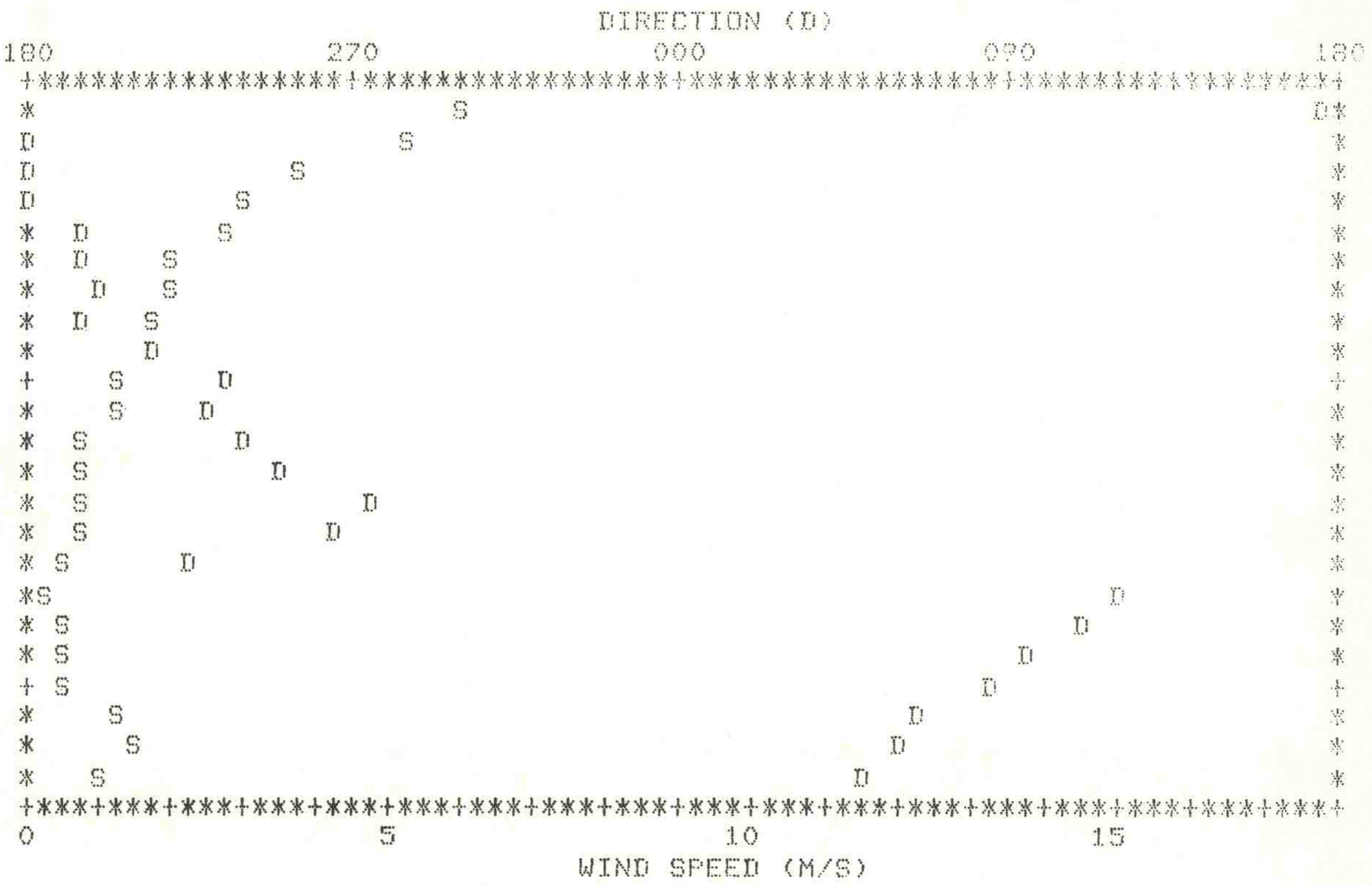
Figure 14.1a.--A sample digital facsimile output and C_T^2 profile from PHOENIX acoustic-sounder data.

ACOUSTIC DOPPLER DATA AVERAGED FOR 15 MIN, 28 SEC.

STARTING TIME
DAY: 261
HOUR: 7
MIN: 20

HEIGHT (M)	WIND SPEED (M/S)	WIND DIRECTION (DEG FM N)
500.	6.1	176.
480.	5.4	181.
460.	4.0	181.
440.	3.1	181.
420.	2.9	198.
400.	2.2	196.
380.	2.2	200.
360.	1.8	199.
340.	1.8	217.
320.	1.4	237.
300.	1.4	233.
280.	1.0	242.
260.	0.8	251.
240.	0.8	278.
220.	0.8	267.
200.	0.6	227.
180.	0.5	122.
160.	0.5	112.
140.	0.7	98.
120.	0.7	86.
100.	1.4	70.
80.	1.6	62.
60.	1.1	54.

WIND SPEED AND DIRECTION PROFILES



KEY:
S = SPEED (100 HZ DOPPLER) D = DIRECTION (100 HZ DOPPLER)

Figure 14.1b.--A digital height profile of wind speed and direction for the same period.

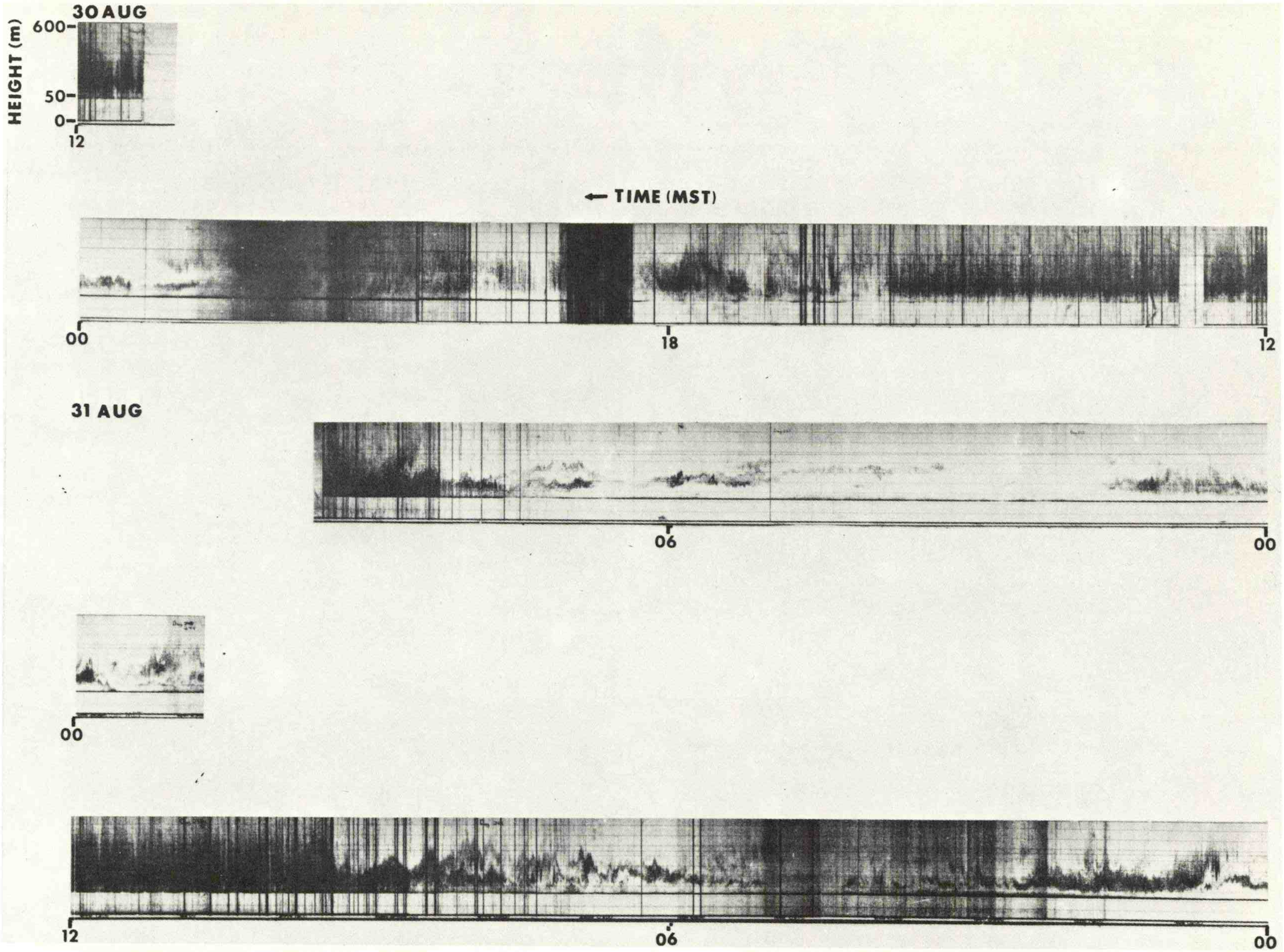


Figure 14.2.--Analog acoustic-sounder facsimile records for the PHOENIX experiment.

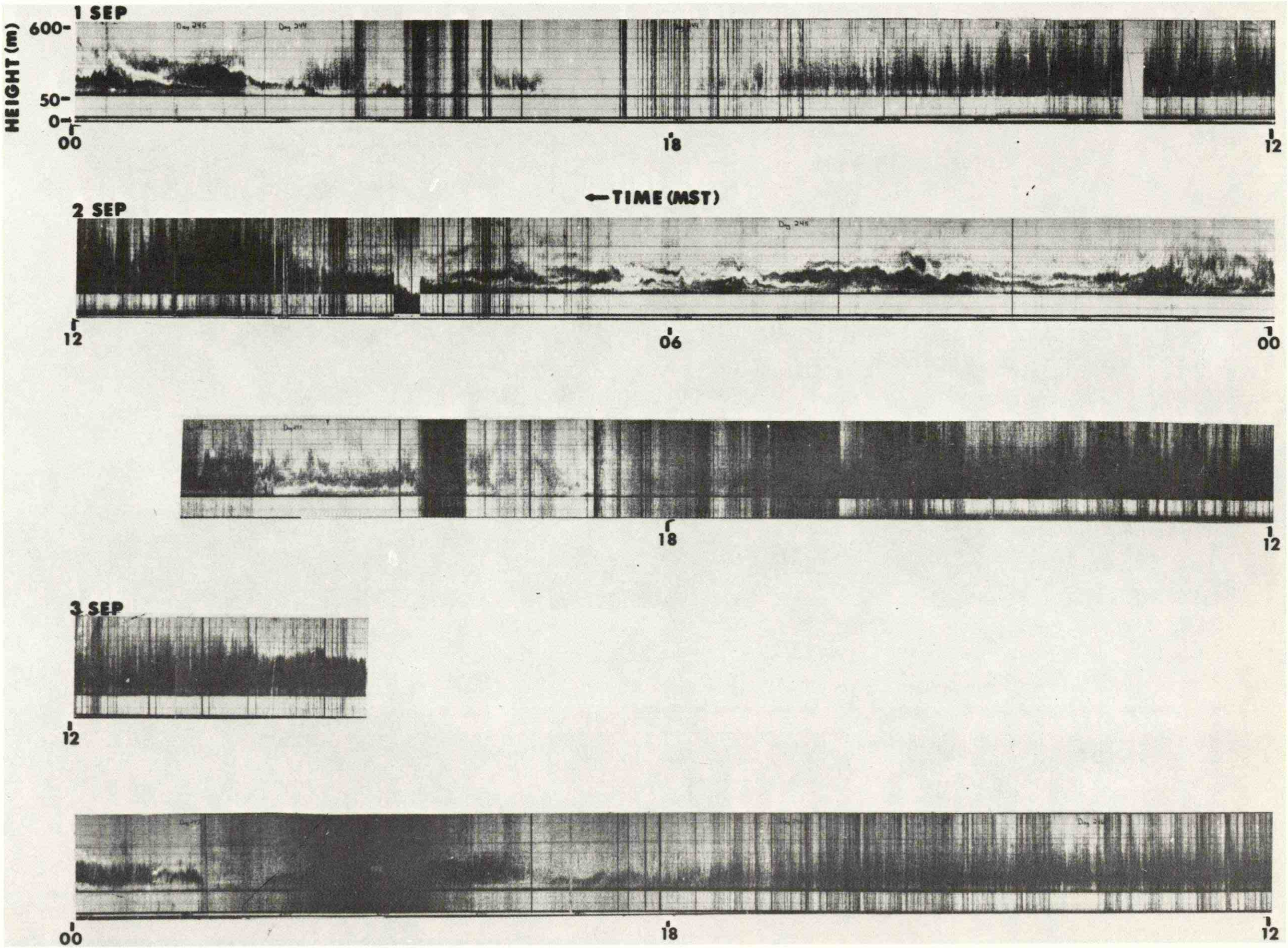


Figure 14.2.--Continued.

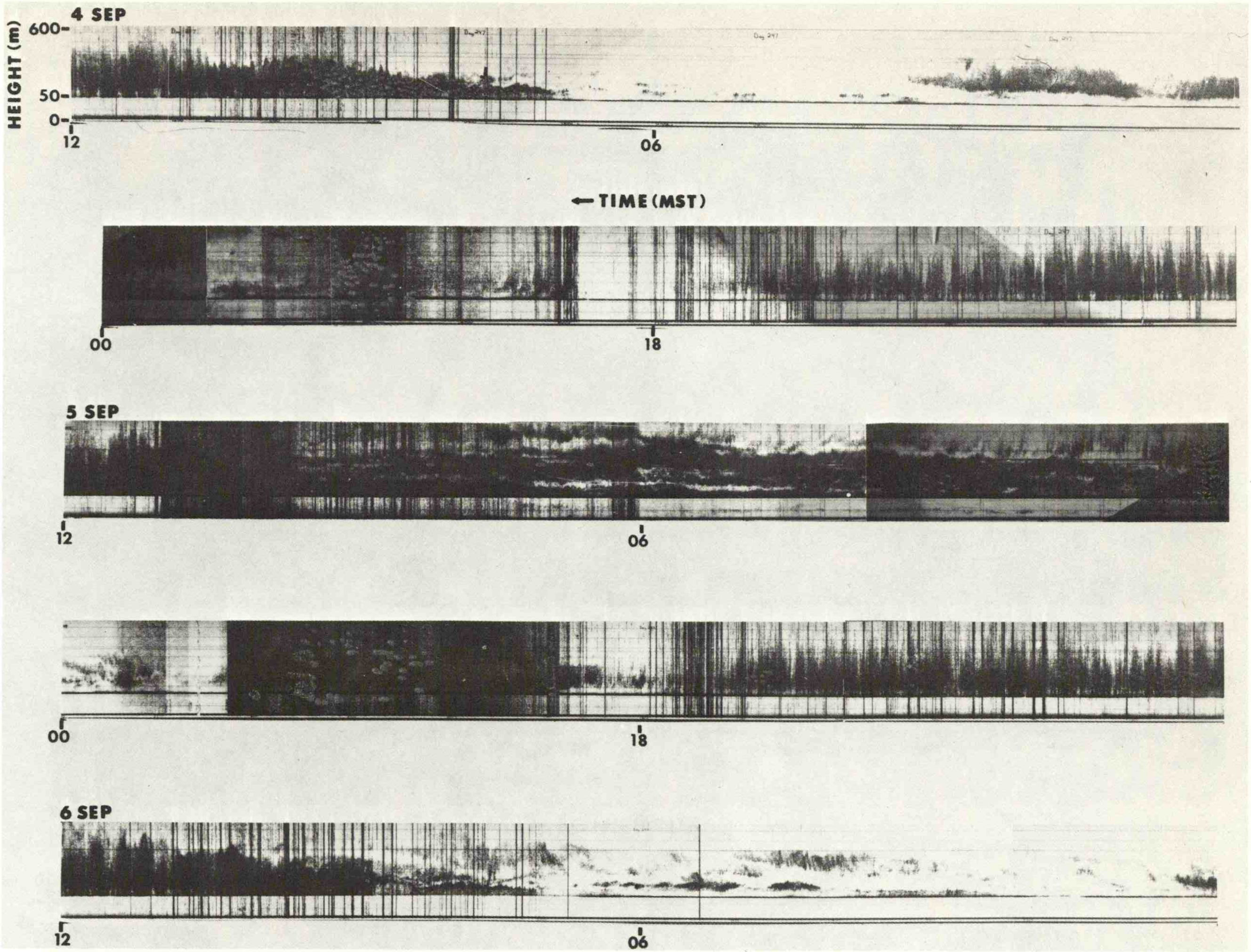


Figure 14.2.--Continued.

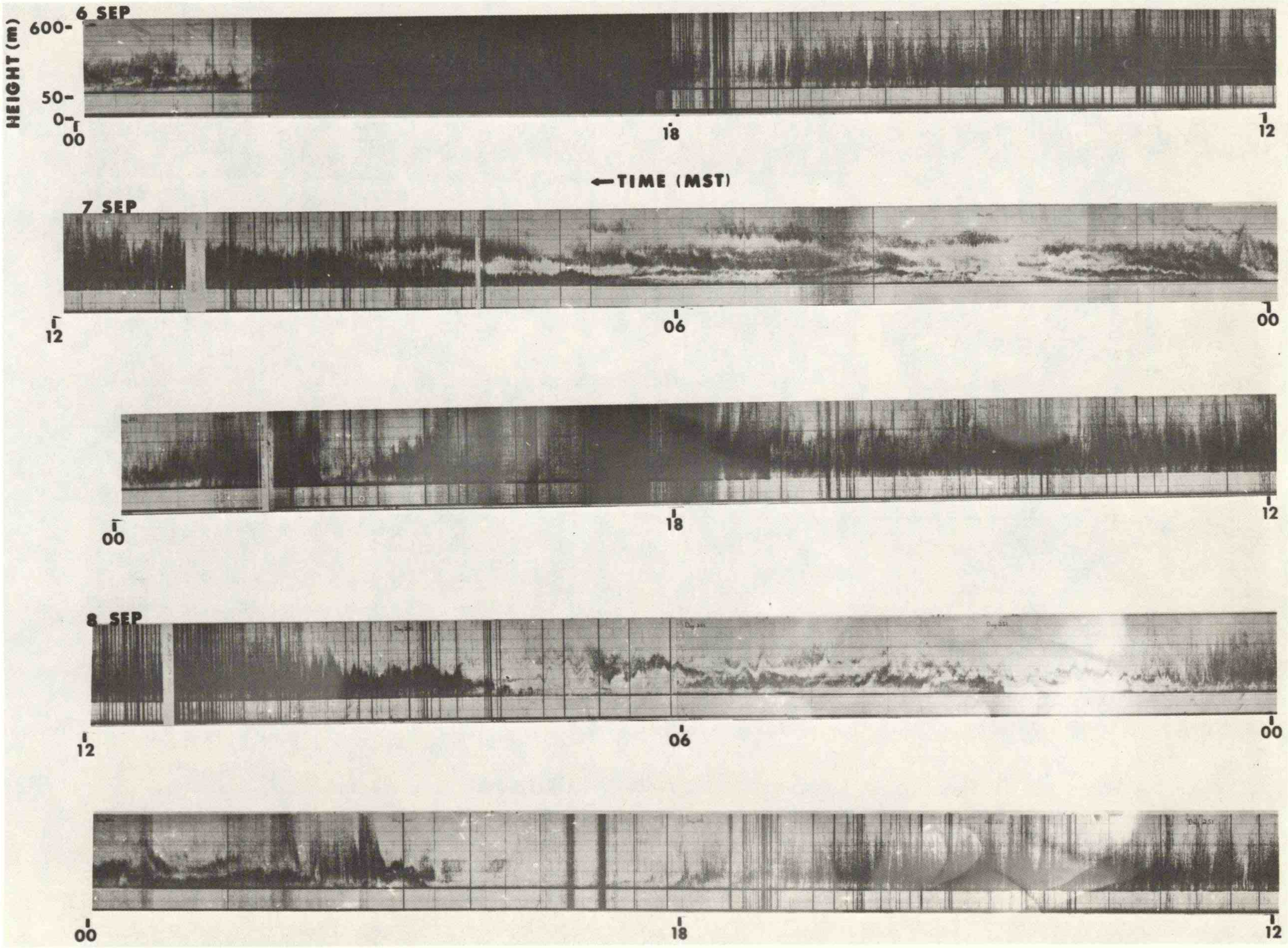


Figure 14.2.--Continued.

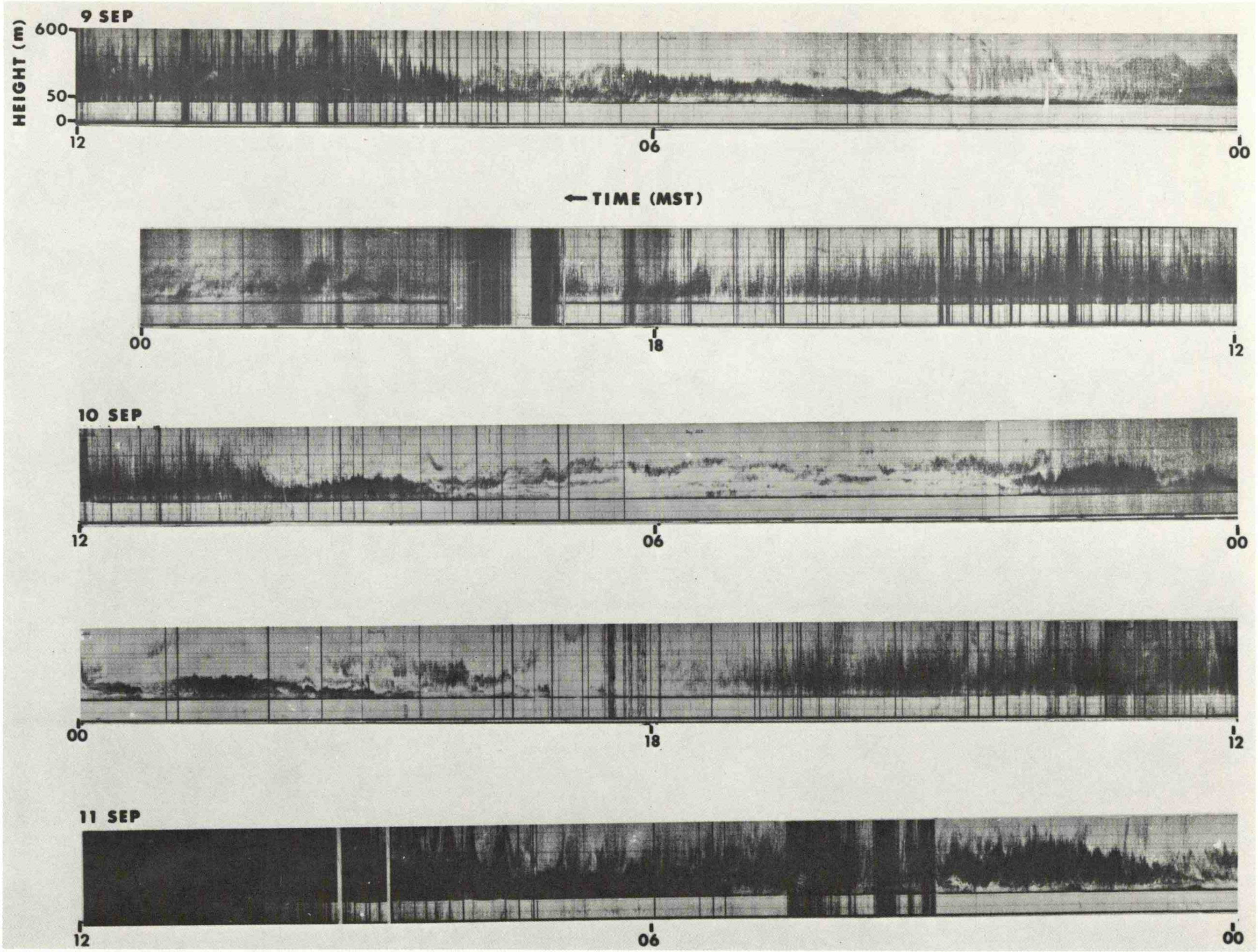


Figure 14.2.--Continued.

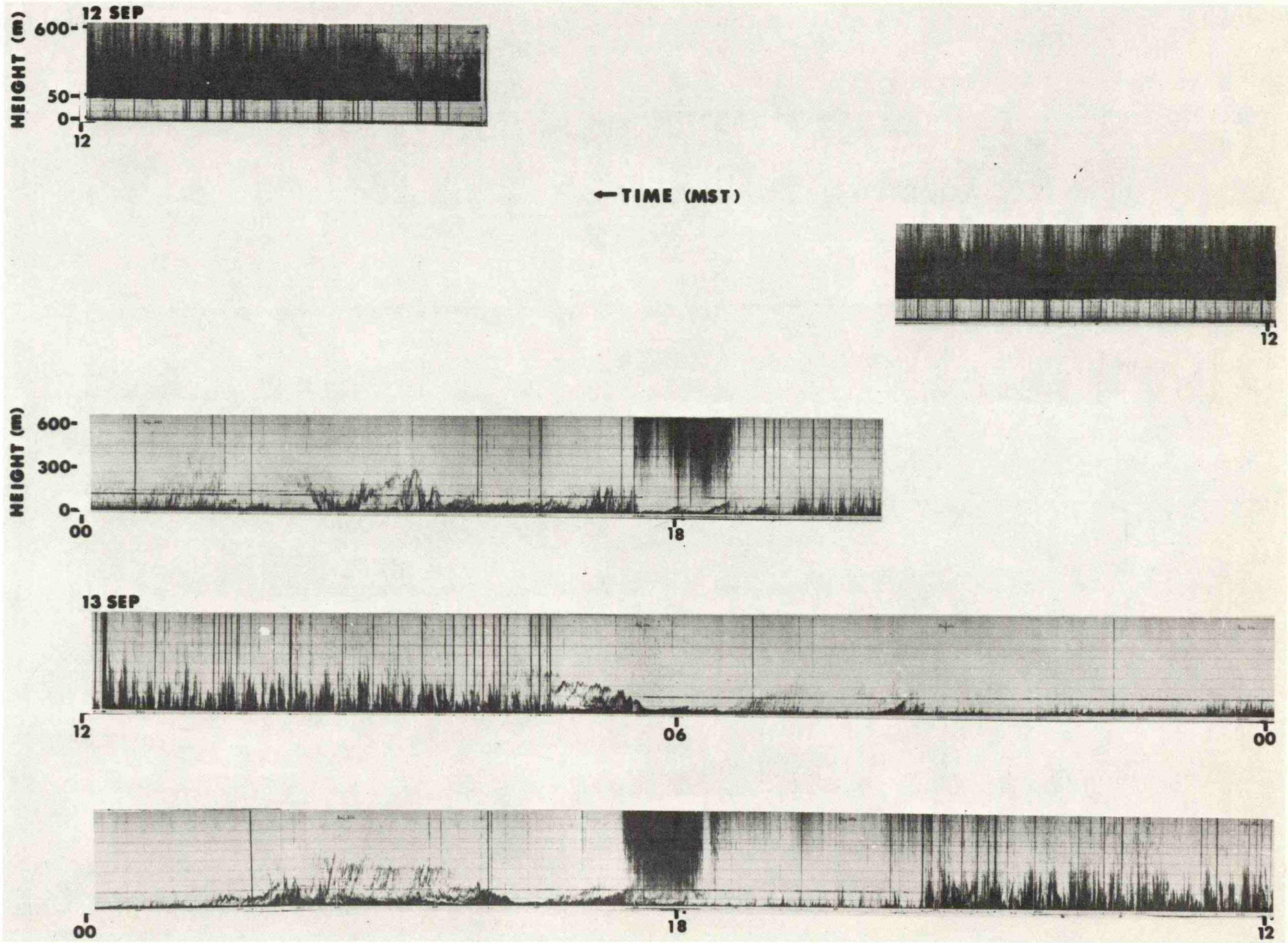


Figure 14.2.--Continued.

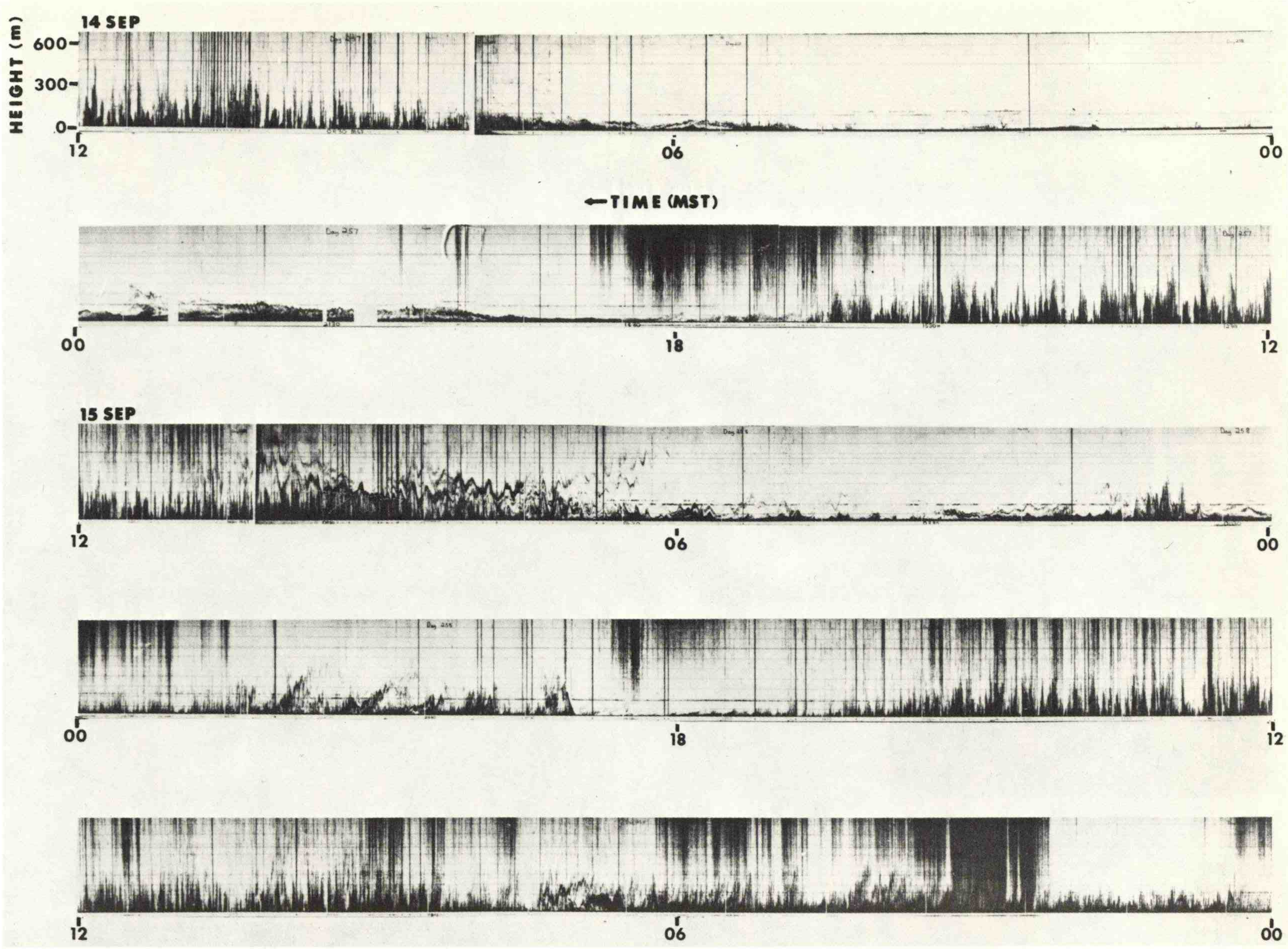


Figure 14.2.--Continued.

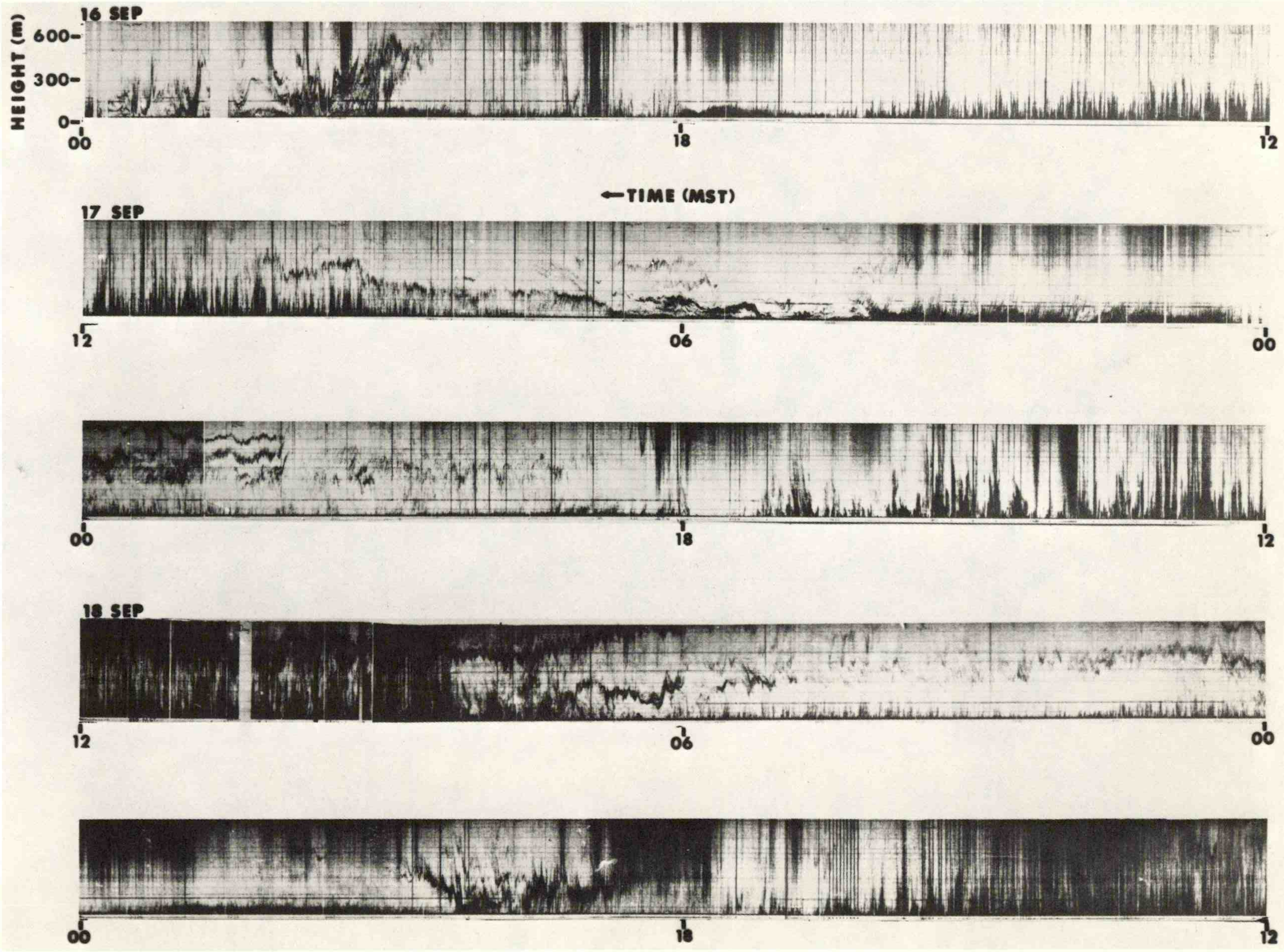


Figure 14.2.--Continued.

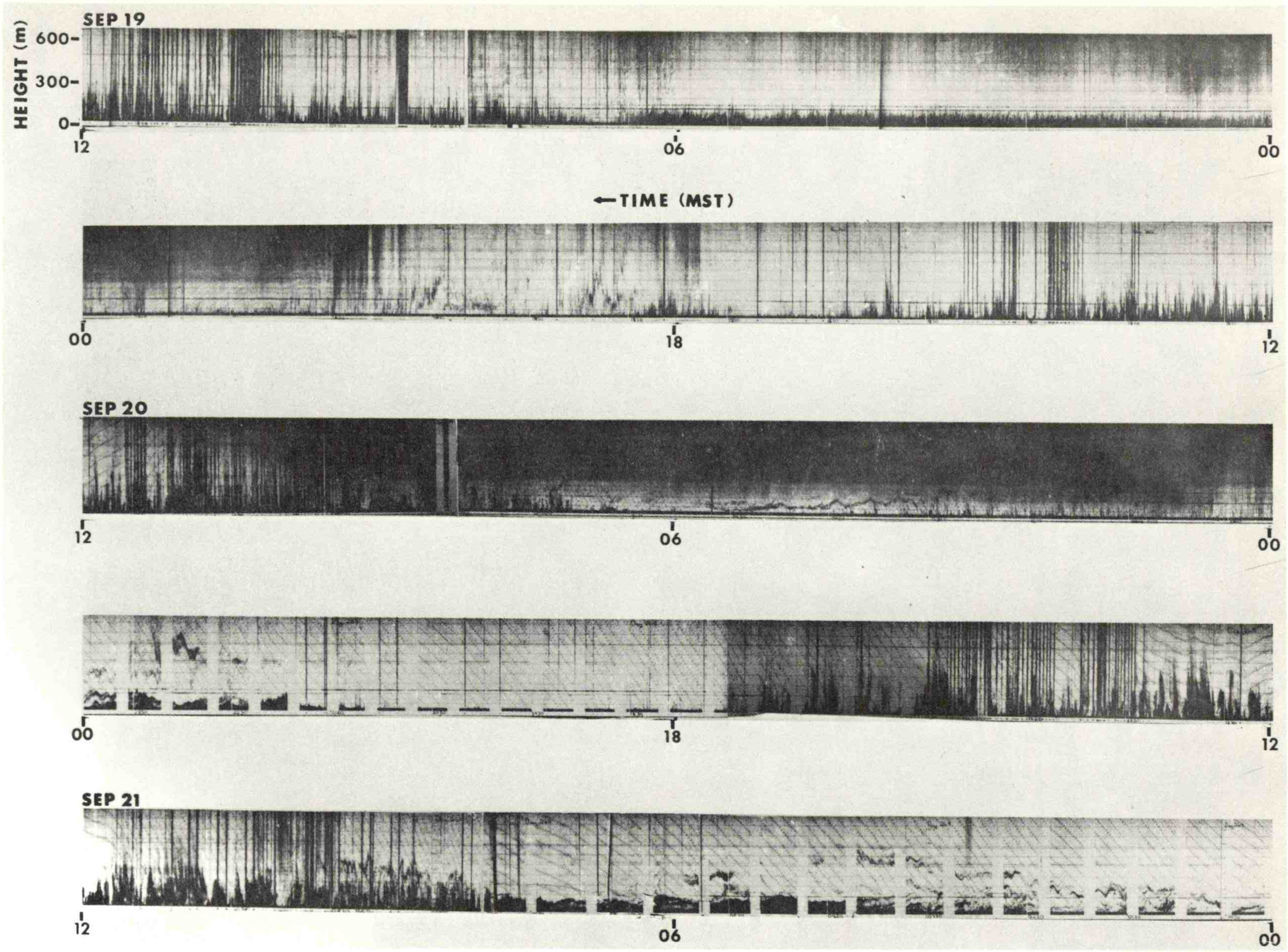


Figure 14.2.--Continued.

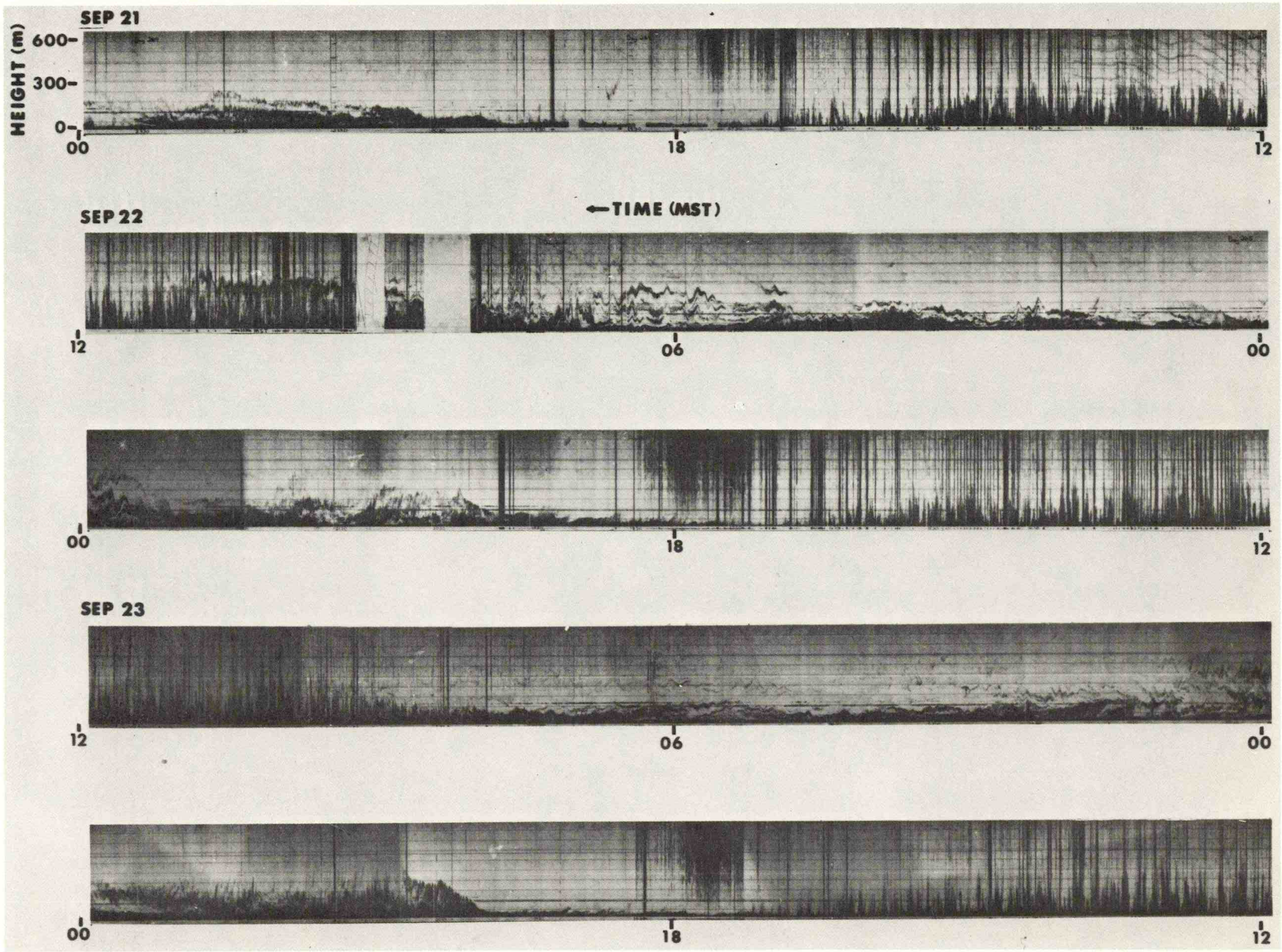


Figure 14.2.--Continued.

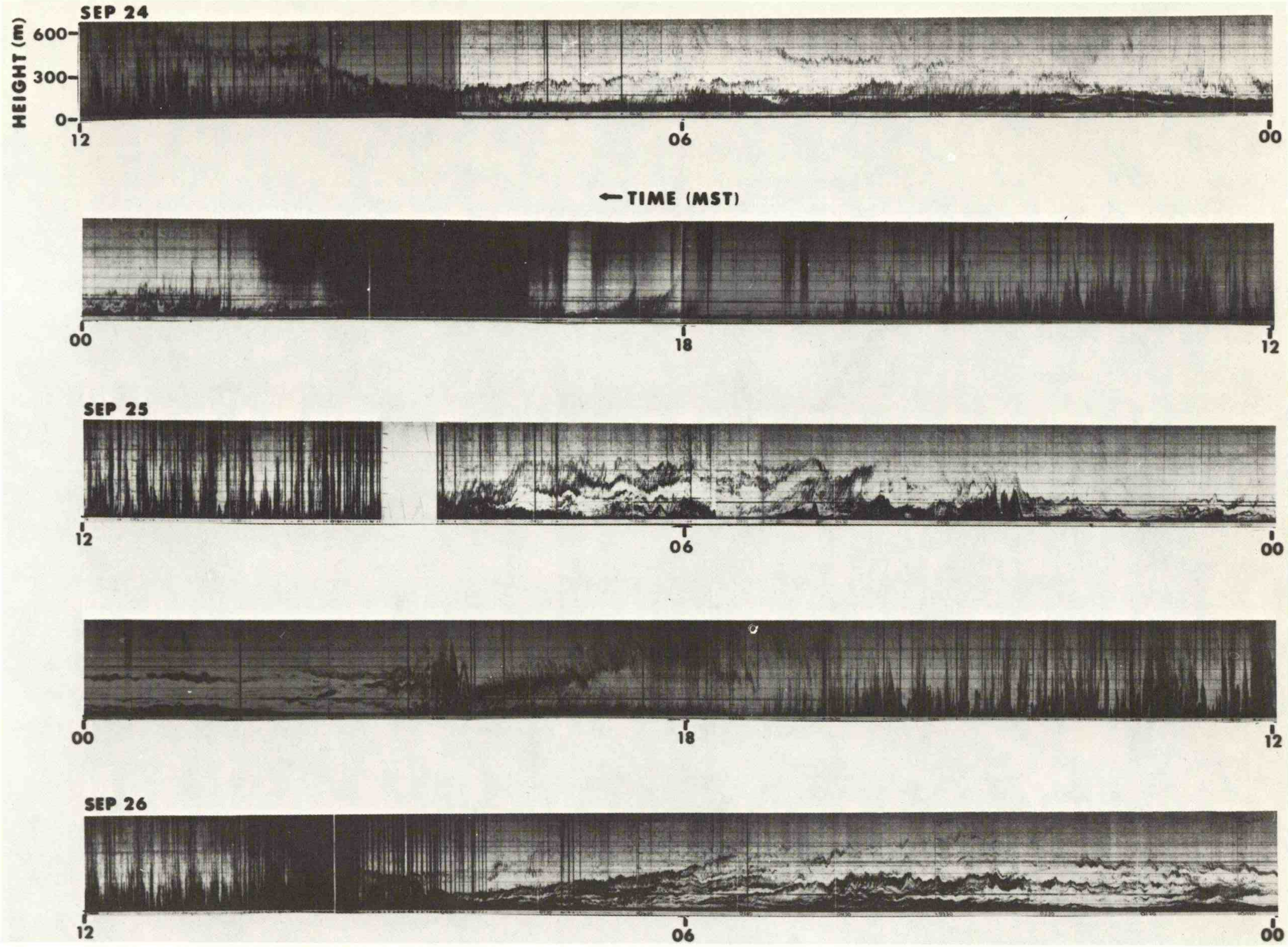


Figure 14.2.--Continued.

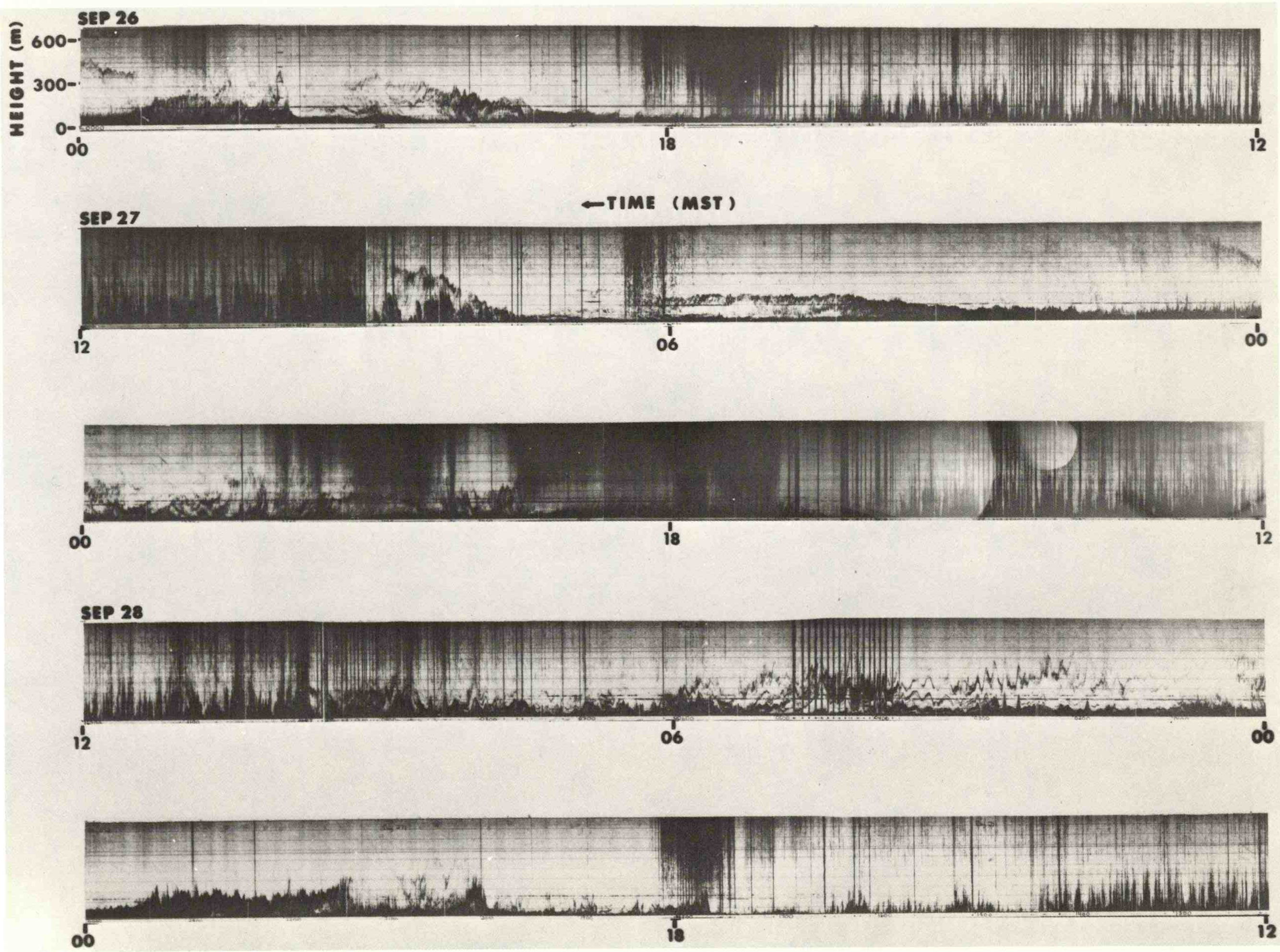


Figure 14.2.--Continued.

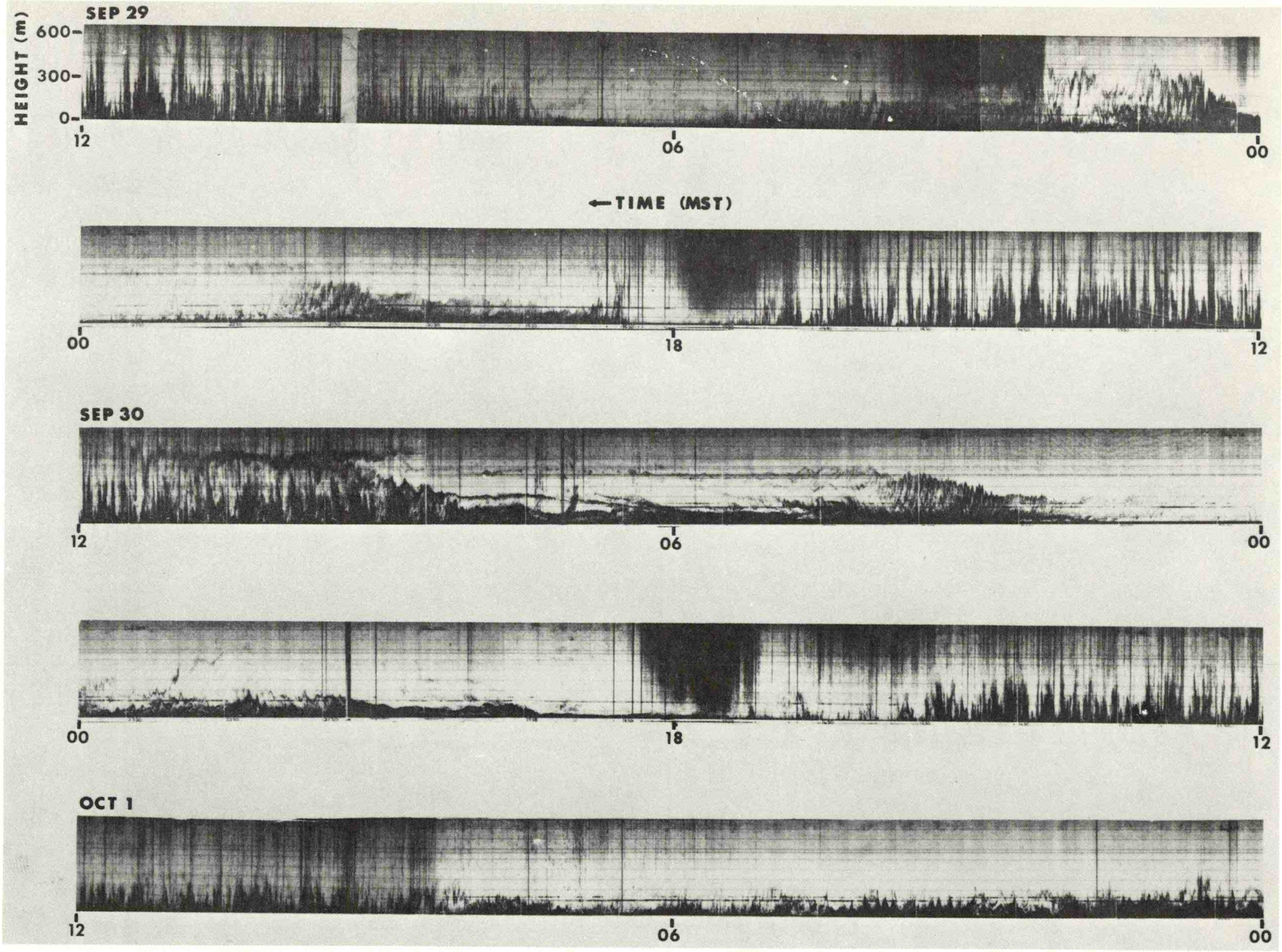


Figure 14.2.--Continued.

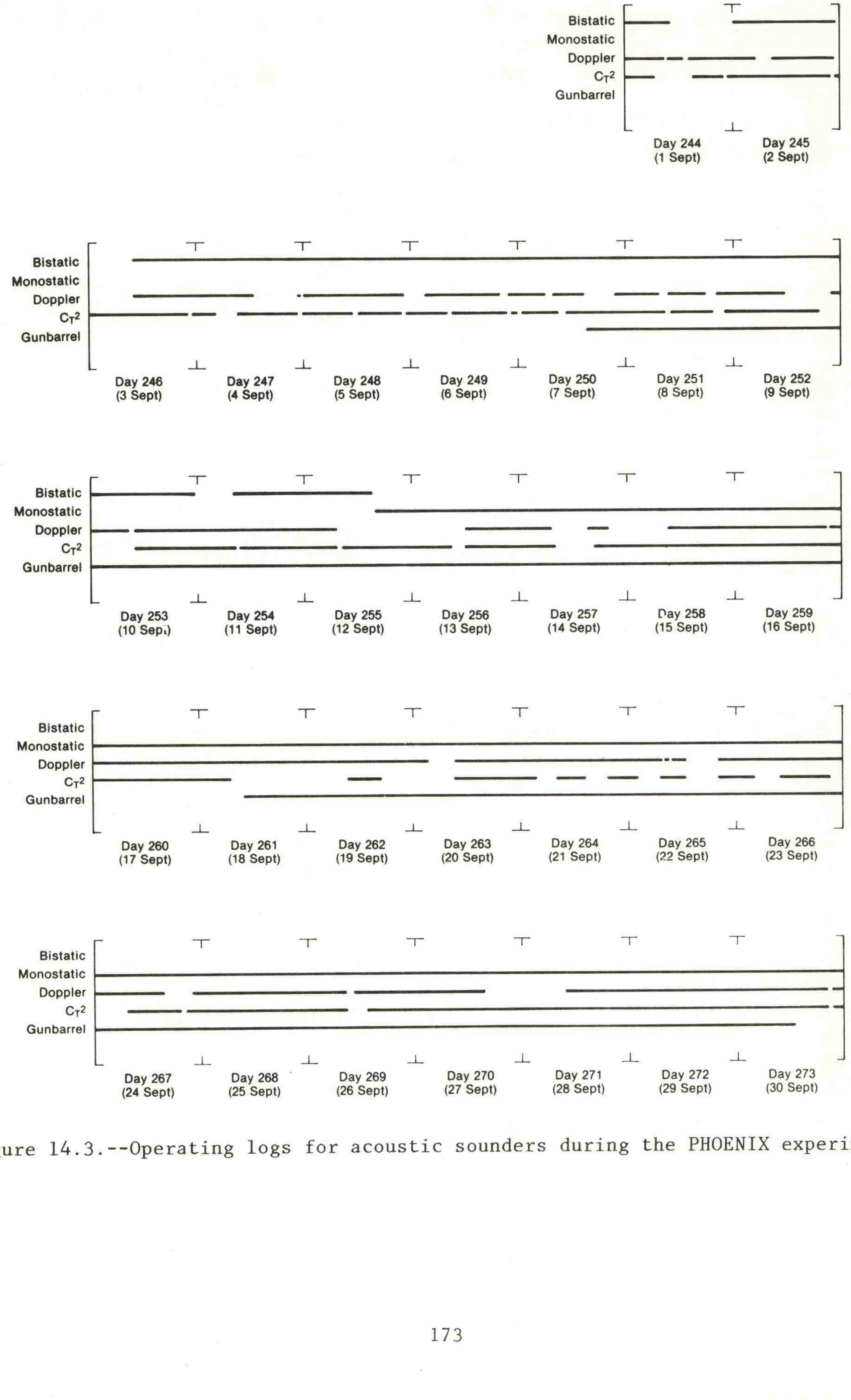


Figure 14.3.--Operating logs for acoustic sounders during the PHOENIX experiment.

Acknowledgments

We wish to acknowledge the help of Joan Birtwistle and Steve Bell for their help in operating the acoustic systems during PHOENIX. Edward J. Owens engineered and constructed the system.

References

Beran, D. W., C. G. Little, and B. C. Willmarth, Acoustic Doppler measurements of vertical velocities in the atmosphere, Nature 230, 160-162 (1971).

Beran, D. W., W. H. Hooke, and S. F. Clifford, Acoustic echo-sounding techniques and their application to gravity-wave, turbulence, and stability studies, Boundary-Layer Meteorol. 4, 133-153 (1973).

Brown, E. H., and F. F. Hall, Jr., Advances in atmospheric acoustics, Geophys. Space Phys. 16, 47-110 (1978).

Gaynor, J. E., Acoustic Doppler measurements of atmospheric boundary layer velocity structure functions and energy dissipation rates, J. Appl. Meteorol. 16, 148-155 (1977).

Gaynor, J. E., and P. A. Mandics, Analysis of the tropical marine boundary layer during GATE using acoustic sounder data, Mon. Weather Rev. 106, 223-232 (1978).

Hall, F. F., Jr., J. G. Edinger, and W. D. Neff, Convective plumes in the planetary boundary layer, investigated with an acoustic echo sounder, J. Appl. Meteorol. 14, 513-523 (1975).

Hall, F. F., Jr., W. D. Neff, and T. V. Frazier, Wind shear observations in thunderstorm density currents, Nature 264, 408-411 (1976).

Hooke, W. H., J. M. Young, and D. W. Beran, Atmospheric waves observed in the planetary boundary layer using an acoustic sounder and a microbarograph array, Boundary-Layer Meteorol. 2, 371-380 (1972).

Hooke, W. H., F. F. Hall, Jr., and E. E. Gossard, Observed generation of an atmospheric gravity wave by shear instability in the mean flow of the planetary boundary layer, Boundary- Layer Meteorol. 5, 29-42 (1973).

Little, C. G., Acoustic methods for the remote probing of the lower atmosphere, Proc. IEEE 57, 571-578 (1969).

McAllister, L. G., Acoustic sounding of the lower troposphere, J. Atmos. Terr. Phys. 30, 1439-1440 (1968).

McAllister, L. G., J. R. Pollard, A. R. Mahoney, and P. J. R. Shaw, Acoustic sounding — a new approach to the study of atmospheric structure, Proc. IEEE 57, 579-587 (1969).

Neff, W. D., Boundary layer research at South Pole Station using acoustic remote sensing, Antarct. J. U. S. 13, 179-181 (1978).

Neff, W. D., and F. F. Hall, Jr., Acoustic remote sensing of the atmospheric boundary layer at the South Pole, Preprints Fourth Symposium on Meteorological Observations and Instrumentation, April 10-14, 1978, Denver, Colo., pp. 357-361, American Meteorological Society, Boston, Mass. (1978).

CHAPTER 15

A BRIEF SUMMARY OF WEATHER CONDITIONS DURING PHOENIX

D. E. Wolfe
Wave Propagation Laboratory
National Oceanic and Atmospheric Administration
Boulder, Colorado 80303

15.1 Introduction

All PHOENIX participants hope to see PHOENIX data receive the widest possible use within the meteorological community. To aid readers in evaluating the suitability of this data set for their particular purposes, as well as to provide a collection of maps and charts to which we can refer in our own publications, we provide here a brief summary of the meteorological conditions over Colorado during September 1978. We present two levels of detail in the synoptic weather analysis as it pertains to PHOENIX. First is a large-scale weather synopsis, focusing on the day-to-day pattern of weather evolving over the northeastern plains of Colorado during September. The second is a more detailed analysis of our localized conditions (both in space and time) as they relate to the BAO site itself. Because of cost and time involved in providing such a detailed analysis we analyzed only three days, September 11, 21, and 26 — both to illustrate the availability of data for such purposes and to look more closely at days of particular interest. September 11 marked a high-wind event at the BAO site; for the 21st and 26th we are interested in carrying out detailed comparisons of various remote-sensors and in-situ estimates of z_i (boundary-layer depth).

15.2 General Weather Synopsis for September 1978

Figures 15.1-15.28, taken from the daily weather map series (published by NOAA's Environmental Data Information Service), show daily surface, 500 mb, maximum and minimum temperature, and precipitation charts for the contiguous United States during September. A full set of three-hourly surface maps, as well as all the upper-air charts for September, has been archived within WPL. Figure 15.29 shows Denver surface pressures and 500-mb heights, surface temperatures, and water-vapor mixing ratios for surface and 700 mb throughout the month. The remainder of this

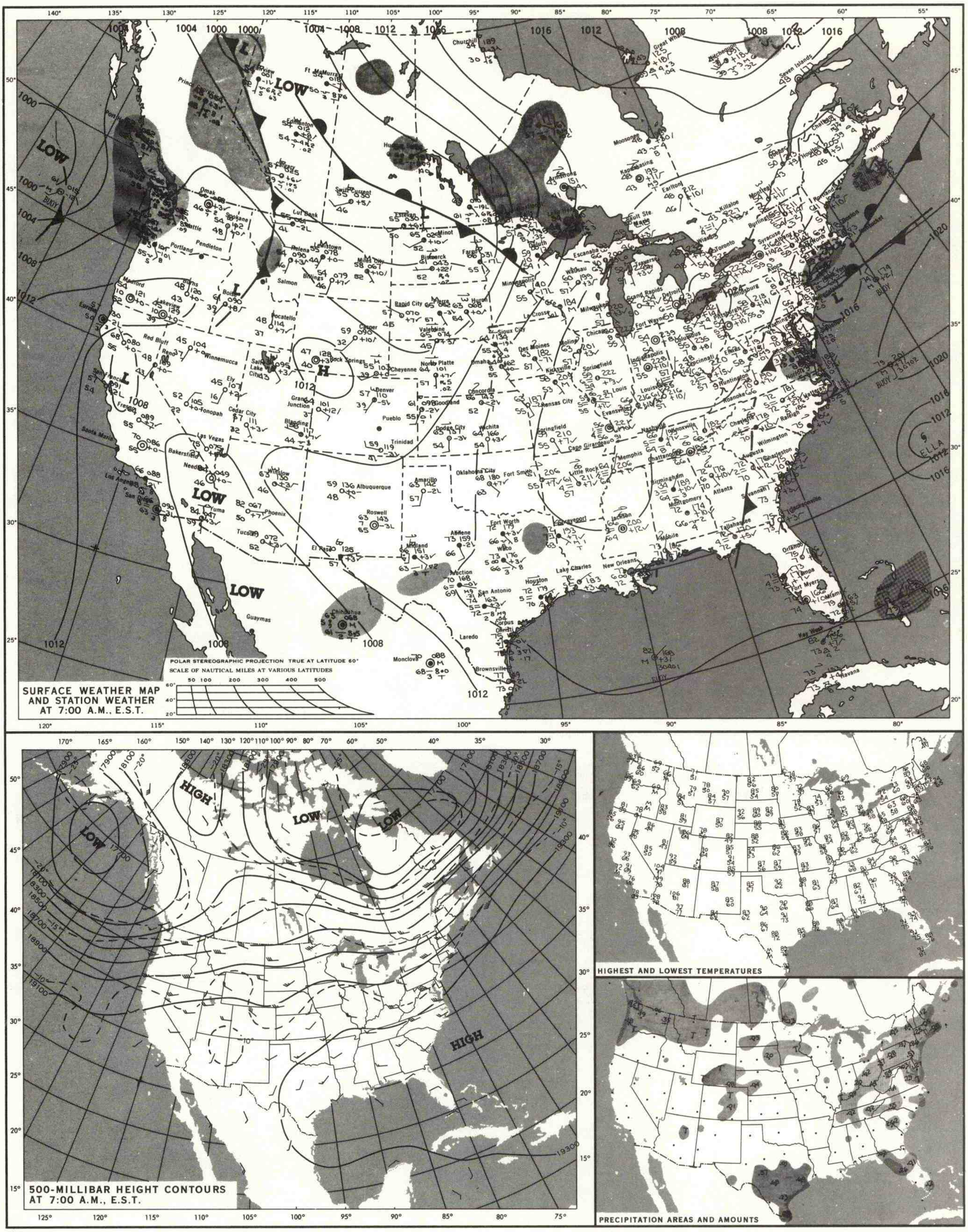


Figure 15.1.--National Weather Service maps for September 1, 1978.

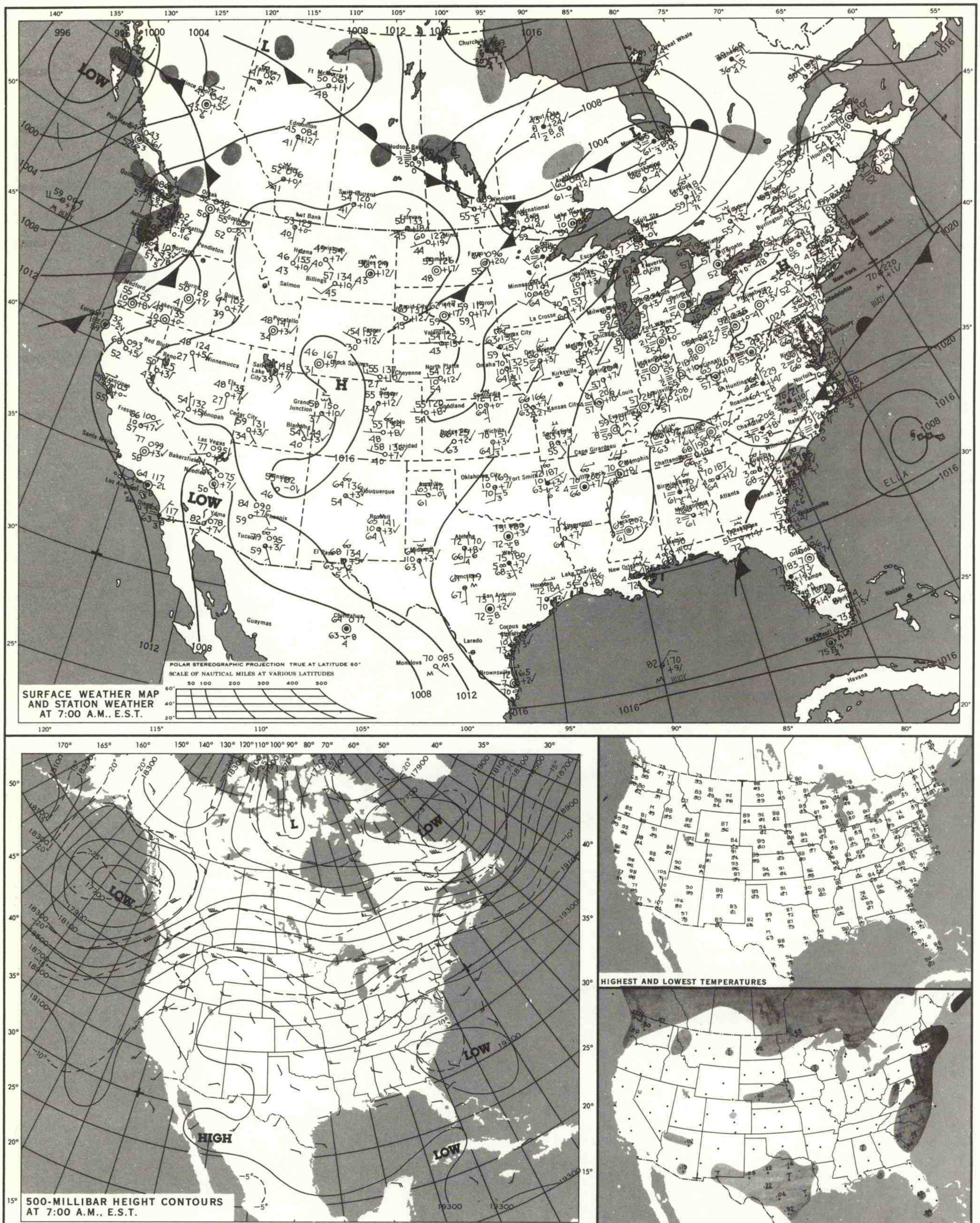


Figure 15.2.--National Weather Service maps for September 2, 1978.

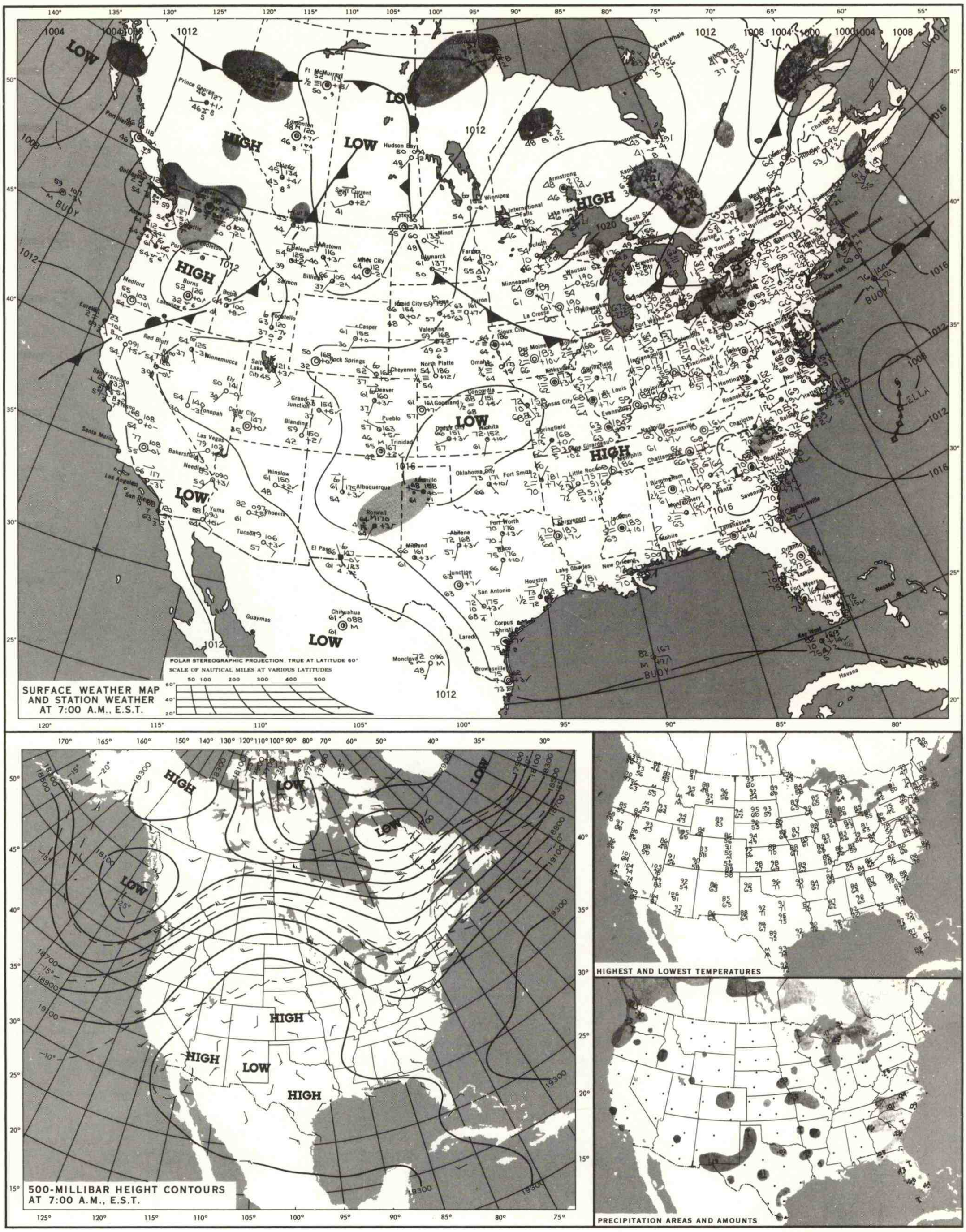


Figure 15.3.--National Weather Service maps for September 3, 1978.

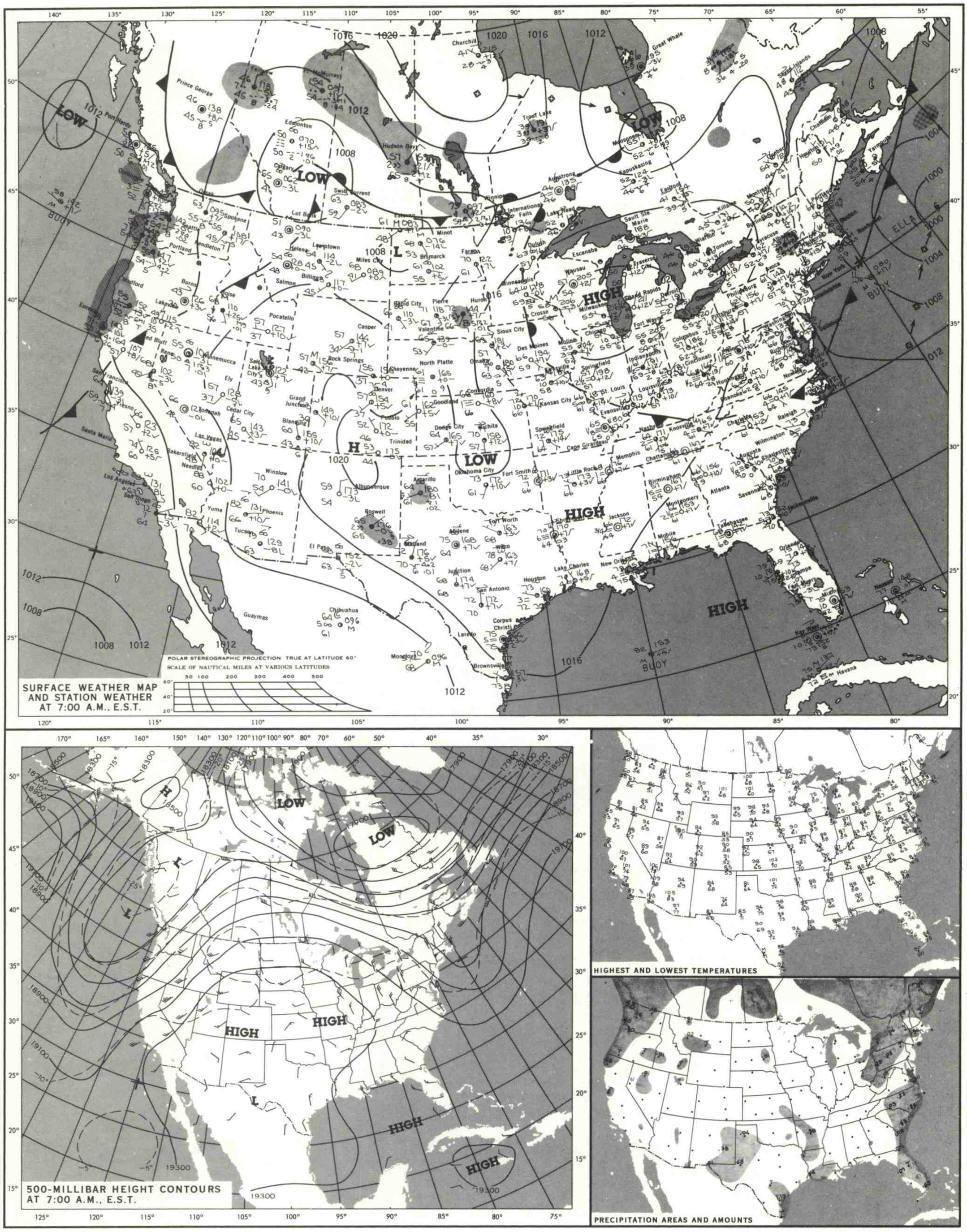


Figure 15.4.--National Weather Service maps for September 4, 1978.

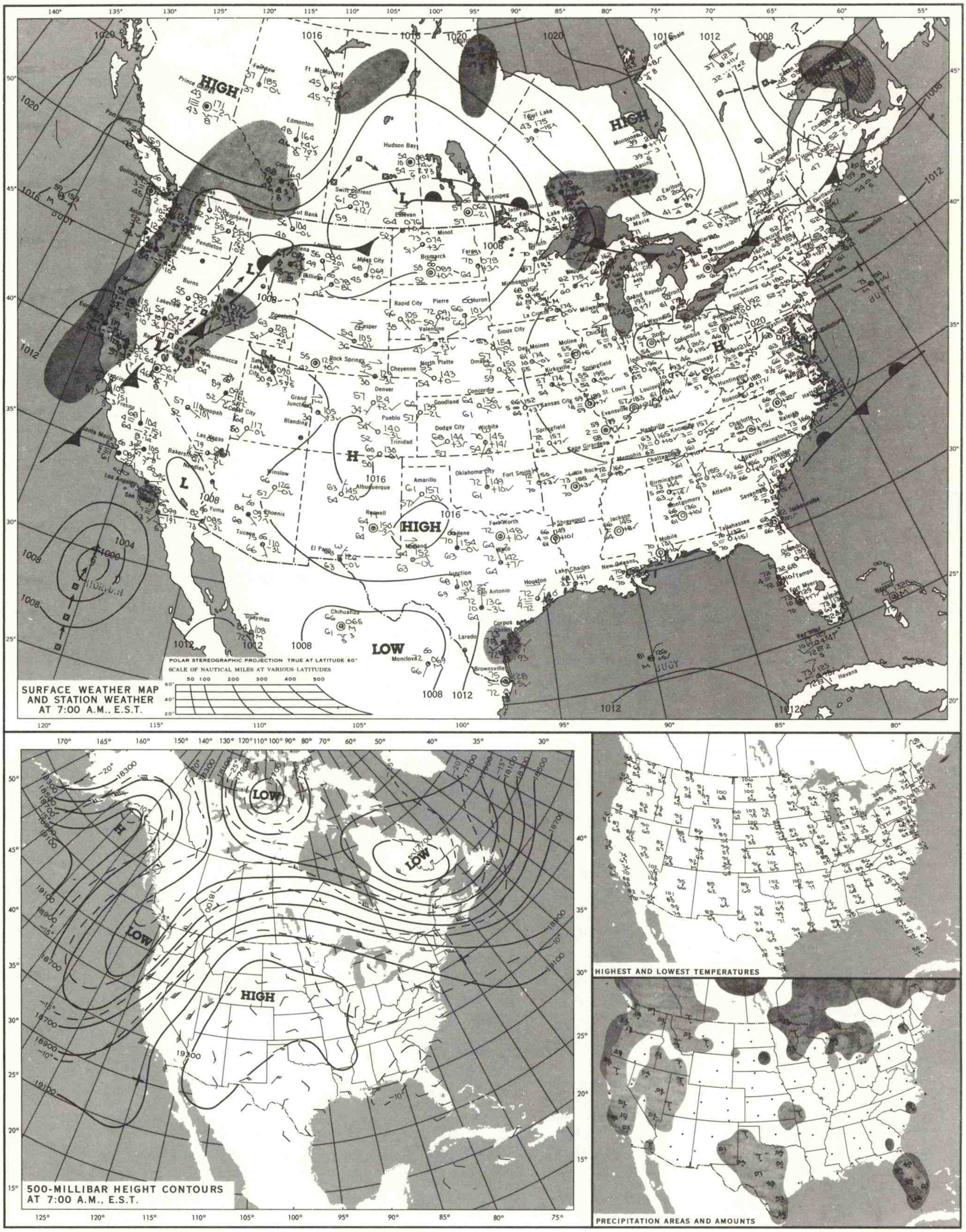


Figure 15.5.--National Weather Service maps for September 5, 1978.

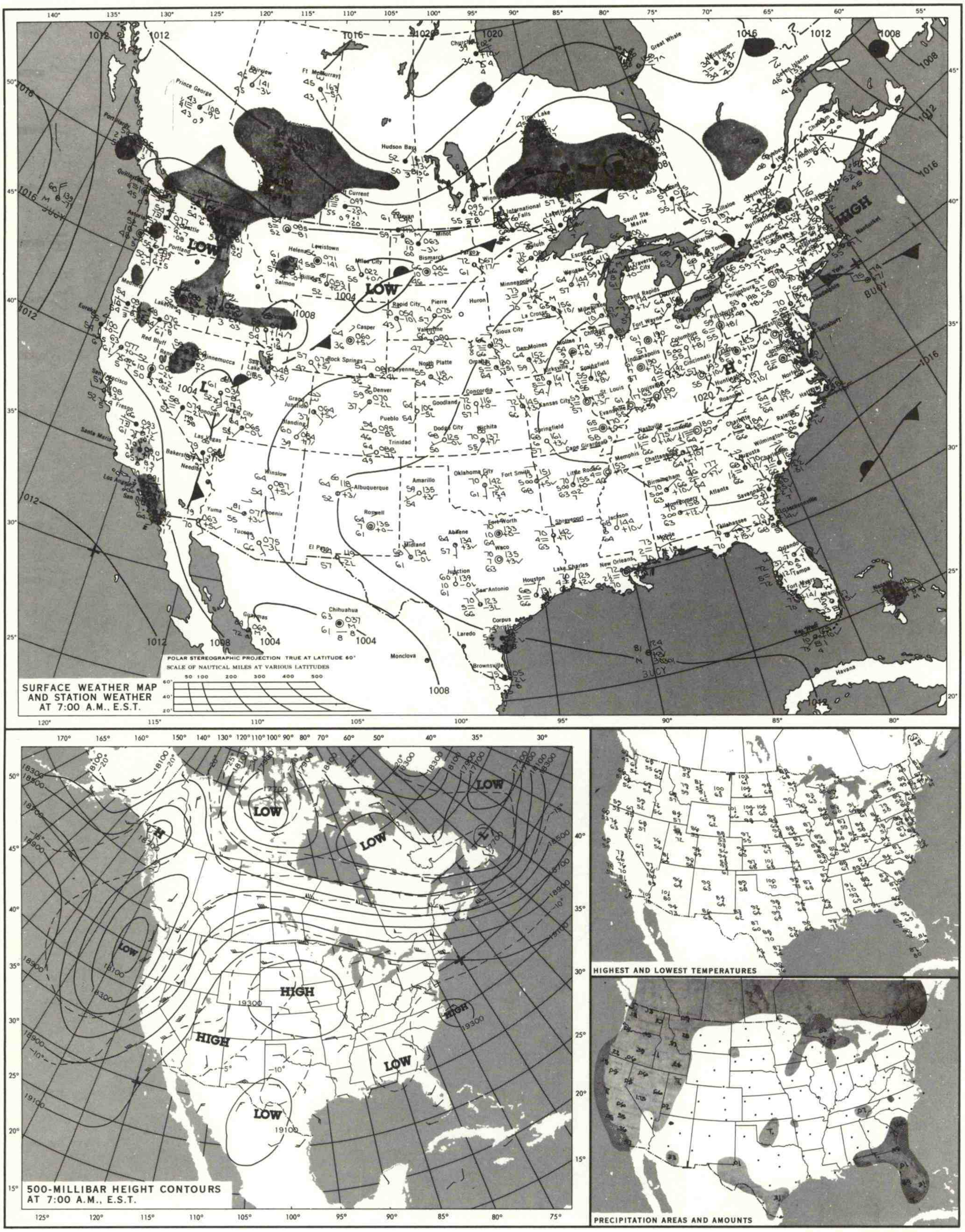
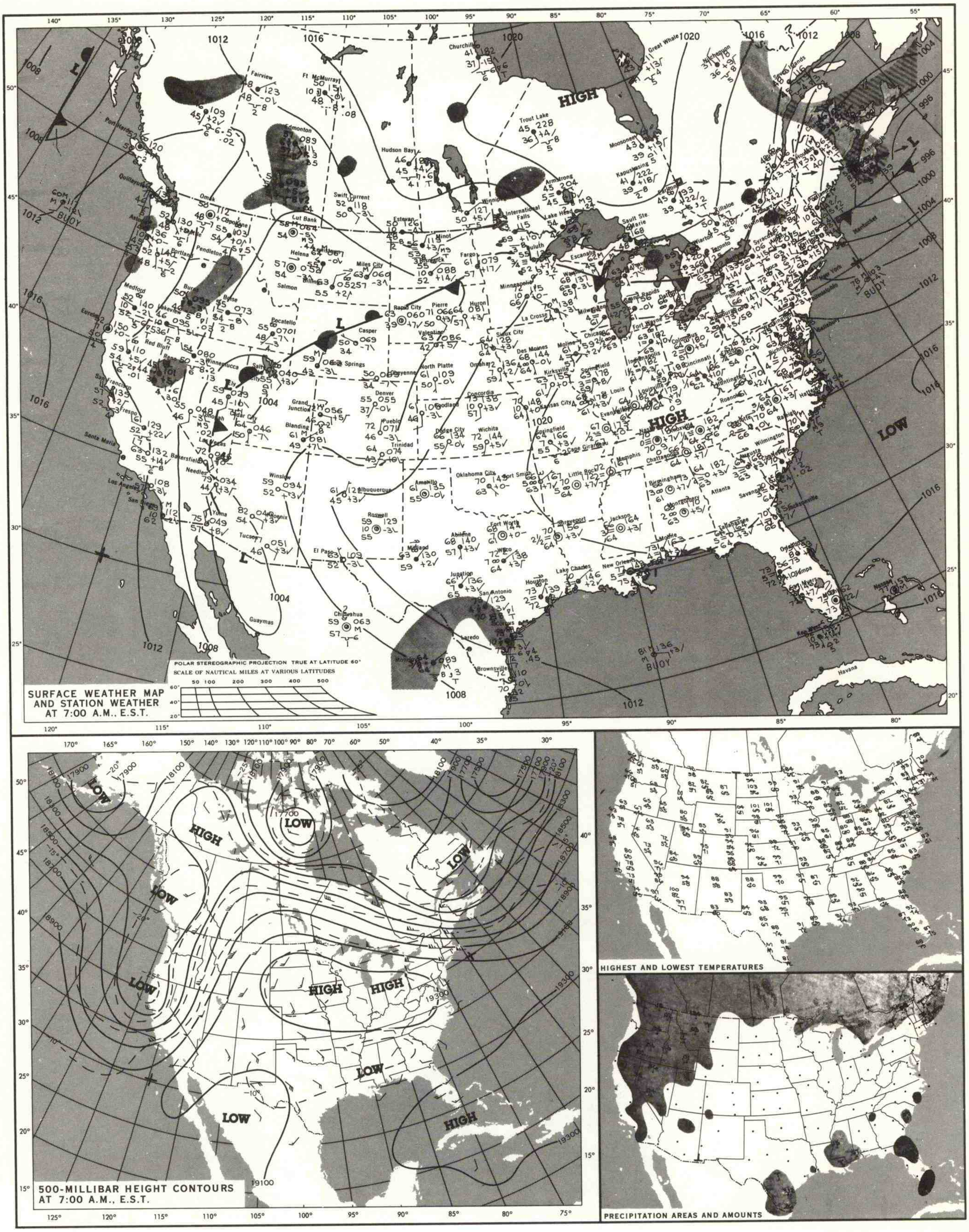


Figure 15.6.--National Weather Service maps for September 6, 1978.


SURFACE WEATHER MAP AND STATION WEATHER AT 7:00 A.M., E.S.T.
POLAR STEREOGRAPHIC PROJECTION TRUE AT LATITUDE 60°
SCALE OF NAUTICAL MILES AT VARIOUS LATITUDES
50 100 200 300 400 500
HIGH
LOW
1012
1016
1020
1004
1008
1000
996
Fairview
Ft McMurray
Edmonton
Hudson Bay
Trout Lake
Great Whale
Churchill
Moosonee
Kapuskasing
Armstrong
Swift Current
Lut Bank
Estevan
Minot
Fargo
Winnipeg
International Falls
Lake Head
Sault Ste. Marie
Billaloe
Toronto
Buffalo
Syracuse
Portland
Pendleton
Helena
Miles City
Bismarck
Salmon
Medford
Burns
Boise
Eureka
Lakeview
Red Bluff
Reno
Winnemucca
Salt Lake City
Ely
Pocatello
Rapid City
Pierre
Huron
Valentine
Casper
Cheyenne
North Platte
Omaha
Sioux City
Des Moines
Minneapolis
Duluth
Escanaba
Milwaukee
La Crosse
Grand Rapids
Detroit
Chicago
Moline
Fort Wayne
Columbus
Cincinnati
Indianapolis
Kirksville
Springfield
Concordia
Goodland
Kansas City
Grand Junction
Blanding
Denver
Pueblo
Dodge City
Wichita
Trinidad
Oklahoma City
Fort Smith
Little Rock
Memphis
Nashville
Louisville
St. Louis
Roanoke
Charleston
Richmond
Hatteras
Raleigh
Wilmington
Augusta
Charlotte
Atlanta
Birmingham
Montgomery
Chattanooga
Savannah
Jacksonville
Tallahassee
Jackson
Shreveport
Fort Worth
Abilene
Midland
Waco
Amarillo
Albuquerque
Roswell
El Paso
Tucson
Phoenix
Yuma
Needles
Winslow
Los Angeles
San Diego
Bakersfield
Fresno
Santa Maria
San Francisco
Quillayute
Port Hardy
Omak
Astoria
Lander
Cape Girardeau
Evansville
Lexington
Huntington
Parkersburg
Pittsburgh
Syracuse
Buffalo
Toronto
Kingston
Ottawa
Montreal
Quebec
Yarmouth
Sydney
Gander
Goose Bay
Nain
Frobisher
Resolute
Eureka
Thule
Iceland
Shannon
Valentia
Scilly
Brest
Paris
Berlin
Prague
Vienna
Munich
Zurich
Rome
Nice
Madrid
Lisbon
Gibraltar
Algiers
Tripoli
Cairo
Dakar
Bermuda
Nassau
Havana
Key West
Miami
Tampa
Orlando
Jacksonville
Charleston
Wilmington
Norfolk
Atlantic City
New York
Boston
Portland
Caribou
Sable Island
Kentucky
Lake Charles
New Orleans
Houston
San Antonio
Laredo
Brownsville
Corpus Christi
Junction
Chihuahua
Guaymas
Mazatlan
Merida
Belize
Kingston
Port au Prince
Caracas
Curacao
Trinidad
Barbados
Antigua
San Juan
Guadeloupe
Martinique
Dominica
St. Lucia
Grenada
Tobago
Georgetown
Paramaribo
Cayenne
Belem
Fortaleza
Natal
Recife
Maceio
Salvador
Rio de Janeiro
Sao Paulo
Santos
Porto Alegre
Montevideo
Buenos Aires
Bahia Blanca
Comodoro Rivadavia
Rio Gallegos
Ushuaia
Stanley
Asuncion
Corumba
Cuiaba
Campo Grande
Belo Horizonte
Brasilia
Goiania
Manaus
Boa Vista
Iquitos
Lima
Arequipa
Antofagasta
Santiago
Concepcion
Valdivia
Puerto Montt
Punta Arenas
Easter Island
Juan Fernandez
Guayaquil
Quito
Bogota
Cali
Medellin
Barranquilla
Maracaibo
Valencia
Caracas
Maturin
Ciudad Bolivar
Boa Vista
Manaus

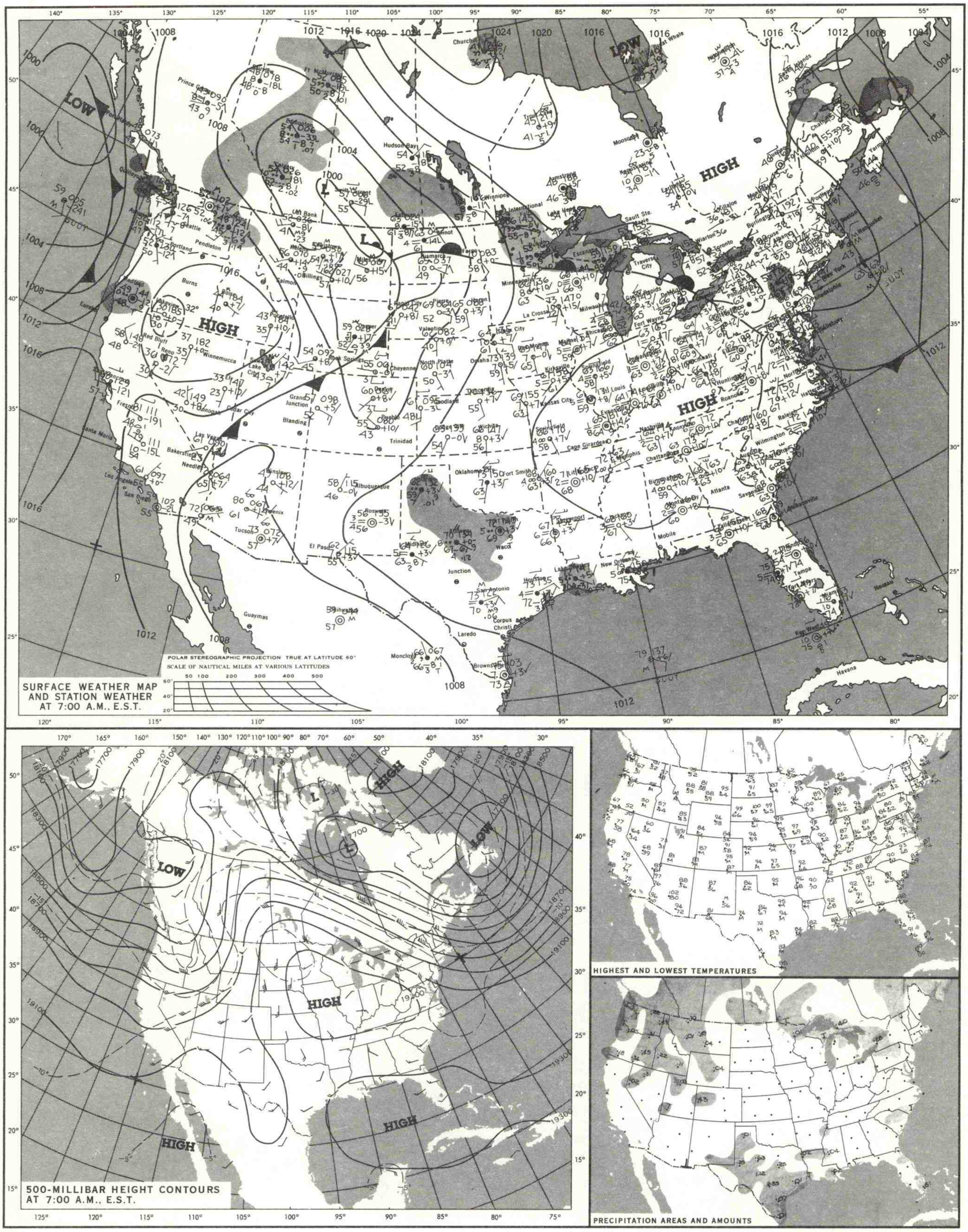


Figure 15.8.--National Weather Service maps for September 8, 1978.

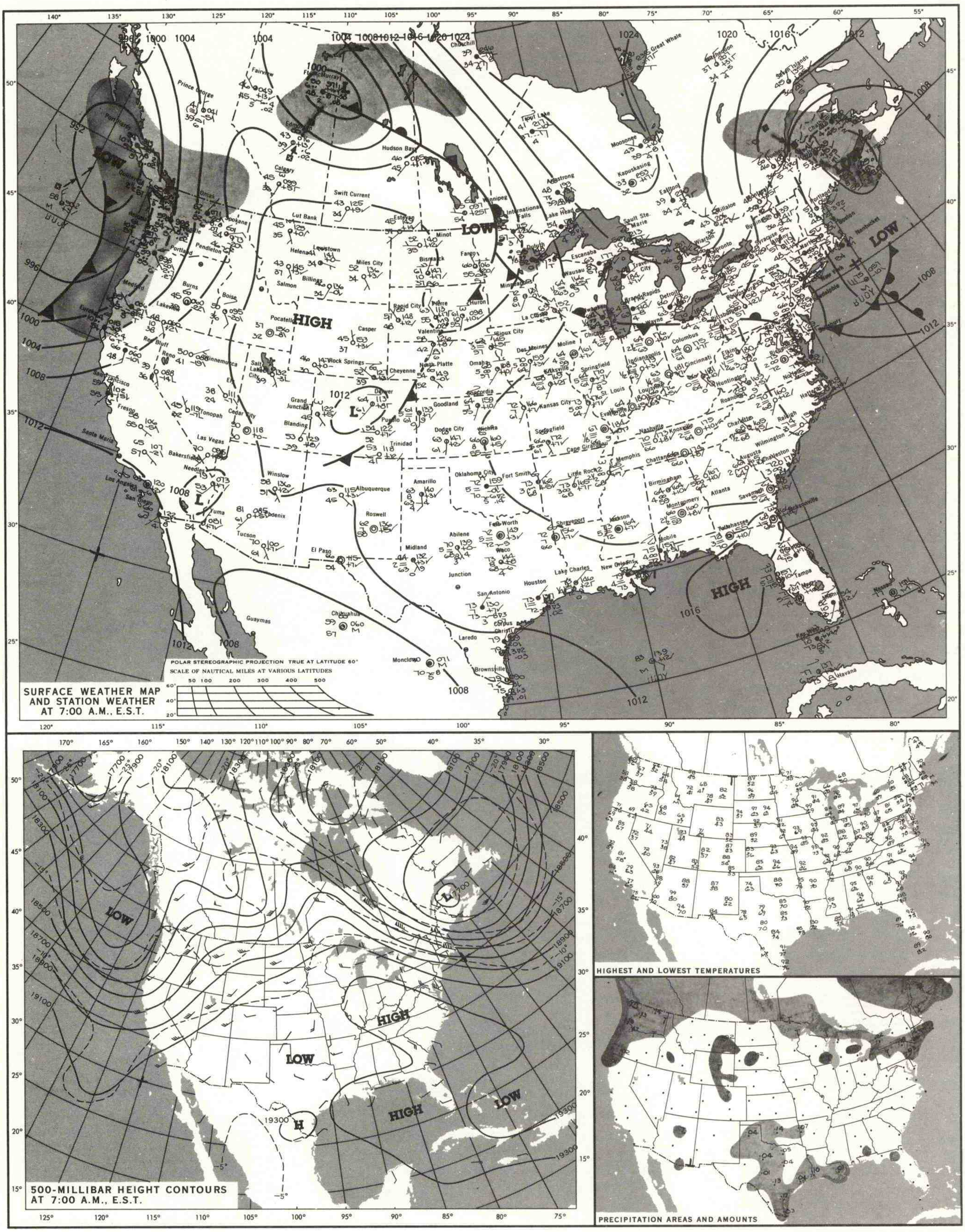


Figure 15.9.--National Weather Service maps for September 9, 1978.

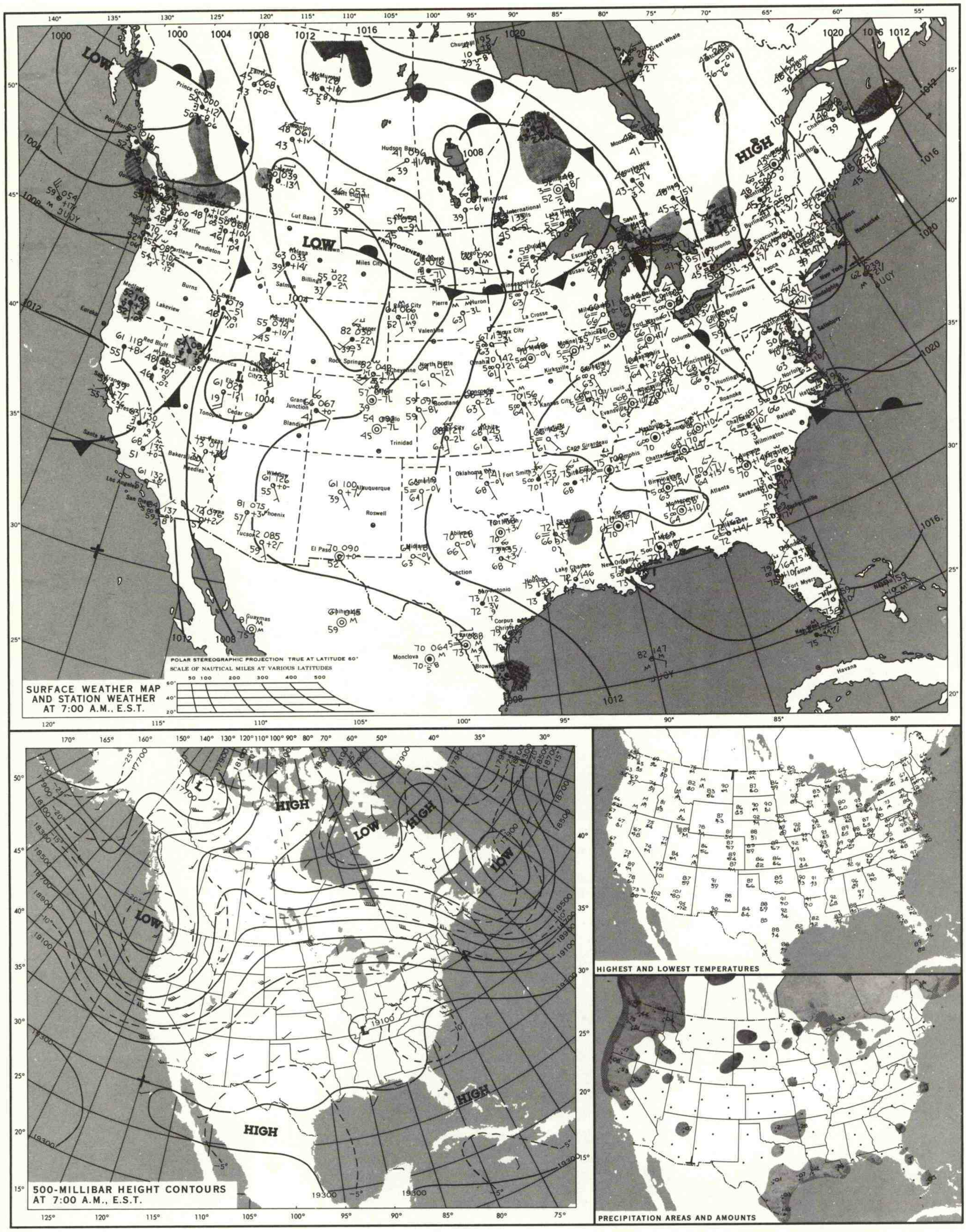


Figure 15.10.--National Weather Service maps for September 10, 1978.

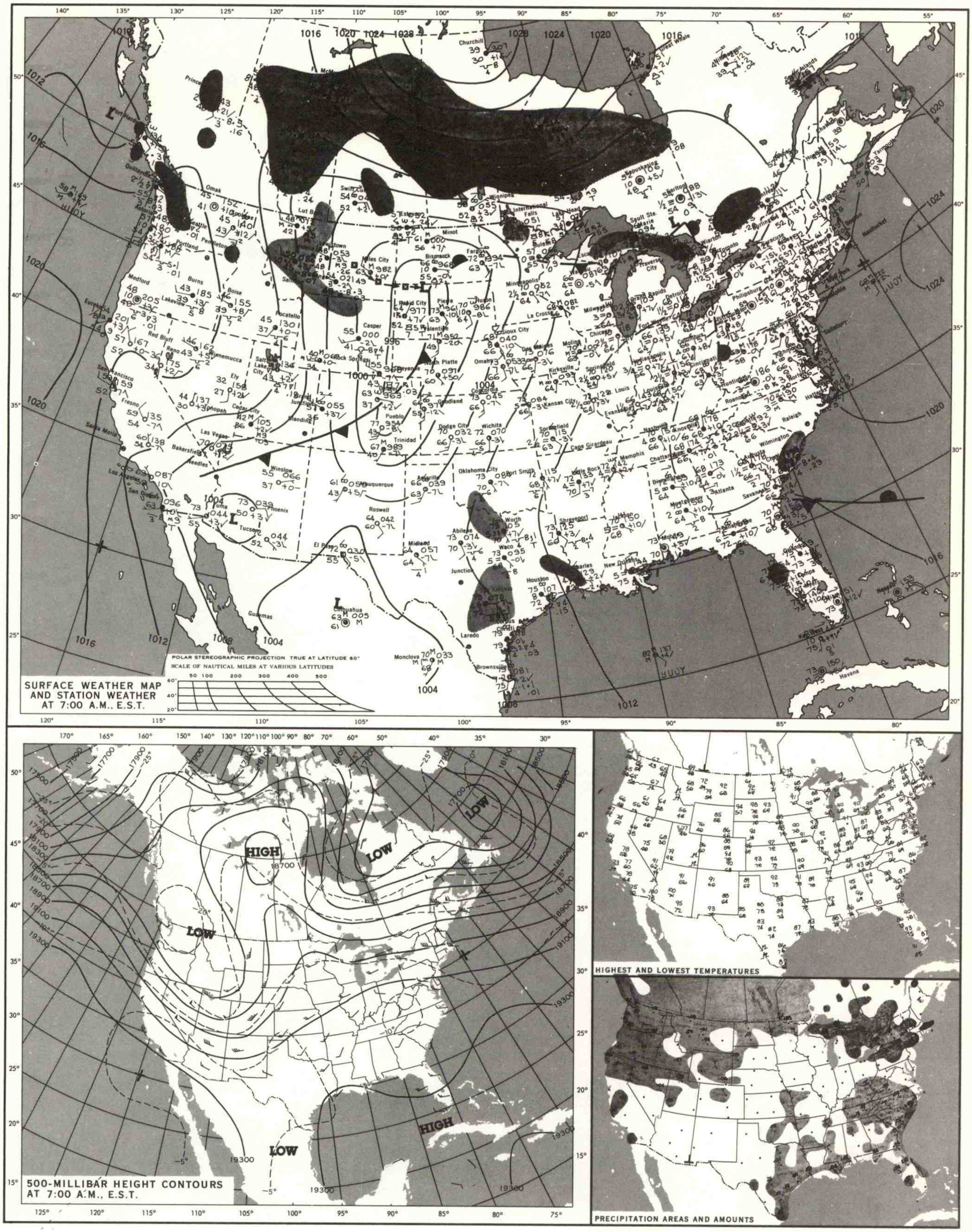


Figure 15.11.--National Weather Service maps for September 11, 1978.

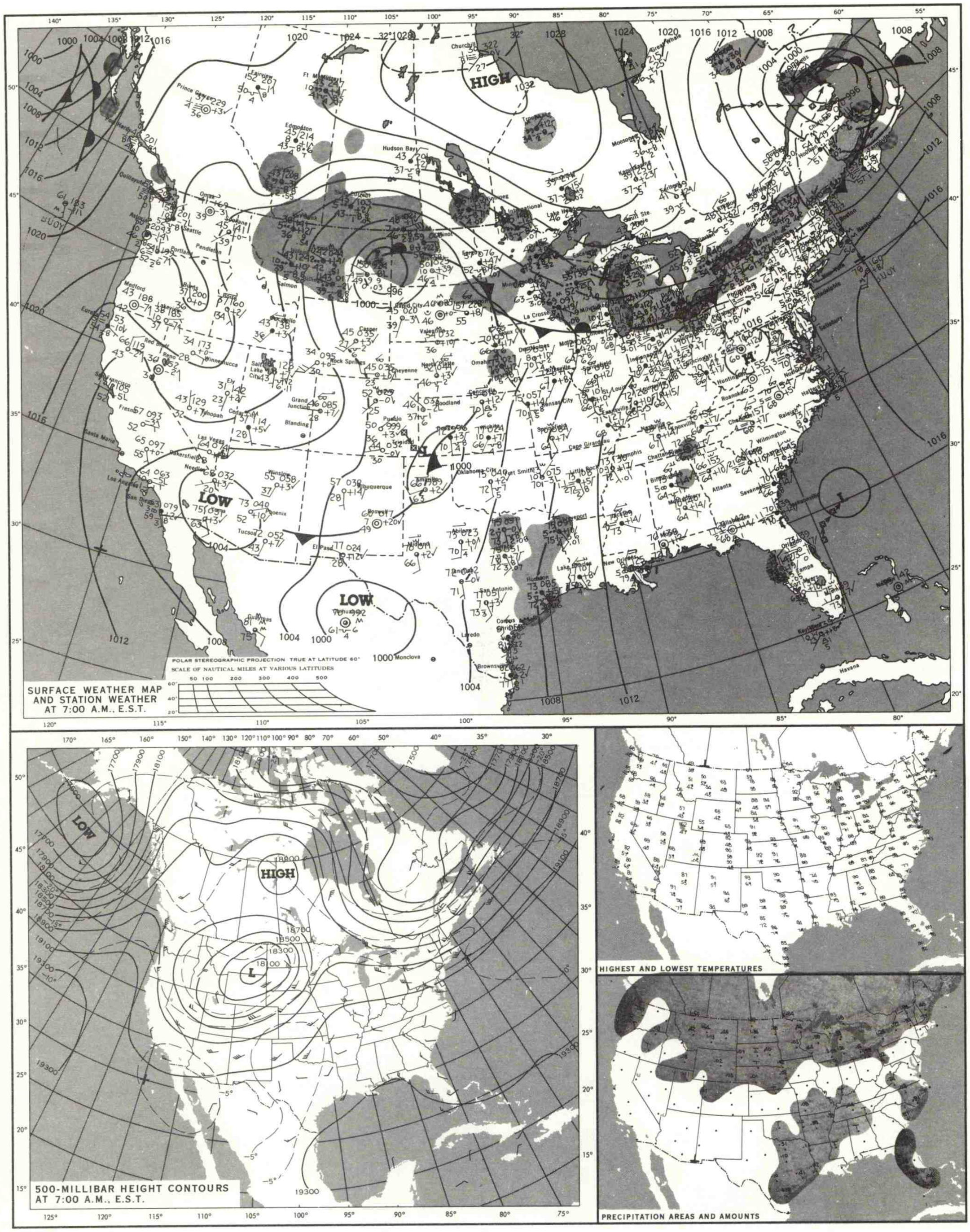


Figure 15.12.--National Weather Service maps for September 12,1978.

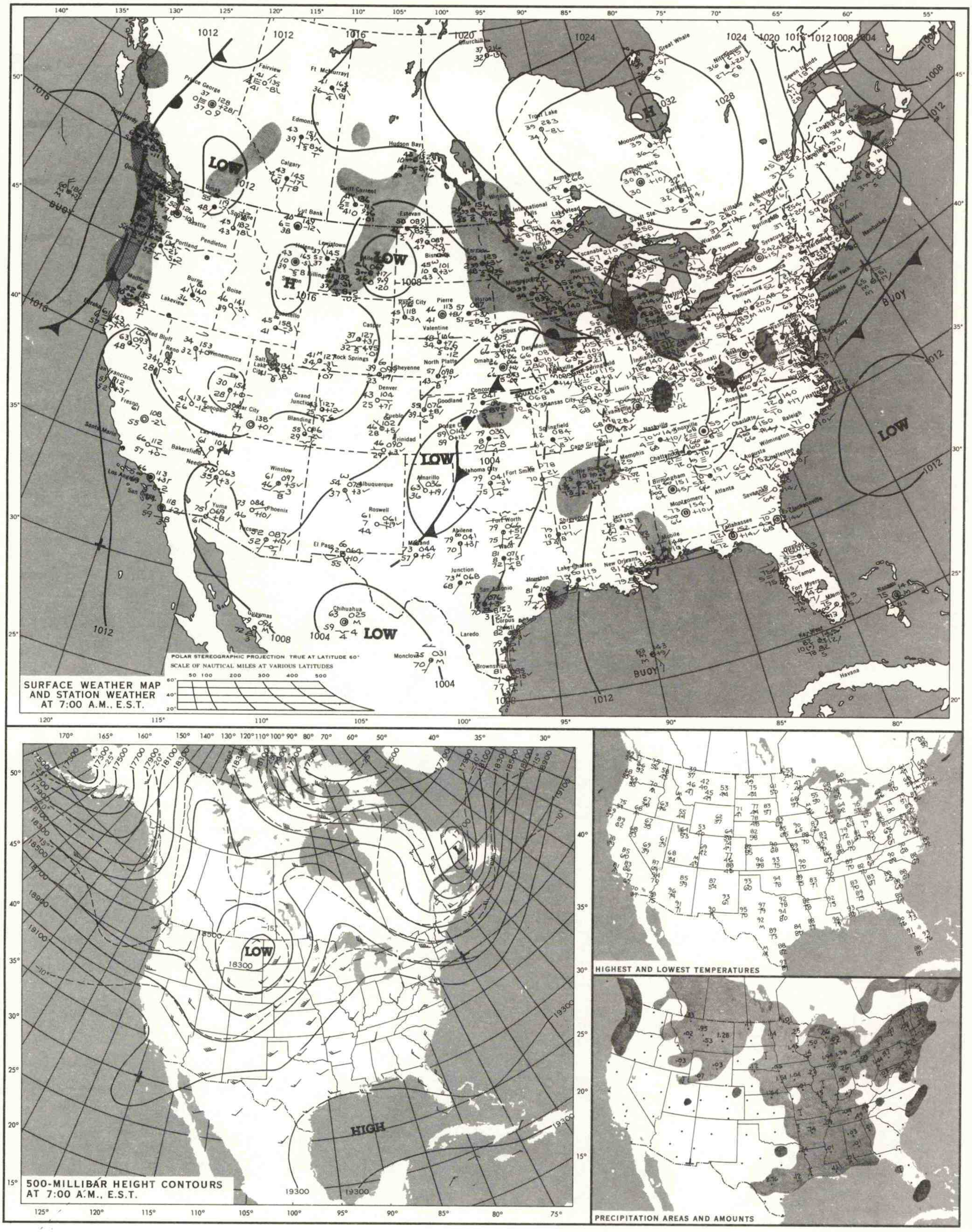


Figure 15.13.--National Weather Service maps for September 13, 1978.

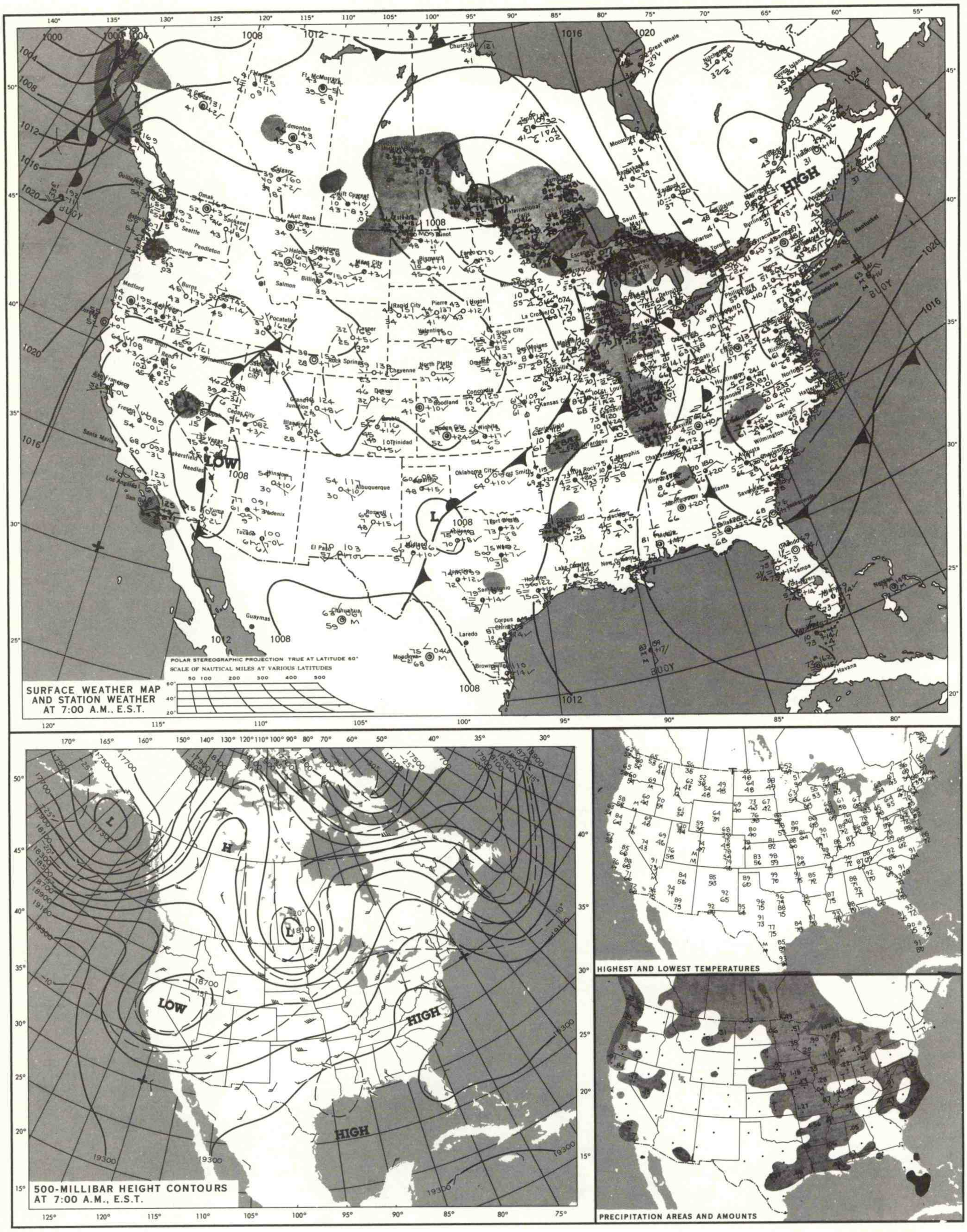


Figure 15.14.--National Weather Service maps for September 14, 1978.

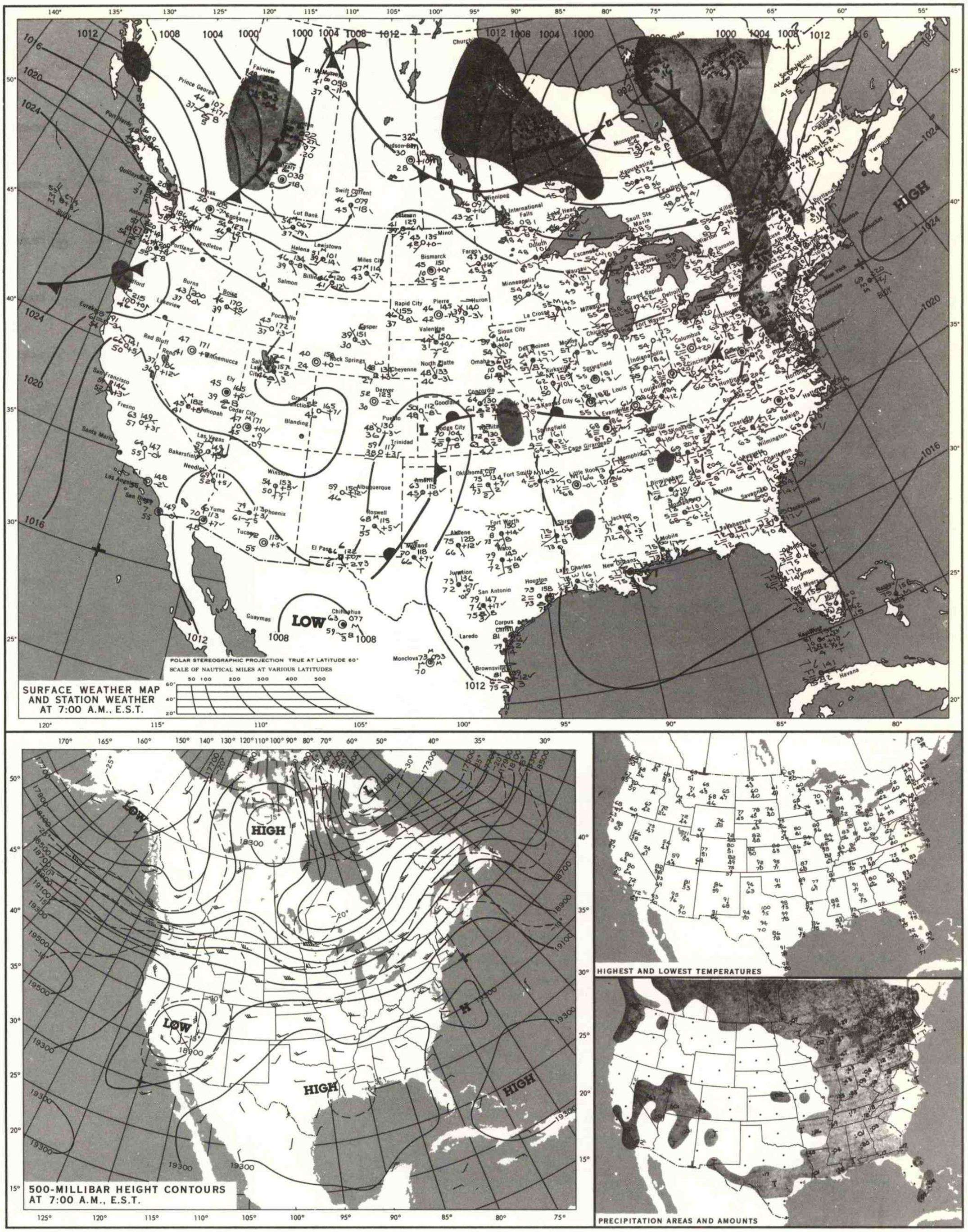


Figure 15.15.--National Weather Service maps for September 15, 1978.

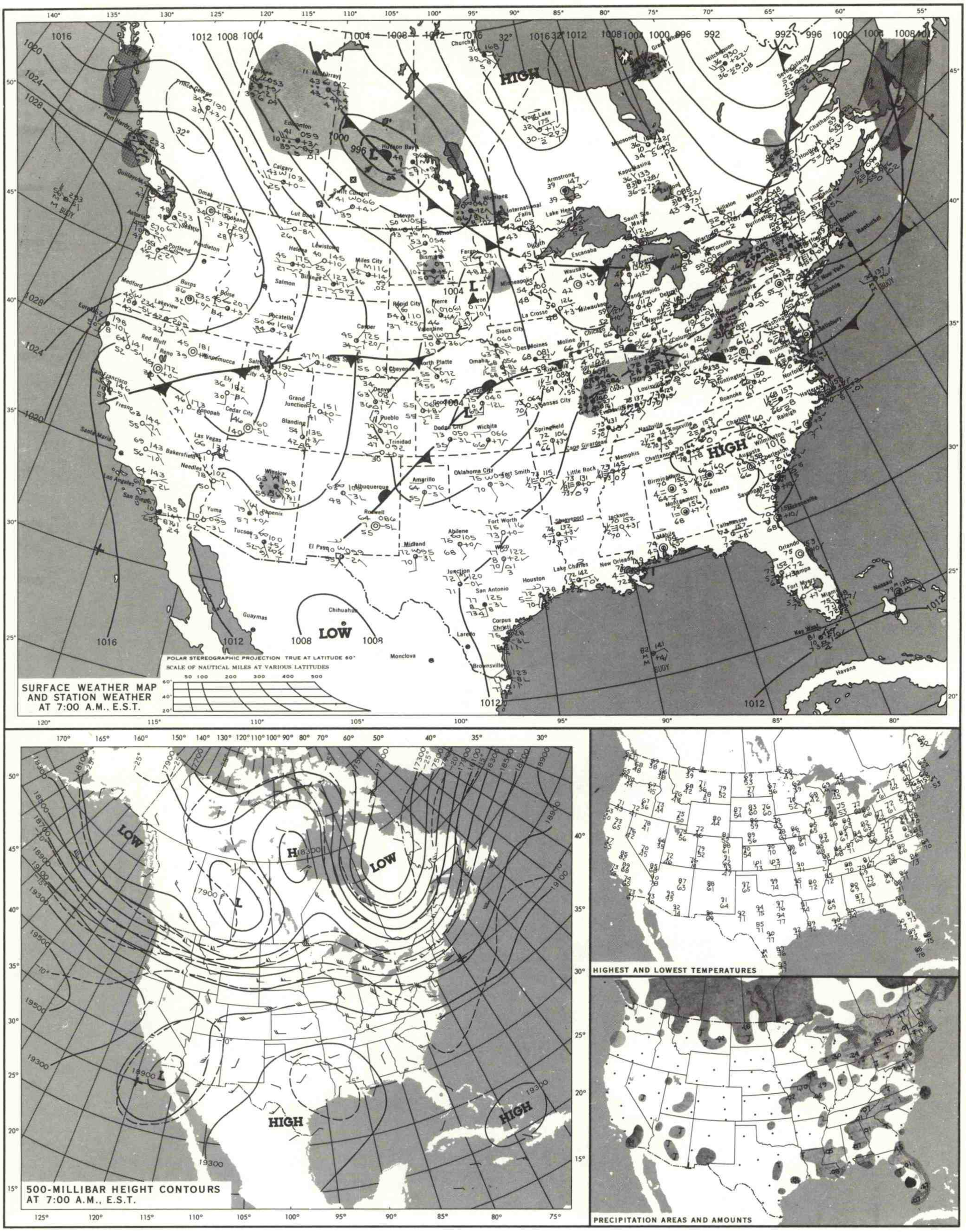


Figure 15.16.--National Weather Service maps for September 16, 1978.

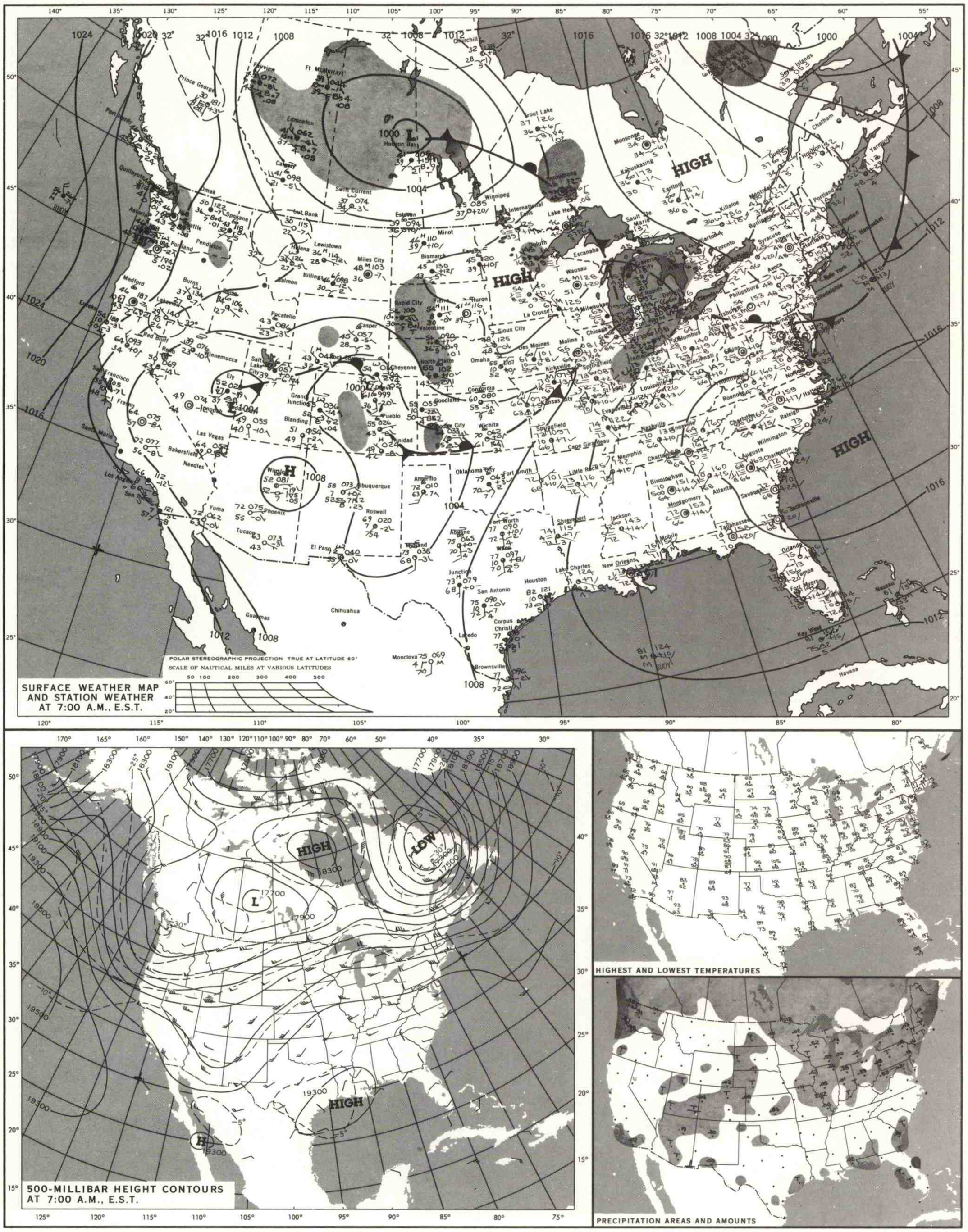


Figure 15.17.--National Weather Service maps for September 17, 1978.

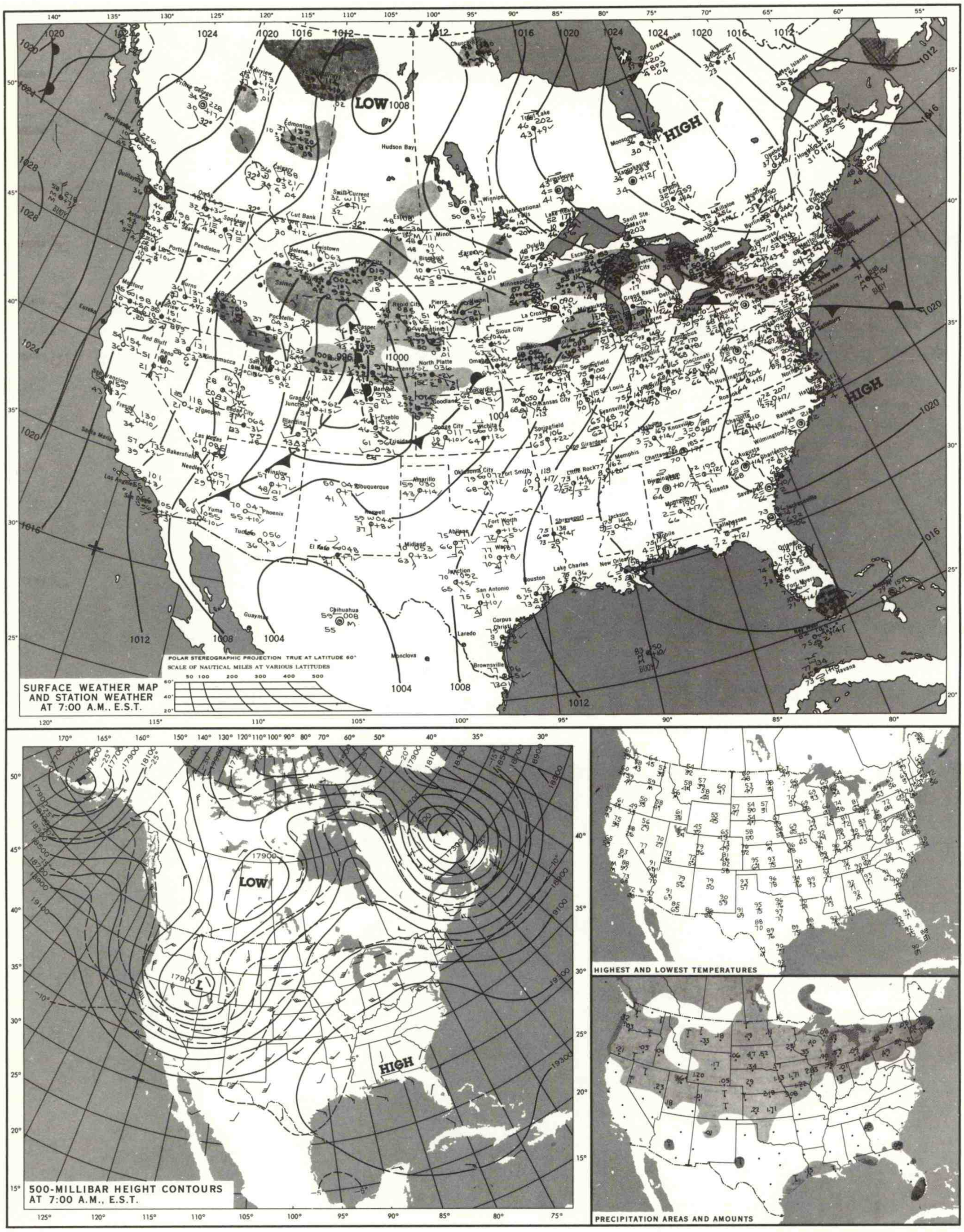


Figure 15.18.--National Weather Service maps for September 18, 1978.

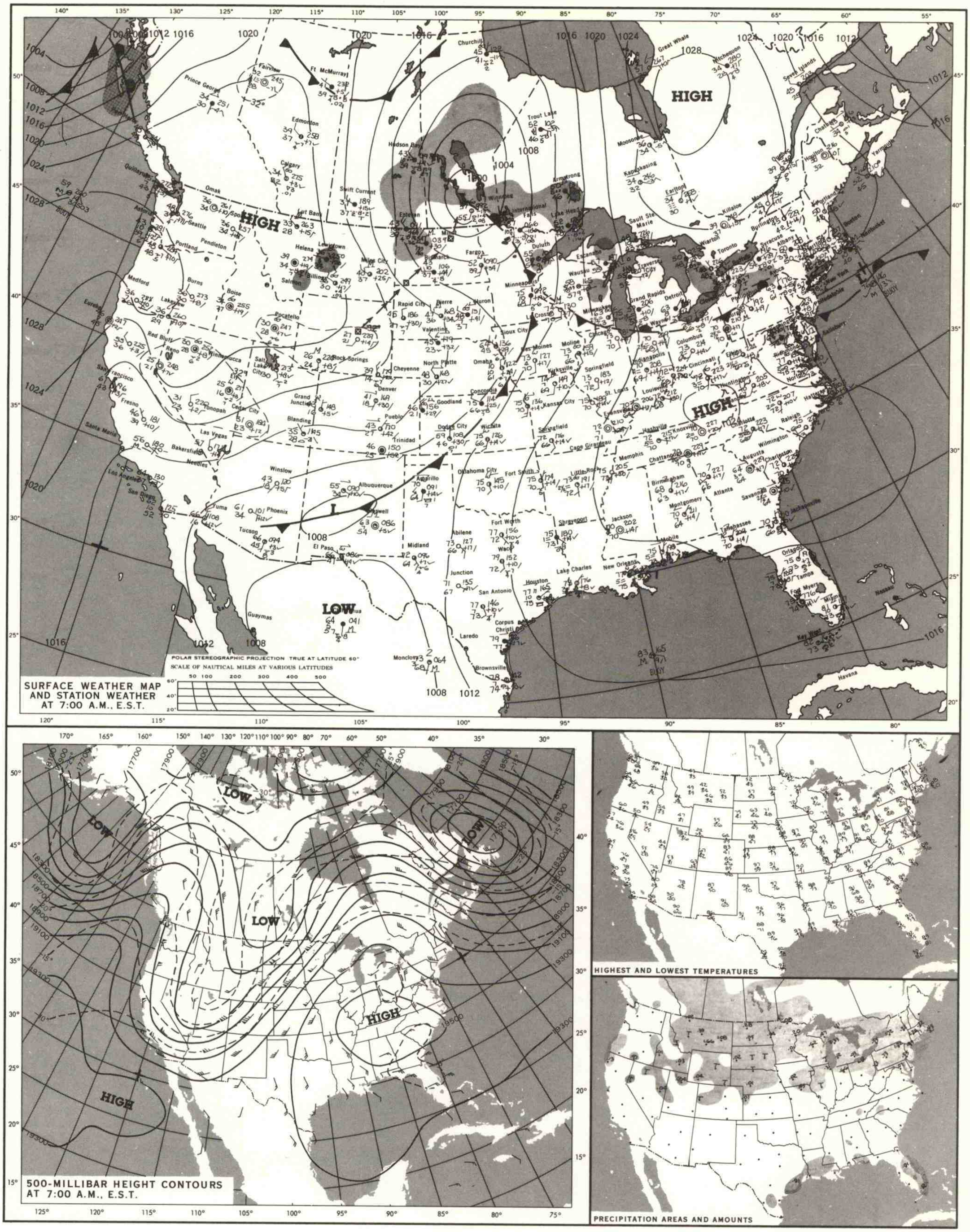


Figure 15.19.--National Weather Service maps for September 19, 1978.

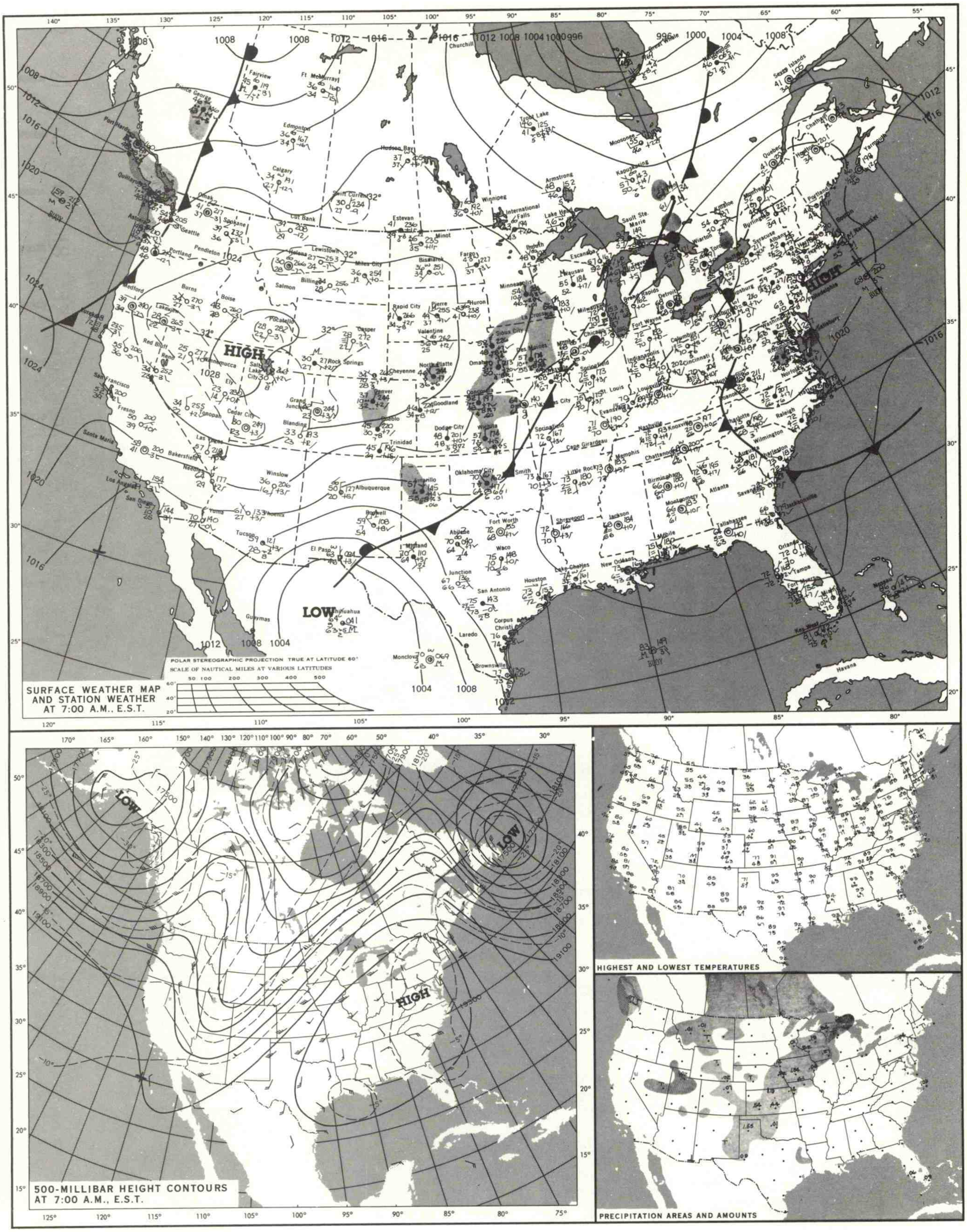


Figure 15.20.--National Weather Service maps for September 20, 1978.

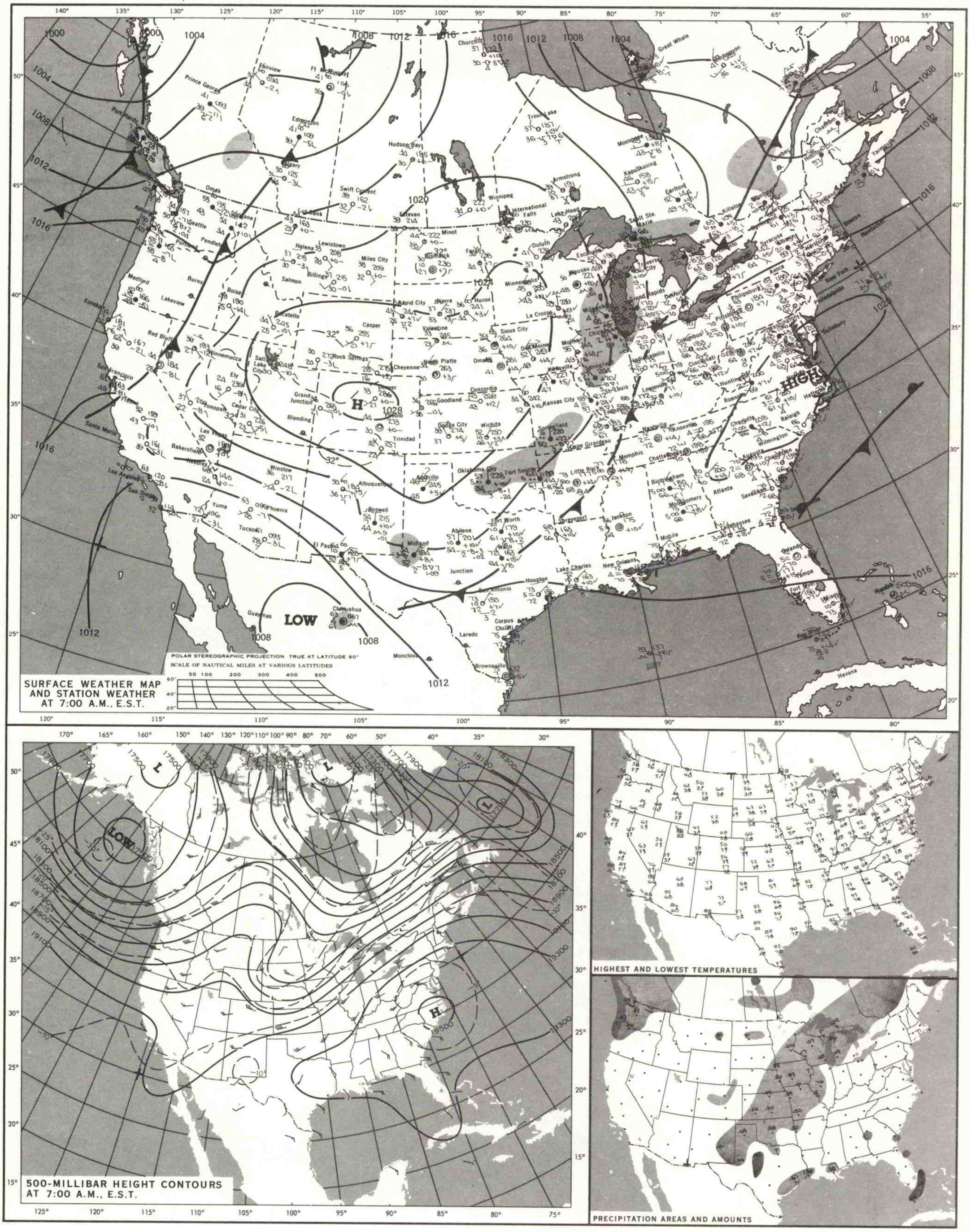


Figure 15.21.--National Weather Service maps for September 21, 1978.

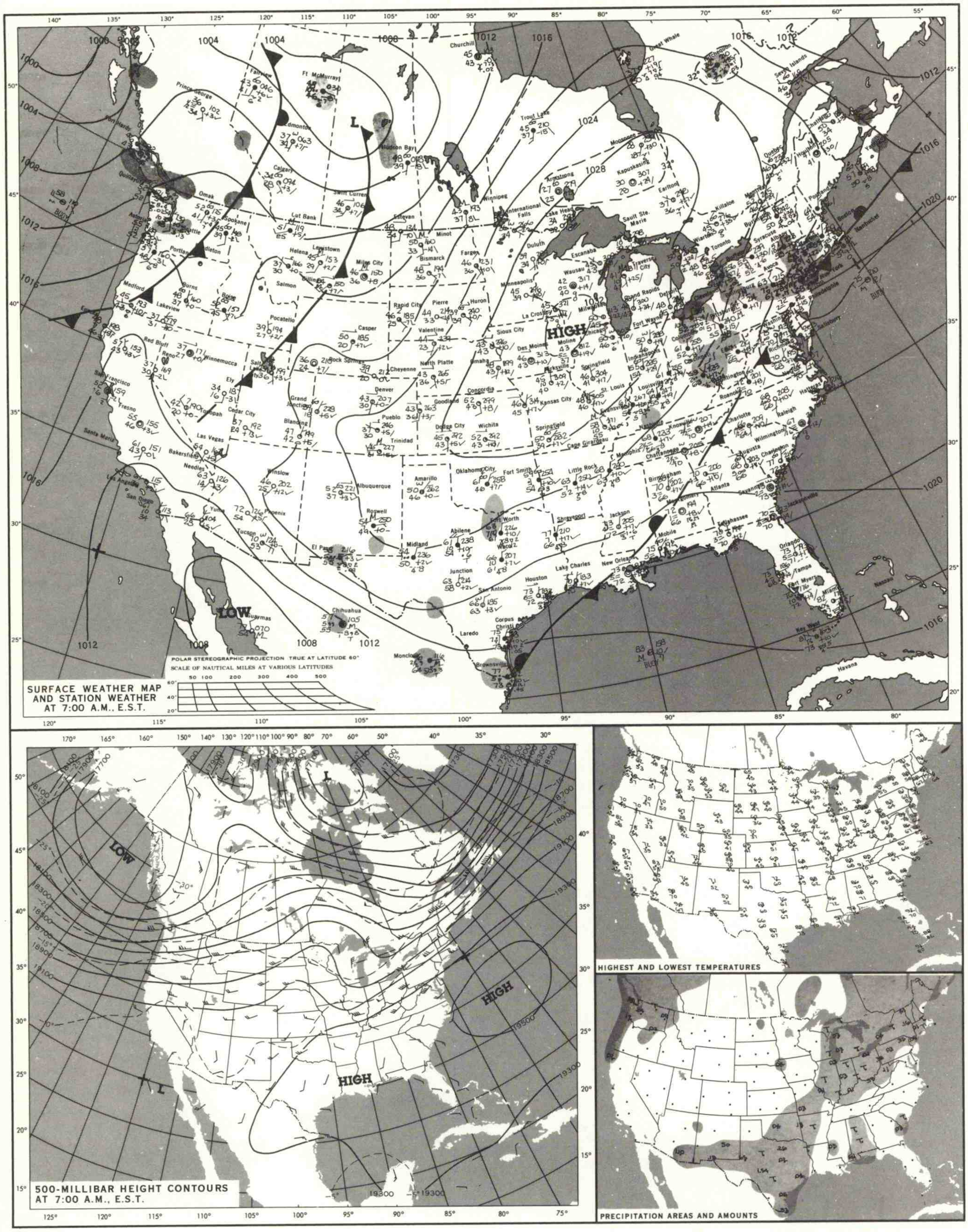


Figure 15.22.--National Weather Service maps for September 22, 1978.

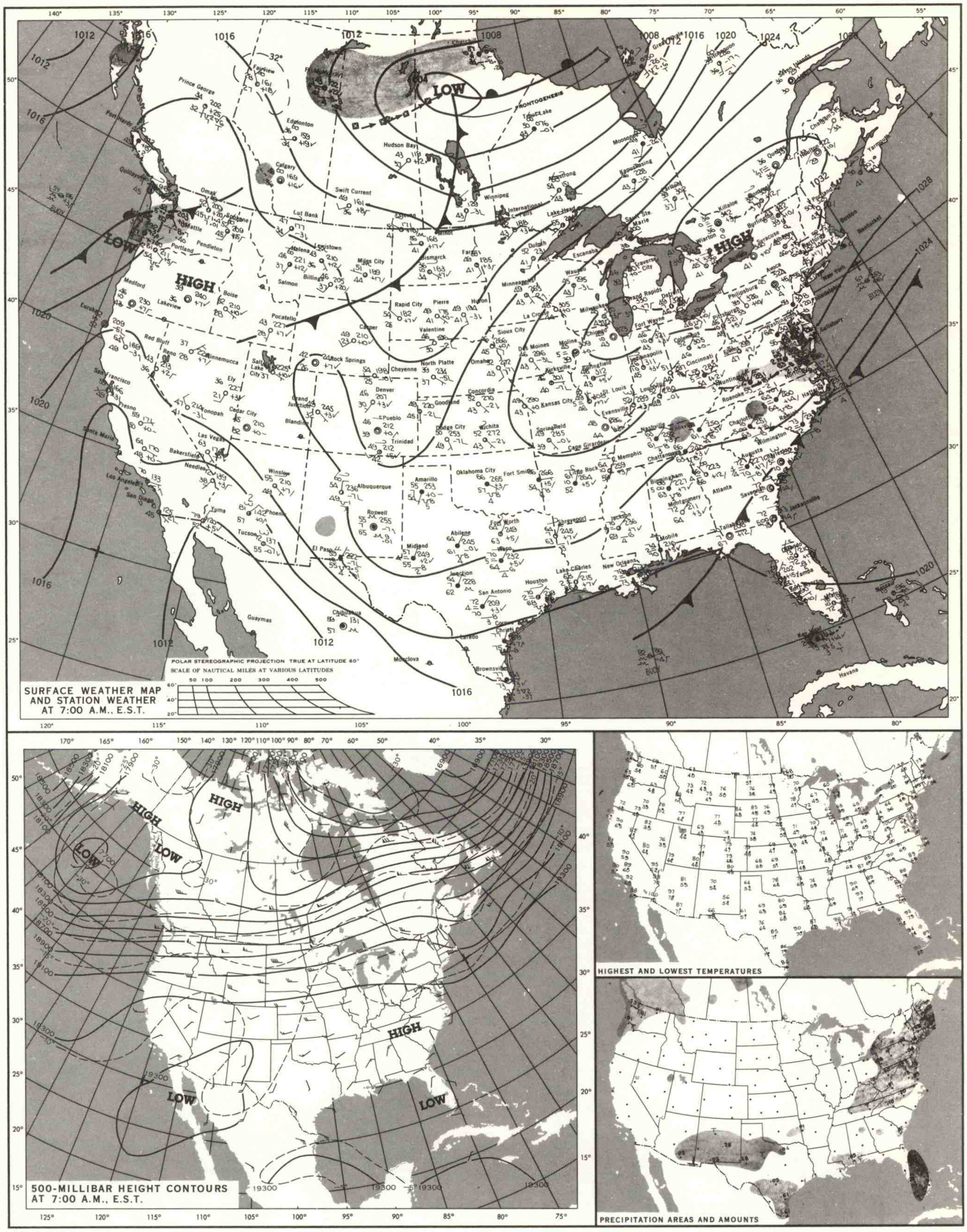


Figure 15.23.--National Weather Service maps for September 23, 1978.

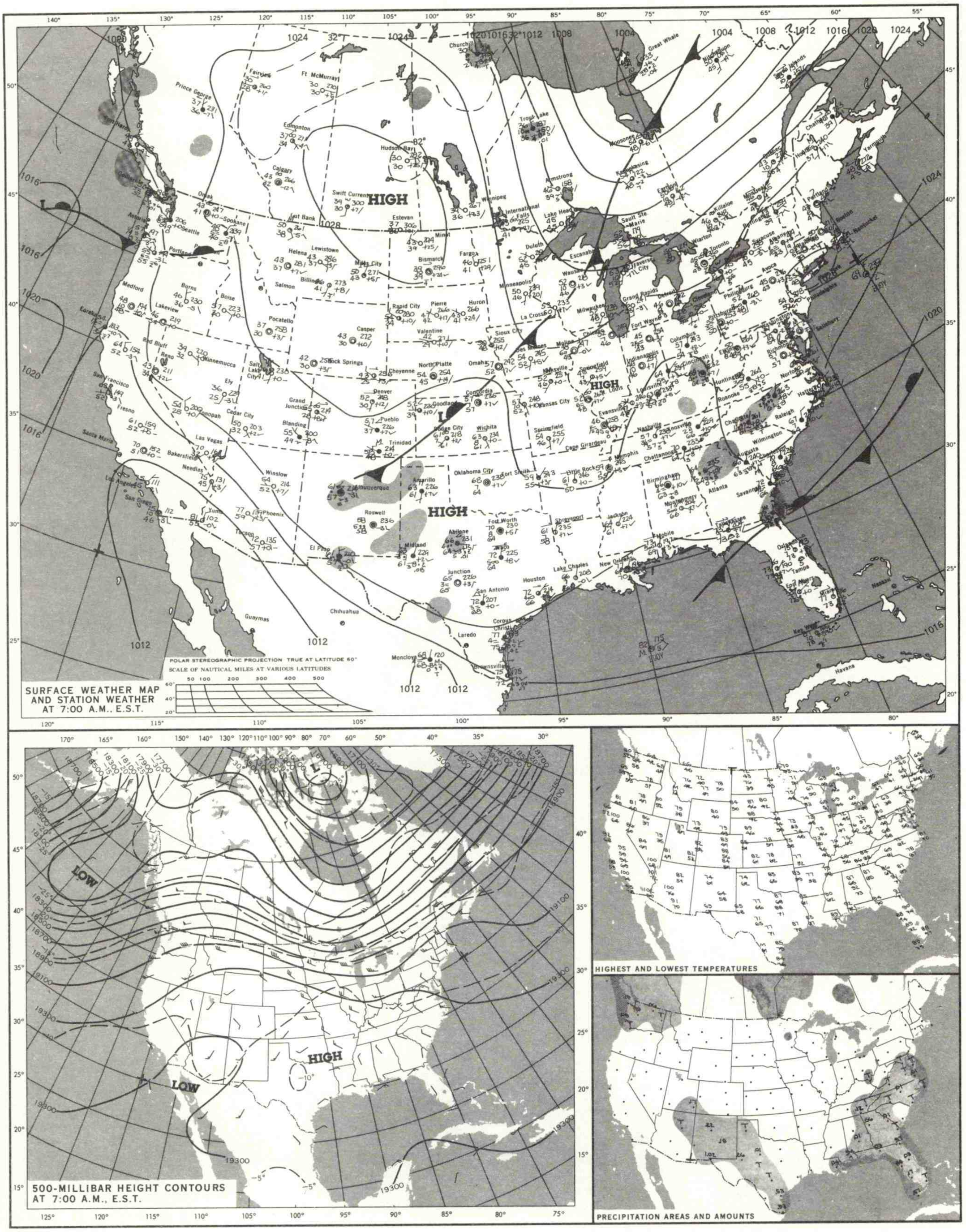


Figure 15.24.--National Weather Service maps for September 24, 1978.

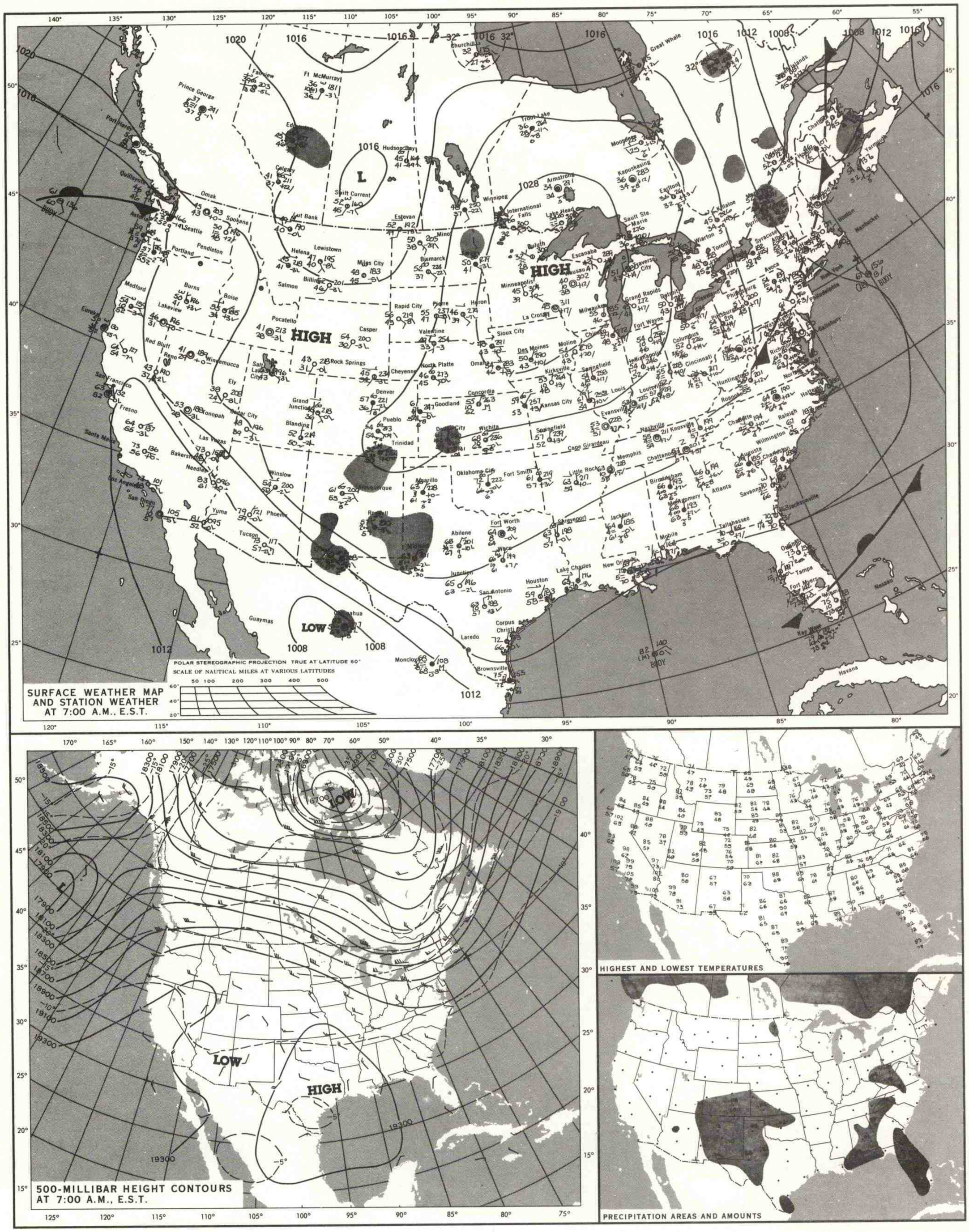


Figure 15.25.--National Weather Service maps for September 25, 1978.

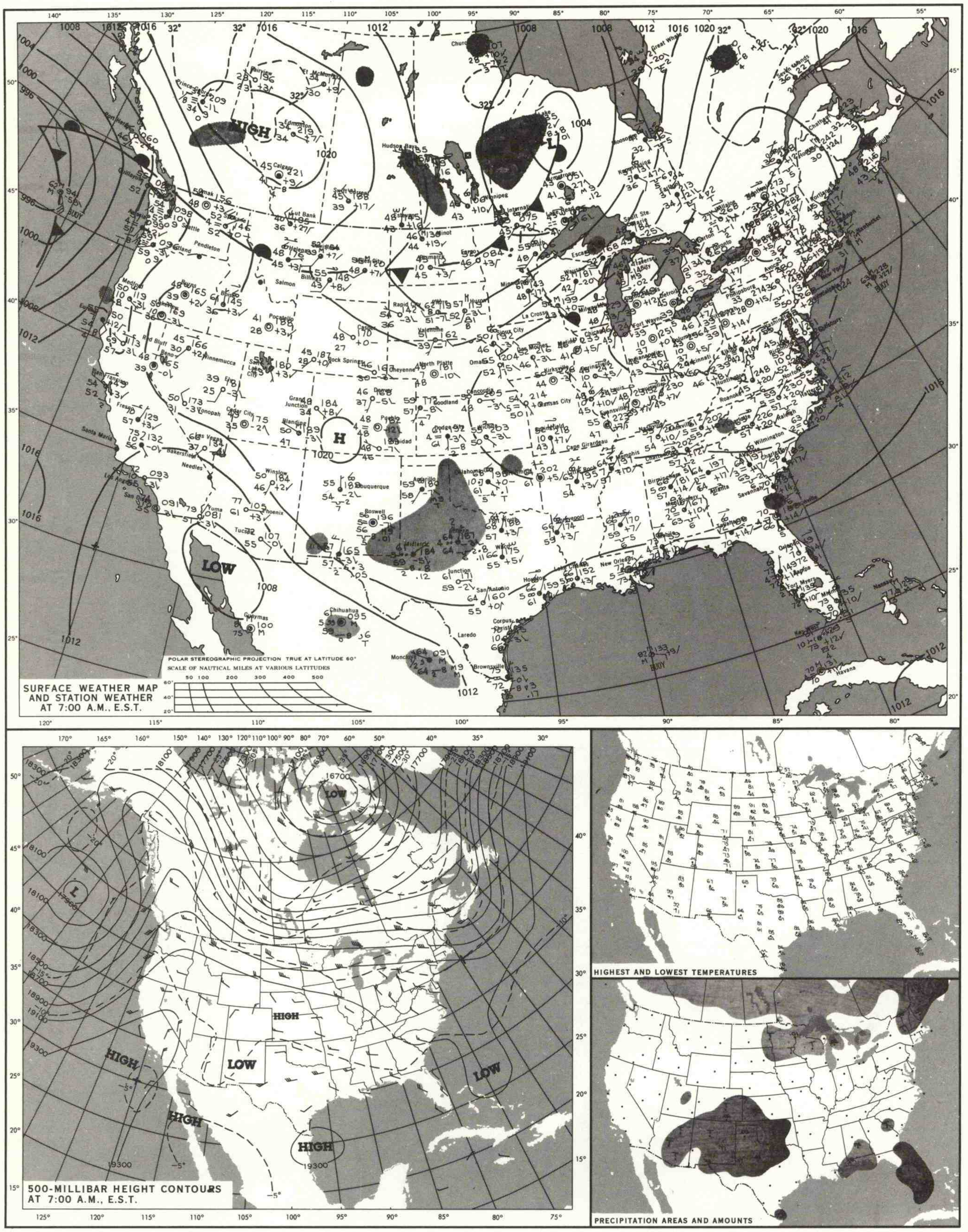


Figure 15.26.--National Weather Service maps for September 26, 1978.

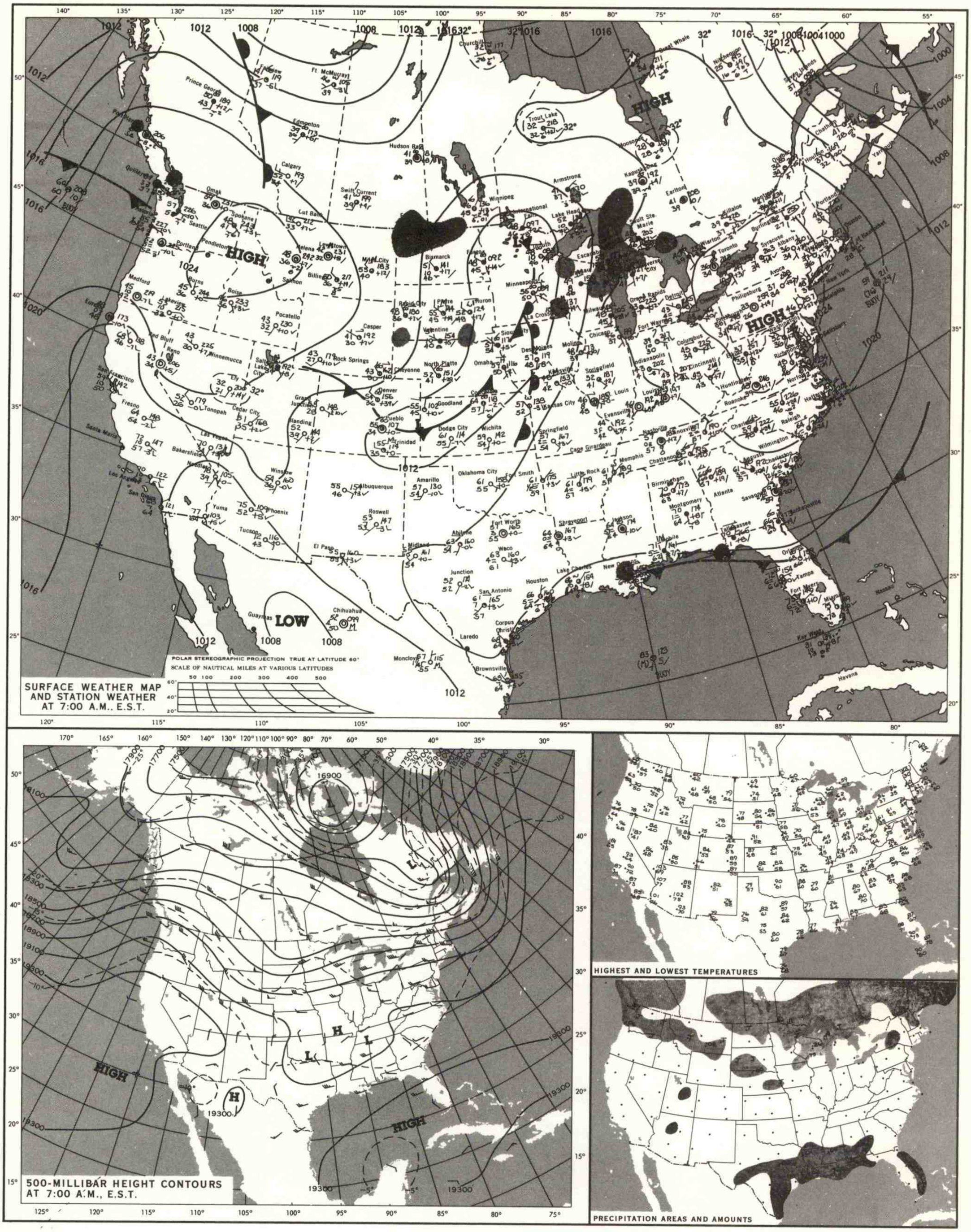


Figure 15.27.--National Weather Service maps for September 29, 1978.

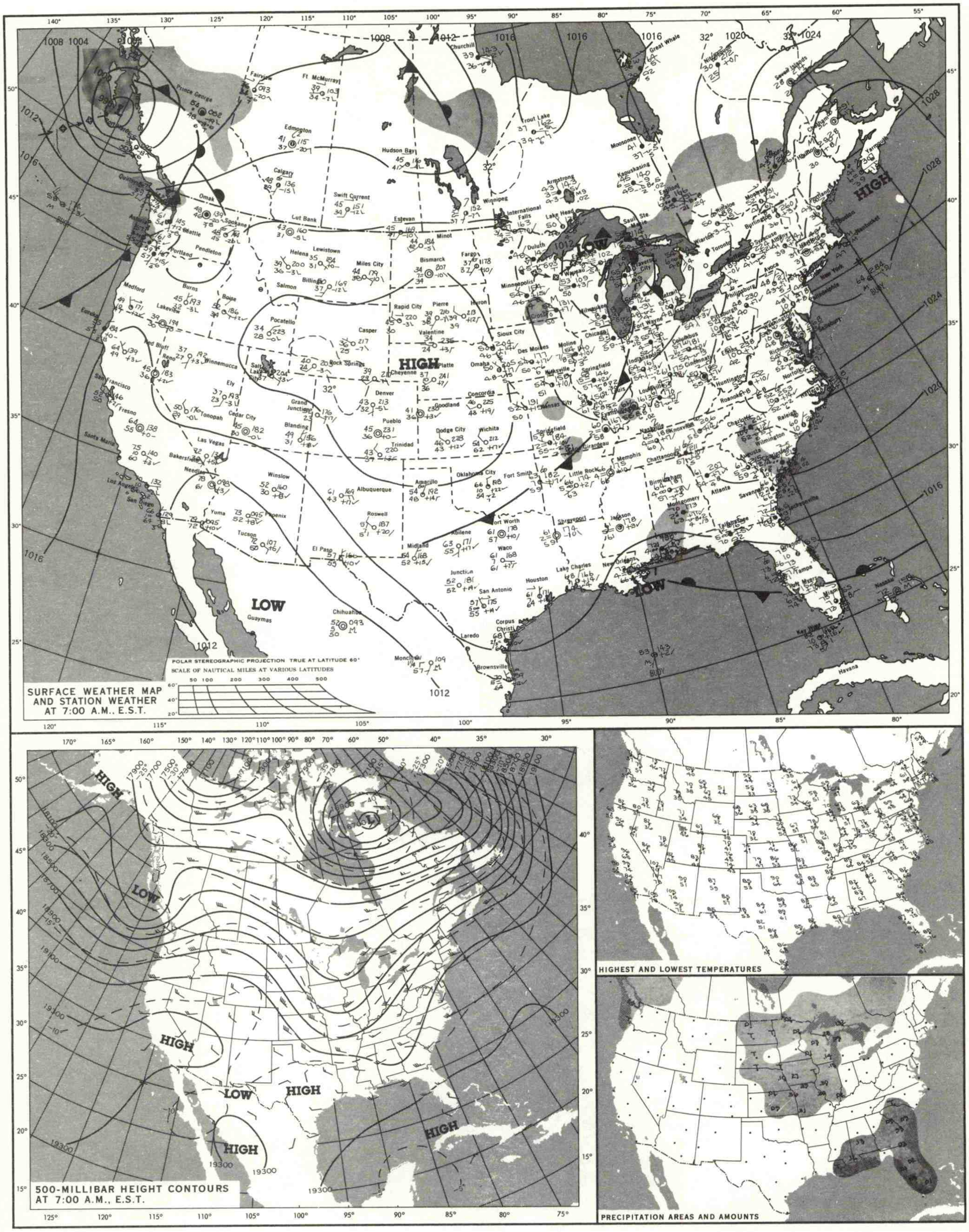


Figure 15.28.--National Weather Service maps for September 30, 1978.

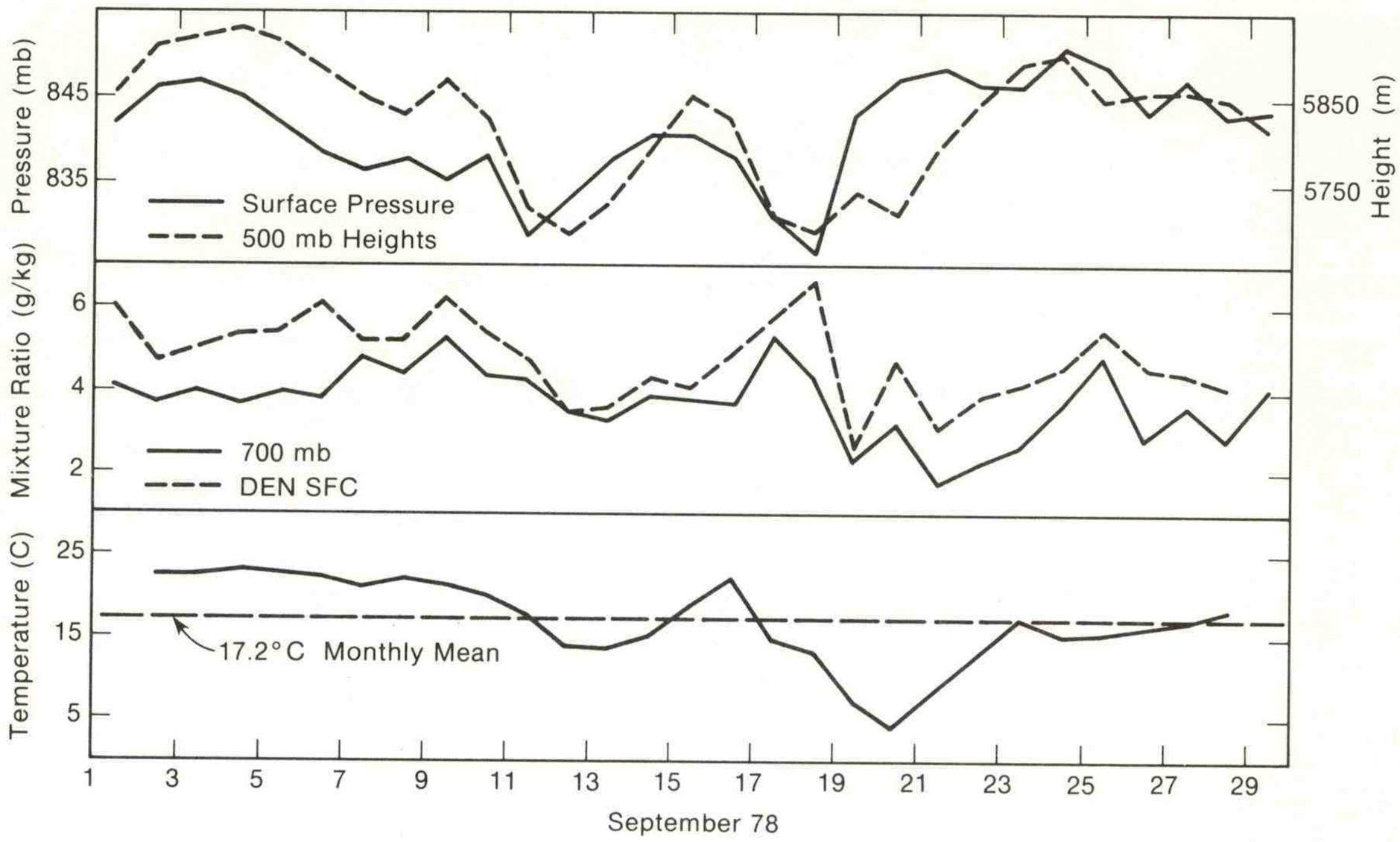


Figure 15.29.--Time series plots of surface pressures and 500-mb heights, mixing ratios at surface and 700 mb, and surface temperature for September (daily means).

section provides written discussion of the weather situation week by week as well as tabular data. Tables provide maximum, minimum, and daily mean temperatures from NCAR PAM data, maximum and daily mean winds (also from PAM data), surface pressure from BAO data, cloud-cover information (2- to 12-h averages) from the National Weather Service, Stapleton Airport Denver, and precipitation data from the BAO.

15.2.1 September 1 and 2: PHOENIX instrument checkout

The PHOENIX planners decided that September 1 and 2 would be a period of instrument checkout; the experiment would then stand down over the Labor Day weekend, and begin in earnest the following Tuesday. Zonal flow characterized both days as high pressure in southwestern Colorado — the so-called "Four Corners High" — carried warm dry air onto the plains at the surface and 700 mb (Figure 15.29). Table 15.1 summarizes the surface information prevailing over the BAO area.

15.2.2 September 3-9: warm and dry

A strong ridge built over Colorado on the 3rd and 4th and extended northward into Montana, keeping the major storm track north. This ridge maintained the warm, dry pattern through September 7. By the 8th the 500 mb ridge had moved eastward and was centered over Minnesota and the Dakotas. This eastward shift in the pattern allowed a modified maritime polar cold front to move across the Rockies, triggering scattered rain showers and moderate thunderstorms on September 8 along with renewed buildup on the 9th. Table 15.2 summarizes pertinent surface data for this week.

15.2.3 September 10-16: high winds

With continued drift of the ridge over the eastern United States, an upper-level trough began to develop and deepen in the Pacific Northwest. About 0330 MST on September 11 a second maritime polar cold front passed through the Denver area. The front moved swiftly, and only light rain fell over the Front Range prior to the frontal passage. Following the front, a significant weather change occurred as the upper-level trough combined with a localized low-pressure center in southeastern Colorado to produce strong downslope winds (Figure 15.30). Anemometers on the BAO tower recorded steady 10-25 m s^{-1} winds from 1000 MST on September 11 until 0100 MST on the 12th. Cooler air behind the front helped keep temperatures on the mild side for September 13, 14, and 15 as moderate southerly flow returned to the area. The system moved quickly onto the Plains, but then stalled over the central United States. By September 16, the same (weakened) system was still over the Midwest, and a 500-mb ridge now prevailed east of the Rockies. Table 15.3 provides surface data for the period.

15.2.4 September 17-23: a touch of winter

A new cool front remained north of Colorado until a weakening of the ridge over the Midwest, and an eastward shift of the Bermuda High on September 17. With this change in pattern, cool air pushed south into eastern Colorado and up against the foothills of the Rocky Mountains. At mid-morning on the 18th a cold front associated with a newly developed low pressure center in southern Wyoming moved onto the plains of eastern Colorado followed by a surge of continental polar air

Table 15.1.--Surface measurements for September 1 and 2

Date	Temp (°C)			Wind Speed (m s^{-1})		Pressure (mb)	Clouds				Precip (in)	
	Min	Max	Daily mean	Max	Daily mean	Daily mean	00-12 MST Amt(1/10)	Type	12-24 MST Amt(1/10)	Type		
1*	--	--	--	--	--	841.7	0		7	Cu,Ac,Ci	0	
2	12.8	31.9	22.1	5.3	1.9	846.1	4	Ac,Ci,Cb	10	Ac,Ci,Cb	0	RW - in area

* Data gathering did not include full day

Table 15.2.--Surface measurements for September 3-9

Date	Temp (°C)			Wind Speed (m s^{-1})		Pressure (mb)	Clouds				Precip (in)	
	Min	Max	Daily mean	Max	Daily mean	Daily mean	00-12 MST Amt(1/10)	Type	12-24 MST Amt(1/10)	Type		
3	12.8	32.2	22.0	6.6	2.8	846.8	4	Ac,Ci	1	Cu	0	
4	11.9	33.3	22.7	2.3	1.4	845.1	1	Cu,Ac	0	Cu	0	
5	13.1	33.7	22.4	3.2	1.7	842.7	0	Cu	0	Cu	0	
6	11.5	32.8	21.9	4.9	1.6	838.3	1	Cu,Ac	0	Cu	0	
7	10.3	29.9	21.0	6.1	2.0	836.3	0	Cu	1	Ac,Ci	0	
8	12.2	30.0	21.1	3.8	1.8	837.7	1	Cu,Ci	8	Cu,Ac	T	RW- in area
9	13.3	29.7	21.3	3.2	1.9	835.2	0	Cu	6	Cu,Ac,Cb	0	

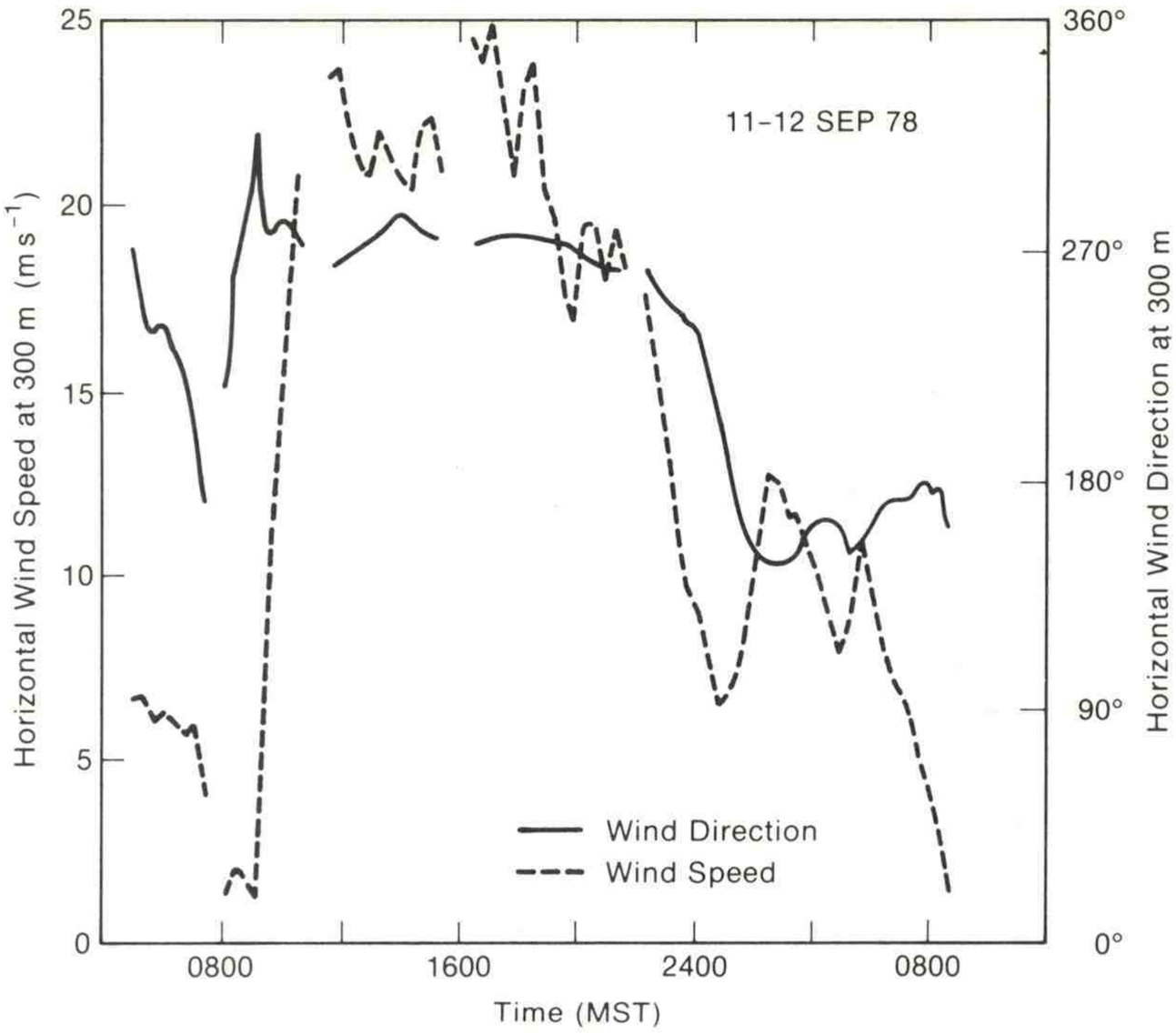


Figure 15.30.--BAO wind speed and direction time series comparison (from PDP 11/70 20-min averages).

out of Canada. This large high pressure cell, centered in Montana, brought light upslope winds (NE) and cold air into eastern Colorado. Scattered light rainfall occurred the evening of September 19 under stratiform skies and temperatures that had dropped some 10°C. Upslope conditions continued during the 20th as the cold air pushed south into Texas. During this influx of dense, cold air, a weak subsidence inversion is visible above the cold air mass in the Denver soundings. Clear skies the morning of September 21 brought freezing temperatures and the first frost since the previous spring. The next several days, September 21-23, saw a gradual warming trend develop. During this same period, upper-air charts show zonal flow across the United States. Table 15.4 summarizes the surface meteorological records during this period.

15.2.5 September 24-29: fall weather

The weather pattern north of Colorado changed quickly as another maritime polar front moved down out of the Pacific Northwest on September 24. This had little effect on Colorado since these outbreaks of cold air were kept north by a ridge developing over the far western United States. Fair weather over eastern Colorado prevailed for the remainder of the PHOENIX experiment as localized

Table 15.3.--Surface measurements for September 10-16

Date	Temp (°C)			Wind Speed (m s^{-1})		Pressure (mb)	Clouds				Precip (in)	
							00-12 MST		12-24 MST			
	Min	Max	Daily mean	Max	Daily mean	Daily mean	Amt(1/10)	Type	Amt(1/10)	Type		
10	11.8	28.9	20.2	6.2	1.8	838.0	2	Ac	8	Ac,Ci,Cb	.08	RW-
11	12.9	22/6	18.3	13.9	7.2	828.5	3	Cu,Ac,Ci	5	Cu,Ac	0	
12	7.9	21.5	14.3	5.9	2.3	833.2	3	Cu,Ac	3	Ac,Ci	0	
13	6.0	22.1	13.8	3.1	1.6	838.0	0	Cu	0	Cu	0	
14	6.5	24.5	15.1	1.9	1.3	841.0	0	--	2	Cu	0	
15	8.3	29.3	18.9	2.8	1.4	841.0	0	Cu	0	Cu	0	
16	17.4	28.7	22.4	4.4	3.1	838.3	2	Cu	7	Cu,Ac	0	RW- in area

Table 15.4.--Surface measurements for September 17-23

Date	Temp (°C)			Wind Speed (m s^{-1})		Pressure (mb)	Clouds				Precip (in)	
							00-12 MST		12-24 MST			
	Min	Max	Daily mean	Max	Daily mean	Daily mean	Amt(1/10)	Type	Amt(1/10)	Type		
17	10.0	19.7	15.30	4.8	2.1	830.9	8	Ac,Ci	6	Sc,Cu,Ac	0	RW- in area
18	8.9	22.0	13.9	6.9	3.3	826.8	9	St,Sc,Ac	4	Cu,Ac	0	F in morning
19	4.0	11.3	7.8	5.4	3.7	843.7	Bldg Cu at 1100		10	St	.04	RW-
20	1.9	9.0	4.6	2.0	1.2	847.8	10	St,Cu	Clearing by 1800		T	R-,L-,S-, in area
21	-1.1	17.5	9.0	1.8	1.0	849.0	0	--	1	Ci	0	
22	1.7	25.3	13.0	2.2	1.3	847.3	2	Ci	0	Cu	0	
23	7.6	27.9	17.6	3.1	1.7	847.1	0	--	2	Cu,Ac	0	

southerly flow continued. Table 15.5 gives the surface values of meteorological parameters for this period.

15.2.6 Forest fires

Two Front Range forest fires are of interest here because they occurred (or flared up) during September 1978, producing smoke plumes and haze that spread over the experimental area. There is indication that particulates from these fires were detected by some of the remote sensors deployed for PHOENIX, notably the lidar. The first fire was the Ouzel Lake fire, which apparently began August 9, 1978, when lightning struck about 100 feet from the Ouzel Lake Trail in the Rocky Mountains near Allenspark, about 40 to 50 km WNW of the BAO. For the next 14 days the fire did little more than smoulder. Then, beginning August 23, the fire flared up and began to spread. On September 1, coincident with the start of PHOENIX, increased winds in the mountains changed the character of the fire to a crowning condition, fire spreading primarily through the tops of the trees. It was at this point that suppression activities began, bringing the fire to a stable condition by September 4. On September 15, westerly winds gusting to 20 to 30 mph caused the fire to intensify. Attempts to contain the fire increased during the next few days, and were aided substantially by rain and snowfall above 9400 feet. However, the fire was not declared officially under control until September 30.

The second fire, the Murphy Gulch fire that burned in Colorado State Forest land southwest of Denver and at one point threatened the extensive Johns-Manville plant there, started the morning of September 10 and was not controlled until September 17. Some 3072 acres of brush, grass, and forest were destroyed by this fire, which was Colorado's largest foothills/urban fire in 25 years. Smoke was greatest on September 10-12, and plumes were reported by the National Weather Service (NWS) at Denver's Stapleton International Airport over the city on September 10, 11, and 14.

15.2.7 September recap

The Colorado high plains experienced unseasonably warm and dry weather for the major portion of September. Most significant storm activity tracked far north of the PHOENIX site, along the Canadian border; only two major disturbances affected eastern Colorado, on September 11 and 18. Convective showers and thunderstorms

Table 15.5.--Surface measurements for September 24-30

Date	Temp (°C)			Wind Speed (m s^{-1})		Pressure (mb)	Clouds				Precip (in)
	Min	Max	Daily mean	Max	Daily mean	Daily mean	00-12 MST Amt(1/10)	00-12 MST Type	12-24 MST Amt(1/10)	12-24 MST Type	
24	8.1	23.0	15.8	4.5	1.8	851.5	8	Ac,Ci	10	Cu,Ac,Cs	0
25	8.4	23.5	16.0	4.3	1.5	849.6	8	Sc,Ac	4	Cu,Ac,Ci	0
26	6.1	27.9	16.9	3.1	1.5	843.9	0	--	2	Cu,Ac,Ci	0
27	8.3	28.0	17.4	3.5	1.8	848.1	0	--	7	Cu,Ac,Ci	0
28	9.6	28.4	19.4	3.7	1.5	843.6	2	Ac,Ci	8	Cu,Ac,Cs	0
29*	7.2	21.0	--	5.3	--	839.0	4	Cu,Ac	1	Cu,Ci	0
30*	5.0	26.6	--	2.1	--	842.7	0	--	2	Cu,Ci	0

* Data gathering did not include full day

were generally limited to the foothills and to the northeast plains. Little convective activity was noted over the PHOENIX site.

Comparison of PHOENIX data with 30-yr means for the Denver area show that September 1978 was characterized by less than 50% normal precipitation and temperatures 0° to 3°C warmer than normal. Figure 15.29 shows unseasonably warm temperatures for the first third of the month, followed by two cold periods, the second of which brought freezing temperatures and snow to parts of Wyoming, Montana, and the Colorado mountains. During the final third of the month temperatures returned to near normal conditions.

15.3 A Closer Look at September 11, 1978

Monday, September 11, 1978, saw a cold front entering northwestern Colorado associated with a 997-mb low centered over the western Dakotas. A wind shift (180° to 310°) along with a weak rise in pressure was reported by the NWS at Denver between 0300 and 0400 MST in conjunction with the frontal passage. Around 0915 MST a second wind shift along with strong westerly winds (Figure 15.30) hit the Boulder area and arrived some 15 min later at the BAO site. Microbarograph charts from the BAO show a small but sharp fall then rise in pressure coinciding with the start of the high winds. With advance notice from Boulder, the BAO staff was able to start a special "raw data" run to collect detailed information on the wind system as it passed through the experimental area. Figure 10.2 of Chapter 10 (Hildebrand, 1979) shows PAM data for the period depicting the westward progress of the strong winds. Figures 15.31 a-e show 6-hourly surface maps, with associated cumulus and thunderstorm activity. These charts include additional station plots, reanalysis of isobars and frontal locations, and a pressure trough. These analyses show two distinct fronts. One, a maritime polar front moving in from the northwest and the second a pocket of cold air moving nearly due south along the front range. In the Denver area, there were early morning clouds including Ac and Ci, with Cu developing about mid-morning and continuing through late afternoon. Following the start of the high winds, a north-south line of Cu began to build east of the BAO site, revealing a possible low-level convergence line caused by the winds. This line of Cu was visible for nearly the entire high wind period. The 500-mb charts (Figures 15.11, 15.32, and 15.12) show a short-wave trough rotating rapidly across Colorado northward, while a second short-wave trough and cut-off low develop over the northern Rockies and Great Basin. Eastward progression of the long-wave

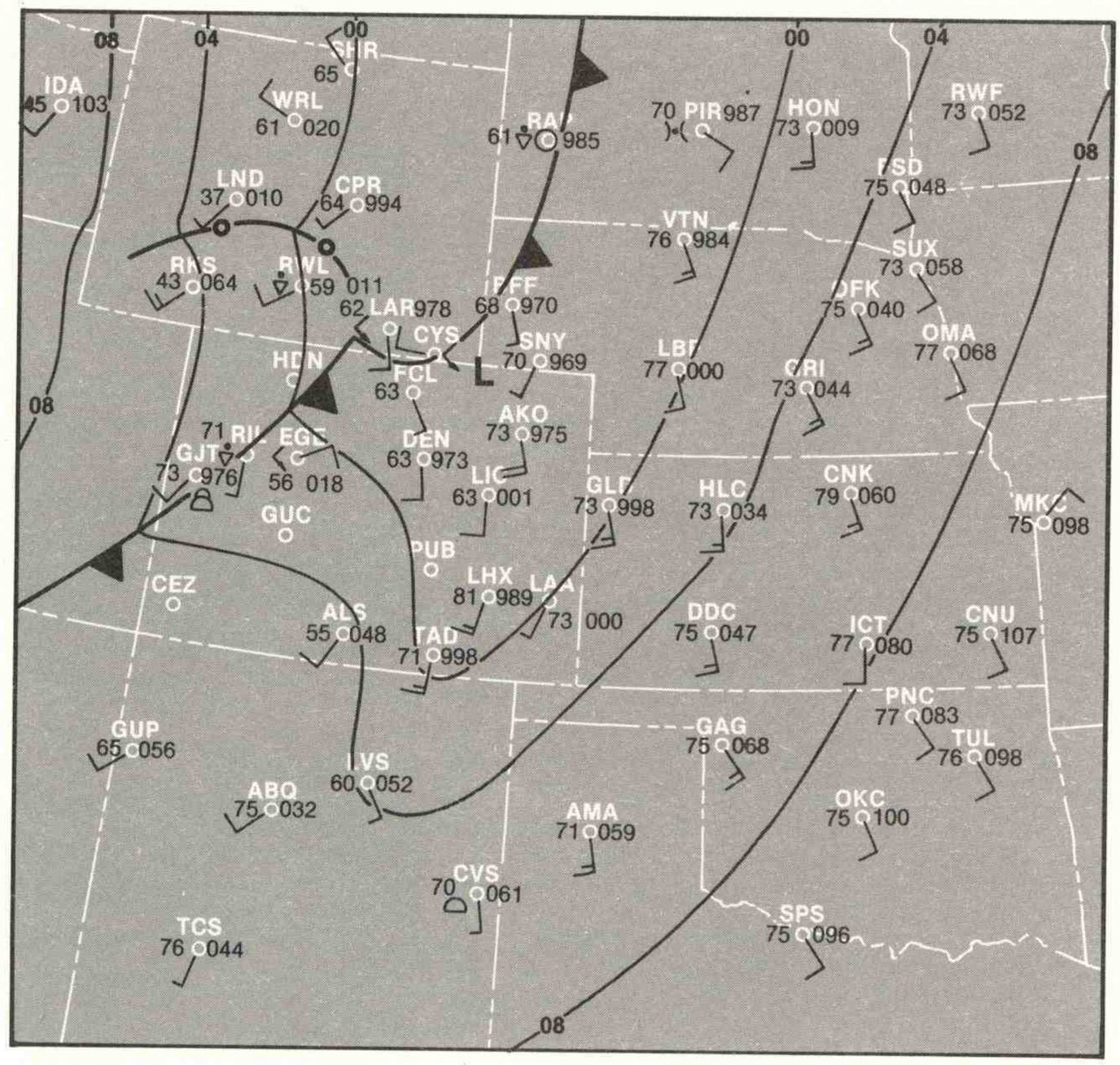


Figure 15.31.--Three-hourly surface weather maps from National Climatic Center, Asheville, N. C. (a) 2300 MST, September 10, 1978.

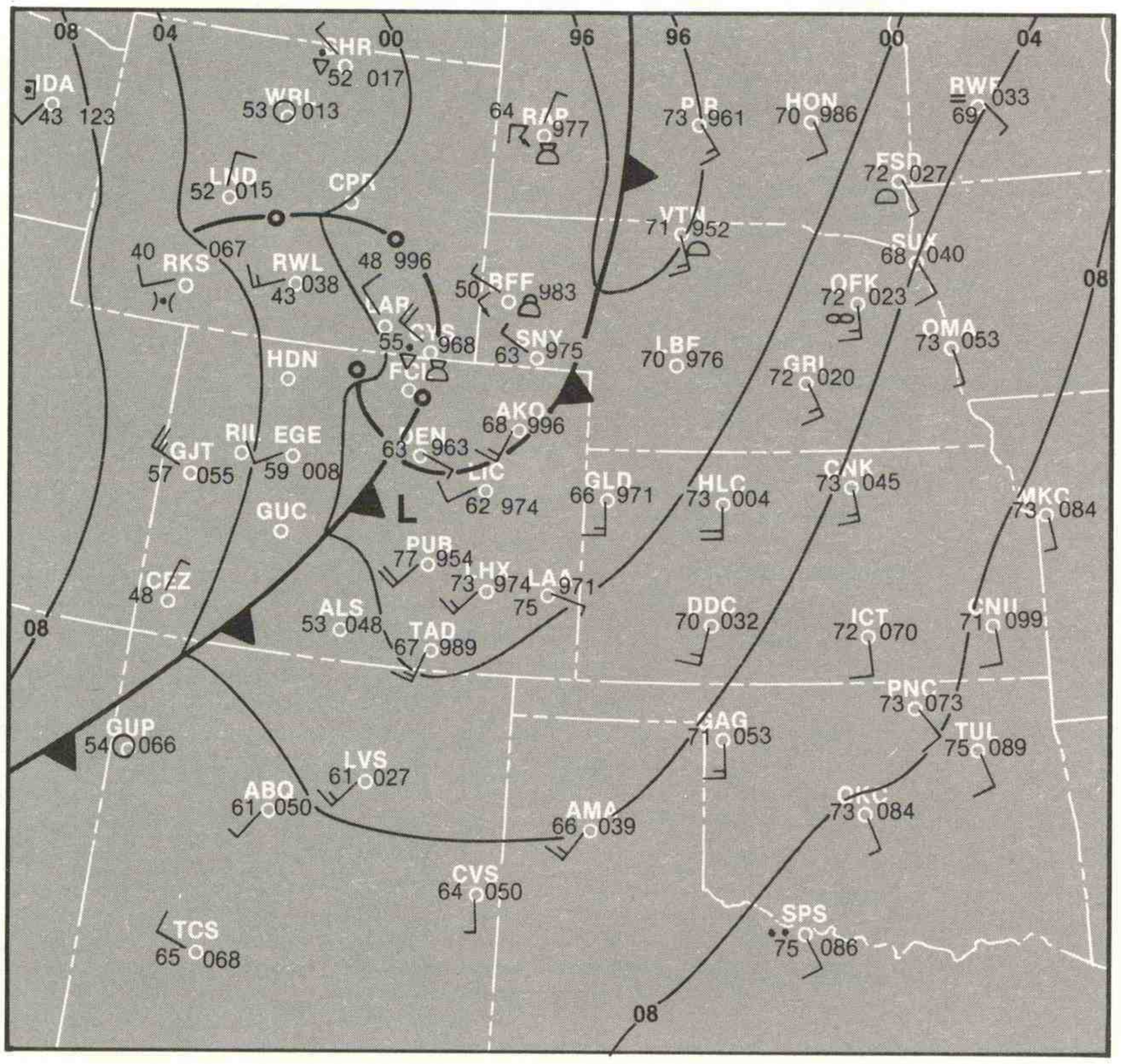


Figure 15.31b.--0200 MST, September 11, 1978.

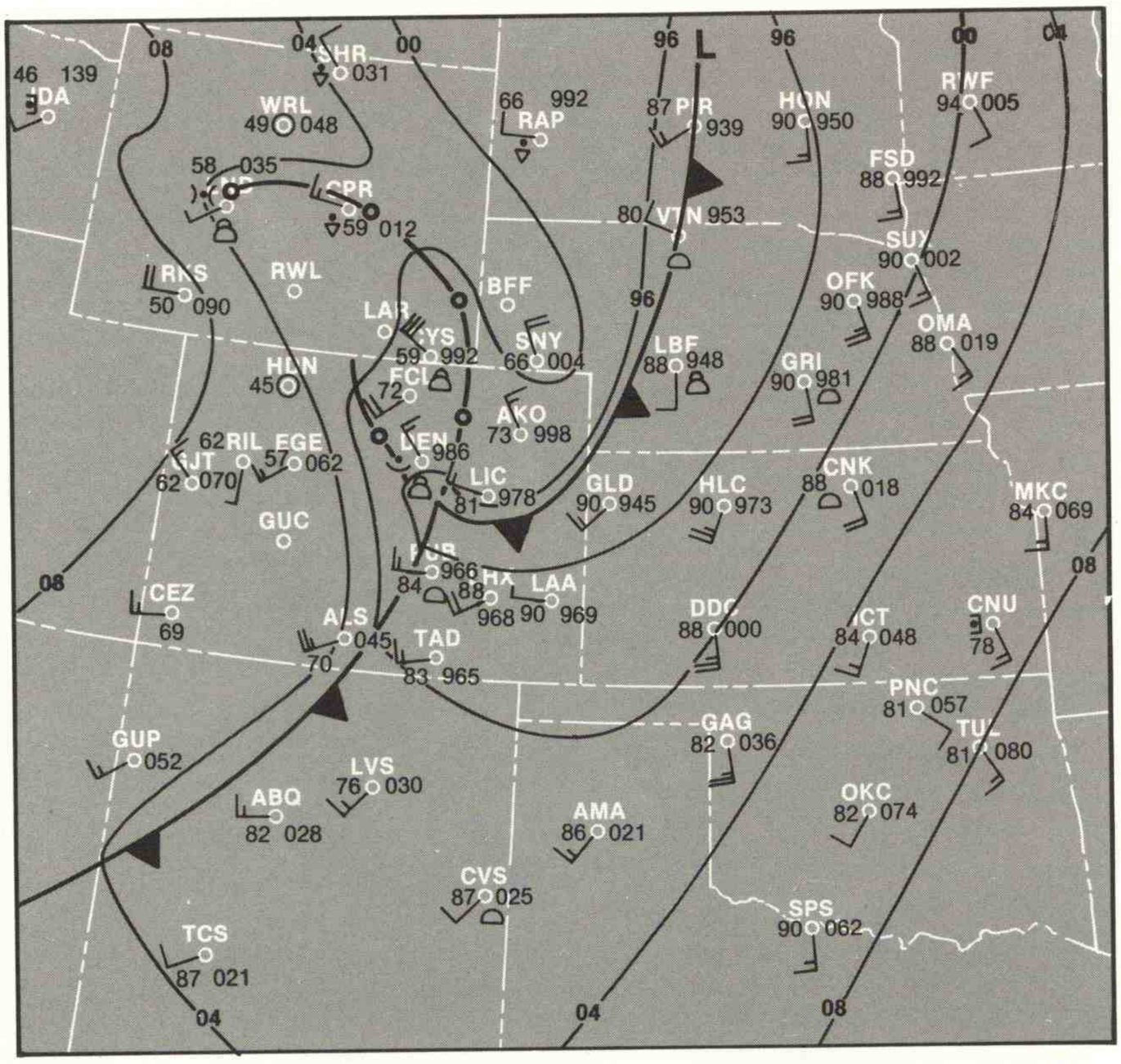


Figure 15.31c.--0500 MST, September 11, 1978.

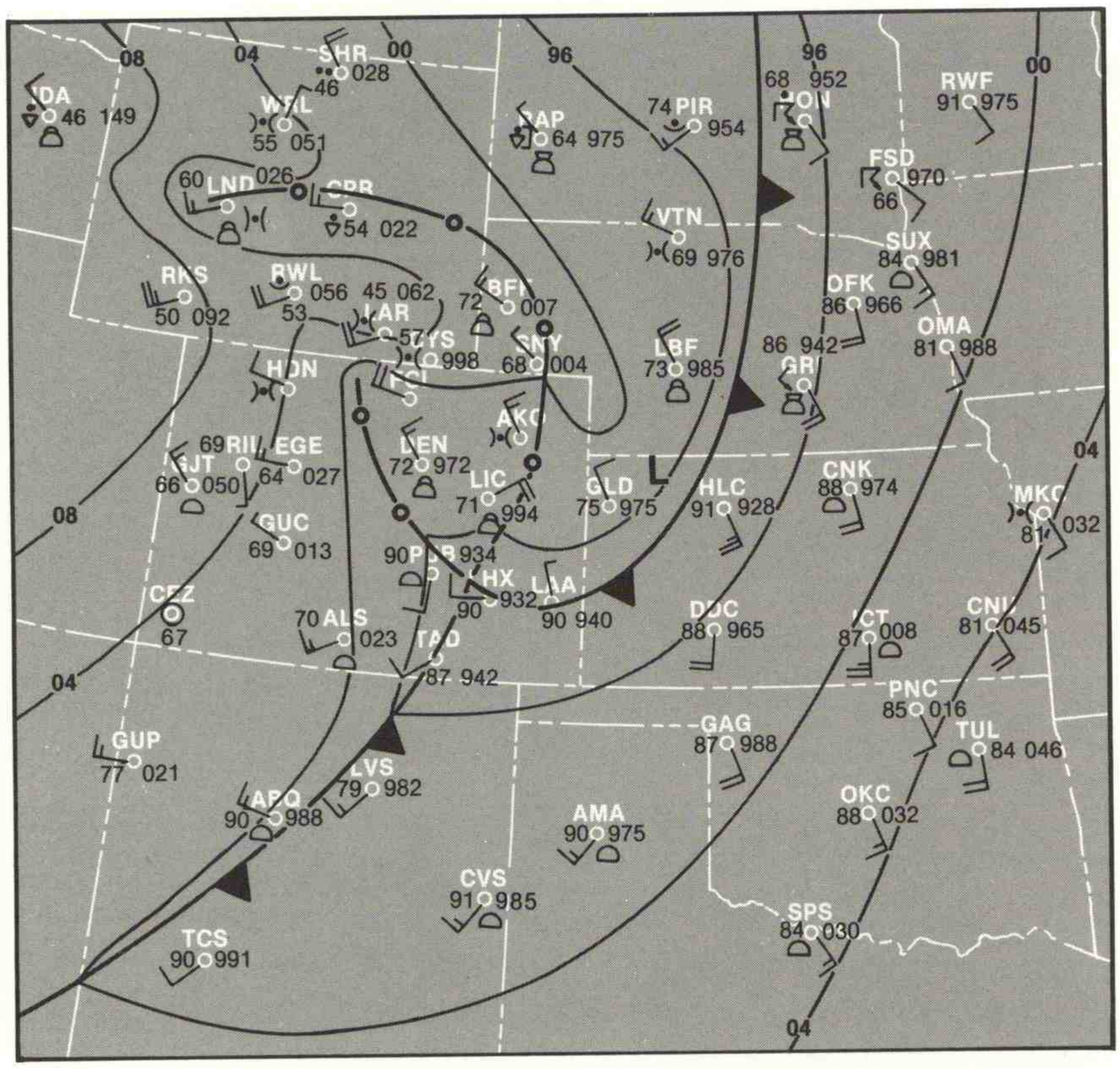


Figure 15.31d.--0800 MST, September 11, 1978.

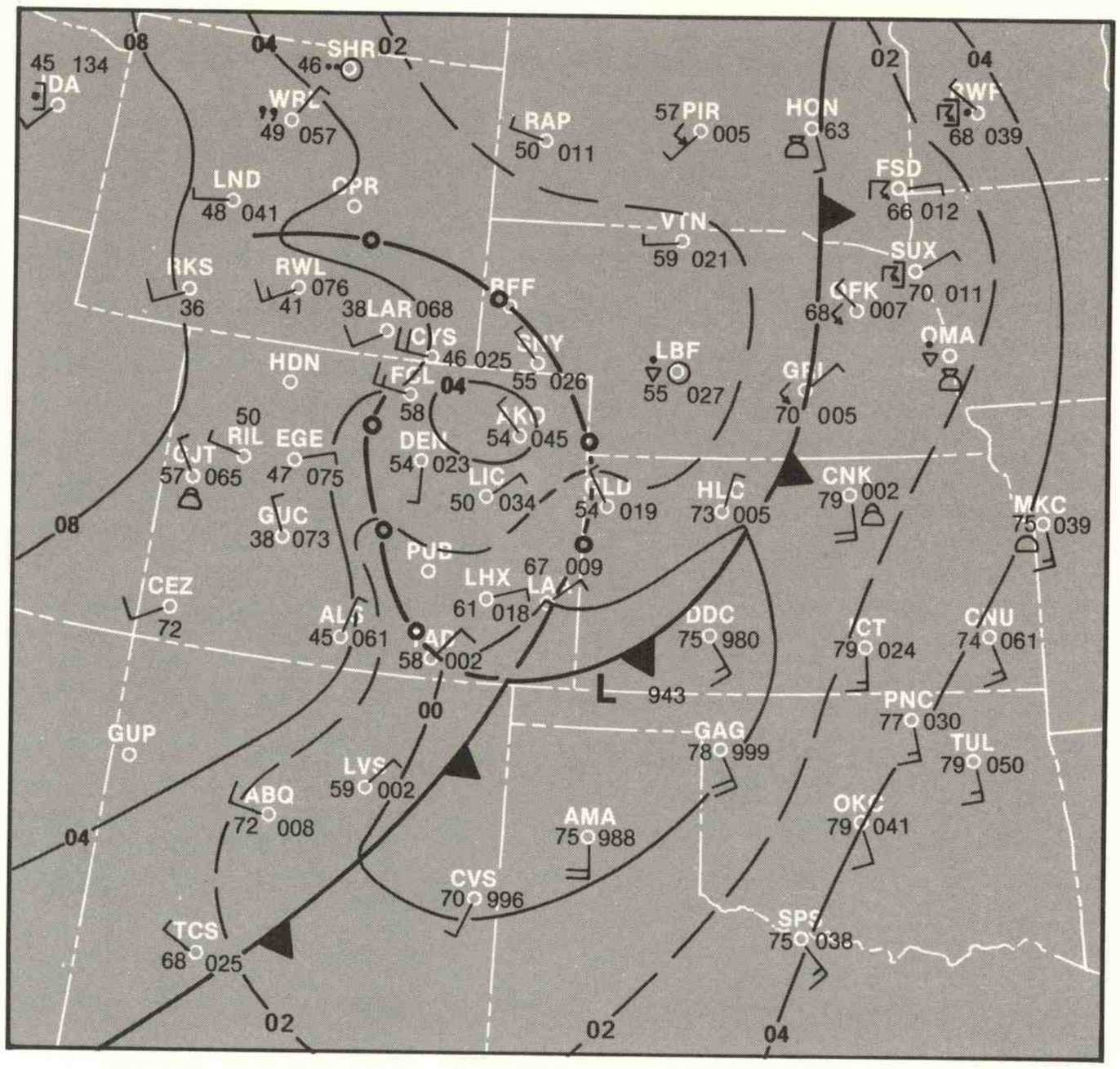


Figure 15.31e.--1100 MST, September 11, 1978.

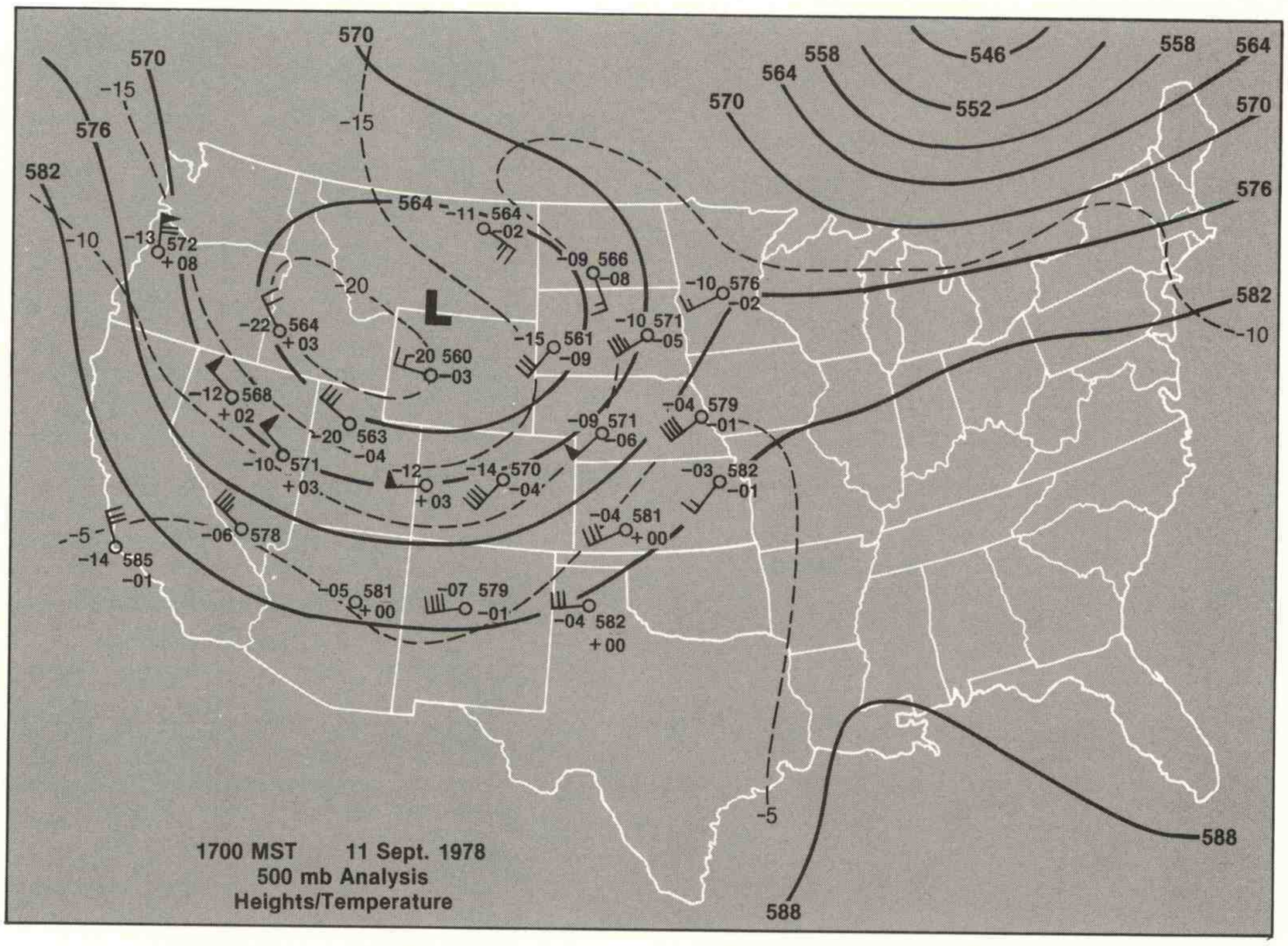


Figure 15.32.--500-mb heights/temperature chart for 1700 MST, September 11, 1978 (from National Climatic Center).

trough was restricted by a blocking ridge over the eastern United States and central Canada. Advection of cold air at 500 mb occurred over Colorado between 0500 and 1700 MST as seen by a 5°C drop in temperature at Denver. Denver rawinsondes (Figure 15.33) show strong upper-level winds moving directly over Denver by late afternoon on the 11th. Even though the September 1978 case might not be classified as a "severe" downslope wind storm, the event's sudden intensity and duration encourage a search for its precise causes. Such an investigation would require much deeper analysis into the chain of events and the interrelations of meteorological features responsible for the wind storm.

Figure 15.34 shows BAO tower winds for the time period depicted in Figure 15.33. Table 15.6 provides additional meteorological data and Table 15.7 describes the sequence of events at the BAO site as recorded on the all-sky camera operated by the lidar group. Figure 15.35 depicts ground-level solar radiation as a function of time and reveals a decrease in intensity that coincides with the onset of a small dust storm kicked up by the high winds. Figure 15.36 shows expanded detail in the time-series of radiation intensity.

15.4 A Closer Look at September 21 and 26

Figures 15.37 a-j and 15.38 a-j show the evolution of meteorological conditions over the Colorado area during September 21 and 26, respectively. These figures are expanded reproductions of the National Meteorological Center charts with a few local stations added on. The 500-mb upper-level patterns provide a good first indication of the differences between the two days. On the 21st a short-wave trough is leaving Colorado while the 26th is a transitional period from zonal flow to a ridge building over the far western United States. Meteorological data provided in Table 15.8 and Figures 15.39 a,b; 15.40 a,b; and 15.41 a,b show September 26 as both warmer and moister with a faster-developing PBL (planetary boundary layer). Figures 15.42 a,b and 15.43 indicate stronger low-level winds and a 90° difference in direction during daylight hours on the 26th. Airplane temperature soundings (Figure 15.44) also give evidence of two different vertical structures. Meteorological conditions over the state on September 26 were generally more complex, a fact revealed by corresponding complexity in the refractive index structure over the site, as observed by the various remote sensors. Comparison of these observations will be discussed in more detail in a paper now in preparation, along with possible meteorological causes.

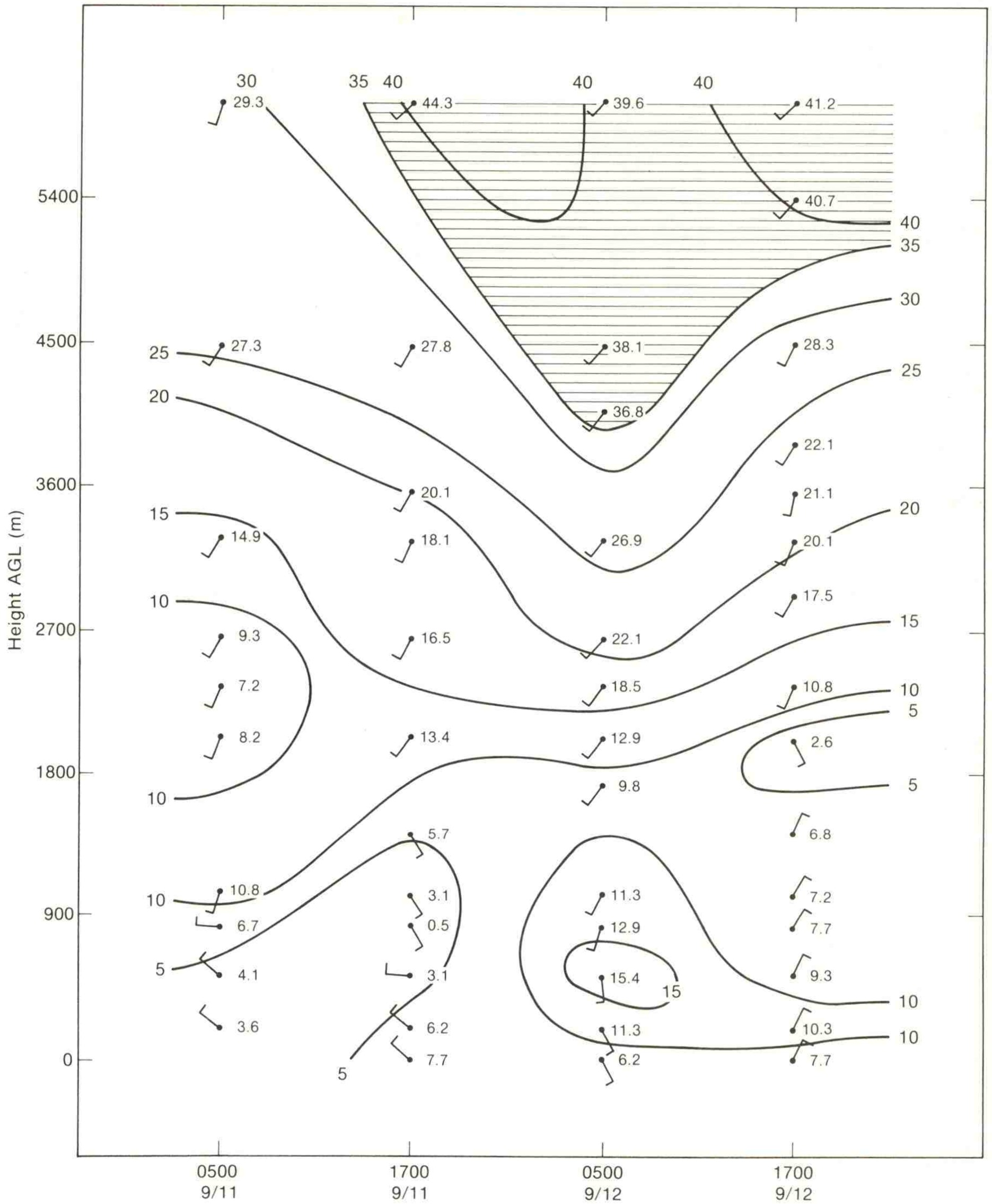


Figure 15.33.--Denver rawinsonde time-series wind speed profiles (m/s), with wind direction flags.

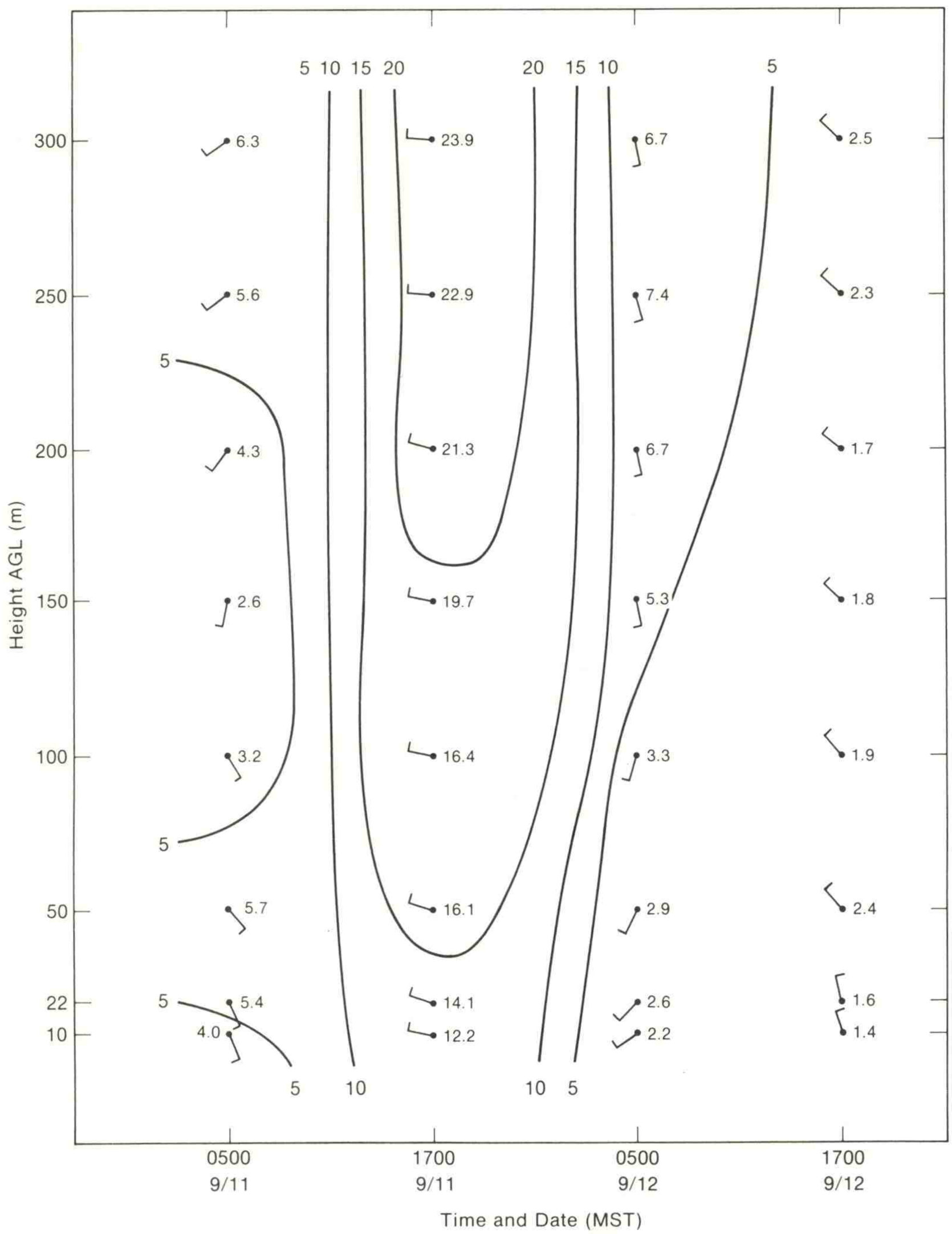


Figure 15.34.--BAO rawinsonde time-series wind speed profiles (m/s), with wind direction flags.

Table 15.6.--Meteorological data for September 11, 1978

Rawinsonde data

Time	Station	Height	stability	Modified Showalter index
0500 MST	DEN	0-340 m	strong stability	5
		340-1800 m	stable	
0902 MST	BAO	0-60 m	conditional instability	-2
		60-1100 m	stable	
		1100-1250 m	conditional instability	
		1250-1400 m	neutral	
		1400-1800 m	stable	
1700 MST	DEN	0-60 m	strong instability	1
		60-1800 m	stable	

Temperatures

min	12.9°C	0400 MST	
max	22.6°C	1400 MST	
mean	18.3°C		

Moisture

surface	4.8 g/kg	Denver daily	
700-mb	4.3 g/kg	average	

Winds

Speed

minimum	0.3 m s^{-1}		
maximum	13.9 m s^{-1}		
peak wind	25 m s^{-1}	(1640 MST)	BAO 300-m

Direction

SSW early morning (4 m s^{-1}) veering NW around 0330 MST, becoming variable before shifting to WNW and increasing to a steady 15 to 20 m s^{-1}. Daytime dominated by strong WNW flow. Nighttime consisting of shifting winds with periods of strong WNW flow.

Table 15.7.--Sequence of events on September 11, 1978, as recorded by all sky camera summary

Time (MST)	Events
0500	Small cumulus puffs appear but dissipate quickly
0530	Size and number of cumulus increase
0545	Sky becomes totally clear
0615	Very small cumulus appear
0745	Sky becomes mostly clear
0845	Deeper cumulus form and move by
0900	Faint "cirrus"* moving overhead
0930	"Cirrus" thickens and cumulus disappear
1000	Thick patches of "cirrus" move by
1030	Sky becomes clear as "cirrus" disappear
1100	"Cirrus" reappear but not as thick
1130-1300	Sky mostly clear with a few "cirrus," line of cumulus along east horizon
1300	More cumulus pass over, but dissipate quickly
1500	Cirrus and cumulus moving across sky; line of cumulus still to east
1600	Cirrus become thickest of day
1630	Increased cumulus activity to east
1645	Sky becoming mostly clear with cumulus still along east horizon
1800	Layer of haze visible to west as sun sets

*This "cirrus" is not in fact cirrus but blowing dust. This was determined (with some difficulty) by comparing its appearance with that of clearly definable cirrus occurring later in day. The dust appears at 0900 MST, becomes quite thick at 0930 until about 1015, then thinner until around 1130. From 1130 until 1245 no clouds can be seen, but some dust or haze still seems visible.

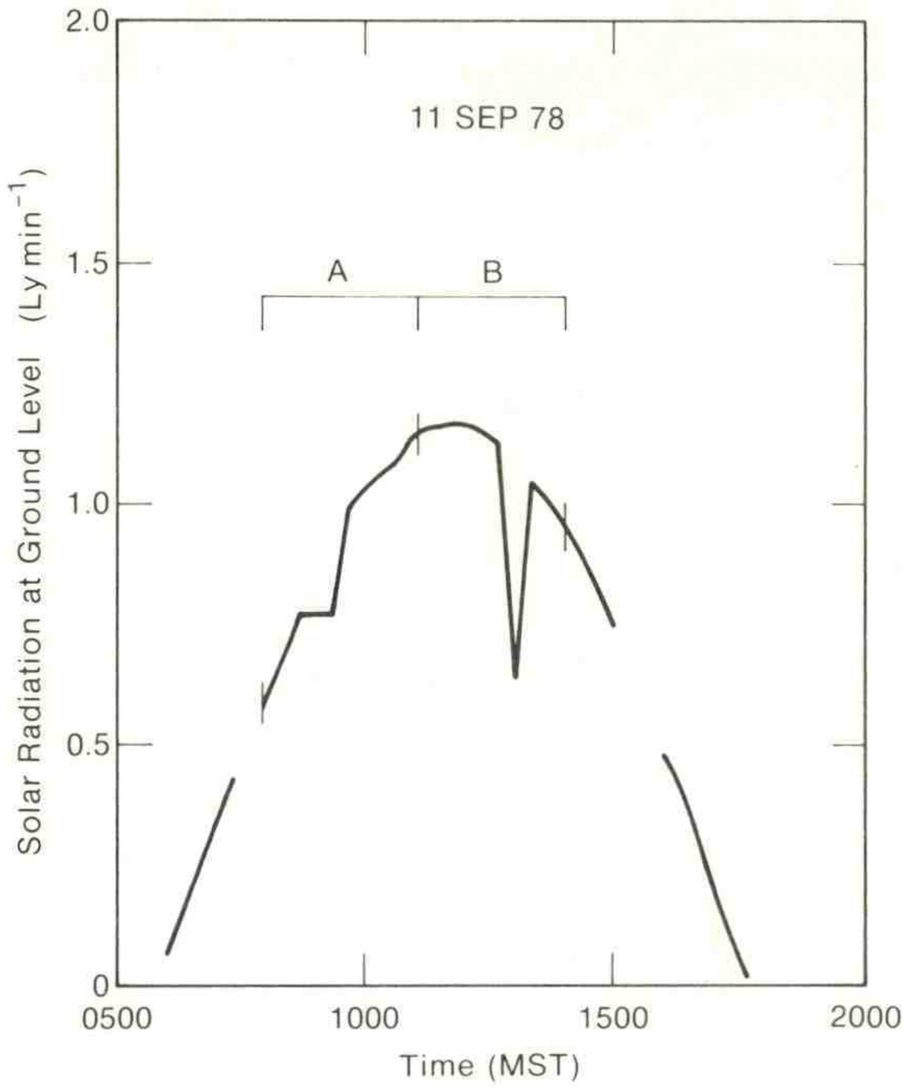


Figure 15.35.--Ground-level solar radiation intensity time-series, direct and diffuse (from PDP 11/70 20-min averages).

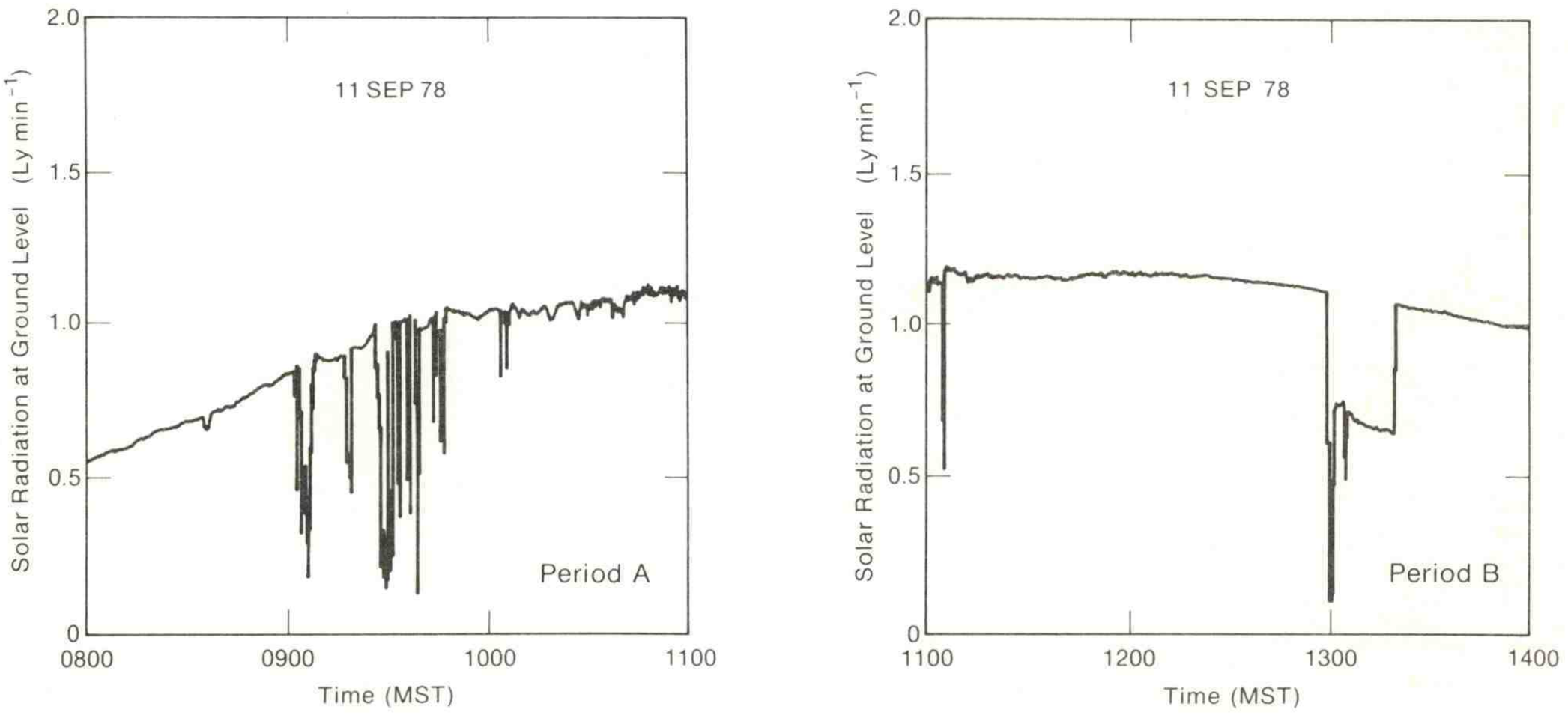


Figure 15.36.--Ground level solar radiation intensity time series (taken from PDP 11/70 10-s averages). Left: 0800-1100 MST; right: 1100-1400 MST.

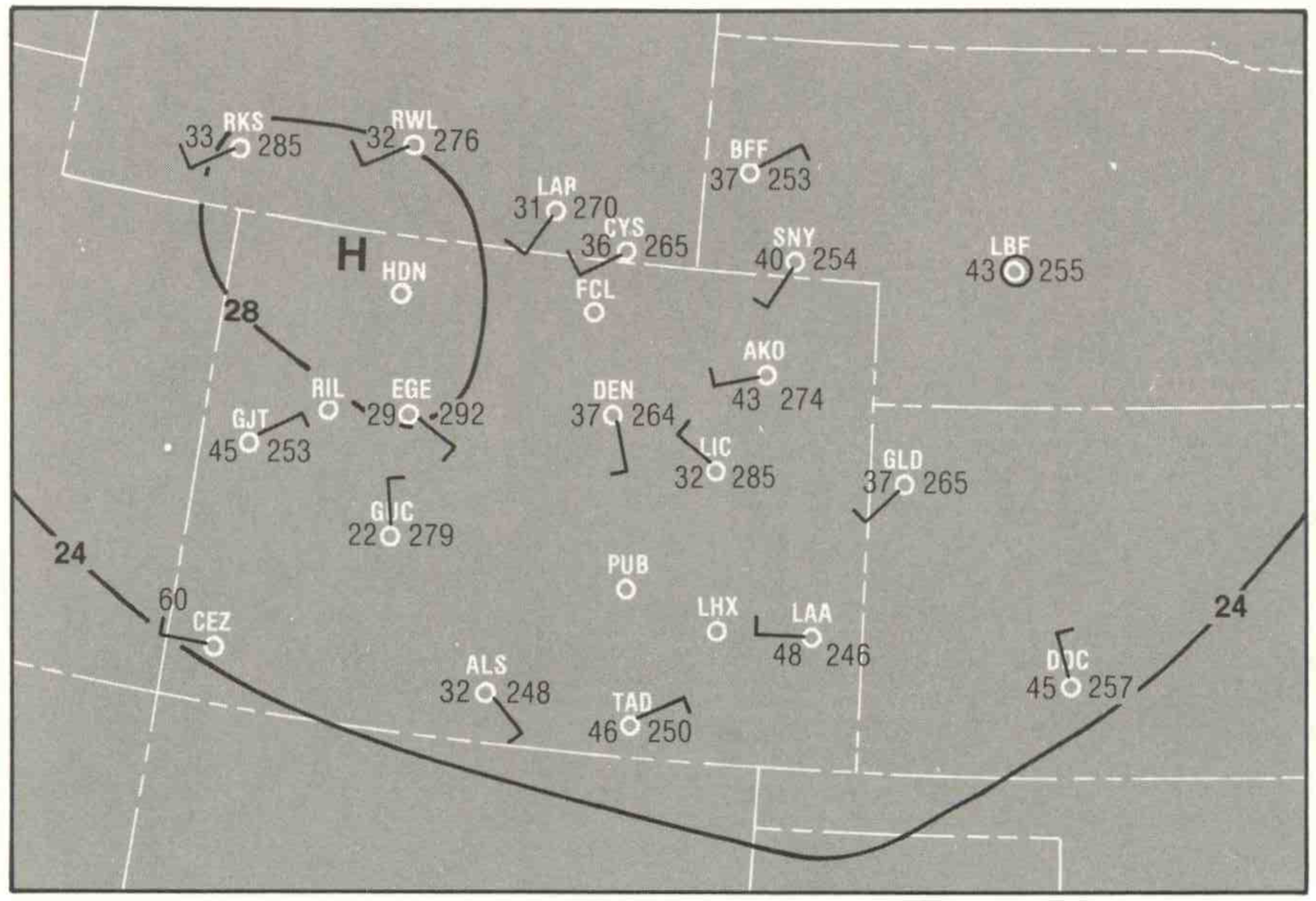


Figure 15.37.--Three-hourly surface weather maps from National Climatic Center, Asheville, N. C. (a) 2300 MST, September 20, 1978.

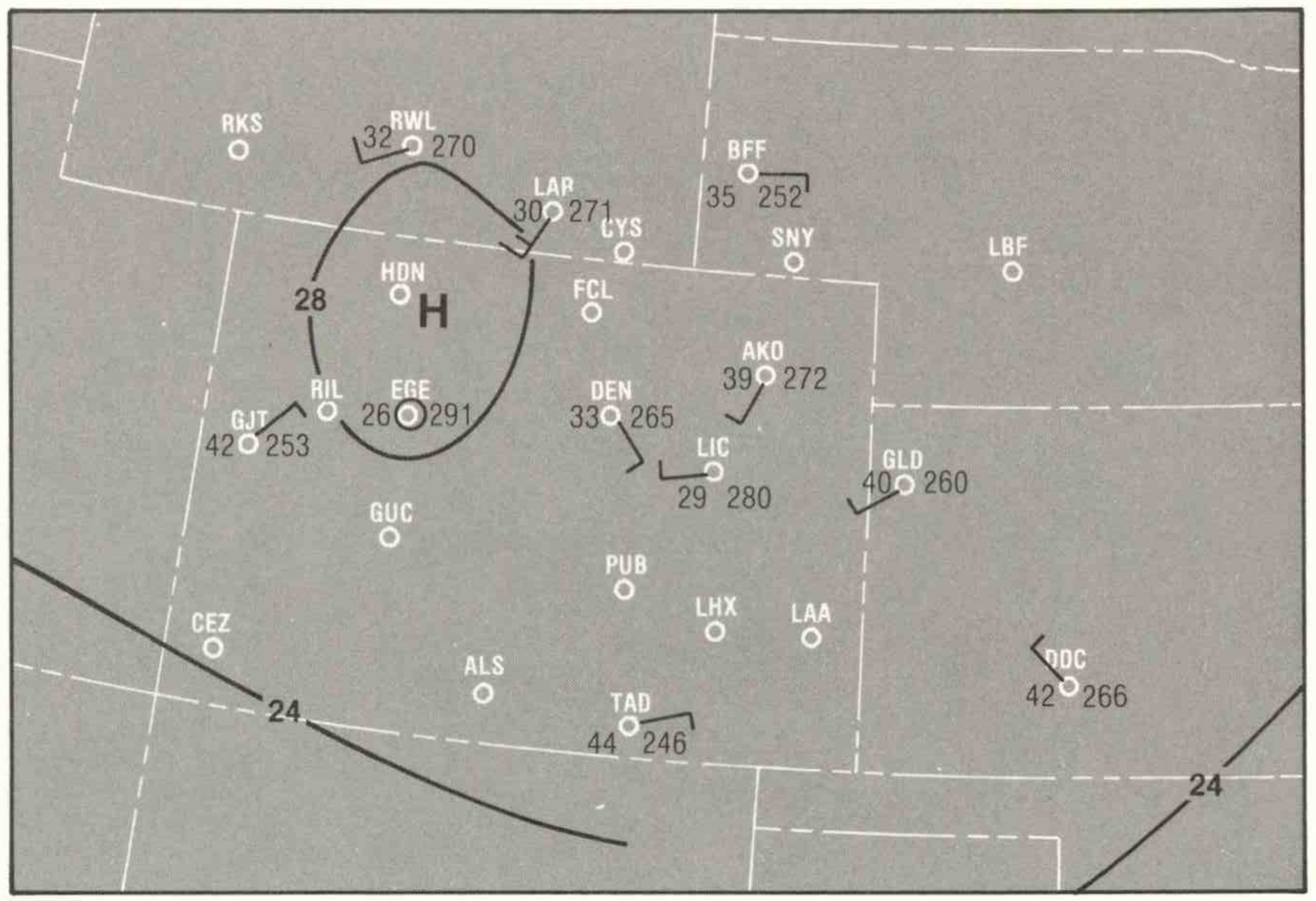


Figure 15.37b.--0200 MST, September 21, 1978.

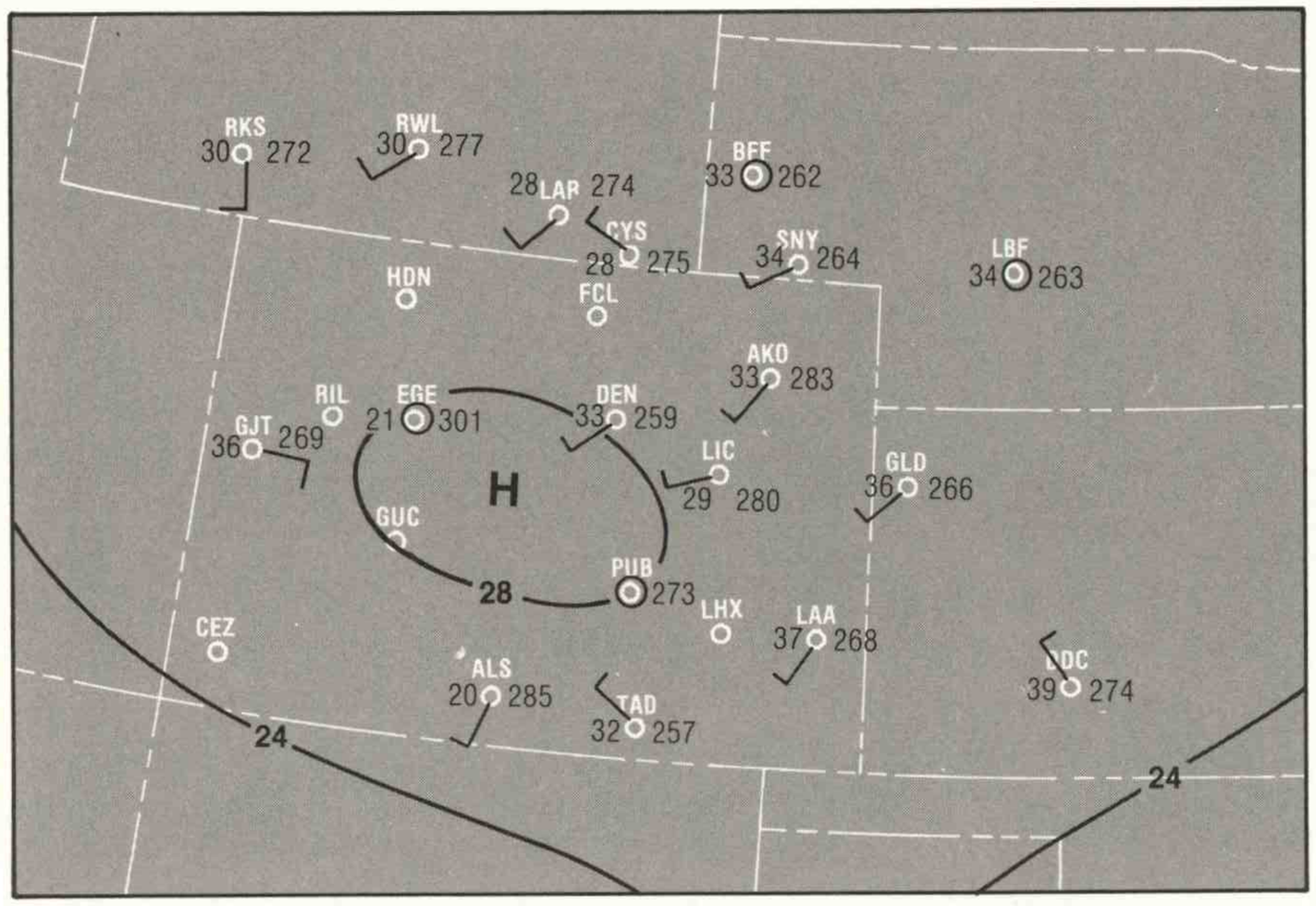


Figure 15.37c.--0500 MST, September 21, 1978.

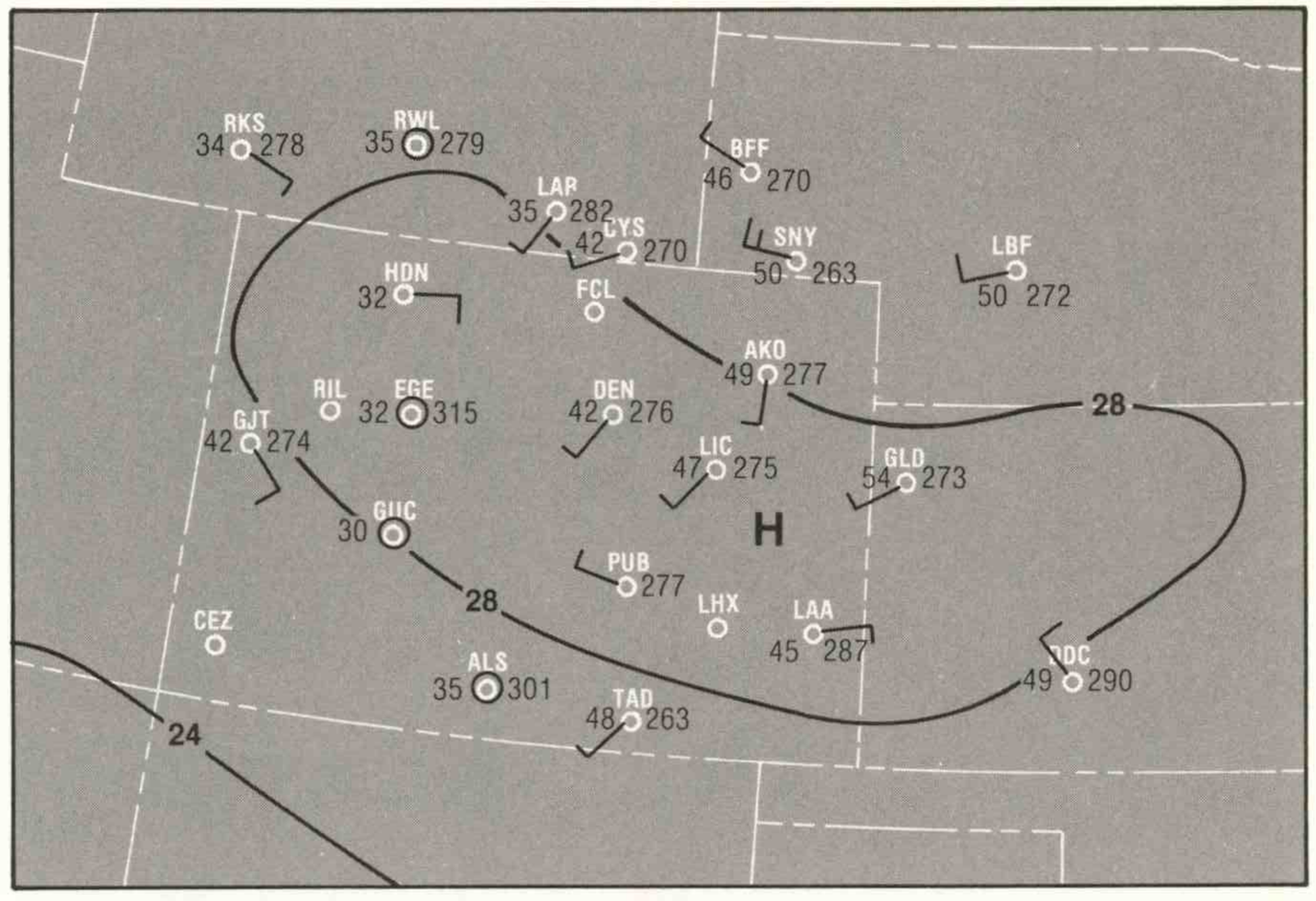


Figure 15.37d.--0800 MST, September 21, 1978.

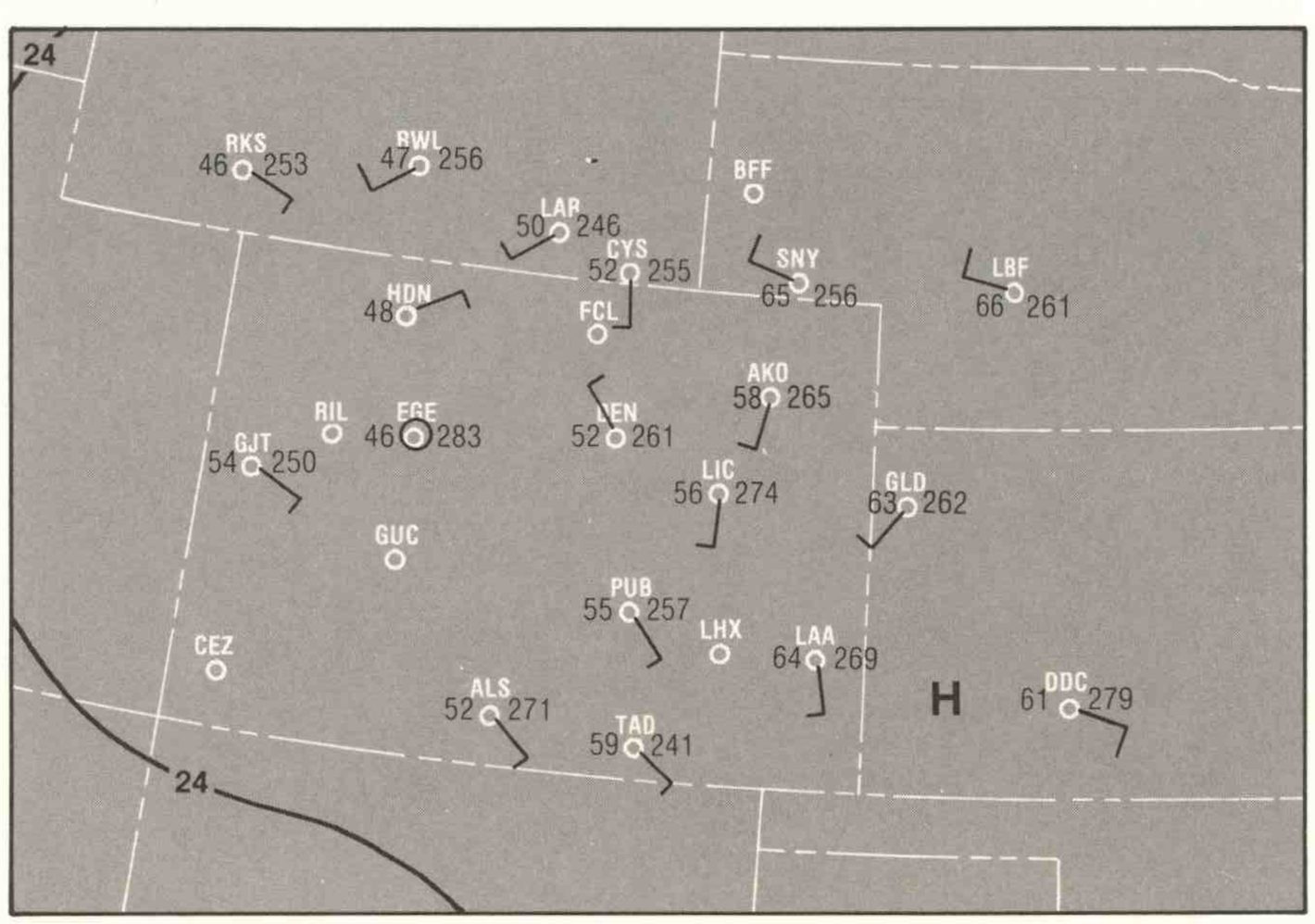


Figure 15.37e.--1100 MST, September 21, 1978.

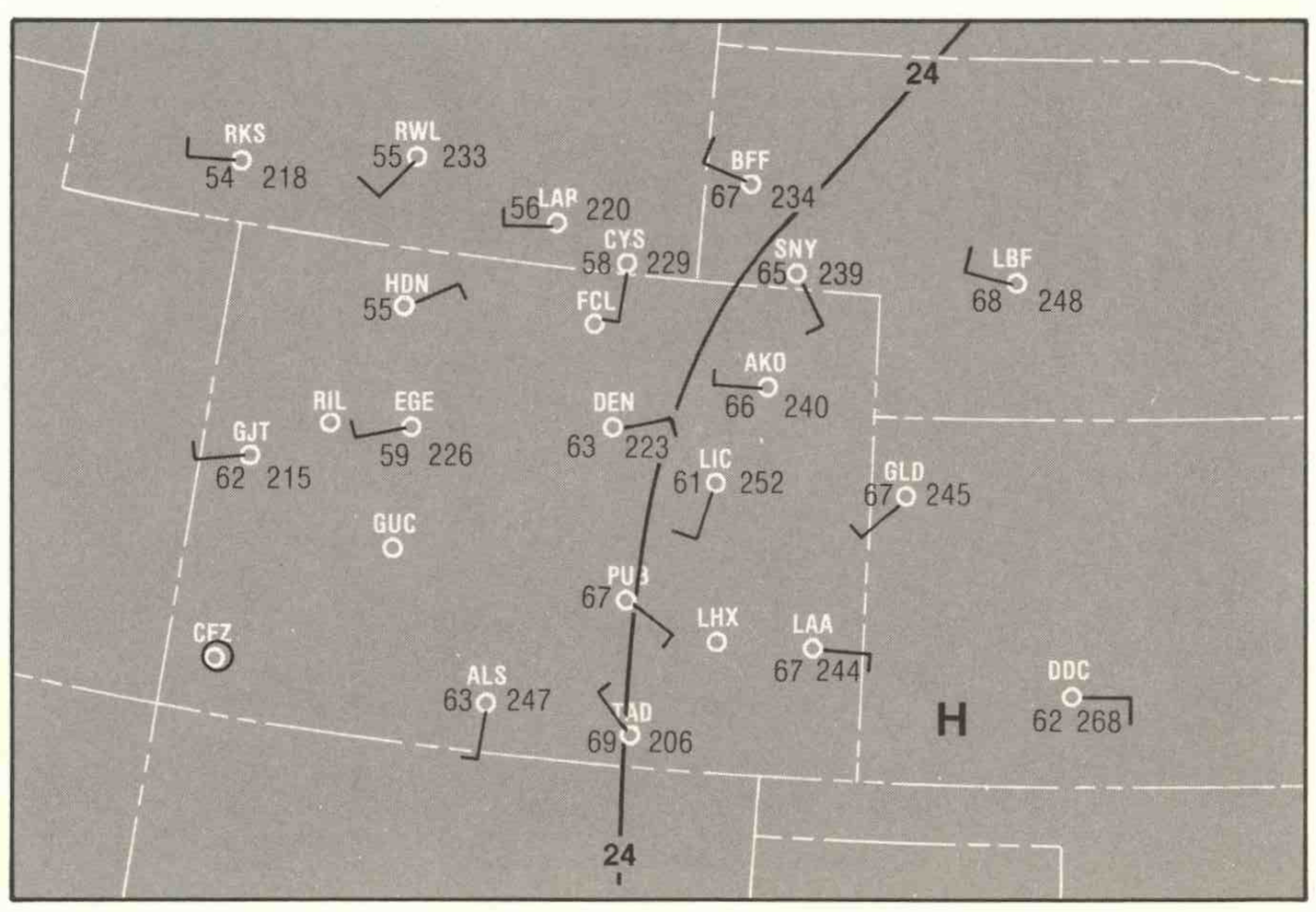


Figure 15.37f.--1400 MST, September 21, 1978.

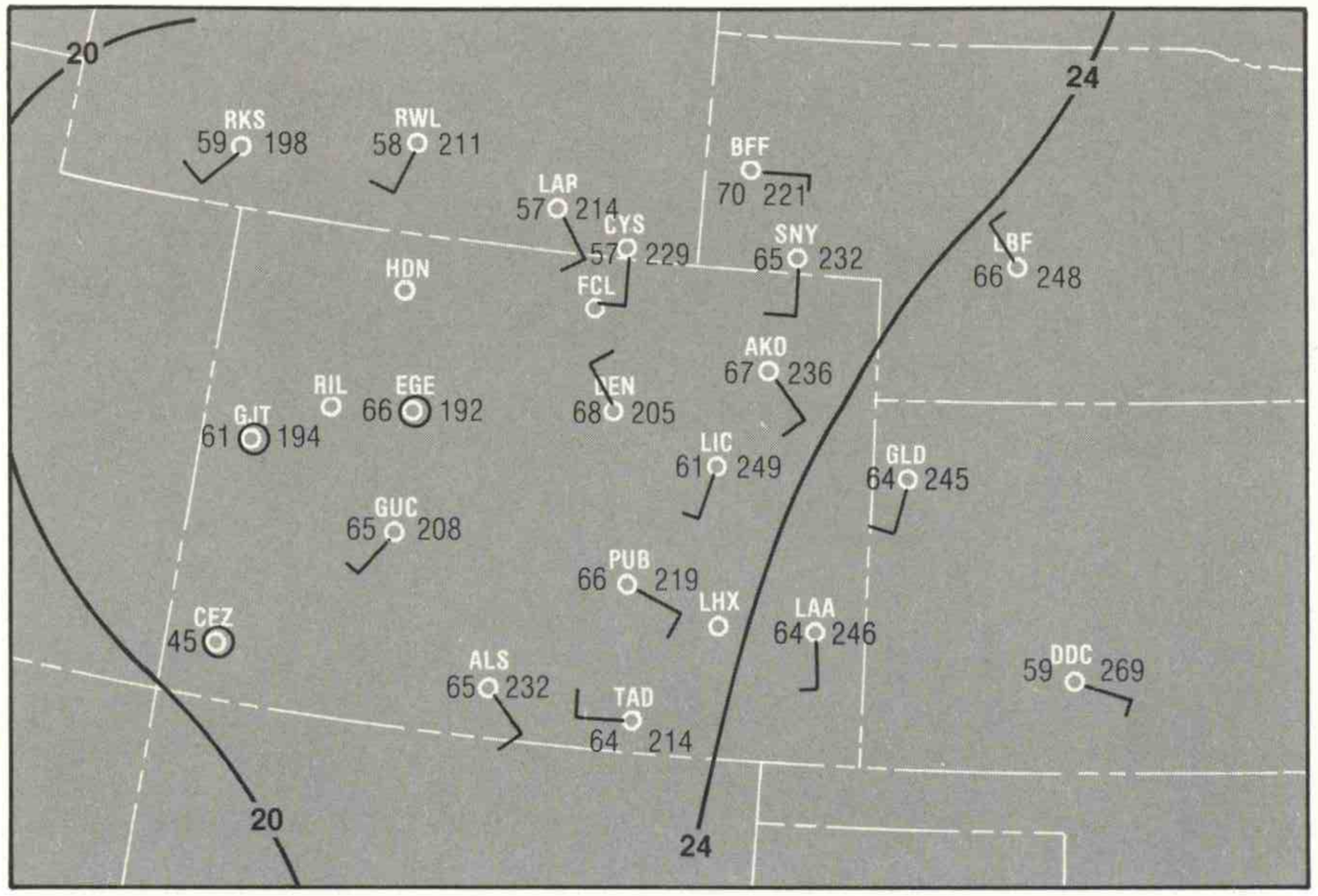


Figure 15.37g.--1700 MST, September 21, 1978.

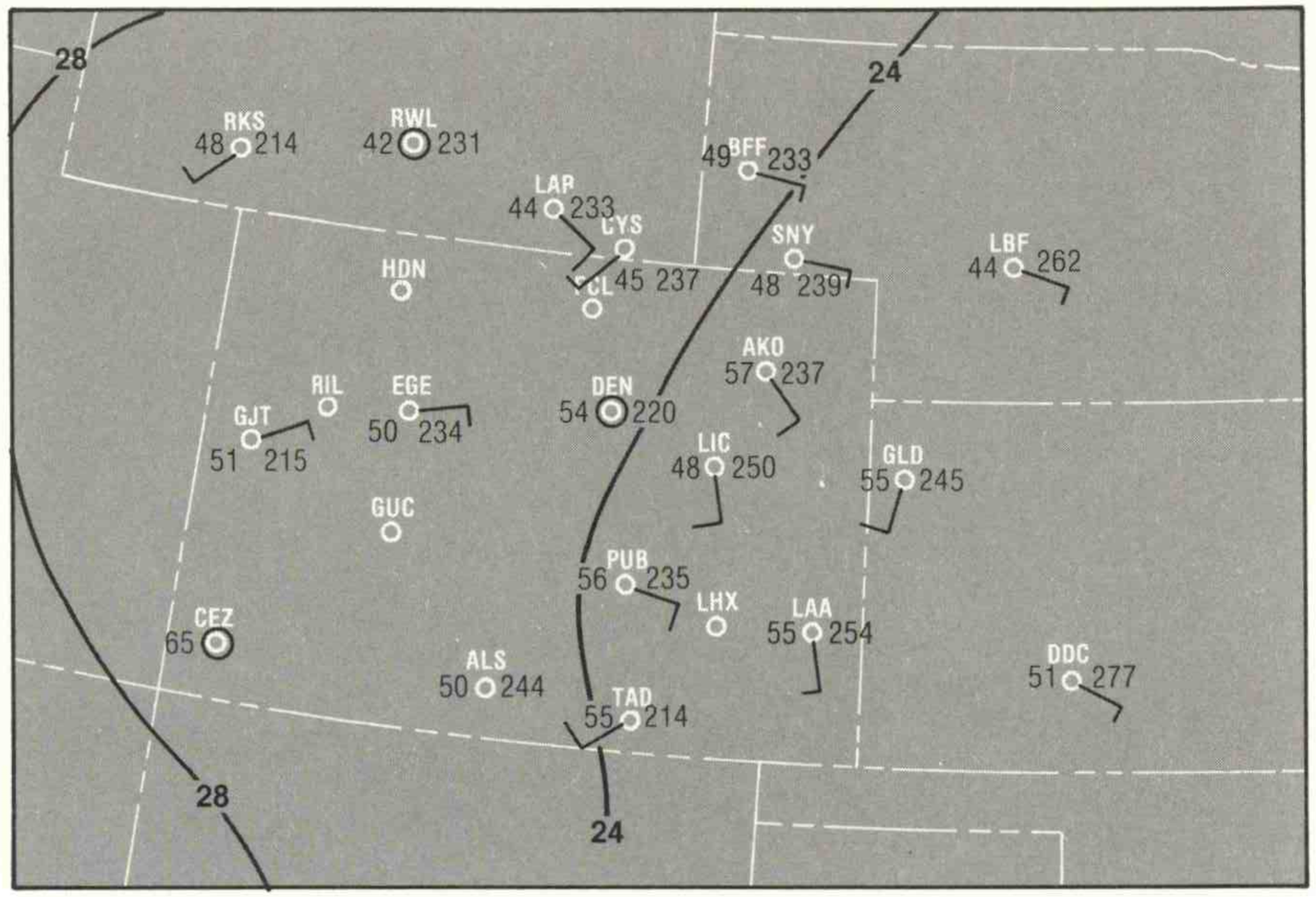


Figure 15.37h.--2000 MST, September 21, 1978.

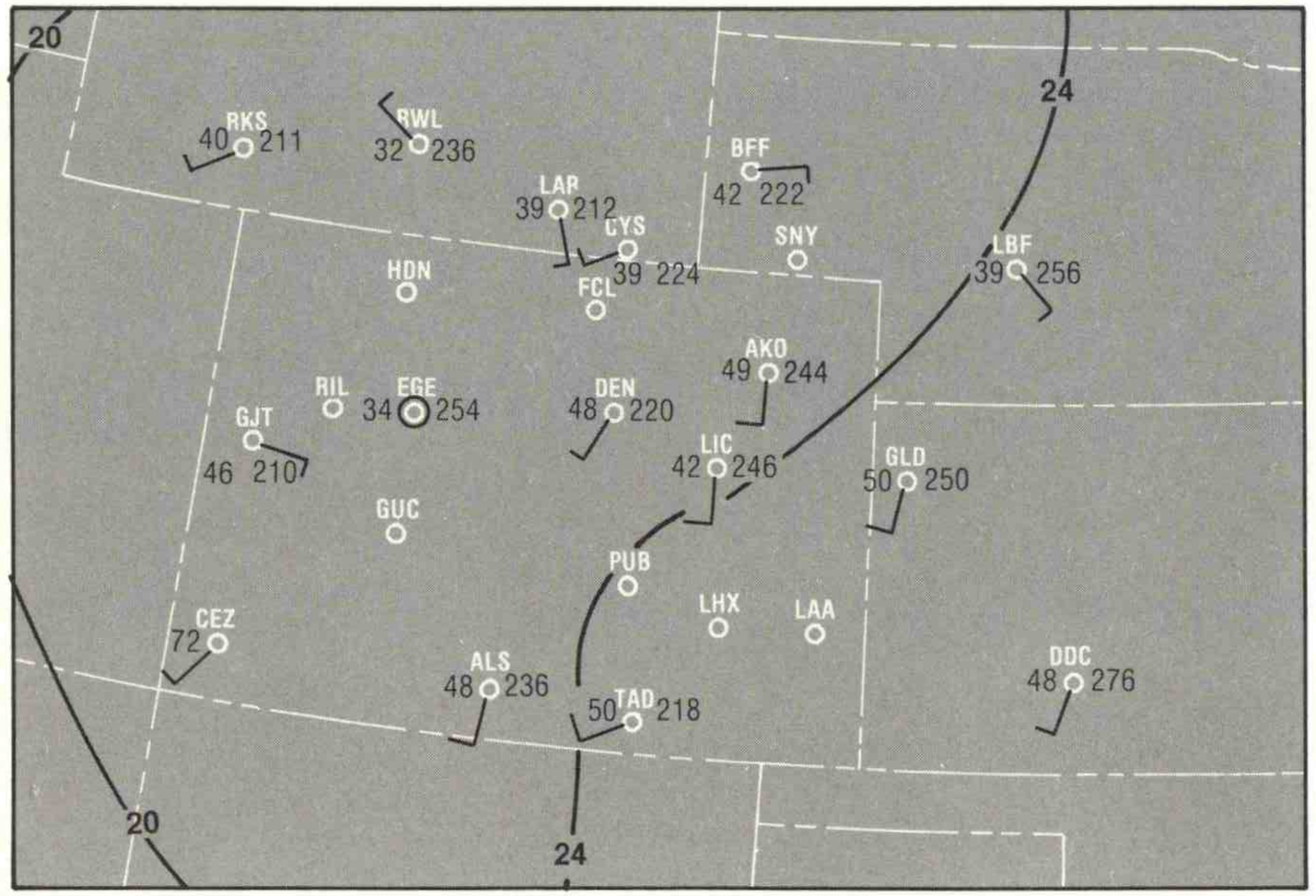


Figure 15.37i.--2300 MST, September 21, 1978.

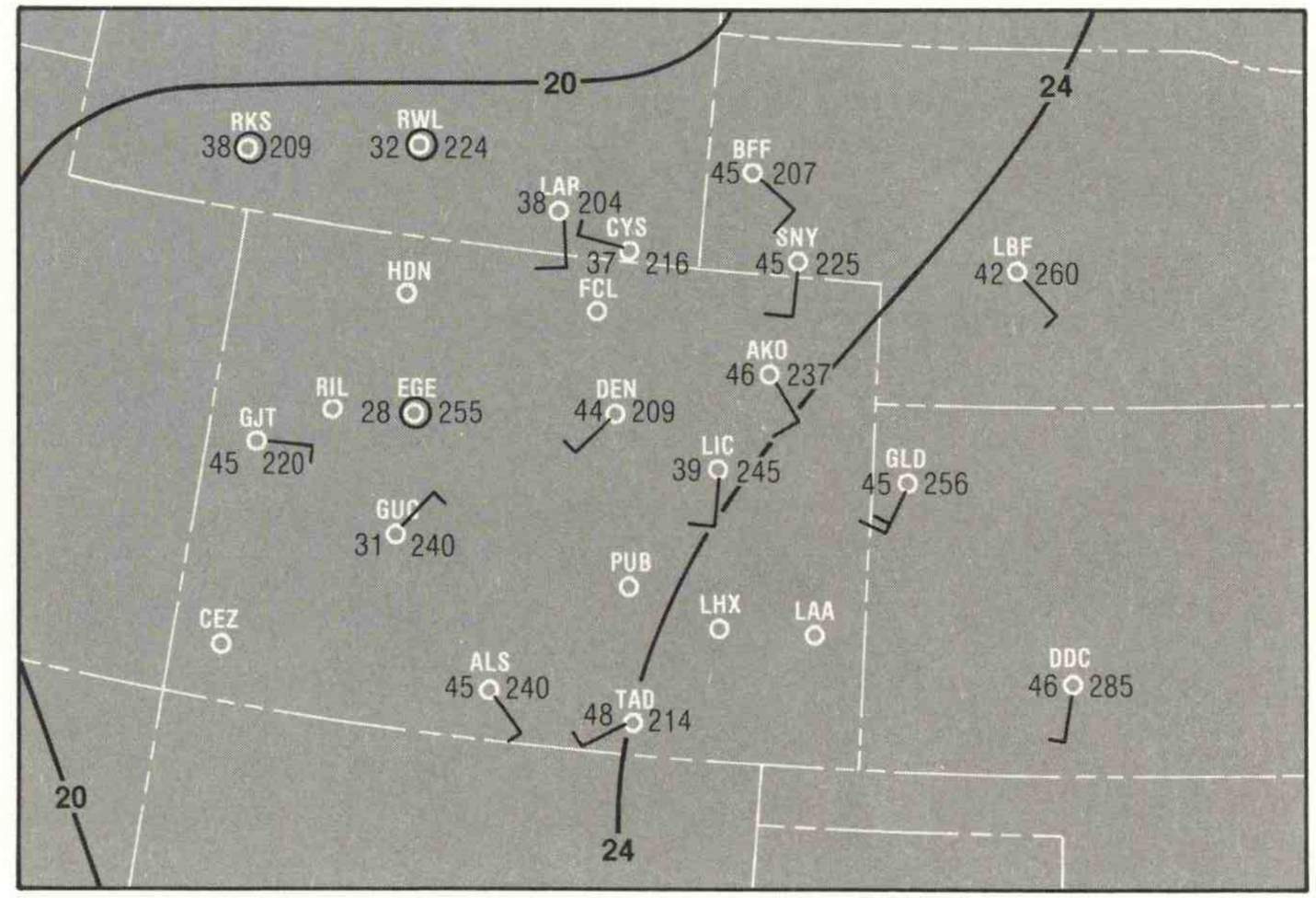


Figure 15.37j.--0200 MST, September 22, 1978.

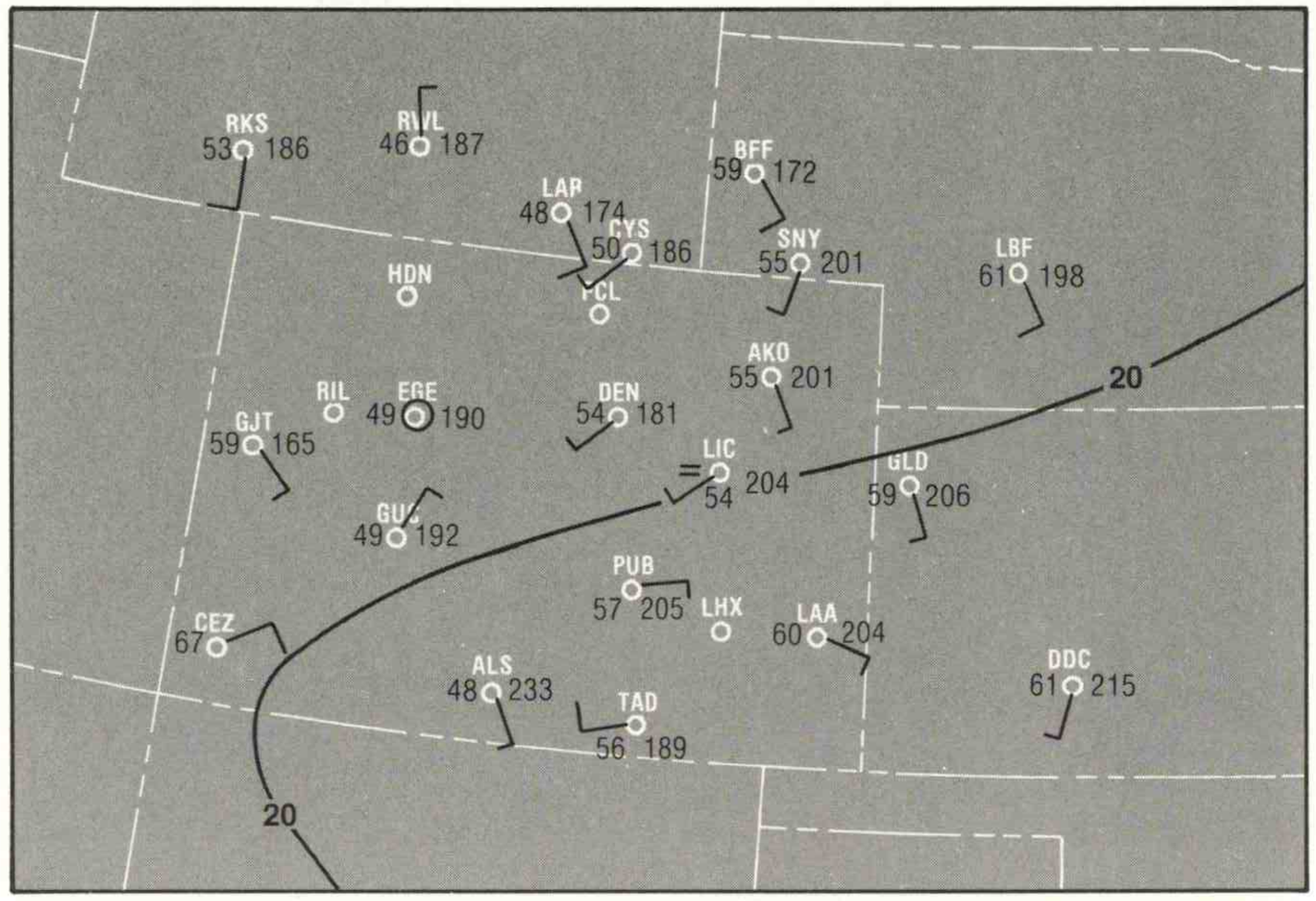


Figure 15.38.--Three-hourly surface weather maps from National Climatic Center, Asheville, N. C. (a) 2300 MST, September 25, 1978.

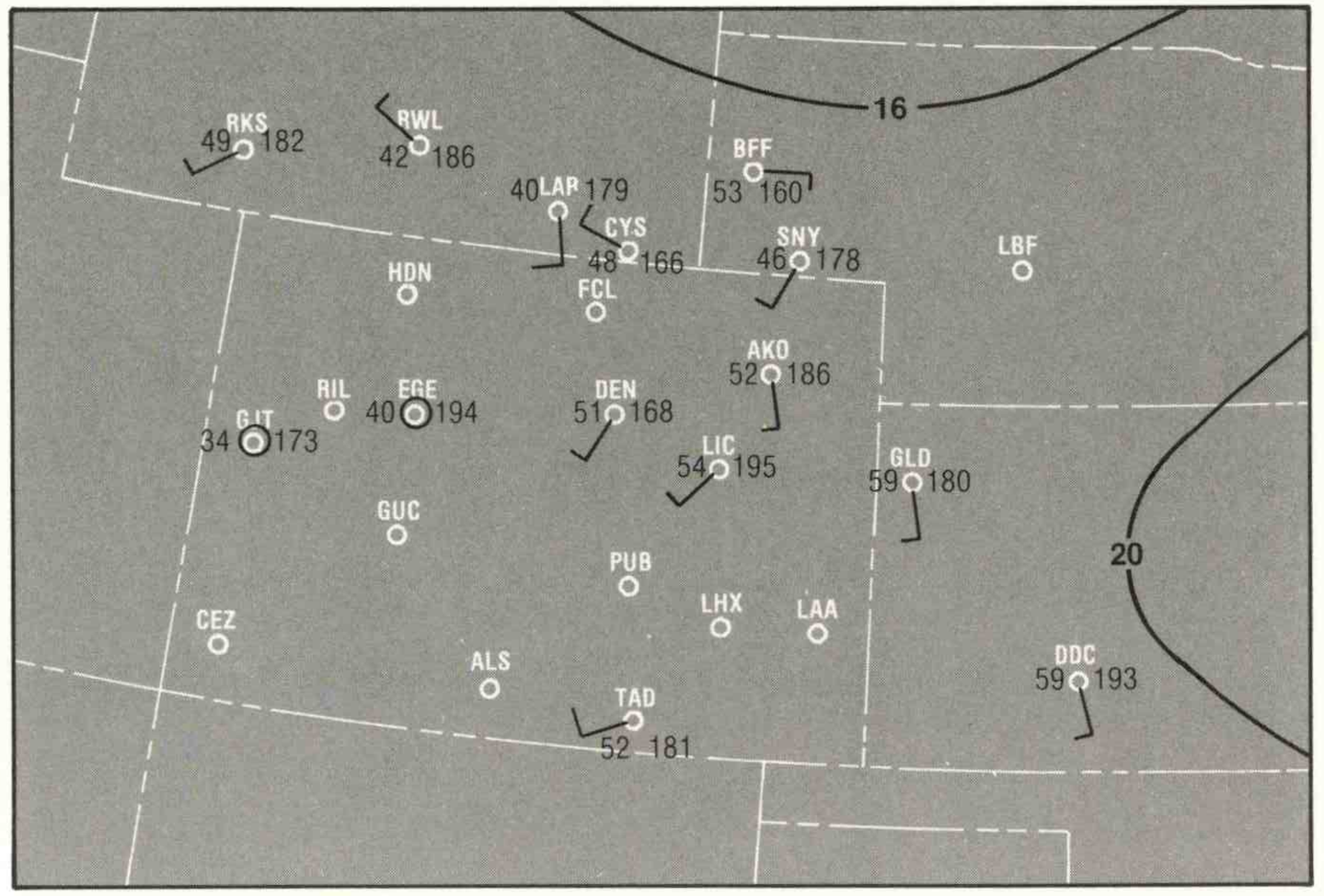


Figure 15.38b.--0200 MST, September 26, 1978.

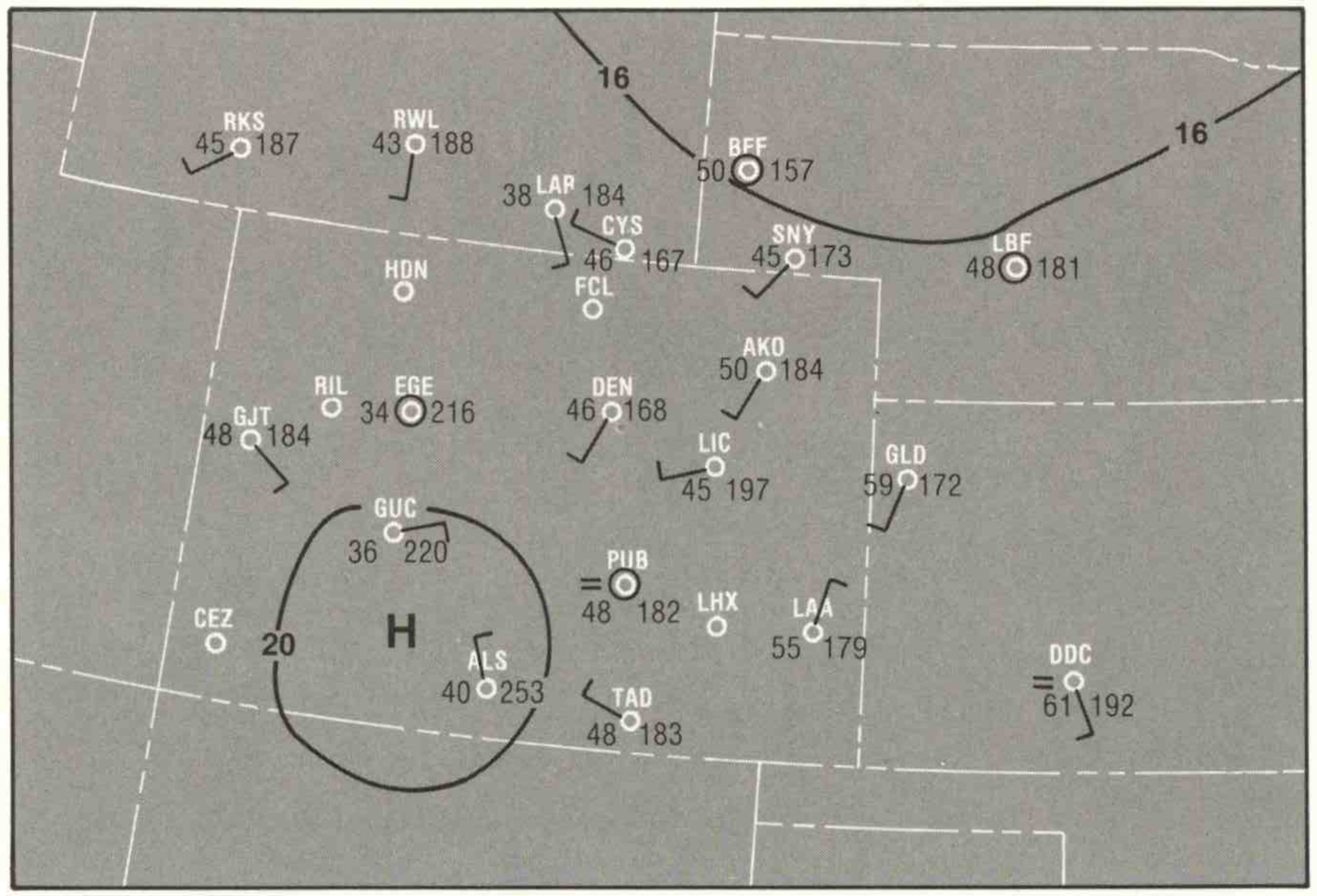


Figure 15.38c.--0500 MST, September 26, 1978.

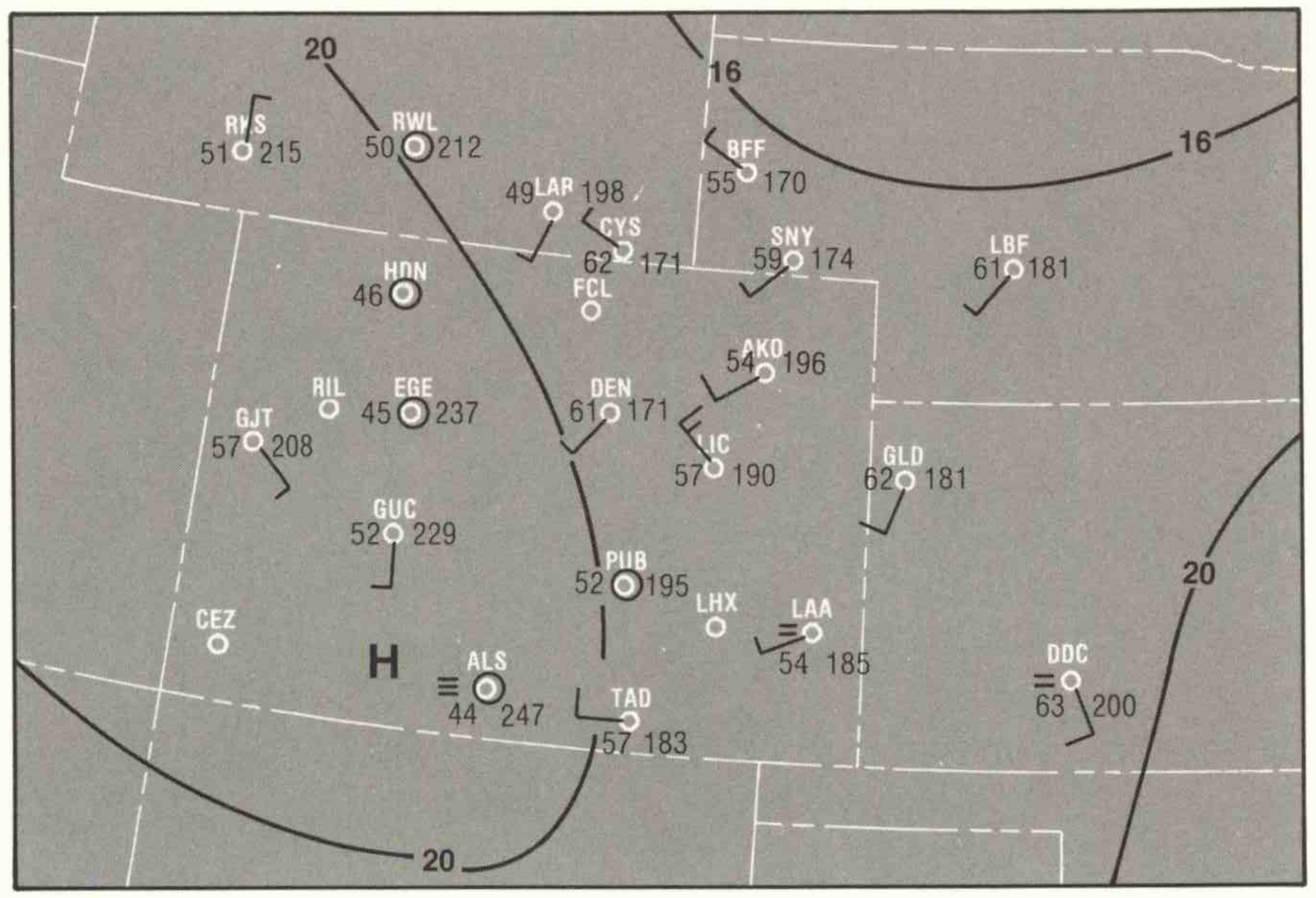


Figure 15.38d.--0800 MST, September 26, 1978.

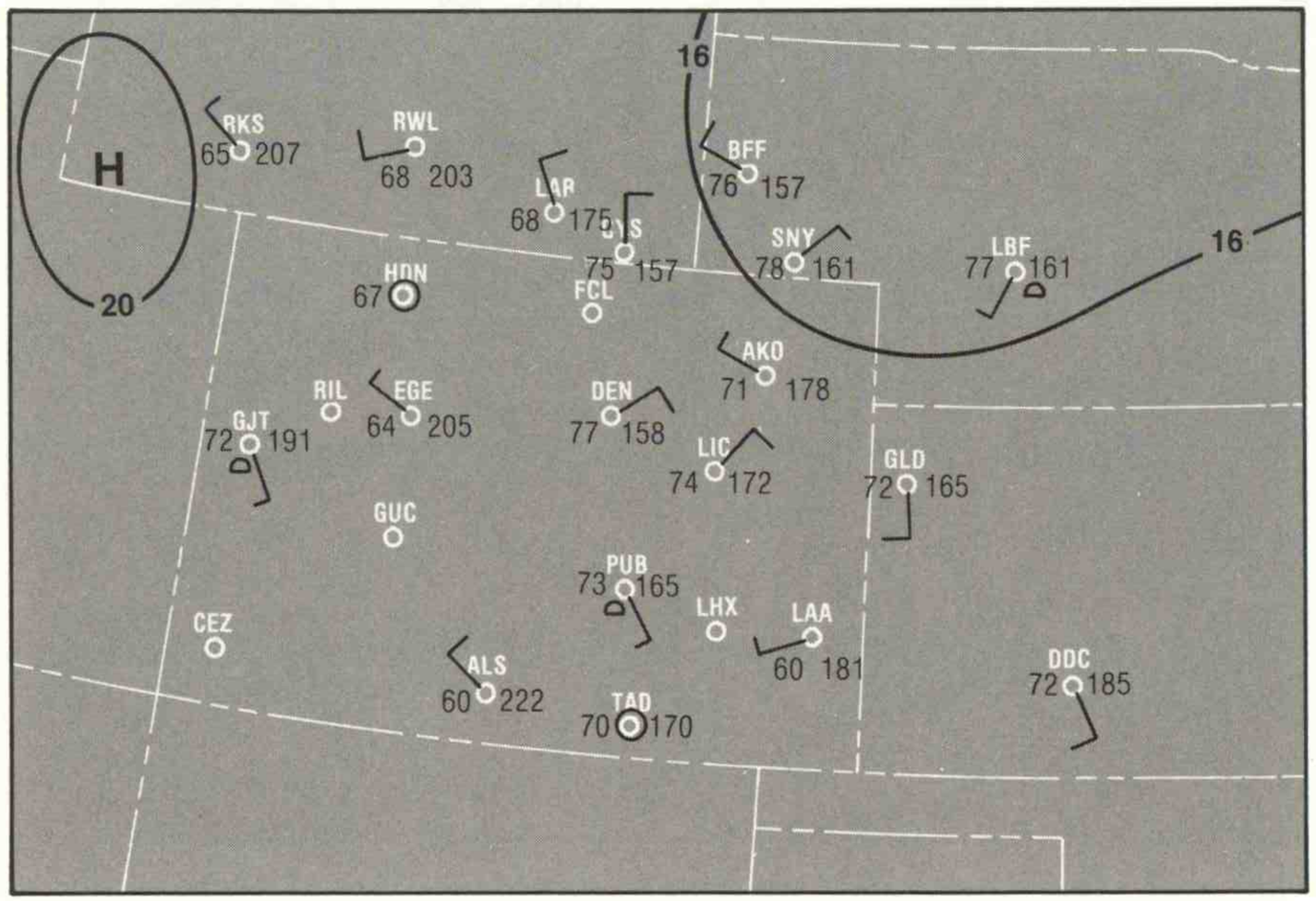


Figure 15.38e.--1100 MST, September 26, 1978.

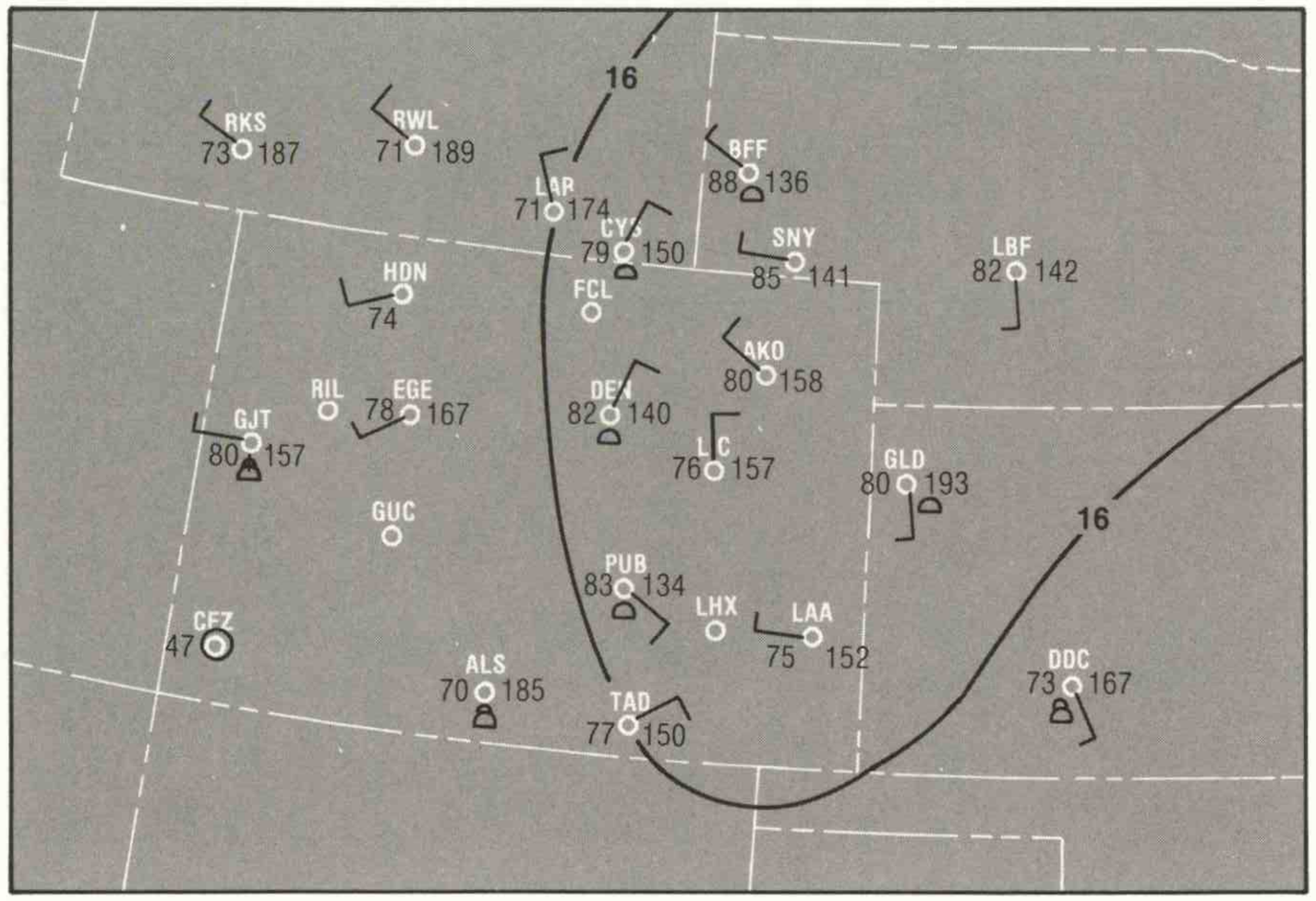


Figure 15.38f.--1400 MST, September 26, 1978.

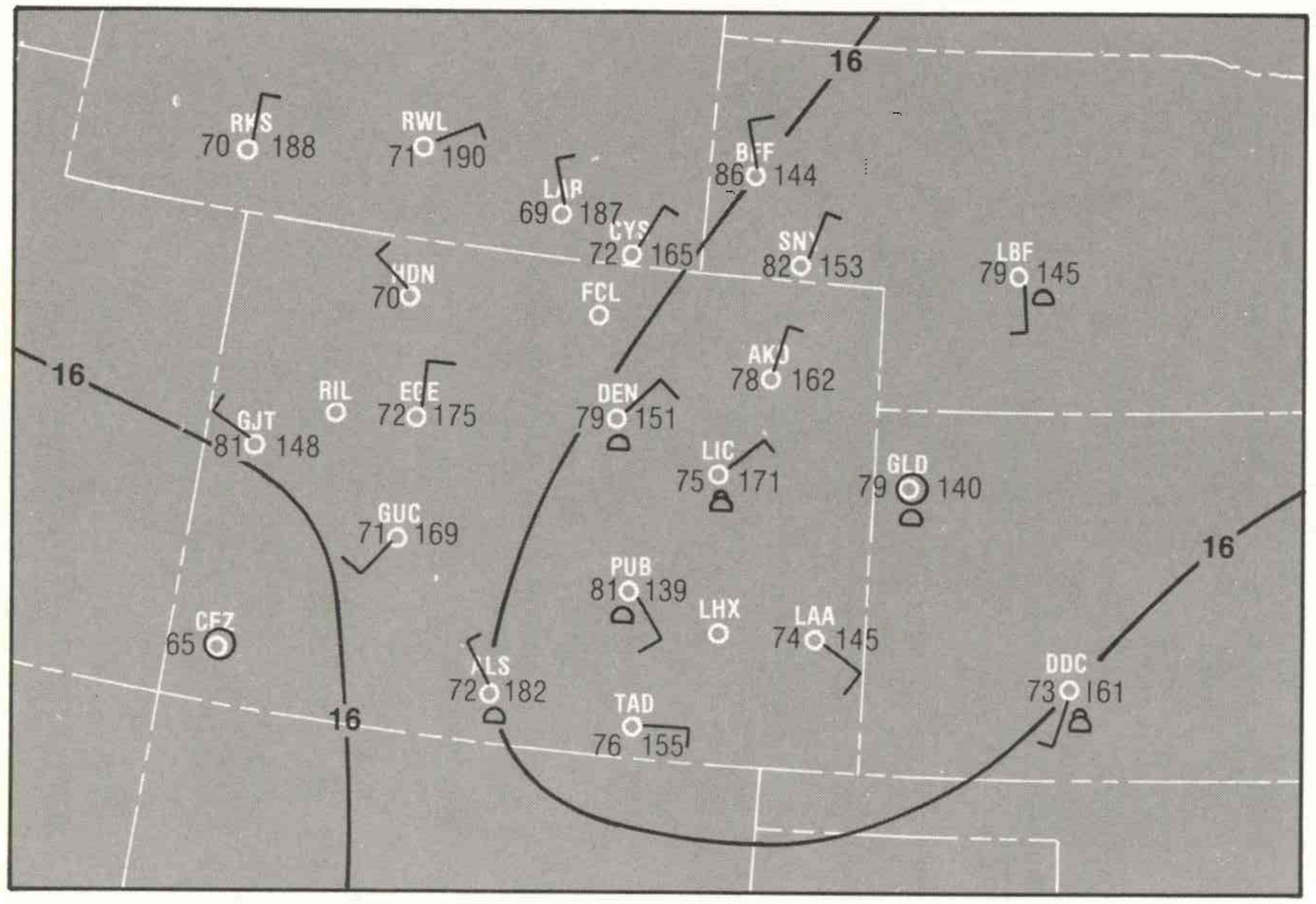


Figure 15.38g.--1700 MST, September 26, 1978.

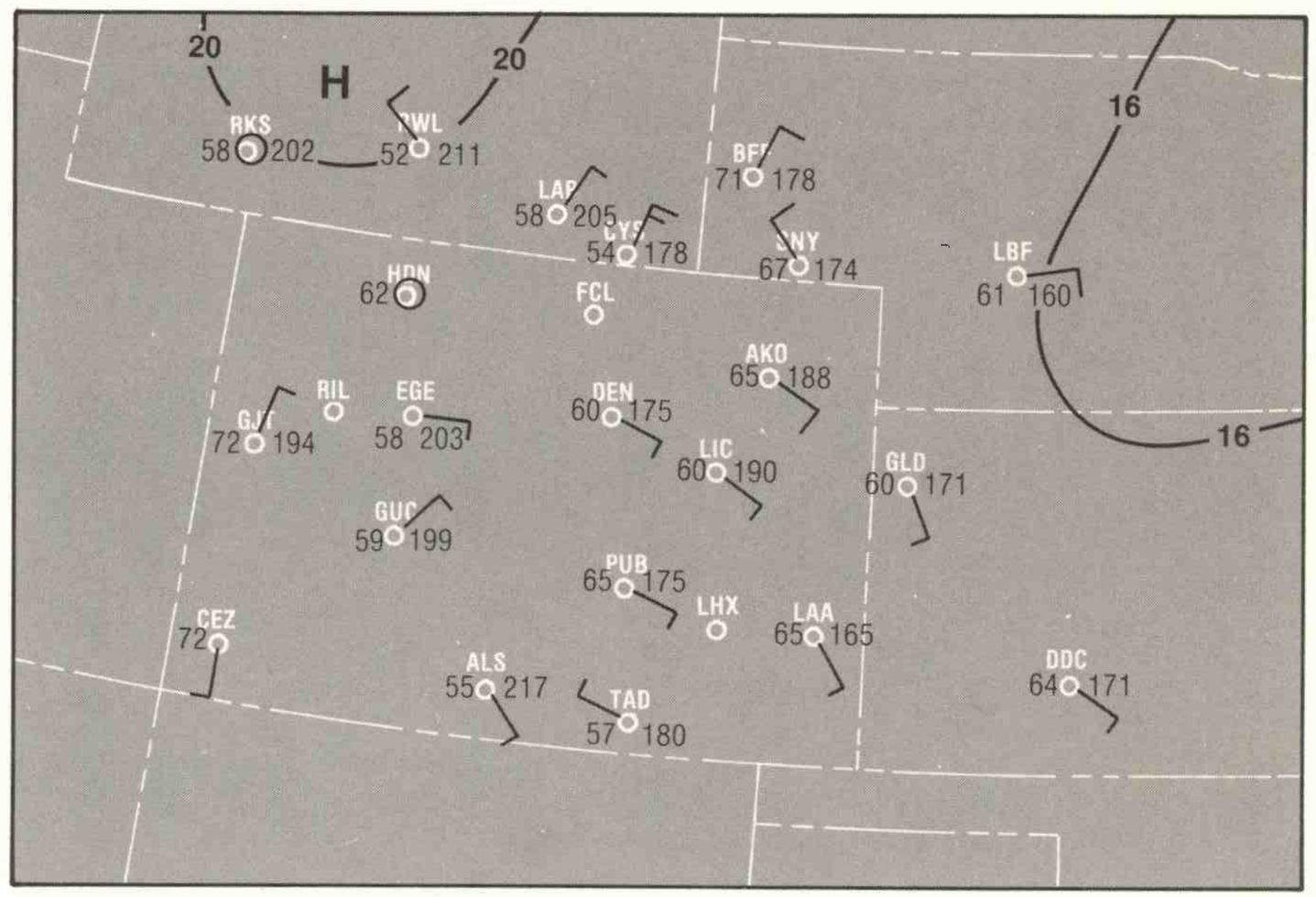


Figure 15.38h.--2000 MST, September 26, 1978.

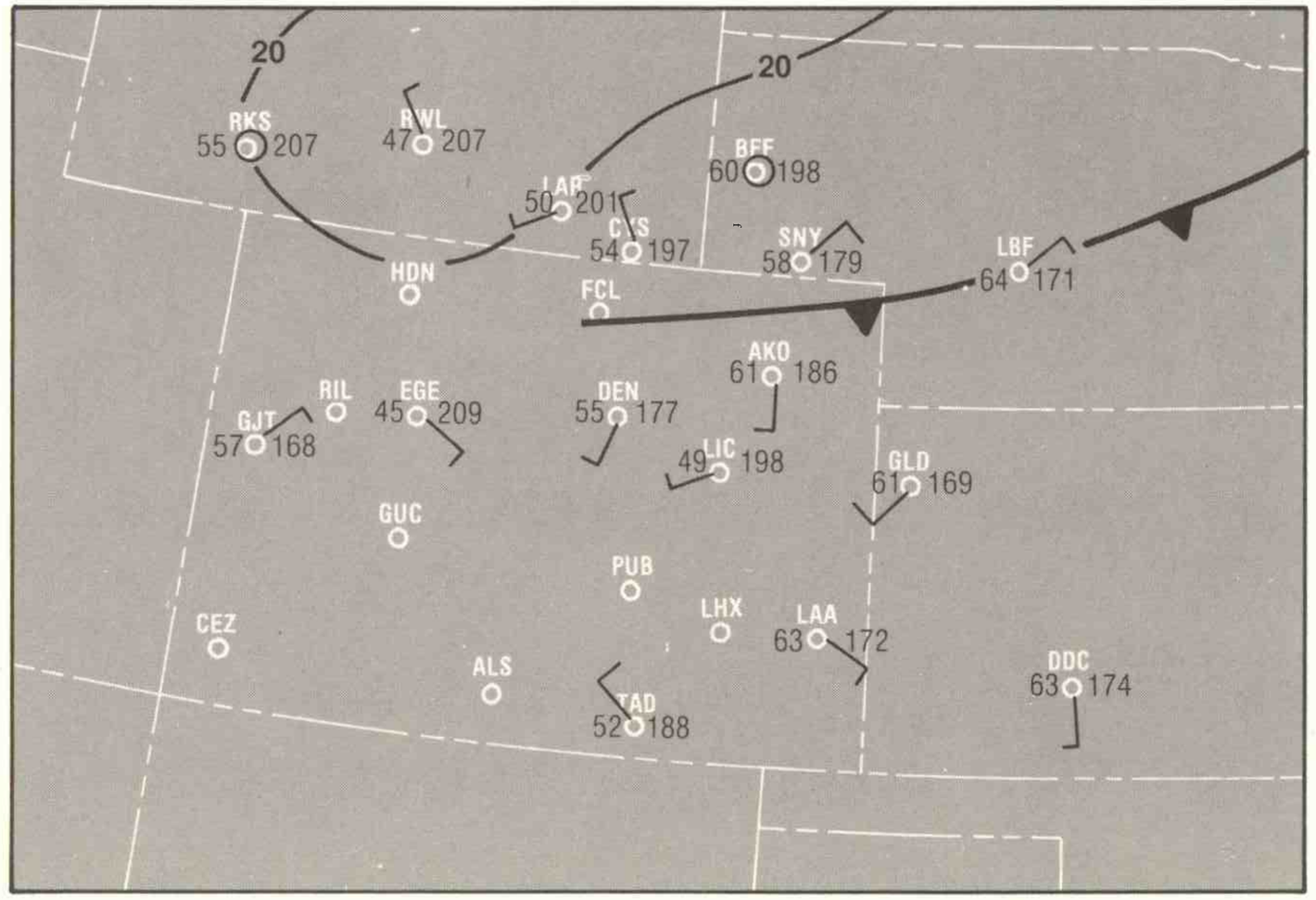


Figure 15.38i.--2300 MST, September 26, 1978.

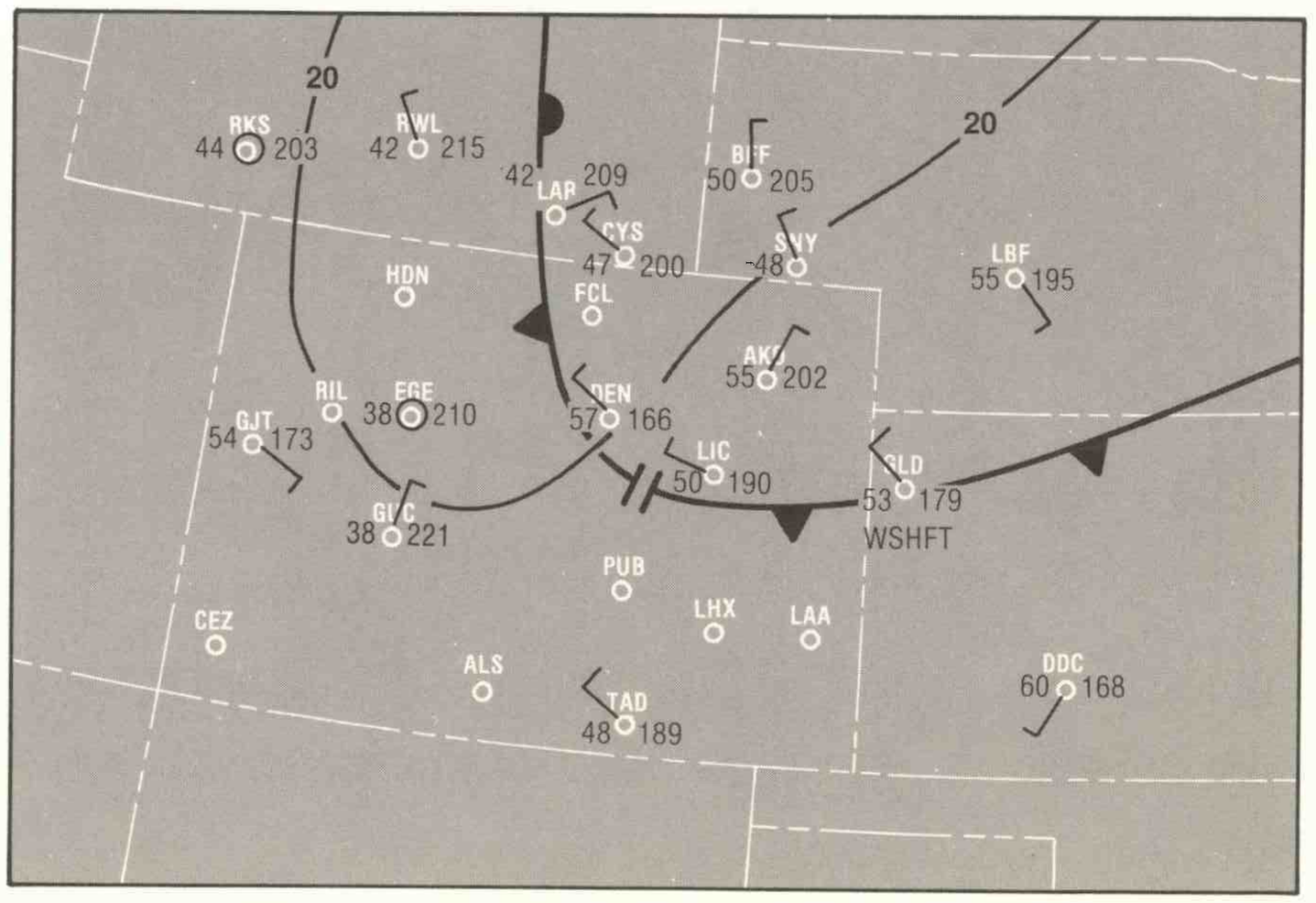


Figure 15.38j.--0200 MST, September 27, 1978.

Table 15.8.--Meteorological data for September 21 and 26, 1978

September 21			September 26		
Temperature			**Temperature**		
Min	-1.1°C	0400 MST	Min	6.1°C	0400 MST
Max	17.5°C	1600 MST	Max	27.9°C	1400 MST
Daily Mean	9.0°C		Daily Mean	16.9°C	
Moisture			**Moisture**		
Surface 1.9 g/kg	Denver daily		Surface 2.9 g/kg	Denver daily	
700 mb 3.0 g/kg	average		700 mb 4.6 g/kg	average	
Major area of moisture to E and SE at 700 mb			Major area of moisture to SE at 700 mb		
Contents restricted to lower 100 meters			Moisture extending up as high as 2700 m AGL		
Winds			**Winds**		
Speed*			Speed*		
Min	.3 m s ^{1}		Min	.5 m s ^{1}	
Max	1.8 m s ^{1}		Max	4.3 m s ^{1}	
Daily Mean	1.0 m s ^{1}		Daily Mean	1.5 m s ^{1}	
*Tower ranges presented in Chapter 2 (Kaimal and Wolfe, 1979)					
Direction			Direction		
NW early morning (< 2 m s ^{1}) shifting slowly to SE around 1100 MST. In late afternoon returning to NW. Daytime dominated by SE flow. Nighttime dominated by NW flow.			NW shifting to NE by 1000 MST (4 m s ^{1}) becoming light around 2000 MST before returning to NW. Daytime dominated by NE flow. Nighttime dominated by NW flow.		
Ht (500 mb)			Ht (500 mb)		
1700 MST 9/20	5700 m		1700 MST 9/25	5850 m	
0500 MST 9/21	5770 m	Denver	0500 MST 9/26	5850 m	Denver
1700 MST 9/21	5820 m		1700 MST 9/26	5870 m	
Stability and Inversions			**Stability and Inversions**		
Tower			Tower		
0000 MST - 1.8°C Surface inversion up tower			0000 MST - 4.5°C Surface inversion up tower		
0600 MST - 2.0°C Surface inversion up tower			0500 MST - 5.0°C Surface inversion up tower		
0700 MST - Lifting of inversion			0720 MST - Lifting of inversion		
0900 MST - Inversion off tower			0900 MST - Inversion off tower		
Rawinsonde Stability (0-1800 m)			**Rawinsonde Stability (0-1800 m)**		
0918 MST	BAO		0542 MST	BAO	
0-100 m	SFC Instability		0-600 m	High stability	
100-1800 m	Stable		600-1500 m	Stable	
Modified Showalter Index 10			Modified Showalter Index 7		
1240 MST	BAO		0954 MST	BAO	
0-100 m	SFC Instability		0-200 M	Conditional instability	
100-200 m	Neutral		200-1800 m	Stable	
200-400 m	Conditional instability				
400-800 m	Stable		Modified Showalter Index 4		
800-950 m	Neutral				
950-1800 m	High stability				
Modified Showalter Index 10					
1700 MST	DEN		1352 MST	BAO	
0-75 m	SFC		0-130 m	High instability	
75-1800 m	Instability		130-1100 m	Fluctuating around neutral	
	Neutral		1100-1800 m	Stable	
Modified Showalter Index 6			Modified Showalter Index 1		
			1700 MST	DEN	
			0-1500 m	Conditional instability	
			1500-1800 m	Stable	
			Modified Showalter Index 2		
Clouds			**Clouds**		
Clear morning			Clear morning		
Ci-Late evening 4/10			Cu - short lived mid-afternoon < 1/10		
			Ac, Ci - Late evening 1/10, 3/10		

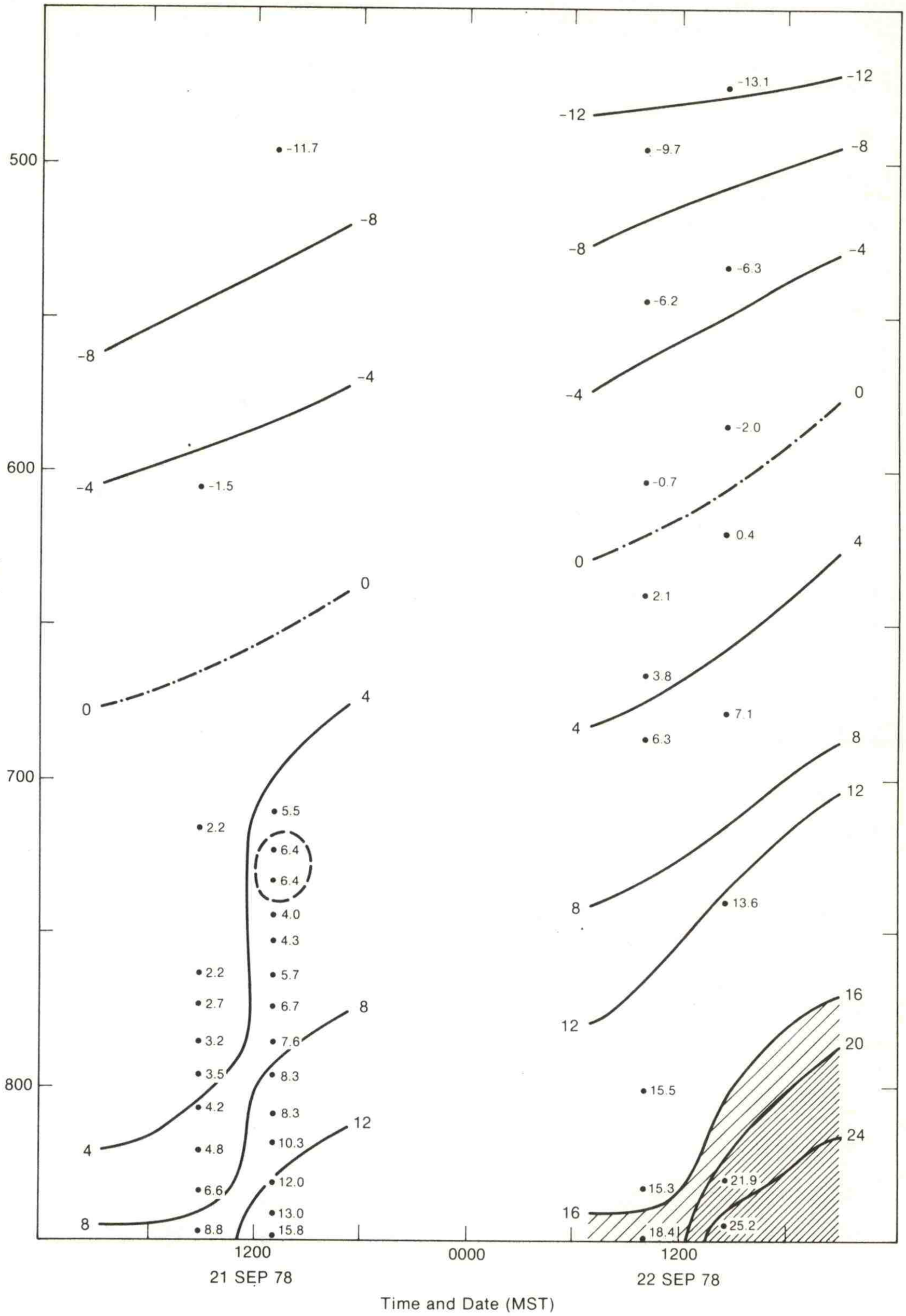


Figure 15.39a.--BAO rawinsonde time-series temperature profiles (C) for September 21-22, 1978.

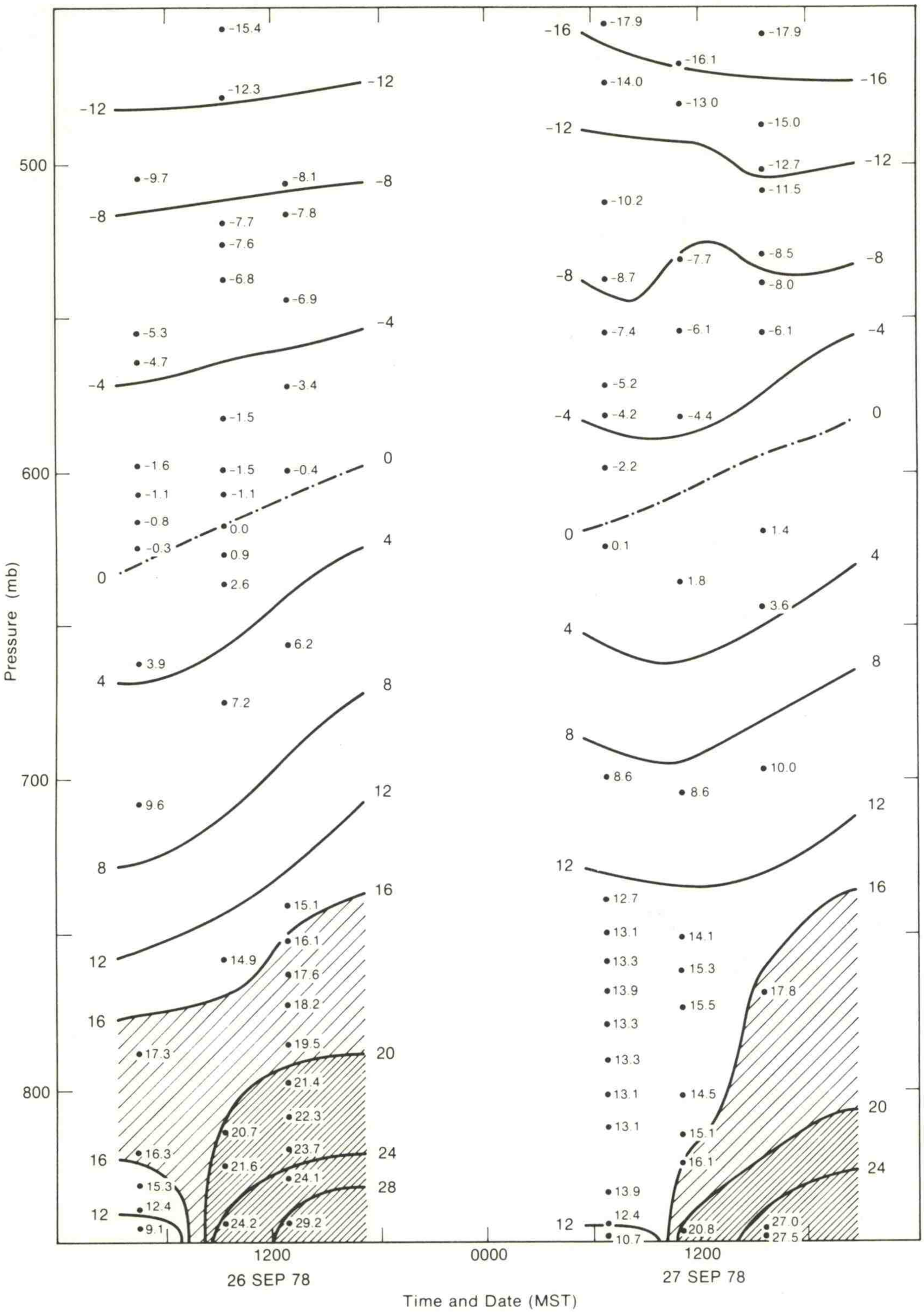


Figure 15.39b.--BAO rawinsonde time-series temperature profiles (C) for September 26-27, 1978.

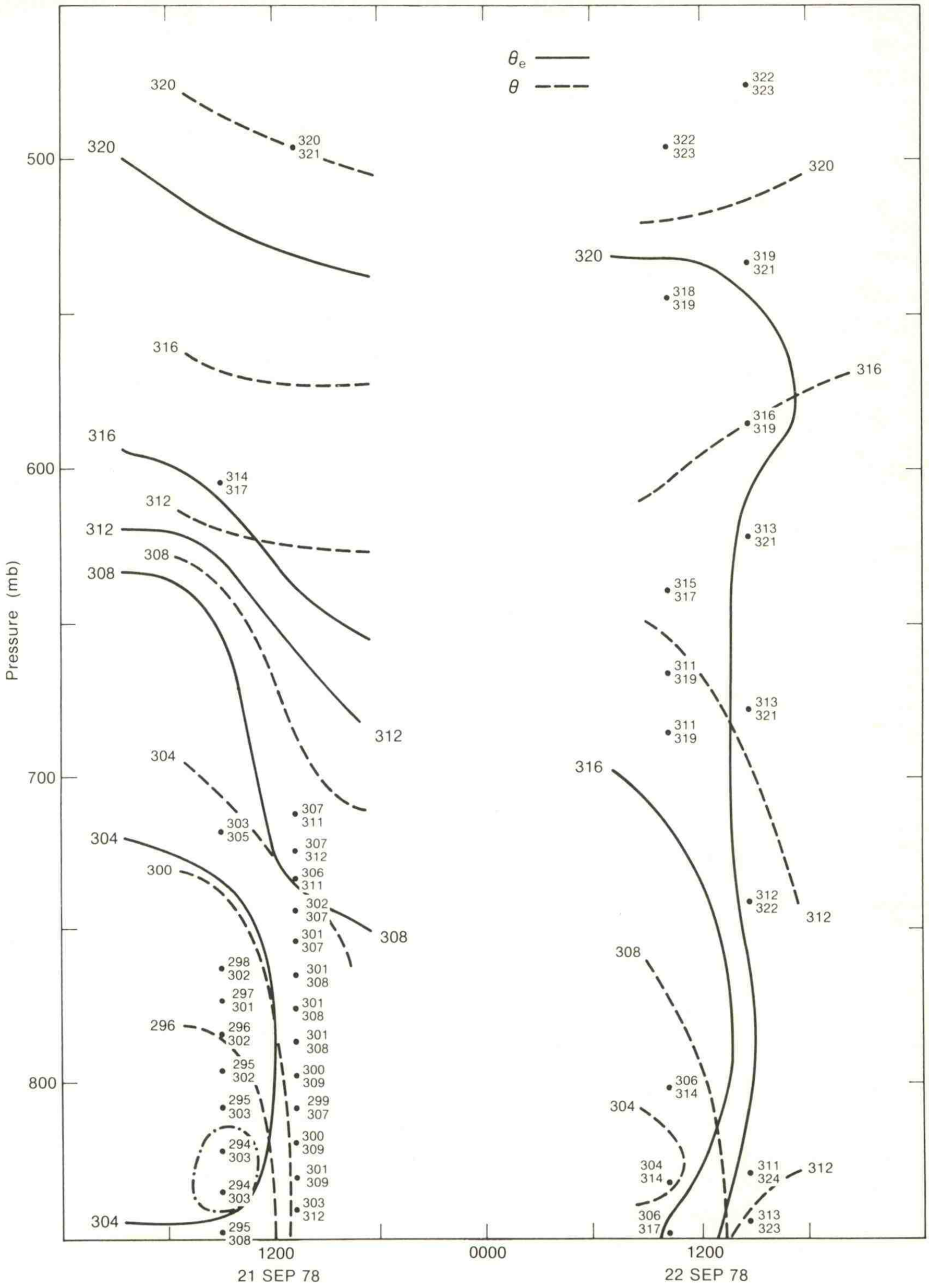


Figure 15.40a.--BAO rawinsonde time-series potential/equivalent-potential temperature profiles (K) for September 21-22, 1978.

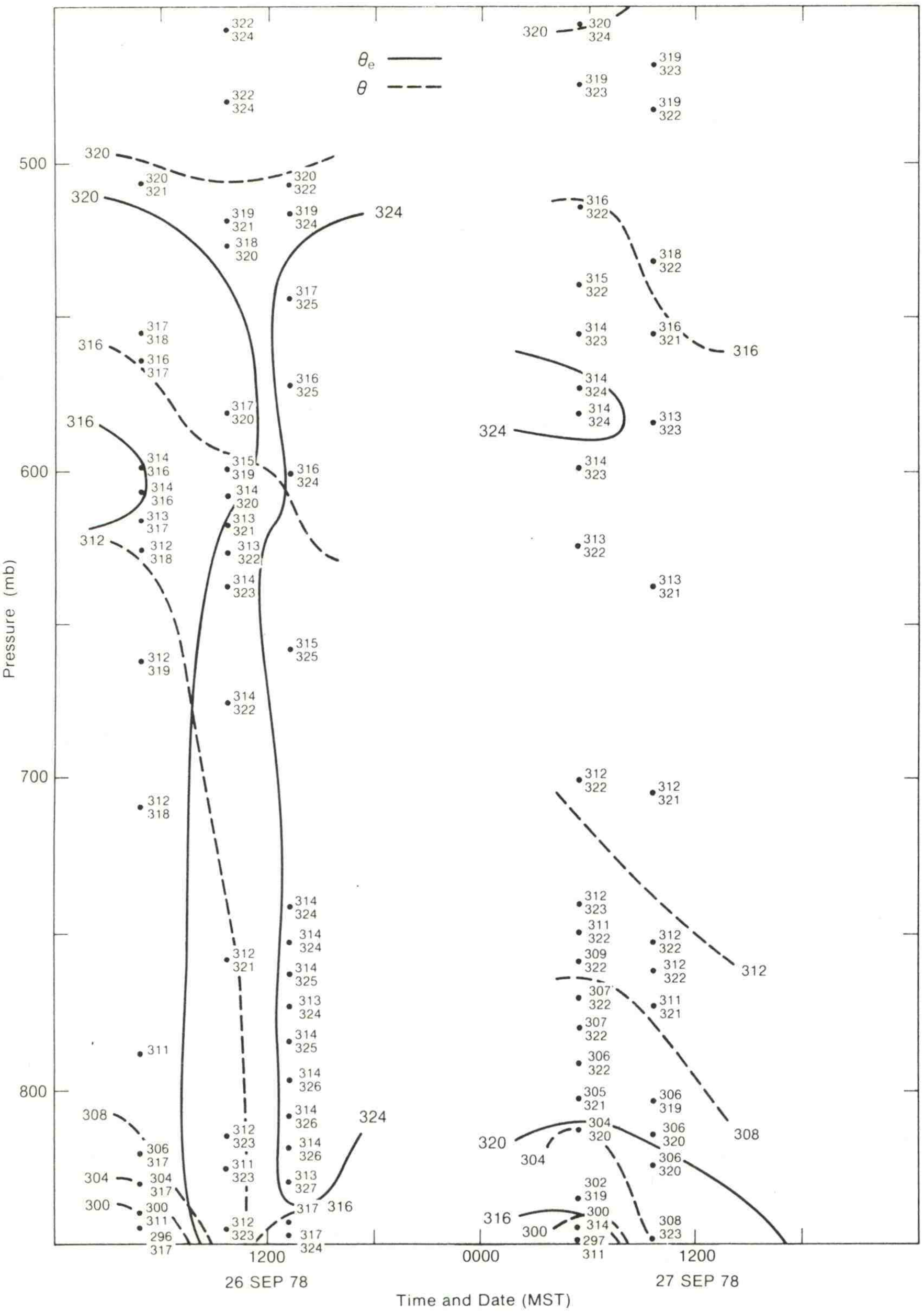


Figure 15.40b.--BAO rawinsonde time-series potential/equivalent-potential temperature profiles (K) for September 26-27, 1978.

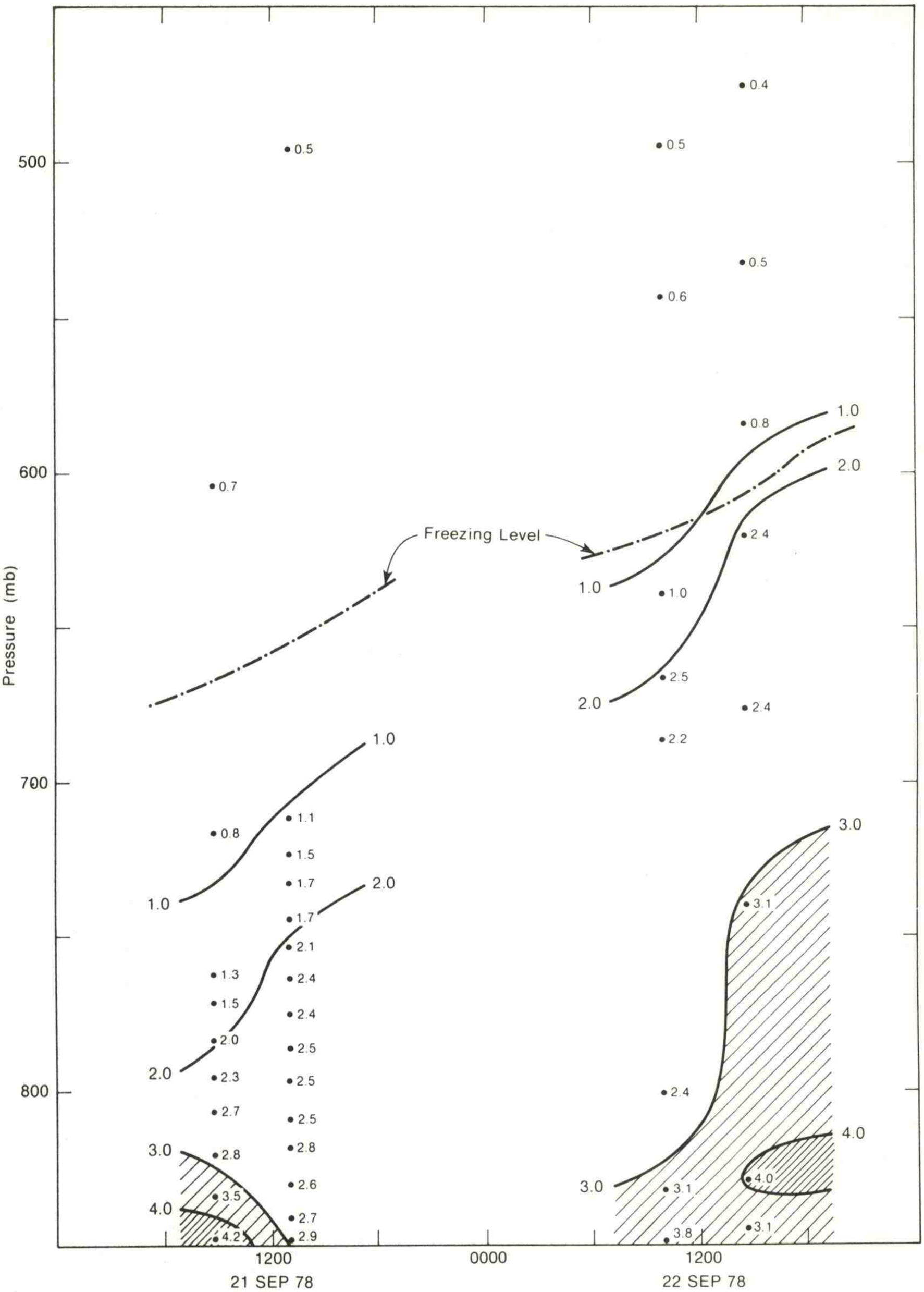


Figure 15.41a.--BAO rawinsonde time-series mixing ratio profiles (g/kg) for September 21-22, 1978.

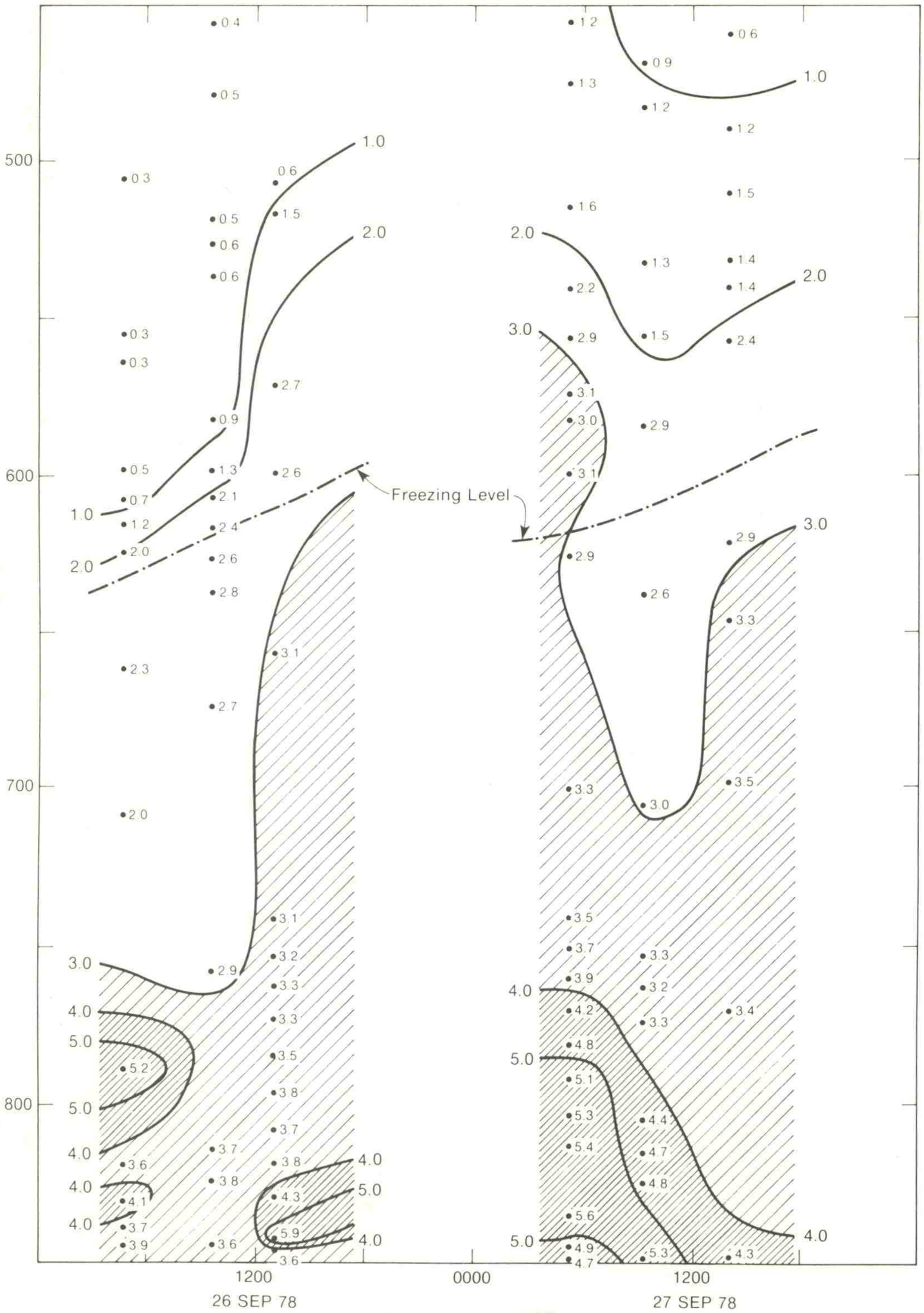


Figure 15.41b.--BAO rawinsonde time-series mixing ratio profiles (g/kg) for September 26-27, 1978.

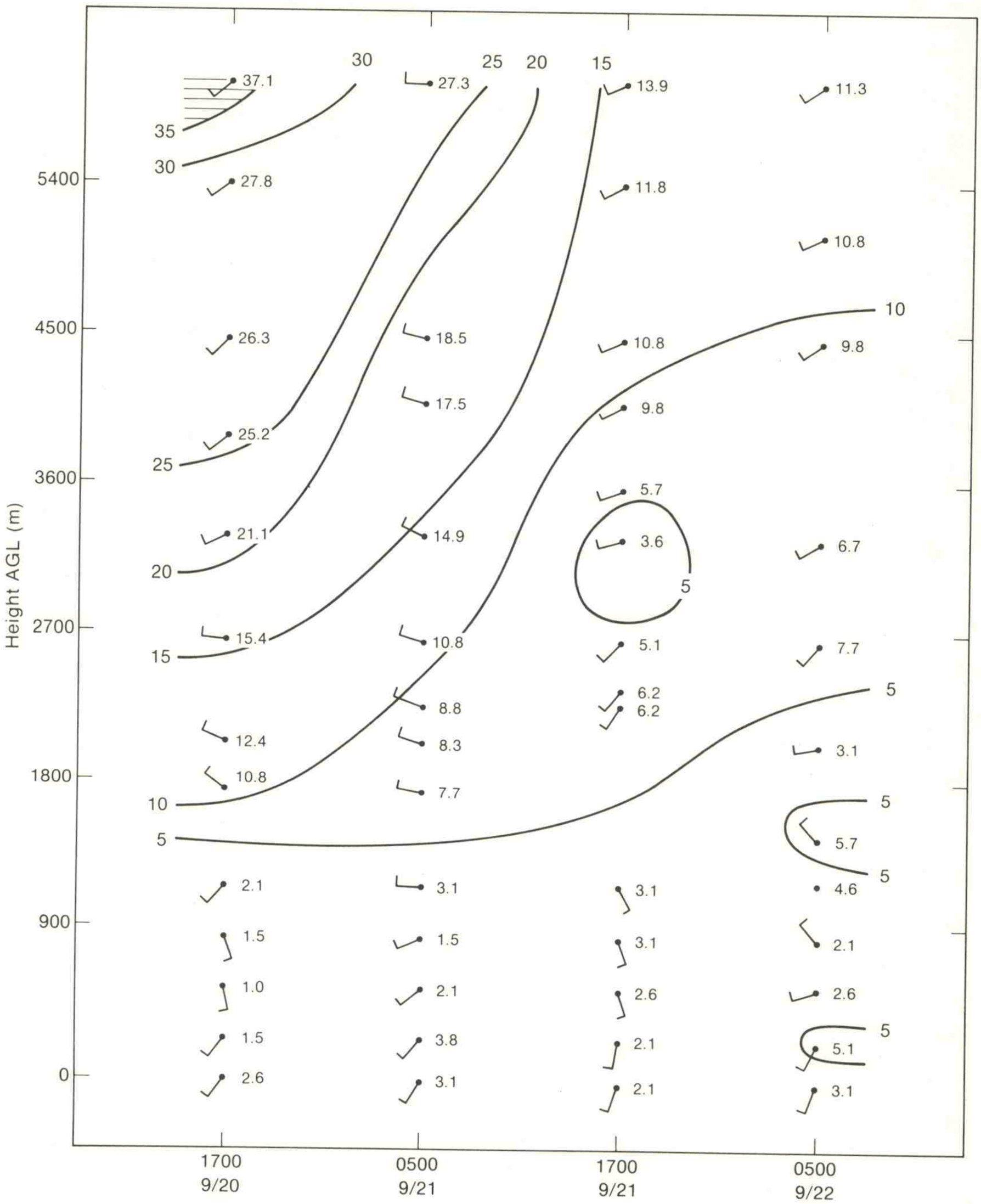


Figure 15.42a.--Denver rawinsonde time-series wind speed profiles (m/s) for September 20-22, with wind direction flags.

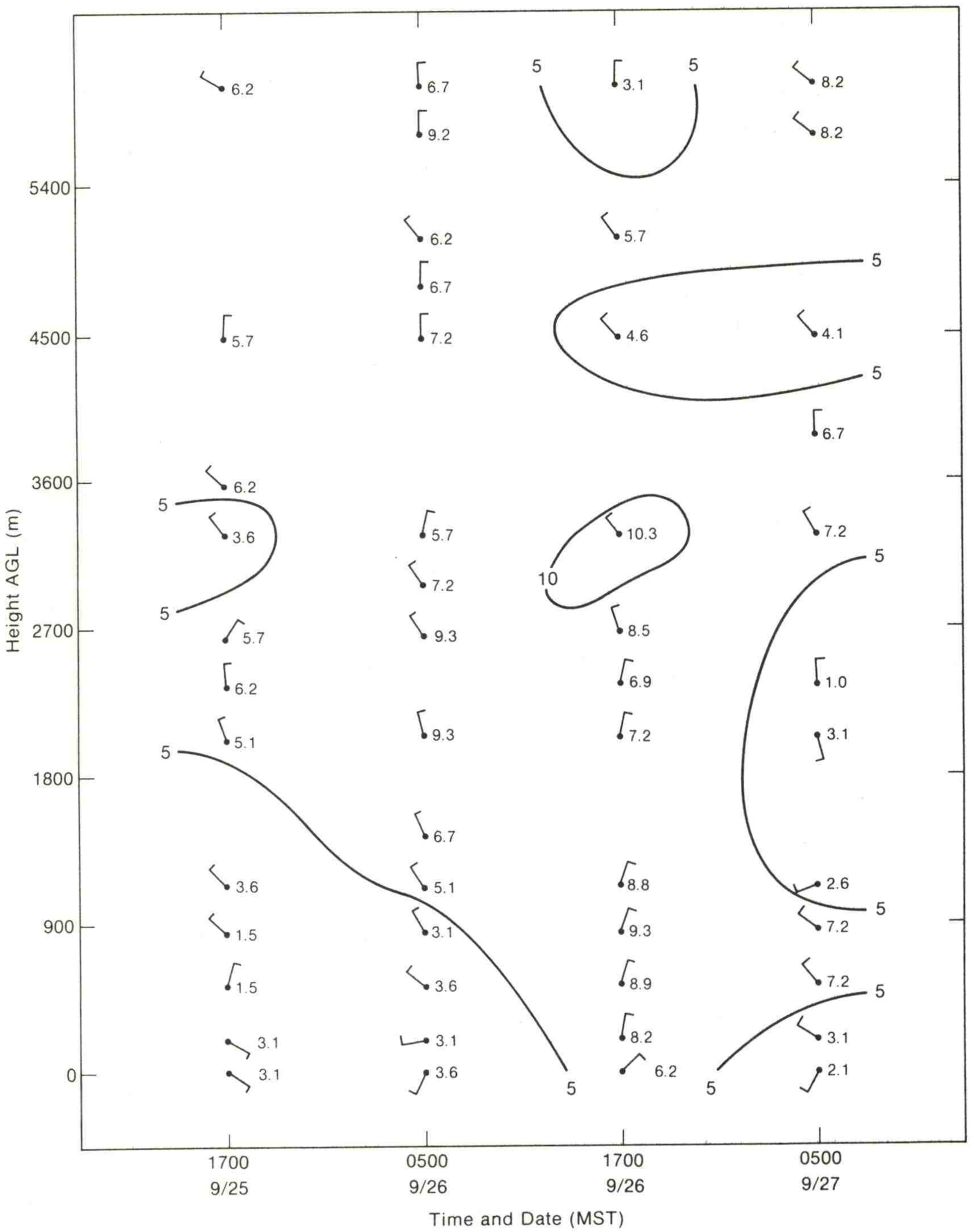


Figure 15.42b.--Denver rawinsonde time-series wind speed profiles (m/s) for September 25-27, wind wind direction flags.

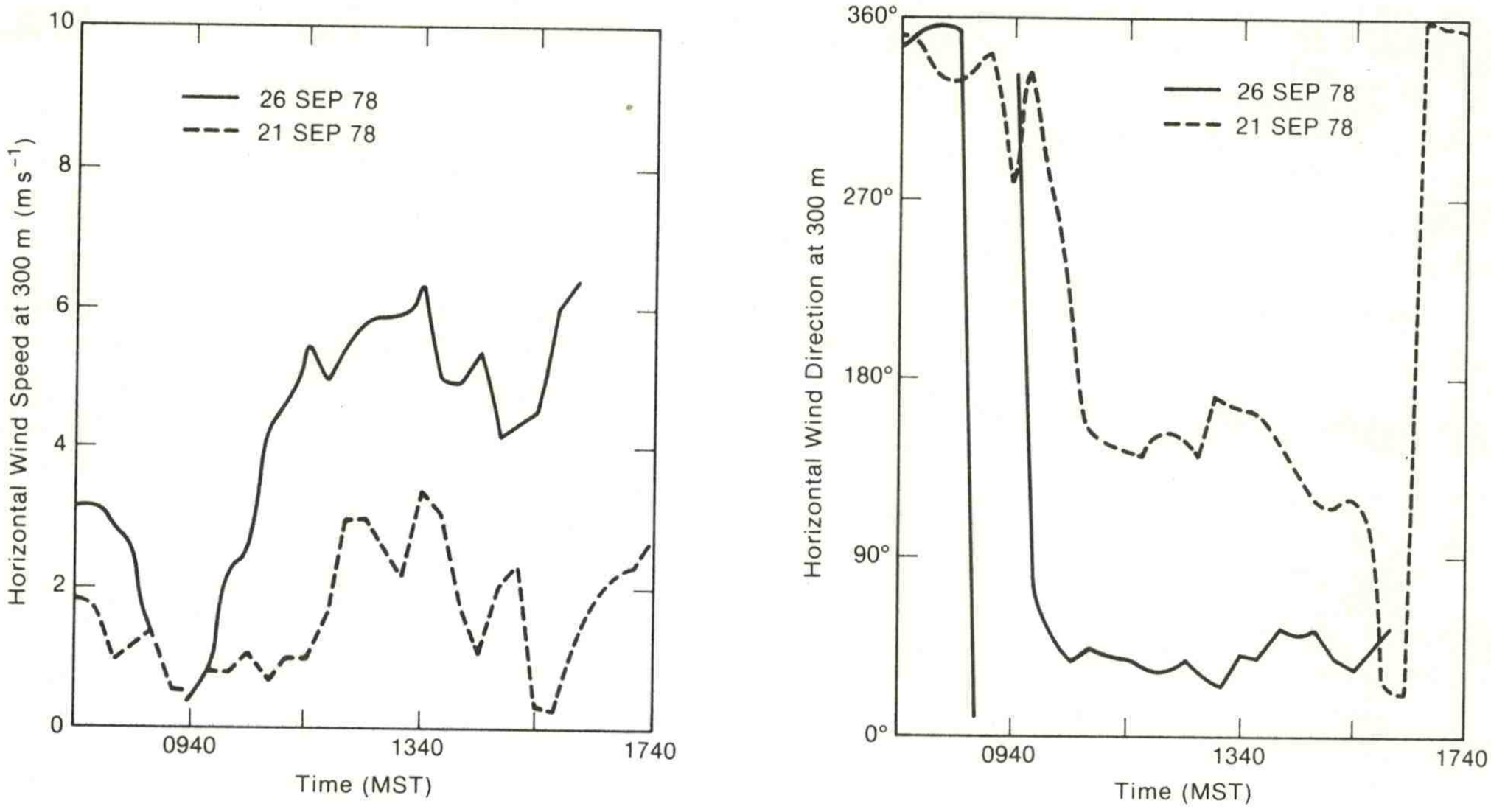


Figure 15.43.--Comparisons of (left) wind speed and (right) wind direction, from PDP 11/70 20-min averages.

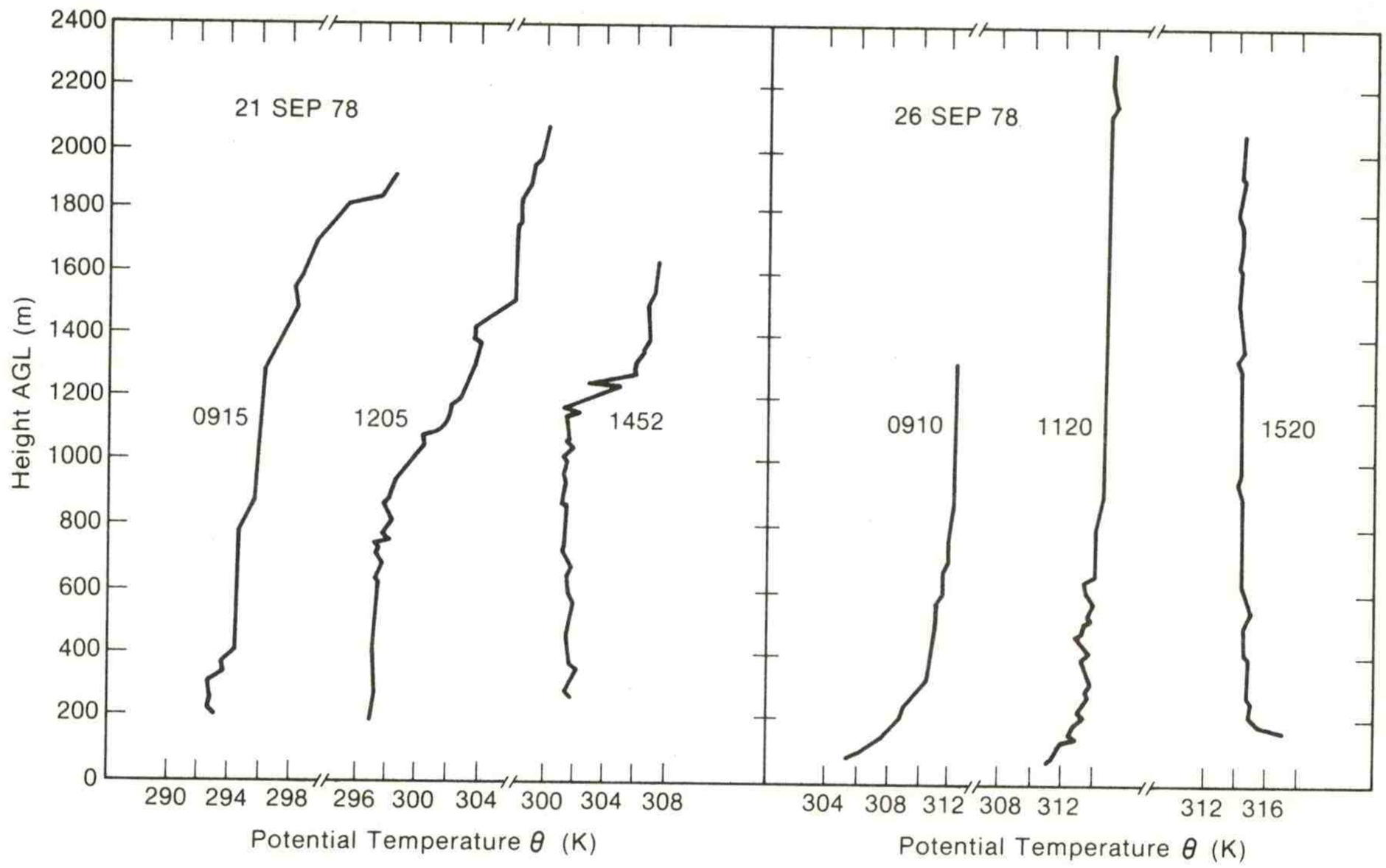


Figure 15.44.--NCAR Queen Air aircraft potential temperature soundings (K).

Acknowledgments

The PHOENIX staff wishes to thank C. F. Chappell, J. M. Fritsch, L. R. Hoxit, and R. A. Maddox of the Atmospheric Physics and Chemistry Laboratory of ERL for their help and consultation in interpretation of the mesoscale weather situations during PHOENIX.

References

Hildebrand, P. H., Portable Automated Mesonet (PAM) observations during PHOENIX, Chapter 10, in Project PHOENIX: The September 1978 Field Operation, William H. Hooke, Ed., NOAA/NCAR Boulder Atmospheric Observatory Rept. No. 1, available from NOAA/ERL, Boulder, Colo., and from NCAR Publications Office, Boulder, Colo. (1979).

Kaimal, J. C., and D. E. Wolfe, BAO site, tower instrumentation, and PHOENIX operations, Chapter 2, in Project PHOENIX: The September 1978 Field Operation, William H. Hooke, Ed., NOAA/NCAR Boulder Atmospheric Observatory Rept. No. 1, available from NOAA/ERL, Boulder, Colo., and from NCAR Publications Office, Boulder, Colo. (1979).

CHAPTER 16

PHOENIX SUMMARY LOGS

William H. Hooke[1], Peter H. Hildebrand[2], and Robert A. Kropfli[1]

To serve the reader interested in which sensors were operating during which periods in PHOENIX, we have included a copy of the daily operations log, a kind of master log compiled as the experiment progressed. There may be some inconsistencies (usually amounting to a few minutes or less) between these and the individual logs included in the previous chapters. Although we have removed some of these inconsistencies, we cannot guarantee the compatibility of the lists. Where discrepancies exist, the individual logs should be considered authoritative until further checking can be made. Unless otherwise noted, as for example in Chapter 15, all times are Mountain Daylight Time (MDT). Aircraft flight times indicated here refer to time in the air rather than actual data runs; for the latter, see Chapter 4.

[1]Wave Propagation Laboratory, National Oceanic and Atmospheric Administration, Boulder, Colorado 80303

[2]National Center for Atmospheric Research, Boulder, Colorado 80307

PHOENIX--Daily Operations Log Date: 9/1/78

Sensor	P.I.	Time/Mode of operation	Comments
CP4	Baynton		Still being deployed
NOAA 1	Kropfli	1053-1151, 1301-1621	Minor gaps
NOAA 2	Kropfli	Same as above	Minor gaps
304	Hildebrand	0900-1204	306 ARIS down for second flight
306	Hildebrand	0900-1200	
CHAFF	Lawrence	Up	Poor dispersion prior to 1030
RFC			
KNOLLENBERG	Derr	--	
SCAMS	Decker	Down	
NEMS	Decker	Down	
MTS	Decker	Down	
FM-CW	Chadwick	Down until noon; no data recorded after noon	
TPQ-11	Pasqualucci	0800-1130, 1340-1530	
LIDAR	Derr	Up	
ACOUSTIC	Brown	Up	
OPTICAL Δ	Lawrence	Up; large Δ up 1000-2400	
PAM	Baynton	Up	The PAM system was up and operating for essentially the entire month. No outage exceeded 1-1/2 hours.
TOWER	Kaimal	1000-1240	
RAWINSONDE	Baynton	No	
CONST-LEVEL BALLOONS	Hanna	1324	

PHOENIX--Daily Operations Log Date: 9/5/78

Sensor	P.I.	Time/Mode of operation	Comments
CP4	Baynton	10 - 11	Too much clutter for good observation
NOAA 1	Kropfli	1120-1215, 1549-1631	
NOAA 2	Kropfli	Same as above	
304	Hildebrand	0830-1200, 1420-1615	Some data recording problems, most data OK.
306	Hildebrand		
CHAFF	Lawrence	0830-1200, 1400-1600	Down midmorning - chaff cutter problems
RFC	---		
KNOLLENBERG	Derr	---	
SCAMS	Decker	Up 0600-1400 (nominal)	Intermittent operation
NEMS	Decker	Up 0600-1400 (nominal)	Intermittent operation
MTS	Decker	Up 0610-1436	
FM-CW	Chadwick	0000-1059 1059-1140 1316-1400	Very strong layers. Knocked out by chaff around noon, when chaff finally reached BAO.
TPQ-11	Pasqualucci	0845-1900 (off from 1100-1300)	
LIDAR	Derr	1000-1300	Intermittent-power problems
ACOUSTIC	Brown	Up 1100-2400	
OPTICAL Δ	Lawrence	(Large Δ) 0000-2400	
PAM	Baynton	Up	
TOWER	Kaimal	Up 0820-1540 (run ended with tape-drive problems)	No data 9/5-9/6 overnight
RAWINSONDE	Baynton	1000-1400	
CONST-LEVEL BALLOONS	Hanna	No	

PHOENIX--Daily Operations Log Date: 9/6/78

Sensor	P.I.	Time/Mode of operation	Comments
CP4	Baynton	--	Ground clutter
NOAA 1	Kropfli	0957-1211; 1402-1549	
NOAA 2	Kropfli	Same as above	
304	Hildebrand	0840-1200; 1315-1545	
306	Hildebrand	0840-1200; 1315-1545	
CHAFF	Lawrence	Up	
RFC	--		
KNOLLENBERG	Derr	--	
SCAMS	Decker	0600-1600	Intermittent
NEMS	Decker	0830-1500	
MTS	Decker	1140-1355	
FM-CW	Chadwick	Up 0853-1431, 1708-2400	Lots of chaff returns
TPQ-11	Pasqualucci	0840-1540	Good data
LIDAR	Derr		Aerosol layer started at 10K feet, went to 18K today. Gordon Lerfald suggested forest fire source.
ACOUSTIC	Brown	Up all day 0000-1800 ?	
OPTICAL Δ	Lawrence	Up; large Δ up 0000-2400	
PAM	Baynton	Up	
TOWER	Kaimal	SR3 Up 0800-0840 SR4 0900-1500 SA1 1700-1000 9/7/78	
RAWINSONDE	Baynton	1000, 1400 nominal	
CONST-LEVEL BALLOONS	Hanna	--	

PHOENIX--Daily Operations Log Date: 9/7/78

Sensor	P.I.	Time/Mode of operation	Comments
CP4	Baynton	Down	
NOAA 1	Kropfli	Up	Clock out - radar support of cloud studies
NOAA 2	Kropfli	Down	
304	Hildebrand	Down	
306	Hildebrand	Down	
CHAFF	Lawrence	Down	
RFC		--	
KNOLLENBERG	Derr	Down	
SCAMS	Decker	Up 0540-1524	
NEMS	Decker	Up 0630-1500 (nominal)	
MTS	Decker	Up 0748-1112	
FM-CW	Chadwick	0000-1003, 1826-0810 (9/8) in Doppler mode 0-4500 in (vertical) 1700-1800 look at echo from strata of clear air returns	No aspect sensitivity
TPQ-11	Pasqualucci	1200-1400	
LIDAR	Derr		Data unreliable
ACOUSTIC	Brown	0000-0820 0840-1641; 2246-2400	
OPTICAL Δ	Lawrence	Up; large Δ up 0000-2400	
PAM	Baynton		
TOWER	Kaimal	0000-1000 average data on SA1.	Sa2:2300 until 1000 MDT on 9/2 in support of Radiometry.
RAWINSONDE	Baynton	0638, 0955	
CONST-LEVEL BALLOONS	Hanna	--	

PHOENIX--Daily Operations Log Date: 9/8/78

Sensor	P.I.	Time/Mode of operation	Comments
CP4	Baynton	--	Hay bale artificial horizon failed to work.
NOAA 1	Kropfli	1109-1503	Clock out during a.m.
NOAA 2	Kropfli	Same as above	
304	Hildebrand	--	
306	Hildebrand	1145-1230	μ-wave refractometer data.
CHAFF	Lawrence	--	
RFC		--	
KNOLLENBERG	Derr	1100-1230	
SCAMS	Decker	0600-1430	
NEMS	Decker	0630-1430	
MTS	Decker	0640-1302	
FM-CW	Chadwick	0000-0810 vertical Doppler 0830-1257 vertical (no Doppler)	9-11000 MSL (feet) layers of strong echoes on TPQ-11. Aircraft profiles from 0-20,000 AGL(Cessna to 19,000)
TPQ-11	Pasqualucci	0850-1540 Suspect both clear air inhomogeneities and aerosol.	Suspect strong aerosol and turbulence layers.
LIDAR	Derr	1030-1430	
ACOUSTIC	Brown	Up 0000-1106 1120-2000	
OPTICAL Δ	Lawrence	Up; large Δ up 0000-2400	
PAM	Baynton	Up	
TOWER	Kaimal	SA3 1500-0800 (9/9)	
RAWINSONDE	Baynton	0633, 1055 profiles	
CONST-LEVEL BALLOONS	Hanna	--	

PHOENIX--Daily Operations Log Date: 9/9/78

Sensor	P.I.	Time/Mode of operation	Comments
CP4	Baynton	Down	Useless because of ground clutter
NOAA 1	Kropfli	0959-1220, 1330-	
NOAA 2	Kropfli	0959-1220, 1330-	
304	Hildebrand	0840-1200 1340-1600	
306	Hildebrand	0840-1200; 1340-1600	
CHAFF	Lawrence	Up	
RFC		--	
KNOLLENBERG	Derr	--	
SCAMS	Decker	--	
NEMS	Decker	--	
MTS	Decker	--	
FM-CW	Chadwick	Down	
TPQ-11	Pasqualucci	Up all day 0850-1627	
LIDAR	Derr	Down	
ACOUSTIC	Brown	Up	Lightning hit
OPTICAL Δ	Lawrence	Large Δ up 0000-2400	
PAM	Baynton	Up	
TOWER	Kaimal	SA3 Up 0000-8000, SR5 0840-1600 SA4 1620-1940 SA5 2220-0540 (9/11)	
RAWINSONDE	Baynton	1000, 1400 nominal	
CONST-LEVEL BALLOONS	Hanna	--	

PHOENIX--Daily Operations Log Date: 9/10/78

Sensor	P.I.	Time/Mode of operation	Comments
CP4	Baynton	--	
NOAA 1	Kropfli	--	
NOAA 2	Kropfli	--	
304	Hildebrand	--	
306	Hildebrand	--	
CHAFF	Lawrence	--	
RFC		--	
KNOLLENBERG	Derr	--	
SCAMS	Decker	--	
NEMS	Decker	--	
MTS	Decker	--	
FM-CW	Chadwick	Down until 1800, began run 1822-2400	
TPQ-11	Pasqualucci	--	
LIDAR	Derr	--	
ACOUSTIC	Brown	0000-2400	
OPTICAL Δ	Lawrence	Large Δ up 0000-2400	
PAM	Baynton	Up	
TOWER	Kaimal	Restored after power failure SA5 0000-2400	
RAWINSONDE	Baynton	--	
CONST-LEVEL BALLOONS	Hanna	--	

PHOENIX--Daily Operations Log Date: 9/11/78

Sensor	P.I.	Time/Mode of operation	Comments
CP4	Baynton	Down	
NOAA 1	Kropfli	Down	
NOAA 2	Kropfli	Down	
304	Hildebrand	Down	
306	Hildebrand	Down	
CHAFF	Lawrence	Down	
RFC		--	
KNOLLENBERG	Derr	Down--unable to take off from Boulder Airport because of high winds.	
SCAMS	Decker	0540-1330	
NEMS	Decker	0546-continuing until 1400 next day	
MTS	Decker	0634-1110	Stop because of winds, cart tipped over
FM-CW	Chadwick	0000-1038 5 VAD'S 1536-1654	
TPQ-11	Pasqualucci	0932-1600	
LIDAR	Derr	0900-1200	
ACOUSTIC	Brown	Up 0000-2400	
OPTICAL Δ	Lawrence	Up 0000-1100, 1815-2400	Some data off scale
PAM	Baynton	Up	
TOWER	Kaimal	0900-through the night 0500-2400 fast data run (prompted by wind) runs SA5, SR6-SR10	Good tower data on transition Winds greater than 5 meters from SW
RAWINSONDE	Baynton	1000	
CONST-LEVEL BALLOONS	Hanna	--	

PHOENIX--Daily Operations Log Date: 9/12/78

Sensor	P.I.	Time/Mode of operation	Comments
CP4	Baynton	--	
NOAA 1	Kropfli	--	
NOAA 2	Kropfli	--	
304	Hildebrand	--	
306	Hildebrand	--	
CHAFF	Lawrence	--	
RFC		--	
KNOLLENBERG	Derr		
SCAMS	Decker	1200-1400	Equipment failure--high winds blew off shield, etc.
NEMS	Decker	0000 (see log for 9/11) - 1400	
MTS	Decker	0723-1400	
FM-CW	Chadwick	1038-1114, 1150-1327, 1715-2400	
TPQ-11	Pasqualucci	--	Maintenance
LIDAR	Derr		Data unreliable
ACOUSTIC	Brown	0700-2400	
OPTICAL Δ	Lawrence	0000-2400	
PAM	Baynton		
TOWER	Kaimal	Up--high speed SR10 0000-0930, SA6 0930-1300, SA7 1730-2400	
RAWINSONDE	Baynton	0632, 0945	
CONST-LEVEL BALLOONS	Hanna	--	

PHOENIX--Daily Operations Log Date: 9/13/78

Sensor	P.I.	Time/Mode of operation	Comments
CP4	Baynton	--	
NOAA 1	Kropfli	--	
NOAA 2	Kropfli		
304	Hildebrand	--	
306	Hildebrand	--	
CHAFF	Lawrence	--	
RFC		--	
KNOLLENBERG	Derr	--	
SCAMS	Decker	0600-1400	
NEMS	Decker	0600-1400	
MTS	Decker	0600-1400	
FM-CW	Chadwick	Up 0000-0909 0939-2400 (but power failure sometime during night)	Disk crashed. Almost no insects on this day.
TPQ-11	Pasqualucci	-- maintenance	
LIDAR	Derr		Data unreliable
ACOUSTIC	Brown	Up 0000-2400	
OPTICAL Δ	Lawrence	0000-2400	
PAM	Baynton	Up	
TOWER	Kaimal	SA7 Overnight-1400; SA8 1900-2400	
RAWINSONDE	Baynton	0633, 0941	
CONST-LEVEL BALLOONS	Hanna	--	

PHOENIX--Daily Operations Log Date: 9/14/78

Sensor	P.I.	Time/Mode of operation	Comments
CP4	Baynton	--	Moved to new site; much less ground clutter.
NOAA 1	Kropfli	--	Moved to new site; much less ground clutter.
NOAA 2	Kropfli	--	Moved to new site; much less ground clutter.
304	Hildebrand	--	
306	Hildebrand	--	
CHAFF	Lawrence	--	
RFC		--	
KNOLLENBERG	Derr	--	
SCAMS	Decker	0530-1405	
NEMS	Decker	0535-1315	
MTS	Decker	0600-1306	
FM-CW	Chadwick	0000-0845 1631-2400	
TPQ-11	Pasqualucci	0940-1506	
LIDAR	Derr		Data unreliable
ACOUSTIC	Brown	1640-2400	System hung up at some point betweeen 0800-1640.
OPTICAL Δ	Lawrence	0000-2400	
PAM	Baynton	Up	
TOWER	Kaimal	SA8 0000-1230 SA9 1720-2400	
RAWINSONDE	Baynton	0633, 0942	
CONST-LEVEL BALLOONS	Hanna	--	

PHOENIX--Daily Operations Log Date: 9/15/78

Sensor	P.I.	Time/Mode of operation	Comments
CP4	Baynton		
NOAA 1	Kropfli	1429-1614	
NOAA 2	Kropfli	Same as above	
304	Hildebrand	--	
306	Hildebrand	--	
CHAFF	Lawrence	Up and operating	
RFC		--	
KNOLLENBERG	Derr		
SCAMS	Decker	0535-1345	
NEMS	Decker	0545-1325	
MTS	Decker	0600-1355	
FM-CW	Chadwick	0000-1007; 1456-2400	
TPQ-11	Pasqualucci	0920-1628	
LIDAR	Derr		Data unreliable
ACOUSTIC	Brown	0840-2400	
OPTICAL Δ	Lawrence	0000-2400	
PAM	Baynton	Up	
TOWER	Kaimal	SA9 0000-1020	
		SA10 1040-1400	
		SA11 1620-2400	
RAWINSONDE	Baynton	1003	
CONST-LEVEL BALLOONS	Hanna	--	

PHOENIX--Daily Operations Log Date: 9/16/78

Sensor	P.I.	Time/Mode of operation	Comments
CP4	Baynton	--	
NOAA 1	Kropfli	--	
NOAA 2	Kropfli	--	
304	Hildebrand	--	
306	Hildebrand	--	
CHAFF	Lawrence	--	
RFC		--	
KNOLLENBERG	Derr		
SCAMS	Decker	--	
NEMS	Decker	--	
MTS	Decker		
FM-CW	Chadwick	0000-1200 one VAD 1224 elevation 110° (West) 1242-2400	
TPQ-11	Pasqualucci	--	
LIDAR	Derr	--	
ACOUSTIC	Brown	0000-2220	
OPTICAL Δ	Lawrence	0000-2400	
PAM	Baynton	Up	
TOWER	Kaimal	SA11 0000-2400	
RAWINSONDE	Baynton	--	
CONST-LEVEL BALLOONS	Hanna	--	

PHOENIX--Daily Operations Log Date: 9/17/78

Sensor	P.I.	Time/Mode of operation	Comments
CP4	Baynton	--	
NOAA 1	Kropfli	--	
NOAA 2	Kropfli	--	
304	Hildebrand	--	
306	Hildebrand	--	
CHAFF	Lawrence	--	
RFC		--	
KNOLLENBERG	Derr	--	
SCAMS	Decker	--	
NEMS	Decker	--	
MTS	Decker	--	
FM-CW	Chadwick	110° Doppler Vertical, rough only 0000-1111; 1130-1440 (9/18)	
TPQ-11	Pasqualucci	1100-1300	
LIDAR	Derr	1130-1300	
ACOUSTIC	Brown	0000-2400	
OPTICAL Δ	Lawrence	0000-0400, 0630-2400	
PAM	Baynton	Up	
TOWER	Kaimal	SA11 0000-1800	
RAWINSONDE	Baynton	--	
CONST-LEVEL BALLOONS	Hanna	--	

PHOENIX--Daily Operations Log Date: 9/18/78

Sensor	P.I.	Time/Mode of operation	Comments
CP4	Baynton	1352-1655	
NOAA 1	Kropfli	1352-1655	
NOAA 2	Kropfli	1352-1655	
304	Hildebrand	--	
306	Hildebrand	--	
CHAFF	Lawrence		
RFC		--	
KNOLLENBERG	Derr	0928- 1500-1724 nominal	
SCAMS	Decker	0550-1607	
NEMS	Decker	0735-1607	Heavy mist
MTS	Decker	0601-1400	
FM-CW	Chadwick	0000-1440; 3 VAD's 1550-1640; vertical mode 1640-2400	
TPQ-11	Pasqualucci	0855-1725	
LIDAR	Derr	0900-1727	
ACOUSTIC	Brown	0000-0830	
OPTICAL Δ	Lawrence	0000-0140, 0700-2400	
PAM	Baynton	Up	
TOWER	Kaimal	SR11 0720-1700 SA12 1720-2400	
RAWINSONDE	Baynton	1000	
CONST-LEVEL BALLOONS	Hanna	Two 20-minute runs in afternoon, 1551-1612, 1352-1419	

PHOENIX--Daily Operations Log Date: 9/19/78

Sensor	P.I.	Time/Mode of operation	Comments
CP4	Baynton	Same as below	
NOAA 1	Kropfli	1058-1235, 1506-1521	
NOAA 2	Kropfli	Same as above	
304	Hildebrand	--	
306	Hildebrand	--	
CHAFF	Lawrence		
RFC		--	
KNOLLENBERG	Derr	About 1100-1230, 1500-1600	
SCAMS	Decker	0532-1654	
NEMS	Decker	0545-1654	
MTS	Decker	0000-1617	
FM-CW	Chadwick	(1309-1625 clouds) 0000-1000 1100-1200 1200-1625 1635-2400	Lots of chaff around noon. Run terminated by equipment problem.
TPQ-11	Pasqualucci	1014-1645	
LIDAR	Derr	1022-1630	
ACOUSTIC	Brown	1000-1720	
OPTICAL Δ	Lawrence	0000-2400	
PAM	Baynton	Up	
TOWER	Kaimal	SA12 0000-0940 SR12 0940-1640 SA13 1700-2400	
RAWINSONDE	Baynton	0959, 1343	
CONST-LEVEL BALLOONS	Hanna	--	

PHOENIX--Daily Operations Log Date: 9/20/78

Sensor	P.I.	Time/Mode of operation	Comments
CP4	Baynton	Same as below	
NOAA 1	Kropfli	1130-1305	
NOAA 2	Kropfli	Same as above	
304	Hildebrand	--	
306	Hildebrand	--	
CHAFF	Lawrence		
RFC		--	
KNOLLENBERG	Derr	1015-1234 1425-1618	
SCAMS	Decker	0606-0822 (shut down by rain) 0942-1950	
NEMS	Decker	0616-0822 (shut down by rain) 1003-0400 (rain all night)	
MTS	Decker	0605-0822 (shut down by rain) 0942-1555	
FM-CW	Chadwick	0000-0850, 1155-1200, 1207-1633, 1638-2400	Knollenberg plane caused saturation. Terminated by power failure.
TPQ-11	Pasqualucci	0956-1618	
LIDAR	Derr	1000-1619	
ACOUSTIC	Brown	0808-0000	
OPTICAL Δ	Lawrence	0000-0200, 0900-2400	Wind suspiciously low 02-09; may be OK.
PAM	Baynton	Up	
TOWER	Kaimal	SA13 0000-0845 SR13 0900-1420 SR14 1420-1700	
RAWINSONDE	Baynton		
CONST-LEVEL BALLOONS	Hanna	1337-1427	

PHOENIX--Daily Operations Log Date: 9/21/78

Sensor	P.I.	Time/Mode of operation	Comments
CP4	Baynton	Same as below	
NOAA 1	Kropfli	1117-1729	
NOAA 2	Kropfli	Same as above	
304	Hildebrand	0905-1225; 1446-1731	
306	Hildebrand	0905-0936; 1105-1239; 1446-1720	
CHAFF	Lawrence		
RFC		--	
KNOLLENBERG	Derr	--	
SCAMS	Decker	0646-1941	
NEMS	Decker	0000-0458	
MTS	Decker	0605-1625	
FM-CW	Chadwick	0000-0938, 0951-1357, 1738-2400	Chaff returns saturated at 1120
TPQ-11	Pasqualucci	0908-1515	
LIDAR	Derr	0845-1500	
ACOUSTIC	Brown	0000-0420 0750-1500	
OPTICAL Δ	Lawrence	0000-0130; 0230-2400	
PAM	Baynton	Up	
TOWER	Kaimal	SA14 0140-0820 SR15 0840-1640 SR16 1640-1920 SA15 2020-2400	
RAWINSONDE	Baynton		
CONST-LEVEL BALLOONS	Hanna	--	

PHOENIX--Daily Operations Log Date: 9/22/78

Sensor	P.I.	Time/Mode of operation	Comments
CP4	Baynton	Same as below	
NOAA 1	Kropfli	1145-1838	
NOAA 2	Kropfli	Same as above	
304	Hildebrand	0930-1203; 1646-1842	
306	Hildebrand	0928-0944; 1326-1551; 1630-1803	
CHAFF	Lawrence		
RFC		--	
KNOLLENBERG	Derr	1320-1630	
SCAMS	Decker	0644-1542	
NEMS	Decker	0653-1438	
MTS	Decker	0605-1555	
FM-CW	Chadwick	(Noise on FM/CW) 0000-0922; stopped tape at 0920 power failure -1314-2400	
TPQ-11	Pasqualucci	0915-1815	
LIDAR	Derr	1030-1638	
ACOUSTIC	Brown	0000-0219 0925-? 1900-?	
OPTICAL Δ	Lawrence	0000-2400	
PAM	Baynton	Up	
TOWER	Kaimal	SA15 0000-0820 SR17 0840-1920 SA16 1940-2400	
RAWINSONDE	Baynton		
CONST-LEVEL BALLOONS	Hanna	--	

PHOENIX--Daily Operations Log Date: 9/23/78

Sensor	P.I.	Time/Mode of operation	Comments
CP4	Baynton	--	
NOAA 1	Kropfli	--	
NOAA 2	Kropfli	--	
304	Hildebrand	--	
306	Hildebrand	--	
CHAFF	Lawrence	--	
RFC		--	
KNOLLENBERG	Derr	--	
SCAMS	Decker	--	
NEMS	Decker	--	
MTS	Decker	--	
FM-CW	Chadwick	0000-1218; shut down for weekend	
TPQ-11	Pasqualucci	--	
LIDAR	Derr	--	
ACOUSTIC	Brown		
OPTICAL Δ	Lawrence	0000-2400	
PAM	Baynton	Up	
TOWER	Kaimal	SA16 0000-2400	
RAWINSONDE	Baynton	--	
CONST-LEVEL BALLOONS	Hanna	--	

PHOENIX--Daily Operations Log Date: 9/24/78

Sensor	P.I.	Time/Mode of operation	Comments
CP4	Baynton	--	
NOAA 1	Kropfli	--	
NOAA 2	Kropfli	--	
304	Hildebrand	--	
306	Hildebrand	--	
CHAFF	Lawrence	--	
RFC		--	
KNOLLENBERG	Derr	--	
SCAMS	Decker	--	
NEMS	Decker	--	
MTS	Decker	--	
FM-CW	Chadwick	1746-2400	
TPQ-11	Pasqualucci	--	
LIDAR	Derr	--	
ACOUSTIC	Brown	0905-? 2204-2400	
OPTICAL Δ	Lawrence	0000-2400	
PAM	Baynton	Up	
TOWER	Kaimal	SA16 0000-1500 SA17 2322-2400	
RAWINSONDE	Baynton	--	
CONST-LEVEL BALLOONS	Hanna	--	

PHOENIX--Daily Operations Log Date: 9/25/78

Sensor	P.I.	Time/Mode of operation	Comments
CP4	Baynton	Same as below	
NOAA 1	Kropfli	1316-1357 1401-1737	
NOAA 2	Kropfli	Same as above	
304	Hildebrand	0918-1055 calibration run (tower fly bys)	
306	Hildebrand	0918-1055 calibration run (tower fly bys)	
CHAFF	Lawrence		
RFC		--	
KNOLLENBERG	Derr		
SCAMS	Decker	0610-1440	
NEMS	Decker	0630-	
MTS	Decker	0606-1400	
FM-CW	Chadwick	Saturated by chaff 0000-1217 1700-2400	
TPQ-11	Pasqualucci	--	Maintenance
LIDAR	Derr	--	
ACOUSTIC	Brown	0000-0929	
OPTICAL Δ	Lawrence	0000-2400	
PAM	Baynton	Up	
TOWER	Kaimal	SA17 0000-0742 SR18 (plane calibration) 0800-1040 SA18 2020-2400	
RAWINSONDE	Baynton	0630	
CONST-LEVEL BALLOONS	Hanna	--	

PHOENIX--Daily Operations Log Date: 9/26/78

Sensor	P.I.	Time/Mode of operation	Comments
CP4	Baynton	Same as below	
NOAA 1	Kropfli	1141-1250, 1409-1842	
NOAA 2	Kropfli	Same as above	
304	Hildebrand	1235-1529; 1613-1858	
306	Hildebrand	0807-1148; 1610-1855	
CHAFF	Lawrence		
RFC		--	
KNOLLENBERG	Derr	0915-1230	
SCAMS	Decker	0620-2400	Dew on μ wave antennas
NEMS	Decker	0620-2400	
MTS	Decker	0606-2400	
FM-CW	Chadwick	0000-1209 (wiped out by chaff)	Strong returns in a.m.
TPQ-11	Pasqualucci	0753-	
LIDAR	Derr	0750-	
ACOUSTIC	Brown	1000-	
OPTICAL Δ	Lawrence	0000-2400	
PAM	Baynton	Up	
TOWER	Kaimal	SA18 0000-0540 SR19 0600-1022 SR20 1040-1740 SR21 1820-2340	
RAWINSONDE	Baynton	0630, 1000, 1500	
CONST-LEVEL BALLOONS	Hanna	--	

Power failure on BAO site about 1022

PHOENIX--Daily Operations Log Date: 9/27/78

Sensor	P.I.	Time/Mode of operation	Comments
CP4	Baynton		
NOAA 1	Kropfli	1101-1702	
NOAA 2	Kropfli		
304	Hildebrand	1625-1857	
306	Hildebrand	0921-1210; 1257-1526; 1625-1845	
CHAFF	Lawrence		
RFC			
KNOLLENBERG	Derr		
SCAMS	Decker	0000-1900	
NEMS	Decker	0000-1900	
MTS	Decker	0000-1900	
FM-CW	Chadwick	Down	
TPQ-11	Pasqualucci		
LIDAR	Derr		
ACOUSTIC	Brown		
OPTICAL Δ	Lawrence	0000-1800; one light burned out at 1800	
PAM	Baynton	Up	
TOWER	Kaimal	SR22 0000-1320 SR23 1400-1820 SR24 1840-2000 SA19 2040-2400	
RAWINSONDE	Baynton	0630-1000, 1500	
CONST-LEVEL BALLOONS	Hanna	--	

PHOENIX--Daily Operations Log Date: 9/28/78

Sensor	P.I.	Time/Mode of operation	Comments
CP4	Baynton	--	
NOAA 1	Kropfli	--	
NOAA 2	Kropfli	--	
304	Hildebrand	--	
306	Hildebrand	0941-1128	
CHAFF	Lawrence	--	
RFC			
KNOLLENBERG	Derr		
SCAMS	Decker	0625-1200	
NEMS	Decker	0625-1200	
MTS	Decker	0600-1158	
FM-CW	Chadwick		
TPQ-11	Pasqualucci		
LIDAR	Derr		
ACOUSTIC	Brown		
OPTICAL Δ	Lawrence	1230-2400	
PAM	Baynton	Up	
TOWER	Kaimal	SA19 0000-1100	
RAWINSONDE	Baynton		
CONST-LEVEL BALLOONS	Hanna	--	

PHOENIX--Daily Operations Log Date: 9/29/78

Sensor	P.I.	Time/Mode of operation	Comments
CP4	Baynton		
NOAA 1	Kropfli		
NOAA 2	Kropfli		
304	Hildebrand		
306	Hildebrand		
CHAFF	Lawrence		
RFC			
KNOLLENBERG	Derr		
SCAMS	Decker		
NEMS	Decker		
MTS	Decker		
FM-CW	Chadwick		
TPQ-11	Pasqualucci		
LIDAR	Derr		
ACOUSTIC	Brown		
OPTICAL Δ	Lawrence	0000-2400	
PAM	Baynton		
TOWER	Kaimal		
RAWINSONDE	Baynton		
CONST-LEVEL BALLOONS	Hanna		

PHOENIX--Daily Operations Log Date: 9/30/78

Sensor	P.I.	Time/Mode of operation	Comments
CP4	Baynton		
NOAA 1	Kropfli		
NOAA 2	Kropfli		
304	Hildebrand		
306	Hildebrand		
CHAFF	Lawrence		
RFC			
KNOLLENBERG	Derr		
SCAMS	Decker		
NEMS	Decker		
MTS	Decker		
FM-CW	Chadwick		
TPQ-11	Pasqualucci		
LIDAR	Derr		
ACOUSTIC	Brown		
OPTICAL Δ	Lawrence	0000-2400	
PAM	Baynton		
TOWER	Kaimal		
RAWINSONDE	Baynton		
CONST-LEVEL BALLOONS	Hanna		

CHAPTER 17

INTERACTIVE ACCESS TO THE BAO DATA

Robert S. Lawrence and Margot H. Ackley
Wave Propagation Laboratory
National Oceanic and Atmospheric Administration
Boulder, Colorado 80303

17.1 Introduction

The measurements made by the standard instruments at and near the BAO tower, along with the signals from several special data channels, are recorded by a dedicated computer system and, through that system, are available for interactive use by scientists working at remote terminals. Considerable effort has been devoted to making this BAO computer system easy to use, flexible, self-teaching, and friendly. For example, all the documentation needed to use the system is kept in the computer and is available at any time to any terminal. Samples of this documentation appear in the figures described below. The system will produce low-resolution graphs on character-printing terminals and more refined graphs on any of several commonly used types of graphics terminals. Data remain in the computer for several weeks; after that, they may be retrieved from the tape library. Low-resolution, 20-min averages of the data, called "descriptors," are permanently available from the computer.

17.2 The Organization of Data in the Computer

Although the sampling rate of many of the BAO instruments is 10 samples per second, it is impractical to store so much in the computer. Instead, 10-s averages, 10-s grab samples, 20-min average spectra, and 20-min averages of various statistical moments are stored. More details about these various kinds of data appear in Figure 17.1. The arcane symbols in Figure 17.1 are explained in multi-page lists available on the computer. Figure 17.2 is an excerpt from such a list.

The data files just described fill the available memory of the computer in about two weeks of continuous operation of the BAO. After those data have been

archived on tape, it is convenient to retain, in the computer, a detailed description of the contents of the tapes. This is done with the descriptors of each data channel. Figure 17.3 shows the first page of a list available on the computer enumerating the 179 descriptors defined to date.

17.3 Standard Programs for Inspecting the Data

A number of standard computer programs are available for inspection of the data. Some print numerical summaries; others produce graphs. One elaborate standard program, named PIDGIN, permits flexible interaction with the data (see Section 17.4).

The user first approaching a terminal to work with the BAO data needs to know what data are available in the computer. The first step is to use the program AVL. Figure 17.4 shows output from AVL made in August 1979 when the PHOENIX data were still in the computer. The number associated with each hour tells how many of the 20-min archival periods in that hour were filled with data. It is easy to pick out from this display the long data runs made on September 11-12 and September 26-27, 1978.

The next step in the user's search for appropriate data to analyze might be to look at some of the descriptors. The standard program PLD plots the descriptors. Figure 17.5 shows the result of using an ordinary character-printing terminal to check the wind speed at 10 m height on September 11 and 12, 1978. Naturally, a graphics terminal would have given a more detailed plot. A tabulation of the same descriptors can be summoned by use of the standard program DSCRD. Figure 17.6 shows an example, tabulating wind speed and also direction at 10 m height. DSCRD, like all standard programs, is described in documents that are available from the computer. Figure 17.7 shows the documentation for DSCRD. A different way to get a quick look at summaries of the data is through the summary sheets produced by the standard program SUM. Figure 17.8 shows one such sheet; another appears as Figure 2.8 of Chapter 2 (Kaimal and Wolfe, 1979).

The details of the data, either time series or scatter plots, can be obtained through use of the standard program PLT. Figures 17.9a and b provide examples. Tabulations are given by program BAORD.

```
                    GENERAL BAO DATA INFORMATION
                             24AUG79

Data available through the BAO PDP-11/70 Computer System consist of
several kinds. The kind of data is determined by the location of the in-
strument, the method of data collection, and the method of data reduc-
tion. Current kinds of data are:

                    A       -       Averages
                    B       -       Boulder Wind Network
                    G       -       Grab Samples
                    M       -       Moments
                    S       -       Spectra

With the exception of Kind B Data, the data originate from the "Standard
BAO Data" channels recorded at or near the BAO Tower at Erie, Colorado.
Channels 1 through 50 are "high-speed" data channels and are normally
recorded at 10 samples per second. Channels 51 through 199 are "low-
speed" data channels and are normally recorded at 1 sample per second.
Channels 200 through 299 are for Kind B Data and are normally recorded
at 1 sample per minute. Channels 300 through 499 are utilized for the
results of spectral (Kind S) calculations. Channels 500 through 799
are utilized for the results of moment (Kind M) calculations. For de-
tails concerning the calculations used for "Standard BAO Data" channels
see "NOAA Instrumentation At The Boulder Atmospheric Observatory", J. C.
Kaimal, from the Proceedings of the Fourth Symposium on Meteorological
Observations and Instrumentation, April 10-14, 1978, Denver, Colorado.
**********************************************************************

                          KIND A DATA
                             24AUG79

Kind A Data are 10-second block averages of the "Standard BAO Data"
channels at or near the Tower. Kind A Data are calculated for all avail-
able height levels on the Tower and for all available ground instruments
near the Tower. The data have been averaged for storage on the PDP-11/70
disk system and for archiving.
**********************************************************************

                          KIND B DATA
                             12AUG79

Kind B Data are grab samples taken once every minute. At present, such
data are taken only from the Boulder Wind Network.
**********************************************************************

                          KIND G DATA
                             24AUG79

Kind G Data are grab samples taken once every 10 seconds from the "Stan-
dard BAO Data" channels at or near the Tower. Normally, grab samples
are taken from the fast response channels only. Kind G Data are cal-
culated for all available height levels on the Tower and for all avail-
able ground instruments near the Tower. The grab samples are used for
storage on the PDP-11/70 disk system and for archiving.
**********************************************************************
```

Figure 17.1.--The computer-resident documentation that describes the five kinds of BAO data files.

KIND M DATA
24AUG79

Kind M Data consist of first, second, and third moments; and certain quantities derived from the moments of selected channels. Available moment data include, but is not limited to, the following:

First Moments:	VW, VS, U, V, W, TH, T, TD, DP, P, SR, OTVN, OTVSE, OTVSW, CN2N, CN2SE, CN2SW, PVS, PVD
Second Moments:	UU, VV, WW, TT, UV, VW, UT, VT, UW, WT
Third Moments:	UVW, UWW, VWW, UUW, VVW, WWW, UWT, VWT, WWT, WTT

Derived Quantities: VH, AZ, AS, L, OTS, OTD, CONV, CN2, DPRMS

Kind M data are calculated for all available height levels on the Tower. The data are used for storage on the PDP-11/70 disk system and for archiving.

****

KIND S DATA
24AUG79

Kind S Data are smoothed spectral and cross spectral estimates, of which both consist of power spectral density times frequency. A 1024 point Fourier Transform is computed approximately every 2 minutes for each channel of interest. These spectra are first averaged over time for the entire archival period and then block averaged over a set number of non-overlapping frequency intervals, usually 22. The frequencies are selected so as to give roughly equal spacing of center frequencies on a logarithmic scale with a density of approximately 10 frequency blocks per decade. Available data include, but are not limited to, the following:

Power Spectra:	PSU, PSV, PSW, PST
Cospectra:	CSWU, CSWV, CSWT, CSUT, CSUV
Quad Spectra:	QSWU, QSWV, QSWT, QSUT, QSUV

Normalized Frequencies - (Hz)

(To get actual frequencies multiply by sampling freq. in points/second)

0.97656E-03	0.32227E-01
0.19531E-02	0.41992E-01
0.29297E-02	0.54688E-01
0.39063E-02	0.71289E-01
0.48828E-02	0.92773E-01
0.63477E-02	0.12061
0.83008E-02	0.15625
0.10742E-01	0.20264
0.14160E-01	0.26270
0.19043E-01	0.34082
0.24902E-01	0.44238

Horizontal quantities are given parallel and perpendicular to the mean.

****

[21,21]KIND.DOC

Figure 17.1.--Continued.

KIND A DATA
21SEP79

Kind A data are composed of data quantities whose resulting sampling rate is 120 points per archival period and whose independent variable is time. To date, the data consists only of quantities derived from the "Standard BAO Data" channels at or near the Tower. Currently, A data consists of 10 second block averages. Kind A data are calculated for all available height levels on the Tower and for all available ground instruments in the vicinity of the Tower. The data are stored on the PDP-11/70 on-line disk system and then later archived to magnetic tape.

DATA INDENTIFICATION CODE (DTIC) ASSIGNMENTS ARE:

DTIC	DATA ASSIGNMENT
1	VW(1) Horizontal wind component (sonic) from the West at 10 meters height. (Meters/second).
2	VW(2) Horizontal wind component (sonic) from the West at 22 meters height. (Meters/second).
3	VW(3) Horizontal wind component (sonic) from the West at 50 meters height. (Meters/second).
4	VW(4) Horizontal wind component (sonic) from the West at 100 meters height. (Meters/second).
5	VW(5) Horizontal wind component (sonic) from the West at 150 meters height. (Meters/second).
6	VW(6) Horizontal wind component (sonic) from the West at 200 meters height. (Meters/second).
7	VW(7) Horizontal wind component (sonic) from the West at 250 meters height. (Meters/second).
8	VW(8) Horizontal wind component (sonic) from the West at 300 meters height. (Meters/second).
9	VS(1) Horizontal wind component (sonic) from the South at 10 meters height. (Meters/second).
10	VS(2) Horizontal wind component (sonic) from the South at 22 meters height. (Meters/second).
11	VS(3) Horizontal wind component (sonic) from the South at 50 meters height. (Meters/second).
12	VS(4) Horizontal wind component (sonic) from the South at 100 meters height. (Meters/second).
13	VS(5) Horizontal wind component (sonic) from the South at 150 meters height. (Meters/second).

Figure 17.2.--The first page of the computer-resident list of channel numbers for BAO data of Kind A.

GENERAL BAO DESCRIPTOR INFORMATION
21SEP79

A Descriptor gives low resolution information about some specified data quantity at the rate of 1 value per archival period.

The following table gives the definition of each Descriptor Identification Code (DSIC). Descriptor values range from -127 through 127. A value of zero always indicates that no data exists. A value of 127 or -127 is always a singular case (see descriptions below) and should not be used in the linear conversion formula. A negative value always indicates that some data were misssing or had non-zero Defect Codes during the 20-minute archival period.

In the definitions that follow, the symbol J is used to denote the non-zero absolute value of the Descriptor. DTIC means "Data Identification Code". Meanings of the various DTICs can be found in [21,21]xHDR.INF where x is replaced by the one character code for Kind of data (A,B,G,M S, etc.). The linear conversion formula provides the necessary information for conversion from relative values to the actual engineering units of the particular DSIC.

Descriptors 69 through 137 have a special meaning. They contain "defect codes" that indicate any known or suspected defects in the associated primary data channels. The primary channels are those DTICs which are used in the calculation of any of the resulting DTICs or DSICs. The meaning of the Defect Code is:

0	No known or suspected defects.
2	Defective data noted by comparison of channels., e.g. a kinky profile.
4	Defective data noted by the appearance of the data in an individual channel, e.g. occasional spikes or discontinuities
6	The instrument was on the leeward side of the Tower.
8	Some data points are missing.
9	The sensor was inoperative.

The descriptors are currently stored on the PDP-11/70 on-line disk system for an indefinite period of time.

DESCRIPTOR IDENTIFICATION CODE (DSIC) ASSIGNMENTS ARE:

DSIC	DESCRIPTOR ASSIGNMENT
0	Vacant
1	Mean Westerly Wind from Table Mtn. to RB-3; corresponds to DTIC = 200 J-50 Meters/second. J=127; Laser beam obscured during part of interval.
2	Average horizontal wind speed at 10 meters height. (J-1)/2 Meters/second.
3	Average horizontal wind speed at 22 meters height. (J-1)/2 Meters/second.
4	Average horizontal wind speed at 50 meters height.

Figure 17.3.--The first page of the computer-resident list of descriptor identification codes. A total of 179 codes have been defined to date.

AVAILABLE DATA OF KIND A 19-AUG-79 09:02

DATE	HOUR 0						6						12						18					
780901.	0	0	0	0	0	0	0	0	0	3	3	2	0	0	0	0	0	0	0	0	0	0	0	0
780905.	0	0	0	0	0	0	0	2	3	3	3	3	3	3	1	0	0	0	0	0	0	0	0	0
780906.	0	0	0	0	0	0	0	2	3	3	3	2	3	1	0	0	0	0	0	0	0	0	0	0
780909.	0	0	0	0	0	0	0	1	3	3	3	3	3	3	3	0	0	0	0	0	0	0	0	0
780911.	0	0	0	0	0	3	3	2	3	3	3	3	3	3	3	1	3	3	3	3	3	2	3	3
780912.	3	3	3	3	3	3	3	3	1	0	0	0	0	0	0	0	0	0	0	0	0	0	0	0
780918.	0	0	0	0	0	0	2	3	3	3	2	3	3	3	2	3	0	0	0	0	0	0	0	0
780919.	0	0	0	0	0	0	0	0	1	3	3	3	3	3	3	2	0	0	0	0	0	0	0	0
780920.	0	0	0	0	0	0	0	0	3	3	3	3	3	3	3	3	0	0	0	0	0	0	0	0
780921.	0	0	0	0	0	0	0	1	3	3	3	3	3	3	3	3	3	3	1	0	0	0	0	0
780922.	0	0	0	0	0	0	0	1	3	3	3	3	3	3	3	3	3	3	0	0	0	0	0	0
780925.	0	0	0	0	0	0	0	3	3	2	0	0	0	0	0	0	0	0	0	0	0	0	0	0
780926.	0	0	0	0	0	3	3	3	3	2	3	3	3	3	3	3	2	2	3	3	2	2	1	3
780927.	3	3	3	3	3	3	3	3	3	3	3	3	1	3	3	3	3	2	3	0	0	0	0	0

Figure 17.4.--A computer-generated table of data available from the PHOENIX experiment. The number associated with each hour gives the number of 20-min archival periods for which data of Kind A exist.

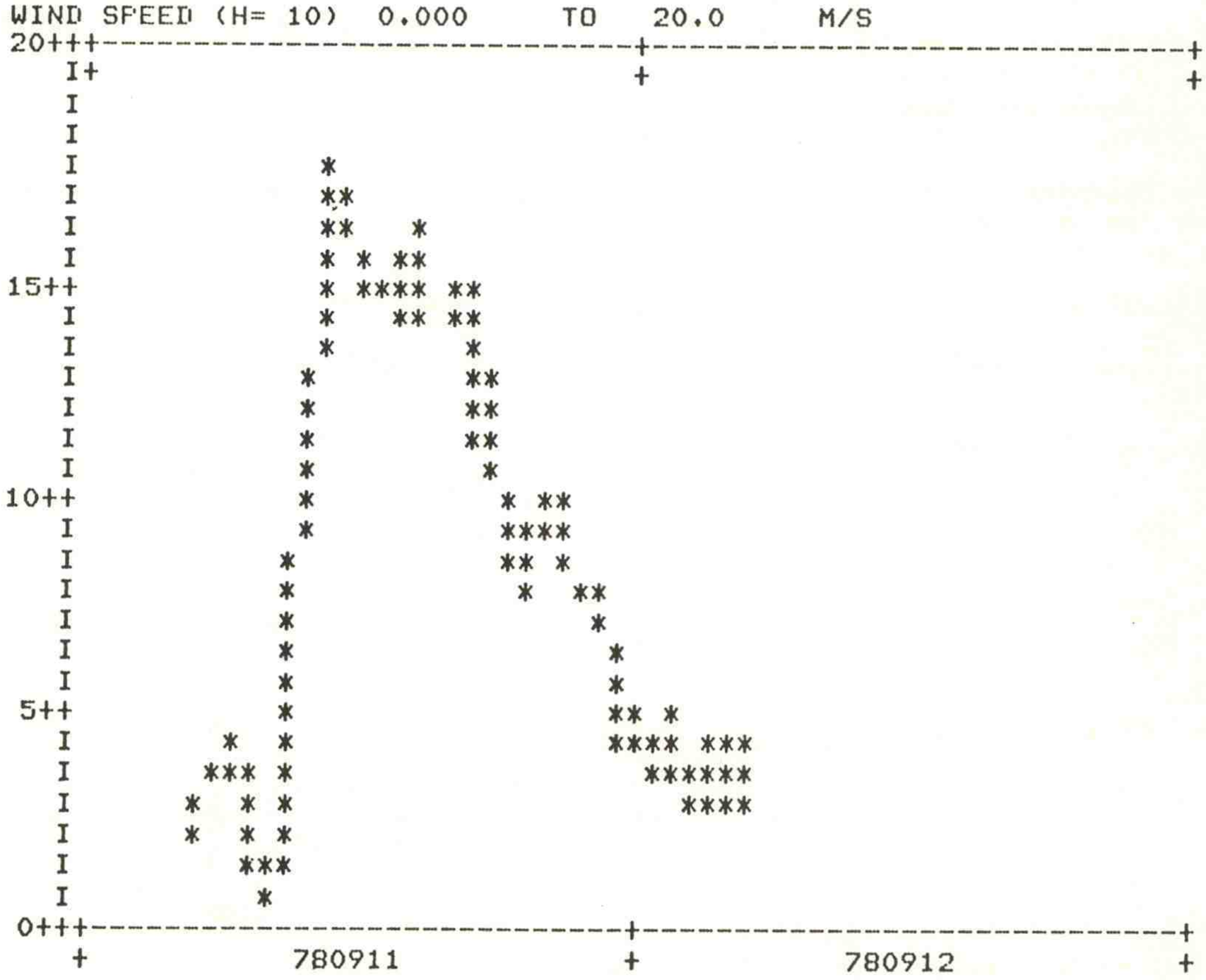


Figure 17.5.--A plot, made by the standard program PLD, of the descriptors for wind speed at 10 m height for two consecutive days of the PHOENIX experiment.

```
>RUN $DSCRD
INPUT 1 TO 3 DESCRIPTOR IDENTIFICATION CODES: 2,10
DATE: 780911
TIME (HHMM) = 0000
HOW MANY DESCRIPTORS? 144
 SOME DESCRIPTORS MISSING
TYPE EVERY NTH.  N = 3
780911.  5.00    5   2.00        49   144.
780911.  6.00    8   3.50       114   339.
780911.  7.00   10   4.50       113   336.
780911.  8.00    2  0.500        36   105.
780911.  9.00    5   2.00        74   219.
780911. 10.00   25   12.0        38   111.
780911. 11.00   36   17.5        31   90.0
780911. 12.00   32   15.5        33   96.0
780911. 13.00   30   14.5        37   108.
780911. 14.00   29   14.0        37   108.
780911. 15.00   29   14.0        35   102.
780911. 16.00   31   15.0        34   99.0
780911. 17.00   28   13.5        34   99.0
780911. 18.00   24   11.5        35   102.
780911. 19.00   18   8.50        34   99.0
780911. 20.00   20   9.50        34   99.0
780911. 21.00   18   8.50        29   84.0
780911. 22.00   17   8.00        30   87.0
780911. 23.00   15   7.00        29   84.0
780912.  0.00   11   5.00         8   21.0
780912.  1.00    8   3.50         2   3.00
780912.  2.00    9   4.00         4   9.00
780912.  3.00    8   3.50       116   345.
780912.  4.00    7   3.00         5   12.0
780912.  5.00    8   3.50       106   315.
```

Figure 17.6.--A tabulation of the 10-m wind-speed and wind-direction descriptors for September 11-12, 1978. Every third descriptor is shown. The first two columns give date and time. Columns 3 and 5 are the actual descriptors as stored in the computer. Columns 4 and 6 are the conversions of those descriptors to engineering units. In this case they are wind speed (m/s) and direction (degrees).

DSCRD

FORTRAN PROGRAM
PDP-11; F4P

Robert S. Lawrence
NOAA, WPL
IDENT:17APR79

1. GENERAL DESCRIPTION
   Given a list of Descriptor Identification Codes (DSIC), a starting date and time, and the number of points per DSIC, DSCRD reads the appropriate BAO Descriptor files and lists the specified values.

2. USAGE
   REQUIRED INPUT
   1. List of DSIC's.
      The list may be of the general form of: I,J-M,N where J-M indicates all DSIC's including and between J and M. All DSIC's must be unique. A maximum of 3 DSIC's is allowed.
   2. Starting Date of Descriptors.
      Three options are available to the User.
      a. Date in the form of YYMMDD.
      b. The User may simply type T, for Today. If this option is selected, the computer verifies the current computer date by immediately printing it out.
      c. The User may also type T-N, where N is some positive integer number. The starting date will then be N days ago from the current computer date. Verification of starting date is the same as for T option.
   3. Starting Time of Descriptors.
      Time is entered in the form of HHMM.
   4. NPPC, number of points per DSIC to list. Maximum number is 1000.
   5. If NPPC is greater than 10, then the User may specify that every Nth point per DSIC be typed.

3. USER NOTES
   A. Output device is the User's terminal and formatted for terminals of width greater than 70 columns.
   B. Along with the requested data, DSCRD also lists the corresponding date and time. Time is in the form of HH.MM. Both unscaled and scaled values are listed for each DSIC.
   C. If any of the requested Descriptors is missing, the program will issue a message indicating such.

4. LOADING INFORMATION
   To use, type: RUN $DSCRD

DSCRD: Reads BAO Descriptor files and lists Descriptors.

Figure 17.7.--The computer-resident documentation of the standard program DSCRD.

BOULDER ATMOSPHERIC OBSERVATORY DATA SUMMARY

AVERAGING PERIOD= 20.00 MIN 21 SEP 78 1200 MST

Z[M]	VWES	VSOU	W	VH	AZ	PVS	PVD	T	TD	L
10	-1.50	0.59	-0.11	1.61	111.	1.94	108.	13.54	-4.36	-1.91
22	-1.69	0.78	-0.25	1.86	115.	2.11	112.	13.15	-4.97	-1.58
50	-1.99	0.99	-0.42	2.22	117.	2.38	117.	12.85	-4.97	*******
100	-1.71	1.09	-0.49	2.03	122.	2.24	127.	12.23	-4.91	-0.34
150	-1.28	1.37	-0.61	1.88	137.	******	****	11.53	-5.19	*******
200	-1.24	1.26	-0.37	1.77	135.	1.94	135.	10.28	-4.79	*******
250	-1.22	1.08	-0.26	1.63	132.	******	****	10.35	-5.40	*******
300	-1.06	1.28	-0.13	1.66	140.	2.04	133.	9.91	-5.30	*******

Z[M]	UU	VV	WW	TT	UV	VW	UT	VT	UW	WT
10	1.1221	1.9952	0.2789	0.4707	0.5371	0.0048	0.0078	0.2125	-0.0287	0.2122
22	0.8773	1.9138	0.4779	0.2301	0.3248	-0.0700	0.0211	0.1411	-0.0254	0.2129
50	0.9382	1.7686	0.7791	0.1261	0.2358	-0.0933	-0.0166	0.0596	0.0489	0.1729
100	1.1941	0.8639	0.8635	0.0731	0.1228	-0.0250	-0.0790	0.0193	-0.0062	0.1174
150	1.7963	0.6762	0.8379	0.0417	-0.1446	0.0088	0.0741	0.0381	0.0449	0.0473
200	1.2336	0.6867	0.7293	0.0318	0.0101	0.0387	-0.0311	0.0184	-0.1226	0.0403
250	1.1678	0.7056	0.7394	0.0347	0.2078	0.0759	-0.0208	0.0418	-0.1746	0.0167
300	0.8461	0.7159	1.0114	0.0343	-0.0119	-0.0276	0.0407	0.0669	-0.2025	-0.0362

Z[M]	UVW	UWW	VWW	UUW	VVW	WWW	UWT	VWT	WWT	WTT
10	-0.01269	-0.00609	0.00546	0.03253	0.03595	0.02270	-0.00688	0.04527	0.04824	0.10331
22	-0.05913	-0.02329	-0.02306	-0.02191	0.15245	0.11151	-0.02360	0.03128	0.09475	0.11743
50	0.03602	0.11981	-0.15342	0.06315	0.40836	0.27901	-0.00971	-0.01374	0.13454	0.09812
100	0.09677	0.19558	0.02401	-0.03104	0.18938	0.41623	-0.02578	0.02176	0.02420	0.02215
150	0.07675	0.31259	0.06342	0.40827	0.23830	0.41573	0.03330	0.01806	0.01245	0.02085
200	0.01083	0.25890	0.09704	0.44099	0.18604	0.46357	-0.01694	-0.01373	0.01046	0.01280
250	-0.04055	-0.17368	-0.09250	0.40599	0.09531	0.15880	-0.02361	-0.03705	-0.03312	0.00082
300	-0.05847	-0.17566	-0.25082	0.20698	0.07476	0.69115	0.02132	-0.02513	-0.09370	0.00112

OPTICAL TRIANGLE

V [M/SEC]	AZ[DEG]	CONV[1/SEC]	LOG10 CN-SQR
0.77	120.	-0.00683	0.22430

RMS PRESSURE VALUES [MICROBARS]

STN 1	STN 2	STN 3	STN 4	STN 5
3.996	5.788	4.955	6.933	6.058

PRESSURE[MB]
848.14

SOLAR RAD[LY/MIN]
1.12

Figure 17.8.--A 20-min summary sheet produced by the standard program SUM.

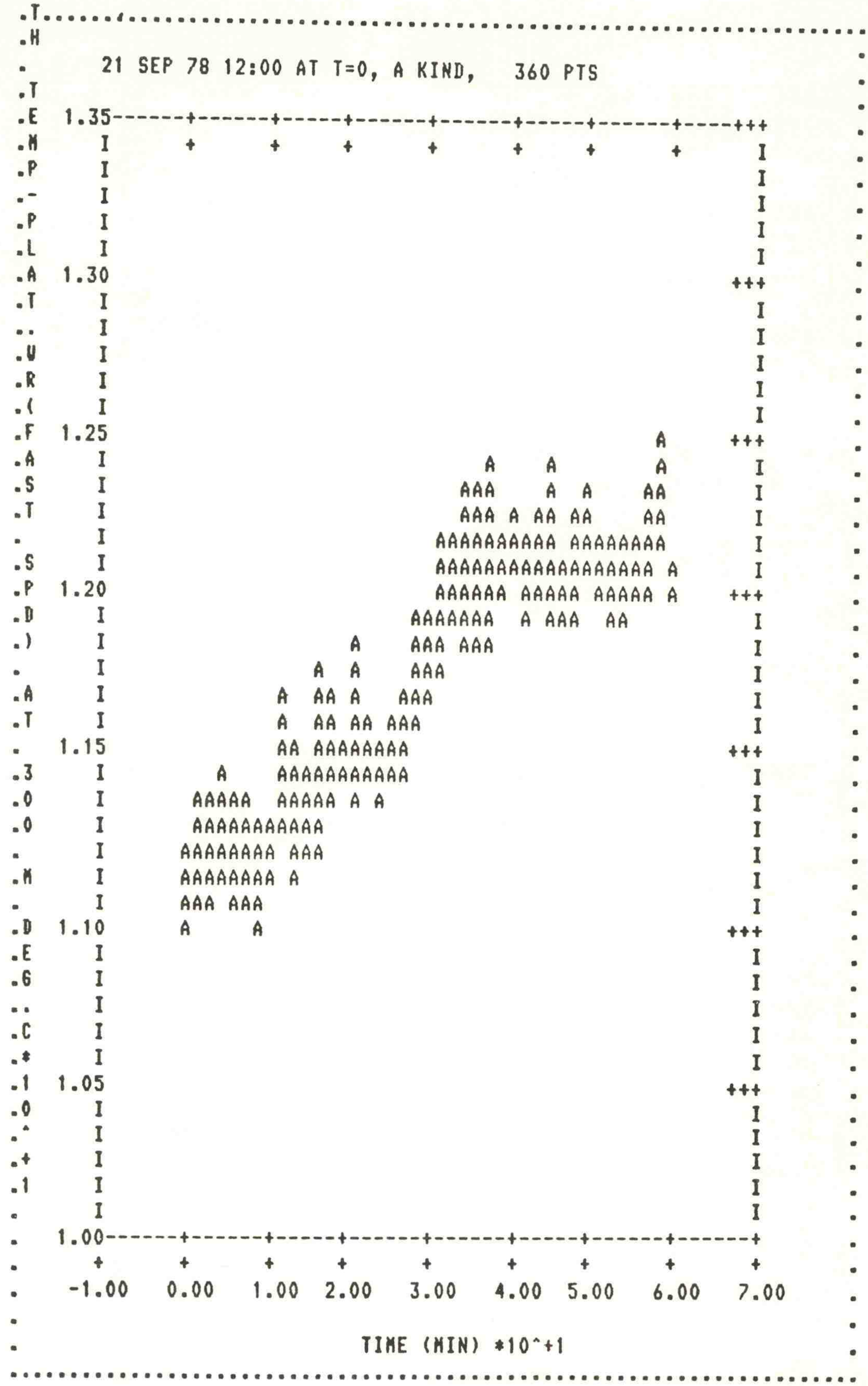


Figure 17.9a.--An example of a 1-h plot of temperature, made by the standard program PLT using an ordinary character-printing terminal.

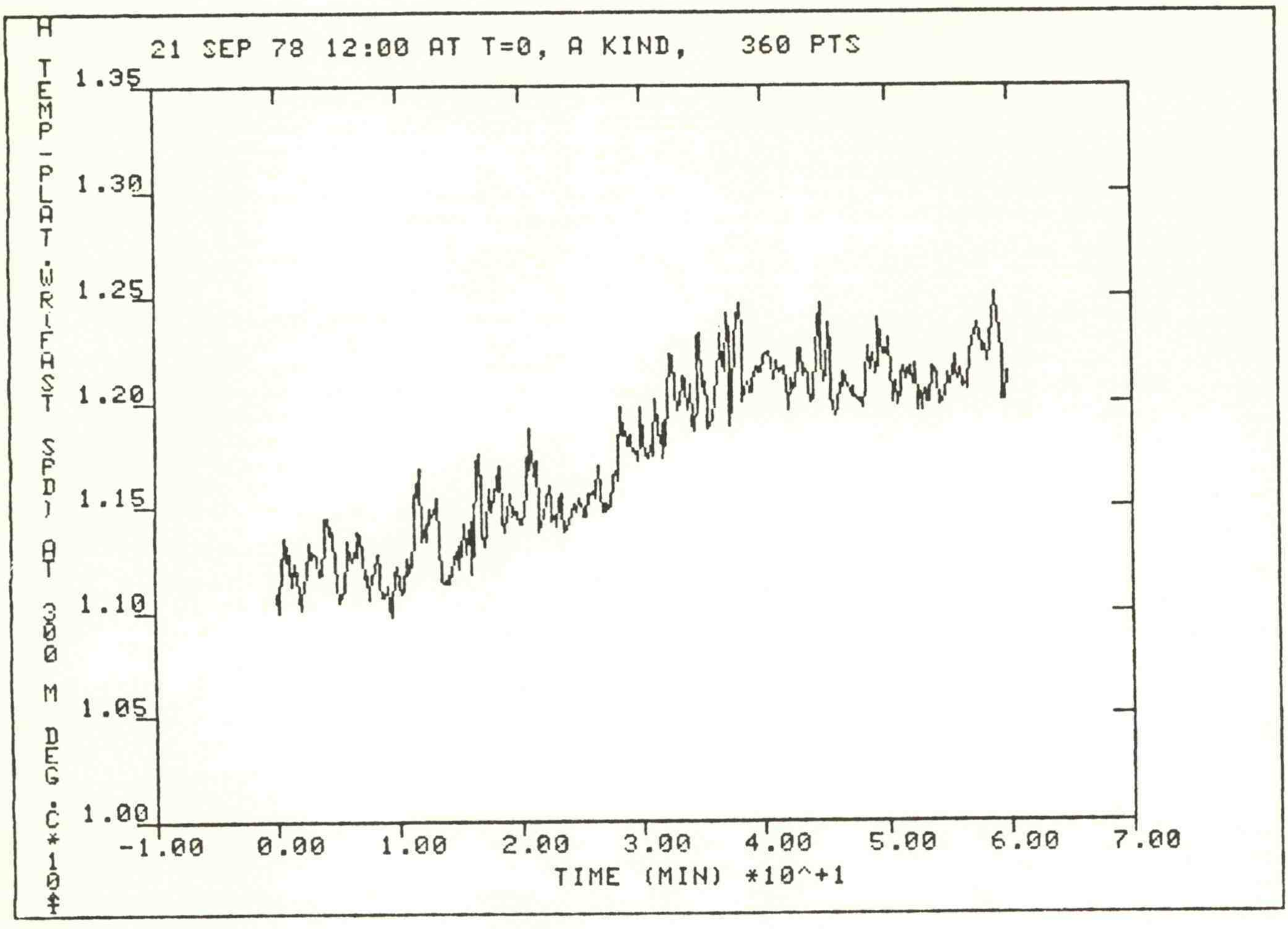


Figure 17.9b.--The plot shown in 17.9a, displayed on a graphics terminal.

17.4 The PIDGIN Language for Manipulating the Data

For the user who must perform some manipulations of the data but does not wish to write specialized computer programs, the PIDGIN language is available. As its name implies, PIDGIN consists of English words used singly and without syntax. More detailed information is transmitted through a plain-English question-and-answer process. Figures 17.10 and 17.11, excerpted from the PIDGIN User's Manual, give a hint of the scope of PIDGIN.

17.5 Custom-Built Computer Programs

The most flexible way to manipulate the BAO data is, of course, with custom-built programs. The BAO computer uses the FORTRAN programming language, and a

Basic PIDGIN Philosophy

The Scientist in today's world of high speed data acquisition is traditionally faced with the problem of being able to obtain previews of the data and to perform basic manipulations and analyses of that data on a timely basis. The ideal solution would be to provide an interactive system by which the Scientist could easily access data and perform the above mentioned tasks.

To this end, PIDGIN was created.

PIDGIN was designed under the assumption that its User has little or no familiarity with computer languages or interactive data processing. Therefore, interactive guidance and question/answer consistency would be needed. All interaction between the User and PIDGIN is in an English-like structure. The User communicates with PIDGIN through the issuance of simple single word Directives. In turn, if an individual Directive needs to further communicate with the User, it does so with easily understandable queries. Each Directive is designed to perform a single well-defined task.

In order to guide the User through an interactive session, PIDGIN was designed with many friendly and easy-to-use features. Perhaps the most prominent of these, is the HELP feature. In response to any question or PIDGIN prompt character (#), the User may type HELP. PIDGIN will then respond accordingly with an appropriate message depending upon its current operation. All input is checked for a proper response. If an invalid response is received by PIDGIN, the User is then so advised. PIDGIN helps the User by supplying the ranges or discrete values of acceptable input. Other features include standardization of question and answer formats and recovery from erroneous operations, data anomalies, and User-induced errors.

Another prominent feature of PIDGIN is that it imposes no limitations or scientific judgments upon the manner in which the User manipulates the data. Only mathematical operations are checked for their validity and consistency with pre-defined procedures. In the event that PIDGIN encounters an operation or situation requiring Deviation from this feature the User is always informed of this non-standard manipulation.

PIDGIN is forever growing and changing to meet the needs of the Users through the implementation of additional Directives or the modification of existing Directives. Such modification is another feature of PIDGIN.

In summary, PIDGIN is:

1. friendly and easy to use,
2. makes no scientific judgments,
3. is expandable as the needs of the Users grow.

Figure 17.10.--An excerpt from the introduction to the PIDGIN User's Manual.

TABLE OF PIDGIN DIRECTIVES

FULL	BRIEF	DESCRIPTION
ADD	ADD	Increments Workfile data by a given value
ANTILG	ALG	Calculates antilogs of Workfile data
BACK	BK	Backspaces one question
BOOK	BO	Lists all available User Directives
BRIEF	BF	Short form of questions and error messages
-BRIEF	-BF	Long form of questions and error messages
CMPRES	CMP	Compresses Workfile data
COSINE	COS	Calculates cosine of Workfile data
DATE	DT	Returns computer date in YYMMDD format
DELETE	DEL	Removes Procedure/Response file
DIVIDE	DIV	Divides Workfile data by a given value
DSIC	DSIC	Sets Descriptor Identification Code mode
DTIC	DTIC	Sets Data Identification Code mode
DUMP	DP	Outputs contents of Workfile
ECHO	EC	Echo of Procedure/Response files
-ECHO	-EC	No echo of Procedure/Response files
END	END	Terminates creation of a Procedure file
ERASE	ERS	Removes a specified Workfile
EXIT	EX	Exit from PIDGIN to System or the Directive level
FIND	FD	Moves requested BAO data into a Workfile
HELP	HP	Responds with information about input requirements
HISTO	HI	Gives a histogram
LIST	LI	Lists Workfiles in use
LOGLN	LOG	Calculates logarithms of Workfile data
MULTPY	MUL	Multiplies Workfile data by a given factor
NULL	NULL	Null Directive for PIDGIN debugging
PLOT	PLT	Plots Workfile data
POWER	PWR	Calculates the Nth power of Workfile data
QUIT	QT	Ends a recursive question set
ROOT	RT	Calculates the Nth root of Workfile data
SAVE	SV	Starts creation of a Procedure file
SETPLT	STP	Sets plotting mode - Vector or Dot
SETSCL	STS	Sets User defined data scales - Minimum and Maximum
SETTRM	STM	Sets terminal width and height characteristics
SINE	SIN	Calculates sine of Workfile data
STAT	ST	Gives several statistics including a histogram
SUBTRT	SUB	Decrements Workfile data by a given value
TIME	TM	Returns computer time in HHMM format
TOP	TP	Returns to start of Directive's question
TOWER	TWR	Description of standard instruments on the Tower
TRUST	TRU	Use all data regardless of quality
-TRUST	-TRU	Replace all defective data with -1.1E38
XECUTE	XE	Starts execution of a Procedure file

Figure 17.11.--A list of the PIDGIN directives that are presently available.

limited amount of computer time is available for this purpose. A fully documented library of nearly 200 subroutines is available for data manipulation, statistical calculations, and plotting. Procedures are also available for making abstract tapes of the data for use on other computers.

17.6 Access Arrangements

Prospective users of the BAO computer system should contact Dr. J. C. Kaimal (commercial phone (303) 499-1000 ext. 6263, FTS 323-6263).

Reference

Kaimal, J. C., and D. E. Wolfe, BAO site, tower instrumentation, and PHOENIX operations, Chapter 2, in Project PHOENIX: The September 1978 Field Operation, W. H. Hooke, Ed., NOAA/NCAR Boulder Atmospheric Observatory Rept. No. 1, available from NOAA/ERL, Boulder, Colo., and from NCAR Publication Office, Boulder, Colo. (1979).

* U. S. GOVERNMENT PRINTING OFFICE: 1980-O-677-138/3

NOAA CENTRAL LIBRARY
CIRC QC851 .B6 no.1
Project Phoenix: the Septe
3 8398 0003 2154 1

PROJECT PHOENIX

